Highly Fluorinated Chiral Sensors for Enantioselective Fluorescent Recognition

Chao Wang
Chibi, China

Bachelor of Science
Renmin University of China, 2012

A Dissertation presented to the Graduate Faculty
of the University of Virginia in Candidacy for the Degree of
Doctor of Philosophy

Department of Chemistry

University of Virginia
May, 2017 Degree will be Conferred

Abstract

Various kinds of fluorinated organic sensors using 1, 1'-Bi-2-naphthol (BINOL) as the chiral core have been developed for the fluorescent recognition of chiral molecules. This study is potentially applicable for rapid enantiomeric excess determination and high throughput catalyst screening.

A perfluoroalkyl diketone compound is synthesized as the first enantioselective fluorescent sensor in a fluorous solvent. Within a certain concentration range one enantiomer causes 1200-2000 folds fluorescent enhancement to the sensor, while the other one only gives 10-50 folds enhancement. Light scattering studies show the formation of aggregates with different particle sizes when the two enantiomers interact with the sensor. The substantial difference enables visual discrimination of two enantiomers with naked eyes. A series of similar sensors are also prepared and their fluorescence responses in various fluorinated solvents are studied.

A facile amide bond formation is utilized for the enantioselective recognition of various amines for the first time. A dramatic solvent effect is observed for the reaction of amine with the H_8BINOL-based perfluoroalkyl ketone. In DMF, cleavage of the perfluoroalkl group to form amides is observed but not in other solvents. This provides a new direction for the design of molecular sensors for amine recognition. A series of other highly fluorinated ketones are also synthesized for the enantioselective sensing of amino acid anions in DMSO. The best enantioselectivity was observed in the case of serine with *ef* values up to 10 when excess amount of serine is used.

A BINAM-based ketone sensor is found to show ratiometric sensing toward diamines, which enables the simultaneous determination of both concentration and ee

values. It also shows moderate enantioselectivity toward amino acids and hydroxyl acids. Moreover, fluorescent dyes have been conjugated to the chiral binaphthyl structure for the sensing of hydroxyl acids and amines at long emission wavelengths.

Acknowledgement

Firstly my appreciation goes to Dr. Lin Pu. Without the support and advise from him, none of the chemistry discoveries mentioned here were possible. The innovative ideas from him have inspired me frequently in the projects. I can always learn something new from him in the discussion. I have been feeling lucky to have an advisor like him that is so knowledgeable and patient and willing to help. My gratitude also goes to my committee members Dr. Brent Gunnoe, Dr. James Demas, Dr. Glenn Mcgarvey and Dr. Jiang He for their academic advise. I am thankful for the help from Dr. Ian Harrison, as well as many other faculty and staffs in the department.

I also would like to thank the former and current members in *Pu* lab. They helped me a lot either in the research or in my daily life. To name a few, they are Xiangfeng Guo, Xuemin Duan, Shanyong Chen, Shuangxi Gu, Wencai Huang, Zhilian Liu, Bin Zhao, Hui Wu, Shanshan Yu, Wei Chen, Xuepeng Zhang, Jun Ying, Shifeng Nian, Sheldon Wu, Gengyu Du, Chaoyuan Zeng, Elaine Wu and Parastoo Anbaei. I am also thankful to all of my friends in chemistry department and in the university.

Lastly I would like to thank my parents and siblings for their enduring support. Their love and care is the greatest fortune of my life. They always support my choice in my career development. They are there to provide me guidance whenever I need.

Table of Content

Abstract ...... **ii**

Acknowledgement ...... **iv**

Table of Content ...... **v**

List of Figures ...... **x**

List of Schemes ...... **xxix**

List of Tables ...... **xxxii**

Chapter 1. Fluorescent Sensor for Chiral Recognition **1**

- **1.1. Importance of chiral molecules** **1**
- **1.2. Current techniques for chiral analysis** **2**
  - 1.2.1. Chiral HPLC and GC for analysis 2
  - 1.2.2. NMR for chiral analysis 3
  - 1.2.3. Circular dichroism for chiral analysis 5
  - 1.2.4. Chiral capillary electrophoresis (CE) 6
- **1.3. Technique evolution for high-throughput screening (HTS)** **7**
  - 1.3.1. HPLC-CD 8
  - 1.3.2. UV-Vis 9
  - 1.3.3. IR-thermography 10
  - 1.3.4. Mass spectrometry 10
- **1.4. Fluorescence in chiral analysis** **12**
  - 1.4.1. Fluorescence sensors 12

1.4.2. Sensors based on non-covalent bondings 14

1.4.2. Sensors based on dynamic covalent reactions. 19

1.4.3. Sensing based on metal complex. 22

1.5. References 24

Chapter 2. Fluorinated molecules in catalysis, separation, and optical studies 29

2.1. Introduction of fluorous chemistry 29

2.2. Fluorous molecules in catalysis and separation 30

2.3. Optical studies of fluorous molecules 33

2.4. References 36

Chapter 3. Enantioselective Fluorescent Recognition in Fluorous Phase: Enhanced Reactivity and Expanded Chiral Recognition 38

3.1. Introduction 38

3.2. Results & Discussion 41

3.2.1. Synthesis of the sensor 41

3.2.2. Study of the interactions of the sensor and amine in organic solvents 42

3.2.3. Study the interactions of sensor and amine in fluorous solvents 46

3.2.4. Fluorescence recognition of other chiral amines 56

3.2.5. Enantiomeric excess determination using fluorescence 64

3.2.6. Further exploration of fluorescent sensing in fluorous solvents 65

3.3. Conclusion 78

3.4. Experimental section 80

3.4.1. General information 80

3.4.2. Sample preparations 81

3.4.3. Synthesis and characterization 83

3.5. References 90

Chapter 4. Enantioselective Detection of Amines and Amino Acids by Amide Formation from Perfluoroalkyl Ketones 91

4.1. Introduction 91

4.2. Results & Discussion 93

4.2.1. Synthetic routes of compounds 93

4.2.2. Solvent-dependent fluorescence response 95

4.2.3. Time-dependent fluorescence response 99

4.2.4. Enantioselective recognition of sensor to the amine 102

4.2.5. Mechanism studies between the reaction of sensor and amine 104

4.2.6. Fluorescence recognition of unfunctional amines 114

4.2.7. Fluorescence recognition of functional amines 119

4.2.8. Fluorescence response of BINOL-based sensor to amines 127

4.2.9 Achiral fluorinated ketones for amine sensing 132

4.2.10. Sensing of amino acids using amide formation 134

4.3. Conclusion 156

4.4. Experimental part 157

4.4.1. General data 157

4.4.2. Sample preparation for fluorescence measurement: 158

4.4.3. Synthesis and characterization 159

4.4.4. Mass spectroscopic studies 175

4.5. References 176

Chapter 5. A fluorinated BINAM derived sensor for chiral recognition 178

5.1. Design and synthesis of (*S*)-5.1 178

5.2. Fluorescence response of (*S*)-5.1 to chiral molecules 180

5.3. Mechanism studies 183

5.4. Conclusion 186

5.5. Experimental part 186

5.5.1. General data 186

5.5.2. Synthesis and characterization 187

5.6. References 188

Chapter 6. Highly fluorinated aldehyde sensors for chiral recognition in fluorous phase 189

6.1. Introduction 189

6.2. Results & Discussion 190

6.3. Conclusion 218

6.4. Experimental part 219

6.5. References 219

Chapter 7. Attempted research: conjugation of fluorophore with chiral backbone for enantioselective recognition 228

7.1. Introduction 228

7.2. Results & Discussion 228

7.2.1 Enantioselective recognition of chiral acid 228

7.2.2. Enantioselective recognition of amines with Resorufin conjugate 235

7.3. Conclusion 243

7.4. Experimental part 243

7.5. References 247

Appendix 249

Appendix for Chapter 3 249

Appendix for Chapter 4 261

Appendix for Chapter 5 285

Appendix for Chapter 6 287

Appendix for Chapter 7 296

List of Figures

Figure 1- 1. A typical setup for M.S. in HTS.. 11

Figure 1- 2. Methods used in fluorescence sensing 13

Figure 1- 3. Three-point interaction between a chiral host and guest............................. 13

Figure 1- 4. Emission spectra of **6**, **8** or **9** with or without hydroxyl acid. 16

Figure 1- 5. Structure of **1.11** and its fluorescence response to mandelic acid. 17

Figure 1- 6. Interactions of **1.15** with hydroxyl acids and the fluorescence response..... 17

Figure 2-1. Examples of fluorinated drugs. 29

Figure 2-2. F-rhodamine dyes synthesized by Kölmel *et al.* 33

Figure 2-3. A perylene diimide dye synthesized by Luca *et al.*...................................... 34

Figure 2-4. Various fluorous polyaromatics synthesized by Sun *et al.* 35

Figure 3-1. Structures of chiral amines used in this study... 42

Figure 3-2. Fluorescence spectra of (*S*)-**3.6** (0.08 mM) with or without (*R*)-**3.7** and (*S*)-**3.7** (5 mM) using dichloromethane as solvent. Spectra were recorded at 1 h, 3 h, 5 h, 7 h, 10 h and 23 h after mixing. λ_{ex}= 290 nm, slit 2/2 nm. 43

Figure 3-3. NMR titration of (*R*)-**3.7** (2 mM in $CDCl_3$) to (*S*)-**3.6** (0.02 mM in 0.4 mL $CDCl_3$). ^{1}H NMR spectra were recorded with the addition of the **3.7** in the following amounts: 0, 1, 3, 5, 10, 15, 20, 30 and 40 μL. These volumes correspond to 0, 0.2, 0.6, 1.0, 2.0, 3.0, 4.0, 6.0, and 8.0 equiv. of **3.7** respectively.^{19}F NMR spectra were recorded with the addition of 0, 4.0, 6.0 and 8.0 equiv. of **3.7**... 43

Figure 3- 4. NMR titration of (*S*)-**3.7** (2 mM in $CDCl_3$) to (*S*)-**3.6** (0.02 mM in 0.4 mL $CDCl_3$). ^{1}H NMR spectra were recorded with the addition of the (*S*)-**3.7** solution in the following amounts: 1, 3, 5, 7.5, 10, 15, 20, 30 and 40 μL. These correspond to 0.2, 0.6, 1.0, 1.5, 2.0, 3.0, 4.0, 6.0, and 8.0 equiv. respectively. ^{19}F NMR spectra were recorded with the addition of 0, 4.0, 6.0 and 8.0 equivalents of (*S*)-**3.7**. 45

Figure 3-5. Fluorescence spectra of (*S*)-**3.6** (8.0 x 10^{-5} M) in the presence of (*R*)-**3.7** (a) and (*S*)-**3.7** (b) with a concentration range of 0.5 to 5 mM (Spectra were recorded 1h after mixing. Solvent: 4% DCM/FC-72, λ_{ex} = 290 nm, slit 2/2 nm).(c)Fluorescent intensity at λ_{em} = 420 nm versus the concentration of (*R*)-**3.7** or (*S*)-**3.7** (Error bars were obtained with 4 independent measurements) and (d) effect of the reaction time. 47

Figure 3-6. Fluorescence spectra of (*R*)-**3.6** (8.0 x 10^{-5} M) in the presence of (*R*)-**3.7** (a) and (*S*)-**3.7** (b) within the concentration range from 0.5 mM to 5 mM. Fluorescence intensity at λ_{em} = 420 nm versus the concentration of (*R*)-**3.7** or (*S*)-**3.7** (c) and effect of the reaction time in 4 h plotted with error bars (d). Spectra were recorded 1 h after mixing. Solvent: 4% DCM/FC-72, excited at 290 nm, slit 2/2 nm. 48

Figure 3-7. UV-Vis absorption spectra of (*S*)-**3.6** (0.08 mM) with or without (*R*)-**3.7** (left) and (*S*)-**3.7** (right) ranging from 0.5 mM to 5 mM in 4% DCM/FC-72 respectively. 49

Figure 3-8. Excitation spectra of (*S*)-**3.6** (0.08 mM) with (*R*)-**3.7** or (*S*)-**3.7** (5.0 mM). Spectra were recorded 1h after mixing the solution. Solvent: 4% DCM / FC-72, λ_{em}= 420 nm, slit 2/2 nm. 49

Figure 3- 9. Titration of (*S*)-**3.6** (0.8 mM, 10 mL in FC-72) with 0, 2, 4, 5, 6, 7, 8, 10 and 12 equiv. of (*R*)- or (*S*)-**3.7** solutions in CH_2Cl_2 (0.8 M) (from left to right). 50

Figure 3-10. Photos of (*S*)-**3.6** (8.0×10^{-4} M, 4% CH_2Cl_2 / FC-72) treated with (a) 10 equiv. (*R*)-**3.7** (left) and 10 equiv. (*S*)-**3.7** (right), and (b) under a UV-lamp (λ= 254 nm). 51

Figure 3-11. Photos for the reactions of (*S*)-**3.6** with (*R*)-**3.7** or (*S*)-**3.7** at various concentrations. From left to right: 0.08 mM (*S*)-**3.6** with 1 mM (*R*)- or (*S*)-**3.7**; 0.08 mM (*S*)-**3.6** with 5.0 mM (*R*)- or (*S*)-**3.7** under UV-lamp; 0.8 mM (*S*)-**3.6** with 5.0 mM (*R*)- or (*S*)-**3.7**. 51

Figure 3-12. ^{1}H NMR and ^{19}F NMR of the isolated complex from (*S*)-**3.6** + (*R*)-**3.7** and (*S*)-**3.6** + (*S*)-**3.7** in $CDCl_3$. (Note: the $CDCl_3$ used here was treated with K_2CO_3 overnight and then filtered through a pipet packed with dry neutral alumina to remove trace amount of acid and H_2O).......... 53

Figure 3- 13. DLS data and spectra for (*S*)-3.6 + (*R*)-3.7 and (*S*)-3.6 + (*S*)-3.7. 55

Figure 3-14. Fluorescence spectra of (*S*)-**3.6** (0.08 mM) in the presence of (*R*)-**3.11** (left) or (*S*)-**3.11**(right) with a concentration range of 1 to 5 mM. Spectra were recorded 1 h after mixing the solution. Solvent: 4% DCM/FC-72, λ_{ex} = 290 nm, slit 2/2 nm... 57

Figure 3-15. Fluorescent intensity of (*S*)-**3.6** against the concentration of (*R*)-**3.11** or (*S*)-**3.11** at 420 nm.Four independent experiments were conducted (left), and an averaged diagram with error bar was plotted (right). 57

Figure 3- 16. Fluorescent intensity at 420 nm recorded at 1, 2, 3 and 4 h after the mixtures of (*S*)-**3.6**+ (*R*)-**3.11** and (*S*)-**3.6**+ (*S*)-**3.11** were prepared.......... 58

Figure 3-17. Fluorescence spectra of (*S*)-**3.6** (0.08 mM) in the presence of (*R*)-**3.12** (left) or (*S*)-**3.12** (right) with a concentration range of 0.5 to 5 mM. Recorded 1 h after mixing the solution. Solvent: 4% DCM / FC-72, λ_{ex} = 290 nm, slit 2/2 nm. 58

Figure 3-18. Fluorescence intensity of (*S*)-**3.6** against the concentration of (*R*)-**3.12** or (*S*)-**3.12** at 425 nm. Spectra were recorded 1h after mixing the solution. Four independent experiments were conducted (left), and an averaged diagram with error bar was plotted (right). 59

Figure 3- 19. Fluorescence spectra of (*S*)-**3.6** (0.08 mM) in the presence of (*R*)-**3.13** (left) or (*S*)-**3.13** (right) with a concentration range of 0.6 to 5 mM. Spectra were recorded 1 h after mixing. Solvent: 4% DCM/FC-72, λ_{exc}= 290 nm, slit 2/2 nm.................. 59

Figure 3- 20. Fluorescent intensity of (*S*)-**3.6** against the concentration of (*R*)-**3.13** or (*S*)-**3.13** at 423 nm. Four independent experiments were conducted (left), and an averaged diagram with error bar was plotted (right). 60

Figure 3-21. Fluorescent intensity of (*S*)-**3.6** at 423 nm recorded at 1, 2 and 4 h after the mixtures of (*S*)-**3.6** + (*R*)-**3.13** and (*S*)-**3.6** + (*S*)-**3.13** were prepared...................... 60

Figure 3-22. Fluorescence spectra of (*S*)-**3.6** (0.08 mM) in the presence of (*R*)-**3.14** (left) or (*S*)-**3.14** (right) with a concentration range of 0.2 to 2.0 mM. Spectra were recorded 1 h after mixing the solution. Solvent: 4% DCM/FC-72, λ_{ex} = 290 nm, slit 3/3 nm. 61

Figure 3- 23. Fluorescent intensity of (*S*)-**3.6** against the concentration of (*R*)-**3.14** or (*S*)-**3.14** at 423 nm. Four independent experiments were conducted (left), and an averaged diagram with error bar was plotted (right). 61

Figure 3-24. Fluorescent intensity at 423 nm recorded at 1 h, 2 h, and 4 h after the mixtures of (*S*)-**3.6** + (*R*)-**3.14** and (*S*)-**3.6** + (*S*)-3.**14** were made. 62

Figure 3-25. Fluorescence spectra of (*R*)-**3.6** (8.0 x 10^{-5} M) in the presence of (*R*)-**3.14** (left) and (*S*)-**3.14** (right) within the concentration range from 0.2 mM to 2 mM. Spectra were recorded 1h after mixing. Solvent: 4% DCM/FC-72, excited at 290 nm, slit 3/3 nm. 62

Figure 3-26. Fluorescent intensity at 423 nm recorded at 1h after the mixtures of (*R*)-**3.6** + (*R*)-**3.14** and (*R*)-**3.6** + (*S*)-**3.14** were made. 63

Figure 3-27. Fluorescent response of (*S*)-**3.6** (8.0 x 10^{-5} M) toward **3.7** (5 mM) at various enantiomeric excess [*ee* = (*R*-*S*)/(*R*+*S*). Reaction time = 1 h. Solvent: 4% CH_2Cl_2 / FC-72, λ_{em} = 420 nm, λ_{ex} = 290 nm, slit: 2/2 nm. The red line is obtained from a second order non-linear fitting]. 64

Figure 3-28. Fluorescent intensity of (*S*)-**3.6** at 420 nm were plotted against the *ee* values obtained for various functional chiral amines **3.11** – **3.14**...................................... 65

Figure 3- 29. Fluorescence spectra of (*S*)-**3.18** (0.08 mM) in different solvents excited at 290 nm, slit 3/3 nm. 67

Figure 3- 30. Fluorescence response of (*S*)-**3.18** (0.08 mM) to 2-aminobutanol (5 mM) in FC72 / 4% DCM (λ_{ex} = 290 nm, slit 2/2 nm) 1h after mixing. 68

Figure 3- 31. Fluorescence spectra in fluorous and organic phase of **3.18** (0.08 mM) with or without addition of (*R*)- or (*S*)-**3.7** (5 mM). 68

Figure 3- 32. Fluorescence response of (*S*)-**3.18** (0.08 mM) to 2-aminobutanol (5 mM) in different solvents (λ_{ex} = 290 nm, slit 2/2 nm). 69

Figure 3- 33. Fluorescence response of (*S*)-**3.18** (0.08 mM) to **3.7** (5 mM) in 0.2mL DCM / 4.8 mL FC72, with addition of excess DCM from 0.3 mL to 4.8 mL......... 70

Figure 3- 34. Fluorescence response of (*S*)-**3.18** (0.08 mM) to 2-aminobutanol (5 mM) in 4% THF/$MeOC_4F_9$ (left) and effects of THF composition to emission (right) (λ_{ex} =290 nm, slit 2/2 nm).. 71

Figure 3- 35. Fluorescence spectra of (*S*)-**3.18** (0.08 mM) with addition of (1*R*, 2*R*)- or (1*S*, 2*S*) –**3.14** (5 mM) in 2%DCM/FC72 (λ_{ex} = 290 nm, slit 2/2 nm). 72

Figure 3- 36. Fluorescence spectra of (*S*)-**3.18** (0.08 mM) with addition of (1*R*, 2*R*)- or (1*S*, 2*S*) –**3.14** (5 mM) in different solvents (λ_{ex} = 290 nm, slit 2/2 nm)................. 72

Figure 3- 37. Fluorescence spectra of (*S*)-**3.18** (0.08 mM) with addition of **3.22**, **23** or **24** (2 mM) in 2% DCM / FC72 (λ_{ex} = 290 nm, slit 2/2 nm).. 73

Figure 3- 38. Fluorescence spectra of (*S*)-**3.18** (0.08 mM) with addition of **3.25** (2 to 5 mM) in 2% DCM / FC72 (λ_{ex} =290 nm, slit 2/2 nm). 74

Figure 3- 39. Fluorescence spectra of (*S*)-**3.18** (0.08 mM) with addition of other chiral molecules (5 mM) in 2%DCM / FC72 (λ_{ex} = 290 nm, slit 2/2 nm)......................... 75

Figure 3- 40. Fluorescence spectra of (*S*)-**3.20** (0.08 mM) with the addition of (*R*) or (*S*)-**3.7** (5 mM) at 5 min (a); Fluorescence change over time for (*R*)-**3.7** (b); Fluorescence change over time for (*S*)-**3.7** (b); Fluorescence intensity at 423 nm was plotted against time (d). (λ_{ex} = 290 nm, slit 3/3 nm).. 76

Figure 3- 41. Fluorescence spectra of (*S*)-**3.20** with (*R*) or (*S*)-**3.7** in CF_3-C_6F_5 over time (λ_{ex} = 290 nm, left) and fluorescence spectra when λ_{ex} = 290 nm (right)................ 78

Figure 3- 42. Fluorescence spectra of (*S*)-**3.20** with (*R*) or (*S*)-**3.7** in CH_3-C_6H_5 or CF_3-C_6H_5 over time (λ_{ex} = 290 nm).. 78

Figure 4-1. Structures of sensor (*S*)-**4.1** and (*S*)-**4.2**. 92

Figure 4-2. Structures of the Chiral Substrates studied. 94

Figure 4-3. Fluorescence spectra of (*S*)-**4.2** (0.1 mM) in the presence of (*R*)-**4.3** or (*S*)-**4.3** (5 mM) in various solvents: FC-72 (perfluorohexane), DCM, THF, CH_3OH and Hexane. (λ_{ex}= 332 nm, slit = 3/3 nm). ……………………………………………………………96

Figure 4-4. Fluorescence spectra of (*S*)-**4.2** (0.1 mM) in the presence of (*R*)-**4.3** or (*S*)-**4.3** (5 mM) in DMF under the same conditions.. 97

Figure 4-5. Fluorescence spectra of (*S*)-**4.2** (0.04 to 0.40 mM) in the presence of (*R*)-2-amino-1-propanol (5 mM, left) or (*S*)-2-amino-1-propanol (5 mM, right) in FC-72 (λ_{ex}= 332 nm, slit = 3/3 nm)... 97

Figure 4-6. Fluorescence spectra of (*S*)-**4.2** (0.1 mM) in the presence of (*R*)- or (*S*)-2-amino-1-propanol (5 mM) in various solvents: DMF, THF, DCM, MeOH and Hexane. (λ_{ex}= 332 nm, slit = 3/3 nm). 98

Figure 4-7. Fluorescence spectra of (*S*)-**4.2** (0.1 mM) with (*S*)-**4.3** (a) and (*R*)-**4.3** (5.0 mM) (b) in DMF recorded over 10 h. Fluorescence intensity at λ = 458 nm versus time (c). Image of (*S*)-**4.2** (0.1 mM) with (*S*)-**4.3** (5 mM) under UV irradiation (d). (λ_{ex} = 332 nm, slit = 2/2 nm). 100

Figure 4-8. Fluorescence spectra of (*S*)-**4.2** (0.01 mM) with (*R*)-**4.3** or (*S*)-**4.3** (3 mM) in 0.5 mL DMF / 4.5 mL THF over 4 h, and fluorescence intensity at 458 nm was plotted against time (λ_{ex} = 332 nm, slit = 3/3 nm). 101

Figure 4-9. Fluorescence spectra of (*S*)-**4.2** (0.01 mM) with (1*R*, 2*S*)-**4.15** or (1*S*, 2*R*)-**4.15** (5 mM) in 0.5 mL DMF/4.5 mL THF over 4 h, and fluorescence intensity at 460 nm was plotted against time (λ_{ex} = 332 nm, slit = 2/2 nm). 101

Figure 4-10. Fluorescence spectra of (*S*)-**4.2** (0.01 mM) with (*S*)-**4.3** (a) and (*R*)-**4.3** (b). Fluorescence intensity at λ = 458 nm versus the amine concentration (c), and *ee* of **4.3** (3 mM) (d). (λ_{ex} = 332 nm, slit = 3/3 nm, solvent: 10% DMF/THF). (Error bars were obtained on three independent measurements) **.** 103

Figure 4-11. Fluorescence spectra of (*R*)-**4.2** (0.01 mM) with amine **4.3** from 60 to 300 equiv., and the fluorescence intensity at λ = 458 nm was plotted against the equivalents. [λ_{ex} = 332 nm, slit = 3/3 nm, solvent: DMF/THF(1:9 v/v)]. 104

Figure 4-12. UV-Vis and/or emission spectra of (*S*, *S*)-**4.9** (a), (*S*, *R*)-**4.9** (b), (*S*, *R*, *S*)-**4.16** (c) in DMF (Conc. is 0.01 mM for all; slit = 2/2 nm, λ_{ex} = 322 nm for emission spectra). 106

Figure 4-13. UV-Vis spectra of (*S*)-**4.2** (0.1 mM) with (*S*)-**4.3** (200 eq) recorded over 3 h (a), and absorption changes at λ_{max} = 290, 322, and 432 nm were plotted against time (b). The percentage change of absorption was also plotted (c). Graph (d) shows the linear fitting of percentage absorption change during 1 – 3h intervals at 322 nm.. 108

Figure 4-14. UV-Vis spectra of (*S*)-**4.2** (0.1 mM) with (*R*)-**4.3** (200 eq) recorded over 3 h (a), and absorption changes at λ_{max} = 290, 322, and 432 nm were plotted against time (b). The percentage change of absorption was also plotted (c). Graph (d) shows the linear fitting of percentage absorption change during 1-3h intervals at 322 nm. ... 109

Figure 4-15. ^{19}F NMR spectra recorded in DMF for the reaction of (*S*)-**4.2** with **4.3**... 111

Figure 4-16. ^{1}H and ^{19}F NMR spectra were recorded in $CDCl_3$ over 22 h. (*S*)-**4.2** (0.025 mmol) and amine (*S*)-**4.3** (10 eq) was mixed in $CDCl_3$ (0.4 mL). 112

Figure 4-17. The observed *ef* values when (*S*)-**4.2** (0.01 mM) was interacted with the (*R*)- and (*S*)-enantiomers of various amine (3.0 mM). 114

Figure 4-18. Fluorescence spectra of (*S*)-**4.2** (0.01 mM) with amine **4.11** from 60 to 300 eq, and the fluorescence intensity at λ = 458 nm was plotted against the equivalents. 115

Figure 4-19. Enantiomeric excess correlation for the fluorescent responses of (*S*)-**4.2** (0.01 mM) toward **4.11** (200 eq). Fluorescence intensity at λ = 458 nm was plotted against the ee values, and a 1st order linear fitting was applied. 116

Figure 4-20. Fluorescence spectra of (*S*)-**4.2** (0.01 mM) with amine **12** from 60 to 300 equivalents, and the fluorescence intensity at λ = 458 nm was plotted against the amine equivalents. 116

Figure 4-21. Enantiomeric excess correlation of the fluorescence responses of (*S*)-**4.2** (0.01 mM) toward **4.12** (180 eq). Fluorescence intensity at λ = 458 nm was plotted against ee values, and a 1st order linear fitting was applied. 117

Figure 4-22. Fluorescence spectra of (*S*)-**4.2** (0.01 mM) with amine **4.13** from 60 to 300 eq, and the fluorescence intensity at λ = 463 nm was plotted against the equivalents. 117

Figure 4-23. Enantiomeric excess correlation for the fluorescence responses of (*S*)-**4.2** (0.01 mM) toward **4.13** (200 eq). Fluorescence intensity at λ = 463 nm was plotted against the *ee* values, and a 1st order linear fitting was applied. 118

Figure 4-24. Fluorescence spectra of (*S*)-**4.2** (0.01 mM) with amine **4.14** from 60 to 300 eq, and fluorescence intensity at λ = 458 nm was plotted against the equivalents. 119

Figure 4- 25. The observed *ef* values when (*S*)-**4.2** (0.01 mM) was interacted with the (*R*)- and (*S*)-enantiomers of various functional chiral amines at 1 mM (or 3 mM for **4.17** and **4.20**). 120

Figure 4-26. Fluorescence spectra of (*S*)-**4.2** (0.01 mM) with (*S*, *S*)-**4.17** (a) and (*R*, *R*)-**4.17** (b). Fluorescence intensity at λ = 463 nm versus the amino alcohol concentration (c), and ee correlation of **4.17** (3.0 mM) (d) were plotted separately (slit = 3/3 nm). 121

Figure 4-27. Fluorescence spectra of (*S*)-**4.2** (0.01 mM) with amino alcohol **4.15** from 20 to 200 eq, and fluorescence intensity at λ = 460 nm was plotted against the equivalence (slit = 2/2 nm). 122

Figure 4-28. Enantiomeric excess correlation of fluorescence spectra for (*S*)-**4.2** (0.01mM) and **4.15** (50 eq). Fluorescence intensity at λ = 460 nm was plotted against the *ee* values, and a 2nd order nonlinear fitting was applied (slit = 2/2 nm). 122

Figure 4-29. Fluorescence spectra of (*S*)-**4.2** (0.01 mM) with amino alcohol **4.18** from 20 to 200 eq, and the fluorescence intensity at λ = 460 nm was plotted against the equivalence (slit = 2/2 nm). 123

Figure 4-30. Enantiomeric excess correlation of fluorescence spectra for (*S*)-**4.2** (0.01 mM) and **4.18** (100 eq). Fluorescence intensity at λ = 460 nm was plotted against the *ee* values, and a 2nd order nonlinear fitting was applied (slit = 2/2 nm). 124

Figure 4-31. Fluorescence spectra of (*S*)-**4.2** (0.01 mM) with **4.19** from 20 to 200 eq, and fluorescence intensity at λ = 460 nm was plotted against the equivalence (slit=2/2nm). 124

Figure 4- 32. Fluorescence spectra of (*S*)-**4.2** (0.01 mM) with diamine **4.20** from 60 to 300 eq recorded 3 h after reaction, and fluorescence intensity at λ = 384 and 462 nm was plotted against the equivalents. The intensity ratio (I_{462}/I_{384}) was also plotted against the equivalent (slit = 3/3 nm).......... 125

Figure 4-33. Fluorescence spectra of (*S*)-**4.2** (0.01 mM) with diamine **21** from 20 to 200 eq, and fluorescence intensity at λ = 460 nm was plotted against the equivalence (slit = 2/2 nm).......... 126

Figure 4-34. Enantiomeric excess correlation of fluorescence spectra for (*S*)-**4.2** (0.01 mM) and **4.21** (50 eq). Fluorescence intensity at λ = 460 nm was plotted against the *ee* values, and a 1st order linear fitting was applied (slit = 2/2 nm). 127

Figure 4-35. Fluorescence spectra of (*S*)-**4.1** (0.1 mM) in the presence of (*R*)-**4.3** or (*S*)-**4.3** (5 mM) in various solvents: FC-72, DMF, DCM, methanol, THF and hexane (λ_{ex}= 332 nm, slit = 2/2 nm).......... 128

Figure 4-36. Fluorescence spectra of (*S*)-**4.1** (0.1 mM) with (*R*)-**4.3** or (*S*)-**4.3** (5 mM) in DMF recorded over 10 h, and fluorescence intensity at λ = 501 nm was plotted against the reaction time (λ_{ex} = 390 nm, slit = 2/2 nm).......... 129

Figure 4-37. Fluorescence spectra of (*S*)-**4.1** (0.1 mM) with (1*R*, 2*S*)-**4.15** or (1*S*, 2*R*)-**4.15** (5 mM) in DMF recorded over 10 h, and fluorescence intensity at λ = 501 nm was plotted against the reaction time (λ_{ex} = 390 nm, slit = 2/2 nm). 130

Figure 4- 38. UV-Vis and fluorescence of (*S*, *R*, *S*)-**4.22**. 131

Figure 4- 39. Emission spectra of **4.23-4.26** (0.05 mM) treated with 2 enantiomer of Nonrephedrine (2 mM) in DMF (λ_{ex} =290 nm, slit = 3.0/3.0 nm)......................... 133

Figure 4- 40. Emission spectra of (*S*)-**4.33** (0.3 mM, 5 mL) in DMF (left) or DMSO (right) with addition of amino acid solid (2 mg).. 136

Figure 4- 41. Emission spectra of (*S*)-**4.33** with addition of amino acid in DMSO (left) or water (right). 136

Figure 4- 42. Emission spectra of (*S*)-**4.33** (0.2 mM) with addition of amino acid (2 mM) in 0.4% Water/DMSO.. 137

Figure 4- 43. Emission of (*S*)-**4.32** (0.1 mM) with addition of L-Arg at different equivalents (0-10 eq) in 2% Water/DMSO.. 137

Figure 4- 44. Emission spectra of (*S*)-**4.32** (0.05 mM) with addition of HCl or NaOH(3 M) from 1 µL to 100 µL in 10% water/DMSO... 138

Figure 4- 45. Emission spectra of (*S*)-**4.32** (0.01 mM) treated with KF, KOAc or KBr (50eq). 139

Figure 4- 46. Fluorescence spectra of (*S*)-**4.32** (0.01 mM) with addition of D- or L-Serine (1-20 eq) in DMSO. Fluorescence intensity at 500 nm was plotted against equivalents of serine (λ_{ex} = 363 nm, slit = 3.0/3.0 nm, t = 3h). 140

Figure 4- 47. Fluorescence spectra of (*S*)-**4.32** (0.01 mmol) with addition of serine (10 eq) in different *ee* values and emission intensity at 500 nm was plotted against *ee* values (t = 3h). 141

Figure 4- 48. Emission intensity at 500 nm for of (*S*)-**4.32** (2 µM, 50 µM and 200 µM) with addition of serine (t = 3h). 141

Figure 4- 49. Fluorescence spectra of (*S*)-**4.32** (0.01 mM) with addition of D- or L-Serine (200 eq) in DMSO. Fluorescence intensity at 500 nm was plotted against time.... 142

Figure 4- 50. Fluorescence spectra of (*R*)-**4.32** (0.01 mM) with addition of D- or L-Serine (200 eq) in DMSO tracked overtime. 143

Figure 4- 51. Fluorescence spectra of (*S*)-**4.32** (0.01 mM) with addition of D- or L-cysteine (1-20 eq) in DMSO. Fluorescence intensity at 500 nm was plotted against equivalents 144

Figure 4- 52. Fluorescence spectra of (*S*)-**4.32** (0.01mM) with addition of D- or L-threonine in DMSO 3h after reaction. Fluorescence intensity at 500 nm was plotted against equivalents. 145

Figure 4- 53. Fluorescence spectra of (*S*)-**4.32** (0.01 mM) with addition of D- or L-allo-threonine in DMSO 3h after reaction. Fluorescence intensity at 500 nm was plotted against equivalents. 146

Figure 4- 54. Fluorescence spectra of (*S*)-**4.32** (0.01 mM) with addition of D- or L-lysine in DMSO 3 h after reaction. Fluorescence intensity at 500 nm was plotted against equivalents. 146

Figure 4- 55. Fluorescence spectra of (*S*)-**4.32** (0.01 mM) with addition of D- or L-valine from 1 to 16 equivalents in DMSO 3h after reaction. 147

Figure 4- 56. Fluorescence spectra of (*S*)-**4.32** (0.01 mM) with addition of D- or L-tryptophan from 1 to 16 equivalents in DMSO 3 h after reaction. 148

Figure 4- 57. Fluorescence spectra of (*S*)-**4.33** (0.01mM) treated with D- or L-serine in DMSO. Emission at 457 nm was plotted against the concentration of serine. 149

Figure 4- 58. Fluorescence spectra of (*S*)-**4.32** (0.01 mM) with addition of D- or L-serine in DCM 3 h after reaction.. 148

Figure 4- 59. Fluorescence spectra of (*S*)-**4.32** (0.01 mM) with addition of D- or L-serine in DMF 3 h after reaction. 149

Figure 4- 60. Fluorescence spectra of (*S*)-**4.33** (0.01 mM) treated with D- or L-tryptophan in DMSO. Emission intensity at 415 nm was plotted against the concentration of tryptophan. 150

Figure 4- 61. Fluorescence spectra of (*S*)-**4.33** (0.01 mM) treated with D- or L-valine in DMSO. Emission intensity at 415 nm was plotted against the concentration of valine. 151

Figure 4- 62. Fluorescence spectra of **4.35** (0.05 mM) with addition of 10 eq D- or L-serine excite at 340 nm in DMSO. 152

Figure 4- 63. Fluorescence spectra of **4.35** (0.05 mM) + **4.32** (0.05 mM) with addition of 0.5 mM D- or L-serine excited at 363 nm in DMSO. 153

Figure 4- 64. Fluorescence spectra of (*S*)-**4.38** and (*R*)- or (*S*)-2-amino-1-butanol diluted with various solvents to a total of 2mL after reacting in DMF (0.2 mL) for 2h (λ_{ex} = 300 nm, slit 3/3 nm). 154

Figure 4- 65. Fluorescence spectra of (*S*)-**4.38** with (*R*) or (*S*)- 2-amino-1-butanol in various solvents (λ_{ex} = 300 nm). 155

Figure 4- 66. Fluorescence spectra of (*S*)-**4.38** with (*R*) or (*S*)-**4.3** in various solvents (λ_{ex} = 300 nm). 156

Figure 5- 1. Fluorescence spectra of (*S*)-**5.1** (0.01mM) in various solvents. (λ_{ex} = 290 nm, slit = 3.0/3.0 nm). The ratios of mixed solvents are 1/1 (v/v). 179

Figure 5- 2. Fluorescence spectra of (*S*)-**5.1** (0.01 mM) with L-serine (1.0 mM) in H_2O / CH_3CN with different ratios (λ_{ex} = 290 nm, slit = 3.0/3.0 nm). 179

Figure 5- 3. Fluorescence spectra of (*S*)-**5.1** (0.01 mM) with the addition of different amino acids (1.0 mM). (λ_{ex} = 290 nm, slit = 3.0 / 3.0 nm, CH_3CN / H_2O=4.5 / 0.5 mL).. 180

Figure 5- 4. Fluorescence spectra of (*S*)-**5.1** (0.01 mM) with the addition of hydroxyl acids (5.0 mM). (λ_{ex} =290 nm, slit = 3.0/3.0 nm, solvent: CH_2Cl_2). 181

Figure 5- 5. Fluorescence spectra of (*S*)-**5.1** (0.01 mM) with (*R*, *R*)-DAH (top left) or (*S*, *S*)-DAH (top right) at various concentrations; Fluorescence intensity at 474 nm was plotted against the conc. (bottom left) and *ee* (bottom right). 2nd-order fitting was applied. (λ_{ex} = 290 nm, slit = 3.0/3.0 nm, solvent: CH_2Cl_2) 182

Figure 5- 6. ^{19}F NMR titration of (*R*, *R*)-DAH or (*S*, *S*)-DAH to (*S*)-**5.1** in $CDCl_3$....... 184

Figure 6- 1. Structures of chiral amines studied. 191

Figure 6- 2. Fluorescence spectra of (*S*)-**6.1** (0.02 mM left) and (*S*)-BINOL-CHO (0.02 mM, right) treated with (*R*)- or (*S*)-**6.8** in methanol under the existence of zinc acetate (0.02 mM) (λ_{ex} = 330 nm, slit 3/3 nm). Fluorescence intensity at 525 nm was plotted against the equivalents of **6.8**.. 192

Figure 6- 3. Fluorescence spectra of (*S*)-**6.1** (0.02 mM left) and (*S*)-BINOL-CHO (0.02 mM, right) treated with (*R*)- or (*S*)-leucine in methanol under the existence of zinc acetate (0.02 mM) and TBAOH (10 eq) (λ_{ex}=330 nm, slit 3/3 nm). Fluorescence intensity at 525 nm was plotted against the equivalents of leucine. 193

Figure 6- 4. Fluorescence spectra of (*S*)-**6.1** (0.02 mM, left) and (*S*)-BINOL-CHO (0.02 mM, right) treated with (*R*)- or (*S*)-**6.8** in toluene under the existence of zinc acetate (0.02 mM) (λ_{ex} = 330 nm, slit 3/3 nm). The photo shows the emission under UV-lamp irradiation at 1eq of **6.8**. 194

Figure 6- 5. Fluorescence spectra of (*S*)-**6.2** (0.05 mM) with DAH (0.4-10 eq) in FC-72 (4% DCM, λ_{ex} = 320 nm, slit 3/3 nm). 197

Figure 6- 6. Fluorescence spectra of (*S*)-**6.2** (0.05 mM) with DAH (4 eq) in various solvents (λ_{ex} = 320 nm, slit 3/3 nm). 197

Figure 6- 7. Correlation of *ee* to fluorescence intensity in a DCM/FC-72 biphasic system (λ_{ex} = 320 nm, slit 3/3 nm). Emission intensities at 395 nm were plotted against *ee* values. 199

Figure 6- 8. Fluorescence spectra of (*S*)-**6.3** (0.01 mM) with DAH (1-10 eq) in FC-72/ 2% DCM recorded 1 h after mixing (λ_{ex} = 335 nm, slit 3/3 nm). 202

Figure 6- 9. Fluorescence spectra of (*S*)-**6.3** (0.01 mM) with DAH (10 eq) in different solvents recorded 3 h after mixing (λ_{ex} = 335 nm, slit 3/3 nm). 202

Figure 6- 10. Fluorescence spectra of (*S*)-**6.3** (0.1 mM) with DAH (10 eq, left) and **6.8** (20 eq, right) in FC-72 recorded 3 h, 6 h, 9 h after mixing (λ_{ex} = 335 nm, slit 2/2 nm). 203

Figure 6- 11. Fluorescence spectra of (*S*)-**6.3** (0.01 mM)+ (1*S*, 2*S*)-DAH (1 eq) with addition of **6.8** (4-40 eq) in 4% DCM/FC-72. Emission intensity at 412 nm was plotted against equivalents of **6.8**.. 205

Figure 6- 12. Fluorescence spectra of (*S*)-**6.3** (0.05 mM) in FC-72 (2 mL), with DAH at different equivalents in the methanol (0.5 mL) layer (λ_{ex} = 335 nm, slit 2/2 nm). . 206

Figure 6- 13. Fluorescence spectra of (*S*)-**6.3** (0.05 mM) in FC-72 (2 mL), with DAH at 8 eq or 32 eq and zinc acetate (1 eq) in the methanol (0.5 mL) layer (λ_{ex} = 335nm, slit 2/2 nm). 207

Figure 6- 14. Fluorescence spectra of (*S*)-**6.3** (0.05 mM) in FC-72 (2 mL), and DAH (8 eq) with or without and zinc acetate (1 eq) in methanol (0.5 mL) layer (λ_{ex} = 335 nm, slit 2/2 nm). 208

Figure 6- 15. Fluorescence spectra of (*S*)-**6.3** (0.05 mM) in FC-72 (2 mL), and DAH (8 eq) in methanol from 1 mL to 6 mL (λ_{ex} = 335 nm, slit 2/2 nm). 208

Figure 6- 16. Fluorescence spectra of (*S*)-**6.3** (0.05 mM) in FC-72 (2 mL), and DAH (8 eq) in different solvents (0.5 mL) (λ_{ex} = 335 nm, slit 2/2 nm). 209

Figure 6- 17. Fluorescence spectra of (*S*)-**6.3** (0.05 mM) in FC-72 (2 mL), and DAH at 2-20 eq in DMF (0.5 mL) (λ_{ex} = 335 nm, slit 2/2 nm). Fluorescence intensity at 430 nm was plotted against equivalents of DAH. 210

Figure 6- 18. Relationship between *ee* and emission intensity in a FC-72/methanol biphasic system. Emission intensities at 420 nm were plotted against *ee* values ([**6.3**] = 0.05 mM, [rrDAH + ssDAH] = 8 eq, λ_{ex} = 335 nm, slit 2/2 nm). 211

Figure 6- 19. Fluorescence spectra of (*S*)-**6.3** at various concentrations in FC-72 (2 mL), and DAH (0.4 mM) in 0.5 mL methanol (λ_{ex} = 335 nm, slit 2/2 nm). 213

Figure 6- 20. Fluorescence spectra of (*S*)-**6.3** (5 μM) in FC-72 (2 mL). **6.8** (36 eq) with or without zinc acetate (1 eq) were added in methanol (0.5 mL) layer (λ_{ex} = 335 nm, slit 2/2 nm). 214

Figure 6- 21. Fluorescence spectra of (*S*)-**6.3** (0.05 mM) in FC-72 (2 mL), with various kinds of amino alcohols (16 eq) in 0.5 mL methanol (λ_{ex} = 335 nm, slit 2/2 nm). . 214

Figure 6- 22. Fluorescence spectra of (*S*)-**6.3** (0.05 mM) in FC-72 (2 mL), with amino acids (Ser or Cys, 16 eq) in 0.5 mL methanol (5% of H_2O, λ_{ex} = 335 nm, slit 2/2 nm). 215

Figure 6- 23. Fluorescence spectra of (*S*)-**6.4** (0.05 mM) in FC-72 (2 mL), with 1-8 eq of DAH in 0.5 mL methanol (λ_{ex} = 335 nm, slit 2/2 nm). 216

Figure 6- 24. Fluorescence spectra of (*S*)-**6.4**-PEA (5 μM) + DAH (10 eq) with Zn(II) (1 eq) in THF or methanol (λ_{ex} = 340 nm, slit 1/1 nm). 217

Figure 6- 25. Fluorescence spectra of (*S*)-**6.4**-PEA (5 μM) + DAH (10 eq) with or without Cu(II) (1 eq) in THF or methanol (λ_{ex} = 340 nm, slit 1/1 nm). 217

Figure 6- 26. Fluorescence spectra of (*S*)-**6.4**-PEA (5 μM) + DAH (10 eq) with Yb(III) (1 eq) in THF or methanol (λ_{ex} = 340 nm, slit 1/1 nm). 218

Figure 7- 1. Fluorescence spectra of (*S*)-**7.1** (0.01 mM) in different solvents (λ_{ex} = 530 nm, slit = 3.0/3.0 nm). 230

Figure 7- 2. Fluorescence spectra of (*S*)-**7.1** (0.01 mM) with or without addition of hydroxyl acids (5 mM). (λ_{ex} = 530 nm, slit = 5.0 / 5.0 nm, Solvent: CH_3CN). 231

Figure 7- 3. Fluorescence spectra of (*S*)-**7.1** (0.01 mM) with addition of mandelic acid at various concentrations. Fluorescence intensity at 580nm was plotted against concentration. (λ_{ex} = 530 nm, slit = 5.0/5.0 nm, solvent: CH_3CN) 232

Figure 7- 4. Fluorescence spectra of (*S*)-**7.1** (0.01 mM) with addition of Zn(II) at various equivalents. (λ_{ex} = 530 nm, slit = 2.0/2.0 nm, solvent: methanol). 233

Figure 7- 5. Fluorescence spectra of (*S*)-**7.1** (0.01 mM) + chiral acids (0.1 mM) with or without $ZnCl_2$ (0.1 mM). (λ_{ex} =530 nm, slit = 2.0/2.0 nm, solvent: methanol). 234

Figure 7- 6. UV-Vis absorption spectra of (*S*)-**7.1** (0.01 mM) with addition MA (5 mM) in methanol (left), and its circular dichroism spectra (right). 235

Figure 7- 7. Fluorescence spectra of (*S*)-**7.2** (0.05 mM) in various solvents (λ_{ex} = 332 nm, slit 2/2 nm). 237

Figure 7- 8. Fluorescence spectra of (*S*)-**7.2** with addition of *RR* or *SS*-DAH over 1-8 h. 238

Figure 7- 9. Fluorescence spectra of (*S*)-**7.2** (0.05 mM) with DAH (5 mM) in various solvents overtime. 239

Figure 7- 10. Fluorescence spectra of (*S*)-**7.2** (0.05 mM) with serine (5 mM) in 10% H_2O/ DMF overtime. 240

Figure 7- 11. Fluorescence spectra of (*S*)-**7.2** (0.05 mM) and DAH (5 mM) with additive (0.05 mM) in various solvents at 3 h after mixing.. 241

Figure 7- 12. Fluorescence spectra of (*S*)-**7.2** (0.05 mM) and 2-amino-1-butanol (5 mM) with or without additive (0.05 mM) in various solvents at 3 h after mixing. 242

List of Schemes

Scheme 1- 1. Analysis of chiral molecule mixtures with resolving agents....................... 2

Scheme 1- 2. Moshers's acid in NMR resolution. 4

Scheme 1- 3. Chiroptical CD sensors developed by Wolf *et al.* 6

Scheme 1- 4. HPLC screening in the reduction of ketone to alcohol................................ 8

Scheme 1- 5. GC screening for the addition of nitroalkenes... 8

Scheme 1- 6. HPLC-CD screening in the addition of aldehyde.. 9

Scheme 1- 7. UV-Vis screening in lipase catalyzed hydrolysis.. 9

Scheme 1- 8. Salen-catalyzed epoxide ring-opening reaction... 10

Scheme 1- 9. Lipase catalyzed kinetic resolution of alcohol. 11

Scheme 1- 10. Interaction of mandelic acid with sensor... 15

Scheme 1- 11. Examples of dynamic covalent reactions. 20

Scheme 1- 12. Fluorescence recognition of glucose using boronate ester formation. 21

Scheme 1- 13. Sensing of chiral amine through imine exchange using **1.24**................. 22

Scheme 1- 14. Sensing of amino acids using Cu(II) complex. 23

Scheme 1- 15. Enantioselective gel-collapse by amino alcohol...................................... 23

Scheme 1- 16. Fluorescence quenching of Cd(II) MOF by amino alcohols................... 24

Scheme 2- 1. A general strategy of fluorous separation.. 31

Scheme 2- 2. Aerobic oxidation of alcohols to aldehydes with fluorous catalyst............ 31

Scheme 2- 3. Ir-catalyzed asymmetric ketone reduction using fluorous ligands............ 32

Scheme 2- 4. Kinetic resolution of rac-2.3 by fluorous labeling..................................... 32

Scheme 3-1. Hydroformylation in fluorous phase. 38

Scheme 3-2. Fluorous sensors for Histamine recognition reported by Vincent *et al.* 39

Scheme 3-3. Synthesis of sensors (*S*)-**3.6** and (*R*)-**3.6**. 42

Scheme 3-4. Products formed between **3.6** and **3.7** detected by ESI-MS. 52

Scheme 3-5. Proposed reaction routes between the sensor and amino alcohol............... 53

Scheme 3- 6. Synthesis of highly fluorinated (*S*)-**3.18**.. 66

Scheme 3- 7. Chiral molecules to be tested.. 66

Scheme 3- 8. Synthesis of (*S*)-**3.20.** 76

Scheme 4-1. Synthetic routes of sensor (*S*)-**4.2** and (*R*)-**4.2**. 93

Scheme 4-2. Synthetic routes of related amides... 93

Scheme 4-3. Reaction of (*S*)-**4.2** with (*S*)-**4.3** in DMF.. 105

Scheme 4- 4. Synthesis of achiral sensors **4.23** – **4.26**... 132

Scheme 4- 5. Amidation reaction between fluorinated ketone and amine.................... 134

Scheme 4- 6. Synthesis of (*S*)-**4.32** and (*S*)-**4.33**.. 135

Scheme 4- 7. Reaction between (*S*)-**4.32** and (L)-Serine-TBA in DMSO.................... 144

Scheme 4- 8. Synthesis of achiral sensor **4.35**. 152

Scheme 4- 9. Synthesis of (*S*)-**4.38**. 154

Scheme 5- 1. Synthesis of (*S*)-**5.1** from (*S*)-BINAM. 178

Scheme 5- 2. Reactions between (*S*)-**5.1** and DAH.. 185

Scheme 6- 1. A design of rapid *ee* and yield determination using fluorescence........... 189

Scheme 6- 2. Synthesis of (*S*)-**6.1**. 191

Scheme 6- 3. Synthesis of (*S*)-**6.2** containing 4 fluorous ponytails................................ 195

Scheme 6- 4. Attempted synthesis of aldehyde sensor (*S*)-**6.15**.................................... 196

Scheme 6- 5. Synthesis of (*S*)-6.3 and (*S*)-6.4**.**.. 201

Scheme 6- 6. Reaction between **6.3** and DAH to form (*S*)-**6.3**-DAH. 204

Scheme 6- 7. A representative diagram of *ee* determination in a biphasic system. 212

Scheme 6- 8. Synthesis of (*S*)-**6.4**-PEA by condensation. 216

Scheme 7- 1. Synthesis of Rhodamine-BINOL conjugate (*S*)-**7.1**. 229

Scheme 7- 2. Acid/base promoted ring opening/closure of Rhodamine B. 229

Scheme 7- 3. Synthesis of Resorufin-H_8BINOL conjugate (*S*)-**7.2**. 236

Scheme 7- 4. Substitution of Resorufin with amine for ratiometric sensing................. 237

List of Tables

Table 5- 1. The *ef* values of (*S*)-**5.1** to various kinds of chiral molecules. 180

Table 6- 1. A summary of e*f* values of (*S*)-**6.2** toward DAH in various solvents. 199

Table 6- 2. A summary of *ef* values in a 2-phase system for different solvents. 210

Table 7- 1. The *ef* values of (*S*)-**7.1** to hydroxyl acids and amino acids. 233

Chapter 1. Fluorescent Sensor for Chiral Recognition

1.1. Importance of chiral molecules

Chiral molecules are substances that are non-superimposable with their mirror images. The two enantiomers of a chiral molecule are identical in most physical and chemical properties, but function differently or even oppositely in biological systems because of the chiral bio-macromolecules such as proteins, DNA/RNA or carbohydrates.[1] Since the disastrous medical incident regarding thalidomide, the enantiopurity of drug has been strictly inspected by health institutions. Even though enantiomers with opposite biological behaviors like thalidomide are not common, it's widely known that racemic drugs are usually less effective and have more side effects in comparison with those under single enantiomeric forms.[2] In the past decades, enantiopure drugs have taken the dominant position in pharmaceutical markets.[3] By 2002, the annual sales of chiral drugs took up about 39% of all drug sales worldwide. In 2006 the sales increased to 56% and it is expected to reach a top of 95% by 2020. Numerous researches have been conducted for the synthesis, separation and analysis of chiral drugs.[4-5]

Louis Pasteur, a French chemist, pioneered the first chiral resolution of tartaric acid using crystallization in 1858. According to the ICH guidelines recognized in Europe, Japan and United States, the impurity content of the other enantiomer cannot exceed 0.1% in registered enantiopure drugs.[6] Following the need in pharmaceuticals, many traditional techniques have been accommodated for fast and accurate analysis of enantiomeric excess, including chiral HPLC, GC, circular dichroism, capillary electrophoresis, mass spectrometry, IR, fluorescence, and etc.

1.2. Current techniques for chiral analysis

Because enantiomers have identical properties in achiral environment, additional chiral resolving agents (CRA) are always needed to induce the formation of diastereomers, which have different properties and can be analyzed by various techniques.

Scheme 1- 1. Analysis of chiral molecule mixtures with resolving agents.

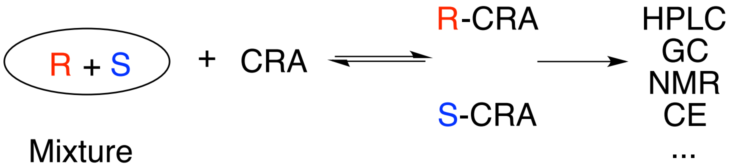

1.2.1. Chiral HPLC and GC for analysis

Chiral HPLC has become the standard in reporting enantiomeric excess (ee = ([R]-[S]) / ([R]+[S])), and takes up more than 50 % of ee determinations.[7] Developed from common HPLC using silica gel or other polymers as stationary phase, chiral HPLC uses chiral stationary phase (CSP) such as polysaccharides or cyclodextrins. Preparative chiral HPLC using chiral sorbent has enabled the separation of racemate in moderate amounts.[8] The selection ability is described by α (where t_2 and t_1 are retention times for two enantiomers and t_0 is the dead time).

$$\alpha = \frac{t_2 - t_0}{t_1 - t_0}, \qquad \Delta\Delta G = -RT ln\alpha$$

The Gibbs free energy difference ($\Delta\Delta G$) between the interactions of the enantiomer with CSP can be calculated from α value. With $\Delta\Delta G$ value as little as 0.5 kJ/mol, the selection α reaches 1.25, enough for an accurate *ee* measurement. It is routine to switch between chiral columns to achieve satisfactory resolution. Though other factors such as temperature, pressure, flow rate and elution composition can be optimized to improve the efficiency, the progress of chiral HPLC is always marked by the discovery of new CSP materials.

In the past decades CSP materials have expanded greatly for the separation of specific molecules that are otherwise difficult.[9] Crown ether-based CSPs have been found to be efficient for primary amines or amino acids at reversed phase conditions.[10] Some protein -based CSPs like bovine serum albumin were especially suitable for the analysis of biomolecules without derivation.[11] Many polymer CSPs fabricated through molecular imprinting or silica-gel surface coating have also been commercialized.[12-13] Future developments of chiral HPLC would focus on discovering both general and task-specific CSP materials, reducing their production cost while increasing durability.

In chiral gas chromatography (GC), cyclodextrin derivatives anchored to polysiloxane are the dominant CSP used. Chiral resolution relies on the gas-liquid interactions, including hydrogen bonding, coordination or inclusion.[14] It has been widely applied to the separation of essential oils and volatile organic compounds.[15] Notably, ionic liquid has emerged as a promising CSP material in recent years for their high stability at elevated temperature and wettability toward silica surface.[16]

1.2.2. NMR for chiral analysis

The first example of chiral analysis using NMR technique was reported by Harry Mosher *et al* at 1969 using the well-known Mosher acid (chloride) to react with chiral amine or alcohol. [17] The diastereomers formed gave a difference in chemical shift of 0.03-0.13 ppm in ^{1}H NMR and 0.11-0.71 ppm in ^{19}F NMR.

Scheme 1- 2. Moshers's acid in NMR resolution.

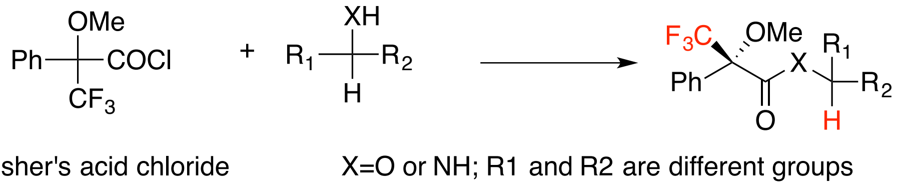
OMe
Ph
COCl
CF3
+
XH
R1
R2
H
F3C
OMe
Ph
X
R1
R2
O
H
Mosher's acid chloride
X=O or NH; R1 and R2 are different groups

The extensive spread of NMR technique has made it a popular tool to determine optical purity and absolute configuration of many kinds of compounds. Compared with chiral HPLC, it has higher tolerance to impurities and can determine *ee* values of many samples in a single experimental setup. It is also more economical and time-efficient. Using ^{1}H, ^{19}F, or ^{31}P NMR, numerous chiral auxiliary agents, most of which are Brønsted acids / bases, transition metal complexes or host-guest receptors, have been explored in-depth.[18] Recent studies focus more on its application in high-throughput analysis, which enables rapid *ee* determination of many samples. Some groups used flow-through NMR screening with auto-sampling to achieve ee measurements up to 1400 / day.[19] Swager *et al* reported a palladium complex with chiral pincer ligands that is capable of resolving mixtures containing 12 amine racemates using ^{19}F NMR.[20]

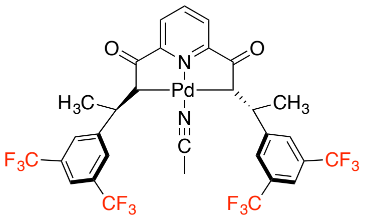
O
N
O
Pd
H3C
CH3
N
C
F3C
CF3
CF3
F3C

Though still limited by substrate scope, line-broadening and resolution, chiral NMR is an important alternative to HPLC when chiral columns are not efficient or sample separations are difficult.

1.2.3. Circular dichroism for chiral analysis

The intrinsic nature of circular dichroism (CD) using polarized light makes it the most straightforward method to determine enantiomeric excess and absolute configuration. A positive or negative CD signal is produced when two enantiomers show different absorption to left-polarized light and right-polarized light. Though having been applied to the study of chiral molecules of all types, it is in the study of biomolecules especially proteins where CD spectroscopy find most of its applications, as well as technique innovations.[21] In studying secondary structures of proteins, CD is the standard method to determine the percentage of α helix and β sheet as they shown characteristic CD spectra under 260nm.[22] However, the use of CD in ee determination has been limited by the fact that most chiral molecules do not have good UV-Vis absorption or only absorbs at far-UV region.

Wolf et al have developed some well-designed chiroptical sensors containing fluorophores to induce CD signals at UV-Vis region for rapid *ee* determination and catalyst screening (Scheme 1-3).[23–26] These probes are CD silent due to free rotations at room temperature. Once the assembly with amine or alcohol occurs, rotation is restricted and CD response is induced with opposite Cotton effects observed for two enantiomers at 300-450 nm ranges. The errors of enantiomeric excess and concentration measurements are generally within 2-10% with regard to the HPLC standard. Remarkably, they demonstrated the feasibility of using CD for high-throughput chiral catalysts screening in Sharpless dihydroxylation, iridium-catalyzed hydrogenation and ketone reduction, without any workup of crude reaction mixtures.

Scheme 1- 3. Chiroptical CD sensors developed by Wolf *et al.*

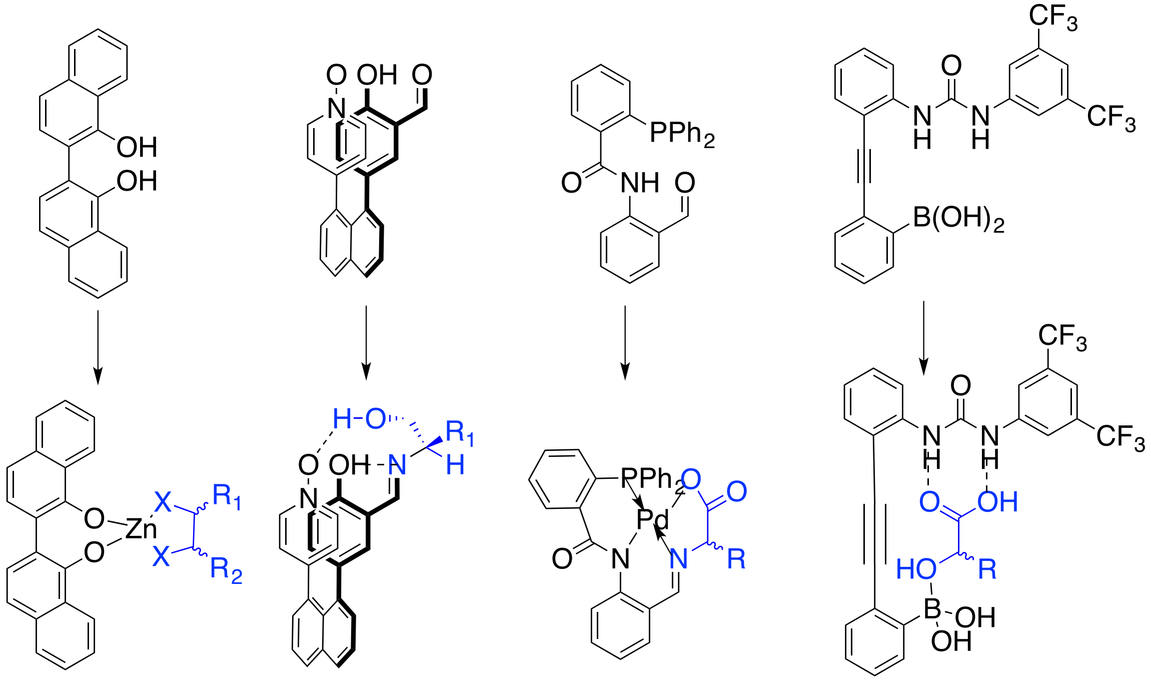
OH
OH
O OH O
N
PPh2
O NH O
CF3
O
N N
H H
CF3
B(OH)2
O
Zn
X R1
X R2
H-O R1
O OH N
H
PPh2 O O
Pd
O N N R
CF3
O
N N
H H
CF3
O OH
HO R
B OH
OH

X= O or N, R is aliphatic or aromatic group.

1.2.4. Chiral capillary electrophoresis (CE)

On the basis of CE, chiral analysis of enantiomers can be achieved with the addition of chiral selectors (CS) that are usually modified cyclodextrins, including neutral, positive or negative charged CDs, to create a chiral environment.[27] Other selectors like chiral crown ethers, macrocyclic antibiotics, proteins, calixarenes, chiral surfactants and ion-pairing reagents have also been well developed in recent years.[28] Electrophoretic mobility of a molecule depends on its effective charge, volume, size, solvent and ionic strength of the medium. Like in chiral HPLC or NMR resolution, a labile complex between the enantiomer (R or S) and chiral selector needs to be formed to achieve mobility differences.

$$\mathrm{R + S + CS \rightleftharpoons R\text{-}CS + C\text{-}CS}$$

Chiral CE has been successfully used in the separation of many drugs in the past decades. Using TM-β-CD as chiral selector, Glowka *et al* separated three racemates, ibuprofen, flurbiprofen and ketoprofen from human serum samples.[29] Other racemates like apomorphine, lactic acid, neurotoxins, methadone, anisodamine have been separated from biological resouces.[27] CE was proved to be convenient in testing the purity of enantiomeric drug assays to as low as 0.05%, and has discovered some drugs that fail to meet the standard as reported.[27] In a case of super high throughput screening, Reetz *et al* adapted a multi-capillary MegaBase CE that was shown to be able to determine over 7000 *ee* values per day in the enzymatic synthesis of amines.[30]

1.3. Technique evolution for high-throughput screening (HTS)

The increasing demand to highly efficient catalysts and development of computing technology has promoted the discovery of asymmetric catalysts using combinatorial methods.[31] Instead of a single design, synthesis and testing cycle, HTS facilitates this process by largely multiplying each step, especially for testing and design. Testing enantiomeric excess (ee) has long been limited by the efficiency of chiral HPLC, which requires the sample to have high purity and takes around half-an-hour for each run, as well as large amount of solvent consumption.

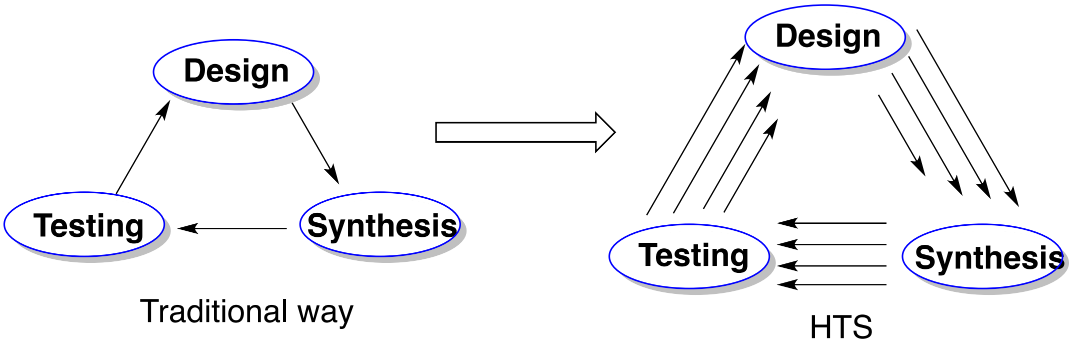

In an early study by Gao *et al*, they used chiral HPLC to screen the substrate scopes of a single catalyst for asymmetric reduction of ketone to alcohol (Scheme 1-4).[32] By dividing the ketones to several groups based on their retention times to avoid spectra overlap, they are able to measure up to eight *ee* values in a single run. A preliminary flash chromatography is required for larger sample amounts.

Scheme 1- 4. HPLC screening in reduction of ketone to alcohol.

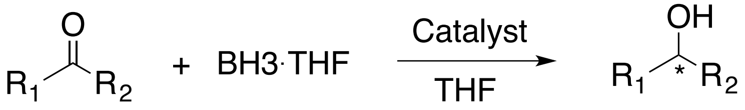

Using a "one-pot, multi-substrate" strategy, Duursma *et al* measured nine ee values in a single run with chiral GC to find out the optimized chiral ligand for asymmetric addition of zinc reagents to nitroalkenes (Scheme 1-5).[33]

Scheme 1- 5. GC screening for the addition of nitroalkenes.

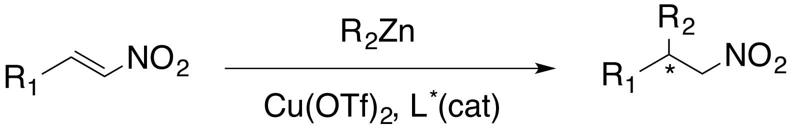

In recent years some companies like Sepmatix have commercialized highly compact 8-channel HPLC screening systems with autosampler to improve efficiency. However, these advanced instruments usually come with high costs and thus have limited implications. Compared with chromatography alone, spectroscopic methods or their couplings with HPLC/GC seem to be more attractive in HTS.

1.3.1. HPLC-CD

Mikami *et al* applied HPLC-CD with a combinatory chemistry factory to screen catalysts for zinc addition to aldehydes (Scheme 1-6).[34] Dozens of catalysts were obtained by a combination of various chiral ligands and activators. They use CD to measure ee and HPLC with common column to measure yield with established standard curves. The best catalysts were discovered to have perfect *ee* and yield values without much labor work.

Scheme 1- 6. HPLC-CD screening in addition of aldehyde.

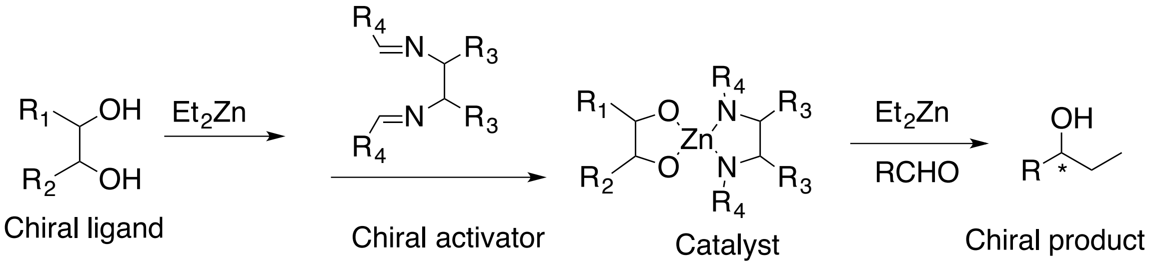

Chiral ligand
Et₂Zn
Chiral activator
Catalyst
Et₂Zn
RCHO
Chiral product

1.3.2. UV-Vis

UV-Vis has also demonstrated its value in HTS in a few cases. In a super HTS manner, Reetz *et al* picked out the best lipases from a library of 30, 000 mutant lipases that synthesize chiral acid with over 90 % *ee* compared with 2 % ee from natural lipase.[35] During screening, they use (*R*)-**1.1** and (*S*)-**1.1** in parallel for each lipase in 96 wells and measure the absorption at 410 nm caused by the formation of nitrophenolate anion. The difference in absorption is directly related to *ee* values.

Scheme 1- 7. UV-Vis screening in lipase catalyzed hydrolysis.

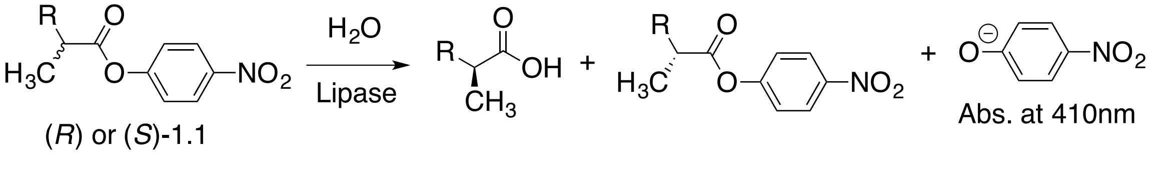

(R) or (S)-1.1
H₂O
Lipase
Abs. at 410nm

1.3.3. IR-thermography

In another example shown in Scheme 1-8, Reetz and his coworkers used IR-thermographic assays for the screening of various kinds of reactions like salen-catalyzed hydrolysis of epoxide to diol.[36] They found that Co(II) salen is more effective than Mn(II) or Cr(II) sales. Using an infrared camera, the temperature increase caused by the reaction can be imaged overtime. In a parallel setup containing *R*, *S* and racemate epoxide separately, it is observed that (*S*)-epoxide with Co(II) salen caused highest temperature increase, followed by Cr(II) and Mn(II).

Scheme 1- 8. Salen-catalyzed epoxide ring-opening reaction.

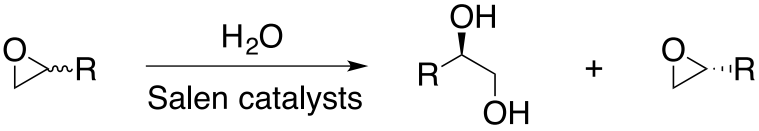

IR-thermography fits well into the need of high-throughput screening. However, this method is more qualitative than quantitative as subtle differences in temperature increase cannot be resolved. With regard to endothermic reactions, “cold spots” have been created for IR imaging.[37]

1.3.4. Mass spectrometry

Mass spectrometry technique has been widely studied for HTS in kinetic resolution and asymmetric transformation.[38] It doesn’t need chromatographic sample purification and can achieve nano-scale *ee* determination.[39] The principle is based on using isotope labeling to make quasi-enantiomers, also known as pseudo-enantiomers, which are assumed to behave as real enantiomers in catalytic reactions but have distinct molecular weights.

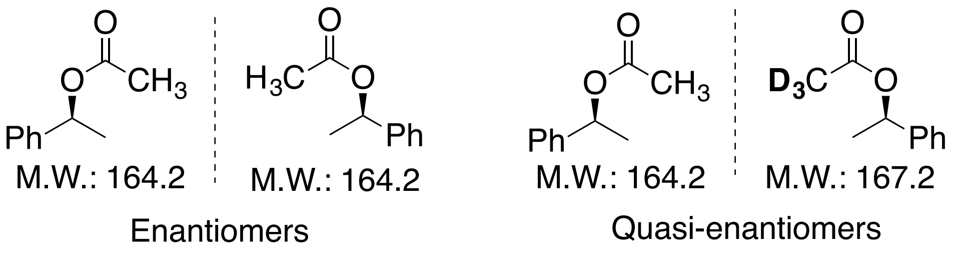
M.W.: 164.2
M.W.: 164.2
Enantiomers
M.W.: 164.2
M.W.: 167.2
Quasi-enantiomers

Reetz *et al* used this method to screen lipase-catalyzed kinetic resolution of phenylethyl acetate. The quasi-enantiomers were mixed at exact 1:1 ratio, and peak intensity ratios of **2** / **3** or **4** / **5** in ESI-MS after reaction can be correlated to the enantiomeric excess. The results obtained are highly consistent with GC results.

Scheme 1- 9. Lipase catalyzed kinetic resolution of alcohol.

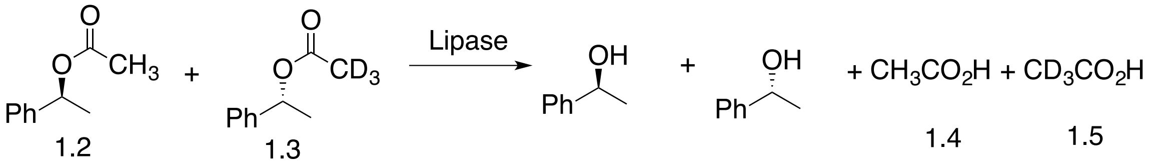
Lipase
+
+
+ CH3CO2H + CD3CO2H
1.2
1.3
1.4
1.5

Using a schematic setup shown in Figure 1-1, they are able to measure more than 1000 ee values accurately within a single day for this reaction. This strategy was also applied to other reactions like enantioselective esterification or hydrolysis of esters.

Figure 1- 1. A typical setup for M.S. in HTS.

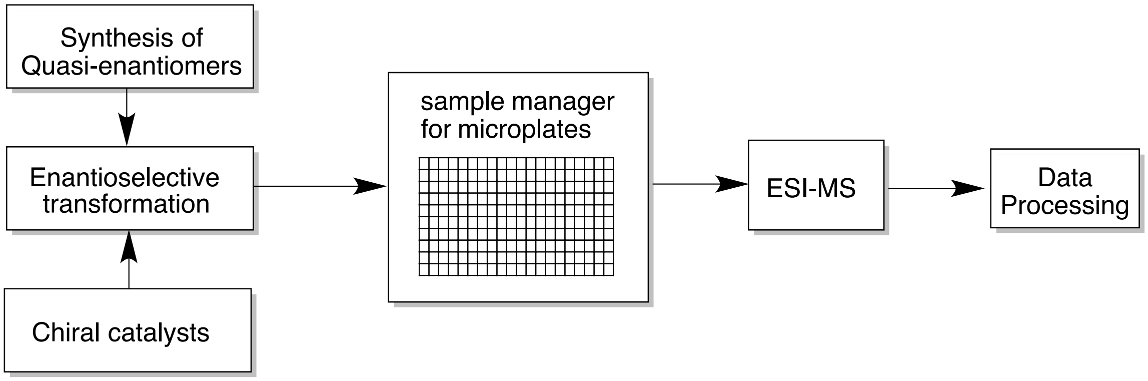
Synthesis of Quasi-enantiomers
Enantioselective transformation
Chiral catalysts
sample manager for microplates
ESI-MS
Data Processing

Remarkably, Pfaltz *et al* reported the use of racemic catalysts for high throughput screening in palladium catalyzed allylic substitutions starting with unequal amount (25:75) of quasi-enantiomers using ESI-MS.[40] This method opens a door for evaluating the efficiency of chiral catalyst when its enantiopure form is not readily available.

1.4. Fluorescence in chiral analysis

1.4.1. Fluorescence sensors

Compared with many other chiral analysis techniques, fluorescence is especially advantageous for its ultrahigh sensitivity that has enabled single molecule detection and non-invasive nature that is suitable for *in vivo* diagnosis. It has been widely used for the sensing and imaging of ions, gases, carbohydrates, pH, protein, DNA, RNA and many other biomolcules.[41] Generally, fluorescence sensing records one of the changes in fluorescence intensity, ratio, lifetime, anisotropy or phase, either positive or negative changes (Figure 1-2). Intensity and intensity ratios are most widely used and easy to carry out, followed by lifetime sensing.[42]

Using fluorescence as a tool for chiral analysis has received a lot of attention in recent years, due to its advantages in high sensitivity, real-time analysis, easy for automation and low cost.[43–45] Because chiral molecules usually only have absorptions at far-UV region, chiral hosts containing chromophores or fluorophores are required to induce emissions at UV-Vis regions. In a three-point model, enantioselectivity in fluorescence originates from the different interactions of two enantiomers with chiral hosts containing fluorophores due to their difference in spatial orientations.

Figure 1- 2. Methods used in fluorescence sensing

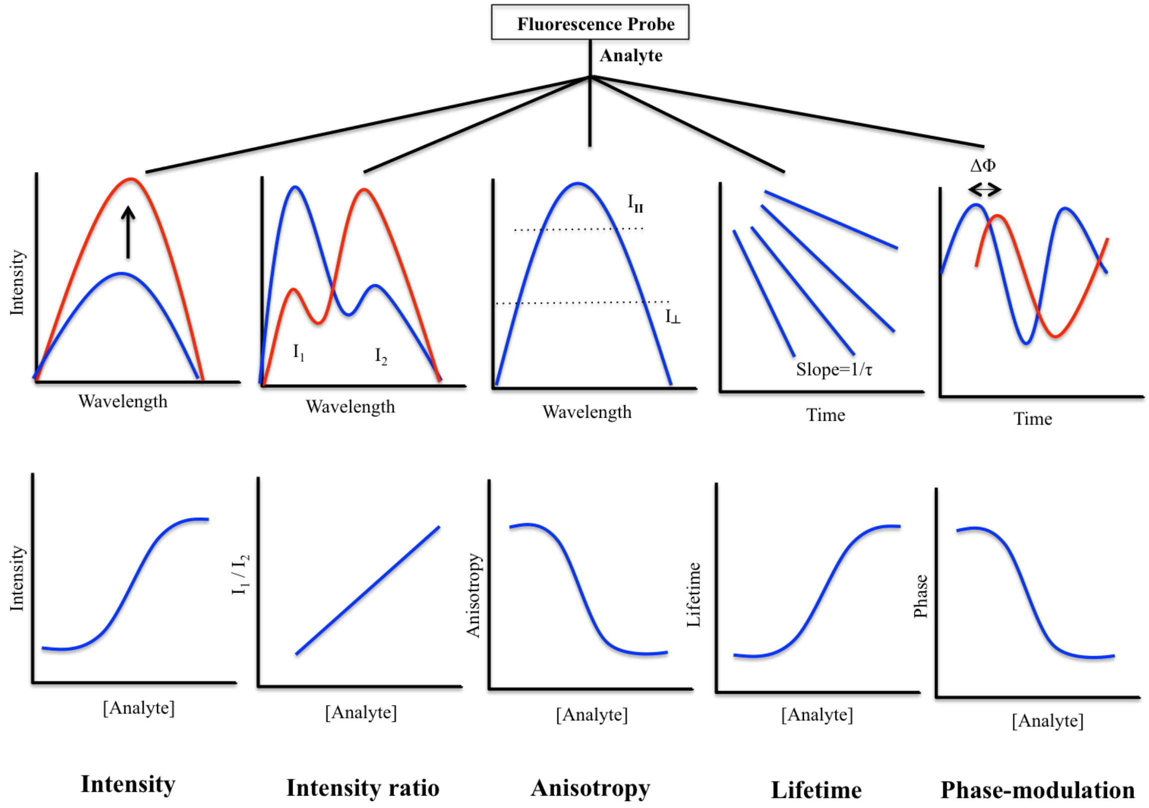
Fluorescence Probe
Analyte
Intensity
Wavelength
I1
I2
Wavelength
I∥
I⊥
Wavelength
Slope=1/τ
Time
ΔΦ
Time
Intensity
[Analyte]
I1 / I2
[Analyte]
Anisotropy
[Analyte]
Lifetime
[Analyte]
Phase
[Analyte]
Intensity
Intensity ratio
Anisotropy
Lifetime
Phase-modulation

Figure 1- 3. Three-point interaction between a chiral host and guest.

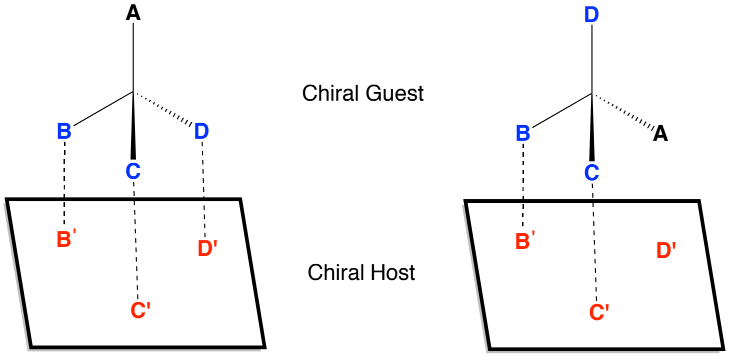
A
B
C
D
B'
D'
C'
Chiral Guest
Chiral Host
D
B
C
A
B'
D'
C'

These interactions can be non-covalent interactions like hydrogen bonding and Van der Waals interactions, or dynamic covalent interactions through formation of imines or boronic esters, or direct asymmetric chemical reactions. For the sensor structures that have been developed, there are inherently chiral Binaphthyl-based chemosensors, boronic ester sensors, Schiff-base derived sensors, macromolecule sensors, metal-complex sensors, polymer-based sensors and etc.[46] Pu *et al* have conducted a wide range of study in using 1,1'-Bi-2-Naphthol (BINOL) as the backbone structures for chirality sensing.[47-48] BINOL has stable chiral configuration at room temperature and both enantiomers are commercially available with low costs. Diversified structural modifications of BINOL are easy to carry out at various positions on its aromatic rings. The naphthol unit is a satisfactory fluorophore and has emissions at the UV-Vis region. The hydroxyl groups are also good hydrogen bonding sites for incoming chiral guests.

1.4.2. Sensors based on non-covalent bondings

Among non-covalent bonding sensors, hydrogen boding networks are the mostly studied ones. In an early study, Parker *et al* used BINOL directly to determine *ee* values of 1–phenylethylamine by observing fluorescence quenching.[46] The quenching resulted from the interaction of the amine with BINOL upon H-bonding. Small difference in Stern-Volmer (K_{sv}) constants is observed for the *R* and *S* enantiomers, with $K_{sv}(R)$ / $K_{sv}(S)$ = 1.09. As an improvement, Beer *et al* used compound BINOL-BODIPY by coupling a BODIPY unit to (*R*)-BINOL and observed better enantioselectivity to the same amine with $K_{sv}(R)$ / $K_{sv}(S)$ = 1.40 at 540 nm.[47]

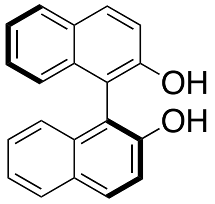

(*S*)-BINOL

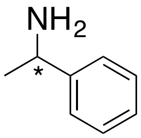

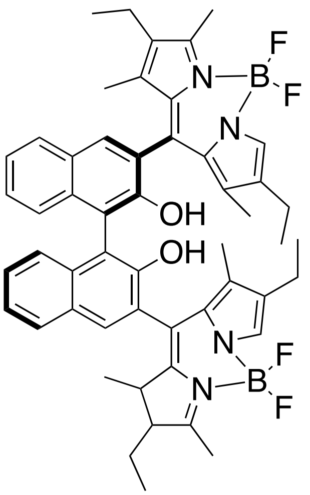

BINOL-BODIPY

In the sensing of α-hydroxyl acids like Mandelic acid (MA), Pu *et al* designed a BisBINOL (*S*)-**1.6** whose fluorescence was quenched by intramolecular hydrogen bonding.[48] The 3-point binding to MA formed complex **1.7** whose fluorescence was restored with enantioselectivity (Scheme 1-10). As shown in Figure 1-4, the addition of (*S*)-mandelic acid gave much large fluorescence enhancement of the sensor than the addition of the *R* enantiomer. The enantiomeric fluorescence enhancement ratio *ef* [= (I_S-I_0) / (I_R-I_0)] is calculated to be 2.49 at 367 nm.

Scheme 1- 10. Interaction of mandelic acid with sensor.

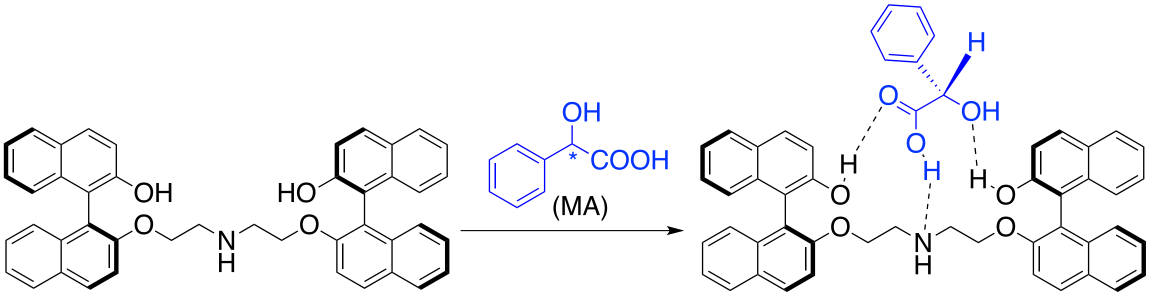

(*S*)-1.6

1.7

Figure 1- 4. Emission spectra of **6**, **8** or **9** with or without hydroxyl acid.

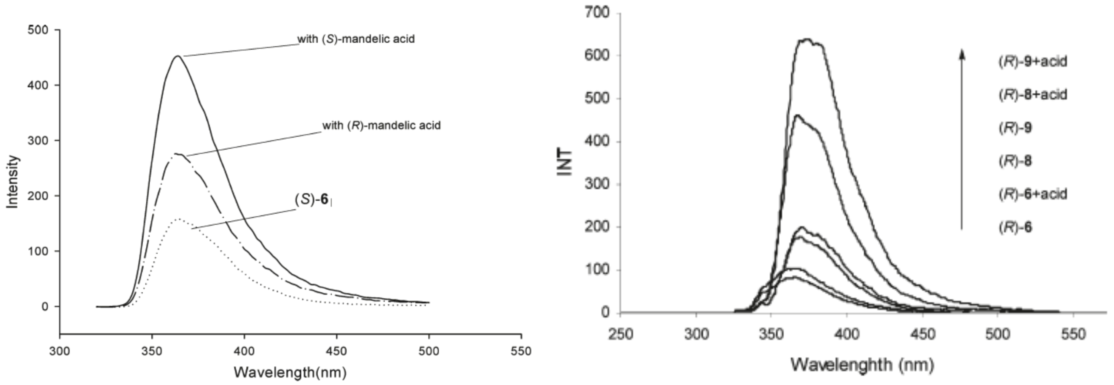

To further improve the selectivity, derivatives **1.8** and **1.9** were synthesized and increased fluorescence enhancements were observed due to the light-harvesting effect from the extended conjugation (Figure 1-4, right).[49]

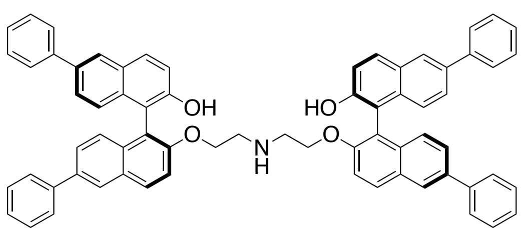

1.8

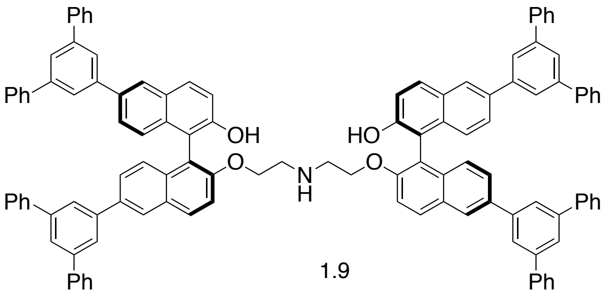

1.9

In another example, macrocycle **1.11** was synthesized to give enantioselective ratiometric response to chiral acids at 365 nm and 424 nm, originated from monomer and excimer emissions separately (Figure 1-5).[50] The hydrogen bond interaction between the chiral cavity of **1.11** with chiral acid is responsible for the fluorescence change. The *ef* values can reach as high as 47 at certain concentration range.

Figure 1- 5. Structure of **1.11** and its fluorescence response to mandelic acid.

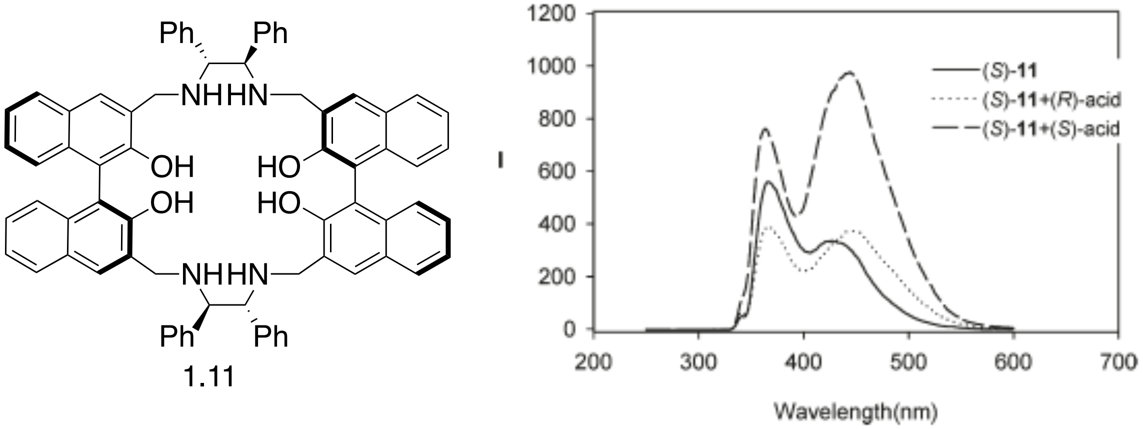

An amino alcohol based sensor **1.15** was also found to show ratiometric response to a wide range of aromatic and aliphatic α-hydroxyl acids through hydrogen bonding with *ef* values up to 26. (Figure 1-6).[51] For phenylactic acid, the (*R*)-form caused 5-fold fluorescence enhancement of sensor while the (*S*)-form gave slight fluorescence quenching at the mono-emission of 375 nm.

Figure 1- 6. Interactions of **1.15** with hydroxyl acids and the fluorescence response.

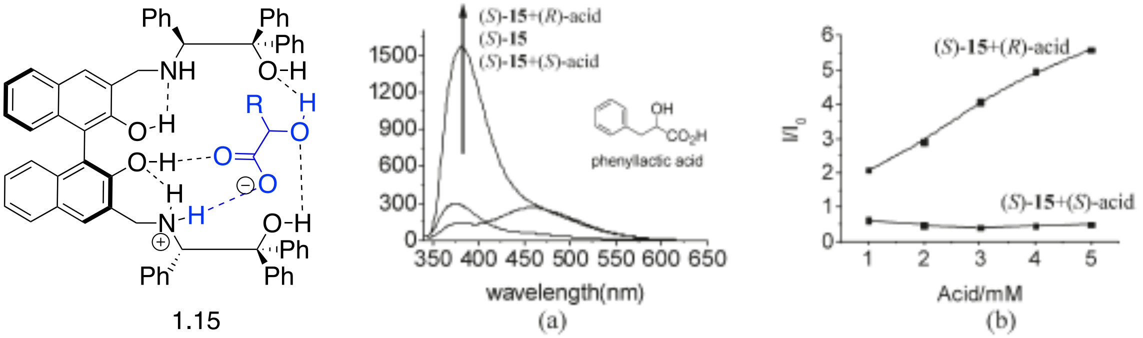

In chiral analysis, both enantiomeric excess and total concentration need to be determined. However, the methods mentioned above are only able to give information on *ee* values at given concentrations. In this regard, a pseudo-enantiomeric pair consisting of

(*S*)-BINOL derived amino alcohol (**1.16**) and (*R)*-H_8BINOL derived amino alcohol (**1.17**) was designed.[52] The (*R)*-H_8BINOL is a partial hydrogenation product of (*R)*-BINOL. The structural similarity between **1.16** and **1.17** allow them to give similar enantioselectivity toward MA as shown in Figure 1-6. However, as the H_8BINOL is less conjugated, the emission occurs at shorter wavelength. A 1:1 mixture of **16**:**17** gives dual emission at 330 nm and 374 nm respectively. With a single measurement, the difference in fluorescence intensity at two peaks can be used to calculate enantiomeric excess, while the sum to calculate total concentration of enantiomers.

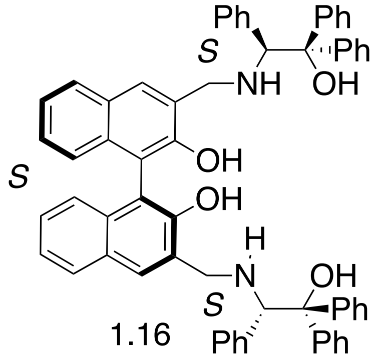
Ph
Ph
S
Ph
NH
OH
OH
S
OH
H
N
OH
S
Ph
Ph
Ph

1.16

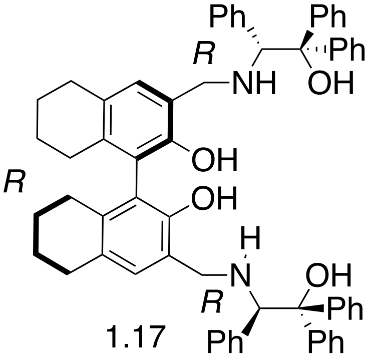
Ph
Ph
R
Ph
NH
OH
OH
R
OH
H
N
OH
R
Ph
Ph
Ph

1.17

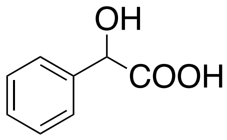

Wolf and his coworker studied on using enantiopure 1,8-diheteroarylnaphthalene derivatives for enantioselective fluorescence quenching by amino acids caused by hydrogen bonding.[53,54] Besides distinct Stern-Volmer quenching constants, different lifetimes were obtained for sensor **1.18** when it interacted chiral N-Boc-Pro. The lifetime reduces to 7.5 ns for L-form and 6.8 ns for D-form respectively, from the original 37 ns.

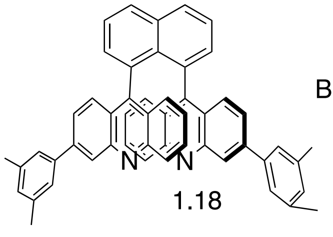

1.18

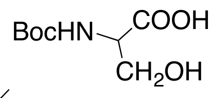
BocHN
COOH
CH2OH

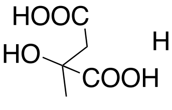
HOOC
HO
COOH

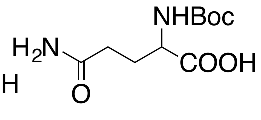
NHBoc
H2N
COOH
O

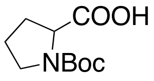

N-Boc-Pro

Many crown-ether based receptors containing BINOL units have also been synthesized for chiral sensing. Hyun *et al* designed sensor **1.19** by incorporating the crown-ether as binding site, BINOL as chiral barrier and dinitrophenylazophenol as chromophore.[55] When treated with primary amino alcohols, different absorption maximum wavelengths up to 43.5 nm and binding constants up to 2.51 times (K_s / K_r) were observed in acetonitrile. The color of **1.19** changed from green-yellow to purple with the addition of (*R*)-phenylalaninol and to blue with the addition of the (*S*)-phenylalaninol.

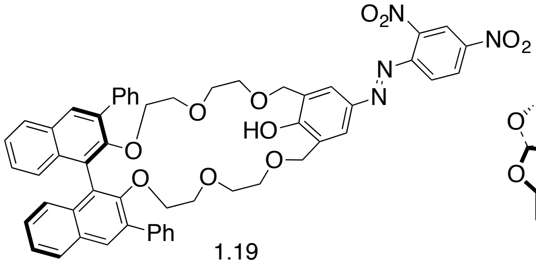

1.19

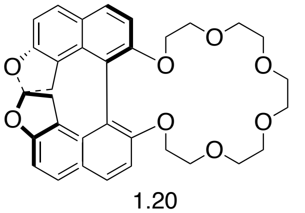

1.20

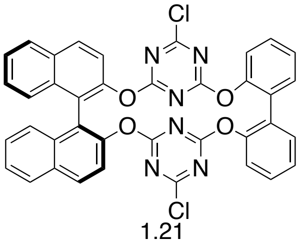

1.21

Using a furo-fused-BINOL based chiral crown (**1.20**), Karnik *et al* reported the enantioselective sensing of phenylethylamine and valine ethyl ester with 2-3 times difference in fluorescence intensity at 367 nm.[56] The chiral molecule formed a 1:1 complex with **1.20** and the association constant was calculated to be $K_r / K_s = 11.30$ for phenylethylamine and 7.02 for valine ester. Additionally, Xu *et al* synthesized a triazine based crown ether (**1.21**) and achieved descent enantioselectivity toward amino acid anions.[57] A 5.4-fold fluorescence enhancement was observed with the addition of D-Ala, while almost no change was observed for L-Ala.

1.4.2. Sensors based on dynamic covalent reactions.

Dynamic covalent chemistry has been developing rapidly in the past decades and has demonstrated great potentials in fluorescence sensing.[58–60] Common dynamic covalent interactions include boronate ester formation, imine formation and exchange, esterification and hemiacetal exchange and etc (Scheme 1-11).[62] Similar to supramolecular interaction, dynamic covalent interaction is also reversible, exchangeable and can reach equilibrium within hours. But it also shares the robustness of covalent chemistry, which makes it less reversible than supramolcular interaction, and in some cases catalyst is needed to reach a rapid equilibrium.

Scheme 1- 11. Examples of dynamic covalent reactions.

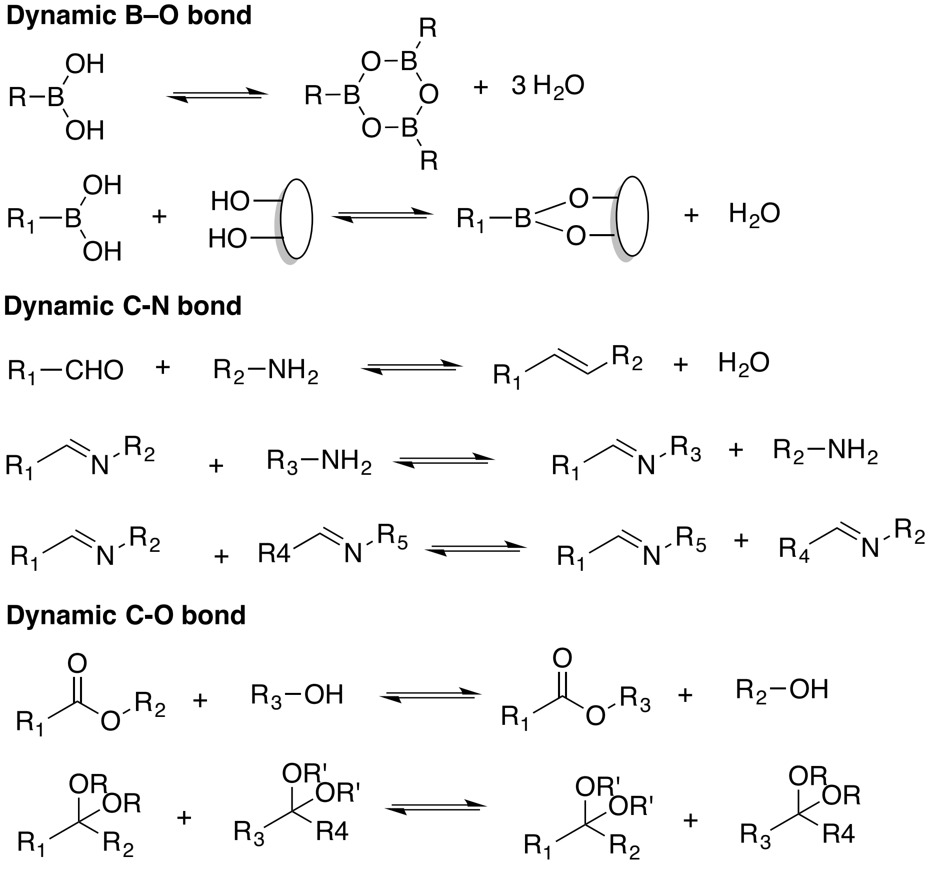

In a pioneering study, James *et al* integrated two boronic acid groups to the chiral BINOL and achieved fluorescence discrimination of D- and L-monosaccharides (Scheme 1-12).[61] Fluorescence of **1.22** was enhanced upon bimodal binding with glucose. The stronger B-O bonding makes it suitable for sensing in water minimizing the interference of its hydrogen bonding. The fluorescence enhancement ratio was 1.93 for glucose and 1.47 for fructose (D / L). Starting from their report, boronic acid motif has become the popular design in the sensing of carbohydrates, alcohols and phenols.[62]

Scheme 1- 12. Fluorescence recognition of glucose using boronate ester formation.

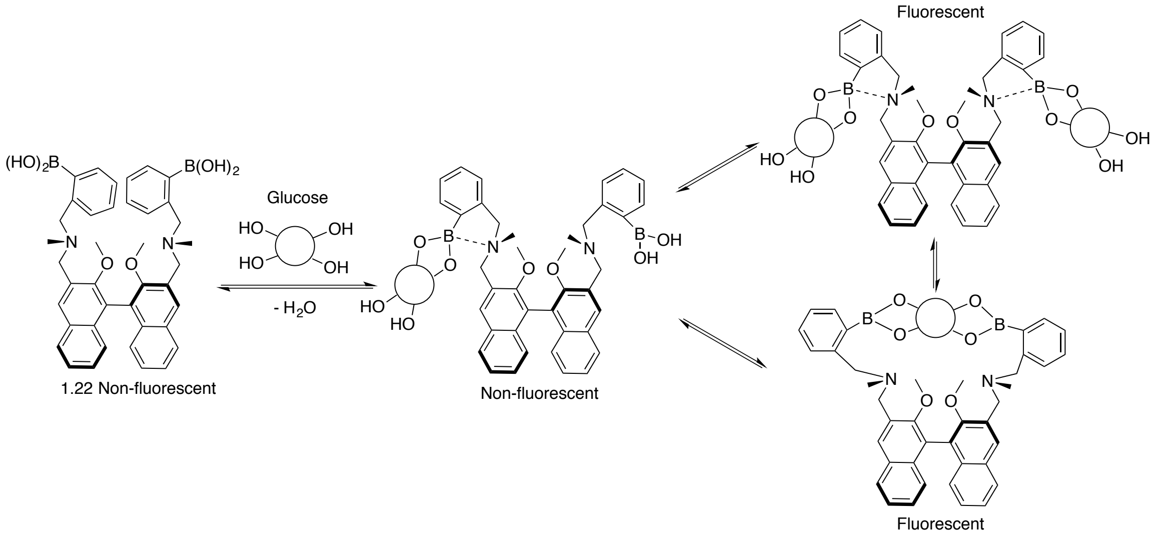
Glucose
- H_2O
1.22 Non-fluorescent
Non-fluorescent
Fluorescent
Fluorescent

Pu *et al* reported using a diformyl-BINOL (**1.23**) in the presence of Zn(II) for enantioselective sensing of amines, amino alcohols and amino acids through imine formation in methanol.[63] The distinct fluorescence intensity at over 500 nm enables visual discrimination of these enantiomers under UV-lamps. The formation of Schiff bases and their complex with Zn(II) was revealed by ESI-MS study. As a necessary component, Zn(II) was assumed to play key roles on inhibiting intramolecular proton transfer and increasing rigidity of the Schiff bases formed.

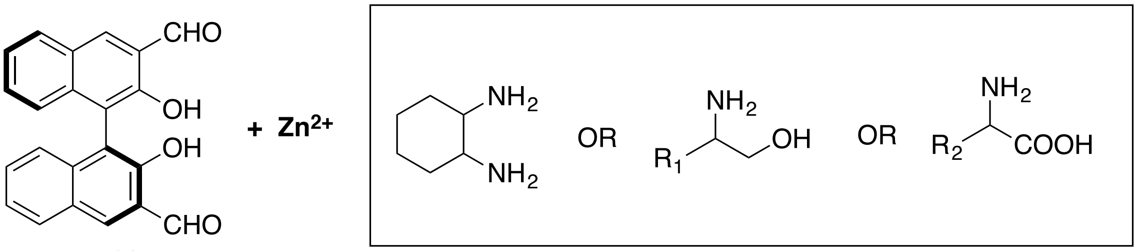
CHO
OH
OH
CHO
+ Zn^{2+}
NH_2
NH_2
OR
NH_2
R_1
OH
OR
NH_2
R_2
COOH

1.23

Moreover, sensor **1.24**, an imine formed by condensation of **1.23** with 2-naphthylamine, can be used to determine the enantiomeric excess and total concentration of chiral amines simultaneously through imine exchange (Scheme 1-13).[64] While **1.24** shows weak emission, the imine **1.25** is strongly emissive at >500 with high enantioselectivity. The naphthylamine restored its emission at 427 nm upon exchange with no enantioselectivity. So fluorescence intensity at 427 nm was used to measure total concentration of chiral amines, while that at > 500 nm was used to measure enantiomeric excess values.

Scheme 1- 13. Sensing of chiral amine through imine exchange using **1.24**.

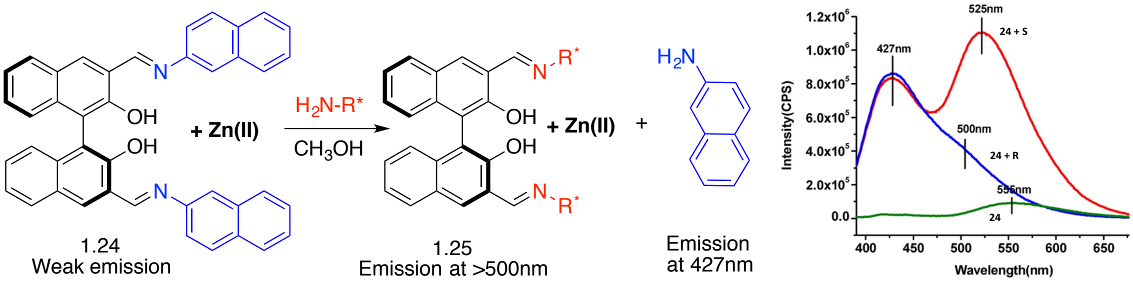
OH
OH
N
N
1.24
Weak emission
+ Zn(II)
H_2N-R*
CH_3OH
N
R*
OH
OH
N
R*
+ Zn(II)
1.25
Emission at >500nm
+
H_2N
Emission
at 427nm
Intensity(CPS)
1.2x10^6
1.0x10^6
8.0x10^5
6.0x10^5
4.0x10^5
2.0x10^5
0.0
525nm
24 + S
427nm
500nm
24 + R
555nm
24
400
450
500
550
600
650
Wavelength(nm)

1.4.3. Sensing based on metal complex.

Besides Zn(II) mentioned above, some other metal ions have also been utilized for enantioselective sensing. Through dynamic ligand exchange, Anslyn et al reported probe **1.26** for enantioselective sensing of amino acids in protic solvents.[65] Titration of **1.26**-Cu(II) to PV formed a 1:1 complex that resulted in a shift of absorption maxima from 445 nm to 645 nm, accompanied by a color change from yellow to blue. Addition of amino acids reversed the process by displacement of PV. The binding favors D-amino acids over the L-forms by a factor of 2-2.5, which can be used for fast *ee* measurements.

Scheme 1- 14. Sensing of amino acids using Cu(II) complex.

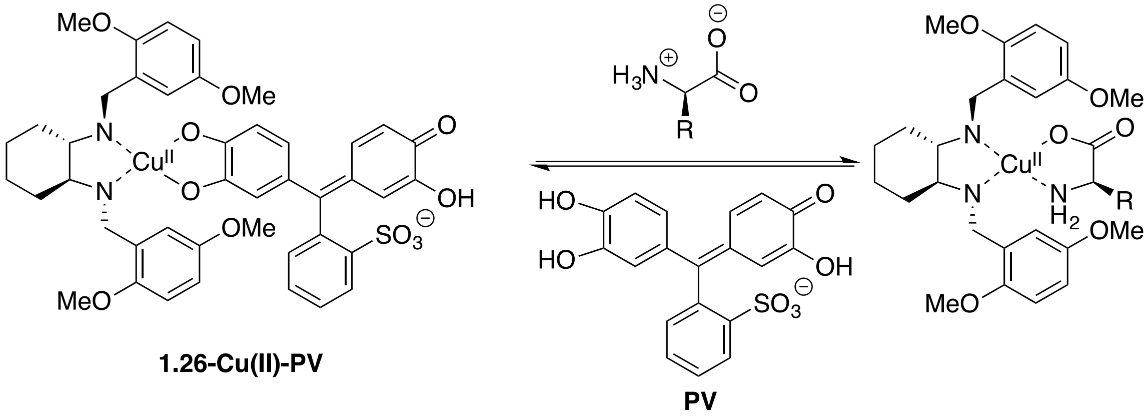
MeO
OMe
N
Cu^II
O
OH
SO3⊖
H3N⊕
R
HO
H2
1.26-Cu(II)-PV
PV

In a rare case, Pu *et al* observed enantioselective gel-collapse from the gel formed by Cu(II) coordination to sensor **1.27** upon sonication.[66] The gel remains stable when treated with (*R*)-phenylglycinol but collapses when (*S*)-phenylglycinol is applied. Stronger fluorescence enhancement was also observed for the (*S*)-enantiomer.

Scheme 1- 15. Enantioselective gel-collapse by amino alcohol.

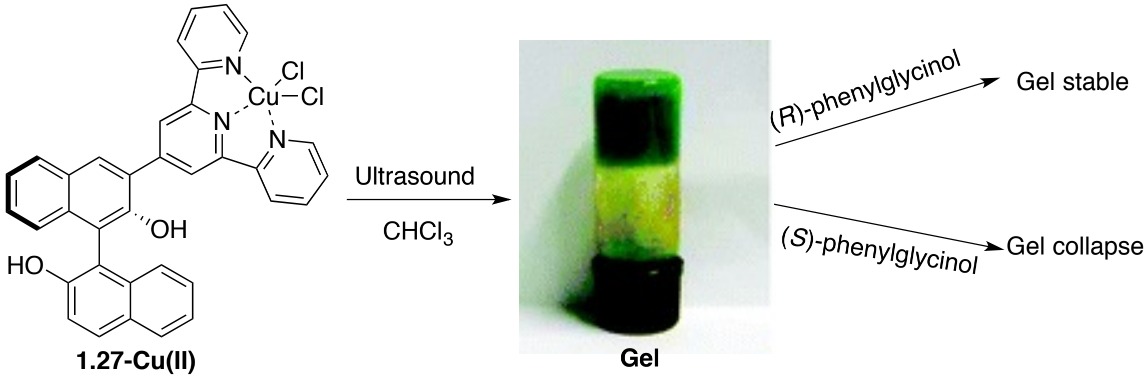
N
Cu
Cl
OH
HO
1.27-Cu(II)
Ultrasound
CHCl3
Gel
(R)-phenylglycinol
Gel stable
(S)-phenylglycinol
Gel collapse

Lin *et al* reported enantioselective sensing of various amino alcohols using the metal-organic framework (MOF) formed by coordination of Cd(II) with ligand **1.28**.[67] Fluorescence of MOF was quenched by amino alcohol and different Stern-Volmer constants were observed for two enantiomers, with K_{sv} (*R*) / K_{sv} (*S*) can reach up to **3.12**.

Scheme 1- 16. Fluorescence quenching of Cd(II) MOF by amino alcohols.

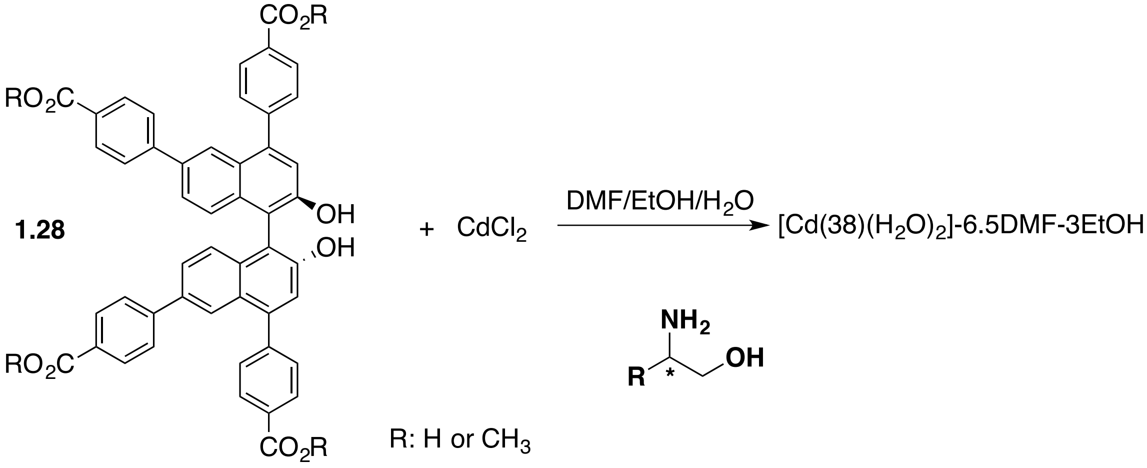

1.5. References

(1) Cecilia Noguez, F. H. *Chirality* **2014**, *26* (April), 553.

(2) Nguyen, L. A.; He, H.; Pham-Huy, C. *Int. J. Biomed. Sci.* **2006**, *2* (2), 85.

(3) Newman, D. J.; Cragg, G. M. *J. Nat. Prod.* **2007**, *70* (3), 461.

(4) Crossley, R. *Chirality and Biological Activity of Drugs*; CRS Press, 1995.

(5) Ganapathy, S. *Chiral Separation Techniques: A Practical Approach*, 3rd ed.; John Wiley & Sons, 2008.

(6) Schmitt, U.; Branch, S. K.; Holzgrabe, U. *J. Sep. ...* **2002**, *25*, 959.

(7) Okamoto, Y.; Ikai, T. *Chem. Soc. Rev.* **2008**, *37* (12), 2593.

(8) Andersson, S.; Allenmark, S. G. *J. Biochem. Biophys. Methods* **2002**, *54* (1–3), 11.

(9) Ward, T. J.; Ward, K. D. *Anal. Chem.* **2012**, *84* (2), 626.

(10) Hyun, M. H.; Han, S. C.; Lipshurtz, B. H.; Shin, Y.-J.; Welch, C. J. *J. Chromat. A* **2001**, *910* (2), 359.

(11) Berthod, A.; Liu, Y.; Bagwill, C.; Armstrong, D. W. *J. Chromat. A* **1996**, *731*, 123.

(12) Fischer, L.; Mueller, R.; Ekberg, B.; Mosbach, K. *J. Am. Chem. Soc.* **1991**, *113*

(24), 9358.

(13) Ikai, T.; Yamamoto, C.; Kamigaito, M.; Okamoto, Y. *Polym. J.* **2006**, *38* (2), 91.

(14) Schurig, V. *J. Chromatogr. A* **1994**, *666*, 111.

(15) Schurig, V. *J. Chromatogr. A* **2001**, *906* (1–2), 275.

(16) Ding, J.; Welton, T.; Armstrong, D. W. *Anal. Chem.* **2004**, *76* (22), 6819.

(17) Dale, J. A.; Dull, D. L.; Mosher, H. *J. Org. Chem.* **1969**, *34* (9), 2543.

(18) Wenzel, T. J. *Discrimination of Chiral Compounds Using NMR Spectroscopy*; Wiley-VCH: Weinheim, 2007.

(19) Reetz, M. T.; Eipper, A.; Tielmann, P.; Mynott, R. *Adv. Synth. Catal.* **2002**, *344* (9), 1008.

(20) Zhao, Y.; Swager, T. M. **2015**, 3221.

(21) Ranjbar, B.; Gill, P. *Chem. Biol. Drug Des.* **2009**, *74* (2), 101.

(22) Chen, Y. H.; Yang, J. T.; Chau, K. H. *Biochemistry* **1974**, *13* (16), 3350.

(23) Santos, Z. A. D. L.; Wolf, C. *J. Am. Chem. Soc.* **2016**.

(24) Bentley, K. W.; Zhang, P.; Wolf, C. *Sci. Adv.* **2016**, *2* (2), e1501162.

(25) Bentley, K. W.; Wolf, C. *J. Am. Chem. Soc.* **2013**, *135* (33), 12200.

(26) Bentley, K. W.; Proano, D.; Wolf, C. *Nat. Commun.* **2016**, *7*, 12539.

(27) Vespalec, R.; Bocek, P. *Electrophoresis* **1999**, *20*, 2579.

(28) Van Eeckhaut, A.; Michotte, Y. *Electrophoresis* **2006**, *27* (14), 2880.

(29) Główka, F. K.; Karaźniewicz, M. *Anal. Chim. Acta* **2005**, *540* (1), 95.

(30) Reetz, M. T.; Kühling, K. M.; Deege, A.; Hinrichs, H.; Belder, D. *Angew. Chemie - Int. Ed.* **2000**, *39* (21), 3891.

(31) Reetz, M. T. *Angew. Chemie - Int. Ed.* **2001**, *40* (2), 284.

(32) Gao, X.; Kagan, H. B. *Chirality* **1998**, *124* (June 1997), 120.

(33) Duursma, A.; Minnaard, A. J.; Feringa, B. L. *Tetrahedron* **2002**, *58* (29), 5773.

(34) Ding, K.; Ishii, A.; Mikami, K. *Angew. Chemie - Int. Ed.* **1999**, *38* (4), 497.

(35) Reetz, M. T.; Zonta, A.; Schimossek, K.; Jaeger, K.-E.; Liebeton, K.; Jaeger, K.-E. *Angew. Chem. Int. Ed. Engl.* **1997**, *36* (24), 2830.

(36) Reetz, M. T.; Becker, M. H.; Kühling, K. M.; Holzwarth, A. *Angew. Chemie - Int. Ed.* **1998**, *37* (19), 2647.

(37) Reetz, M. T.; Becker, M. H.; Liebl, M.; Fürstner, A. *Angew. Chemie - Int. Ed.* **2000**, *39* (7), 1236.

(38) Piovesana, S.; Samperi, R.; Lagan??, A.; Bella, M. *Chem. - A Eur. J.* **2013**, *19* (35), 11478.

(39) Miller, S. M.; Samame, R. A.; Rychnovsky, S. D. *J. Am. Chem. Soc.* **2012**, *134* (50), 20318.

(40) Ebner, C.; Müller, C. A.; Markert, C.; Pfaltz, A. *J. Am. Chem. Soc.* **2011**, *133* (13), 4710.

(41) Alexander, D. *Introduction to Fluorescence Sensing*; Springer, 2009.

(42) Lakowicz, J. R. *Principles of fluorescence spectroscopy*, 3rd ed.; Springer, 2006.

(43) Zhang, X.; Yin, J.; Yoon, J. Recent advances in development of chiral fluorescent and colorimetric sensors. *Chemical Reviews*, 2014, *114*, 4918–4959.

(44) Pu, L.; Pu, L. *Chem. Rev.* **2004**, *104* (3), 1687.

(45) Pu, L. *Acc. Chem. Res.* **2012**, *45* (2), 150.

(46) Parkep, K. S.; A. B. Townshenda; Bale, S. J. *Anal. Proc. Incl. Anal. Commun.* **1995**, *1* (August), 329.

(47) Beer, G.; Daub, J.; Rurack, K. *Chem. Commun.* **2001**, 1138.

(48) Lin, J.; Hu, Q. S.; Xu, M. H.; Pu, L. *J. Am. Chem. Soc.* **2002**, *124* (10), 2088.

(49) Xu, M. H.; Lin, J.; Hu, Q. S.; Pu, L. *J. Am. Chem. Soc.* **2002**, *124* (47), 14239.

(50) Lin, J.; Zhang, H. C.; Pu, L. *Org. Lett.* **2002**, *4* (i), 3638.

(51) Liu, H.-L.; Peng, Q.; Wu, Y.-D.; Chen, D.; Hou, X.-L.; Sabat, M.; Pu, L. *Angew. Chem. Int. Ed. Engl.* **2010**, *49* (3), 602.

(52) Yu, S.; Pu, L. *J. Am. Chem. Soc.* **2010**, *132* (50), 17698.

(53) V, G. U.; Mei, X.; Wolf, C. **2004**, 14736.

(54) Mei, X.; Martin, R. M.; Wolf, C.; V, G. U. *J. Org. Chem.* **2006**, *71*, 2854.

(55) Cho, E. N. R.; Li, Y.; Kim, H. J.; Hyun, M. H. *Chirality* **2011**, *23*, 349.

(56) Upadhyay, S. P.; Pissurlenkar, R. R. S.; Coutinho, E. C.; Karnik, A. V. *J. Org. Chem.* **2007**, *72* (15), 5709.

(57) Xu, K.; Jiao, S.; Yao, W.; Xie, E.; Tang, B.; Wang, C. *Chirality* **2012**, *24* (April), 646.

(58) Simpson, M. G.; Pittelkow, M.; Watson, S. P.; Sanders, J. K. M. *Chem. Rev.* **2006**, *106* (9), 3652.

(59) Jin, Y.; Yu, C.; Denman, R. J.; Zhang, W. *Chem. Soc. Rev.* **2013**, *42* (16), 6634.

(60) You, L.; Zha, D.; Anslyn, E. V. *Chem. Rev.* **2015**, *115* (15), 7840.

(61) James, T. D.; Samankumara Sandanayake, K. R. A.; Shinkai, S. *Nature* **1995**, *374*, 345.

(62) Fang, H.; Kaur, G.; Wang, B. *J. Fluoresc.* **2004**, *14* (5), 481.

(63) Huang, Z.; Yu, S.; Wen, K.; Yu, X.; Pu, L. *Chem. Sci.* **2014**.

(64) Wen, K.; Yu, S.; Huang, Z.; Chen, L.; Xiao, M.; Yu, X.; Pu, L. *J. Am. Chem. Soc.*

2015, *137* (13), 4517.

(65) Folmer-Andersen, J. F.; Lynch, V. M.; Anslyn, E. V. *J. Am. Chem. Soc.* **2005**, *127* (22), 7986.

(66) Chen, X.; Huang, Z.; Chen, S. Y.; Li, K.; Yu, X. Q.; Pu, L. *J. Am. Chem. Soc.* **2010**, *132* (21), 7297.

(67) Wanderley, M. M.; Wang, C.; Wu, C. De; Lin, W. *J. Am. Chem. Soc.* **2012**, *134* (22), 9050.

Chapter 2. Fluorinated molecules in catalysis, separation, and optical studies

2.1. Introduction of fluorous chemistry

Due to the extreme electronegativity of fluorine atom, fluorination of a molecule affects nearly all of its properties, like reactivity, adsorption, distribution, metabolism, and excretion.[1] In the area of pharmaceuticals and agrochemicals, fluorination is an important method to modulate bioactivities of molecules.[2] There is no drug containing fluorine atoms prior to 1957, partially due to the difficulty of preparation. After that, there are more than 150 fluorinated drugs that have been commercialized, occupying a market share of around 20%.[1] These drugs have been widely applied to the treatment of cancer, cardiovascular diseases, infectious diseases, nervous system diseases and etc.[2] The top-selling ones are Prozac (anti-depression drug), Lipitor (reductase inhibitor drug) and Cipro (infection treatment drug), as shown in Figure 2-1.

Figure 2-1. Examples of fluorinated drugs.

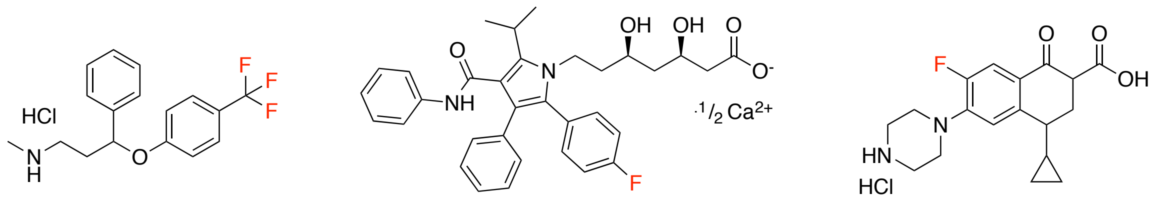

Prozac Lipitor Cliprobay

A few fluorine atoms are usually enough to change the bioactivities of a drug significantly. When the weight percentage of fluorine (wt %) in C(sp3)-F bonds within a molecule exceeds 60%, this molecules is referred to be fluorous, a term introduced by Horváth *et al* in 1994 as an analogue of "aqueous".[3] Fluorocarbons, which are produced by replacing all hydrogen atoms in hydrocarbons to fluorine, are fluorous solvents that are both lipophobic and hydrophobic. The most commonly used fluorous solvents are perfluorinated alkanes like perfluorohexanes (FC-72) and perfluorodecalins (PP6). Fluorous ponytail is fluoroalkyl moiety with the formula $(CH_2)_m(CF_2)_nCF_3$. Ponytail can make a molecule partially or predominantly soluble in fluorous solvent depending on its number and length. At low or room temperature, a biphasic heterogeneous system is formed between fluorous and organic solvents. However, at elevated temperature they are miscible and a single-phase homogeneous systems is formed. In the past two decades, fluorous chemistry has been widely studied in the area of green chemistry, materials chemistry and biomedical systems.[4–6]

2.2. Fluorous molecules in catalysis and separation

The temperature dependent miscibility of fluorous media makes it idea for easy separation and catalyst recycling. As a typical setup shown in Scheme 2-1, the reactant is dissolved in organic phase while the fluorine-tagged catalyst stays in the fluorous phase at room temperature.[4] At elevated temperature, it becomes a homogeneous system where the reaction can proceed smoothly. Upon reaction completion, the system is cooled down and the products will stay in the organic phase with the catalyst retained in the fluorous phase. The products are then isolated by extraction, and the catalyst can also be easily recycled. Another strategy would be allowing the reaction to proceed in a universal solvent. The product can be separated by the addition of organic solvents and catalyst can be recycled by the addition of fluorous solvents.

In an example of copper catalyzed aerobic oxidation of alcohol to aldehyde, a bipyridine catalyst **2.1** bearing two fluorous ponytails was used in the biphasic catalytic system (Scheme 2-2).[7] The reaction turned into homogenous at 90 °C. Upon completion, it was cooled to 0 °C and catalyst **2.1** can be easily recycled from the C_8F_{17} solvent as all other components were kept in C_6H_5Cl. The catalyst can be used for at least 6 cycles as tested without a substantial loss of activity.

Scheme 2- 1. A general strategy of fluorous separation.

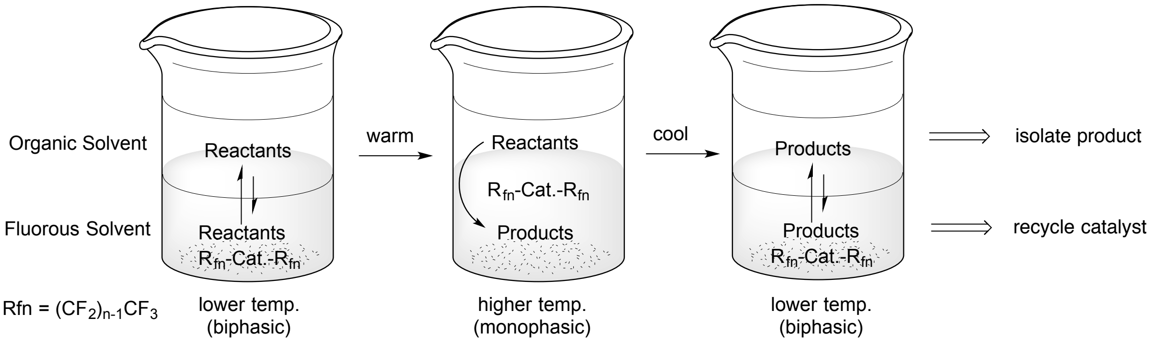
Organic Solvent
Fluorous Solvent
Rfn = (CF2)n-1CF3
Reactants
Reactants
Rfn-Cat.-Rfn
lower temp.
(biphasic)
warm
Reactants
Rfn-Cat.-Rfn
Products
higher temp.
(monophasic)
cool
Products
Products
Rfn-Cat.-Rfn
lower temp.
(biphasic)
isolate product
recycle catalyst

Scheme 2- 2. Aerobic oxidation of alcohols to aldehydes with fluorous catalyst.

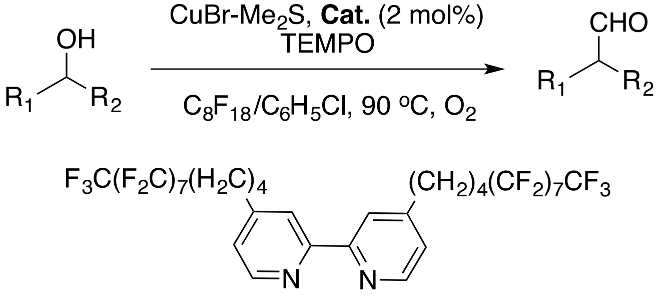
CuBr-Me2S, Cat. (2 mol%)
TEMPO
C8F18/C6H5Cl, 90 ºC, O2
OH
R1
R2
CHO
R1
R2
F3C(F2C)7(H2C)4
(CH2)4(CF2)7CF3
N
N

Catalyst, 2.1

Enantioselective catalysis was also achieved in an iridium-catalyzed reduction of ketones to alcohols using fluorinated diamine ligand **2.2** (Scheme 2-3).[8] The biphasic system consisted of isopropanol / D-100 (mainly n-perfluorooctane). A yield up to 92% and enantioselectivity up to 79% were obtained in the case of acetophenone. However, after four cycles the activity of chiral ligand recovered from D-100 was significantly decreased.

Scheme 2- 3. Ir-catalyzed asymmetric ketone reduction using fluorous ligands.

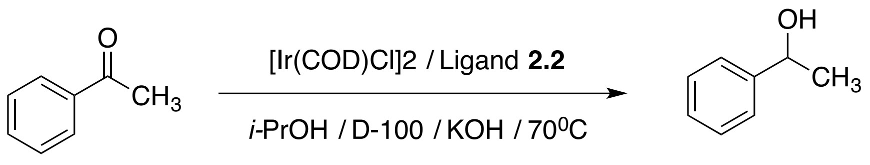
O
CH3
[Ir(COD)Cl]2 / Ligand 2.2
i-PrOH / D-100 / KOH / 70⁰C
OH
CH3

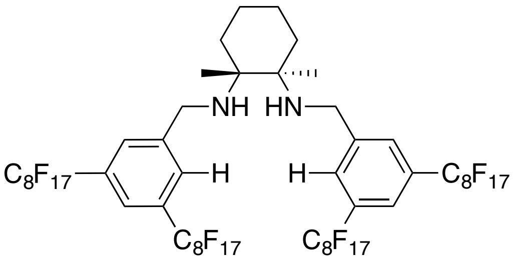
NH
HN
C8F17
H
H
C8F17
C8F17
C8F17

2.2

Cycle	Yield (%)	ee (%)
1	92	69
2	90	79
3	86	59
4	69	58

The advantages of fluorous extraction were obvious when applied to kinetic resolutions (Scheme 2-4).[9] Highly enantioselective esterification of rac-**2.3** was achieved by using enzyme (CAL-B) as the catalyst, with the production of (*R*)-**2.5** and unreacted (*S*)-**2.3**. During work-up, the enzyme was removed by filtration, followed by evaporation to remove volatile components. The residual was re-dissolved in methanol and extracted six times by FC-72, resulting in the separation of (*S*)-**2.3** and (*R*)-**2.5** in two phases with excellent *ee*. (*R*)-**2.3** can be regenerated by removal of the fluorous tag of (*R*)-**2.5**.

Scheme 2- 4. Kinetic resolution of rac-**2.3** by fluorous labeling.

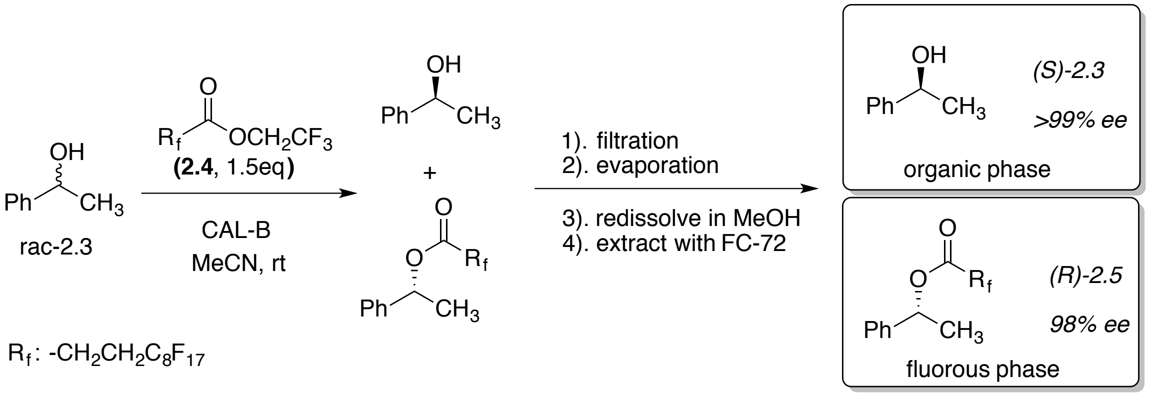
OH
Ph
CH3
rac-2.3
O
Rf
OCH2CF3
(2.4, 1.5eq)
CAL-B
MeCN, rt
OH
Ph
CH3
+
O
O
Rf
Ph
CH3
1). filtration
2). evaporation
3). redissolve in MeOH
4). extract with FC-72
OH
Ph
CH3
(S)-2.3
>99% ee
organic phase
O
O
Rf
Ph
CH3
(R)-2.5
98% ee
fluorous phase
Rf: -CH2CH2C8F17

Besides the liquid-liquid biphasic separation aforementioned, fluorous molecules have also been studied in solid-phase extractions, fluorous flash chromatography and fluorous HPLC.[4]

2.3. Optical studies of fluorous molecules

Optical studies regarding fluorous molecules are still very scarce despite the vast development of fluorous chemistry, mainly due to the lack of fluorinated chromophores or fluorophores, limited availability of fluorous media and synthetic difficulties. Among thousands of fluorophores that were synthesized, there is only a handful of them containing fluorine atoms over 50 wt%.[10]

Kölmel *et al* synthesized three kinds of F-tagged rhodamine dyes (**2.6**, **2.7** and **2.8**) with fluorine content up to 53 wt % (Figure 2-2).[11] These dyes, which are otherwise painful to deal with, can be conveniently separated by fluorous solid-phase extraction using FluoroFlash columns. Spectroscopic studies showed that they had emissions ranging from 520-600 nm and had good extinction coefficients and quantum yields comparable with their analogues. The biocompatibility of these dyes was also maintained as demonstrated by cell imaging studies.

Figure 2-2. F-rhodamine dyes synthesized by Kölmel *et al.*

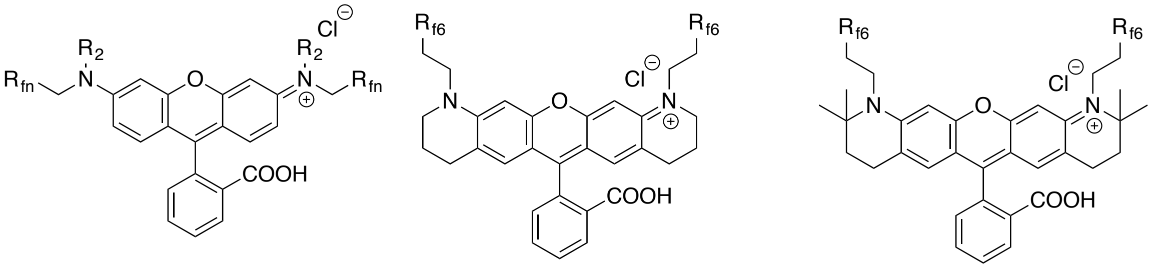

2.6 2.7 2.8

R_{fn} = -(CF2)$_{n-1}$CF$_3$, n=6, 7, or 8. R_2= H or Et.

A perylene diimide dye **2.9** containing significant amount of fluorine atoms was synthesized by Luca *et al* (Figure 2-3).[12] It gave a maximum absorption at 527 nm with an extinction coefficient of 64000 M^{-1} cm^{-1} in chloroform. They used this dye as an electron acceptor in conjugation with another electron donor for the fabrication of optical devices. However, the fluorous properties of **2.9** were not characterized in their study.

Figure 2-3. A perylene diimide dye synthesized by Luca *et al.*

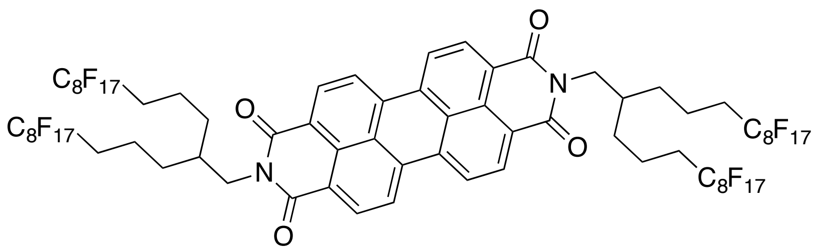

2.9

Sun *et al* synthesized a series of perfluorooctylated fluorophores including anthracene (**2.10**, **2.11**), pyrene (**2.12**), and phenanthroline (**2.13**) to study their photostability (Figure 2-4).[13] By using a mixture of fluorous solvent (perfluorobutyl ethyl ether) and DMSO, the purification was largely simplified, compared with the conventional use of DMSO or DMF only. Under solar light illumination in air for 155 h, it is observed that the photostability of **2.10** – **2**.**13** are all significantly enhanced compared with their non-fluorous analogues. Their photostability in fluorous solvents was found to be 10 times higher than in chloroform solution, even though the oxygen concentration in fluorous solvents is 5-10 times higher than in hydrocarbons.[14] This made the fluorinated dyes superior for the fabrication of organic optical devices.

Figure 2-4. Various fluorous polyaromatics synthesized by Sun *et al.*

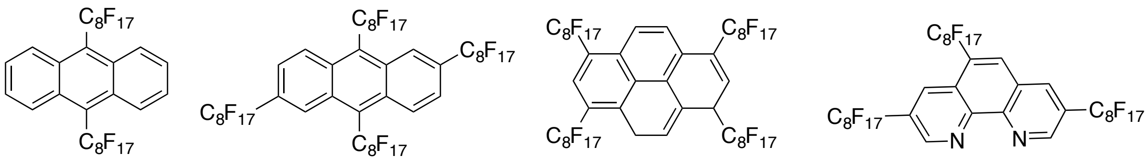

2.10 2.11 2.12 2.13

Figure 2-5. Fluorofluorophores derived from **2.14** by Swager *et al.*

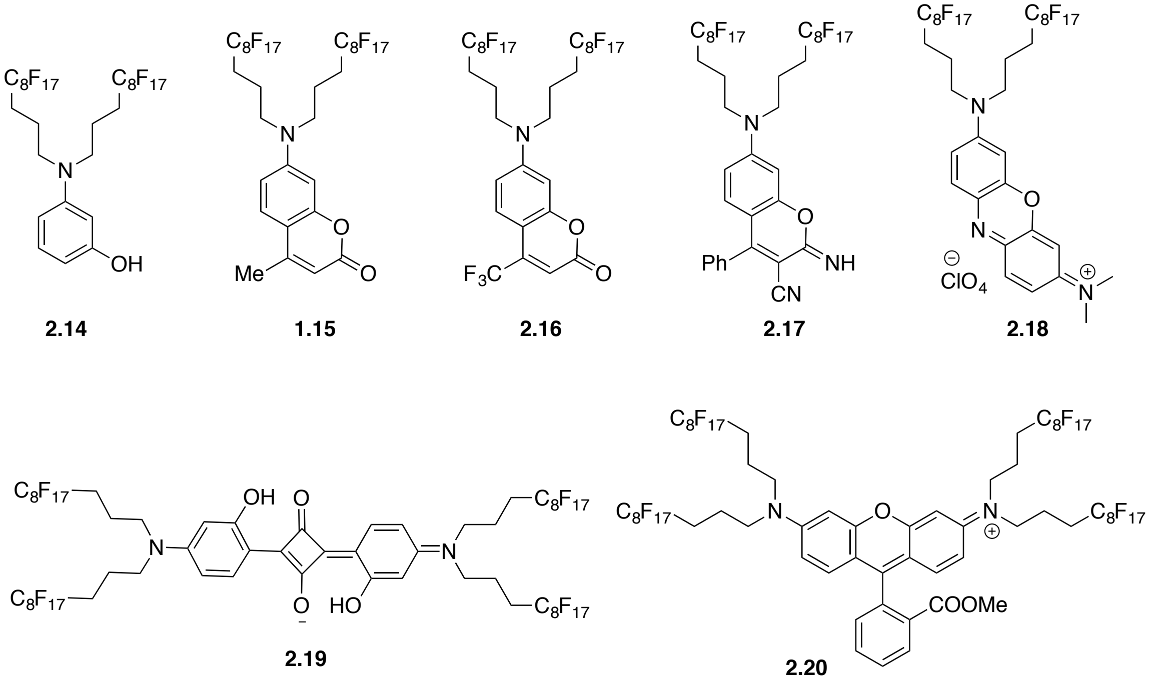

2.14 **1.15** **2.16** **2.17** **2.18** **2.19** **2.20**

Starting with fluorinated aminophenol **2.14**, Swager *et al* reported the highly-efficient synthesis of a series of fluorofluorophores (**2.15**-**2.20**), which refer to fluorophores bearing F-ponytails, with moderate yields (Figure 2-5).[15] These include fluorinated coumarins (**15**, **16**), quinone (**17**), oxazine (**18**), squaraine (**19**) and rhodamine (**20**), whose emissions spread widely over the visible region from 434 nm to 664 nm with quantum yields from 0.16 to 0.89 in ethanol. Strong emission intensity was observed in trifluorotoluene for **17**-**20**, and it is weaker in toluene due to aggregation. These fluorophores are soluble in fluorous solvents containing heteroatoms, but not in fluorocarbons. Fluorescent nanoemulsions can also be prepared with high stability over several weeks. This study would facilitate the use of fluorous fluorophores for *in vivo* imaging.

2.4. References

(1) Müller, K.; Faeh, C.; Diederich, F. *Science* **2007**, *317* (5846), 1881.

(2) Wang, J.; Sánchez-Roselló, M.; Aceña, J. L.; Del Pozo, C.; Sorochinsky, A. E.; Fustero, S.; Soloshonok, V. A.; Liu, H. *Chem. Rev.* **2014**, *114* (4), 2432.

(3) Horvath, I. T.; Rabai, R. *Science* **1994**, *266*, 72.

(4) Gladysz, J.; Curran, D.; Horváth, I. *Handbook of Fluorous Chemistry*; John Wiley & Sons: Weinheim, 2005.

(5) Horvath, I. T. *Acc. Chem. Res.* **1998**, *31* (10), 641.

(6) Zhang, W. *Green Chem.* **2009**, *11* (7), 911.

(7) Betzemeier, B.; Cavazzini, M.; Quici, S.; Knochel, P. *Tetrahedron Lett.* **2000**, *41*, 4343.

(8) Maillard G.; Quici, S.; Valad, B.; Sinou, D., D. P. *Tetrahedron* **2002**, *58*, 3971.

(9) Hungerhoff, B.; Sonnenschein, H.; Theil, F. *Angew. Chemie - Int. Ed.* **2001**, *40* (13), 2492.

(10) Kim, S. H. *Functional Dyes*, 1st editio.; Elsevier Ltd: Amsterdam, 2006.

(11) Kölmel, D. K.; Rudat, B.; Braun, D. M.; Bednarek, C.; Schepers, U.; Bräse, S. *Org. Biomol. Chem.* **2013**, *11* (24), 3954.

(12) De Luca, G.; Liscio, A.; Melucci, M.; Schnitzler, T.; Pisula, W.; Clark, C. G.;

Scolaro, L. M.; Palermo, V.; Müllen, K.; Samorì, P. *J. Mater. Chem.* **2010**, *20* (1), 71.

(13) Sun, H.; Putta, A.; Kloster, J. P.; Tottempudi, U. K. *Chem. Commun.* **2012**, *48* (99), 12085.

(14) R. Battino, T. R. R. and T. T. *J. Phys. Chem. Ref. Data* **1983**, *12*, 163.

(15) Sletten, E. M.; Swager, T. M. *J. Am. Chem. Soc.* **2014**, *136* (39), 13574.

Chapter 3. Enantioselective Fluorescent Recognition in Fluorous Phase: Enhanced Reactivity and Expanded Chiral Recognition

3.1. Introduction

In the past two decades, tremendous amount of research has been conducted on the use of fluorous phase in liquid-liquid separation as described in the previous chapter. The unique hydrophobic and lipophobic properties of the perfluorocarbon-based fluorous solvents have exhibited important advantages in the development of new separation techniques. The pioneering work on the use of fluorous phase in catalysis was reported by Horváth and Rábai in 1994.[1] They designed a Rh-catalyst containing a perfluoroalkyl substituted phosphine ligand, $P[CH_2CH_2(CF_2)_5CF_3]_3$, to catalyze the hydroformylation of 1-decene under CO and H_2 in a fluorous solvent such as a perfluorinated linear alkane or the perfluorinated methylcyclohexane ($CF_3C_6F_{11}$) to form aldehydes (Scheme 3-1). When the reactor was cooled down to room temperature at the completion of reaction, the perfluoroalkyl phosphine coordinated metal catalyst was soluble in the fluorous solvent while the aldehyde products were not. This allowed easy purification of the product as well as easy recovery and reuse of the catalyst.

Scheme 3-1. Hydroformylation in fluorous phase.

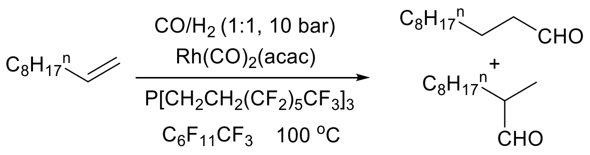

The fluorous-phase-based phase separation technique has been extensively used in synthesis and catalysis. However, very little work was conducted on applying the fluorous chemistry in optical sensing, though there are a few optical studies as mentioned in Chapter 2. There are two reports on using the fluorous phase-based chemistry to develop molecular probes for optical detection.[2,3] In one report, Vincent *et al* described the use of the perfluoroalkyl substituted copper carboxylate complex **3.1** in combination with a tetrapyridylporphyrin **3.2** for the fluorescent detection of histamine.[2] A solution of **3.1** in perfluorohexane can efficiently extract the fluorophore **3.2** from its methylene chloride solution by coordination of the pyridyl group to the Cu(II) center to form the complex **3.1**+**3.2**.

Scheme 3-2. Fluorous sensors used for Histamine recognition reported by Vincent *et al.*

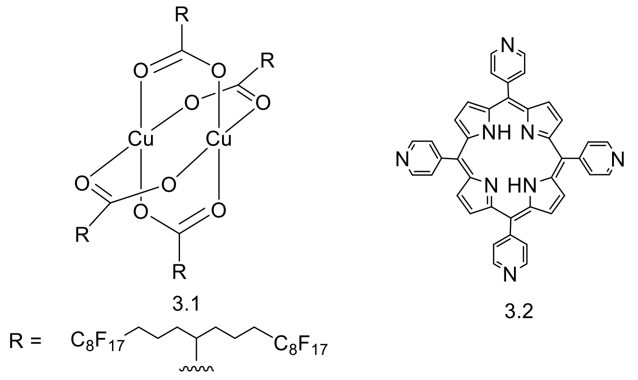

When this two-phase system was treated with histamine, coordination of histamine with the copper complex **3.1** can release the fluorophore **3.2** into the methylene chloride phase. Measuring the increase of the fluorescent intensity of **3.2** in the methylene chloride solution allowed the determination of the concentration of histamine. Using this fluorous-phase-based detection does not require the complex **3.1** + **3.2** and the chromophore **3.2** to have different optical signal because of the phase separation. In another report, selective detection of ethanol by using UV-Vis absorption was observed in a similar manner.[3]

In recent years, the development of enantioselective fluorescent sensors for the recognition of chiral organic molecules has attracted significant research attention.[4] Among the potential applications of these sensors is their use in rapid chiral catalyst screening since fluorescence can provide real time analysis. However, direct addition of a fluorescent sensor into the product mixture of a catalyst screening experiment could cause various degree of uncertainty in fluorescent analysis because of the possible interference from species other than the product.

As a highly sensitive analysis tool, fluorescence measurement can be easily interfered by solvents, catalysts, by-products or even the air. If the product of a screening experiment could be conveniently separated from the reaction mixture, its analysis by using the enantioselective fluorescent sensor should be significantly simplified which should greatly facilitate the high throughput screening of chiral catalysts. The progress of the fluorous phase-based separation has prompted us to propose the use of fluorous phase for enantioselective recognition. We envision that if the enantioselective fluorescent recognition of reaction products could be conducted in fluorous phase, it would be possible to use the fluorous-phase based separation to minimize the interference of other species in the screening experiments since most compounds without a highly fluorinated group are insoluble in fluorous solvents. We studied the first example of enantioselective fluorescent recognition in fluorous phase. In this work we also showed that the fluorous phase-based sensor enhances the reactivity of the previously reported fluorous insoluble sensor with amino alcohols and expands its chiral recognition ability.

This study was inspired by a recent finding in *Pu* lab that the 1,1’-bi-2-naphthol (BINOL)-based chiral trifluoromethyl ketone (*S*)-**3.3** exhibits highly enantioselective fluorescent recognition of trans-1, 2-diaminocyclohexane in CH_2Cl_2.[5] However, the reaction of this compound with amino alcohols was found to be slow in CH_2Cl_2 and not applicable for the fluorescent detection of amino alcohols. (*S*)-**3.3** is insoluble in fluorous solvents such as perfluorohexane (FC-72) since the two trifluoromethyl groups are too short. In order to conduct the fluorescent recognition of chiral amines in fluorous phase, we introduced longer fluorous ponytail groups into **3.3**.

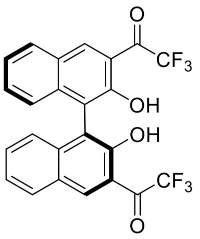

(*S*)-3.3

3.2. Results & Discussion

3.2.1. Synthesis of the sensor

The starting material (*S*)-**3.4** was easily prepared from (*S*)-BINOL using NaH and CH_3OCH_2Cl as reported.[6] As shown in Scheme 3-3, orthometalation of (*S*)-**3.4** with ^nBuLi followed by addition of a perfluoroalkylacyl chloride gave (*S*)-**3.5** with a yield of 72%. It should be noted that fluorous acyl chloride must be used instead of its ester analogue. Removal of the protecting groups of (*S*)-**3.5** using TFA gave (*S*)-**3.6** as an orange powder with 85% yield. (*S*)-**3.6** can also be obtained in a one-pot procedure without the separation of **3.5** in similar yield. This long chain perfluoroalkyl substituted chiral ketone was found to be soluble in fluorous solvents. It can reach a concentration of 0.8 mM in FC-72, enough to be used for optic studies. The solubility is even higher in other more polar fluorous solvents. The enantiomer (*R*)-**3.6** was also synthesized starting with (*R*)-**3.4**.

Scheme 3-3. Synthesis of sensors (*S*)-**3.6** and (*R*)-**3.6**.

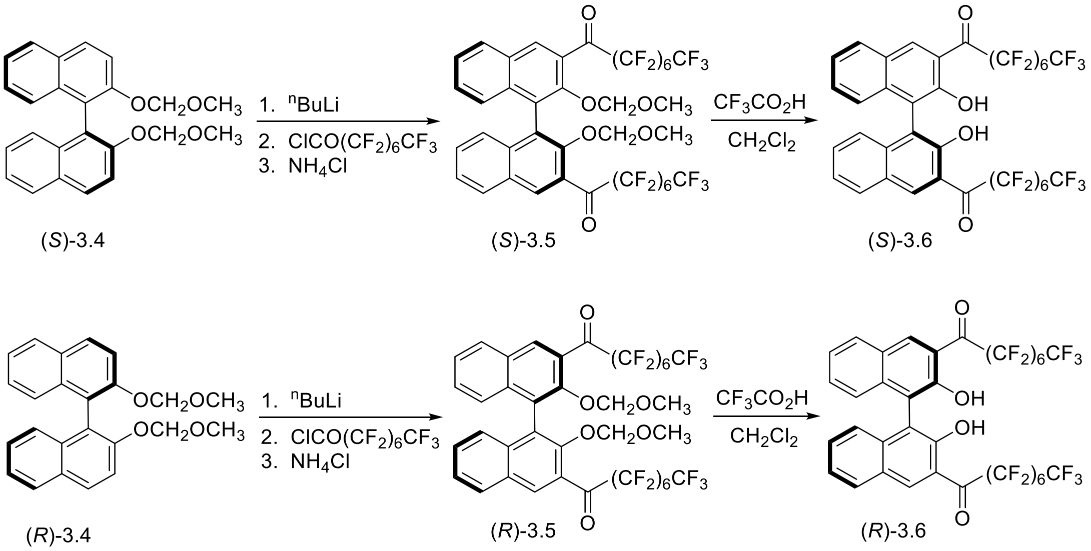
OCH2OCH3
OCH2OCH3
1. nBuLi
2. ClCO(CF2)6CF3
3. NH4Cl
O
(CF2)6CF3
OCH2OCH3
OCH2OCH3
(CF2)6CF3
O
CF3CO2H
CH2Cl2
O
(CF2)6CF3
OH
OH
(CF2)6CF3
O
(S)-3.4
(S)-3.5
(S)-3.6
(R)-3.4
(R)-3.5
(R)-3.6

3.2.2. Study of the interactions of the sensor and amine in organic solvents

Figure 3-1. Structures of chiral amines used in this study.

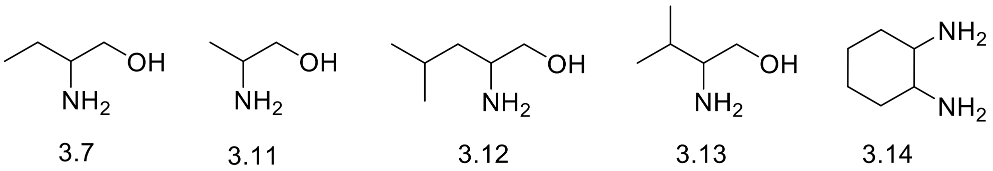
OH
NH2
3.7
OH
NH2
3.11
OH
NH2
3.12
OH
NH2
3.13
NH2
NH2
3.14

We first examined the fluorescent response of (*S*)-**3.6** toward a chiral amino alcohol 2-amino-butanol (**3.7**) in CH_2Cl_2. (*S*)-**3.6** blank gave very weak fluorescent signal in CH_2Cl_2. In the presence of either (*R*)- or (*S*)-2-aminobutanol [(*R*)-**3.7** or (*S*)-**3.7**], the fluorescent signal of (*S*)-**3.6** was still very weak even over a long period of time (Figure 3-2).

Figure 3-2. Fluorescence spectra of (*S*)-**3.6** (0.08 mM) with or without (*R*)-**3.7** and (*S*)-**3.7** (5 mM) using dichloromethane as solvent. Spectra were recorded at 1 h, 3 h, 5 h, 7 h, 10 h and 23 h after mixing, λ_{ex}= 290 nm, slit 2/2 nm.

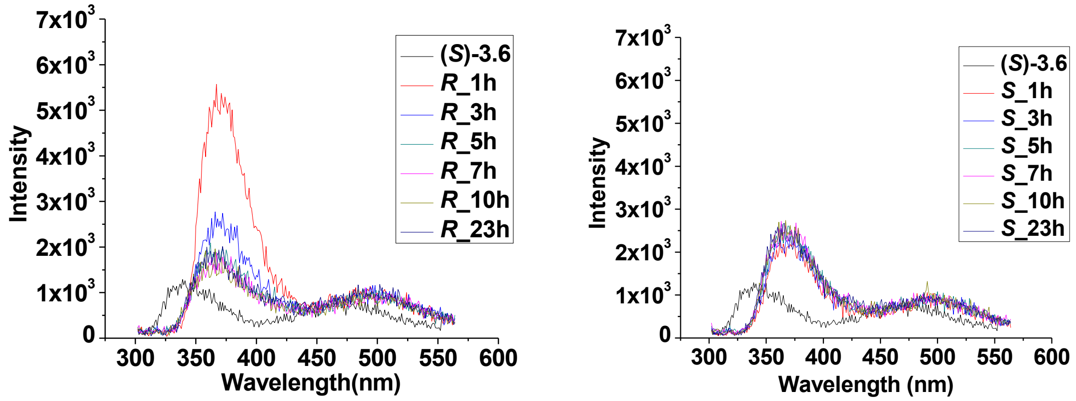

In $CDCl_3$ solution, the ^{1}H NMR spectrum of (*S*)-**3.6** also did not show any change with the addition of either (*R*)-**3.7** or (*S*)-**3.7** except the disappearance of the OH signals of (*S*)-**3.6** at δ 10.58 ppm, due to the base-catalyzed proton exchange in solution (Figure 3-3 and 3-4). Thus, no other chemical reaction was observed for (*S*)-**3.6** with the amino alcohol in chloroform solution. In ^{19}F NMR, no change was observed as well.

Figure 3-3. NMR titration of (*R*)-**3.7** (2 mM in $CDCl_3$) to (*S*)-**3.6** (0.02 mM in 0.4 mL $CDCl_3$). ^{1}H NMR spectra were recorded with the addition of the **3.7** in the following amounts: 0, 1, 3, 5, 10, 15, 20, 30 and 40 μL. These volumes correspond to 0, 0.2, 0.6, 1.0, 2.0, 3.0, 4.0, 6.0, and 8.0 equivalents of **3.7** respectively.^{19}F NMR spectra were recorded with the addition of 0, 4.0, 6.0 and 8.0 equivalents of **3.7**.

^{1}H NMR Spectra

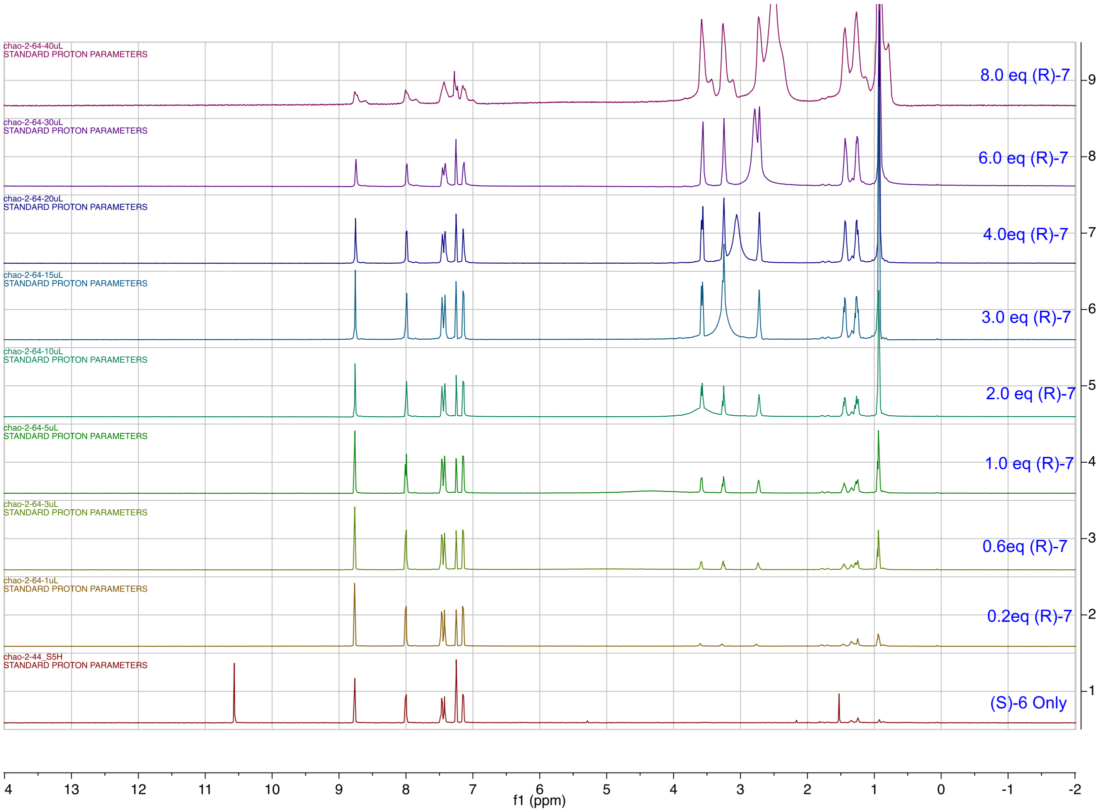

^{19}F NMR Spectra

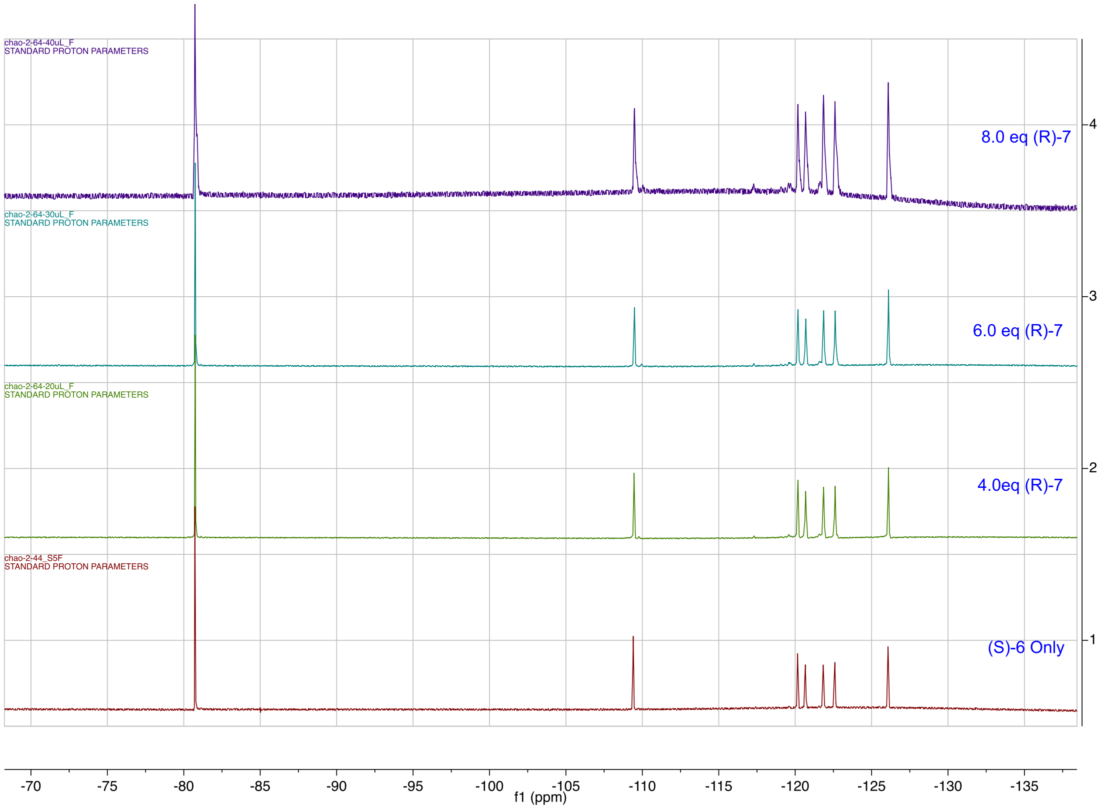

Figure 3- 4. NMR titration of (*S*)-**3.7** (2 mM in $CDCl_3$) to (*S*)-**3.6** (0.02 mM in 0.4 mL $CDCl_3$). ^1H NMR spectra were recorded with the addition of the (*S*)-**3.7** solution in the following amounts: 1, 3, 5, 7.5, 10, 15, 20, 30 and 40 µL. These correspond to 0.2, 0.6, 1.0, 1.5, 2.0, 3.0, 4.0, 6.0, and 8.0 equivalents respectively. ^{19}F NMR spectra were recorded with the addition of 0, 4.0, 6.0 and 8.0 equivalents of (*S*)-**3.7**.

^1H NMR Spectra

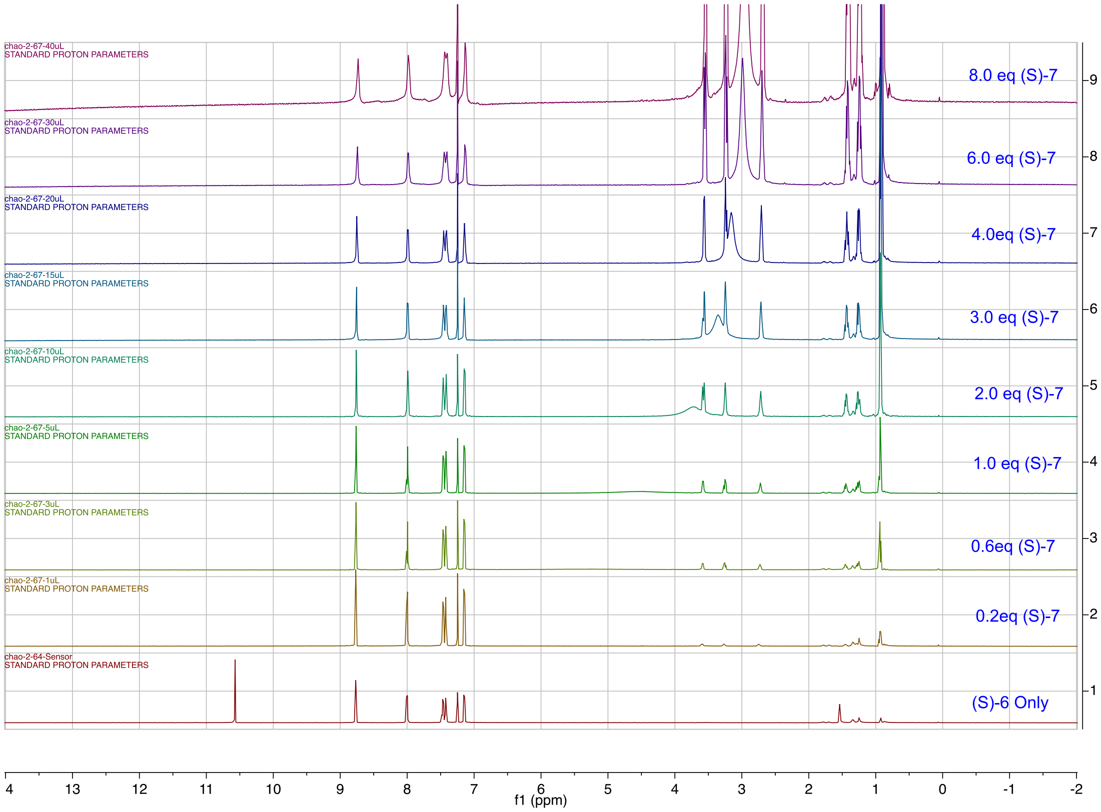

^{19}F NMR Spectra

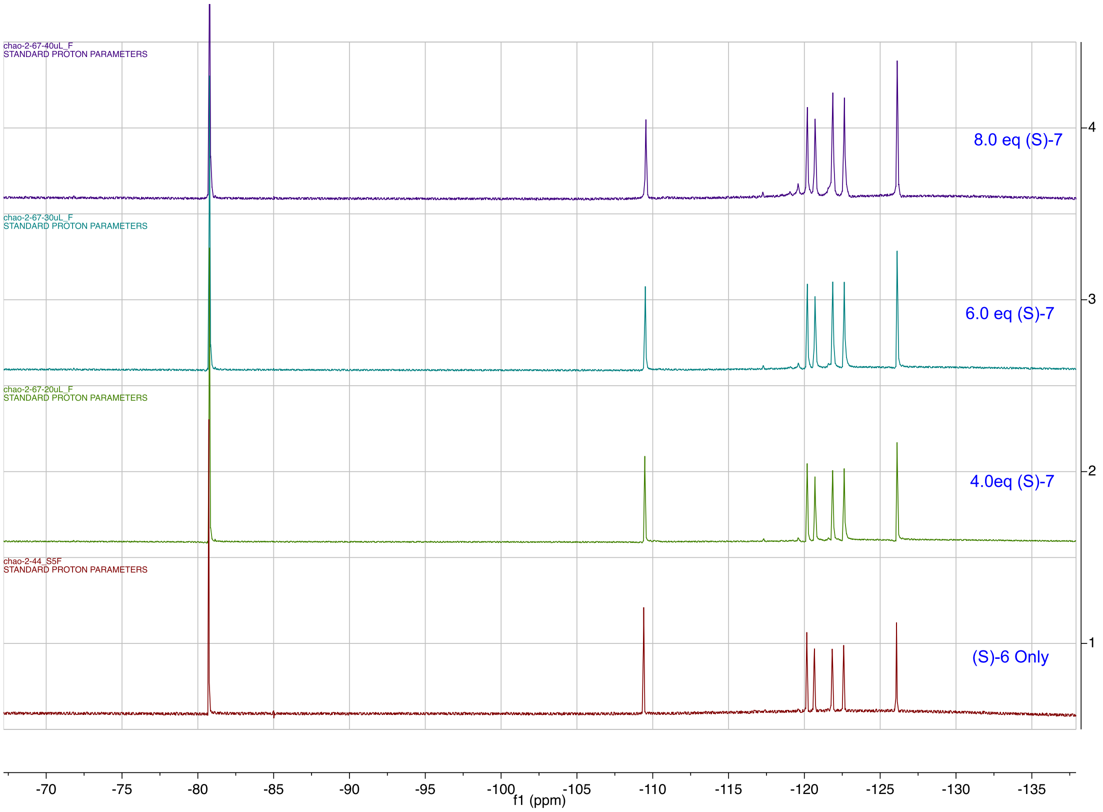

3.2.3. Study the interactions of sensor and amine in fluorous solvents

We then studied the fluorescence response of (*S*)-**3.6** toward the amino alcohol in fluorous phase. In FC-72, (*S*)-**3.6** also showed no fluorescence. When (*S*)-**3.6** (8.0×10^{-5} M) was treated with (*R*)-**3.7** (0.5 – 5 mM) in FC-72 (containing 4% CH_2Cl_2 to dissolve the amino alcohol), large fluorescence enhancement at $\lambda = 420$ nm was observed as shown in Figure 3-5a. However, when (*S*)-**3.6** was treated with the enantiomer (*S*)-**3.7** under the same conditions, little fluorescent response was observed as shown in Figure 3-5b. Thus, (*S*)-**3.6** exhibits highly enantioselective fluorescent recognition of the amino alcohol. Figure c shows the fluorescence responses of (*S*)-**3.6** at $\lambda = 420$ nm when treated with (*R*)- and (*S*)-**3.7** at various concentrations. We also tested the effect of the reaction time on the fluorescent response. As shown in Figure d, the fluorescent responses were relatively stable over the periods of 1 – 4 h.

Figure 3-5. Fluorescence spectra of (*S*)-**3.6** (8.0×10^{-5} M) in the presence of (*R*)-**3.7** (a) and (*S*)-**3.7** (b) with a concentration range of 0.5 to 5 mM (Spectra were recorded 1h after mixing. Solvent: 4% DCM/FC-72, λ_{ex} = 290 nm, slit 2/2 nm).(c)Fluorescent intensity at λ_{em}=420 nm versus the concentration of (*R*)-**3.7** or (*S*)-**3.7** (Error bars were obtained with 4 independent measurements) and (d) effect of the reaction time.

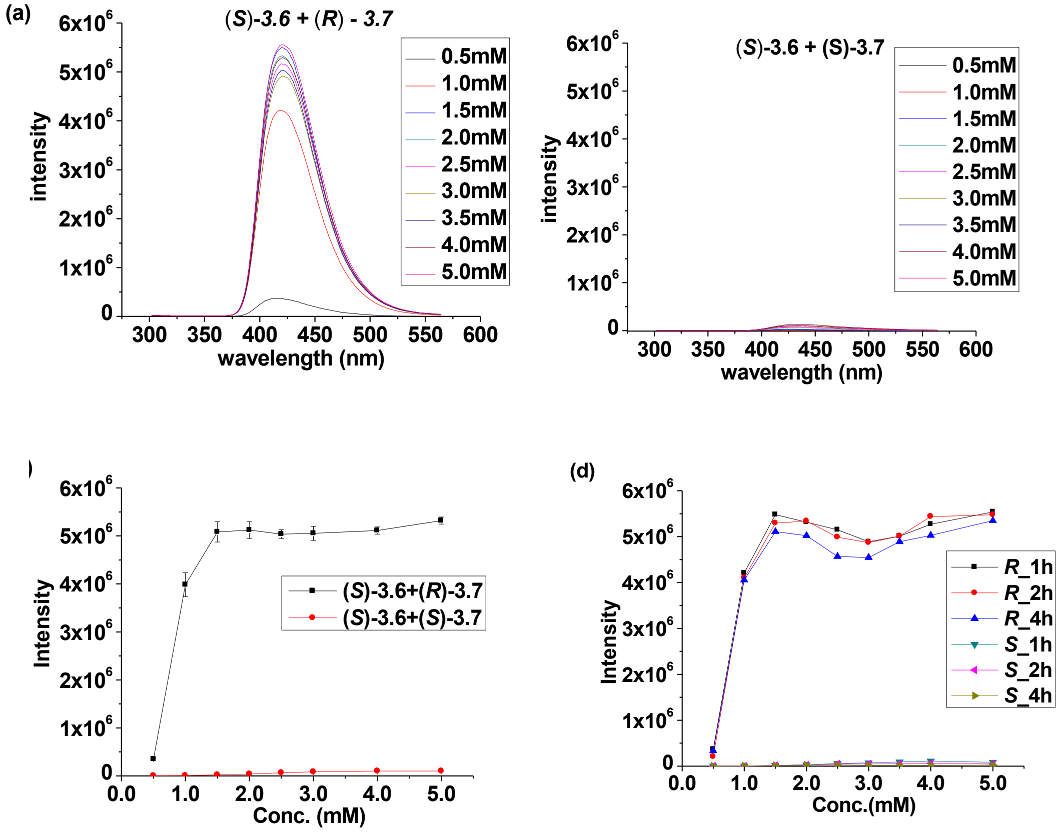

We used the enantiomer (*R*)-**3.6** to verify the results. When (*R*)-**3.6** was used to interact with the amino alcohol in the fluorous phase, large enhancement was observed in the presence of (*S*)-**3.7** with little enhancement in the presence of (*R*)-**3.7** (Figure 3-6). That is, a mirror-image relationship was observed for the fluorescent response of (*S*)-**3.6** versus (*R*)-**3.6** toward the enantiomers of the amino alcohols. This confirms the observed enantioselective fluorescent recognition.

Figure 3-6. Fluorescence spectra of (*R*)-**3.6** (8.0 x 10^{-5} M) in the presence of (*R*)-**3.7** (a) and (*S*)-**3.7** (b) within the concentration range from 0.5 mM to 5 mM. Fluorescence intensity at λ_{emi} = 420 nm versus the concentration of (*R*)-**3.7** or (*S*)-**3.7** (c) and effect of the reaction time in 4 h plotted with error bars (d). Spectra were recorded 1h after mixing. Solvent: 4% DCM/FC-72, excited at 290 nm, slit 2/2 nm.

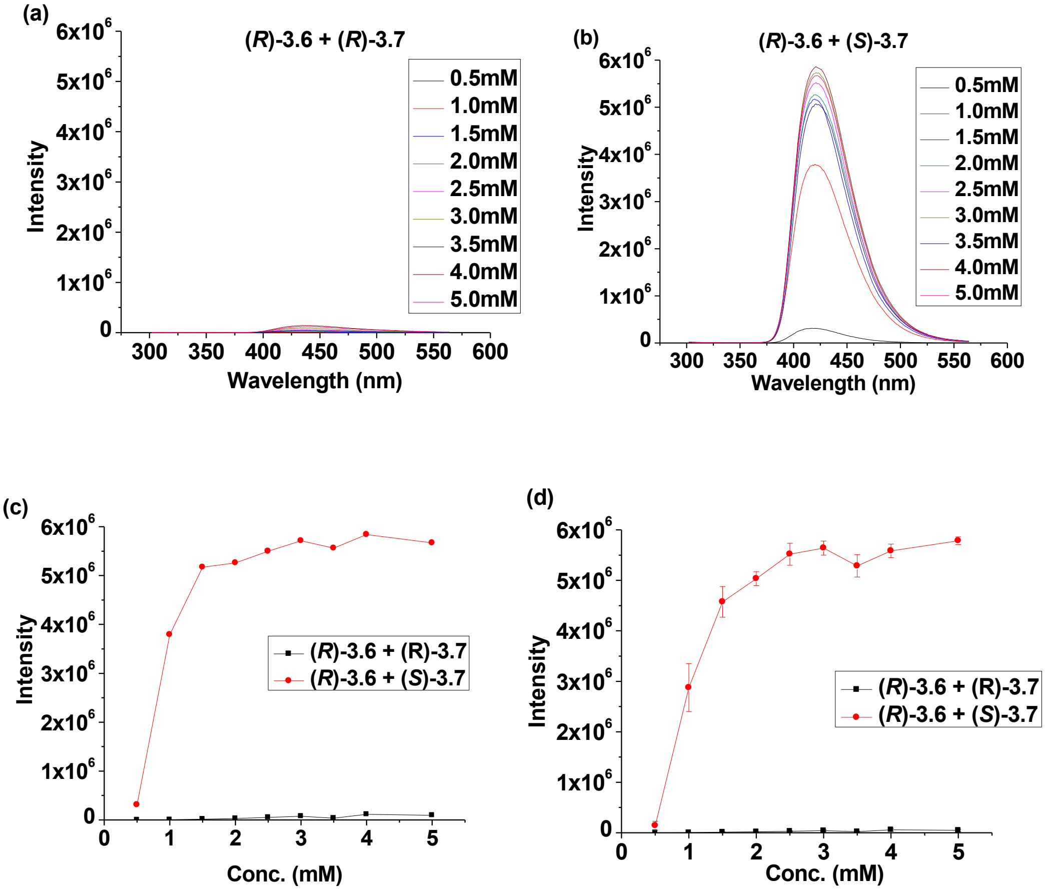

The differences in fluorescence spectra were also reflected in the corresponding UV-Vis spectra as shown in Figure 3-7. (*S*)-**3.6** alone shows four major absorption peaks at 222, 271, 316 and 436 nm respectively. When (*R*)-**3.7** was added, all the fours peaks became diminished, while two new peaks emerged at 239 nm and 360 nm. When (*S*)-**3.7** was added, only the original peaks decreased, with no appearance of new peaks. This means that the fluorescence enhancement was originated from the ground-state reactions between the sensor and the amino alcohol. The elevated baseline of UV-Vis spectra is an indication of heterogeneous absorption, which is consistent with the dynamic light scattering results, which will be discussed later.

Figure 3-7. UV-Vis absorption spectra of (*S*)-**3.6** (0.08 mM) with or without (*R*)-**3.7** (left) and (*S*)-**3.7** (right) ranging from 0.5 mM to 5mM in 4% DCM/FC-72 respectively.

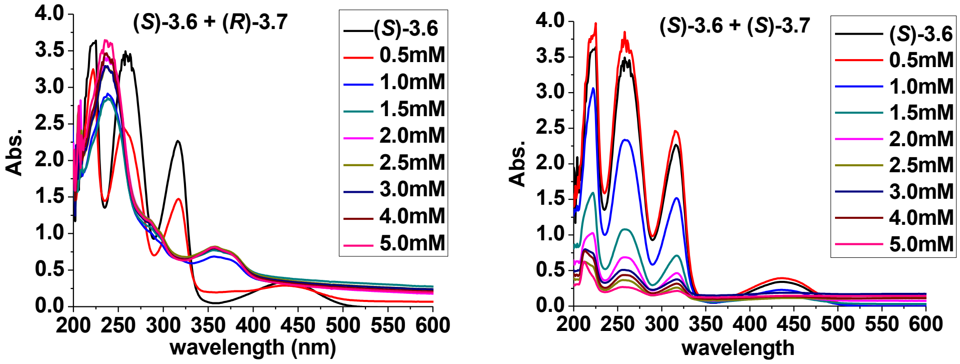

Figure 3-8. Excitation spectra of (*S*)-**3.6** (0.08 mM) with (*R*)-**3.7** or (*S*)-**3.7** (5.0 mM). Spectra were recorded 1 h after mixing the solution. Solvent: 4% DCM / FC-72, λ_{em}= 420 nm, slit 2/2 nm.

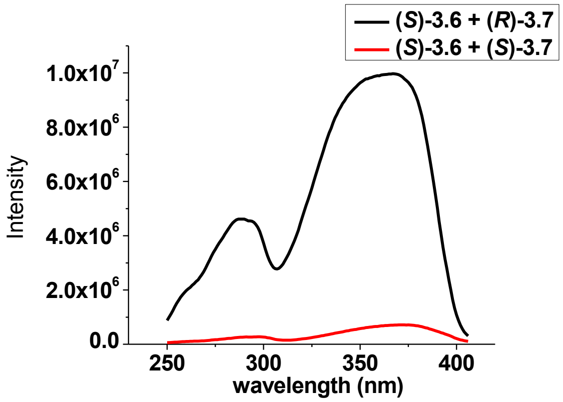

In the excitation spectra shown in Figure 3-8, (*R*)-**3.7** with the sensor displayed two strong excitation peaks at λ_{ex} = 288 nm and 368 nm, while (*S*)-**3.7** only gave very weak excitation intensities at either wavelengths. When sensor (*S*)-**3.6** (8.0 x 10^{-4} M in FC-72) was titrated with amino alcohol, (*R*)-**3.7** changed the color of the solution from yellow to colorless with the formation of very small precipitates visible by eyes. The enantiomer (*S*)-**3.7** also changes the color of the solution but with much less of precipitates formation. When 6eq of (*R*)-**3.7** was added, the color changed completely to white, while 10eq of (*S*)-**3.7** was required to reach this change.

Figure 3- 9. Titration of (*S*)-**3.6** (0.8 mM, 10 mL in FC-72) with 0, 2, 4, 5, 6, 7, 8, 10 and 12 equiv. of (*R*)- or (*S*)-**3.7** solutions in CH_2Cl_2 (0.8 M) (from left to right).

(a). Addition of (*R*)-**3.7** to (*S*)-**3.6**

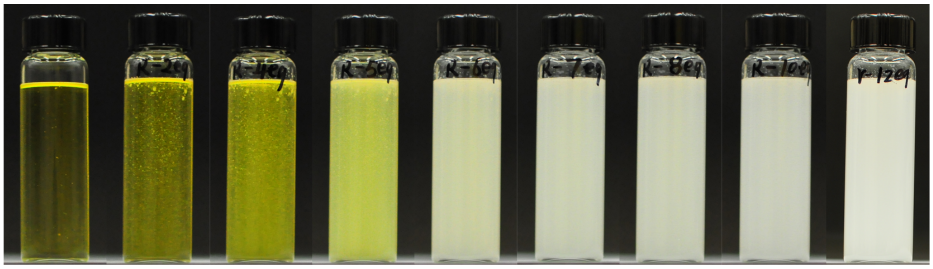

(b). Addition of (*S*)-**3.7** to (*S*)-**3.6**

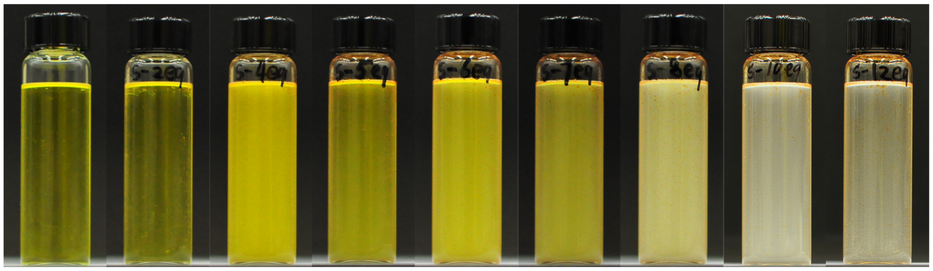

When the concentration of (*S*)-**3.6** was 8.0 x 10^{-4} M in FC-72, addition of (*R*)-**3.7** led to the formation of much more visible precipitates as shown in Figure 3-10a (left).

Figure 3-10. Photos of (*S*)-**3.6** (8.0 x 10^{-4} M, 4 % CH_2Cl_2 / FC-72) treated with (a) 10 equiv. (*R*)-**3.7** (left) and 10 equiv. (*S*)-**3.7** (right), and (b) under a UV-lamp (λ= 254 nm).

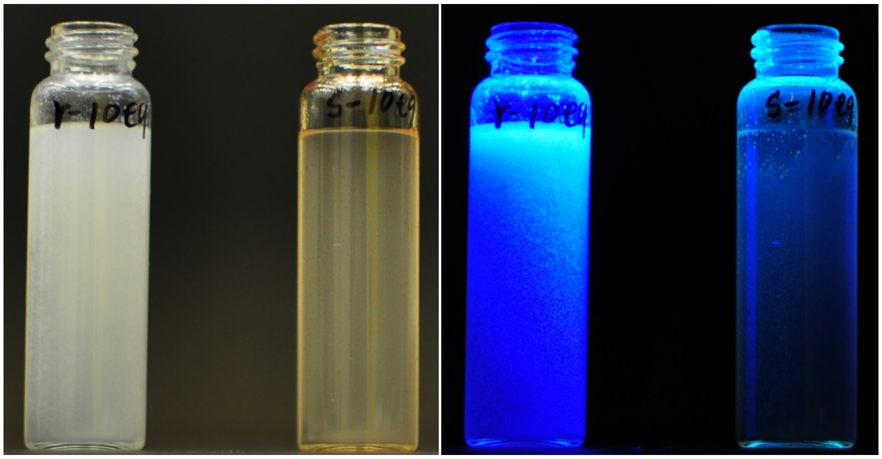

(a) (b)

Figure 3-11. Photos for the reactions of (*S*)-**3.6** with (*R*)-**3.7** or (*S*)-**3.7** at various concentrations. From left to right: 0.08 mM (*S*)-**3.6** with 1 mM (*R*)- or (*S*)-**3.7**; 0.08 mM (*S*)-**3.6** with 5.0 mM (*R*)- or (*S*)-**3.7** under UV-lamp; 0.8 mM (*S*)-**3.6** with 5.0 mM (*R*)- or (*S*)-**3.7**.

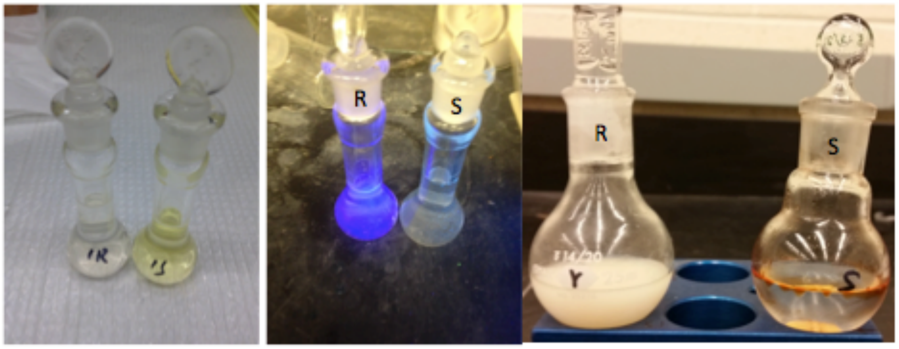

Figure 3-10b (left) shows the strong blue emission of the precipitate formed from (*S*)-**3.6** + (*R*)-**3.7** upon UV irradiation. Although addition of (*S*)-**3.7** also led to a cloudy solution, no solid precipitate was generated, and little fluorescence was observed under UV irradiation (Figure 3-10b, right). Over several hours, the cloud solution formed between (*S*)-**3.6** and (*S*)-**3.7** settled to become a clear solution with the formation of insoluble brown oil on the wall of the reactor (Figure 3-10).

The precipitate generated from the interaction of (*S*)-**3.6** with (*R*)-**3.7** was separated by filtration through filter paper. The IR spectrum of the precipitate shows that the two intense signals at 1661 and 1624 cm^{-1} for the carbonyl groups of (*S*)-**3.6** disappeared, indicating a nucleophilic addition of the amino alcohol to the carbonyl groups (see Appendix). Electron spray mass spectrum of the precipitate displays three peaks at m/z = 1150.1, 1168.1 and 1221.2, which can be assigned to the MH$^+$ peaks of compounds **3.8**, **3.9** and **3.10** respectively (Scheme 3-4).

Scheme 3-4. Products formed between **3.6** and **3.7** detected by ESI-MS.

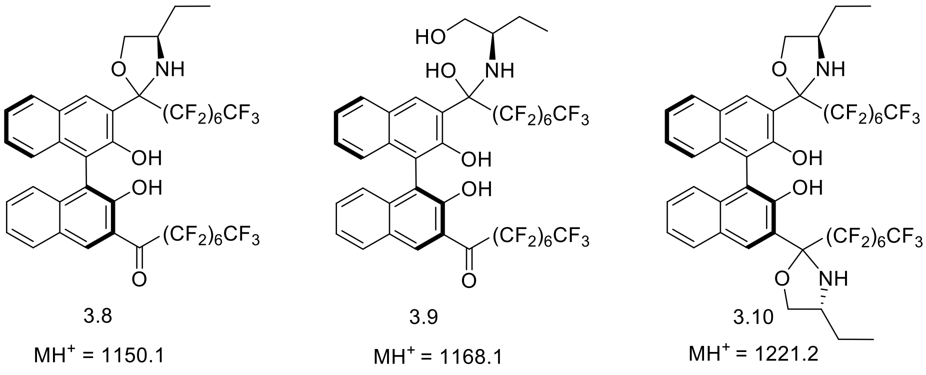

3.8
MH$^+$ = 1150.1

3.9
MH$^+$ = 1168.1

3.10
MH$^+$ = 1221.2

Scheme 3-5. Proposed reaction routes between the sensor and amino alcohol.

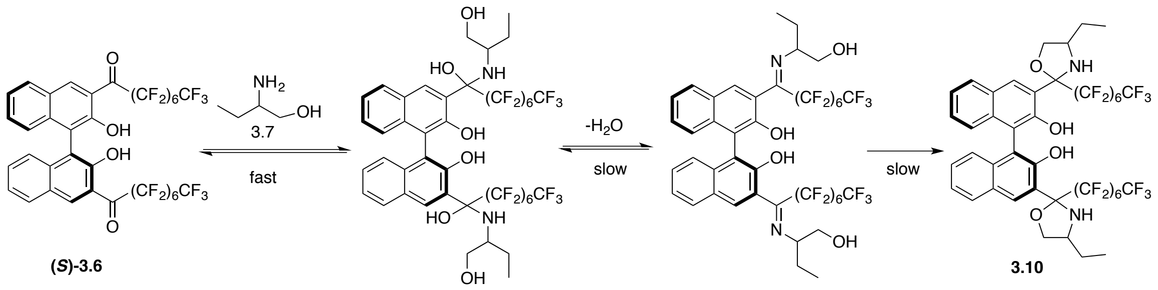

On the basis of the information from ESI-MS, the reaction routes can be easily proposed for the reaction of the sensor with the amino alcohol (Scheme 3-5). This is a common nucleophilic addition of the amino groups to the carbonyl groups, followed by the loss of water molecule to form an imine product, which can further undergo cyclization to form the final product **3.10**. The extremely low solubility of water in FC-12 may be another factor to facilitate the reaction.

We also studied the brown oily adducts formed from the reaction of (*S*)-**3.6** with the enantiomer (*S*)-**3.7** in FC-72. The mass spectrum of the oil shows three peaks at m/z = 1150.1, 1168.1 and 1221.2, indicating the formation of products similar to **3.8** – **3.10**. However, when the precipitate or oil isolated from the reactions was dissolved in $CDCl_3$, ^1H NMR and ^{19}F NMR spectra show that the products were converted back to their starting materials (Figure 3-12). When additional CH_2Cl_2 or $CHCl_3$ was added to the solution displayed in Figure 3-9, it was observed that the color changed back to yellow with the disappearance of emission. Thus, the formation of the nucleophilic addition products is promoted and stabilized by the fluorous solvent.

Figure 3-12. ^1H NMR and ^{19}F NMR of the isolated complex from (*S*)-**3.6** + (*R*)-**3.7** and (*S*)-**3.6** + (*S*)-**3.7** in $CDCl_{3.}$ (Note: the $CDCl_3$ used here was treated with K_2CO_3 overnight and then filtered through a pipet packed with dry neutral alumina to remove trace amount of acid and H_2O).

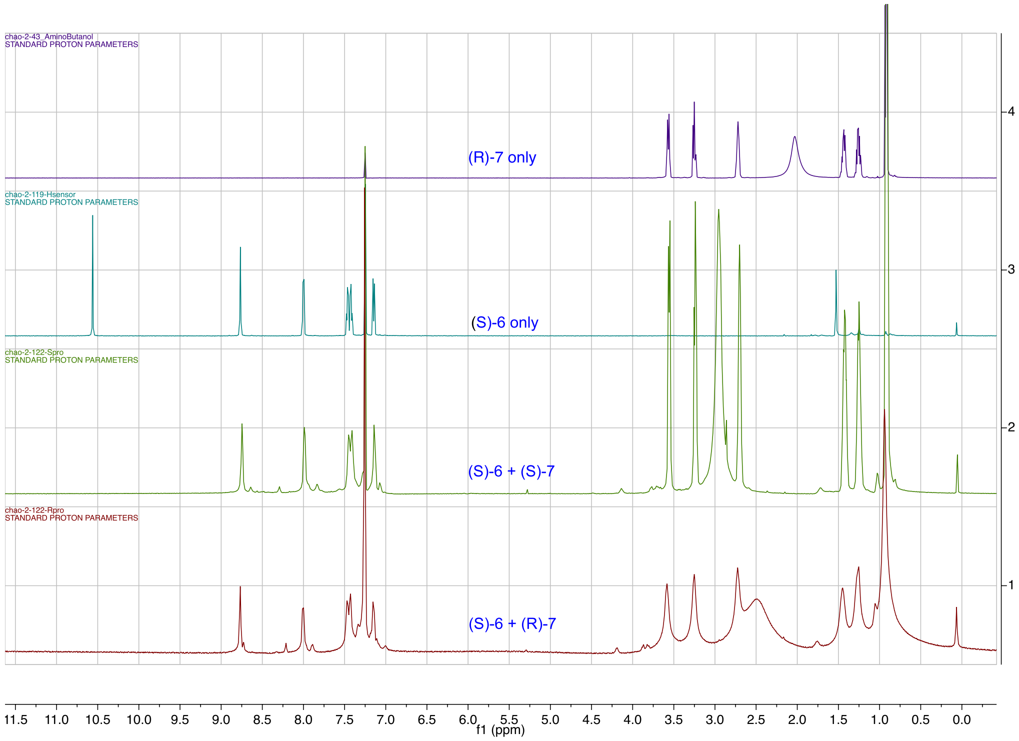

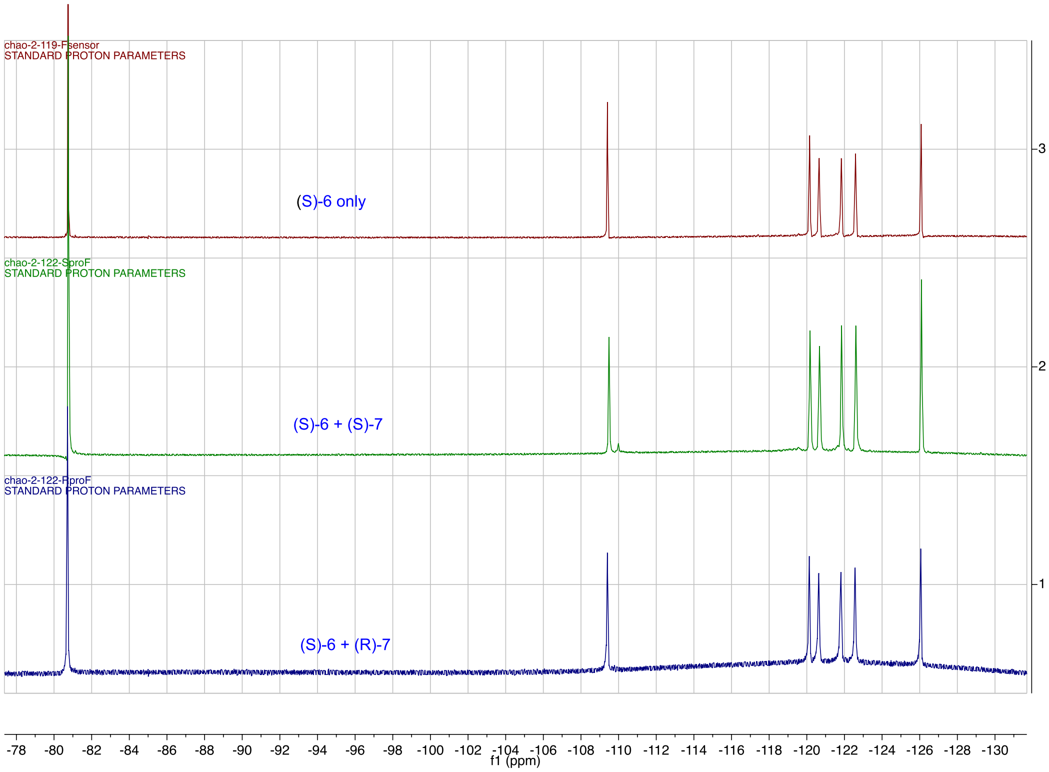

Figure 3- 13. DLS data and spectra for (*S*)-**3.6** + (*R*)-**3.7** and (*S*)-**3.6** + (*S*)-**3.7**.

Type	Start Date/Time	Sample ID	Eff. Diam. (nm)	Polydispersity
DLS	11/28/2014 21:11	(*S*)-**3.6** + (*R*)-**3.7**	587.01	0.49
DLS	11/28/2014 21:13	(*S*)-**3.6** + (*S*)-**3.7**	88.23	0.28

(*S*)-**3.6** + (*R*)-**3.7**

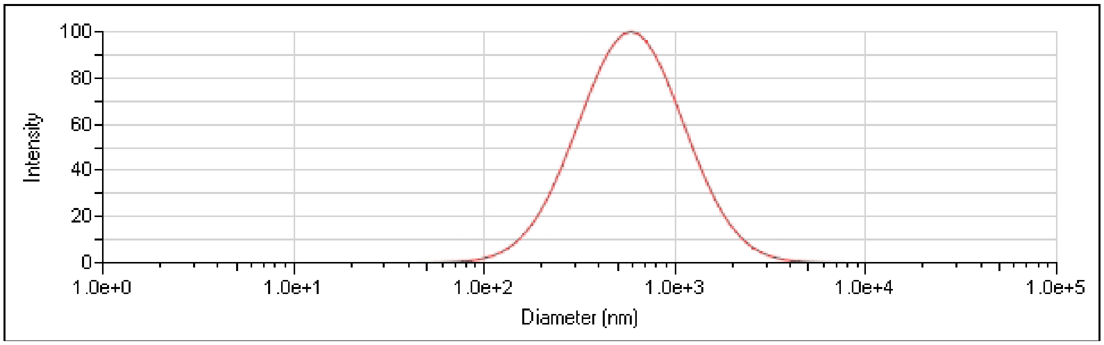

(*S*)-**3.6** + (*S*)-**3.7**

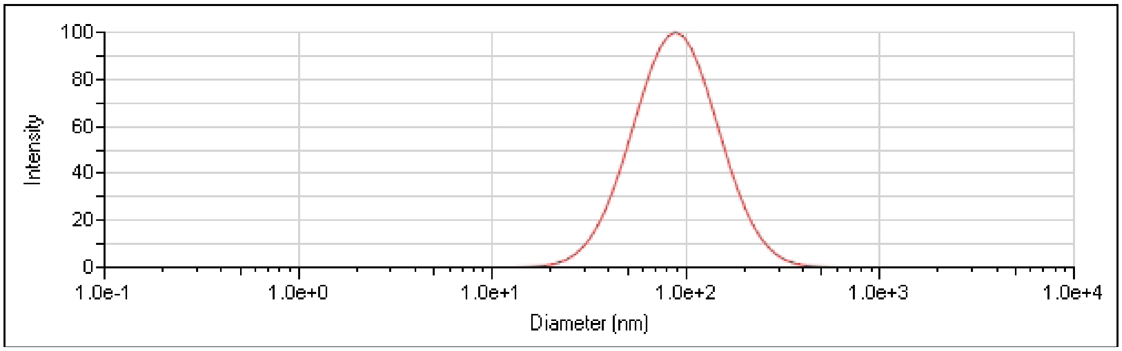

In order to characterize the difference between the two products formed from (*S*)-**3.6** with the two enantiomers of the chiral amino alcohol, we conducted a dynamic light scattering study on the slurry generated from the reaction of (*S*)-**3.6** with (*R*)- and (*S*)-**3.7**. The slurry formed from the reaction of (*S*)-**3.6** (8.0 x 10^{-5} M) with (*R*)-**3.7** (5 mM) in FC-72 (4% CH_2Cl_2) shows a lognormal distribution of the particle sizes of 587 nm, and that formed with (*S*)-**3.7** under the same conditions shows a lognormal distribution of the particle sizes of only 88 nm (Figure 3-13).

Thus, although the reaction of (*S*)-**3.6** with (*R*)- or (*S*)-**3.7** in fluorous solvent gave similar nucleophilic addition products, their intermolecular aggregations are very different. We propose that the white precipitate generated from (*S*)-**3.6** + (*R*)-**3.7** have a more rigid structure, giving the greatly enhanced fluorescence,[7] but the oily slurry generated from (*S*)-**3.6** + (*S*)-**3.7** should have a much more flexible structure, giving no fluorescence enhancement.

3.2.4. Fluorescence recognition of other chiral amines

We studied the fluorescent response of (*S*)-**3.6** toward other chiral amino alcohols or diamines in fluorous solvent. In general, highly enantioselective fluorescent responses have been observed for the chiral functional amines such as **3.11**−**3.14**. For the amino alcohols with concentrations higher than 1 mM, the *R* enantiomers increase the fluorescence of (*S*)-**3.6** by 1200 − 2000-fold, while the *S* enantiomers only increase it by 10−50-fold. For the chiral diamine 14, its (*S*, *S*)-enantiomer increases the fluorescence of (*S*)-**3.6** much more than its (*R*, *R*)-enantiomer.

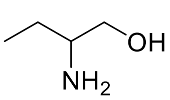

3.7

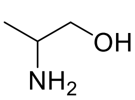

3.11

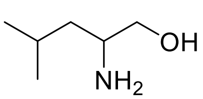

3.12

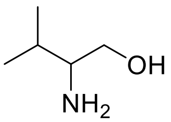

3.13

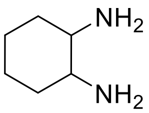

3.14

Figure 3-14. Fluorescence spectra of (*S*)-**3.6** (0.08 mM) in the presence of (*R*)-**3.11** (left) or (*S*)-**3.11** (right) with a concentration range of 1 to 5 mM. Spectra were recorded 1h after mixing the solution. Solvent: 4% DCM / FC-72, λ_{ex} = 290 nm, slit 2/2 nm.

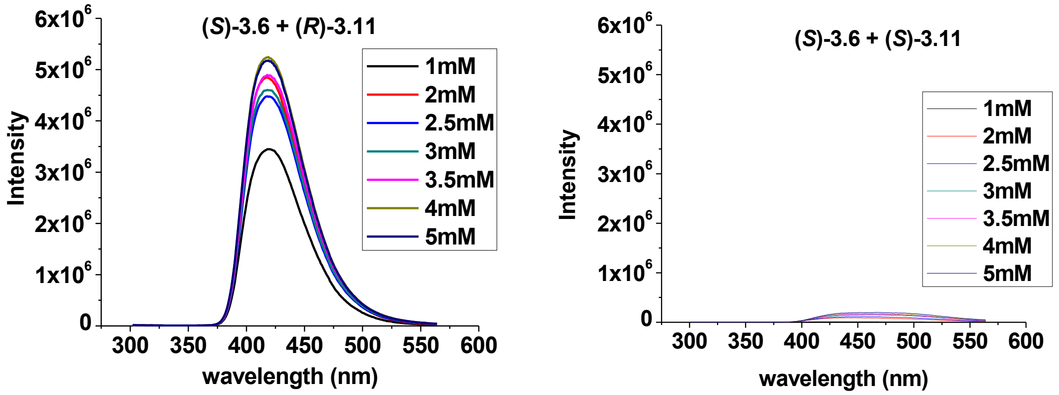

Figure 3-15. Fluorescent intensity of (*S*)-**3.6** against the concentration of (*R*)-**3.11** or (*S*)-**3.11** at 420 nm. Four independent experiments were conducted (left), and an averaged diagram with error bar was plotted (right).

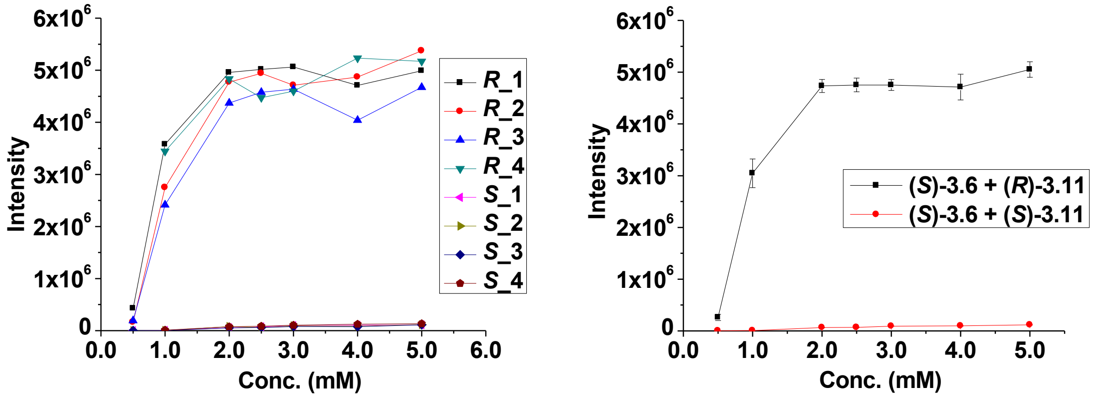

Figure 3- 16. Fluorescent intensity at 420 nm recorded at 1, 2, 3 and 4 h after the mixtures of (*S*)-**3.6** + (*R*)-**3.11** and (*S*)-**3.6** + (*S*)-**3.11** were prepared.

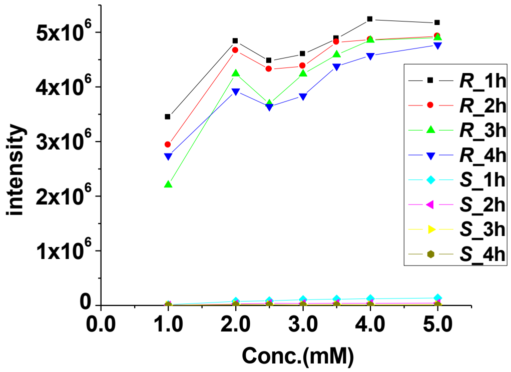

Figure 3-17. Fluorescence spectra of (*S*)-**3.6** (0.08 mM) in the presence of (*R*)-**3.12** (left) or (*S*)-**3.12** (right) with a concentration range of 0.5 to 5 mM. Spectra were recorded 1h after mixing the solution. Solvent: 4% DCM / FC-72, λ_{ex} = 290 nm, slit 2/2 nm.

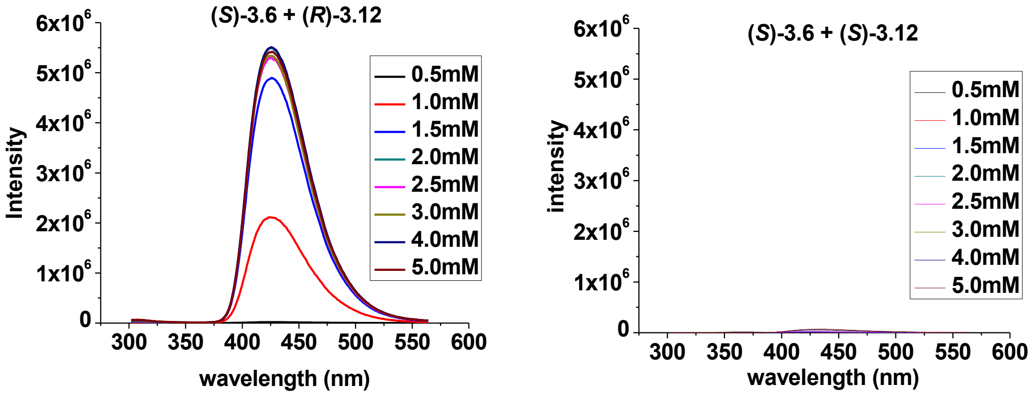

Figure 3-18. Fluorescence intensity of (*S*)-**3.6** against the concentration of (*R*)-**3.12** or (*S*)-**3.12** at 425 nm. Spectra were recorded 1h after mixing the solution. Four independent experiments were conducted (left), and an averaged diagram with error bar was plotted (right).

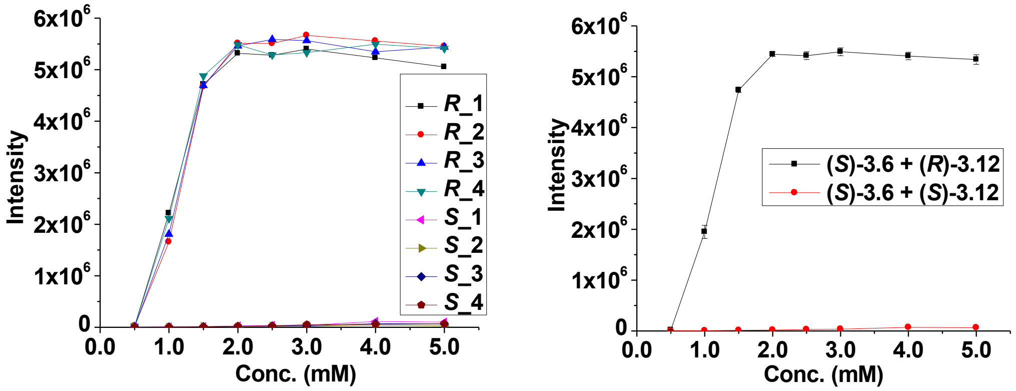

Figure 3- 19. Fluorescence spectra of (*S*)-**3.6** (0.08 mM) in the presence of (*R*)-**3.13** (left) or (*S*)-**3.13** (right) with a concentration range of 0.6 to 5 mM. Spectra were recorded 1 h after mixing. Solvent: 4% DCM/FC-72, λ_{ex}= 290 nm, slit 2/2 nm.

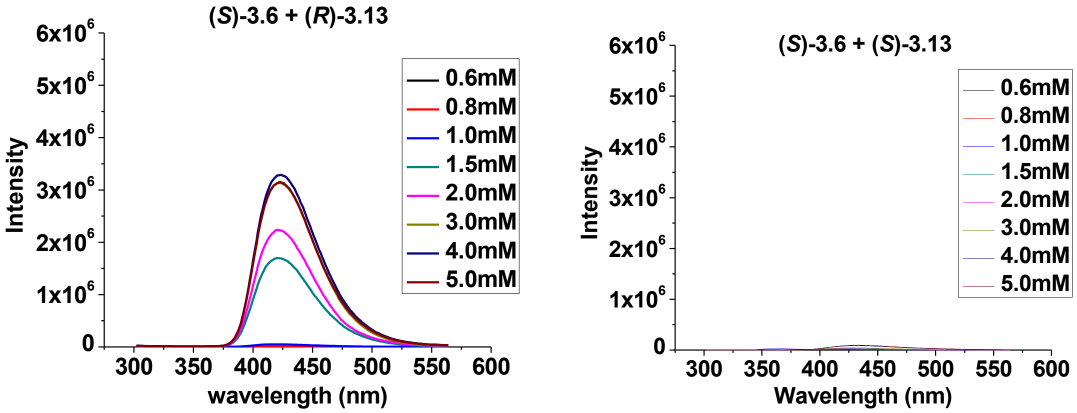

Figure 3- 20. Fluorescent intensity of (*S*)-**3.6** against the concentration of (*R*)-**3.13** or (*S*)-**3.13** at 423 nm. Four independent experiments were conducted (left), and an averaged diagram with error bar was plotted (right).

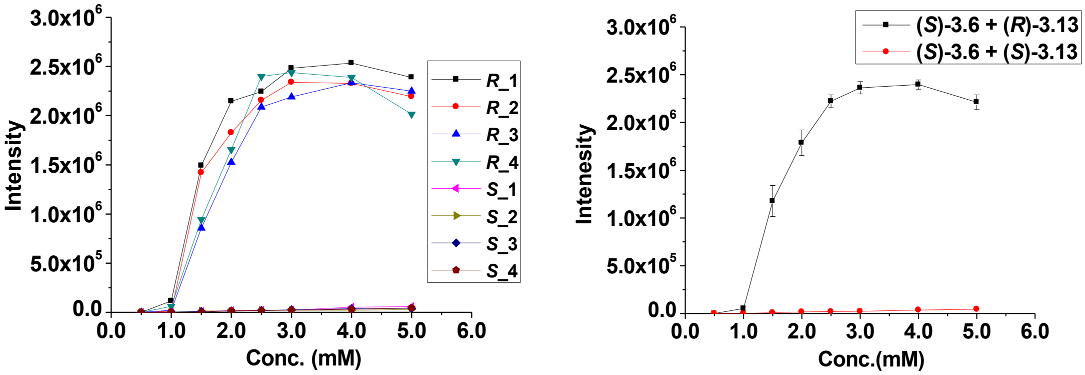

Figure 3-21. Fluorescent intensity of (*S*)-**3.6** at 423 nm recorded at 1, 2 and 4 h after the mixtures of (*S*)-**3.6** + (*R*)-**3.13** and (*S*)-**3.6** + (*S*)-**3.13** were prepared.

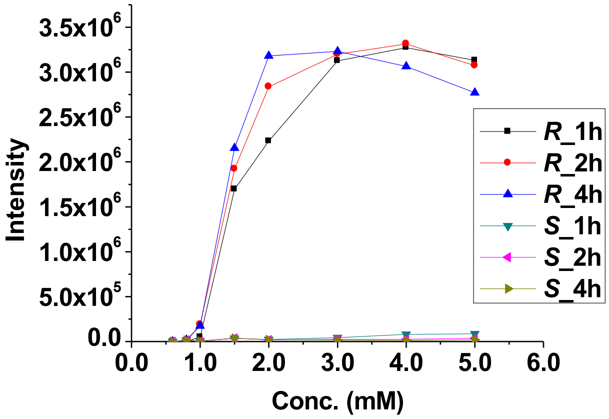

Figure 3-22. Fluorescence spectra of (*S*)-**3.6** (0.08 mM) in the presence of (*R*)-**3.14** (left) or (*S*)-**3.14** (right) with a concentration range of 0.2 to 2.0 mM. Spectra were recorded 1h after mixing the solution. Solvent: 4% DCM / FC-72, λ_{ex} = 290 nm, slit 3/3 nm.

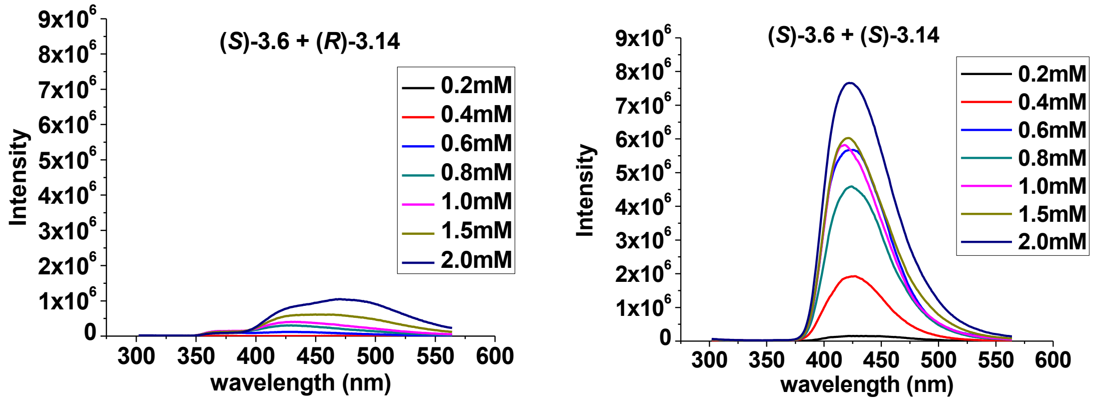

Figure 3- 23. Fluorescent intensity of (*S*)-**3.6** against the concentration of (*R*)-**3.14** or (*S*)-**3.14** at 423 nm. Four independent experiments were conducted (left), and an averaged diagram with error bar was plotted (right).

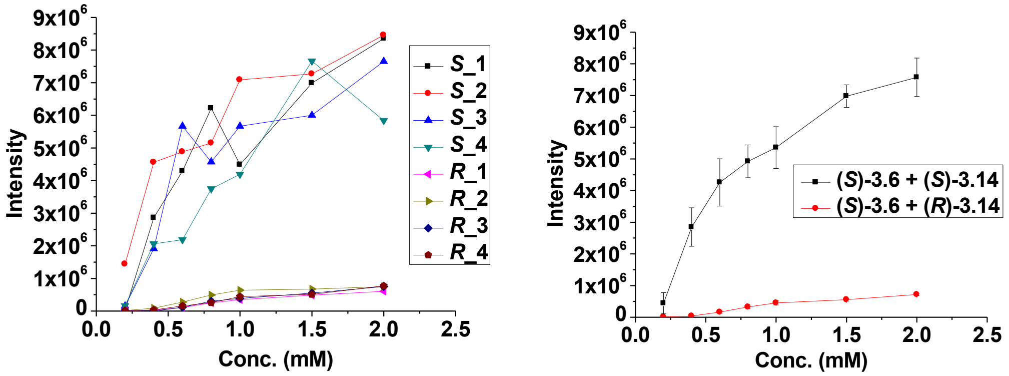

Figure 3-24. Fluorescent intensity at 423 nm recorded at 1 h, 2 h, and 4 h after the mixtures of (*S*)-**3.6** + (*R*)-**3.14** and (*S*)-**3.6** + (*S*)-**3.14** were made.

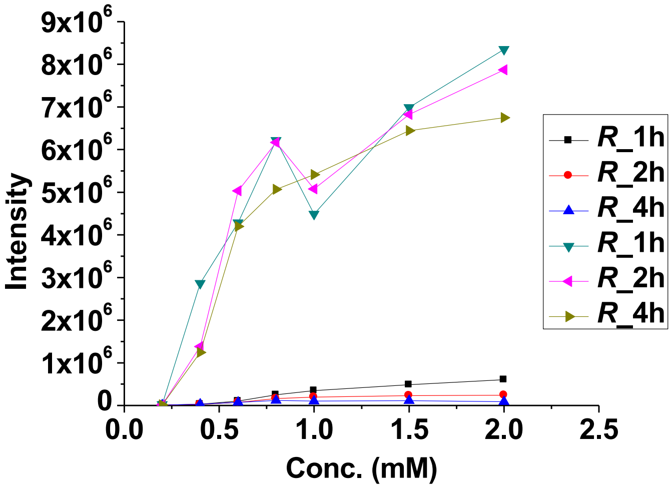

Figure 3-25. Fluorescence spectra of (*R*)-**3.6** (8.0×10^{-5} M) in the presence of (*R*)-**3.14** (left) and (*S*)-**3.14** (right) within the concentration range from 0.2 mM to 2 mM. Spectra were recorded 1 h after mixing. Solvent: 4% DCM/FC-72, excited at 290 nm, slit 3/3 nm.

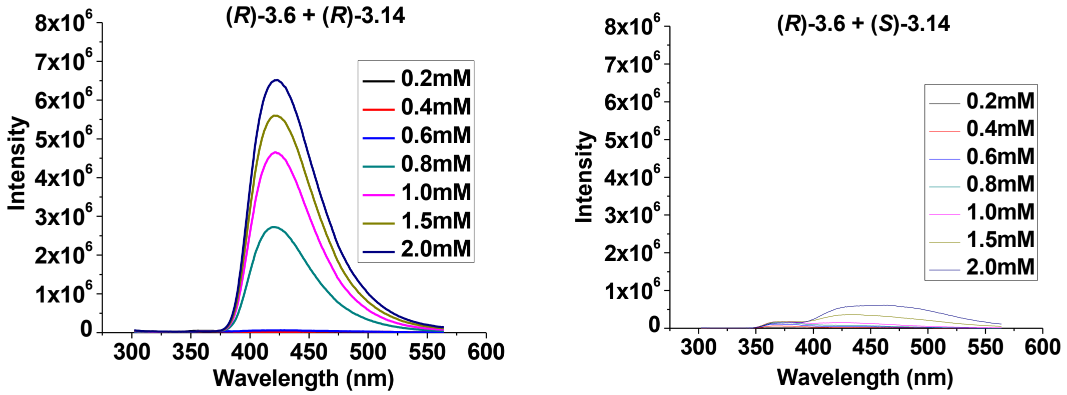

Figure 3-26. Fluorescent intensity at 423 nm recorded at 1h after the mixtures of (*R*)-**3.6** + (*R*)-**3.14** and (*R*)-**3.6** + (*S*)-**3.14** were made.

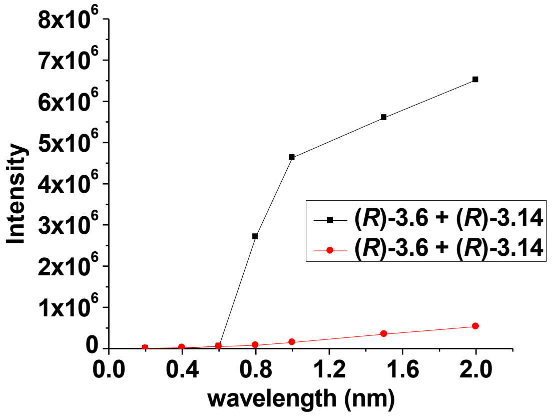

Note that the stability of fluorescence intensity regarding the diamine **3.14** was not as good as other amino alcohols as shown above. This was partially due to its lower compatibility with the fluorous solvent. Nevertheless, when we use (*R*)-**3.6** to verify the enantioselectivity, the spectra were still mirror images of spectra obtained from (*S*)-**3.6** sensor. This confirmed the reliability of this data. We also tested the sensing of aromatic amino alcohols and monoamines, but almost no fluorescence response was obtained. For aromatic amino alcohol, it precipitated out immediately when its DCM solution was added to the FC-72 solution of the sensor, due to its low affinity with fluorous solvent. For monoamines, no substantial reaction and fluorescence enhancement was observed at room temperature. Even though the reaction can be promoted at higher temperature (50 ^{0}C), the enantioselectivity and enhancement ratio were still very limited, accompanied by the low reproducibility.

3.2.5. Enantiomeric excess determination using fluorescence

We also studied the fluorescent response of (*S*)-**3.6** toward the amino alcohol with various enantiomeric compositions. As shown in Figure 3-27, a nonlinear relationship between the fluorescence intensity of (*S*)-**3.6** and the enantiomeric composition of the amino alcohol **3.7** is obtained.

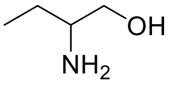
3.7

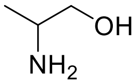
3.11

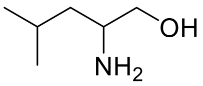
3.12

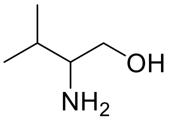
3.13

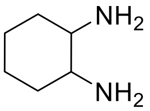
3.14

Figure 3-27. Fluorescent response of (*S*)-**3.6** (8.0 x 10^{-5} M) toward **3.7** (5 mM) at various enantiomeric excess [*ee* = (*R*-*S*) / (*R*+*S*). Reaction time = 1 h. Solvent: 4% CH_2Cl_2 / FC-72, λ_{em} = 420 nm, λ_{ex} = 290 nm, slit: 2/2 nm. The red line is obtained from a second order non-linear fitting].

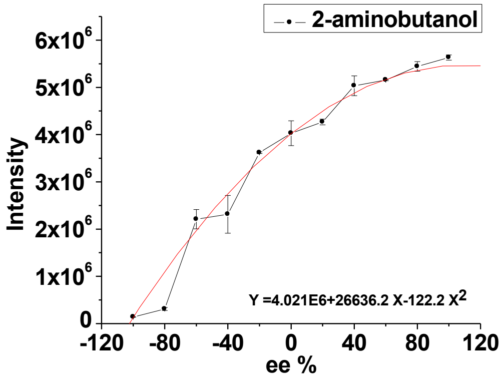

We also built the relationship between *ee* and fluorescence intensity for other amino alcohols (Figure 3-28). This nonlinear relationship is consistent with the proposed fluorescent enhancement mechanism, which has been proved to originate from the aggregation of the sensor-amino alcohol adducts.

Figure 3-28. Fluorescent intensities of (*S*)-**3.6** at 420 nm were plotted against the *ee* values obtained for various functional chiral amines **3.11** – **3.14**.

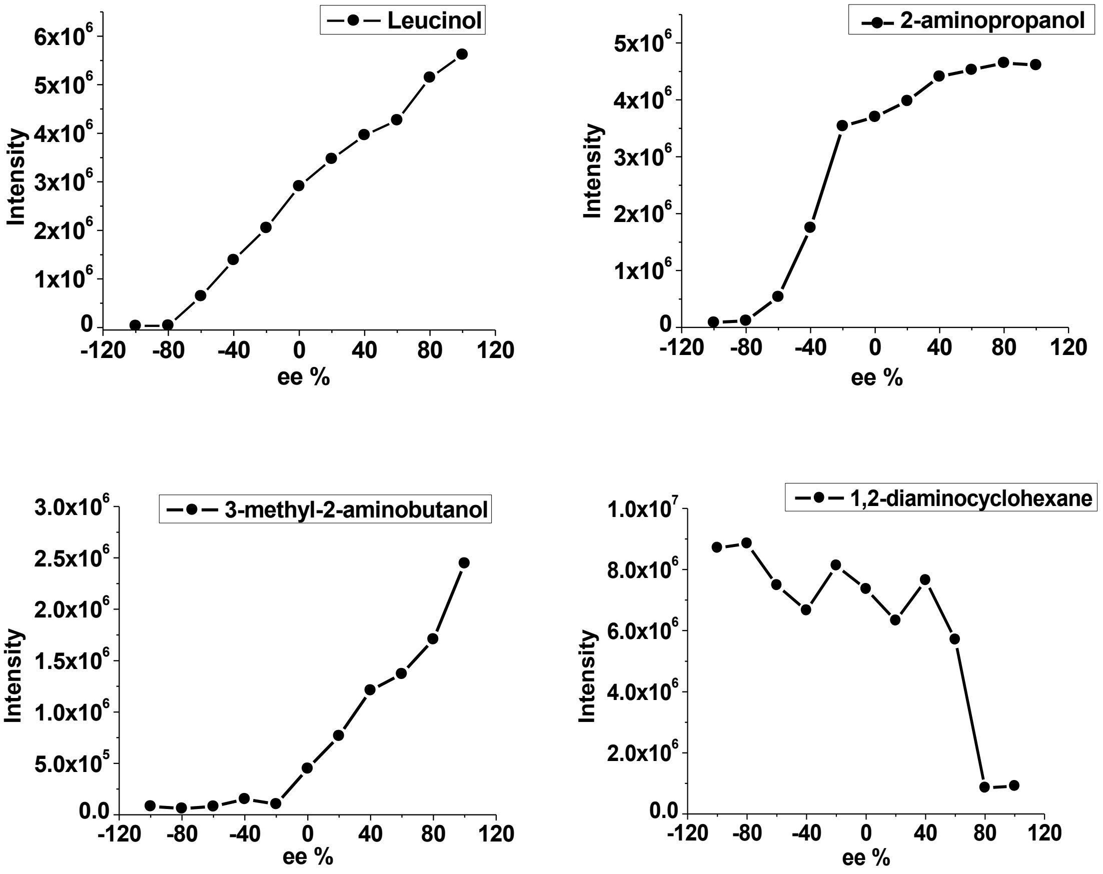

3.2.6. Further exploration of fluorescent sensing in fluorous solvents

We prepared sensor (*S*)-**3.18**, which has two more fluorous ponytails at 6, 6'-position of BINOL, using the procedures depicted in Scheme 3-6. (*S*)-**3.18**, which has a 61.7% weight percentage of fluorine atoms, is highly soluble in FC-72 and hexane, and has low solubility in common organic solvents like DCM, chloroform, THF and acetone. (*S*)-**3.18** is weakly emissive in FC-72, DMC, and hexane as tested, while shows additional emission at 500 nm in THF (Figure 3-29).

Scheme 3- 6. Synthesis of highly fluorinated (*S*)-**3.18**.

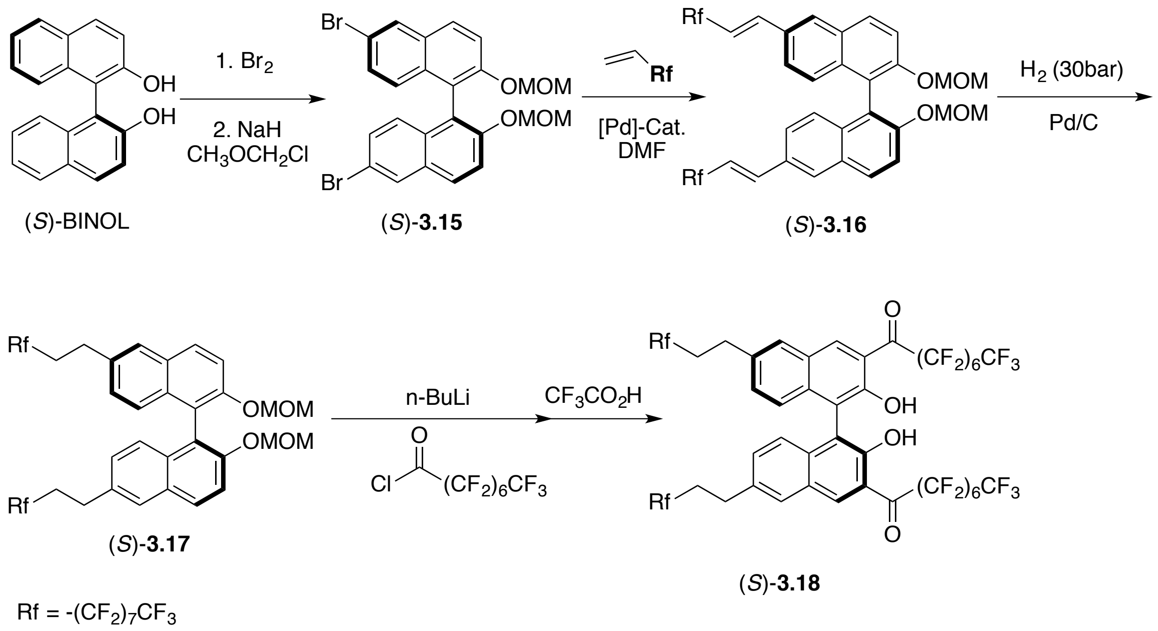
OH
OH
(S)-BINOL
1. Br2
2. NaH
CH3OCH2Cl
Br
OMOM
OMOM
Br
(S)-3.15
Rf
[Pd]-Cat.
DMF
Rf
OMOM
OMOM
Rf
(S)-3.16
H2 (30bar)
Pd/C
Rf
OMOM
OMOM
Rf
(S)-3.17
n-BuLi
O
Cl
(CF2)6CF3
CF3CO2H
Rf
O
(CF2)6CF3
OH
OH
(CF2)6CF3
O
Rf
(S)-3.18
Rf = -(CF2)7CF3

Scheme 3- 7. Chiral molecules studied.

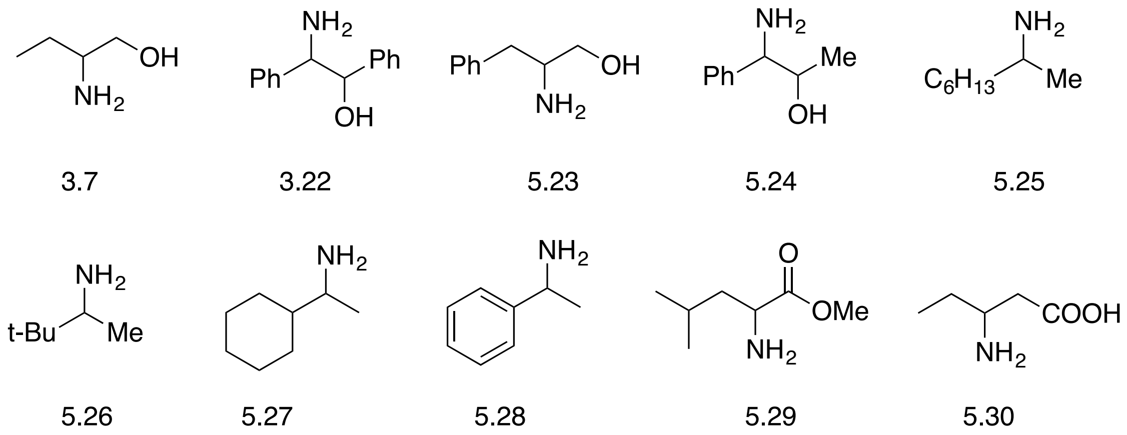
OH
NH2
3.7
NH2
Ph
Ph
OH
3.22
Ph
OH
NH2
5.23
NH2
Ph
Me
OH
5.24
NH2
C6H13
Me
5.25
NH2
t-Bu
Me
5.26
NH2
5.27
NH2
5.28
O
OMe
NH2
5.29
COOH
NH2
5.30

Figure 3- 29. Fluorescence spectra of (*S*)-**3.18** (0.08 mM) in different solvents excited at 290 nm, slit 3/3 nm.

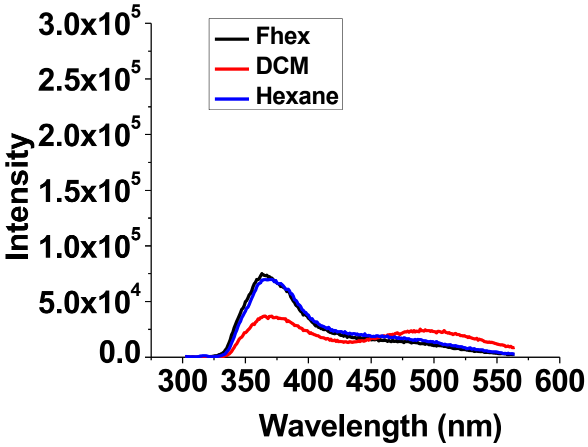

We firstly studied the fluorescence response of (*S*)-**3.18** toward (*R*)- or (*S*)-2-amino-1-butanol (**3.7**) in FC-72 (4% DCM) as shown in Figure 3-30. Similar with the studies of (*S*)-**3.6** described above, addition of (*R*)-**3.7** caused a large fluorescence enhancement at 434 nm, which is around 8 times higher than that of (*S*)-**3.7**. The color of the solution also changed from bright yellow to colorless. In this case, as (*S*)-**3.18** is much more soluble in FC72 than (*S*)-**3.6**, no visible aggregation was observed. Because (*S*)-**3.18** is highly soluble in fluorous phase, we wanted to achieve enantioselectivity in a biphasic system by mixing (*S*)-**3.18** with **3.7** in DCM and measure fluorescence in fluorous phase (Figure 3-31). After addition of FC-72 (5 mL) to the mixture in DCM (5 mL) and allowed a biphasic equilibrium, however, no substantial emission enhancement was observed in either fluorous or organic phase. As observed, no emission was shown in DCM under UV-lamp. After addition of FC-72, it simply extracted the sensor from DCM phase without bringing in the amino alcohol.

Figure 3- 30. Fluorescence response of (*S*)-**3.18** (0.08 mM) to 2-aminobutanol (5 mM) in FC72 / 4% DCM (λ_{ex} = 290 nm, slit 2/2 nm) 1 h after mixing.

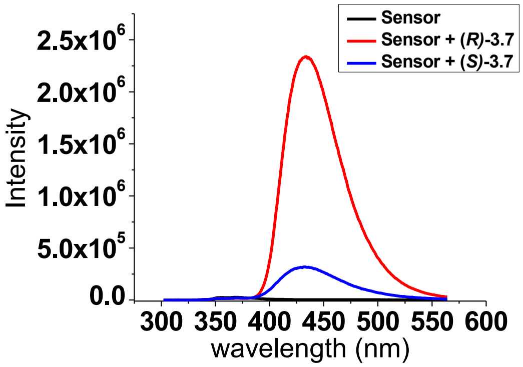

Figure 3- 31. Fluorescence spectra in fluorous and organic phase of **3.18** (0.08 mM) with or without addition of (*R*)- or (*S*)-**3.7** (5 mM).

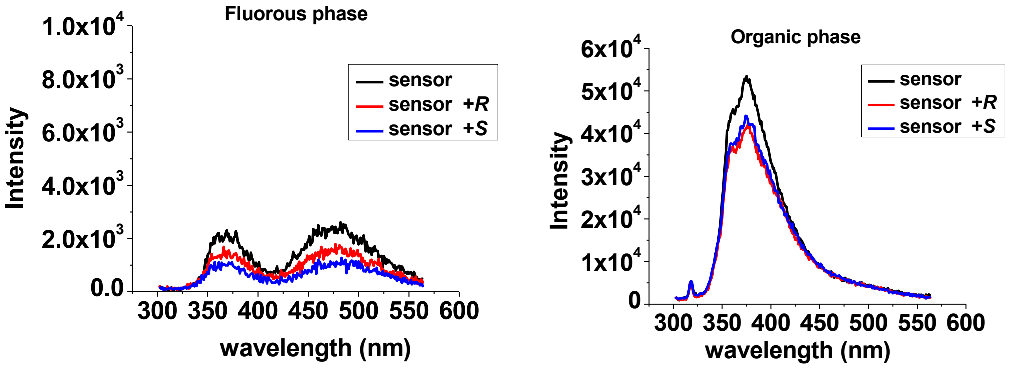

We then tested the fluorescence response in common organic solvents such as diethyl ether, hexane, methanol, acetonitrile, THF and ethyl acetate (Figure 3-32). In diethyl ether, fluorescence quenching was observed at 380 nm and 485 nm with some enantioselectivity. In hexane, fluorescence enhancement at 435 nm was observed with a small *ef* value of 1.15. In methanol, **3.18** blank is highly emissive 370 nm, which was mostly quenched by the addition of amino alcohol. In acetonitrile, only some peak broadening was observed. In THF or ethyl acetate, *ef* values around 2 were observed for both of them. Compared with the ~500-fold fluorescence enhancement and *ef* of 8, the benefits of fluorous solvent are obvious. The reaction between the sensor and amino alcohol in FC-72 is also reversible. To the mixture of (*S*)-**3.18** and (*R*)-**3.7** in 0.2 mL DCM/ 4.8 mL FC72 was titrated with DCM from 0.3 mL to 4.8 mL, the emission disappeared completely when a two-phase solution was formed (Figure 3-33). The color of the solution also turned back to its original yellow color.

Figure 3- 32. Fluorescence response of (*S*)-**3.18** (0.08 mM) to 2-aminobutanol (5 mM) in different solvents (λ_{ex} = 290 nm, slit 2/2 nm).

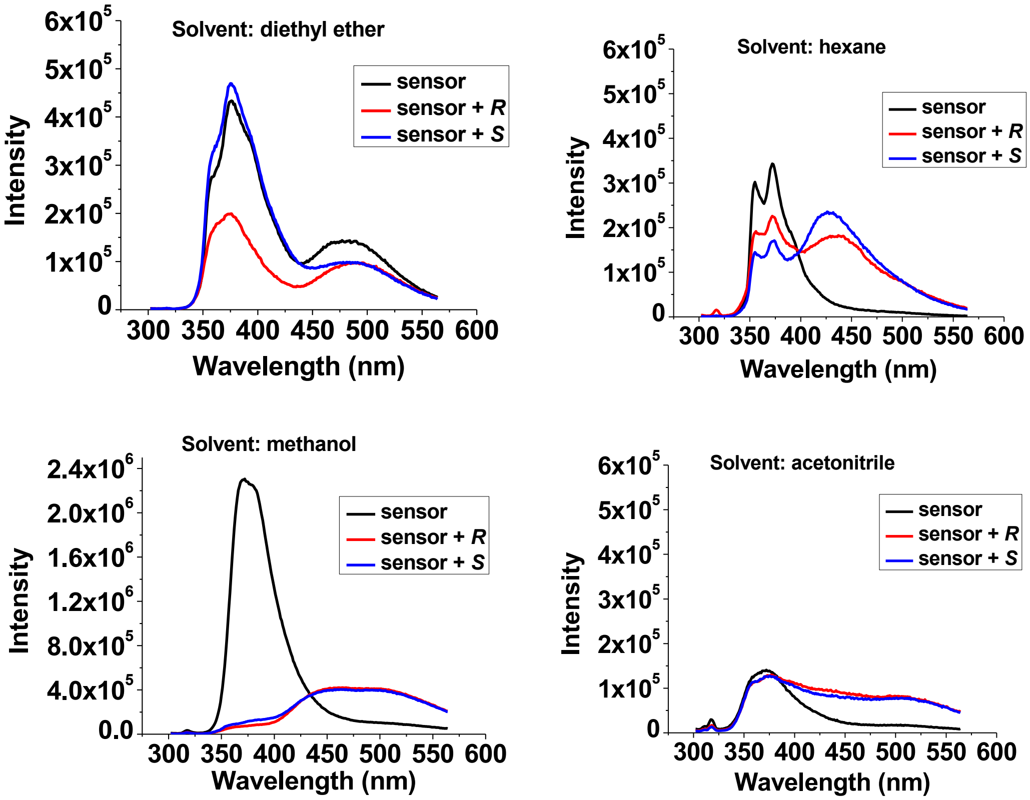

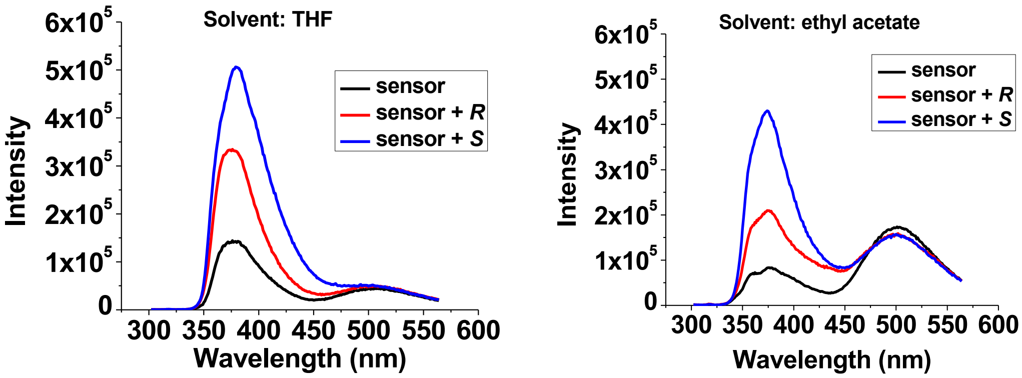

Figure 3- 33. Fluorescence response of (*S*)-**3.18** (0.08 mM) to **3.7** (5 mM) in 0.2 mL DCM / 4.8 mL FC72, with addition of excess DCM from 0.3 mL to 4.8 mL.

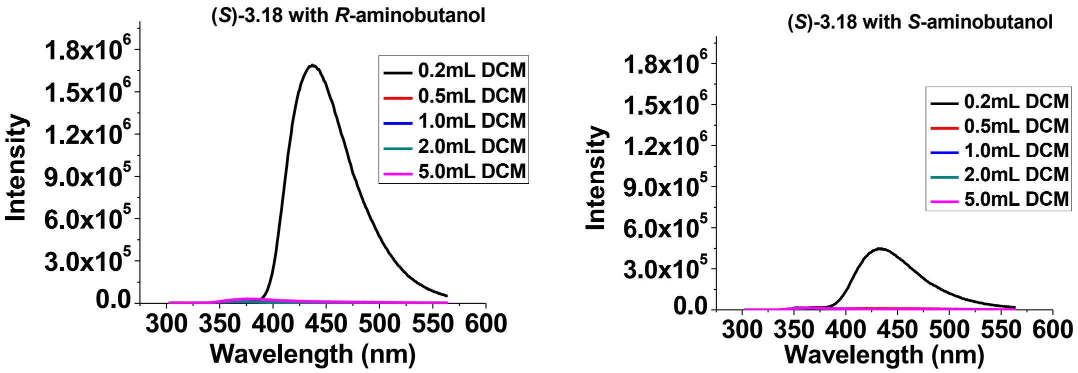

To study the effect of solvent in a single phase, we introduced a partially fluorinated solvent $CH_3OC_4F_9$, which shares the property of fluorous solvents but also miscible with many organic solvents like THF. It is found that even in $CH_3OC_4F_9$, sensor (*S*)-**3.18** still shows highly enantioselective fluorescence toward 2-aminobutanol (**3.7**) as shown in Figure 3-34 (left). When the ratio of THF in the co-solvent system was increased from 0 % to 80 %, the emission at 434 nm decreases gradually and disappears when more than 10 % of THF was used. This concludes that the fluorescence enhancement of (*S*)-**3.18** by amino alcohol requires a dominant fluorous environment.

The enantioselective fluorescence in fluorous solvent also applies to diamino-cyclohexane (**3.14**) as shown in Figure 3-35. It gave an *ef* value of **3.2** with the (1*R*, 2*R*)-enantiomer shows stronger emission than the (1*S*, 2*S*)-one when 0.08 mM of sensor and 5 mM of **3.14** was used. In DCM, good enantioselectivity was maintained at 440 nm but with very low emission intensity. The recognition behavior for **3.14** in hexane was somewhat similar with in FC72 due to their nonpolar nature, but a lower *ef* of 1.7 was obtained. The enantioselectivity also arose from ethyl acetate, with the (1*R*, 2*R*)-**3.14** showed 2.2 times emission intensity of (1*S*, 2*S*)-**3.14** at 450 nm. As with methanol, the situation is identical with the use of 2-amino-1-butanol (**3.7**).

Figure 3- 34. Fluorescence response of (*S*)-**3.18** (0.08 mM) to 2-aminobutanol (5 mM) in 4% THF / $MeOC_4F_9$ (left) and effects of THF composition to emission (right) (λ_{ex} = 290 nm, slit 2/2 nm).

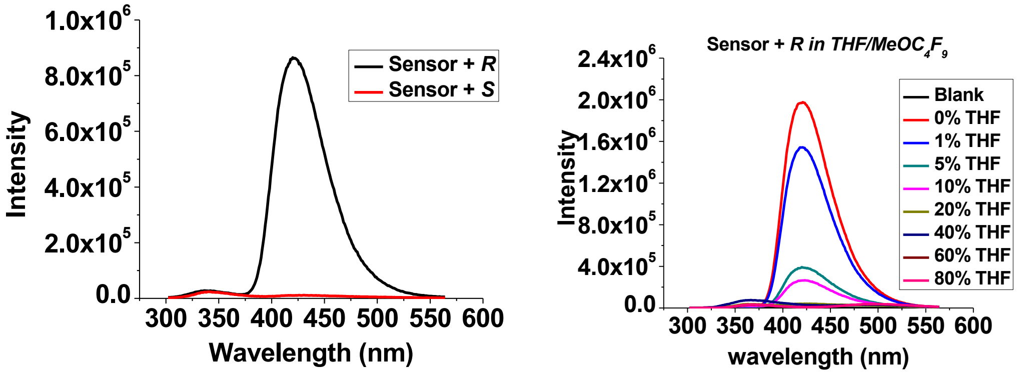

Figure 3- 35. Fluorescence spectra of (*S*)-**3.18** (0.08 mM) with addition of (1*R*, 2*R*)- or (1*S*, 2*S*) –**3.14** (5 mM) in 2 % DCM / FC72 (λ_{ex} =290 nm, slit 2/2 nm).

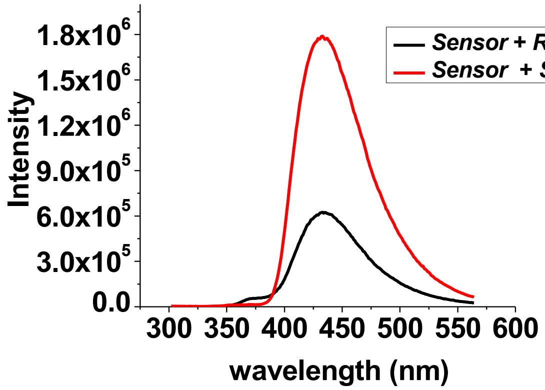

Figure 3- 36. Fluorescence spectra of (*S*)-**3.18** (0.08 mM) with addition of (1*R*, 2*R*)- or (1*S*, 2*S*) –**3.14** (5 mM) in different solvents (λ_{ex} = 290 nm, slit 2/2 nm).

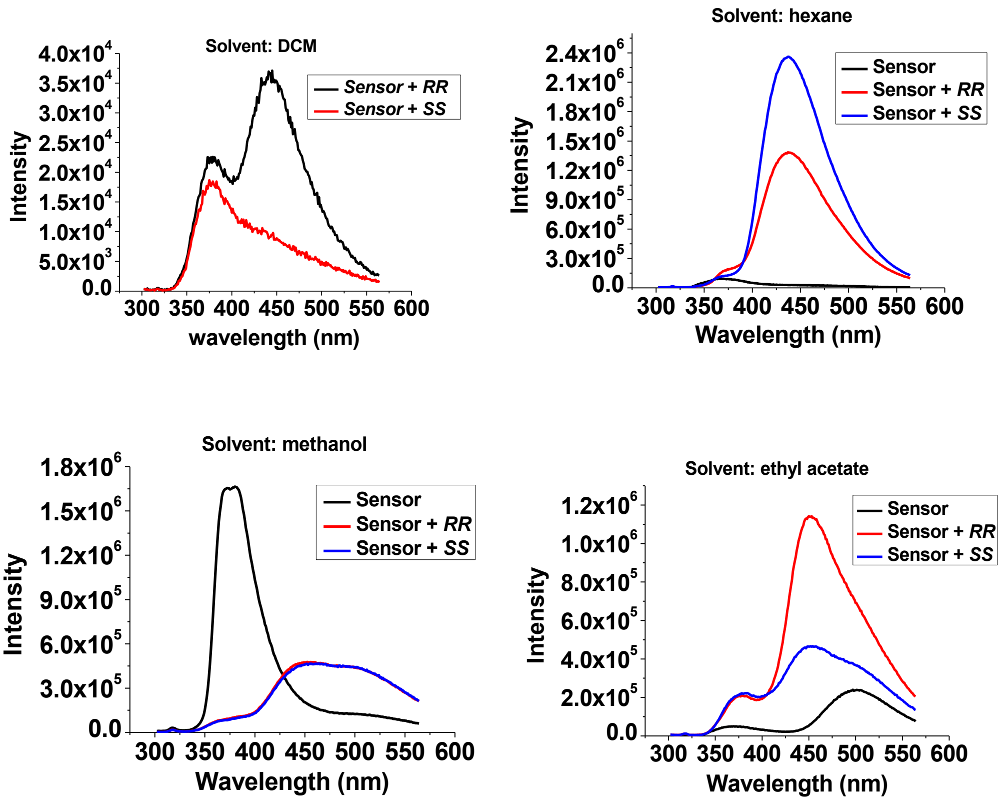

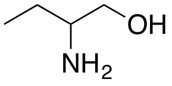

3.7

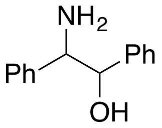

3.22

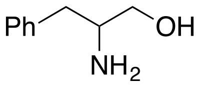

5.23

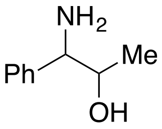

5.24

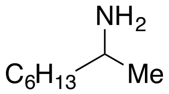

5.25

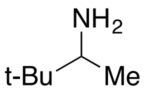

5.26

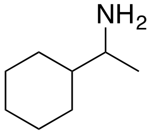

5.27

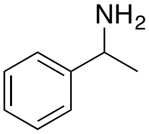

5.28

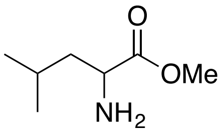

5.29

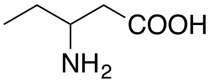

5.30

We tried to expand the scope of chiral recognition to aromatic amino alcohols (**3.22-24**), nonfunctional amines (**3.25-28**) and others as shown in Figure 3-37. (*S*)-**3.18**, though having higher affinity in fluorous solvent compared with BINOL-C_7F_{15}, is still incapable of sensing aromatic amino alcohols since they are too bulky to interact with the sensor in fluorous solvent. At higher concentration of **3.22-24** over 2 mM, they precipitate out immediately in FC72. Though $CH_3OC_4F_9$ has higher tolerance of aromatic alcohols, no emission was observed as well.

Figure 3- 37. Fluorescence spectra of (*S*)-**3.18** (0.08 mM) with addition of **3.22**, **23** or **24** (2 mM) in 2 % DCM / FC72 (λ_{ex} = 290 nm, slit 2/2 nm).

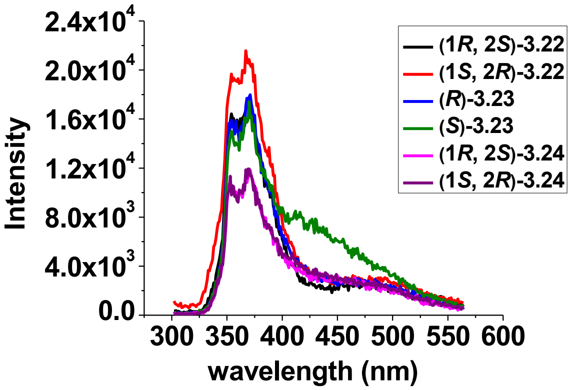

For the nonfunctional 2-aminooctane (**3.25**), we observed intermediate fluorescence enhancement at 434 nm for both enantiomers, but the enantioselectivity was very low (*ef* = 1.15 at 5 mM, Figure 3-38). For the bulky amine **3.23** containing tetra-butyl group, no emission enhancement was observed. Moderate enhancement was also observed with *ef* = 1.5 for amine **3.27** containing a hexyl group. Similar with aromatic amino alcohols, the aromatic amine **3.28** gave no emission change. Thus the interaction of amine with the sensor is highly sensitive to steric effects. For other chiral molecules like hydroxyl acids or amino esters, we observed no fluorescence change as well.

Figure 3- 38. Fluorescence spectra of (*S*)-**3.18** (0.08 mM) with addition of **3.25** (2 to 5 mM) in 2% DCM / FC72 (λ_{ex} = 290 nm, slit 2/2 nm).

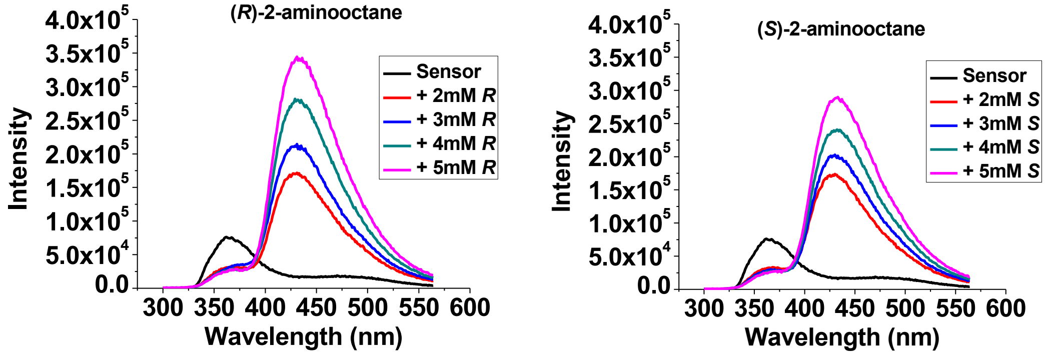

Figure 3- 39. Fluorescence spectra of (*S*)-**3.18** (0.08 mM) with addition of other chiral molecules (5 mM) in 2%DCM / FC72 (λ_{ex} =290 nm, slit 2/2 nm).

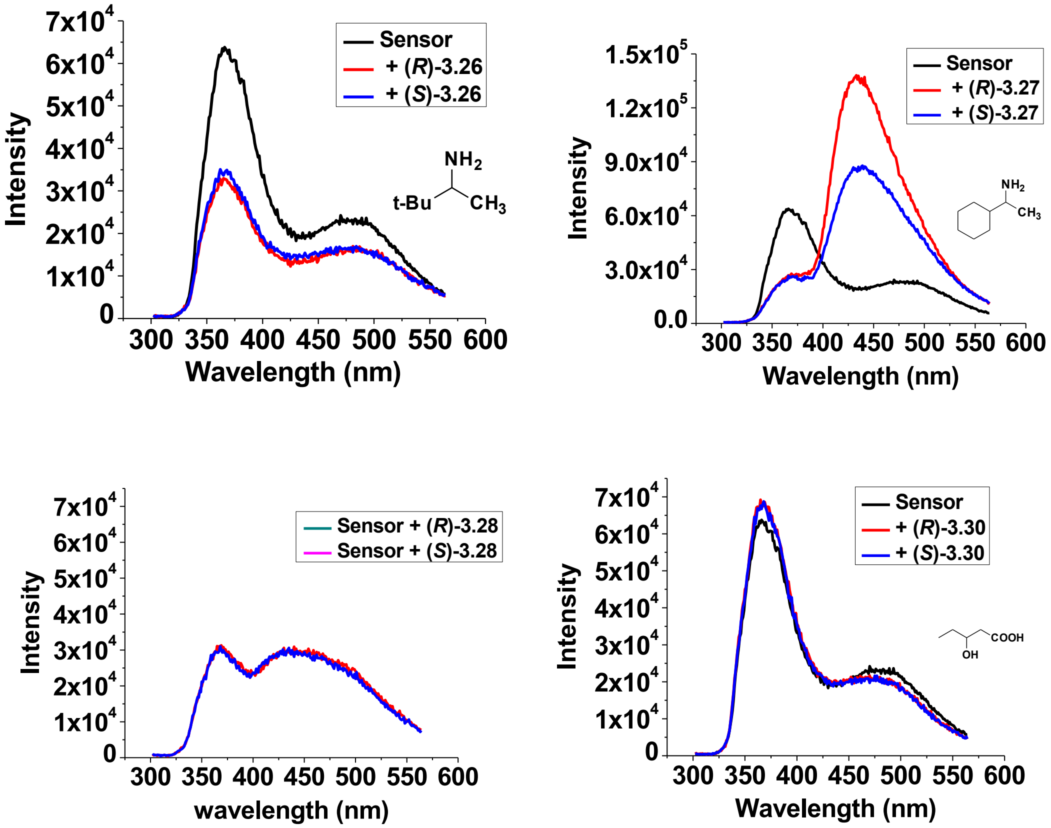

Furthermore, we studied the fluorescence response of (*S*)-**3.20**, a molecule containing much shorter perfluoroalkyl chains, toward chiral amines in fluorous solvents as a comparison with **3.18**. (*S*)-**3.20** was synthesized with a similar protocol as shown in Scheme 3-8. It is expected that (*S*)-**3.20** is insoluble in FC-72 as it doesn't have enough fluorine content. So we turned to $MeOC_4F_9$ as the solvent.

Scheme 3- 8. Synthesis of (*S*)-**3.20**.

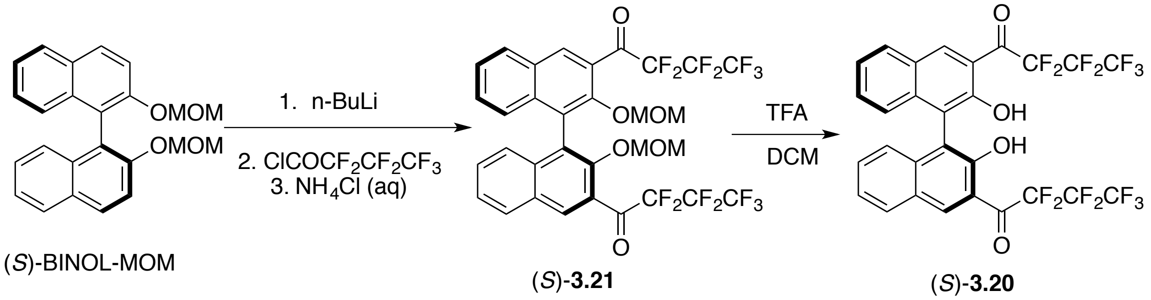
OMOM
OMOM
(S)-BINOL-MOM
1. n-BuLi
2. ClCOCF2CF2CF3
3. NH4Cl (aq)
O
CF2CF2CF3
OMOM
OMOM
CF2CF2CF3
O
(S)-3.21
TFA
DCM
O
CF2CF2CF3
OH
OH
CF2CF2CF3
O
(S)-3.20

Figure 3- 40. Fluorescence spectra of (*S*)-**3.20** (0.08 mM) with the addition of (*R*) or (*S*)-**3.7** (5 mM) at 5 min in $MeOC_4F_9$ (a); Fluorescence change over time for (*R*)-**3.7** (b); Fluorescence change over time for (*S*)-**3.7** (b); Fluorescence intensity at 423 nm was plotted against time (d). (λ_{ex} = 290 nm, slit 3/3 nm)

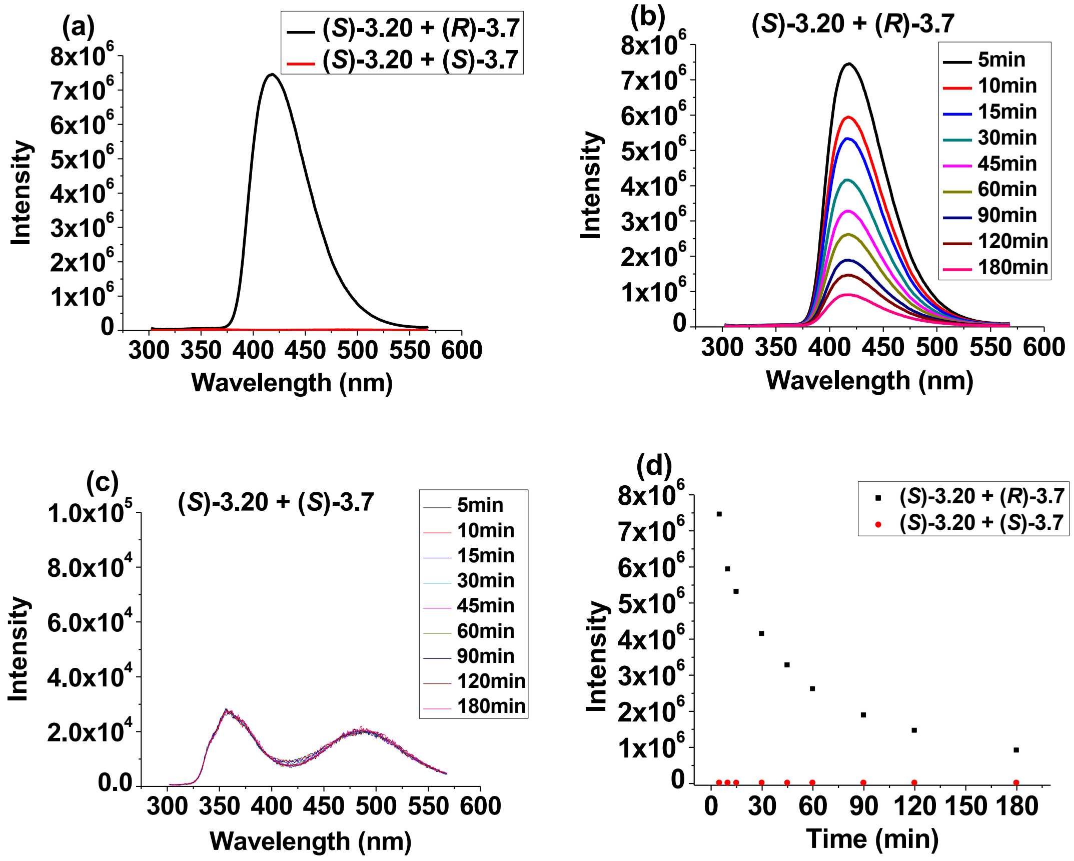

When (*R*)-**3.7** in THF (40 µL, 5 mM) was added to the solution of (*S*)-**3.20** (0.08 mM) in $MeOC_4F_9$, very strong blue emission was observed under a UV-lamp. However when (*S*)-**3.7** was used, no emission was observed (Figure 3-40). This is similar to the use of (*S*)-**3.6** in FC-72 described. However, the emission for the interaction of (*S*)-**3.20** with (*R*)-**3.7** was found to decrease continuously and turned very week after 3 h, while that of (*S*)-**3.20** with (*S*)-**3.7** remained weak all the time. The instability of the fluorescence might due to the fact that the adducts formed between the sensor and amine have better solubility in $MeOC_4F_9$. When the amine was firstly added, it forms local aggregate that produces strong emission. However as the reaction continues, the aggregation is dissolved in $MeOC_4F_9$ and the emission keeps decreasing.

When the solvent was changed to octafluorotoluene (CF_3-C_6F_5), a much better fluorescence stability was observed over 2 h (Figure 3-41). However, the emission intensity and enantioselectivity are both lower than the use of $MeOC_4F_9$. A better enantioselectivity with *ef* = 12 was obtained when the excitation wavelength was shifted to 320 nm to avoid the background emission from the sensor. The importance of a fluorous environment is obvious when the recognition was conducted in common solvents like toluene or trifluorotoluene (Figure 3-42). In this case, only weak emission was observed at the beginning and disappeared soon without enantioselectivity. We also tested the recognition of (*S*)-**3.20** to monoamines and aromatic amino alcohols, however no fluorescence response was observed as well.

Figure 3- 41. Fluorescence spectra of (*S*)-**3.20** with (*R*) or (*S*)-**3.7** in CF_3-C_6F_5 over time (λ_{ex} = 290 nm, left) and fluorescence spectra when λ_{ex} = 320 nm (right).

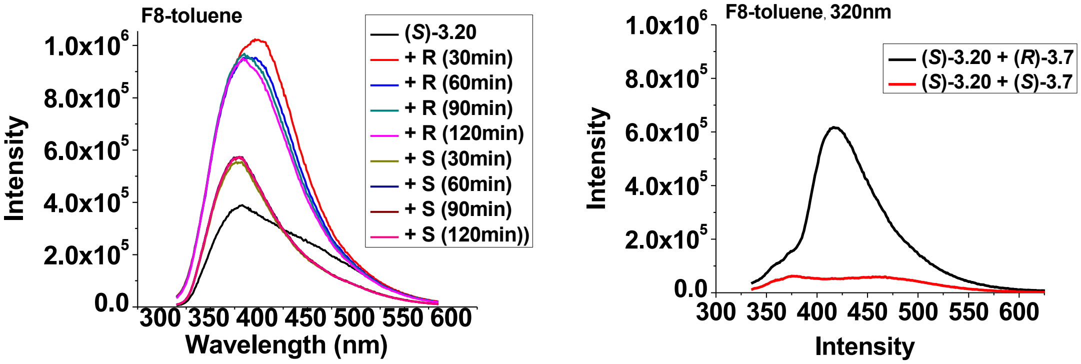

Figure 3- 42. Fluorescence spectra of (*S*)-**3.20** with (*R*) or (*S*)-**3.7** in CH_3-C_6H_5 or CF_3-C_6H_5 over time (λ_{ex} = 290 nm).

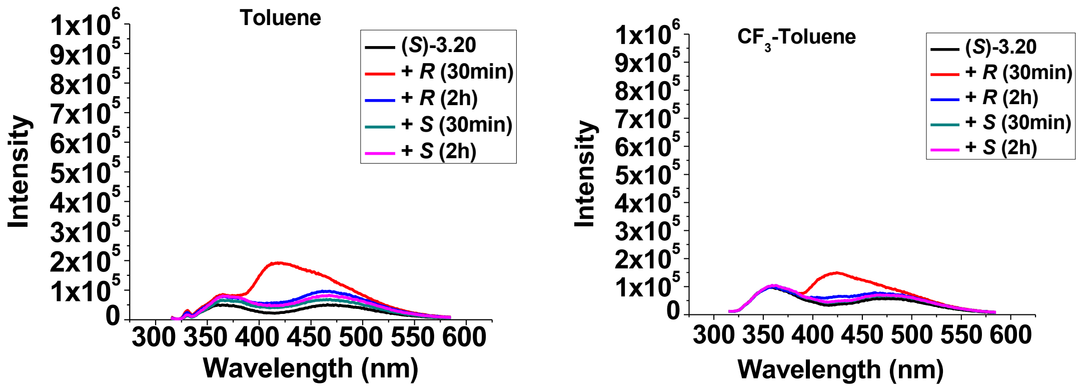

3.3. Conclusion

In summary, we have discovered compound (*S*)-**3.6** as the first enantioselective fluorescent sensor used in fluorous phase. In perfluorohexane solution, (*S*)-**3.6** exhibits greatly enhanced fluorescence when treated with chiral amino alcohols such as (*R*)-**3.7** but little fluorescent response is observed with the enantiomer (*S*)-**3.7**. The fluorous solvent is found to promote the nucleophilic addition of the amino alcohols to the carbonyl groups of (*S*)-**3.6** as shown by IR and mass spectroscopic studies. This is quite remarkable since no such a reaction is observed in a common polar organic solvent like methylene chloride or chloroform. Dynamic light-scattering studies of the sensor and chiral amino alcohol mixtures generated in the fluorous phase demonstrate the formation of aggregates of very different particle sizes from the interaction of the two enantiomers of achiral amino alcohol with the sensor. Thus, the highly enantioselective fluorescent response of (*S*)-**3.6** toward the chiral amino alcohols could be attributed to their very different aggregation forms. The highly enantioselective fluorescent response of (*S*)-**3.6** in fluorous phase is potentially useful for high throughput chiral catalyst screening since the reaction of the sensor with the chiral substrates only occur in the fluorous phase in which most other species should not influence the reaction. The ability of the sensor to determine enantiomeric excess of functional amines using fluorescence also makes it useful in rapid chiral analysis.

By adding two extra fluorous ponytail chains on the 6 and 6' position of BIONL, we synthesized **3.18** with very high fluorine content. Compound **3.18** is highly soluble in various fluorous solvents and maintains excellent enantioselectivity toward aliphatic amino alcohols. However, attempts for two phase sensing were not successful due to the instability of the adducts formed between sensor and amine in the presence of large amount of common organic solvents. It is interesting to find that compound **3.20**, which has relatively low fluorine contents, still displays high enantioselectivity in fluorous solvents but not in organic solvents. However, the emission is highly unstable and decays exponentially overtime. The sets of various sensors with distinct sensing ability will greatly enrich the library of fluorinated sensors, which is still largely an unexplored area. The unique chemical and photo-physical properties of these fluorinated sensors and fluorous solvents make them valuable for further development in rapid analysis and screening.

3.4. Experimental section

3.4.1. General information

All reactions were carried out under N_2 unless otherwise noted. Fluorous reagents were purchased from SynQuest Labs, Inc. All other chemicals were purchased from Sigma Aldrich Chemical Co. or Alfa Aesar. The diamine was distilled before fluorescent measurements. Other chemicals were used without further purification. Methylene chloride and diethyl ether were dried by passing them through activated alumina columns under nitrogen. Optical rotations were measured on a Jasco P-2000 digital polarimeter. NMR spectra were recorded on Varian-300 MHz or Varian-600 MHz spectrometer. Chemical shifts for ^{1}H NMR spectra were reported in parts per million relative to a singlet at 7.26 ppm for deuterated chloroform. Chemical shifts for ^{13}C NMR were reported relative to the centerline of a triplet at 77.16 ppm for deuterated chloroform. The ^{19}F NMR spectra were reported in units of part per million (ppm) relative to trifluoroacetic acid (δ -76.55 ppm) as an external reference. Steady-state fluorescence emission spectra were recorded on Horiba FluoroMax-4 spectrofluorometer. High-resolution mass spectra were obtained from the University of Illinois at Urbana-Champaign (UIUC) Mass Spectrometry Facility. UV-Vis spectra were produced from a Hewlett-Packard 8452A diode-array spectrophotometer. IR spectra were produced on Nicolet iS 5 FT-IR spectrometer. Dynamic light scattering studies were performed on a

NanoBrook 90plus PALS particle size analyzer.

3.4.2. Sample preparations

Preparation of Samples for UV-Vis and Fluorescence Measurement

Compound (*S*)-**3.6** was purified by column chromatography followed by recrystallization and then stored in a refrigerator. The enantiomers of *trans*-1,2-diaminocyclohexane were purchased from Sigma and redistilled under vacuum pump before use. The enantiomers of amino alcohols were also purchased from Sigma, but used without further purification. Stock solutions of (*S*)-**3.6** were freshly prepared with a concentration of 0.8 mM in FC-72, and then diluted to 0.08 mM for each measurement. For amino alcohols, 0.125 M stock solutions were freshly prepared in methylene chloride. For *trans*-1, 2-diaminocyclohexane, a 0.05 M stock solution was prepared. In the fluorescence enhancement study, a sensor solution in FC-72 was mixed with the amino alcohol or diamine solution in methylene chloride at room temperature in a 5 mL volumetric flask and diluted to the desired concentration with FC-72. The mixtures containing 4 % of methylene chloride in FC-72 can be made into a stable single-phase system after rigorous manual shaking. The resulting solution was allowed to stand at room temperature for 1 h before measurement.

Enantiomeric excess (*ee*) correlations

The *ee* was defined as follows: *ee* = (R - *S*) / (*R* + *S*). Solutions containing each amino alcohol in methylene chloride were prepared in 5 mL volumetric flasks with a total concentration of 5mM for a series of *ee* values. This was performed by mixing two enantiomers in varying ratios. In the case of the diamine, a total concentration of 2 mM was used. Then (*S*)-**3.6** in FC-72 was added. Fluorescence spectra were recorded 1h after mixing the solution.

Study of the adducts formed from the reaction of (*S*)-3.6 with (*R*)-3.7 or (*S*)-3.7

Solutions of (*S*)-**3.6** (0.8 mM, 10 mL) in FC-72 were prepared in vials. Solutions of (*R*)-**3.7** or (*S*)-**3.7** (0.8 M, 1 mL) in CH_2Cl_2 were also prepared in vials. The solutions of (*R*)-**3.7** or (*S*)-**3.7** (10 equiv., 0.10 mL) were added to (*S*)-**3.6** in FC-72. After rigorous shaking and allowing the solutions to react for 1 h, precipitate was formed for the reaction of (*R*)-**3.7**, while oil was formed with that of (*S*)-**3.7**. The precipitate was separated by filtration through filter paper. The oil was separated by decanting the bulk solution to leave only the product on the wall of the reaction vessel. The products were dried under a vacuum pump. The NMR spectra of (*S*)-**3.6** + (*R*)-**3.7** (7.8 mg in 0.4 mL $CDCl_3$, partially dissolved) and (*S*)-**3.6** + (*S*)-**3.7** (17 mg in 0.4 mL $CDCl_3$, fully dissolved) was recorded. The $CDCl_3$ used here was treated with K_2CO_3 overnight and then filtered through a pipet packed with dry alumina to remove trace amount of acid and H_2O.

Dynamic light scattering study

Stock solutions of (*S*)-**6** were freshly prepared with a concentration of 0.8 mM in FC-72. Stock solutions of (*R*)- or (*S*)-2-aminobutanol were freshly prepared with a concentration of 0.125 M in CH_2Cl_2. For DLS studies, 0.08 mM (*S*)-**6** was mixed with 1.5 mM (*R*)- or (*S*)-2-aminobutanol at room temperature in 5 mL volumetric flasks. The mixtures containing 4 % of CH_2Cl_2 in FC-72 can be made into a stable single-phase system after rigorous manual shaking. The resulting solution was allowed to stand at room temperature for 1.0 h before measurements. Temperature was set at 25°C. Viscosity and refractive index were set to be 0.67 cp and 1.252 with regard to FC-72.

3.4.3. Synthesis and characterization

Synthesis of (*S*)-1,1'-(2,2'-bis(methoxymethoxy)-[1,1'-binaphthalene]-3,3'-diyl)bis(2,2,3,3,4,4,5,5, 6,6,7,7,8,8,8-pentadecafluorooctan-1-one), (*S*)-3.5.

Under nitrogen, 2, 2'-bis-methoxymethyl-1, 1'-binaphthyl, (*S*)-**3.4** (0.5 mmol, 187 mg), was dissolved in diethyl ether (6 mL). The solution was cooled to 0 ºC, and n-BuLi (2.0 mmol, 2.5 M in hexane, 0.8 mL) was added dropwise. The reaction mixture was stirred at room temperature for 2 h and cooled to -78 °C (dry ice / acetone), and then perfluorooctanoyl chloride (2.0 mmol, 0.5 mL) was added slowly. The reaction mixture was stirred at -78 °C for 2 h, and then warmed to 0 °C to react for 1 h to afford a yellow cream-like mixture. The mixture exhibited a bright green color under the UV-lamp, indicative of (*S*)-**3.5** formation. Saturated aqueous NH_4Cl solution (2 mL) was added to quench the reaction at 0 °C. The organic layer was separated, and the aqueous layer was extracted with dichloromethane (3 × 10 mL). The combined organic extracts were washed with brine, and dried over Na_2SO_4. After evaporation of the solvent, the residue was purified by column chromatography on silica gel eluted with hexane / methylene chloride (1 / 8) to afford compound (*S*)-**3.5** as a yellow oil with a yield of 72 %. ^{1}H NMR (600 MHz, Chloroform-d) δ 8.24 (s, 2H), 8.00 (d, *J* = 8.1 Hz, 2H), 7.53 (t, *J* = 7.4 Hz, 2H), 7.45 (t, *J* = 7.6 Hz, 2H), 7.23 (d, *J* = 8.5 Hz, 2H), 4.66 (dd, *J* = 13.2, 6.0 Hz, 4H), 2.74 (s, 6H). ^{13}C NMR (151 MHz, Chloroform-d) δ 186.95 (t, *J* = 27.8 Hz), 151.56, 136.02, 131.84, 129.86, 129.62, 128.76, 126.71, 126.39, 126.23, 120-106 (m), 100.19, 56.63. ^{19}F NMR (564 MHz, Chloroform-d) δ -80.90 (t, *J* = 9.7 Hz, 6F), -113.82 - -115.32 (m, 4F), -120.77 (s, 4F), -121.11 (s, 4F), -122.02 (s, 4F), -122.76 (s, 4F), -126.22 (s, 4F). HRMS Calcd for $C_{40}H_{20}O_6F_{30}Na$ (MNa+): 1189.0679, Found: 1189.0702. $[\alpha]_D$ = -190.7 (c = 0.6360, $CHCl_3$).

Synthesis of (*S*)-1,1'-(2,2'-dihydroxy-[1,1'-binaphthalene]-3,3'-diyl)bis(2,2,3,3,4,4,5,5,6,6,7,7,8,8,8 -pentadecafluorooctan-1-one), (*S*)-3.6.

After compound (*S*)-**3.5** (1.17 g, 1.0 mmol) was dissolved in a minimum amount of CH_2Cl_2, trifluroacetic acid (3.0 mL) was added slowly at 0 °C, and the mixture was stirred at room temperature for 30 min. Saturated aqueous $NaHCO_3$ solution was added to quench the reaction. The organic layer was separated, and the aqueous layer was extracted with CH_2Cl_2 (3 × 20 mL). The combined organic extracts were washed with brine, and dried over Na_2SO_4. After evaporation of the solvents, the residue was purified by column chromatography on silica gel eluted with hexane/methylene chloride (10 / 1) to afford compound (*S*)-**3.6**, a red-orange powder with a yield of 85 %. ^{1}H NMR (300 MHz, Chloroform-*d*) δ 10.60 (s, 2H), 8.79 (s, 2H), 8.02 (d, J = 7.6 Hz, 2H), 7.47 (m, 4H), 7.16 (d, J = 7.9 Hz, 2H). ^{13}C NMR (151 MHz, Chloroform-*d*) δ 187.63 (t, *J* = 25.6 Hz), 155.09, 138.53, 136.53, 132.37, 131.44, 127.26, 125.31, 124.73, 118.02, 116.79, 118-106(m). ^{19}F NMR (282MHz, Chloroform-*d*) δ -81.16 (t, *J* = 9.7 Hz, 6F), -109.80 (m, 4F), -120.60 (m, 4F), -121.12 (m, 4F), -122.28 (m, 4F), -123.04 (m, 4F), -126.54 (m, 4F). HRMS Calcd for $C_{36}H_{13}O_4F_{30}$ (MH+): 1079.0335, Found:1079.0308. $[\alpha]_D$ = -74.7 (c = 0.400, $CHCl_3$).

Synthesis of (*R*)-1,1'-(2,2'-dihydroxy-[1,1'-binaphthalene]-3,3'-diyl)bis (2,2,3,3,4,4,5,5,6,6,7,7,8,8,8 -pentadecafluorooctan-1-one), (*R*)-3.6.

Compound (*R*)-**3.6**, the enantiomer of (*S*)-**3.6**, was synthesized as an orange powder with a total yield of 59 % in two steps using the same protocol described above but starting with (*R*)-2, 2’-bis-methoxymethyl-1, 1’-binaphthyl. ^{1}H NMR (600 MHz, Chloroform-*d*) δ 10.58 (s, 2H), 8.78 (s, 2H), 8.02 (d, *J* = 8.3 Hz, 2H), 7.46 (m, 4H), 7.16 (d, *J* = 8.4 Hz, 2H). ^{13}C NMR (151 MHz, Chloroform-*d*) δ187.73 (t, *J* = 25.6 Hz), 155.03, 138.46, 136.44, 132.30, 131.38, 127.19, 125.25, 124.67, 117.96, 116.73, 118-106(m). ^{19}F NMR (564 MHz, Chloroform-d) δ -81.16 (t, *J* = 9.6 Hz, 6F), -109.82 (m, 4F), -120.58 (m, 4F), -121.08 (m, 4F), -122.26 (m, 4F), -123.02 (m, 4F), -126.50 (m, 4F). $[\alpha]_D$ = 84.5 (c = 0.400, $CHCl_3$).

Synthesis of ((1E,1'E)-((*S*)-2,2'-bis(methoxymethoxy)-[1,1'-binaphthalene]-6,6'-diyl)bis(ethene-2,1-diyl))bis((1,1,1,2,3,3,4,4,5,5,6,6,7,7,8,8-hexadecafluoro-8λ^3-octan-2-yl)-λ^2-fluorane), (*S*)-3.16

A [Pd]-catalyzed Heck coupling was used to synthesize (*S*)-**3.16**. To a 100 mL round bottom flask was loaded (*S*)-**3.15** (6 mmol, 3.2 g), sodium acetate (15 mmol, 1.2 g). Herrmann's catalyst (2 mol %, 120 mg) was then added in glove box, followed by addition of dry DMF (60 mL) and 1H, 1H, 2H-Perfluoro-1-decene ($CH_2CHC_8F_{17}$, 24 mmol, 6.4 mL). The mixture was heated at 120 °C with rigorous stirring for 24 h under nitrogen. After cooled down to room temperature, the solution was poured into ice water

(150 mL) and extracted with diethyl ether / hexane mixture (30 mL / 10 mL, 5 times). The combined organic extracts were washed with H_2O (100 mL), brine (100 mL) and dried over anhydrous Na_2SO_4. After evaporation of the solvents, the residue was purified by column chromatography on silica gel eluted with hexane/ethyl acetate (20 / 1 to 10 / 1) to afford the compound **3.16** as a white solid in 76% yield. ^{1}H NMR (600 MHz, Chloroform-*d*) δ 7.99 (d, *J* = 9.1 Hz, 2H), 7.94 (s, 2H), 7.64 (d, *J* = 9.1 Hz, 2H), 7.37 (d, *J* = 8.9 Hz, 2H), 7.30 (d, *J* = 16.1 Hz, 2H), 7.14 (d, *J* = 8.9 Hz, 2H), 6.20 (dt, *J* = 15.8, 12.1 Hz, 2H), 5.12 (d, *J* = 6.9 Hz, 2H), 5.03 (d, *J* = 6.9 Hz, 2H), 3.18 (s, 6H). ^{19}F NMR (564 MHz, Chloroform-*d*) δ -80.81 (t, *J* = 10.0 Hz, 6F), -110.81 (dd, *J* = 107.7, 13.8 Hz, 4F), -121.30 – -121.40 (m, 4F), -121. 88 – -121.94 (m, 8F), -122.69 – -122.76 (m, 4F), -123.10 – -123.18 (m, 4F), -126.09 – -126.17 (m, 4F).^{13}C NMR (151 MHz, Chloroform-*d*) δ 154.04, 139.77 (t, *J* = 9.39Hz), 134.86, 130.41, 129.63, 129.61, 129.45, 126.33, 123.90, 120.89, 117.85, 113.88 (t, *J* = 22.6Hz), 118 – 108 (m, weak), 95.09, 56.09.

Synthesis of (((*S*)-2,2'-bis(methoxymethoxy)-[1,1'-binaphthalene]-6,6'-diyl)bis(ethane-2,1-diyl)) bis((1,1,1,2,3,3,4,4,5,5,6,6,7,7,8,8-hexadecafluoro-8λ^3-octan-2-yl)-λ^2-fluorane), (*S*)-3.17

To a high-pressure reactor was added (*S*)-**3.16** (2 mmol, 2.52 g), 10% Pd / C (0.54 g) and 20 mL ethyl acetate. 30 bar of hydrogen gas was then applied. After disconnected with the gas tank, the reactor was place on a stirring plate for 16 h at room temperature. The gas was slowly released and the solution was filtered through Celite to remove Pd / C and washed with ethyl acetate. After evaporation of the solvents, the residue was purified by column chromatography on silica gel eluted with hexane/ethyl acetate (30 / 1 to 10 / 1) to afford compound **3.17** as a white solid in 93 % yield. ^{1}H NMR (600 MHz, Chloroform-*d*) δ 7.90 (d, *J* = 9.1 Hz, 2H), 7.70 (s, 2H), 7.58 (d, *J* = 9.0 Hz, 2H), 7.12 – 7.05 (m, 4H), 5.07 (d, *J* = 6.8 Hz, 2H), 4.97 (d, *J* = 6.7 Hz, 2H), 3.16 (s, 6H), 3.02 (dt, *J* = 12.0, 3.7 Hz, 4H), 2.48 – 2.37 (m, 4H). ^{19}F NMR (564 MHz, Chloroform-*d*) δ -80.80 (dt, *J* = 11.6, 5.7 Hz, 6F), -114.55 (t, *J* = 19.1 Hz, 4F), -121. 64 – -121.72 (m, 4F), -121. 89 – -121.94 (m, 8F), -122.88 – -122.76(m, 4F), -123. 43 – -123.49 (m, 4F), -126.09 – -126.17 (m, 4F). ^{13}C NMR (151 MHz, Chloroform-*d*) δ 152.85, 134.91, 133.05, 130.23, 129.17, 127.32, 126.83, 126.32, 121.41, 117.98, 120.41–106.32 (m, weak), 95.48, 55.94, 33.03, 26.53, 26.50, 26.47.

Synthesis of 1,1'-((1*S*)-6,6'-bis(2-((1,1,1,2,3,3,4,4,5,5,6,6,7,7,8,8-hexadecafluoro-8λ^{3}-octan-2-yl)-λ^{2}-fluoranyl)ethyl)-2,2'-dihydroxy-[1,1'-binaphthalene]-3,3'-diyl) bis (2,2,3,3,4,4,5,5,6,6,7,7,8,8,8-pentadecafluorooctan-1-one), (*S*)-3.18

(1). Compound **3.17** (1.5 mmol, 950 mg) was dissolved in dry diethyl ether (20 mL). The solution was cooled to 0 °C, and n-BuLi (6.0 mmol, 2.4 mL, 2.5 M in hexane,) was added dropwise. The reaction mixture was stirred at room temperature for 2 h and cooled to -78 °C. Then $C_7F_{15}COCl$ (6.0 mmol, 1.5 mL) was added dropwise. The reaction mixture was stirred at -78 °C for 1 h, and then warmed up to 0 °C to react for additional 1 h. Saturated aqueous solution of NH_4Cl (4 mL) was added to quench the reaction at 0 °C. The organic layer was separated, and the aqueous layer was extracted with methylene chloride (4 × 20 mL). The combined organic extracts were washed with brine, and dried over anhydrous Na_2SO_4. After evaporation of the solvents, the mixture was further dried under vacuum pump to yield the red crude product.

(2). The crude product was dissolved in a 30 mL of methylene chloride, and cooled to 0 °C. Trifluroacetic acid (1.5 mL) was added slowly, and the mixture was stirred at room temperature for 1 h. Saturated aqueous solution of $NaHCO_3$ was added slowly to quench the reaction. The organic layer was separated, and the aqueous layer was extracted with CH_2Cl_2 (3 × 20 mL). The combined organic extracts were washed with brine, and dried over anhydrous Na_2SO_4. After evaporation of the solvents, the residue was purified by column chromatography on silica gel eluted with hexane / methylene chloride (15 / 1) to afford compound **3.18** as a red quasi-solid in 68 % yield for two steps. ^{1}H NMR (600 MHz, Chloroform-*d*) δ 10.56 (s, 2H), 8.73 (s, 2H), 7.85 (s, 2H), 7.33 (d, *J* = 10.3 Hz, 2H), 7.13 (d, *J* = 8.8 Hz, 2H), 3.06 (t, *J* = 8.4 Hz, 4H), 2.49 – 2.40(m, 4H). ^{19}F NMR (564 MHz, Chloroform-d) δ -80.70 – -80.95 (m, 12F), -109.51 (t, *J* = 13.3 Hz, 4F), -114.26 – -114.92 (m, 4F), -120.12 – -120.20 (m, 4F), -120.65 – -120.74 (m, 4F), -121.62 – -121.69 (m, 4F), -121. 82 – -122.10 (m, 12F), -122.55 – -122.95 (m, 8F), -123. 39 – -123.51 (m, 4F), -126.02 – -126.28 (m, 8F).

Synthesis of (*S*)-1,1'-(2,2'-dihydroxy-[1,1'-binaphthalene]-3,3'-diyl)bis(2,2,3,3,4,4,4-heptafluorobutan-1-one), (*S*)-3.20

(1). Compound (*S*)-BINOL-MOM (1 mmol, 374 mg) was dissolved in dry diethyl ether (12 mL). The solution was cooled to 0 °C, and n-BuLi (4.0 mmol, 1.6 mL, 2.5 M in hexane,) was added dropwise. The reaction mixture was stirred at room temperature for 2 h and cooled to -78 °C by dry ice / acetone. Then perfluorobutyryl chloride (C_3F_7COCl, 4.0 mmol, 600 μL) was added dropwise. The reaction mixture was stirred at -78 °C for 1 h, and then warmed up to 0 °C to react for additional 1 h to afford a yellow cream-like mixture. Saturated aqueous solution of NH_4Cl (2 mL) was added to quench the reaction at 0 °C. The organic layer was separated, and the aqueous layer was extracted with ethyl acetate (3 × 10 mL). The combined organic extracts were washed with brine, and dried over anhydrous Na_2SO_4. After evaporation of the solvents, the mixture was further dried under vacuum pump to yield a yellow crude product.

(2). The crude product was dissolved in a minimum amount of methylene chloride, and cooled to 0 °C. Trifluroacetic acid (1.0 mL) was added slowly, and the mixture was stirred at room temperature for 1 h. Saturated aqueous solution of $NaHCO_3$ was added slowly to quench the reaction. The organic layer was separated, and the aqueous layer was extracted with CH_2Cl_2 (3 x 10 mL). The combined organic extracts were washed with brine, and dried over anhydrous Na_2SO_4. After evaporation of the solvents, the residue was purified by column chromatography on silica gel eluted with hexane/methylene chloride (10 / 1) to afford compound (*S*)-**3.20** as a red solid in 42 % yield for two steps. ^{1}H NMR (600 MHz, Chloroform-*d*) δ 10.56 (s, 2H), 8.77 (d, *J* = 8.64 Hz, 2H), 8.00 (t, *J* = 8.45 Hz, 2H), 7.49 – 7.40 (m, 4H), 7.15 (t, *J* = 8.45 Hz, 2H,).^{19}F NMR (564 MHz, Chloroform-*d*) δ -79.84 – -79.89 (m, 3F), -110.20 (t, *J* = 8.61 Hz, 2F), -124.76 – -124.77 (m, 2F).^{13}C NMR (151 MHz, Chloroform-*d*) δ 187.58 (t, *J* = 25.42 Hz), 155.03, 138.49, 136.46 (t, *J* = 6.9 Hz), 132.32, 131.36, 127.20, 125.26, 124.68, 117.96, 116.70, 119 – 108 (m, weak).

3.5. References

(1) Horváth, I. T.; Rábai, J. *Science* **1994**, *266*, 72-75.

(2) Bakkari, M. E.; Fronton, B.; Luguya, R.; Vincent, J. -M. *J. Fluor. Chem*. **2006**, *127*, 558–564.

(3) Bakkari, M. E.; Luguya, R.; da Costa, R. C.; Vincent, J.-M. *New J. Chem*. **2008**, *32*, 193–196.

(4) Selected reports on enantioselective fluorescent recognition: (a) Pu, L. *Chem. Rev.* **2004**, *104*, 1687–1716. (b) Leung, D.; Kang, S. O.; Anslyn, E. V. *Chem. Soc. Rev*. **2012**, *41*, 448–479. (c) Accetta, A.; Corradini, R.; Marchelli, R. *Top. Curr. Chem*. **2011**, *300*, 175–216. (d) Pu, L. *Acc. Chem. Res*. **2012**, *45*, 150–163. (e) Zhang, X.; Yin, J.; Yoon, J. *Chem. Rev*. **2014**, *114*, 4918-4959. (a) James, T. D.; Sandanayake, K. R. A. S.; Shinkai, S. *Nature* **1995**, *374*, 345–347. (b) Lin, J.; Hu, Q. -S.; Xu, M. H.; Pu, L. *J. Am. Chem. Soc.* **2002**, *124*, 2088–2089. (a) Zhao, J.-Z.; Fyles, T. M.; James, T. D. *Angew. Chem., Int. Ed.* **2004**, *43*, 3461–3464. (b) Zhu, L.; Anslyn, E. V. *J. Am. Chem. Soc.* **2004**, *126*, 3676–3677. (c) Mei, X. F.; Wolf, C. *J. Am. Chem. Soc.* **2004**, *126*, 14736–14737

(5) Yu, S.; Plunkett, W.; Kim, M.; Pu, L. J. Am. Chem. Soc. 2012, 134, 20282−20285.

(6) Yu, S., Pu, L. *J. Org. Chem*. **2013**, 78, 12671−12680.

(7) A review on aggregation induced emission: Hong, Y.; Lam, J. W. Y.; Tang, B. Z. *Chem. Soc. Rev*. **2011**, 40, 5361−5388.

Chapter 4. Enantioselective Detection of Amines and Amino Acids by Amide Formation from Perfluoroalkyl Ketones

4.1. Introduction

Using fluorescence in chiral recognition can potentially provide a fast analytical tool for high throughput chiral assay. Over the past decade, great progress has been made in this area.[1-3] For example, significant amount of work has been conducted for the fluorescent recognition of chiral amines and high enantioselectivity has been achieved for amines containing additional functional groups such as hydroxyl, amine, ester, carboxylic acid groups.[1, 4-8] These additional functional groups could enhance their bonding interaction with a fluorescent probe and increase the structural rigidity of the host-guest adducts, leading to the observed high enantioselectivity. The fluorescent recognition of unfunctionalized chiral amines normally gives low enantioselectivity except in a few limited cases.[7] The interaction between a fluorescent probe and a chiral amine substrate involves a variety of bonding such as hydrogen bonds, electrostatic attraction, metal coordination, and aminal and imine formation.

Although amide bonds are relatively strong with high structural rigidity, formation of amides has not been used for the enantioselective fluorescent recognition of chiral amines. This could be attributed to the following two factors: (1) High temperature and long reaction time are normally required for the reaction of esters or acids with amines to form amides unless certain activators or catalysts are added which could interfere with the fluorescent measurement and complicate the sensing system; (2) Compounds such as acyl chlorides or ketenes can readily form amides with amines, but these compounds are also highly reactive with other species such as water and alcohols which makes them not suitable as molecular probes.

Figure 4-1. Structures of sensor (*S*)-**4.1** and (*S*)-**4.2**.

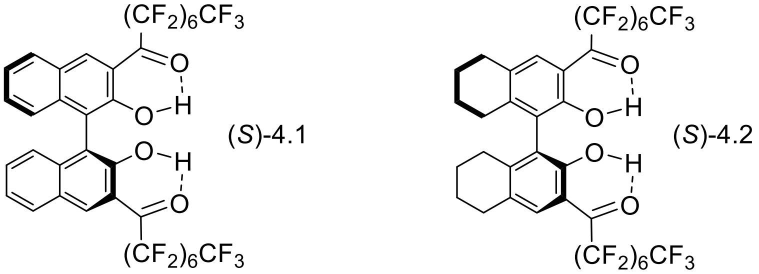

In the last chapter we studied the use of a 1, 1'-Bi-2-Naphthol (BINOL)-based chiral perfluoroalkyl ketone (*S*)-**4.1** for the fluorescent recognition of chiral amino alcohols in the fluorous phase.[8] In perfluorohexane, (*S*)-**4.1** reacts with an amino alcohol to generate a mixture of semiaminal products with highly enantioselective fluorescent enhancements. We recently prepared compound (*S*)-**4.2** as an analogue of (*S*)-**4.1** from the partially hydrogenated BINOL (H_8BINOL). A dramatic solvent effect is discovered for the reaction of (*S*)-**4.2** with chiral amines. In DMF, highly enantioselective fluorescent enhancements for the recognition of both unfunctionalized and functionalized chiral amines have been achieved. On the basis of detailed spectroscopic investigations, we have revealed that the amines react readily with the perfluoroalkyl ketone units of (*S*)-**4.2** to form amide bonds in DMF at room temperature by cleaving the perfluoroalkyl chain off the ketone but not in other solvents such as THF, CH_2Cl_2, hexane and perfluorohexane. These results demonstrate that the amide bond formation from perfluoroalkyl ketones can be used to develop new and efficient enantioselective fluorescent sensors for chiral amines.

4.2. Results & Discussion

4.2.1. Synthetic routes of compounds

Scheme 4-1. Synthetic routes of sensor (*S*)-**4.2** and (*R*)-**4.2**.

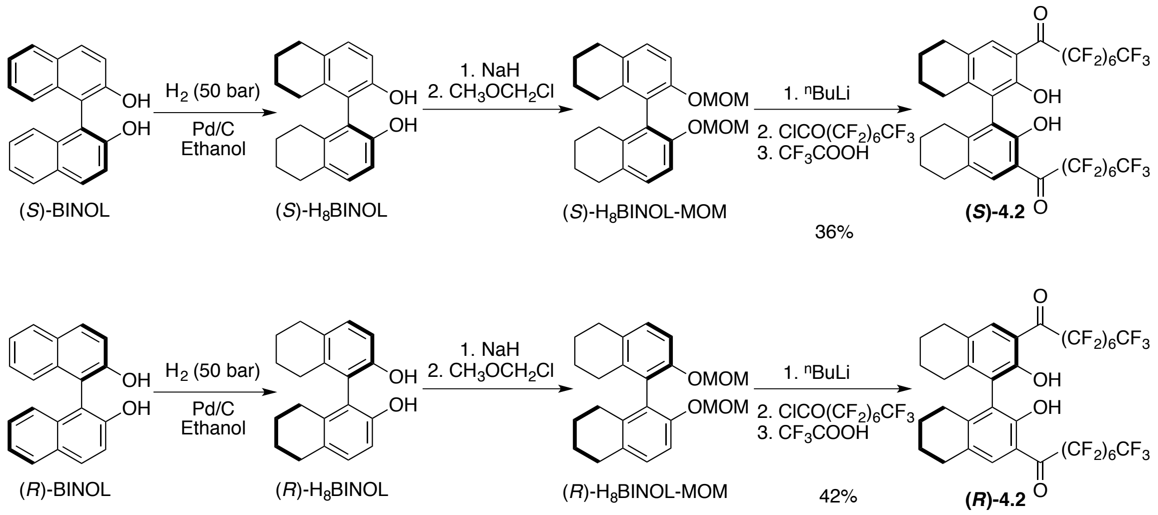
(S)-BINOL
H2 (50 bar)
Pd/C
Ethanol
(S)-H8BINOL
1. NaH
2. CH3OCH2Cl
(S)-H8BINOL-MOM
1. nBuLi
2. ClCO(CF2)6CF3
3. CF3COOH
36%
(S)-4.2
(R)-BINOL
(R)-H8BINOL
(R)-H8BINOL-MOM
42%
(R)-4.2

Scheme 4-2. Synthetic routes of related amides.

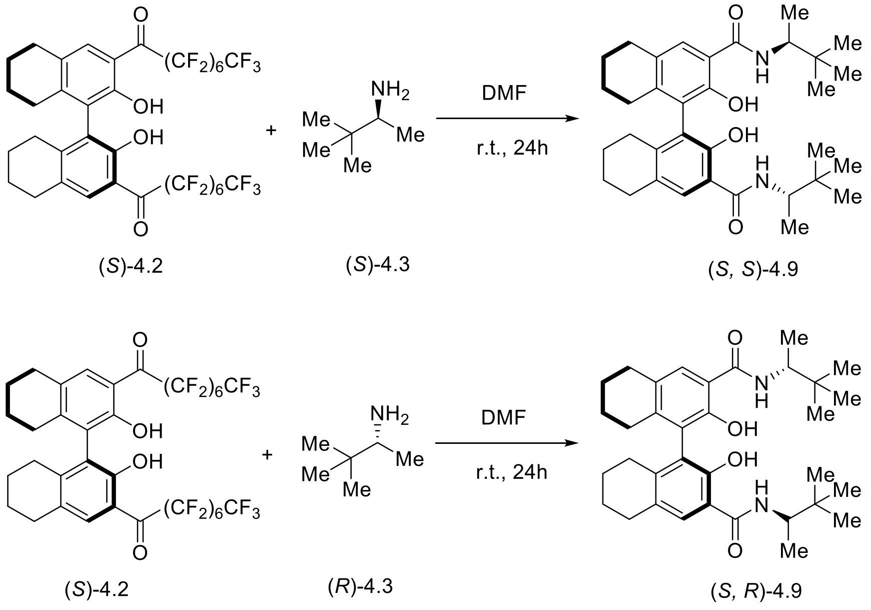
(S)-4.2
(S)-4.3
DMF
r.t., 24h
(S, S)-4.9
(S)-4.2
(R)-4.3
DMF
r.t., 24h
(S, R)-4.9

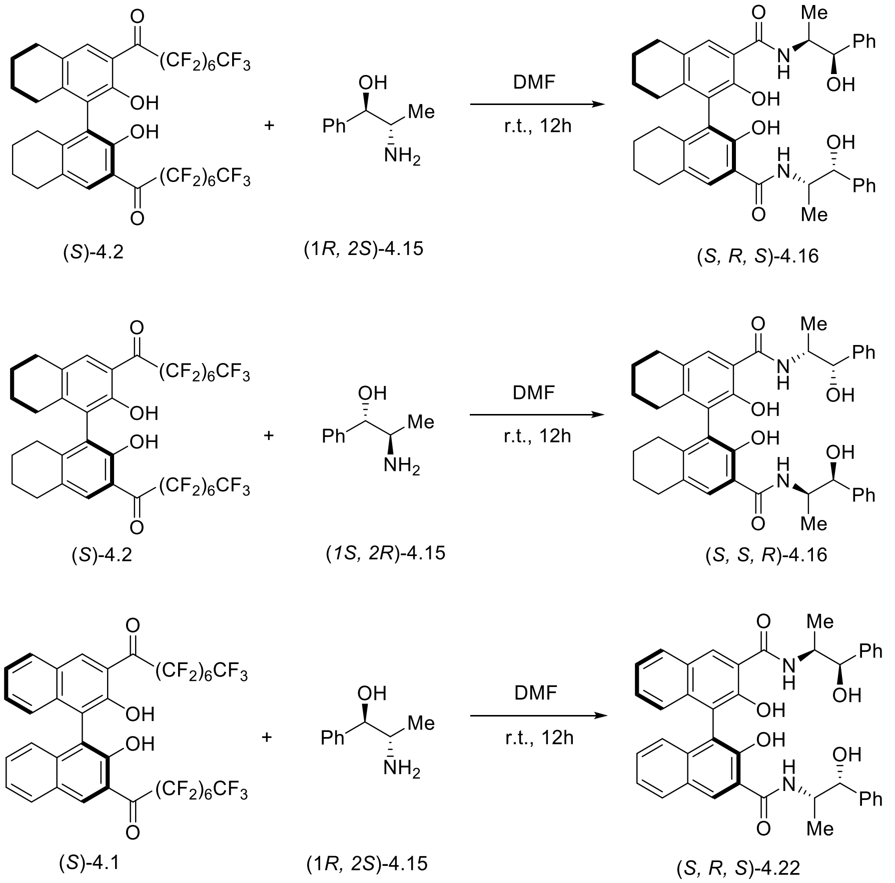
(CF2)6CF3
OH
DMF
r.t., 12h
(S)-4.2
(1R, 2S)-4.15
(S, R, S)-4.16
(1S, 2R)-4.15
(S, S, R)-4.16
(S)-4.1
(S, R, S)-4.22

Figure 4-2. Structures of the chiral substrates.

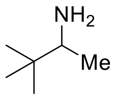

4.3

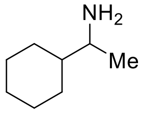

4.11

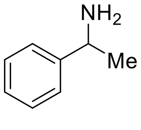

4.12

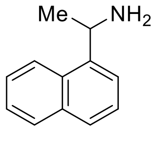

4.13

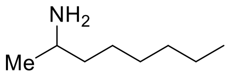

4.14

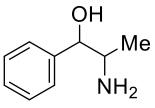

4.15

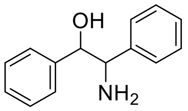

4.17

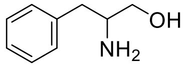

4.18

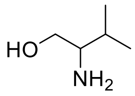

4.19

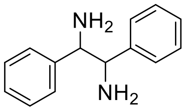

4. 20

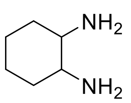

4.21

Compound (*S*)-**4.2** was synthesized by starting from (*S*)-H_8BINOL, which was easily prepared from (*S*)-BINOL using Pd / C catalysed hydrogenation method. (*R*)-**4.2**, the enantiomer of (*S*)-**4.2**, was synthesized using the same procedures for (*S*)-**2** but starting with (*R*)- H_8BINOL. The synthetic procedure of BINOL-based sensor (*S*)-**4.1** can be found in the previous chapter.[8] A series of amides were also prepared from the reaction of these ketones with amines using DMF as the solvent under mild conditions. The detailed procedures and characterization data can be found in the experimental part. The specific optical rotation of (*S*)-**4.2** is $[\alpha]_D$= 18.3 (c = 1.03, $CHCl_3$), very different from that of (*S*)-**4.1** ($[\alpha]_D$ = -74.7). The ^{1}H NMR spectrum of (*S*)-**4.2** in $CDCl_3$ gives a down-field signal at δ 11.28 ppm for its hydroxyl protons, an evidence of strong intramolecular hydrogen bonding, which also exists in all of the amide products listed above.

4.2.2. Solvent-dependent fluorescence response

Compound (*S*)-**4.2** gives very weak fluorescence in various solvents. We studied the fluorescent response of (*S*)-**4.2** (1.0×10^{-4} M) toward the two enantiomers of 3, 3-dimethyl-2-butylamine (**4.3**) (5.0×10^{-3} M), an unfunctionalized chiral amine, in solvents such as FC-72 (perfluorohexane), CH_2Cl_2, THF, methanol and hexane, but only very small change was observed in the fluorescence spectra (Figure 4-3, 4% (v/v) of DCM was used in the case of FC-72 and hexane to dissolve amine). However, when DMF was used as the solvent, large fluorescent enhancement was observed with high enantioselectivity at 450 nm, which is visible under UV-irradiation (Figure 4-4). This is in dramatic contrast with the BINOL-based sensor (*S*)-4.1, which only gives fluorescence response in fluorous solvents due to the formation of aggregation.

Figure 4-3. Fluorescence spectra of (*S*)-**4.2** (0.1 mM) in the presence of (*R*)-**4.3** or (*S*)-**4.3** (5 mM) in various solvents: FC-72 (perfluorohexane), DCM, THF, CH_3OH and Hexane. (λ_{ex}= 332 nm, slit = 3/3 nm).

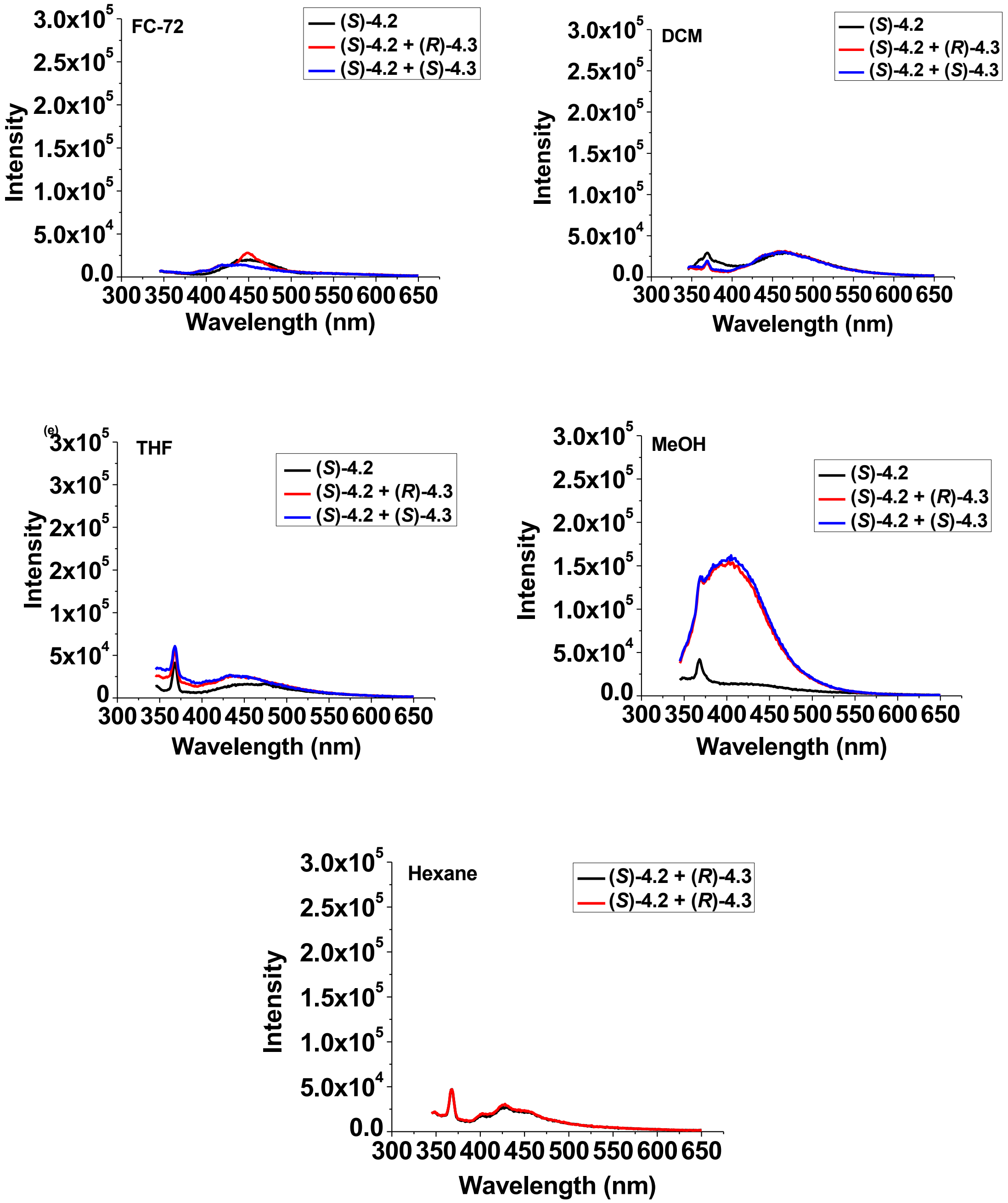

Figure 4-4. Fluorescence spectra of (*S*)-**4.2** (0.1 mM) in the presence of (*R*)-**4.3** or (*S*)-**4.3** (5 mM) in DMF under the same conditions.

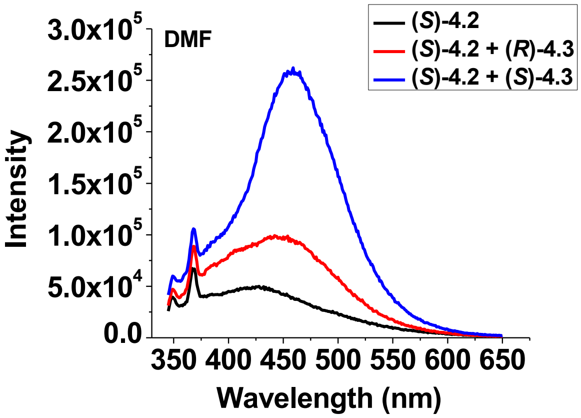

Figure 4-5. Fluorescence spectra of (*S*)-**4.2** (0.04 to 0.40 mM) in the presence of (*R*)-2-amino-1-propanol (5 mM, left) or (*S*)-2-amino-1-propanol (5 mM, right) in FC-72 (λ_{ex}= 332 nm, slit = 3/3 nm).

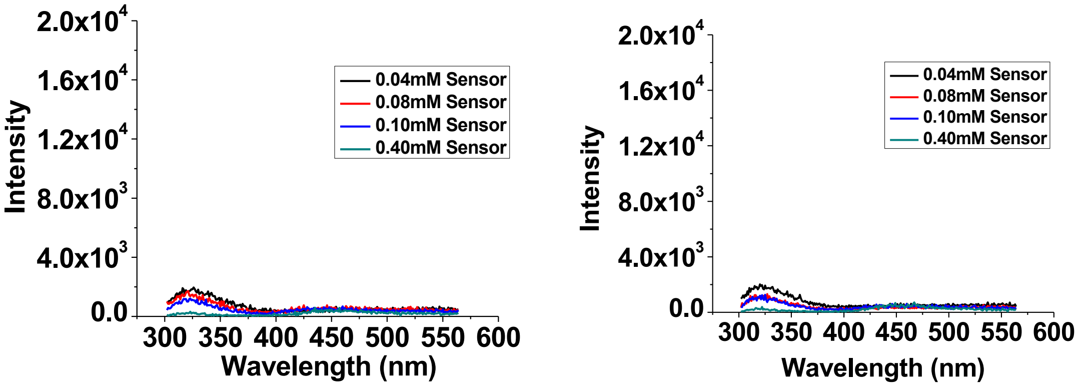

To give a better comparison with the previous study in fluorous solvent, we also conducted the fluorescence response of (*S*)-**4.2** to amino alcohol (*R*)-or (*S*)-2-amino-1-propanol, which is usually more active than monoamines, in various solvents. However, as shown in Figure 4-5, neither aggregation nor fluorescence response was observed in FC-72 even when elevated concentration of (*S*)-**4.2** was used. Similar to the case of **4.3**, enantioselective fluorescence for 2-amino-1-propanol was only observed in DMF but not in other common organic solvents (Figure 4-6). A weaker broad emission in methanol was observed but with no enantioselectivity.

Figure 4-6. Fluorescence spectra of (*S*)-**4.2** (0.1 mM) in the presence of (*R*)- or (*S*)-2-amino-1-propanol (5 mM) in various solvents: DMF, THF, DCM, MeOH and Hexane, λ_{ex}= 332 nm, slit = 3/3 nm.

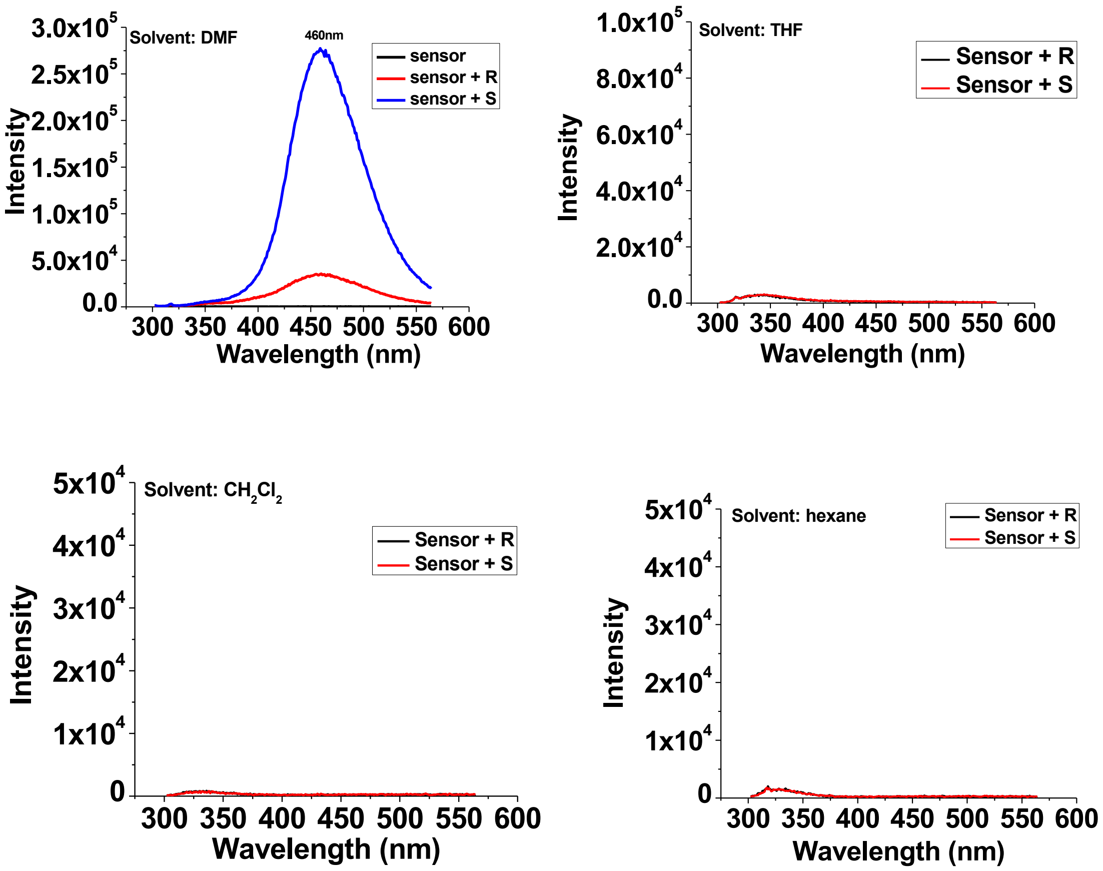

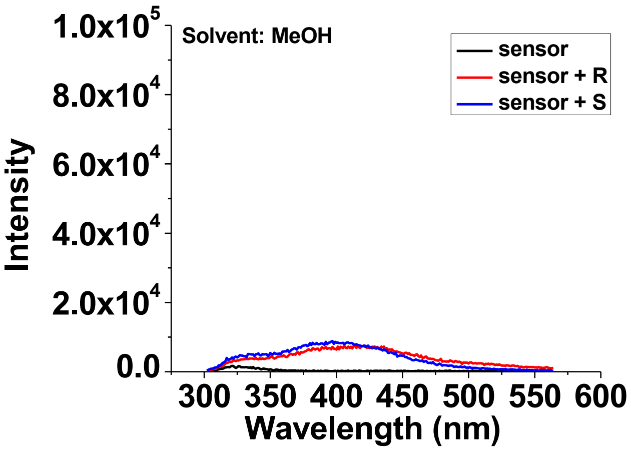

4.2.3. Time-dependent fluorescence response

While adding the amine **4.3** to the sensor (*S*)-**4.2** in DMF, it was observed that fluorescence intensity increased over time. As shown in Figure 4-7 (a-c), over 10 h, the enantiomer (*S*)-**4.3** continuously increased the fluorescence of (*S*)-**4.2** with greater fluorescent enhancement than the opposite enantiomer (*R*)-**4.3** did. The image in Figure 1d shows the strong blue emission of (*S*)-**4.2** in the presence of (*S*)-**4.3** in DMF.

Since little fluorescent response was observed for the interaction of (*S*)-**4.2** with (*S*)- and (*R*)-**4.3** in other solvents such as THF, we tested the use of THF to quench the reaction of (*S*)-**4.2** with the chiral amine in DMF. After (*S*)-**4.2** (0.01 M) was reacted with (*S*)- or (*R*)-**4.3** (3 mM) in DMF (0.5 mL) for 1 h, THF was added to make a total volume of 5 mL and the fluorescence spectra of the resulting solution were monitored over time. As shown in Figure 4-8, there was < 5 % change in the fluorescence intensity within 2 h. That is, addition of THF has effectively quenched the reaction, allowing stable fluorescent responses to be measured at any time. Other solvents like DCM or acetonitrile can also give good quenching effects, but THF yields slightly higher emission intensity.

Figure 4-7. Fluorescence spectra of (*S*)-**4.2** (0.1 mM) with (*S*)-**4.3** (a) and (*R*)-**4.3** (5.0 mM) (b) in DMF recorded over 10 h. Fluorescence intensity at λ=458 nm versus time (c). Image of (*S*)-**4.2** (0.1 mM) with (*S*)-**4.3** (5 mM) under UV irradiation (d). (λ_{ex} = 332 nm, slit = 2/2 nm).

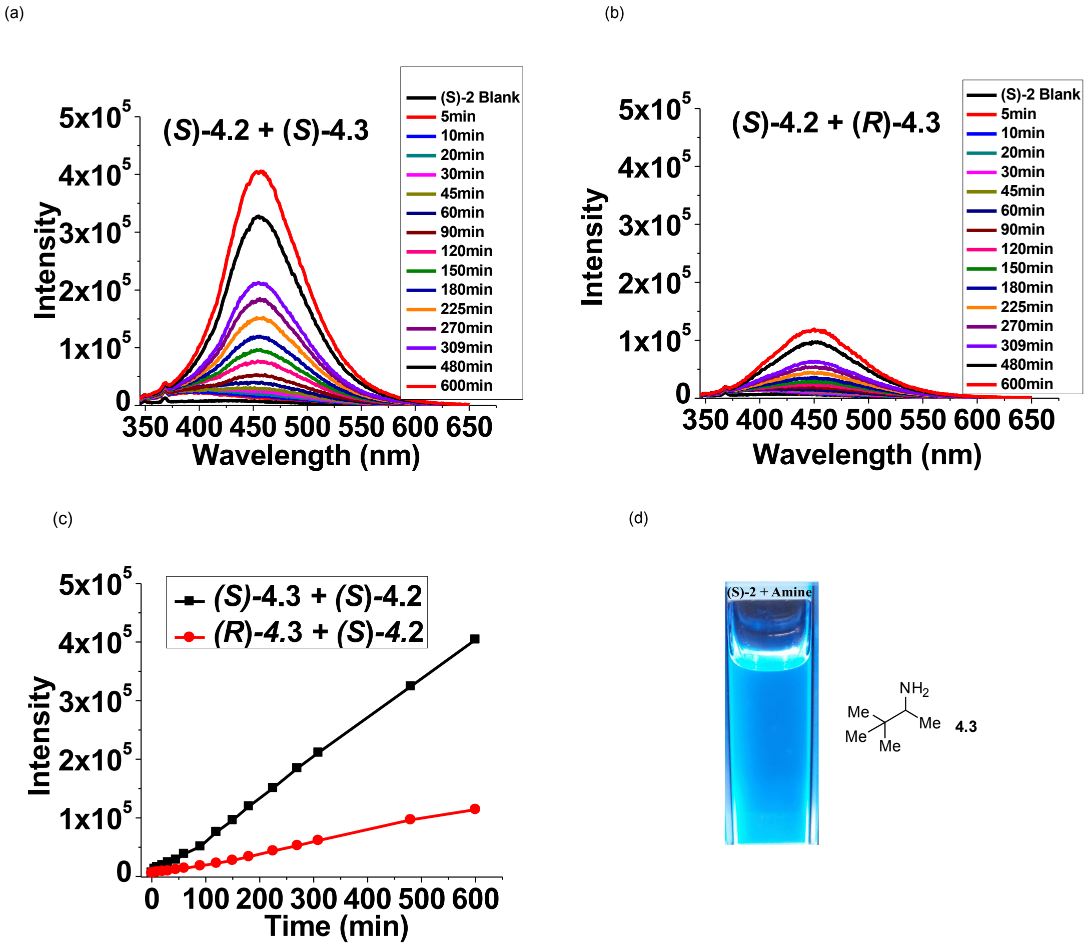
(a) (b) (c) (d)

The quenching by THF also applies to amino alcohols like **4.15** as shown in Figure 4-9, where less than 5 % of fluorescence change was observed 4 hours after quenching. Thus, we conducted the fluorescent measurement for the interaction of (*S*)-**4.2** with various chiral substrates by allowing the reaction to proceed in DMF for 1 h and then quench with the addition of an excess amount of THF.

Figure 4-8. Fluorescence spectra of (*S*)-**4.2** (0.01 mM) with (*R*)-**4.3** or (*S*)-**4.3** (3 mM) in 0.5 mL DMF / 4.5 mL THF over 4 h, and fluorescence intensity at 458 nm was plotted against time (λ_{ex}=332 nm, slit=3/3 nm).

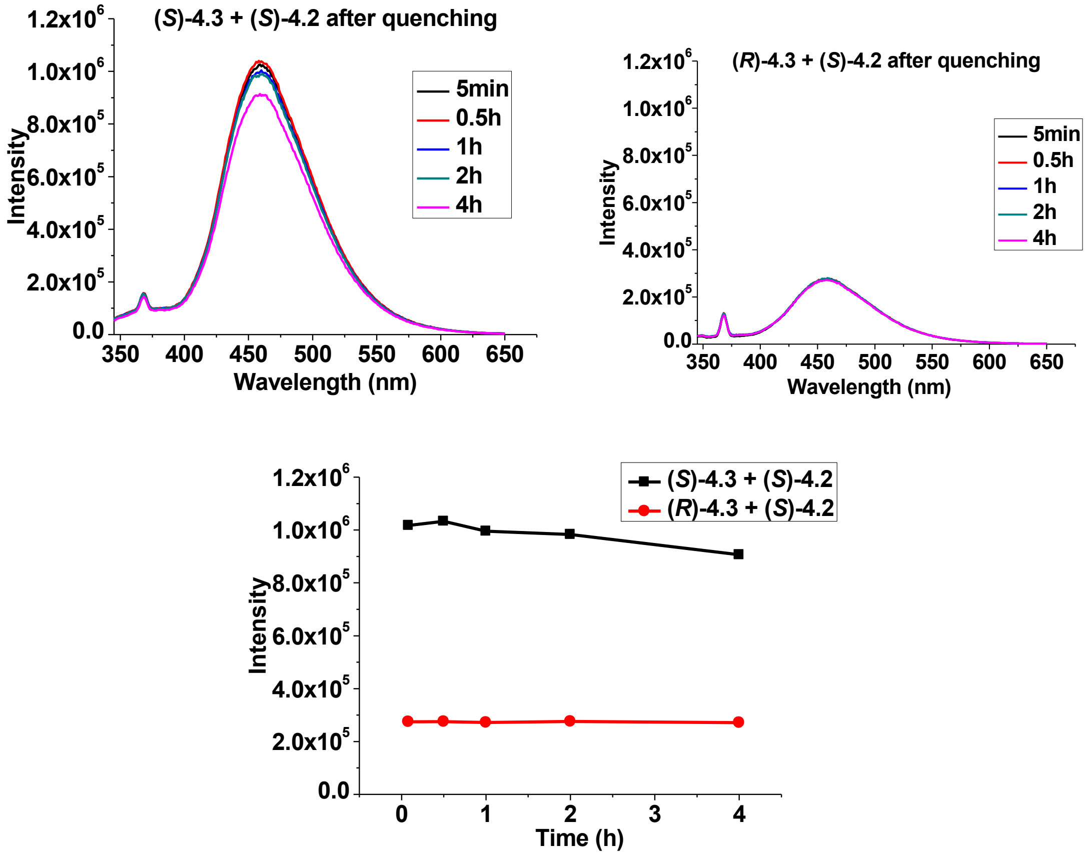

Figure 4-9. Fluorescence spectra of (*S*)-**4.2** (0.01 mM) with (1*R*, 2*S*)-**4.15** or (1*S*, 2*R*)-**4.15** (5 mM) in 0.5 mL DMF/4.5 mL THF over 4 h, and fluorescence intensity at 460 nm was plotted against time (λ_{ex}= 332 nm, slit = 2 / 2 nm).

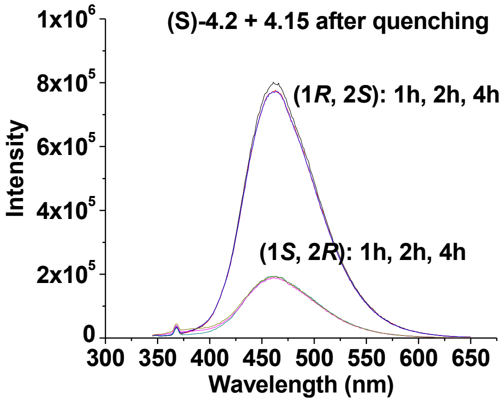

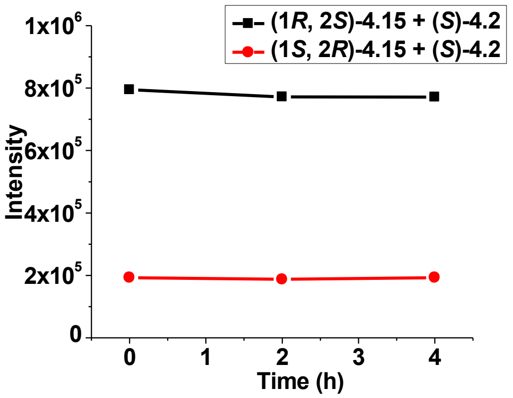

4.2.4. Enantioselective recognition of sensor to the amine

Figures 4-10 (a-c) give the fluorescent responses of (*S*)-**4.2** toward (*S*)- and (*R*)-**4.3**. High enantioselectivity has been achieved with the enantioselective fluorescent enhancement *ef* = 5.0 when the concentration of the amine is 3 mM. Here *ef* = (I_S-I_0) / (I_R-I_0), where I_0 is the initial fluorescence intensity of (*S*)-**4.2**, I_S and I_R are fluorescence intensity in the presence of *S* and *R* amines. We have studied the interaction of (*S*)-**4.2** with the amine at various enantiomeric composition, and obtained the plot of the fluorescence responses of (*S*)-**4.2** against the enantiomeric excess {*ee* % = ([*S*] - [*R*]) / ([*S*] + [*R*])} of the amine as shown in (d). A good 3rd order non-linear relationship can be built between the fluorescence intensity and enantiomeric excess values. Using this plot the enantiomeric composition of the amino alcohol can be easily determined by fluorescent measurement. This is especially useful when considering the difficulty to measure *ee* of amino alcohols using chiral HPCL due to their high polarity and lack of chromophore.

Figure 4-10. Fluorescence spectra of (*S*)-**4.2** (0.01 mM) with (*S*)-**4.3** (a) and (*R*)-**4.3** (b). Fluorescence intensity at λ = 458 nm versus the amine concentration (c), and *ee* of **4.3** (3 mM) (d). (λ_{ex} = 332 nm, slit = 3/3 nm, solvent: 10 % DMF / THF). Error bars were obtained on three independent measurements**.**

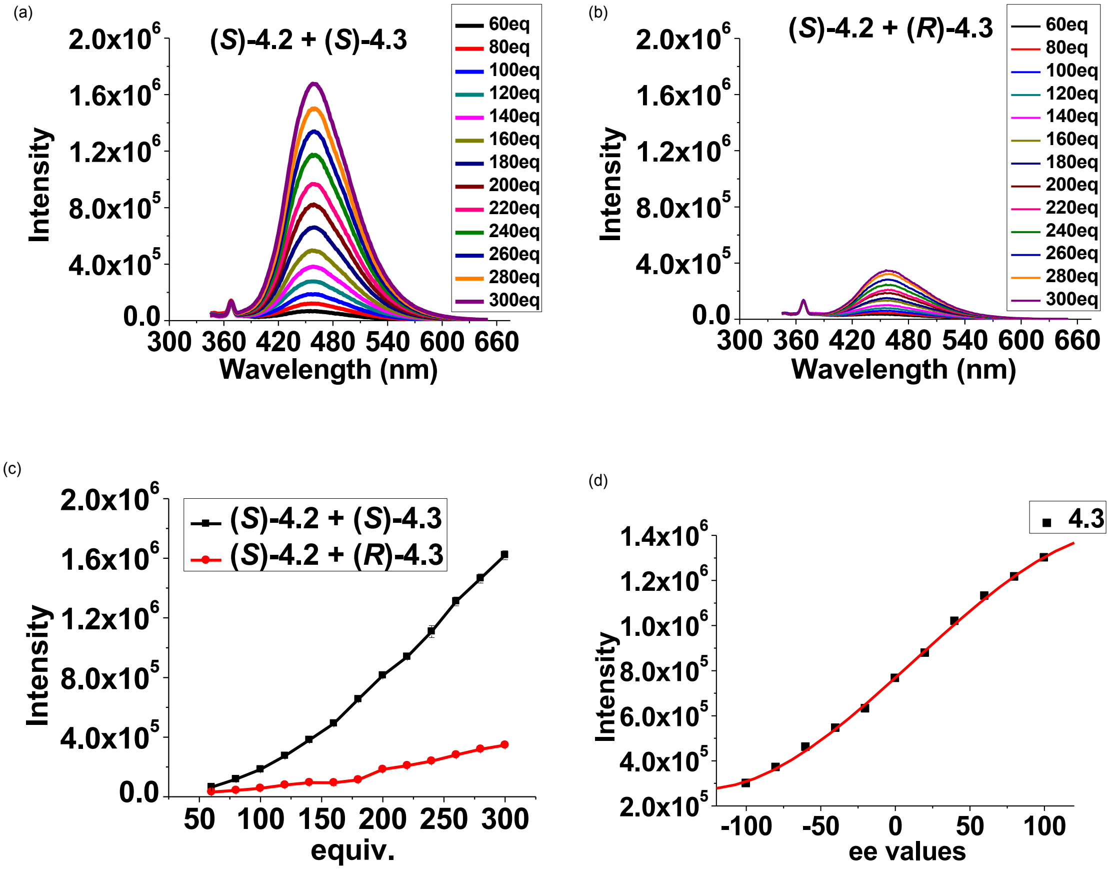

We also prepared (*R*)-**4.2**, the enantiomer of (*S*)-**4.2**, from the corresponding (*R*)-H_8BINOL and studied its fluorescent response toward (*R*)- and (*S*)-**4.3**. In this case, it is the (*R*)-**4.3** that induces stronger emission than its enantiomer (*S*)-**4.3**. The *ef* value is identical with the use of (*S*)-**4.2** (Figure 4-11). Thus, a mirror image relationship with the use of (*S*)-**4.2** in the fluorescent enhancements was established, which confirmed the observed enantioselective recognition.

Figure 4-11. Fluorescence spectra of (*R*)-**4.2** (0.01 mM) with amine **4.3** from 60 to 300 equiv., and the fluorescence intensity at λ = 458 nm was plotted against the equivalents. [λ_{ex}=332 nm, slit=3/3 nm, solvent: DMF/THF (1:9 v / v)].

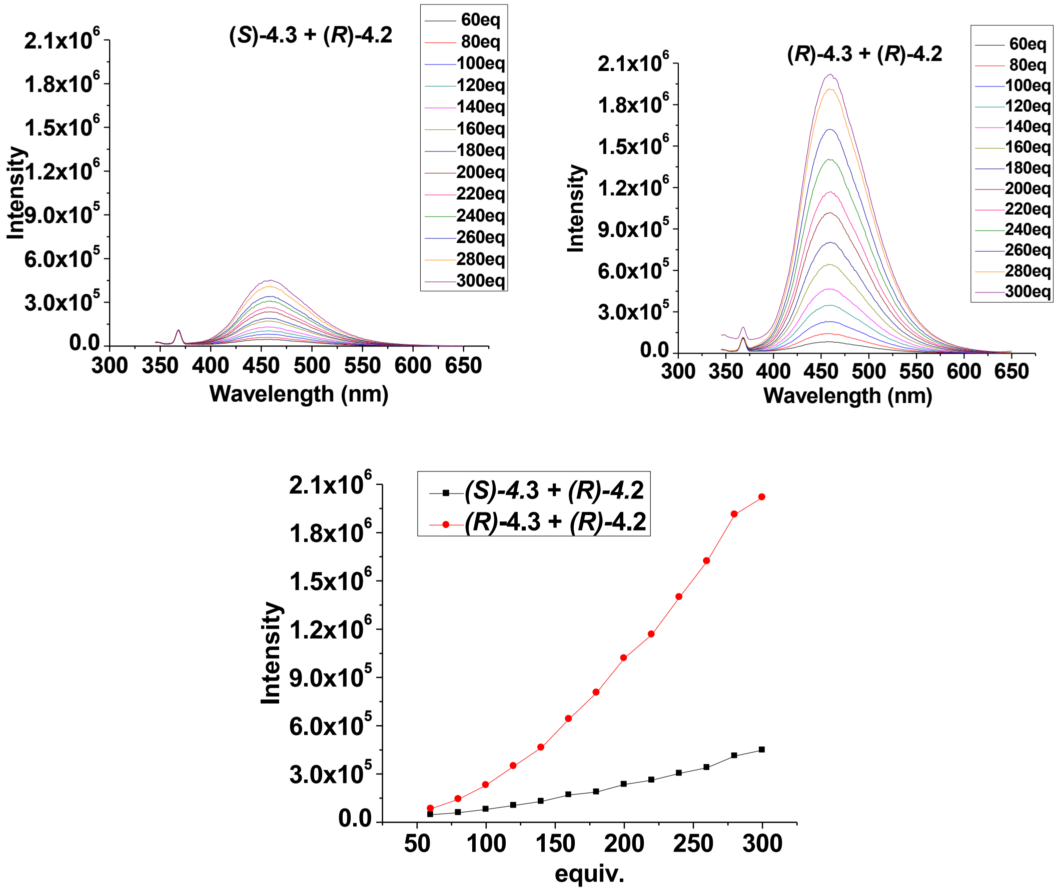

4.2.5. Mechanism studies between the reaction of sensor and amine

In order to understand the nature of the interaction between (*S*)-**4.2** and chiral amine, we have conducted a mass spectroscopic analysis. When (*S*)-**4.2** (0.05 mmol) was mixed with (*S*)-**4.3** (6 eq) in 6 mL DMF, the resulting solution was injected into a mass spectrometer (ES+) to acquire the mass spectra at 0 min, 30 min and 1 h reaction time respectively (see Appendix). On the basis of these mass spectra and isolated final products, the mechanism for the reaction of (*S*)-**4.2** with (*S*)-**4.3** is proposed in Scheme 4-3.

Scheme 4-3. Reaction of (*S*)-**4.2** with (*S*)-**4.3** in DMF.

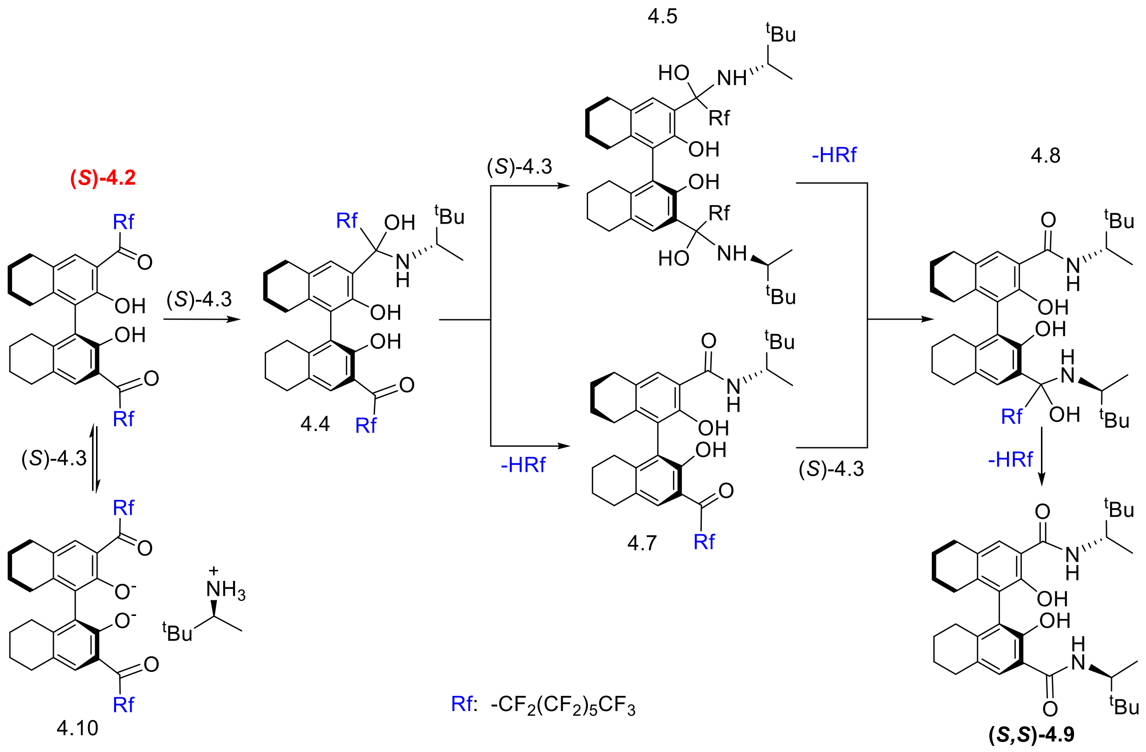
(S)-4.2
Rf
O
OH
OH
O
Rf
(S)-4.3
(S)-4.3
4.10
Rf
O
O-
O-
O
Rf
+
NH3
tBu
Rf
OH
tBu
N
H
OH
OH
O
4.4
Rf
(S)-4.3
-HRf
4.5
tBu
HO
NH
Rf
OH
OH
Rf
HO
NH
tBu
O
tBu
N
H
OH
OH
O
4.7
Rf
-HRf
(S)-4.3
4.8
O
tBu
N
H
OH
OH
H
N
Rf
OH
tBu
-HRf
O
tBu
N
H
OH
OH
H
N
O
tBu
(S,S)-4.9
Rf: -CF2(CF2)5CF3

In the first step, the amine adds to the carbonyl groups of (*S*)-**4.2** to give an intermediate **4.4** corresponding to the observed mass signal at m/z = 1188 for **4.4** + H^+, and an intermediate **4.5** corresponding to m/z = 1220 for **4.5** + H^+ - CF_3 and m/z = 1269 for **4.5** + H^+ - F. Intermediate **4.4** loses the 1-H-perfluoroheptane (HR_f, **4.6**) to give **4.7**, corresponding to the observed mass signal at m/z = 818 for 7 + H^+. Both **4.5** and **4.7** can be converted to 8 by the loss of HR_f and addition of (*S*)-**4.3** respectively. In the mass spectrum taken at 1 h after the mixing of (*S*)-**4.2** and (*S*)-**4.3**, the signal at m/z = 919 rose to be the base peak corresponding to **4.8** + H^+. This demonstrates that in 1 h, the major product in this reaction is **4.8**. No signal corresponding to the final amide product (*S*, *S*)-**4.9** was observed within 1 h. This indicates that the cleavage of the first perfluoroalkyl group off the ketone is much faster than the cleavage of the second one. It is not clear at this stage how the formation of the first amide unit influences the cleavage of the second perfluoroalkyl group. After more extended reaction time, the final product (*S*, *S*)-**4.9** was isolated in 64 % yield and was fully characterized.

The isolated (*S*, *S*)-**4.9** shows emission at λ = 457 nm the same as that observed in Figure 4-10, suggesting that the fluorescent enhancement of (*S*)-**4.2** in the presence of amine should be due to the formation of the arylamide fluorophores in intermediates **4.7** and **4.8**, which share the same arylamide units with (*S*, *S*)-**4.9**. As shown in Figure 4-12, the molar attenuation coefficients are determined to be $1.39 \times 10^4\ M^{-1}\ cm^{-1}$ for (*S*, *S*)-**4.9** and $1.40 \times 10^4\ M^{-1}\ cm^{-1}$ for (*S*, *R*, *S*)-**4.16** at $\lambda_{max} = 322$ nm. The diastereomer (*S*, *R*)-**4.9** was also obtained from the reaction of (*S*)-**4.2** with (*R*)-**4.3**. At the same concentration in DMF solution, these two compounds give identical emission spectra. The large stokes shift is typical for excited-state intramolecular proton transfer that forms zwitterionic structure, which has been widely observed in analogues like salicyaldehyde and salicylamide.[10]

Figure 4-12. UV-Vis and/or emission spectra of (*S*, *S*)-**4.9** (a), (*S*, *R*)-**4.9** (b), (*S*, *R*, *S*)-**4.16** (c) in DMF (Conc. is 0.01 mM for all; slit = 2 / 2 nm, $\lambda_{ex} = 322$ nm for emission spectra).

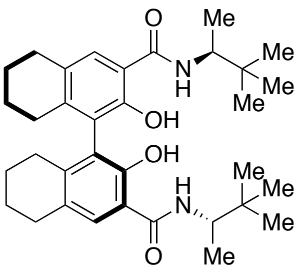
O
Me
N
H
Me
Me
Me
OH
OH
Me
Me
H
N
Me
O
Me

(*S, S*)-4. 9

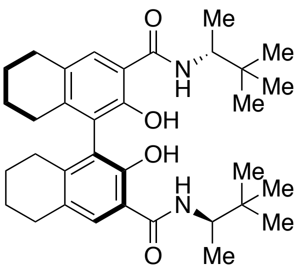
O
Me
N
H
Me
Me
Me
OH
OH
Me
Me
H
N
Me
O
Me

(*S, R*)-4. 9

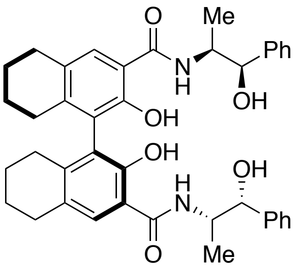
O
Me
Ph
N
H
OH
OH
OH
OH
H
N
Ph
O
Me

(*S, R, S*)-4.16

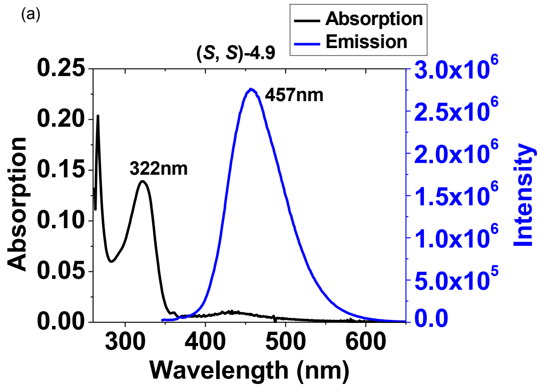

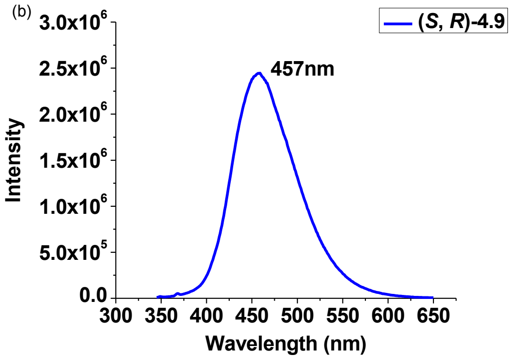

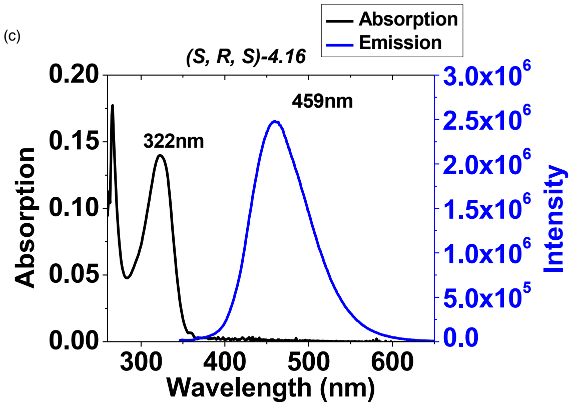

Furthermore, We studied the UV-Vis spectra change upon addition of the amine to (*S*)-**4.2**. A fast deprotonation of (*S*)-**4.2** by the amine to form the intermediate **4.10** as shown in Scheme 4-3 should also occur because of the increased acidity of the phenol hydroxyl groups by the adjacent strongly electron-withdrawing perfluoroalkyl ketone groups. This is supported by the UV-Vis absorption measurement. The samples were prepared by adding (*S*)- or (*R*)-**4.3** (200 equiv, 8.2 μL) directly to (*S*)-**4.2** (0.1 mM in 3 mL DMF) in a 10 × 10 mm cuvette. As shown in Figure 4-13 and 4-14, reaction of (*S*)-**4.2** with (*S*)- or (*R*)-**4.3** led to the immediate appearance of a new and intense broad absorption at a longer wavelength of λ = 432 nm, consistent with the formation of the deprotonated phenolate units in **4.10**. This peak then gradually decreases, accompanied by the growth of absorption at λ = 322 nm, which corresponds to the formation of the arylamide units in the intermediates such as **4.7** and **4.8** since the isolated arylamide product **4.9** gives a predominate absorption at this position.

Figure 4-13. UV-Vis spectra of (*S*)-**4.2** (0.1 mM) with (*S*)-**4.3** (200 eq) recorded over 3 h (a), and absorption changes at λ_{max} = 290, 322, and 432 nm were plotted against time (b). The percentage change of absorption was also plotted (c). Graph (d) shows the linear fitting of percentage absorption change during 1 – 3 h intervals at 322 nm.

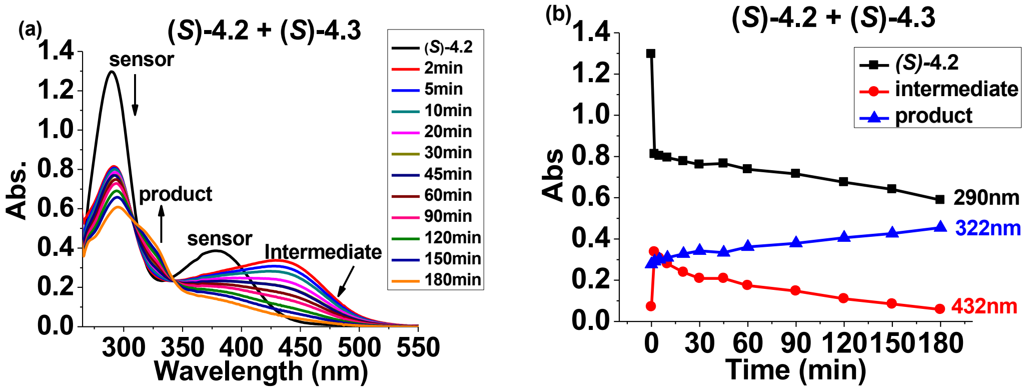

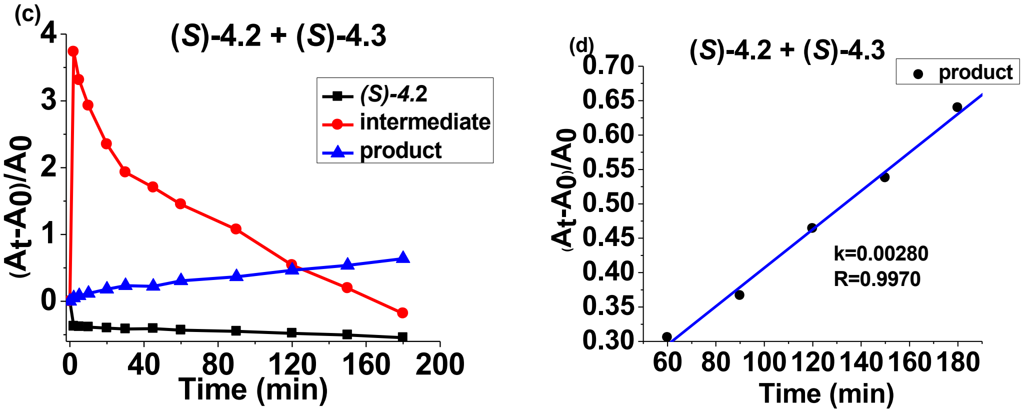

Figure 4-14. UV-Vis spectra of (*S*)-**4.2** (0.1 mM) with (*R*)-**4.3** (200 eq) recorded over 3 h (a), and absorption changes at λ_{max} = 290, 322, and 432 nm were plotted against time (b). The percentage change of absorption was also plotted (c). Graph (d) shows the linear fitting of percentage absorption change during 1-3 h intervals at 322 nm.

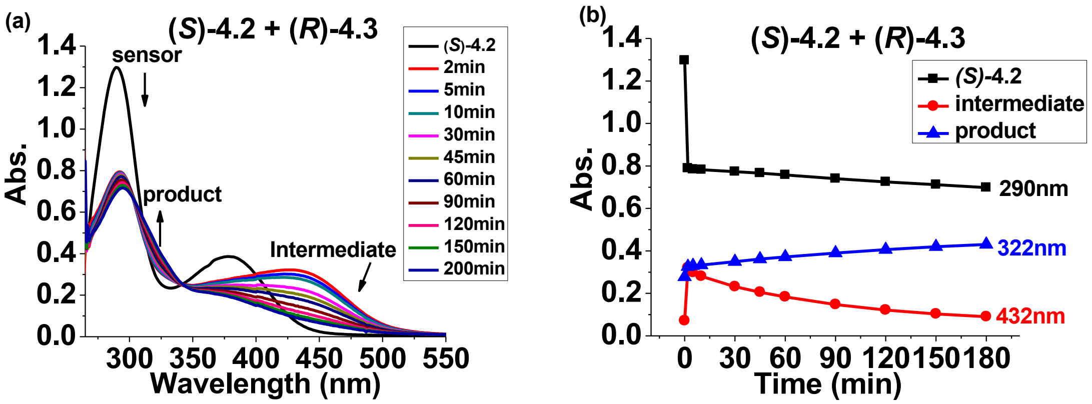

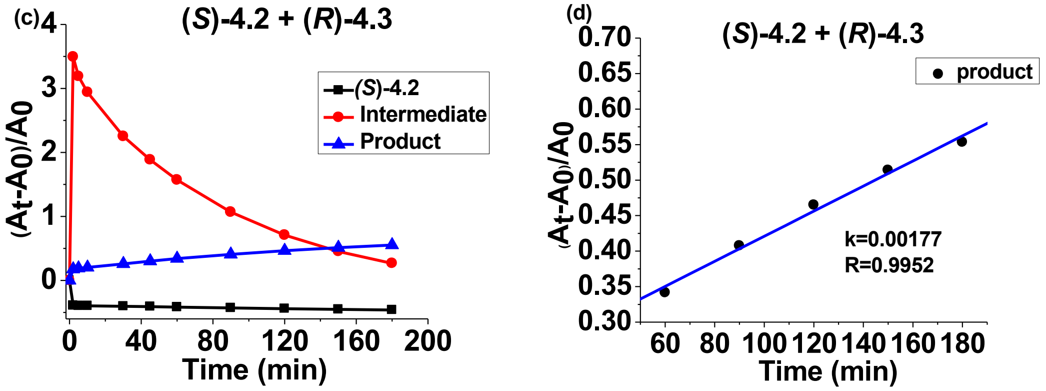

The absorptions at 290, 432, and 322 nm correspond to the starting material, intermediates and final products respectively. In figure (c) of 4-13 and 4-14, the change of absorption at these three wavelengths was plotted against time. The percentage change of absorption was defined as $(A_t-A_0) / A_0$, where A_t is the absorption at various times and A_0 is the absorption at t = 0. Absorption at 290 nm keeps decreasing, corresponding to the consumption of the sensor. Absorption of the intermediates at 432 nm starts to decrease gradually overtime following an immediate increase within the first 2 minutes. Absorption at 322 nm keeps increasing corresponding to the formation of amide products. Although two enantiomers of the amine gave similar reaction pathways, the reaction rate for (*S*)-amine is faster than that of (*R*)-amine as indicated by the slope in the linear regression of absorption change in figure (d) of 4-13 and 4-14. The former one gave a slope of 0.00280, while the latter one gave a slope of 0.00177. This is consistent with the time-dependent fluorescence study in Figure 4-7. Together, it is demonstrated that the observed enantioselective fluorescent response is due to the different reaction rate of (*S*)-**4.2** with the two enantiomers of the chiral amine.

The mechanism depicted in Scheme 4-3 is further supported by our NMR analysis. Compound (*S*)-**4.2** (0.025 mmol) was treated with the amine (*S*)-**4.3** (10 eq) in

DMF (0.4 mL), and the reaction was monitored by using ^{19}F NMR spectroscopy. Acetone-d_6 sealed in a capillary tube was placed in the NMR tube for field locking.

Figure 4-15. ^{19}F NMR spectra recorded in DMF for the reaction of (*S*)-**4.2** with **4.3**.

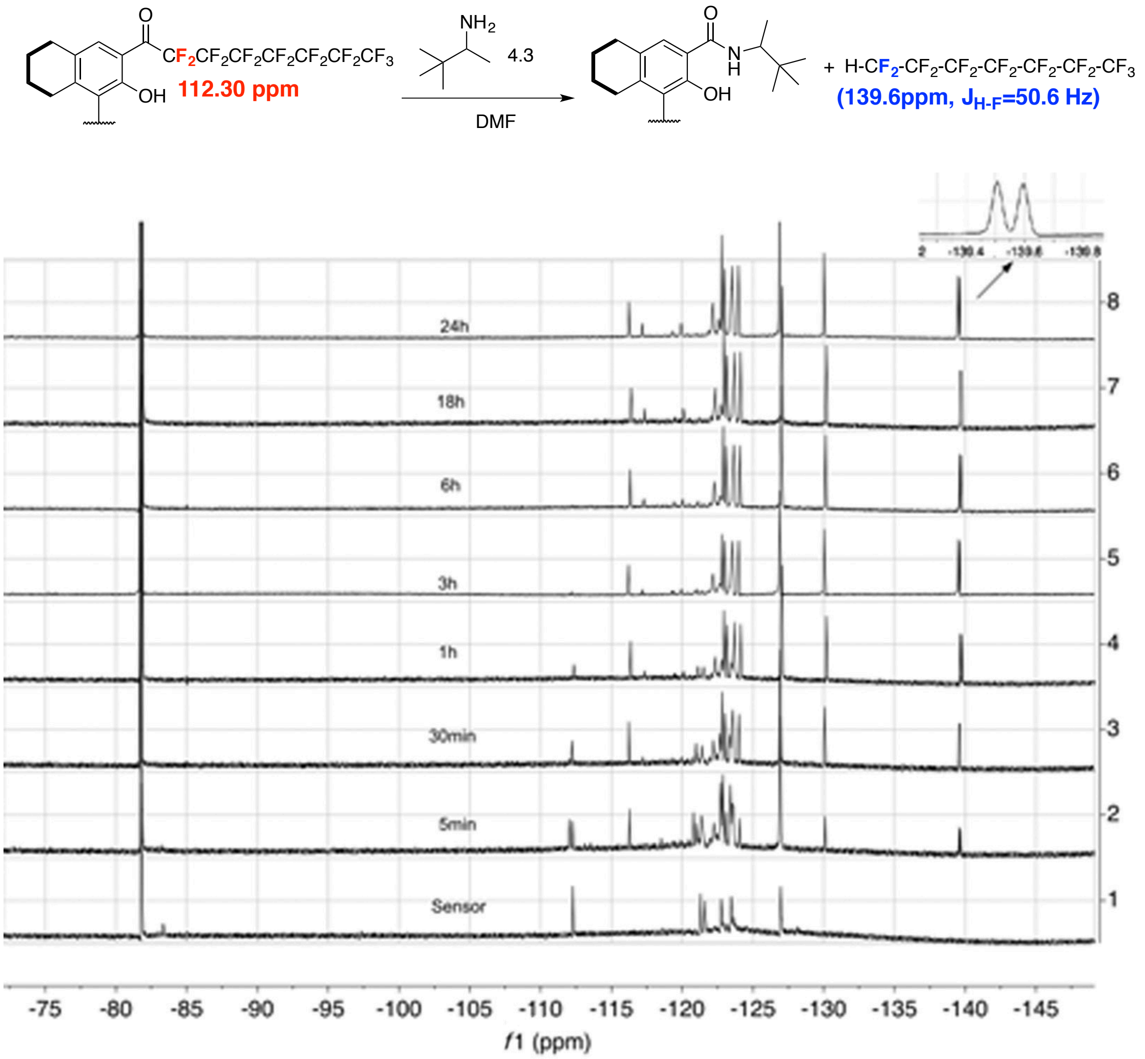

As shown in Figure 4-15, within 5 min, a new peak appeared at δ -112.04 ppm, very close to the original signal at δ -112.30 [-COCF$_2$- of (*S*)-**4.2**]. This new signal could be attributed to the –COCF$_2$- units of the intermediate **4.4** or **4.7** shown in Scheme 4-3. A new signal at δ -139.6 (d, *J* = 50.6 Hz) in the ^{19}F NMR spectra can be assigned to the

HCF_2- unit of 1-H-perfluoroheptane (**4.6**, HR_f). Other signals at δ -130.03, -126.88, -122.80, -123.01 and -81.71 can also be attributed to **4.6** according to the literature.[11] In 3 h, (*S*)-**4.2** was almost completely consumed with the formation of HR_f as the major fluorinated product. The additional signals in the spectra could be attributed to the proposed intermediates such as **4.4**, **4.5**, **4.7** or **4.10**.

The reaction between sensor (*S*)-**4.2** (0.025 mmol) and amine (*S*)-**4.3** (10 eq) in $CDCl_3$ (0.4 mL) was also monitored by NMR spectroscopy. As shown in Figure 4-16, when (*S*)-**4.2** was treated with (*S*)-**4.3** in $CDCl_3$, there was no change in the ^{1}H NMR signals of (*S*)-**4.2** except the disappearance of the acidic OH signal at δ11.28 ppm due to the base-promoted deprotonation and fast proton exchange. No major reaction between (*S*)-**4.2** and the amine was observed. This is consistent with the observed little fluorescent response of (*S*)-**4.2** toward (*S*)-**4.3** in CH_2Cl_2. In ^{19}F NMR, only minor changes were observed without the formation of HR_f (**4.6**). The new and weak signals observed could be attributed to those of the perfluoroalkyl groups of the deprotonated intermediate **4.10**. No further reaction was observed from this deprotonated intermediate in $CDCl_3$.

Figure 4-16. ^{1}H and ^{19}F NMR spectra were recorded in $CDCl_3$ over 22 h. (*S*)-**4.2** (0.025 mmol) and amine (*S*)-**4.3** (10 eq) was mixed in $CDCl_3$ (0.4 mL).

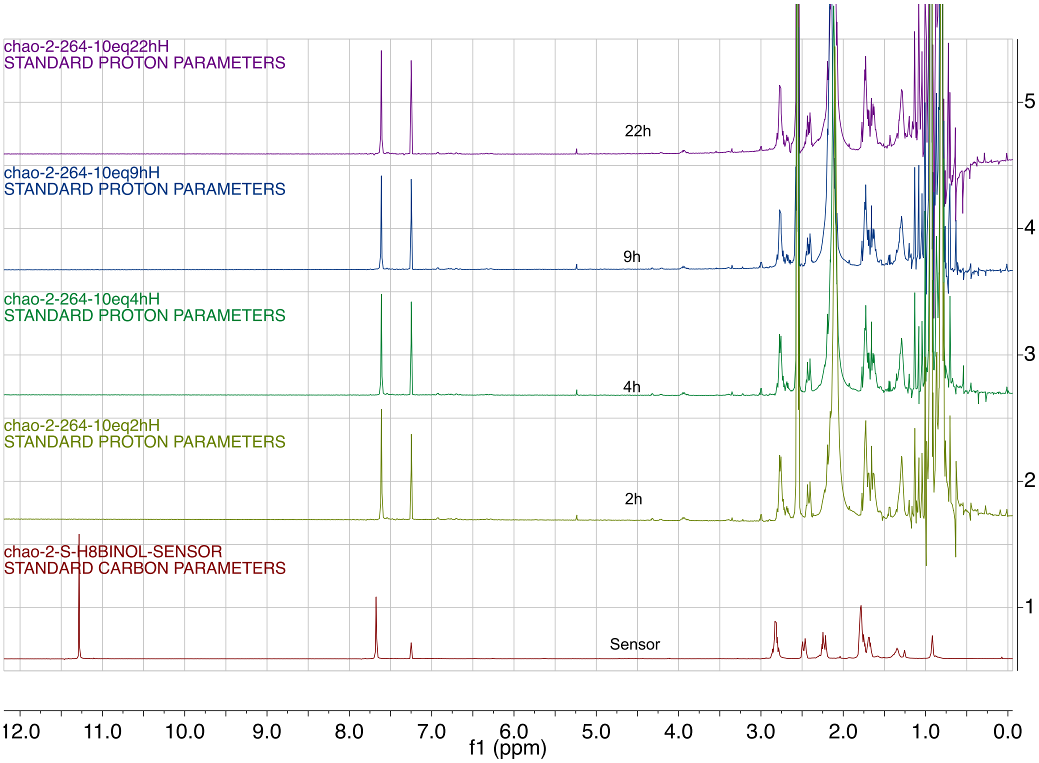
chao-2-264-10eq22hH
STANDARD PROTON PARAMETERS
22h
chao-2-264-10eq9hH
STANDARD PROTON PARAMETERS
9h
chao-2-264-10eq4hH
STANDARD PROTON PARAMETERS
4h
chao-2-264-10eq2hH
STANDARD PROTON PARAMETERS
2h
chao-2-S-H8BINOL-SENSOR
STANDARD CARBON PARAMETERS
Sensor
5
4
3
2
1
12.0
11.0
10.0
9.0
8.0
7.0
6.0
5.0
4.0
3.0
2.0
1.0
0.0
f1 (ppm)

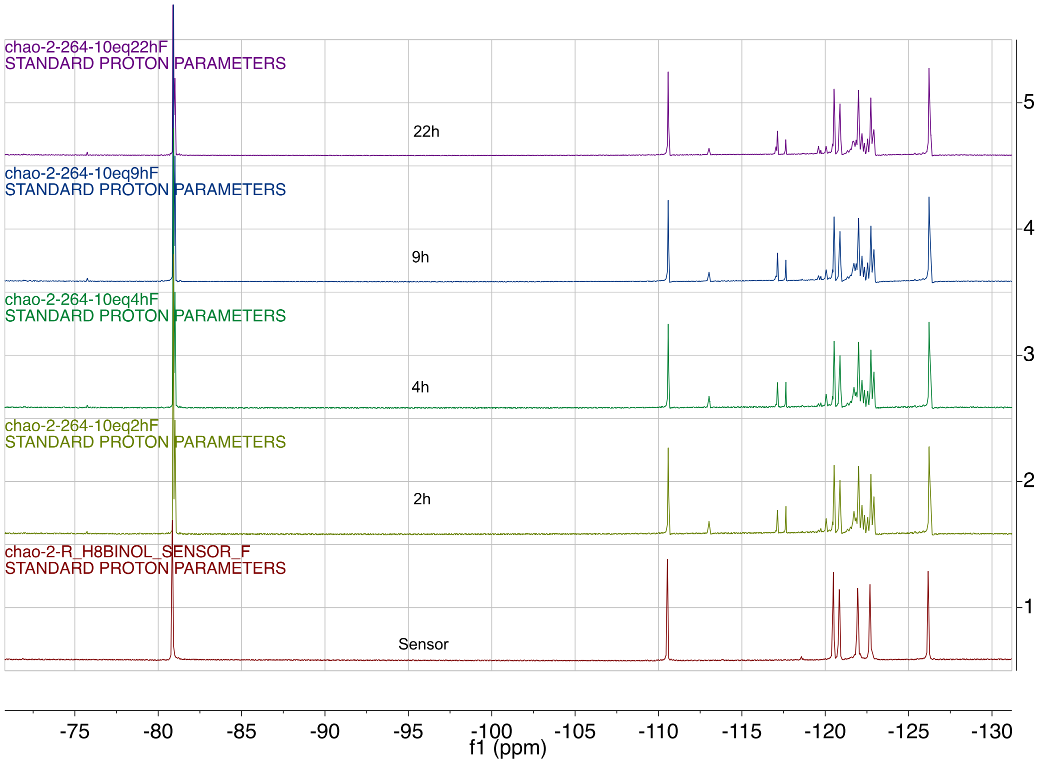
chao-2-264-10eq22hF
STANDARD PROTON PARAMETERS
22h
chao-2-264-10eq9hF
STANDARD PROTON PARAMETERS
9h
chao-2-264-10eq4hF
STANDARD PROTON PARAMETERS
4h
chao-2-264-10eq2hF
STANDARD PROTON PARAMETERS
2h
chao-2-R_H8BINOL_SENSOR_F
STANDARD PROTON PARAMETERS
Sensor
5
4
3
2
1
-75
-80
-85
-90
-95
-100
-105
-110
-115
-120
-125
-130
f1 (ppm)

4.2.6. Fluorescence recognition of unfunctional amines

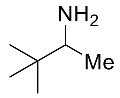

4.3

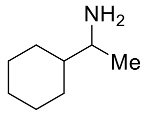

4.11

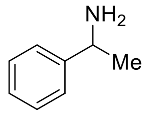

4.12

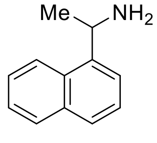

4.13

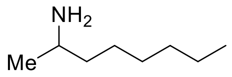

4.14

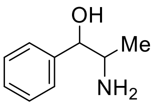

4.15

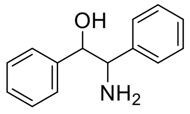

4.17

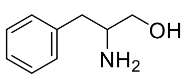

4.18

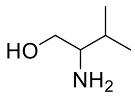

4.19

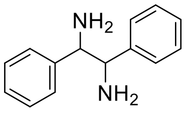

4. 20

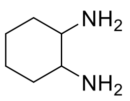

4.21

We have studied the fluorescent response of (*S*)-**4.2** in the presence of additional unfunctionalized chiral amines. Under the same conditions used for the interaction with **4.3**, enantioselective fluorescent enhancements were observed for the interaction of (*S*)-**4.2** with these amines. The observed *ef* values are given in Figure 4-17. It shows that (*S*)-**4.2** exhibits high enantioselectivity in the fluorescent recognition of compounds **4.3** and **4.13** that contain bulky substituents adjacent to the chiral center, medium enantioselectivity for compounds **4.11** and **4.12** that contain medium sized substituents, and low enantioselective for compound **4.14** that contains a less sterically hindered primary alkyl group adjacent to the chiral center. The fluorescence spectra were summarized as shown from figure 4-18 to 4-24. For all of them, the spectra were taken in DMF/THF (1:9 v/v) with an excitation wavelength λ_{ex} of 332 nm and slit of 2/2nm. In enantiomeric excess correlation, ee is still defined as ee = ([*S*] - [*R*]) / ([*S*] + [*R*]),

Figure 4-17. The observed *ef* values when (*S*)-**4.2** (0.01 mM) was interacted with the (*R*)- and (*S*)-enantiomers of various amine (3.0 mM).

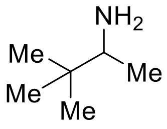

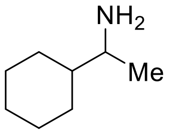

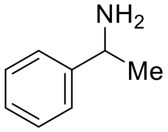

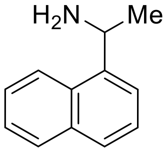

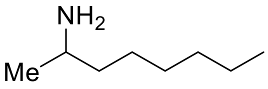

	4.3	**4.11**	**4.12**	**4.13**	**4.14**
ef:	5.0	2.1	2.5	4.9	1.2

Figure 4-18. Fluorescence spectra of (*S*)-**4.2** (0.01 mM) with amine **4.11** from 60 to 300 eq, and the fluorescence intensity at λ = 458 nm was plotted against the equivalents.

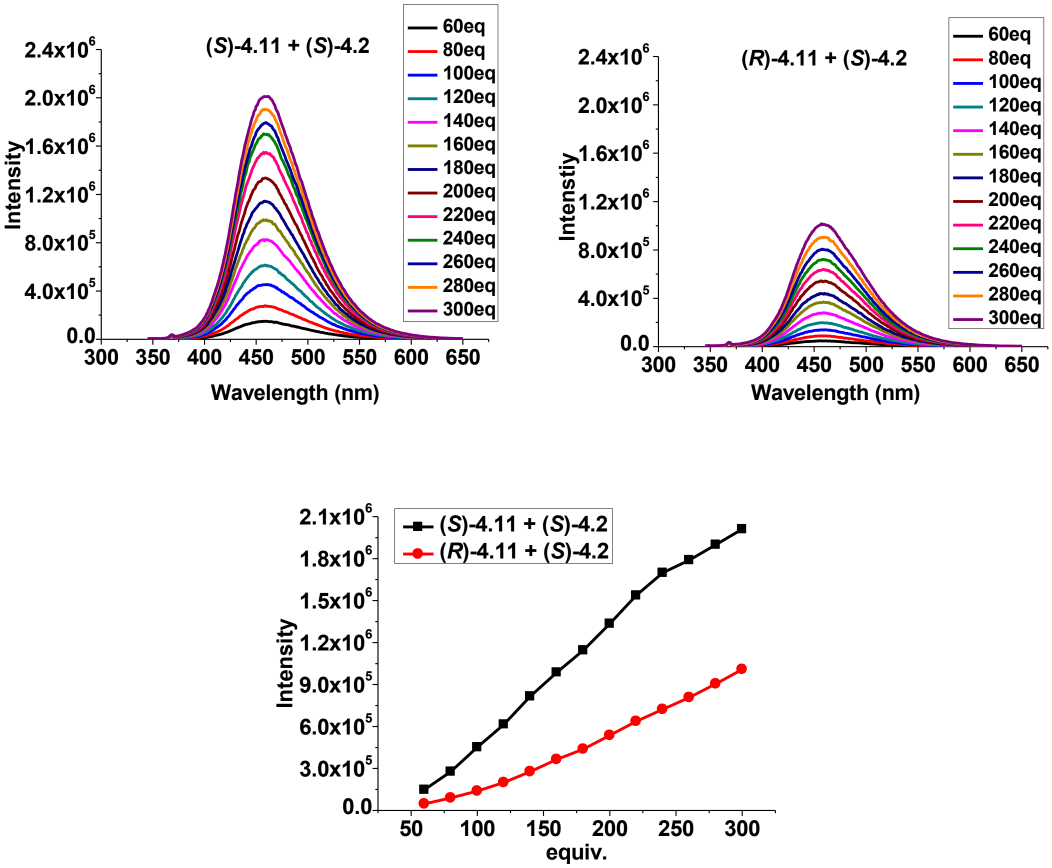

Figure 4-19. Enantiomeric excess correlation for the fluorescent responses of (*S*)-**4.2** (0.01 mM) toward **4.11** (200 eq). Fluorescence intensity at λ = 458 nm was plotted against the *ee* values, and a 1st order linear fitting was applied.

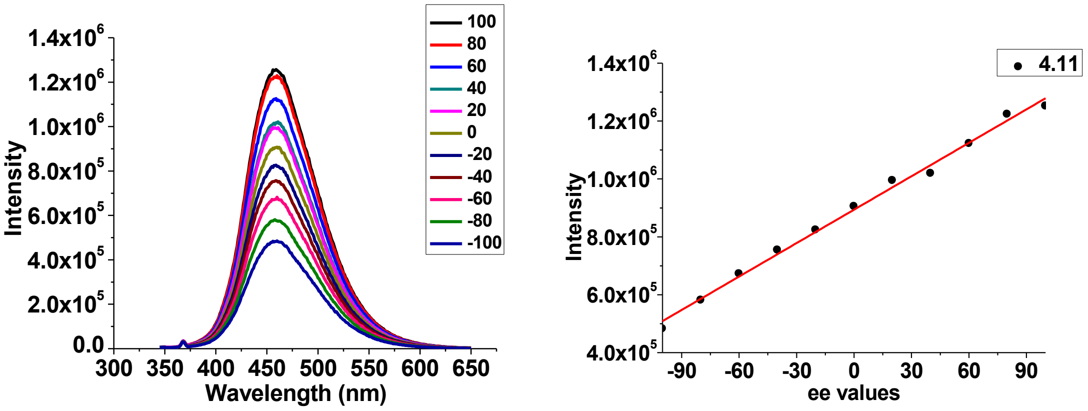

Figure 4-20. Fluorescence spectra of (*S*)-**4.2** (0.01 mM) with amine **12** from 60 to 300 equiv., and the fluorescence intensity at λ = 458 nm was plotted against the amine equivalents.

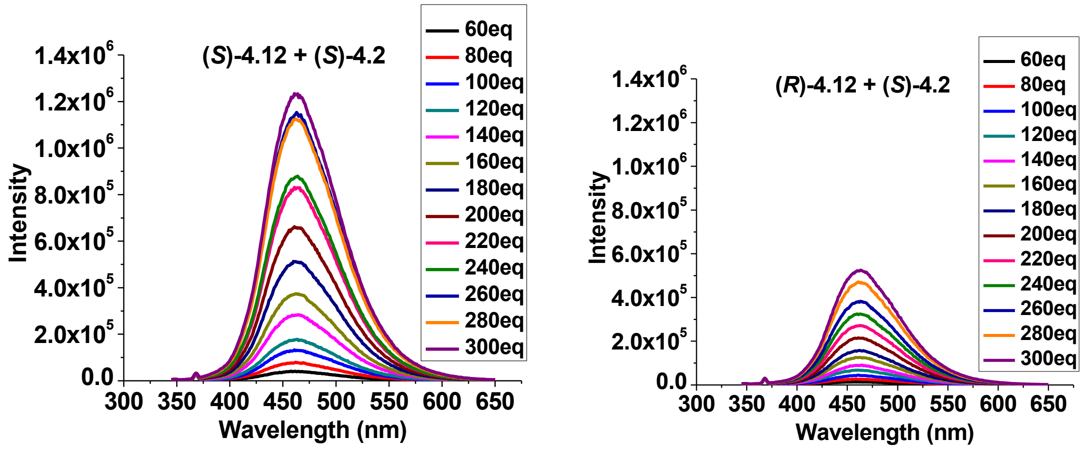

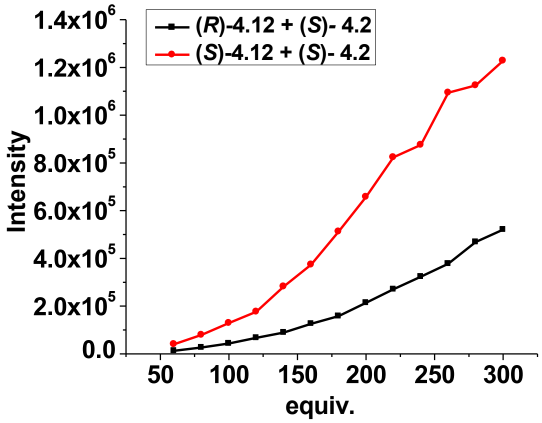

Figure 4-21. Enantiomeric excess correlation of the fluorescence responses of (*S*)-**4.2** (0.01 mM) toward **4.12** (180 eq). Fluorescence intensity at λ = 458 nm was plotted against *ee* values, and a 1st order linear fitting was applied.

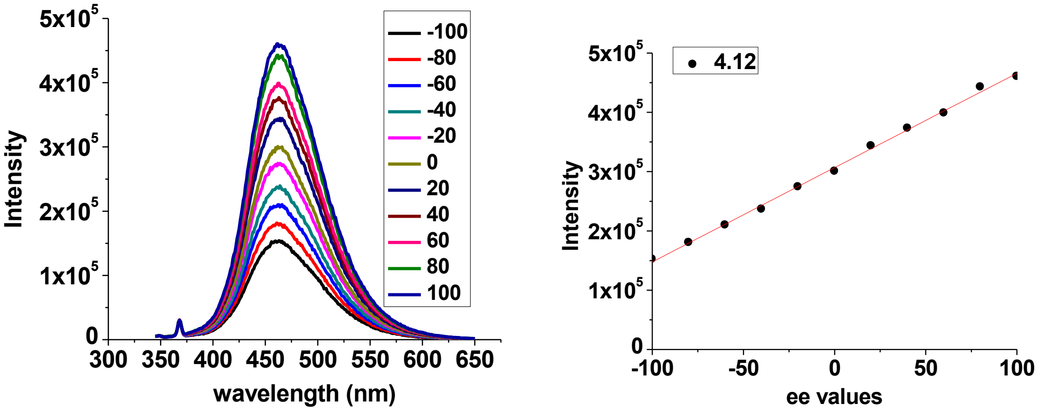

Figure 4-22. Fluorescence spectra of (*S*)-**4.2** (0.01 mM) with amine **4.13** from 60 to 300 eq, and the fluorescence intensity at λ = 463 nm was plotted against the equivalents.

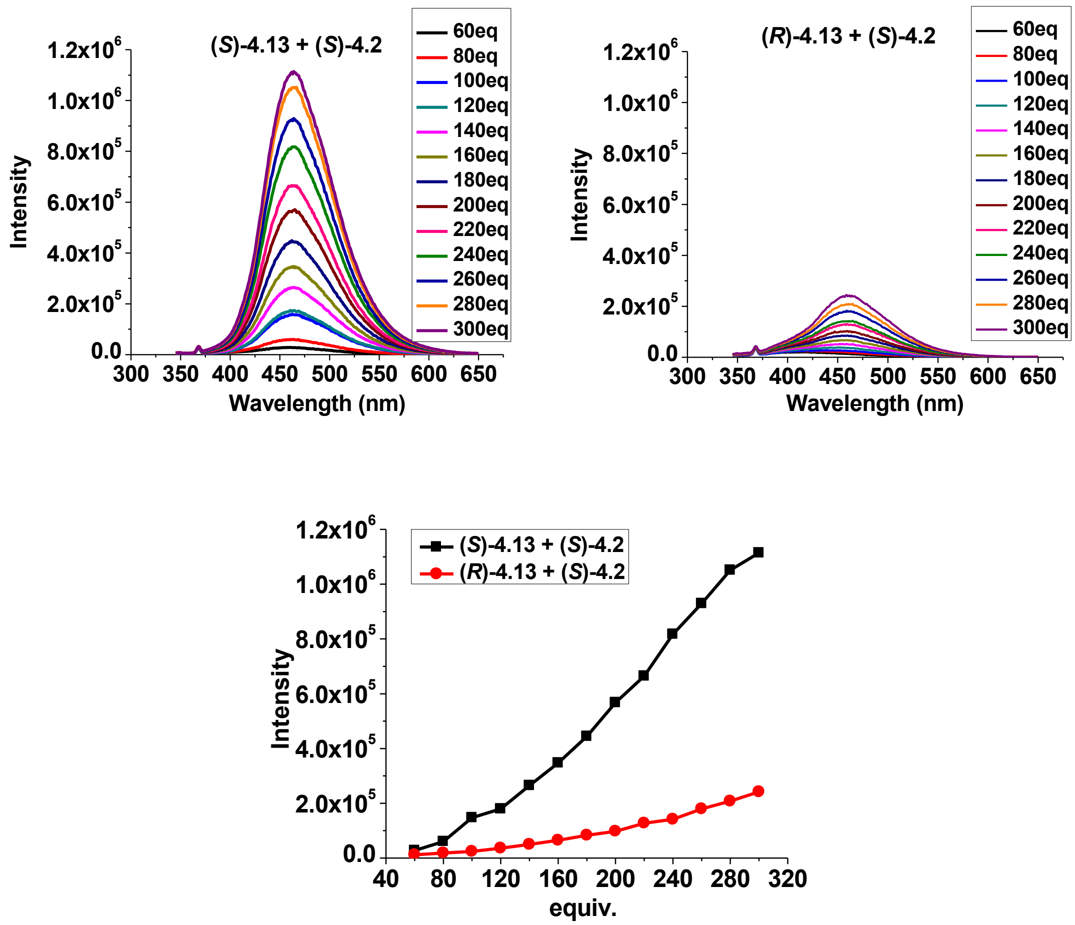

Figure 4-23. Enantiomeric excess correlation for the fluorescence responses of (*S*)-**4.2** (0.01 mM) toward **4.13** (200 eq). Fluorescence intensity at λ = 463 nm was plotted against the *ee* values, and a 1st order linear fitting was applied.

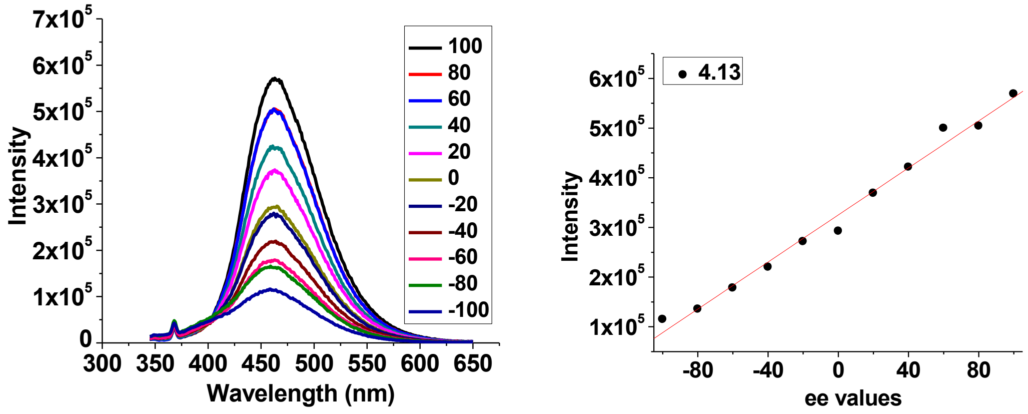

Figure 4-24. Fluorescence spectra of (*S*)-**4.2** (0.01 mM) with amine **4.14** from 60 to 300 eq, and fluorescence intensity at λ = 458 nm was plotted against the equivalents.

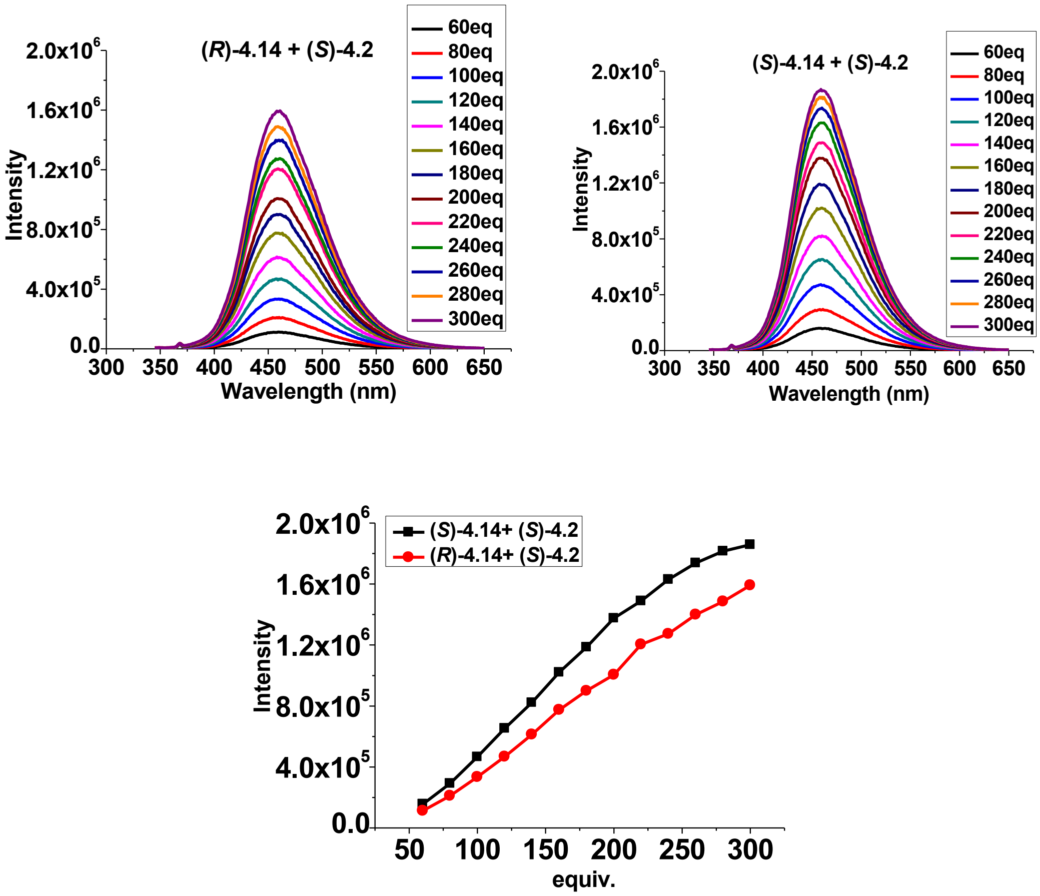

4.2.7. Fluorescence recognition of functional amines

Compound (*S*)-**4.2** is also reacted with the functionalized chiral amines in DMF. For example, when (*S*)-**4.2** was reacted with the amino alcohol (1*R*, 2*S*)-**4.15** in DMF at room temperature, the corresponding amide product (*S*, *R*, *S*)-**4.16** was isolated in 77 % yield. Under the same conditions, the diastereomer (*S*, *S*, *R*)-**4.16** was isolated from the reaction of (*S*)-**4.2** with (1*S*, 2*R*)-**4.15** in 70% yield. Enantioselective fluorescence enhancements of (*S*)-**4.2** toward these substrates in DMF were observed. Similar to the reaction of **4.3** with (*S*)-**4.2**, the reaction of (*S*)-**4.2** with these functional chiral amines can be quenched by dilution with THF to give stable fluorescent response. Fluorescence spectra were recorded after the reactions were conducted in DMF for 1 h (3 h for compounds **4.17** and **4.20**) and quenched with excess THF to give stable fluorescent response. The fluorescent responses of (*S*)-**4.2** toward a number of functional chiral amines as listed in Figure 4-25 have been investigated. It demonstrates that (*S*)-**4.2** is also a very good fluorescent sensor for the enantioselective recognition of functional chiral amines. The *ef* values of various functional chiral amines in the presence of (*S*)-**4.2** can reach up to 12.1 in the case of **4.17**.

Figure 4- 25. The observed *ef* values when (*S*)-**4.2** (0.01 mM) was interacted with the (*R*)- and (*S*)-enantiomers of various functional chiral amines at 1 mM (or 3 mM for **4.17** and **4.20**).

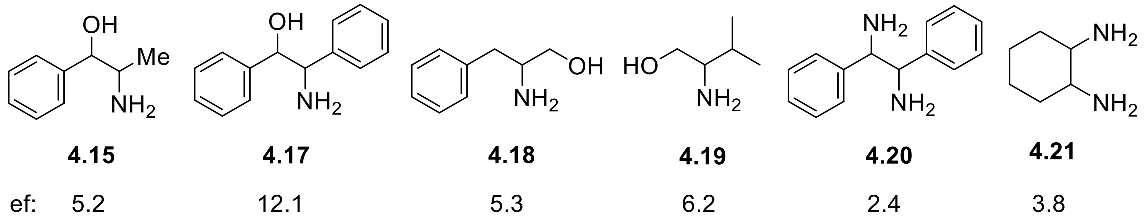

Figure 4-26 to 4-34 gave the fluorescence spectra for the highly enantioselective recognition of these functional chiral amine by using (*S*)-**4.2**. For all of them, the spectra were taken in DMF / THF (1 : 9 v / v) with an excitation wavelength λ_{ex} of 332 nm. We also measured the fluorescent responses of (*S*)-**4.2** toward amino alcohols at various enantiomeric compositions and plotted the fluorescence intensity against *ee* values.

Thus, using the plot, the enantiomeric composition of functional amines can also be determined by fluorescence measurement.

Figure 4-26. Fluorescence spectra of (*S*)-**4.2** (0.01 mM) with (*S*, *S*)-**4.17** (a) and (*R*, *R*)-**4.17** (b). Fluorescence intensity at λ = 463 nm versus the amino alcohol concentration (c), and ee correlation of **4.17** (3.0 mM) (d) were plotted separately (slit = 3/3 nm).

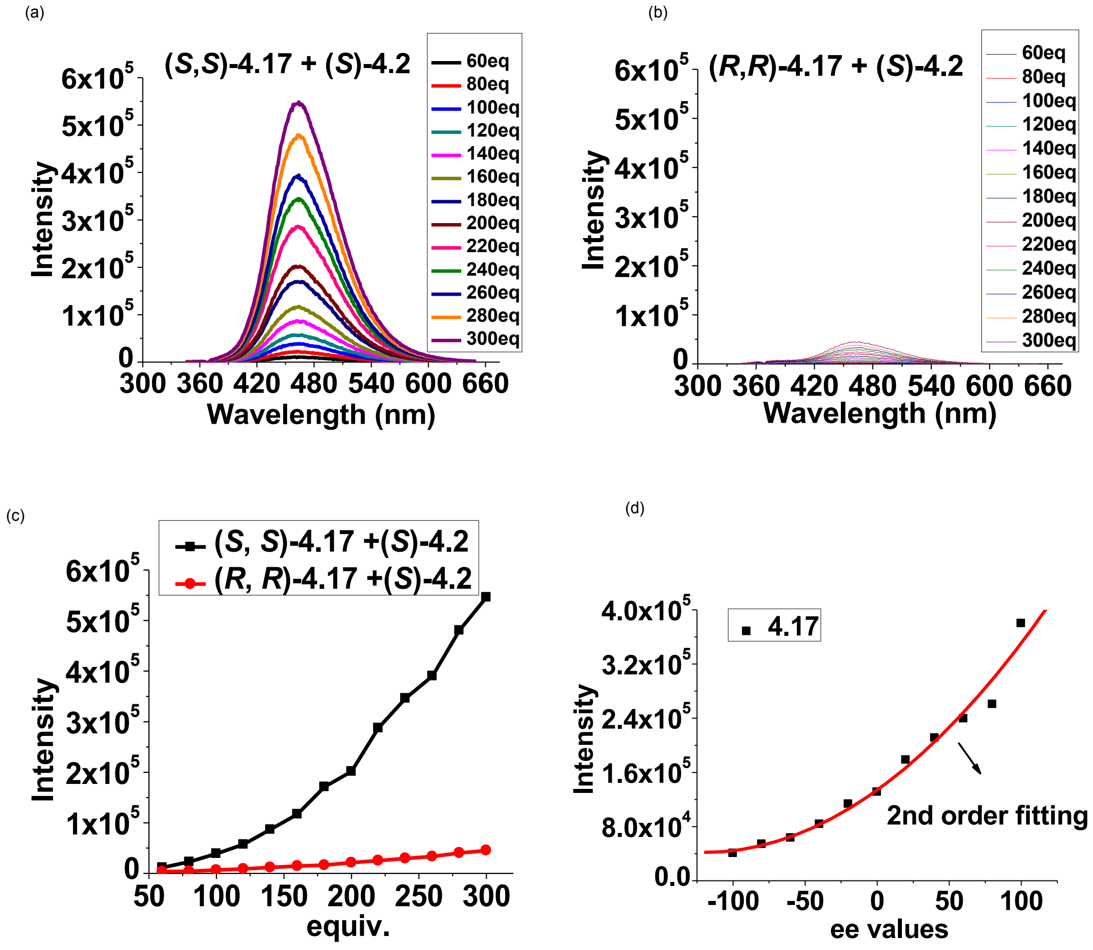

Figure 4-27. Fluorescence spectra of (*S*)-**4.2** (0.01 mM) with amino alcohol **4.15** from 20 to 200 eq, and fluorescence intensity at λ = 460 nm was plotted against the equivalence (slit=2/2 nm).

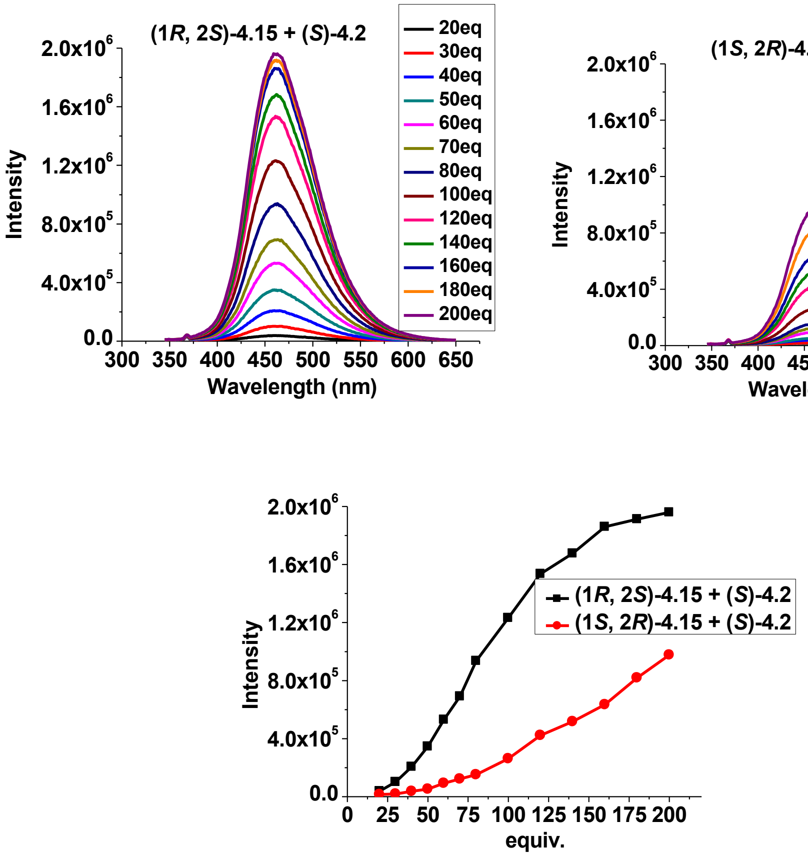

Figure 4-28. Enantiomeric excess correlation of fluorescence spectra for (*S*)-**4.2** (0.01 mM) and **4.15** (50 eq). Fluorescence intensity at λ = 460 nm was plotted against the *ee* values, and a 2nd order nonlinear fitting was applied (slit = 2 / 2 nm).

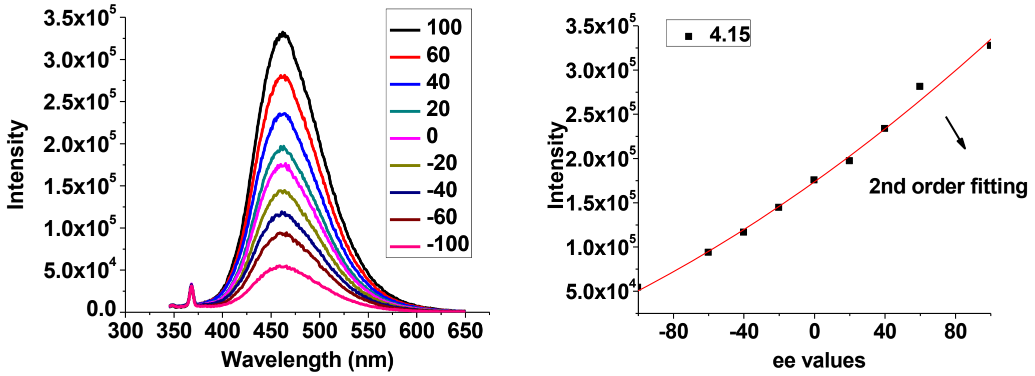

Figure 4-29. Fluorescence spectra of (*S*)-**4.2** (0.01 mM) with amino alcohol **4.18** from 20 to 200 eq, and the fluorescence intensity at λ = 460 nm was plotted against the equivalence (slit = 2 / 2 nm).

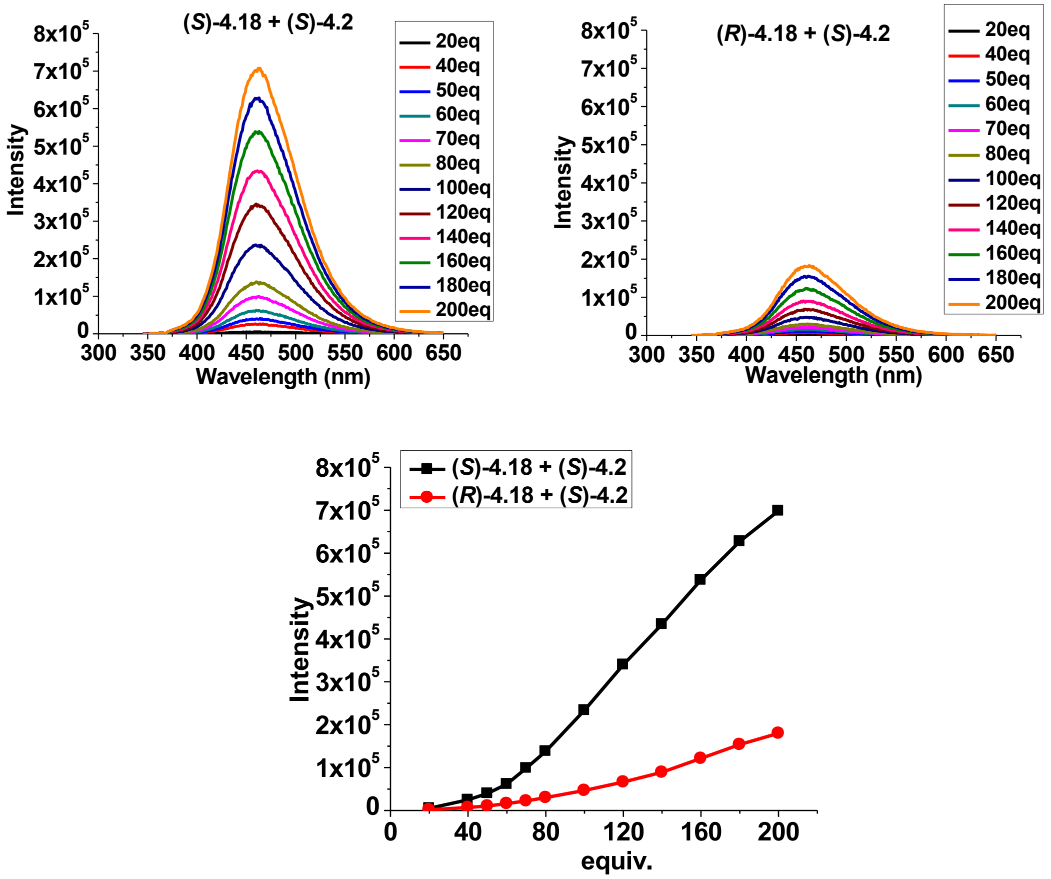

Figure 4-30. Enantiomeric excess correlation of fluorescence spectra for (*S*)-**4.2** (0.01 mM) and **4.18** (100 eq). Fluorescence intensity at λ = 460 nm was plotted against the *ee* values, and a 2nd order nonlinear fitting was applied (slit = 2 / 2 nm).

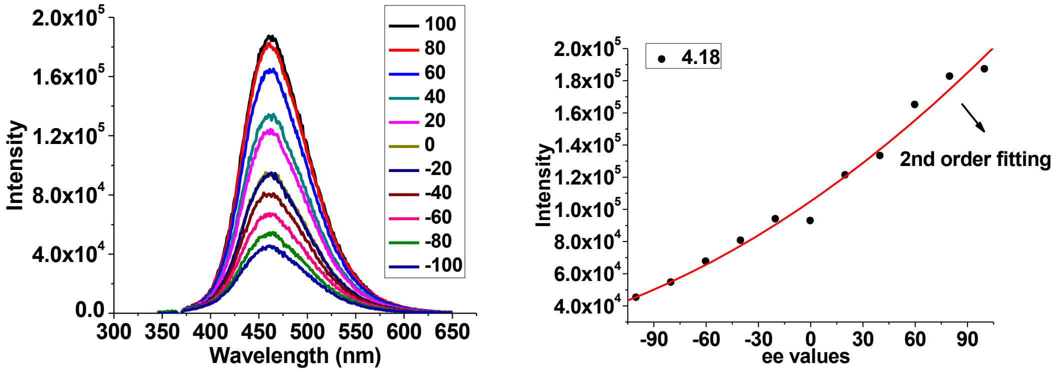

Figure 4-31. Fluorescence spectra of (*S*)-**4.2** (0.01 mM) with **4.19** from 20 to 200 eq, and fluorescence intensity at λ = 460 nm was plotted against the equivalence (slit = 2 / 2 nm).

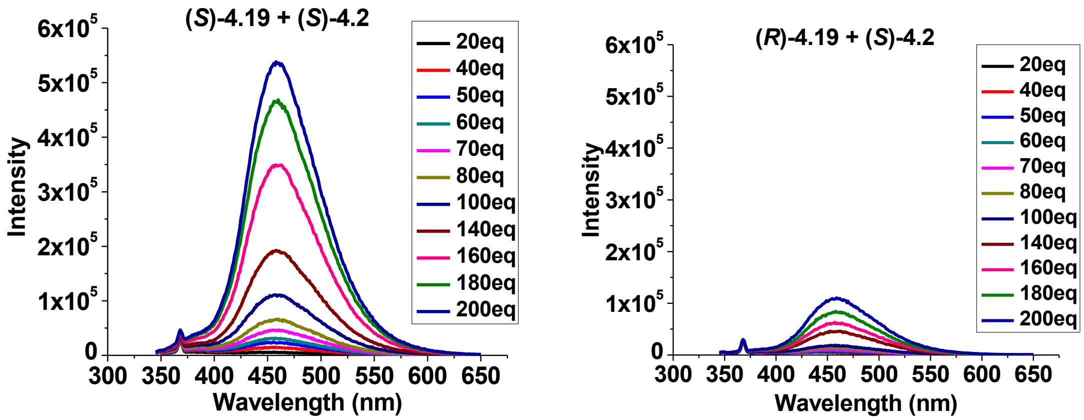

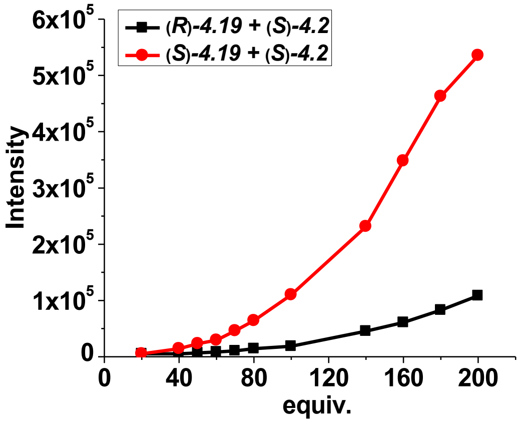

Different from other amines, **4.20** results in two emission peaks at 384 nm and 462 nm (Figure 4-32). While the emission at 384 nm is identical for two enantiomers and can be used to determine their total concentrations, emission at 462 nm is enantioselective and can be used to determine the enantiomeric excess of two enantiomers.

Figure 4- 32. Fluorescence spectra of (*S*)-**4.2** (0.01 mM) with diamine **4.20** from 60 to 300 eq recorded 3 h after reaction, and fluorescence intensity at λ = 384 and 462 nm was plotted against the equivalents. The intensity ratio (I_{462} / I_{384}) was also plotted against the equivalent (slit = 3 / 3 nm).

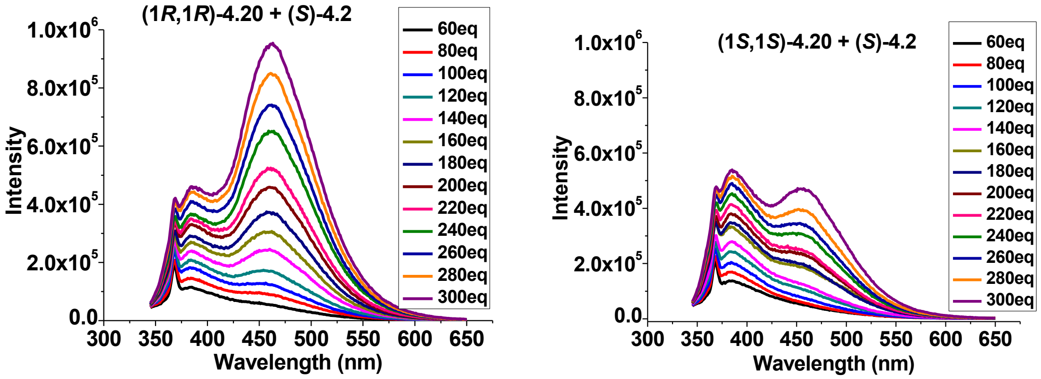

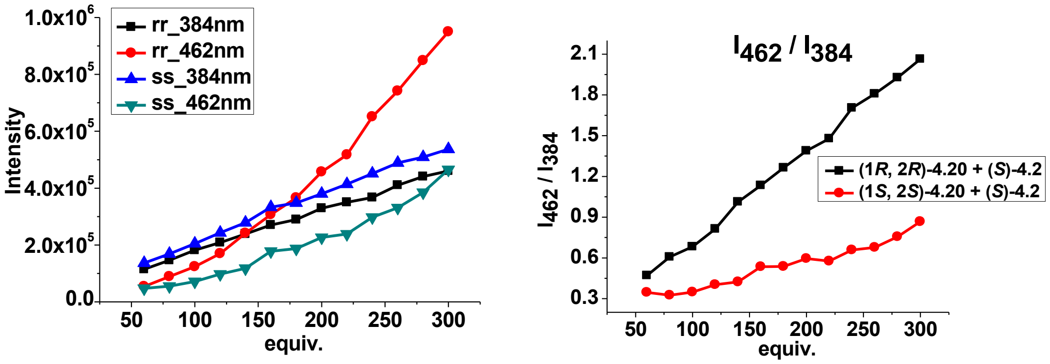

Figure 4-33. Fluorescence spectra of (*S*)-**4.2** (0.01mM) with diamine **21** from 20 to 200eq, and fluorescence intensity at λ = 460 nm was plotted against the equivalence (slit = 2/2 nm).

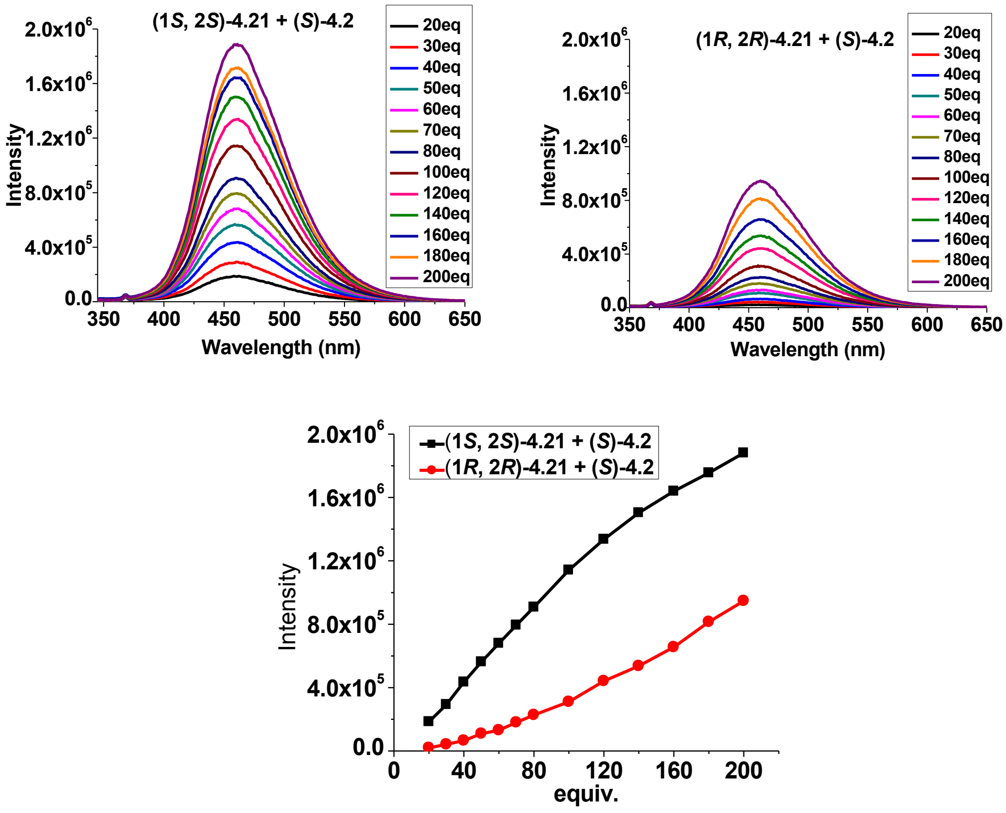

Figure 4-34. Enantiomeric excess correlation of fluorescence spectra for (*S*)-**4.2** (0.01 mM) and **4.21** (50 eq). Fluorescence intensity at λ= 460 nm was plotted against the *ee* values, and a 1st order linear fitting was applied (slit = 2 / 2 nm).

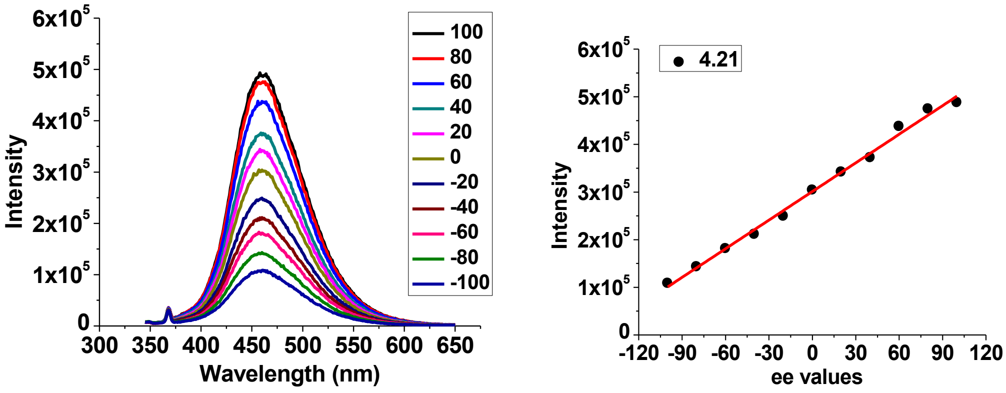

4.2.8. Fluorescence response of BINOL-based sensor to amines

We examined the fluorescent response of the BINOL-based perfluoroalkyl ketone (*S*)-**4.1** toward the chiral amine (*R*)- and (*S*)-**4.3** in various solvents including FC-72, DMF, CH_2Cl_2, methanol, THF and hexane, as shown in Figure 4-35. In general, the fluorescence intensities of (*S*)-**4.1** upon treatment with both enantiomers of this unfunctionalized amine remained to be very weak in each solvent tested. In methanol, (*S*)-**4.1** gave strong background fluorescence, possibly due to the formation of hemiacetal. This fluorescence can be quenched with the addition of amine without enantioselectivity, through the formation of stronger intermolecular hydrogen bonding with the sensor.

Figure 4-35. Fluorescence spectra of (*S*)-**4.1** (0.1 mM) in the presence of (*R*)-**4.3** or (*S*)-**4.3** (5 mM) in various solvents: FC-72, DMF, DCM, methanol, THF and hexane (λ_{ex}= 332 nm, slit = 2/2 nm).

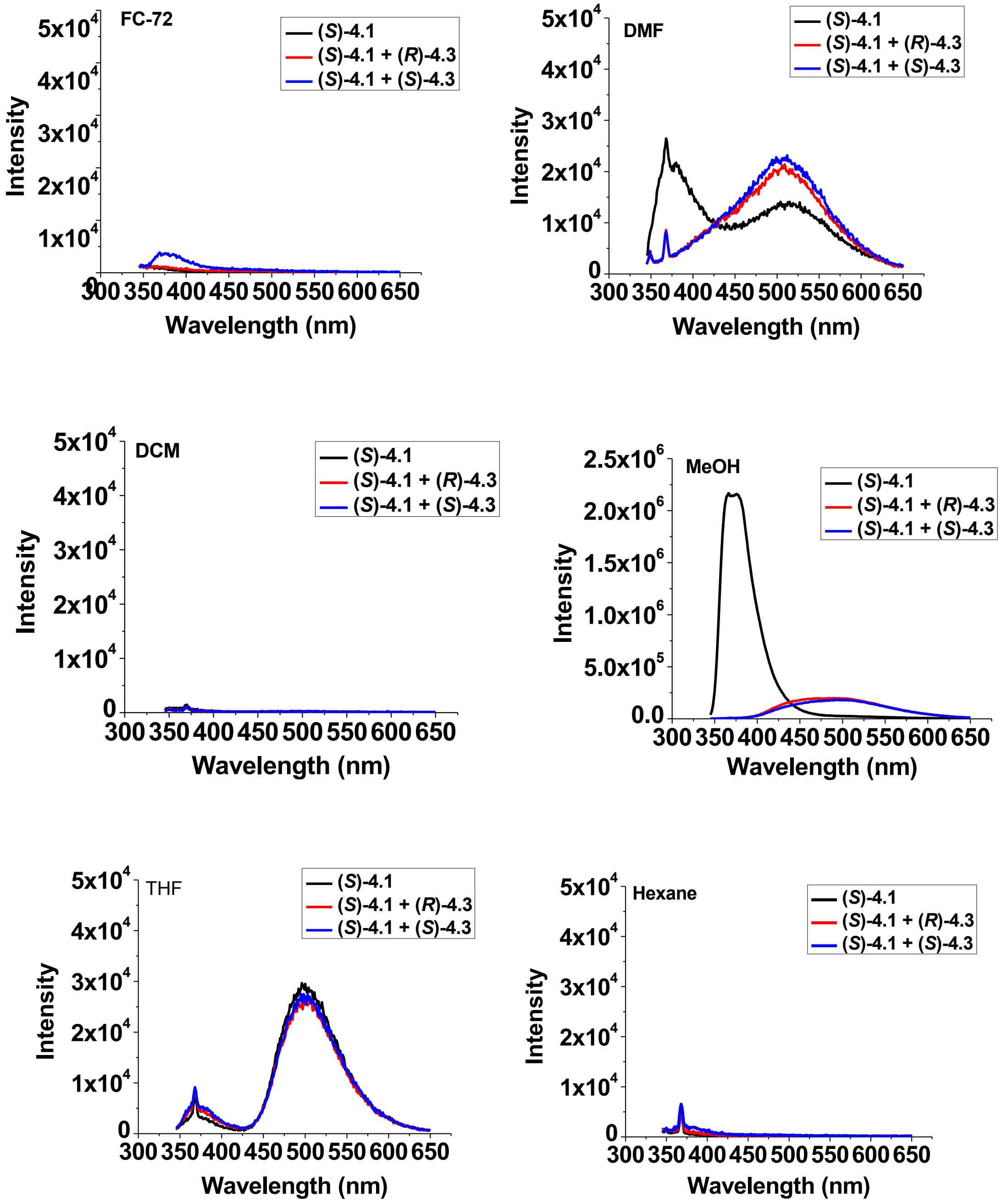

In DMF, (*S*)-**4.1** gave small fluorescence enhancement at 501 nm when treated with amine **4.3**, which was studied in detail over 10 hours as shown in figure 4-36. The fluorescence intensity is much lower compared with the use of (*S*)-**4.2**. We plotted the fluorescence intensity at 501 nm against the time, and it revealed that the *ef* value was only 1.1, which represented very little enantioselectivity.

Figure 4-36. Fluorescence spectra of (*S*)-**4.1** (0.1 mM) with (*R*)-**4.3** or (*S*)-**4.3** (5 mM) in DMF recorded over 10 h, and fluorescence intensity at λ = 501 nm was plotted against the reaction time (λ_{ex} = 390 nm, slit = 2 / 2 nm).

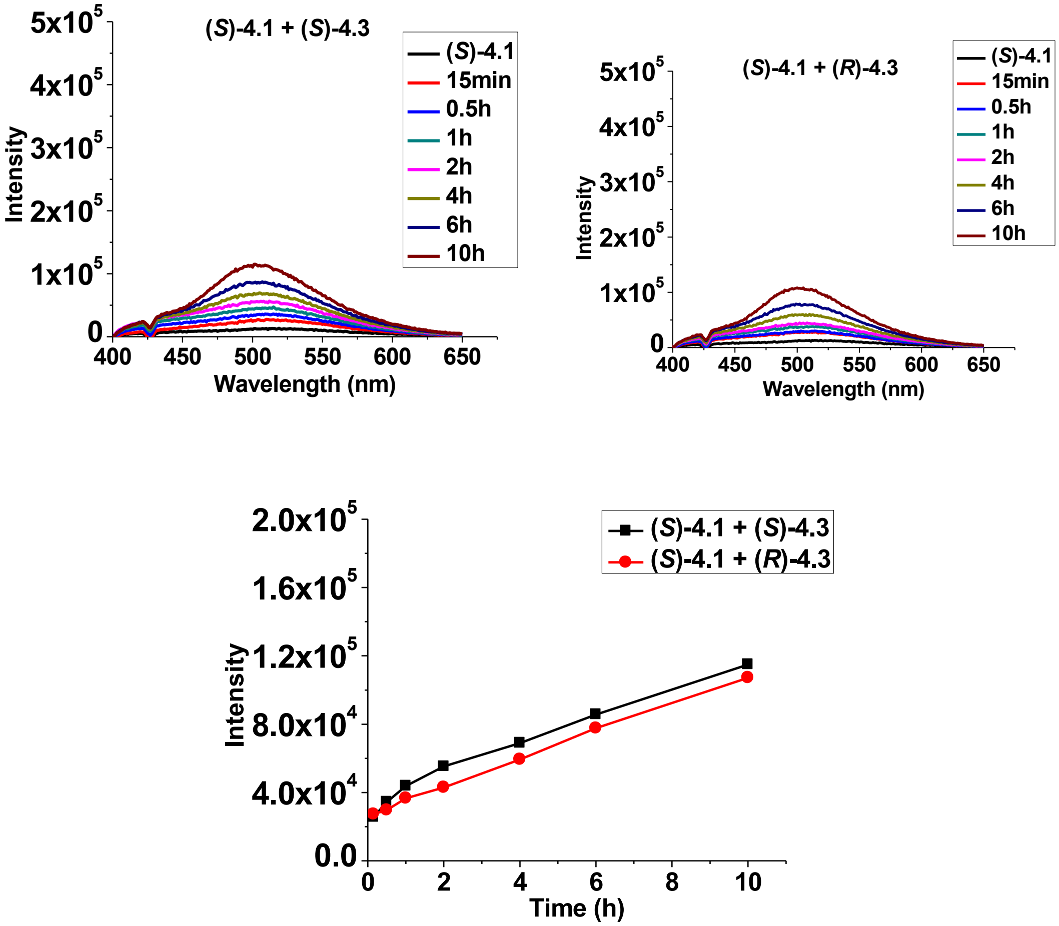

We also treated (*S*)-**4.1** with functional amine **4.15**, which is more active than **4.3**. However, the fluorescence enhancement was still very weak and almost no enantioselectivity was observed, as shown in figure 4-37. In comparison with the use of (*S*)-**4.2**, (*S*)-**4.1** gave much weaker fluorescence intensity and almost no enantioselectivity toward both nonfunctionalized and functionalized amines.

Figure 4-37. Fluorescence spectra of (*S*)-**4.1** (0.1 mM) with (1*R*, 2*S*)-**4.15** or (1*S*, 2*R*)-**4.15** (5 mM) in DMF recorded over 10 h, and fluorescence intensity at λ = 501 nm was plotted against the reaction time (λ_{ex} = 390 nm, slit = 2 / 2 nm).

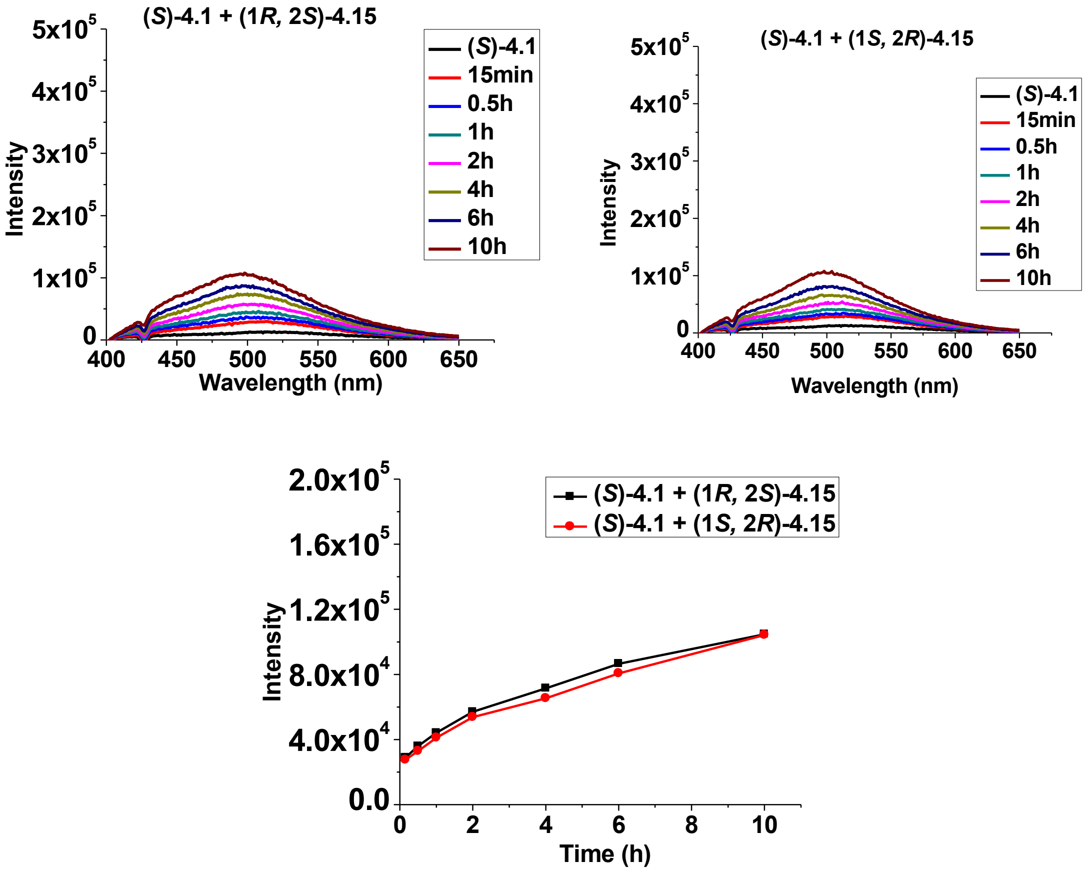

Figure 4- 38. UV-Vis and fluorescence of (*S*, *R*, *S*)-**4.22**.

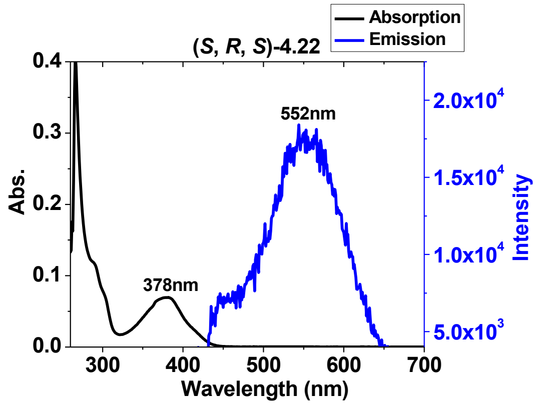

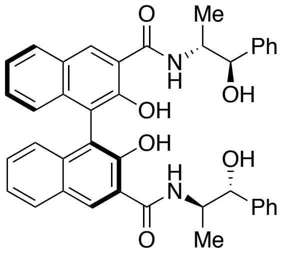

(*S*, *R*, *S*)-4.22

Product from (*S*)-4.1 with (1*R*, 2*S*)-4.15

It is found that the corresponding amide product (*S*, *R*, *S*)-**4.22** was also generated from the reaction of (*S*)-**4.1** with (1*R*, 2*S*)-**4.22** in close to quantitative yield. However, the isolated (*S*, *R*, *S*)-**4.22** gave only very weak fluorescence at 552 nm. Its fluorescence intensity is only about 1% of that of **4.9** or **4.16** at the same concentration excited at their maximum absorption wavelength. The molar attenuation coefficients at λ_{max} = 322 nm is 6.93×10^3 M^{-1} cm^{-1} for **4.22**, much smaller than that of **4.9** or **4.16** as well. One possible explanation for the much weaker emission of the amide product from the BINOL derivative (*S*)-**4.1** than that from the H_8BINOL derivative (*S*)-**4.2** might be the more restricted rotation around the 1, 1'-bond of the H_8BINOL-based amide due to the increased size of the sp^3 hybridized carbons in the partially hydrogenated naphthyl rings. Thus, the H_8BINOL-based compound (*S*)-**4.2** in DMF has greatly improved the enantioselective fluorescent enhancement of (*S*)-**4.1** toward the chiral amines.

4.2.9 Achiral fluorinated ketones for amine sensing

As an extension of the discoveries described above, we systematically studied the fluorescence performance of various kinds of fluorinated ketone sensors for the recognition of molecules bearing amino groups, especially amino acids.

Scheme 4- 4. Synthesis of achiral sensors **4.23** - **4.26**.

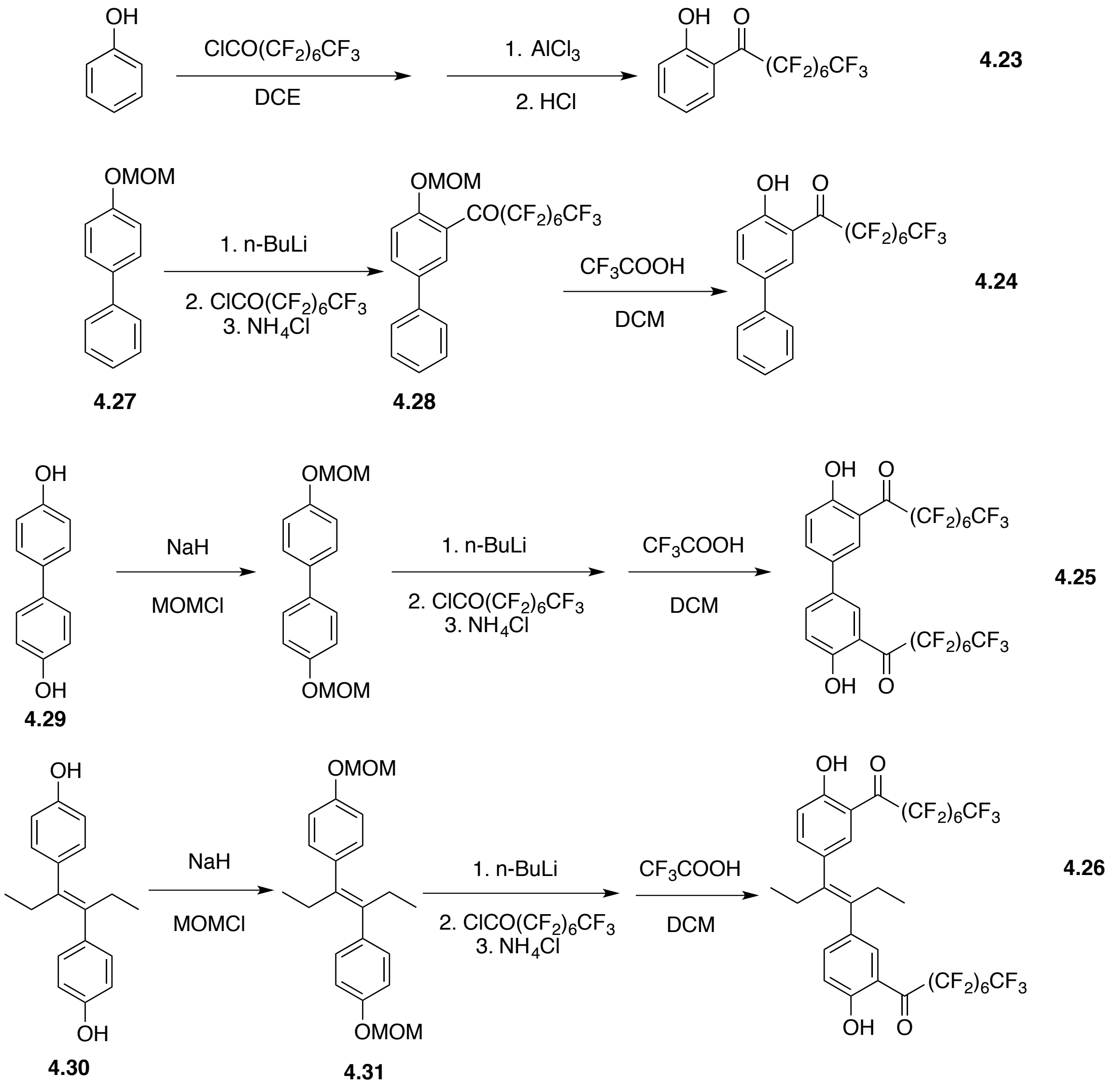
OH
ClCO(CF2)6CF3
DCE
1. AlCl3
2. HCl
OH O
(CF2)6CF3
4.23
OMOM
1. n-BuLi
2. ClCO(CF2)6CF3
3. NH4Cl
OMOM
CO(CF2)6CF3
CF3COOH
DCM
OH O
(CF2)6CF3
4.24
4.27
4.28
OH
NaH
MOMCl
OMOM
1. n-BuLi
2. ClCO(CF2)6CF3
3. NH4Cl
CF3COOH
DCM
OH O
(CF2)6CF3
4.25
(CF2)6CF3
OH O
OH
OMOM
4.29
OH
NaH
MOMCl
OMOM
1. n-BuLi
2. ClCO(CF2)6CF3
3. NH4Cl
CF3COOH
DCM
OH O
(CF2)6CF3
4.26
(CF2)6CF3
OH O
OH
OMOM
4.30
4.31

The synthetic routes of achiral sensors are shown in Scheme 4-4. In general, the desired products are obtained by a successive protection, orthometalation and deprotection process, except for **4.23** that is obtained through Fries rearrangement. We want to use **4.23-4.26** to test the tunability of emission wavelength when the sensors interact with amines through amide formation. As shown in Figure 4-39, these sensors are non- or very weakly emissive in DMF. For each of them, addition of either enantiomer (1*R*, 2*S*)- or (1*S*, 2*R*)-Nonrephedrine gave strong fluorescence enhancement with identical intensity due to the achiral nature of the sensor. The emission wavelength ranges from 432 nm (for **4.23)** to 465 nm (for **4.25**), which is close to the emission observed for the H_8BINOL sensor above. Besides this amino alcohol tested here, this sensing mechanism works for other monoamines as well. They can be regarded as a new group of general sensors for primary amines.

Figure 4- 39. Emission spectra of **4.23-4.26** (0.05 mM) treated with the two enantiomer of Nonrephedrine (2 mM) in DMF (λ_{ex} = 290 nm, slit = 3.0 / 3.0 nm).

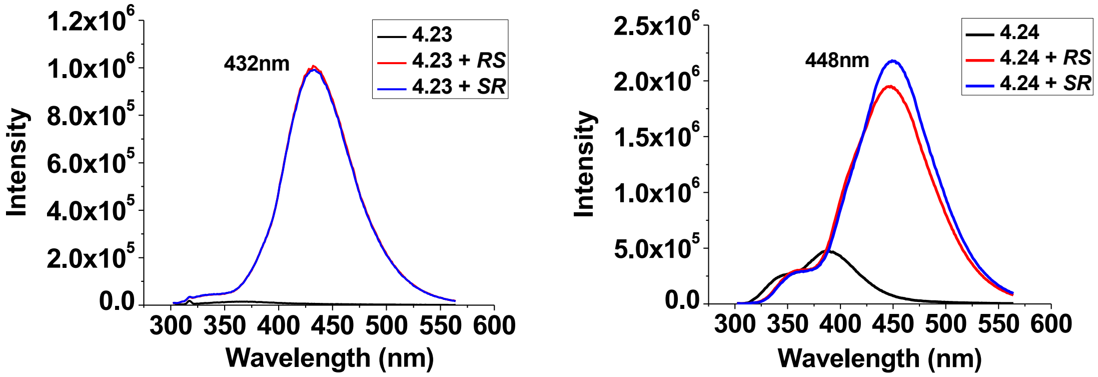

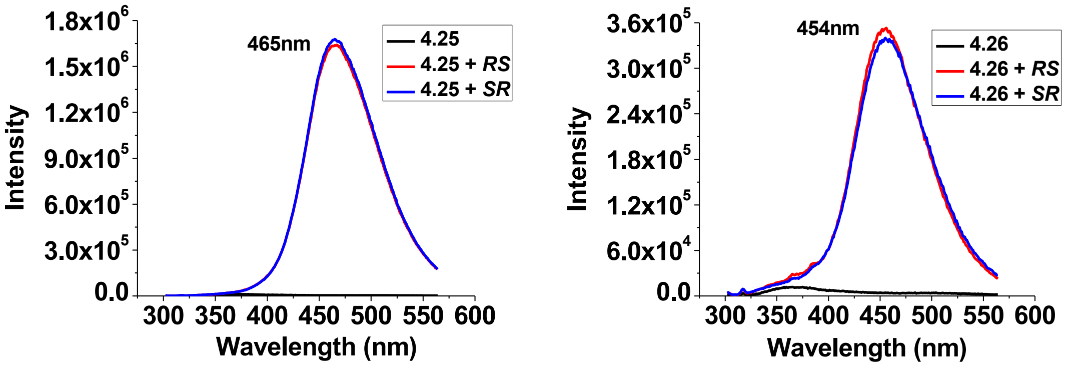

4.2.10. Sensing of amino acids using amide formation

Scheme 4- 5. Amidation reaction between fluorinated ketone and amine.

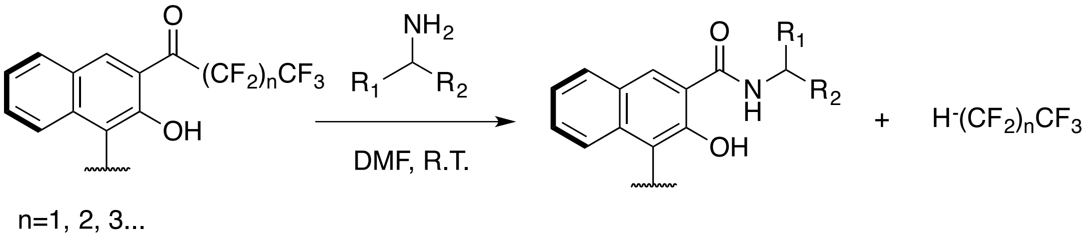

We studied the effects of the fluorous chain lengths on the amidation reaction. As shown in Scheme 4-5, this amidation occurs in DMF when *n* is equal to or greater than 1. When *n* = 1, this reaction proceeds very slowly and complete conversion was not observed even after 24 h of reaction, which make it not suitable for fluorescent sensing. With longer chain lengths, this reaction can finish within a few hours as indicated by TLC. For n = 0, which is a CF_3 ketone, amidation was not observed. It tends to undergo a nucleophilic addition at higher temperature.

Scheme 4- 6. Synthesis of (*S*)-**4.32** and (*S*)-**4.33**.

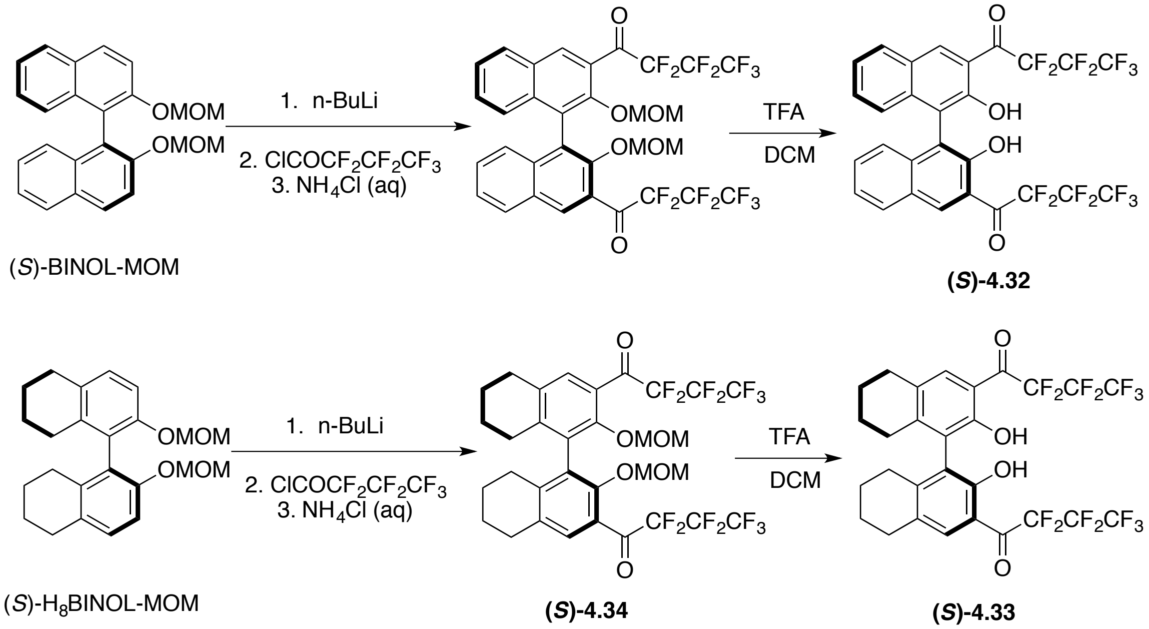
OMOM
OMOM
(S)-BINOL-MOM
1. n-BuLi
2. ClCOCF2CF2CF3
3. NH4Cl (aq)
O
CF2CF2CF3
OMOM
OMOM
CF2CF2CF3
O
TFA
DCM
O
CF2CF2CF3
OH
OH
CF2CF2CF3
O
(S)-4.32
OMOM
OMOM
(S)-H8BINOL-MOM
1. n-BuLi
2. ClCOCF2CF2CF3
3. NH4Cl (aq)
(S)-4.34
TFA
DCM
(S)-4.33

Because the ketones containing -C_3F_7 are efficient enough for amidation in DMF, we prepared two sensors (*S*)-**4.32** and (*S*)-**4.33**. The existence of free phenol hydroxyl groups makes the sensors sensitive to pH variations. When (*S*)-**4.33** was treated with amino acids in DMF, no fluorescence enhancement was observed (Figure 4-40, left). In the more polar DMSO solution, basic amino acids like arginine gave rise to strong fluorescence enhancement due to the deprotonation of hydroxyl groups caused by the pH increase (Figure 4-40, right). With the addition of small amount of water to dissolve amino acids, the selectivity over lysine and arginine was still observed (Figure 4-41, left). When the sensing was performed in aqueous solution (with 4% DMSO to dissolved the sensor), the overall emission intensity was much weaker.

Figure 4- 40. Emission spectra of (*S*)-**4.33** (0.3 mM, 5 mL) in DMF (left) or DMSO (right) with addition of amino acid solid (2 mg).

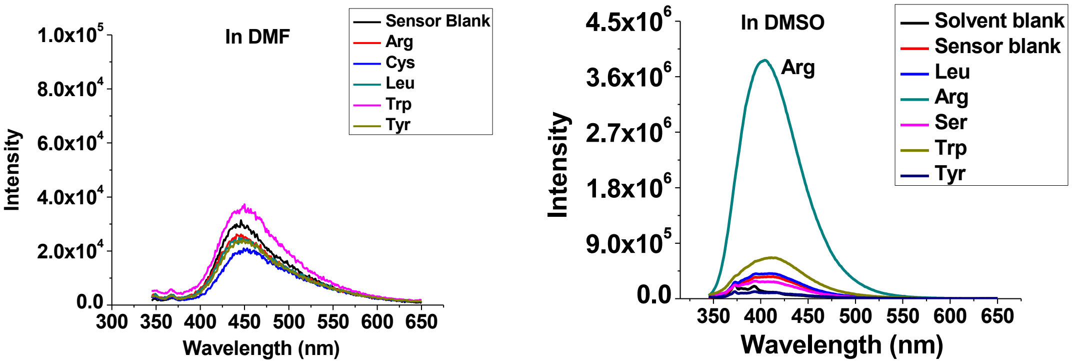

Figure 4- 41. Emission spectra of (*S*)-**4.33** with addition of amino acid in DMSO (left) or water (right).

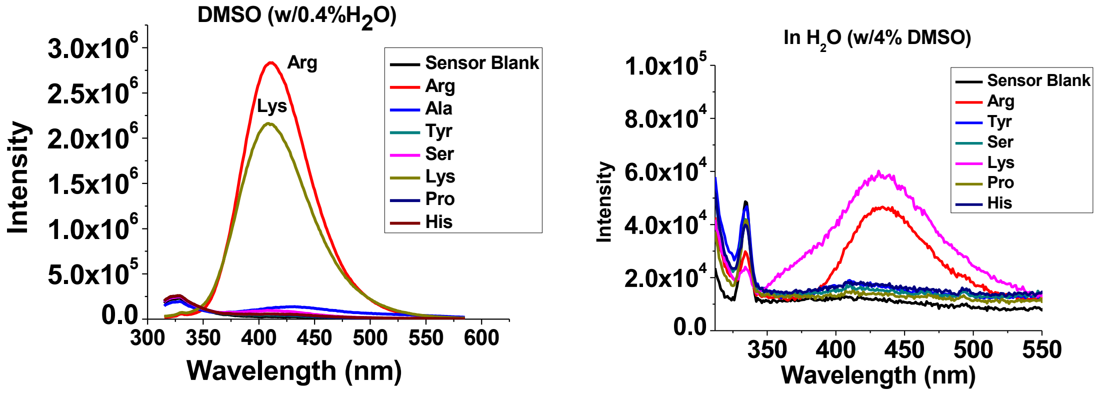

When two enantiomers of lysine or arginine was added to the sensor (*S*)-**4.33** in DMSO, the enantioselectivity was not observed for lysine and very small for arginine as shown in Figure 4-42. Thus (*S*)-**4.33** was not ideal for chiral recognition of free amino acids. Similar with (*S*)-**4.33**, the BINOL-based (*S*)-**4.32** also gave selective emission toward basic amino acids in DMSO but at longer wavelength (500 nm). As shown in Figure 4-43, with the addition of arginine to (*S*)-**4.32**, fluorescence intensity at 500 nm increased up to 9-folds until 9 eq of arginine was used. Further addition of excess amino acids resulted in fluorescence quenching.

Figure 4- 42. Emission spectra of (*S*)-**4.33** (0.2 mM) with addition of amino acid (2 mM) in 0.4 % Water / DMSO.

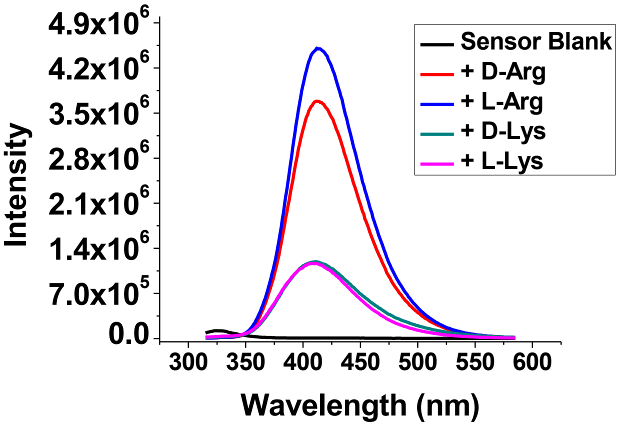

Figure 4- 43. Emission of (*S*)-**4.32** (0.1 mM) with addition of L-Arg at different equivalents (0-10 eq) in 2 % Water / DMSO.

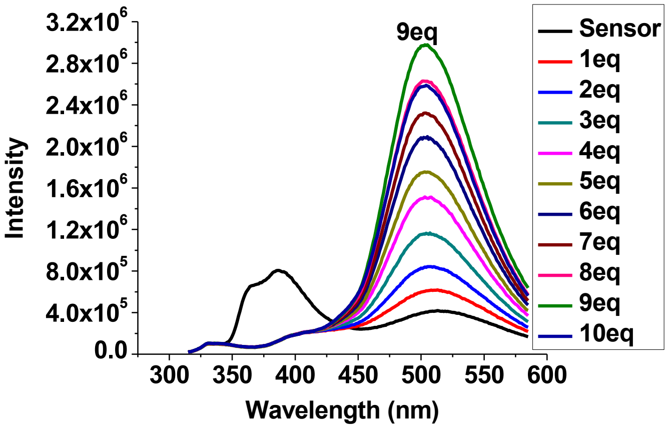

We monitored the reaction between (*S*)-**4.32** and arginine in DMSO-d^6 using ^{1}H and ^{19}F NMR, neither the formation of amide nor the cleavage of fluorous chains were observed. This means that the fluorescence turn-on is a consequence of pH change. Figure 4-44 was the emission spectra when (*S*)-**4.32** was titrated with HCl or NaOH to adjust the pH from 1.52 to 12.78 (pH was shown in the parenthesis). In an acidic environment, fluorescence change at 370 nm is insignificant. Deprotonation of hydroxyl group in basic environment gave rise to the emission at 500 nm, which is consistent with the emission observed with arginine as well as the emission of naphthol.

Figure 4- 44. Emission spectra of (*S*)-**4.32** (0.05 mM) with addition of HCl or NaOH(3M) from 1 μL to 100 μL in 10 % water / DMSO.

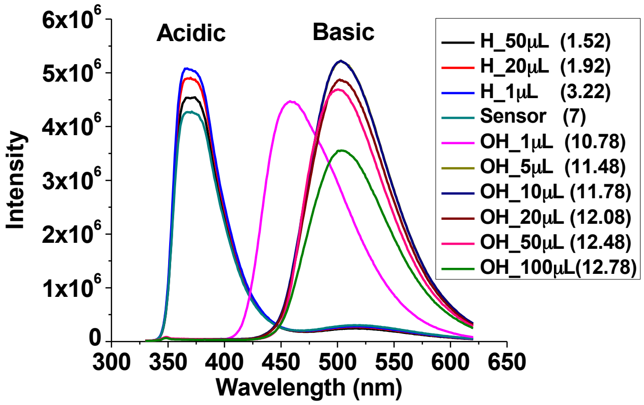

As the sensor is highly sensitive to pH, it can be used for selective sensing of anions like F$^-$, AcO$^-$ and Br$^-$. As shown in Figure 4-45, addition of 50eq of KF in water results in a more basic solution and strong emission at 500 nm was observed. The less basic KOAc resulted in emission at 460 nm, while the neutral solution with KBr gave no fluorescence change.

Figure 4- 45. Emission spectra of (*S*)-**4.32** (0.01 mM) treated with KF, KOAc or KBr (50 eq).

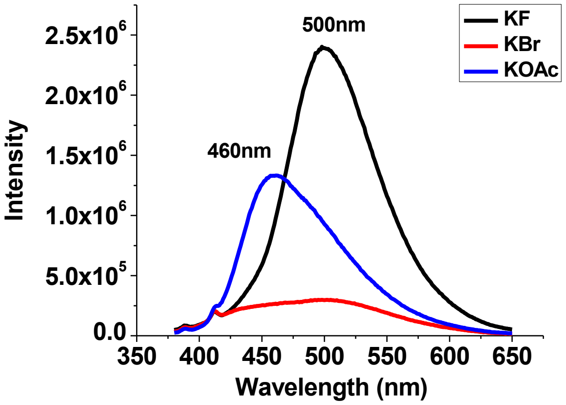

In an effort to achieve enantioselective sensing of amino acids (AAs), we treated the amino acids with tetrabutylammonium hydroxide (TBAOH) and obtained the anionic forms of amino acids (TBA-AAs), which is a kind of ionic liquid. In the following part, all amino acids used in the measurements are in their anionic forms. The TBA-AAs obtained are highly soluble in organic solvents and are more reactive toward ketone sensors. When D-serine or L-serine was added to the sensor (*S*)-**4.32** in DMSO, the former one gave weaker emission intensity at 500 nm than the latter one (Figure 4-46). Fluorescence intensity reached its maximum when 10 eq of serine were used, then it started to decrease. At 10 eq, the emission intensity of L-serine is about twice of D-serine.

Figure 4- 46. Fluorescence spectra of (*S*)-**4.32** (0.01 mM) with addition of D- or L-serine (1-20 eq) in DMSO. Fluorescence intensity at 500 nm was plotted against equivalents of serine (λ_{ex} =363 nm, slit = 3.0 / 3.0 nm, t = 3 h).

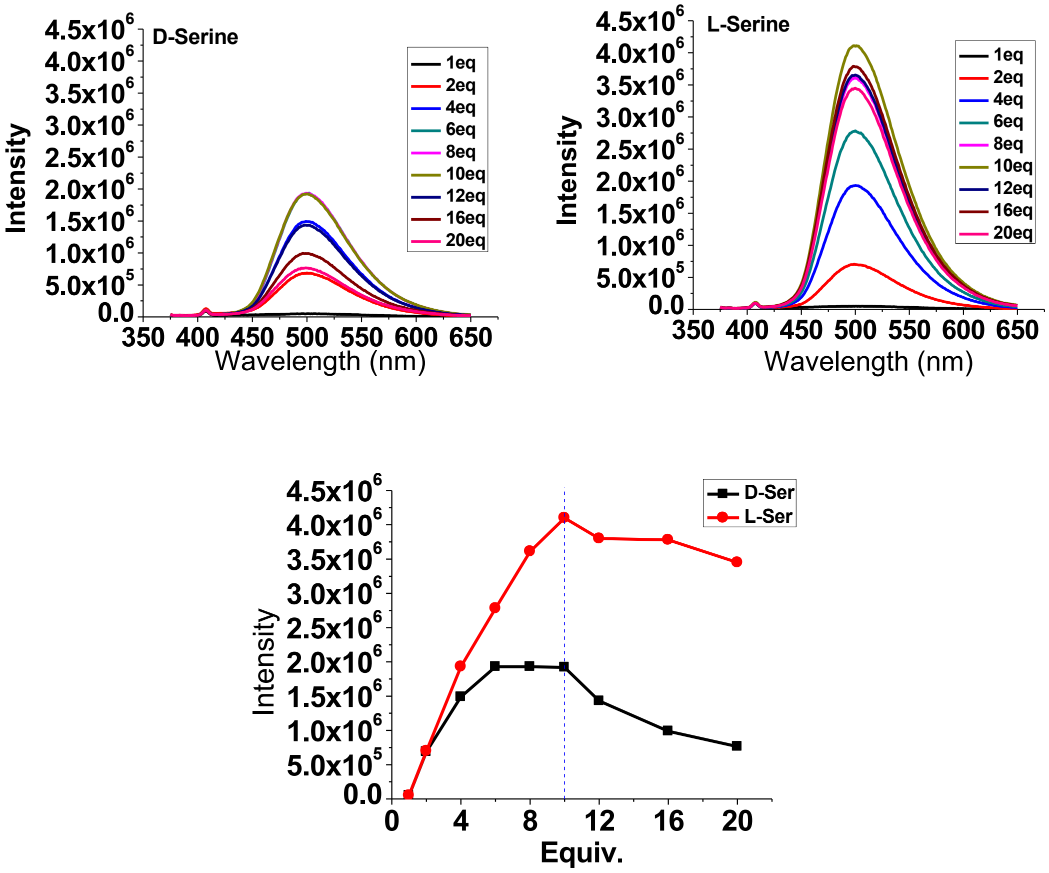

The different emission intensity observed can be used to determine enantiomeric excess values (ee = $\frac{[L]-[D]}{[L]+[D]}$) of serine containing two enantiomers in different compositions. As shown in Figure 4-47, emission at 500 nm increases gradually as *ee* changes from -100 to 100. Using the plot, *ee* values of any mixtures containing the two enantiomers of serine can be easily measured.

Figure 4- 47. Fluorescence spectra of (*S*)-**4.32** (0.01 mmol) with addition of serine (10 eq) in different *ee* values and emission intensity at 500 nm was plotted against *ee* values (t = 3 h).

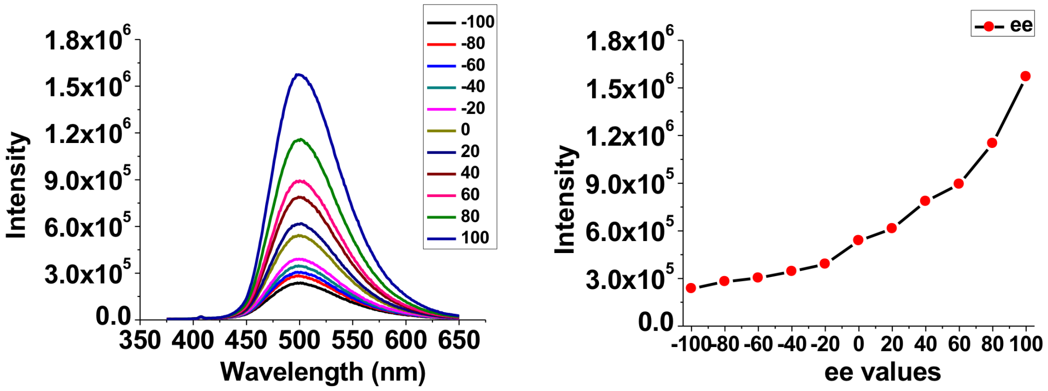

Figure 4- 48. Emission intensity at 500 nm for of (*S*)-**4.32** (2 μM, 50 μM and 200 μM) with addition of serine (t = 3 h).

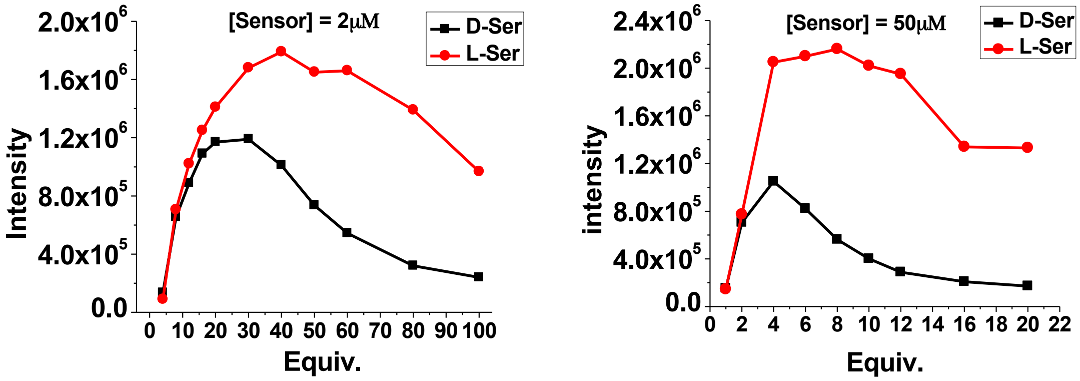

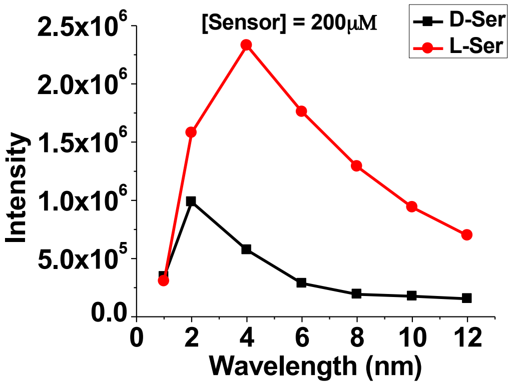

We studied the effects of sensor concentration to the sensing of serine (Figure 4-48). At higher concentration of (*S*)-**4.32**, maximum emission intensity was achieved with smaller equivalents of serine. We also noted that when large excess of serine was added, enantioselectivity was even higher. We tracked the fluorescence change when 200eq of serine was added to (*S*)-**4.32**. As shown in Figure 4-49, fluorescence for L-serine increased overtime while that of D-serine barely changes. Over 9h, the *ef* values increases from 3.5 to 10.5 [*ef* was defined as $(I_L-I_0) / (I_D-I_0)$].

Figure 4- 49. Fluorescence spectra of (*S*)-**4.32** (0.01 mM) with addition of D- or L-Serine (200 eq) in DMSO. Fluorescence intensity at 500 nm was plotted against time.

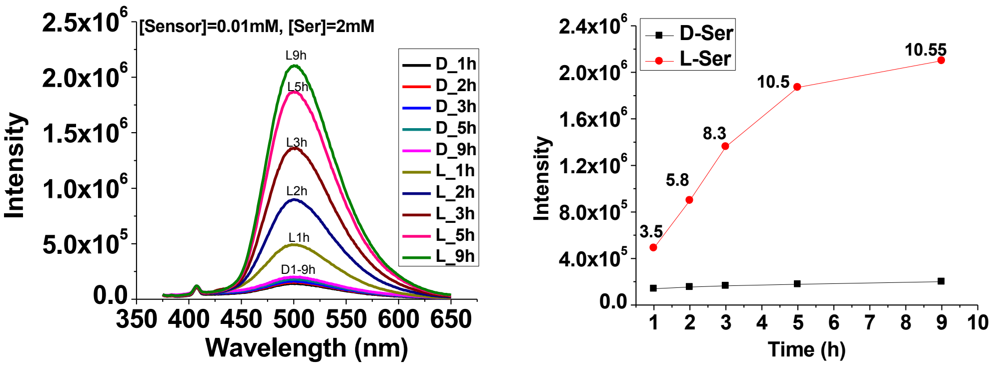

When (*R*)-**4.32**, the enantiomer of (*S*)-**4.32** was used, it is the D-serine that give stronger emission than the L-serine (Figure 4-50). This difference is significant enough to enable visual discrimination of the two enantiomers under UV-irradiation, with the D-serine gave strong green emission while the L-serine is weakly emissive. The mirror-image relationship confirms the reliability of this enantioselectivity.

Figure 4- 50. Fluorescence spectra of (*R*)-**4.32** (0.01 mM) with addition of D- or L-Serine (200 eq) in DMSO tracked overtime.

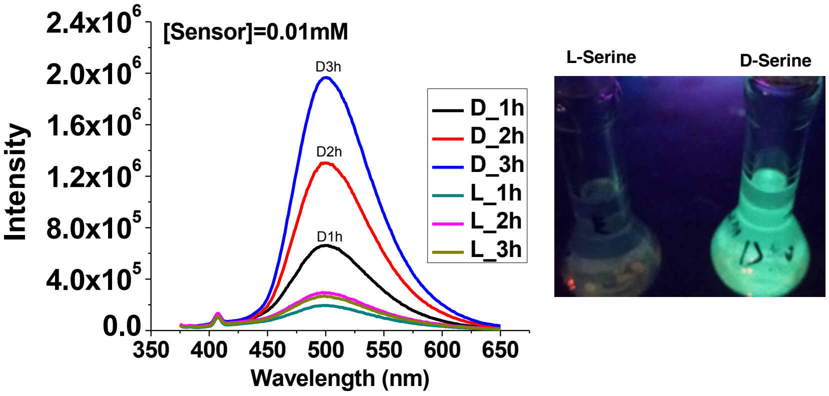

To study this fluorescence turn-on mechanism, we conducted a reaction between the sensor and serine in DMSO (Scheme 4-7). After treatment with HCl, the amide product was separated quantitatively and was characterized. This shows that even though free amino acid is incapable for the amidation process, its anionic form has increased activity toward the sensor and can be recognized with good enantioselectivity.

We further tested the enantioselectivity of (*S*)-**4.32** toward other amino acid anions (TBA as cation) as shown in Figure 5-51 to 5-56. A reaction time of 3 h, excitation wavelength of 363 nm and slit of 3 / 3 nm were applied to all measurements.

While cysteine gave an *ef* value up to 2.0 and threonine up to 2.8, the others like *Allo*-Thr, Lys, Val and Trp resulted *ef* values less than 1.5. Different from other amino acids, L-cysteine gave a stronger emission than its D-enantiomer and no quenching was observed in the concentration range, as shown in Figure 4-51. So among all the amino acids tested, serine gave the highest enantioselective fluorescent response toward (*S*)-4.32.

Scheme 4- 7. Reaction between (*S*)-**4.32** and (L)-Serine-TBA in DMSO.

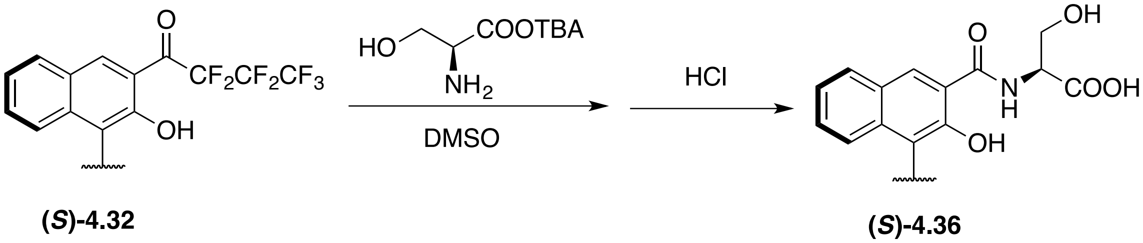

Figure 4- 51. Fluorescence spectra of (*S*)-**4.32** (0.01 mM) with addition of D- or L-cysteine (1-20 eq) in DMSO. Fluorescence intensity at 500 nm was plotted against equivalents.

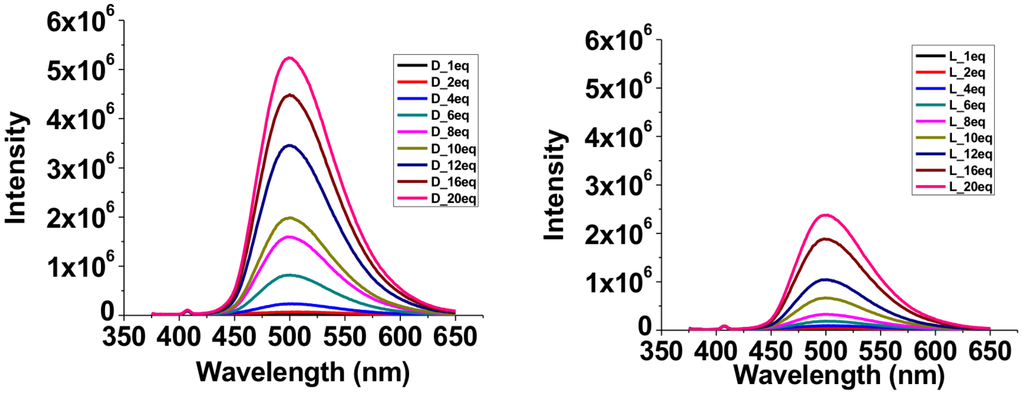

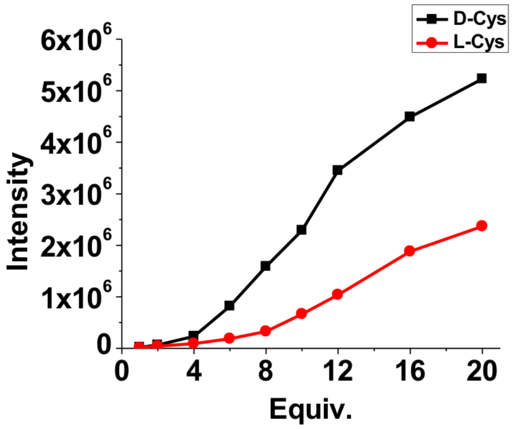

Figure 4- 52. Fluorescence spectra of (*S*)-**4.32** (0.01 mM) with addition of D- or L-threonine in DMSO 3 h after reaction. Fluorescence intensity at 500 nm was plotted against equivalents.

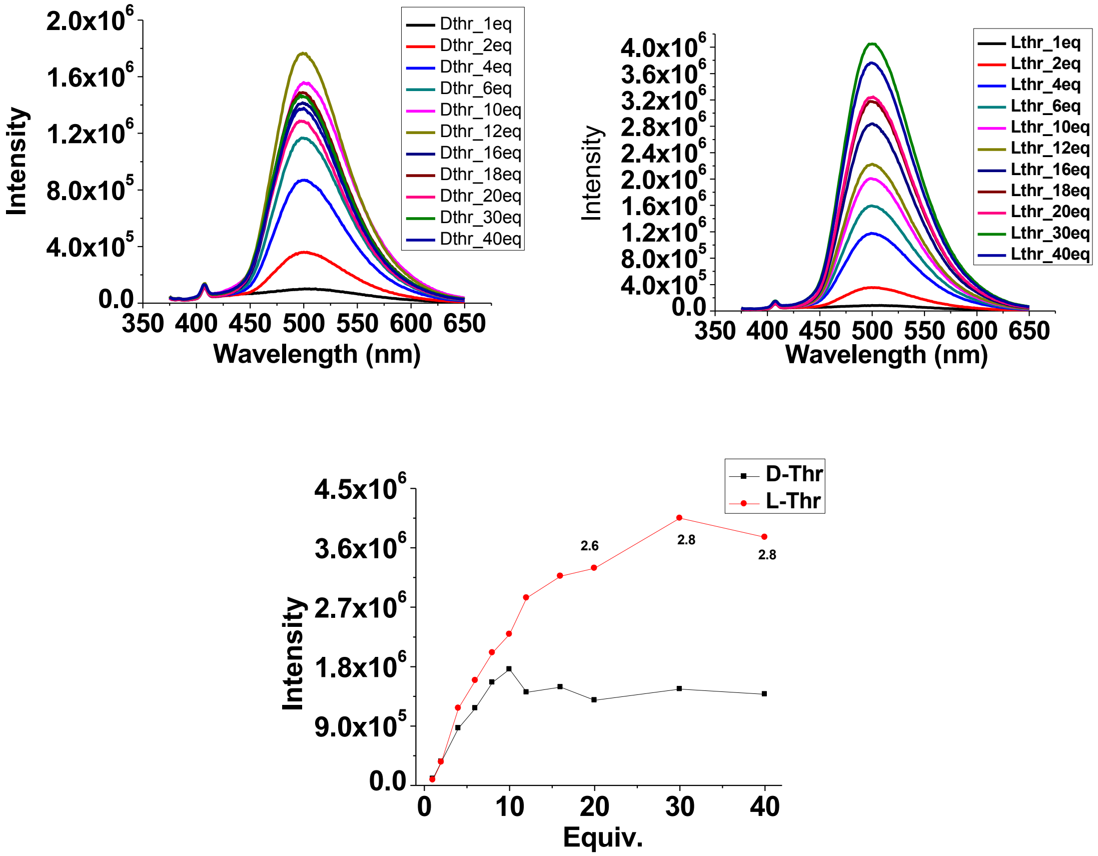

Figure 4- 53. Fluorescence spectra of (*S*)-**4.32** (0.01 mM) with addition of D- or L-allo-threonine in DMSO 3 h after reaction. Fluorescence intensity at 500 nm was plotted against equivalents.

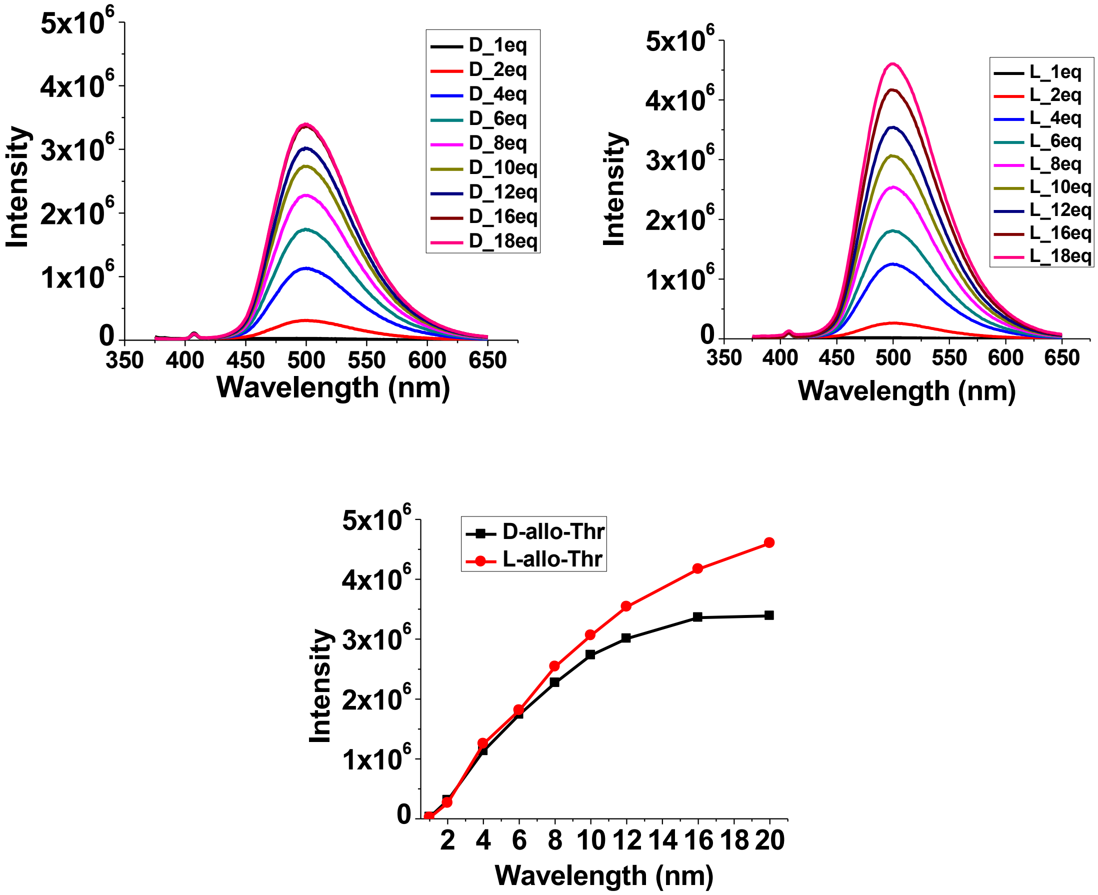

Figure 4- 54. Fluorescence spectra of (*S*)-**4.32** (0.01 mM) with addition of D- or L-lysine in DMSO 3 h after reaction. Fluorescence intensity at 500 nm was plotted against equivalents.

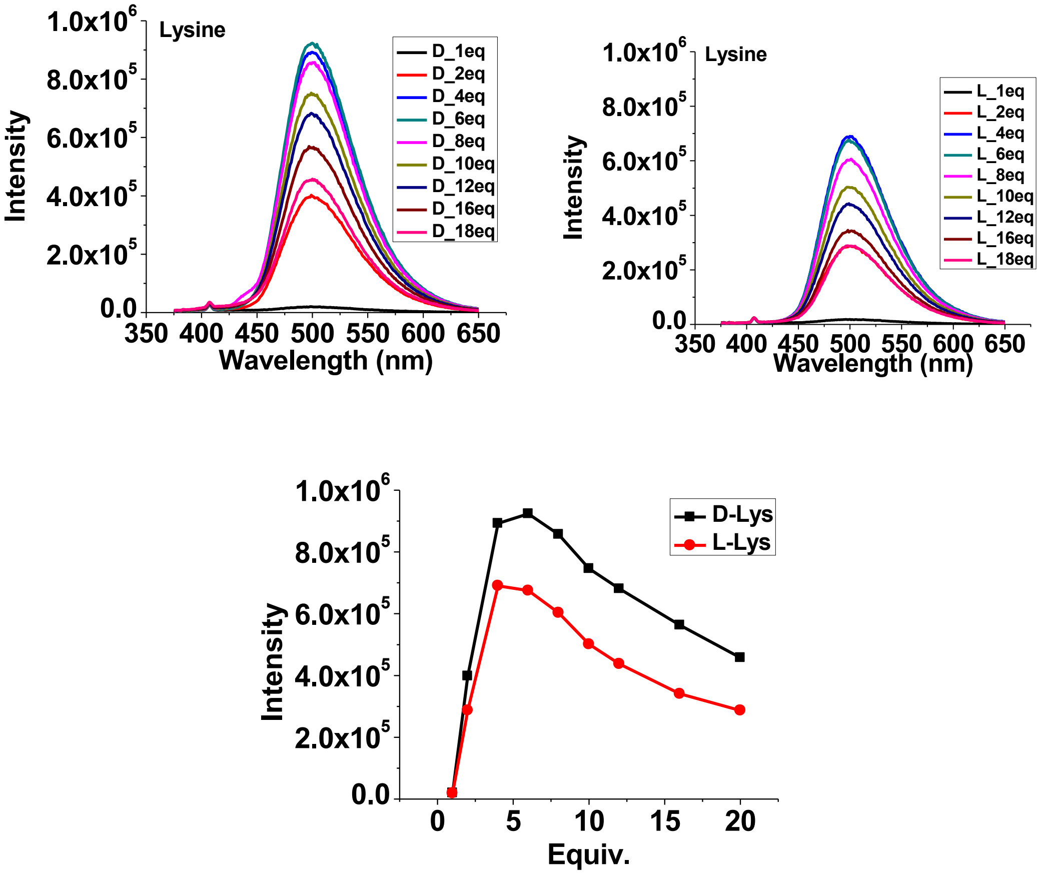

Figure 4- 55. Fluorescence spectra of (*S*)-**4.32** (0.01 mM) with addition of D- or L-valine from 1 to 16 equivalents in DMSO 3 h after reaction.

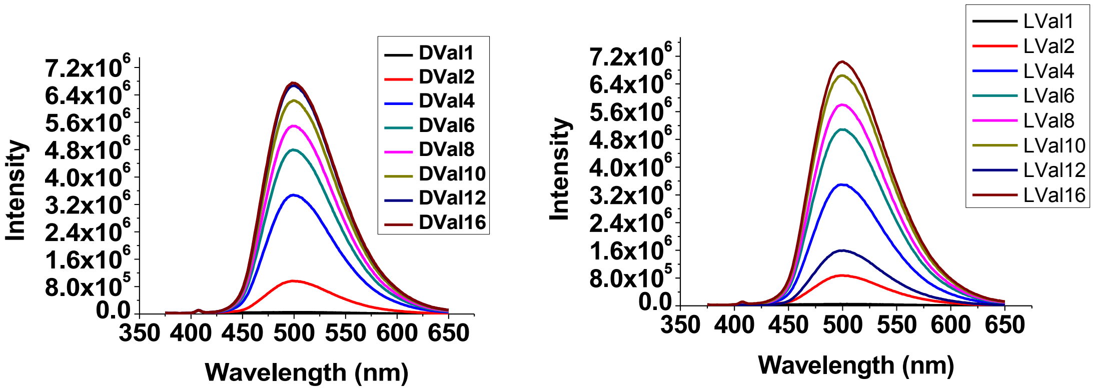

Figure 4- 56. Fluorescence spectra of (*S*)-**4.32** (0.01 mM) with addition of D- or L-tryptophan from 1 to 16 equivalents in DMSO 3 h after reaction.

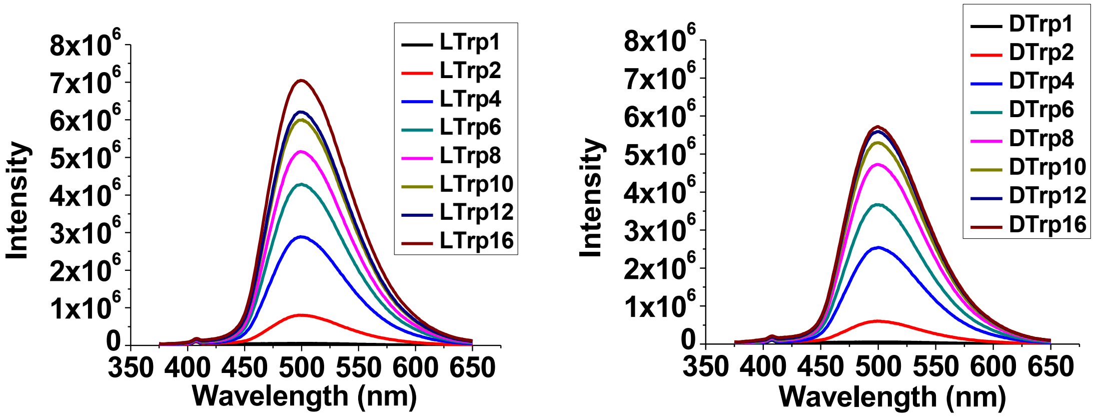

We compared the recognition to serine in other solvents like DCM and DMF (Figure 4-57, 58). In DCM, fluorescence enhancement was observed at 380 and 290 nm without enantioselectivity. No emission was observed at 500 nm, indicating the absence of amide formation. In DMF, the amide was formed readily with emission enhancement at 500 nm, but no enantioselectivity was present.

Figure 4- 57. Fluorescence spectra of (*S*)-**4.32** (0.01 mM) with addition of D- or L-serine in DCM 3 h after reaction.

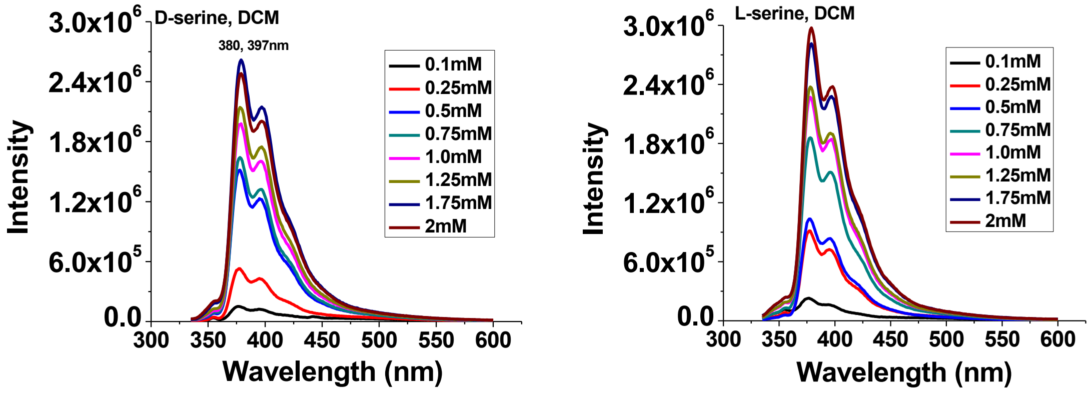

Figure 4- 58. Fluorescence spectra of (*S*)-**4.32** (0.01 mM) with addition of D- or L-serine in DMF 3 h after reaction.

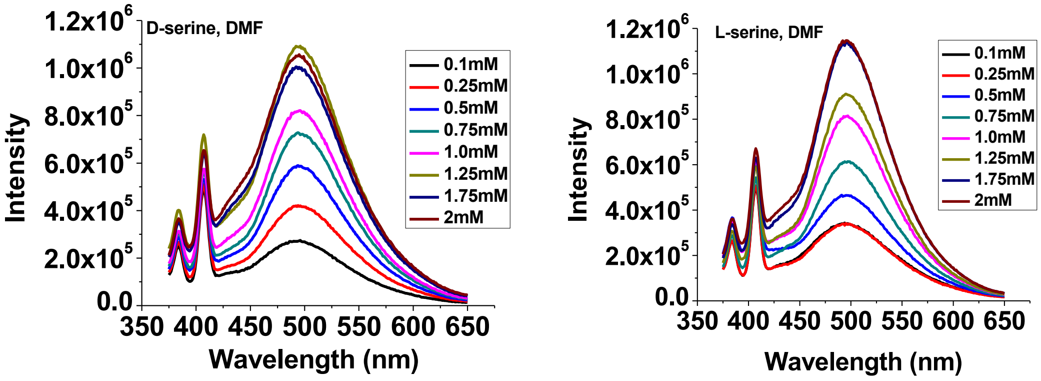

In terms of (*S*)-**4.33**, it is also able to give moderate enantioselectivity toward serine with emission enhancement at 457 nm (Figure 4-59 to 61). However, the enantioselectivity toward other amino acids like tryptophan or valine was negligible. They also gave emission at 415 nm, shorter than the emission with serine found at 457 nm. The increased enantioselectivity and emission wavelength of serine might be attributed to the existence of extra hydroxyl group that can provide additional hydrogen bonding sites to form more rigid networks.

Figure 4- 59. Fluorescence spectra of (*S*)-**4.33** (0.01 mM) treated with D- or L-serine in DMSO. Emission intensity at 457 nm was plotted against the concentration of serine.

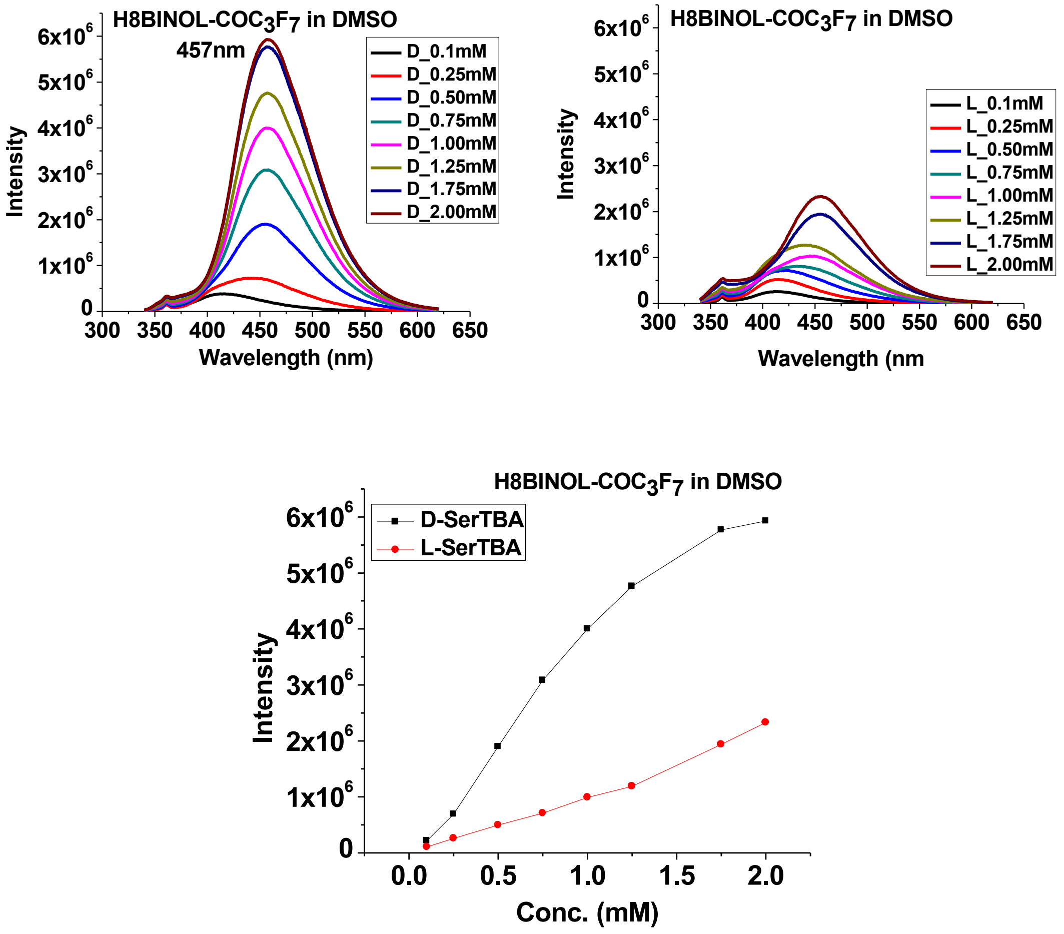

Figure 4-60. Fluorescence spectra of (*S*)-**4.33** (0.01 mM) treated with D- or L-tryptophan in DMSO. Emission intensity at 415 nm was plotted against the concentration of tryptophan.

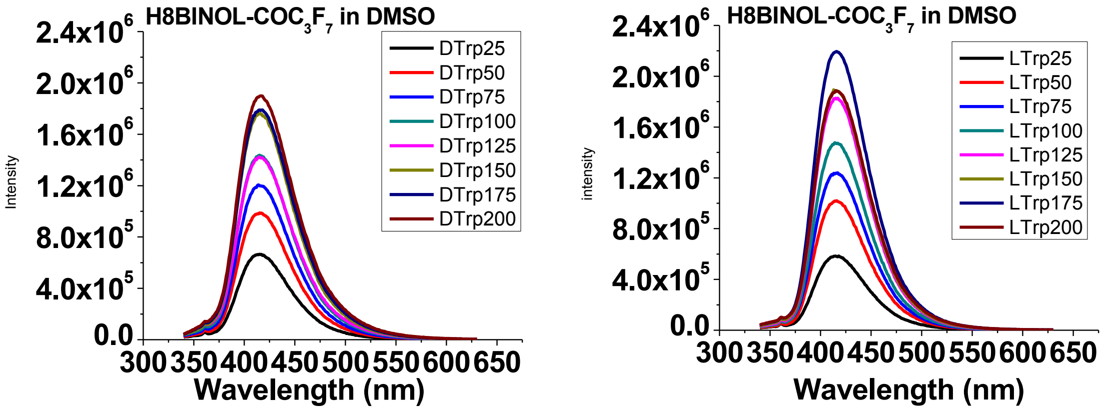

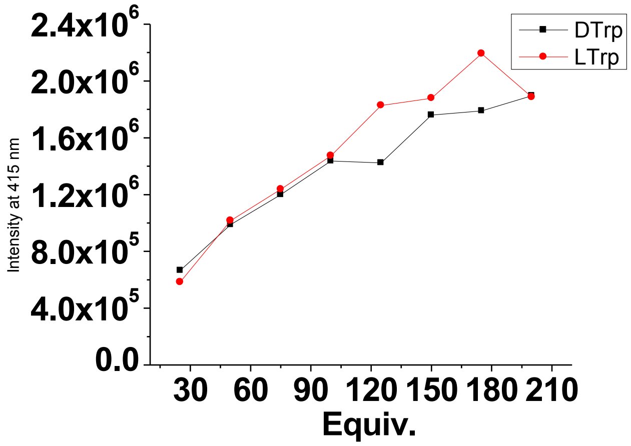

Figure 4-61. Fluorescence spectra of (*S*)-**4.33** (0.01 mM) treated with D- or L-valine in DMSO. Emission intensity at 415 nm was plotted against the concentration of valine.

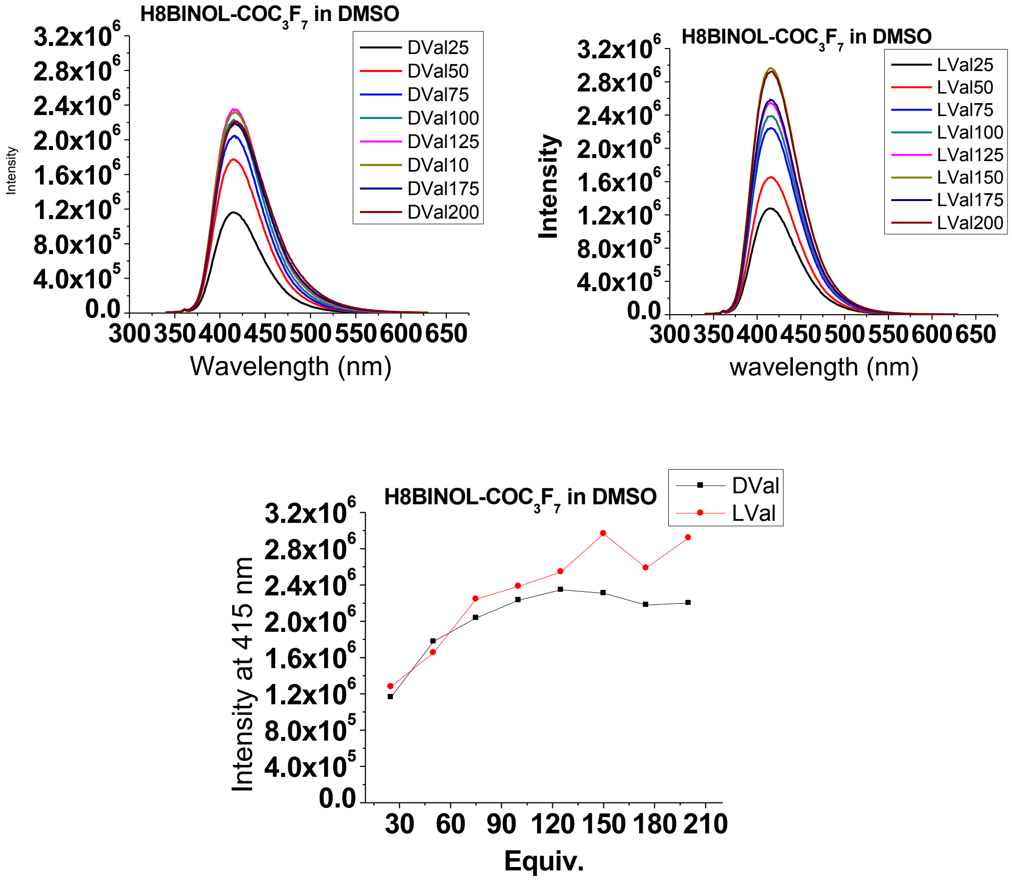

In an effort to achieve simultaneous determination of concentration and *ee*, we prepared the achiral sensor **4.35** (Scheme 4-8), an analogue of **4.24** but with shorter fluorous chains, which is necessary to make it soluble in DMSO.

Scheme 4- 8. Synthesis of achiral sensor **4.35**.

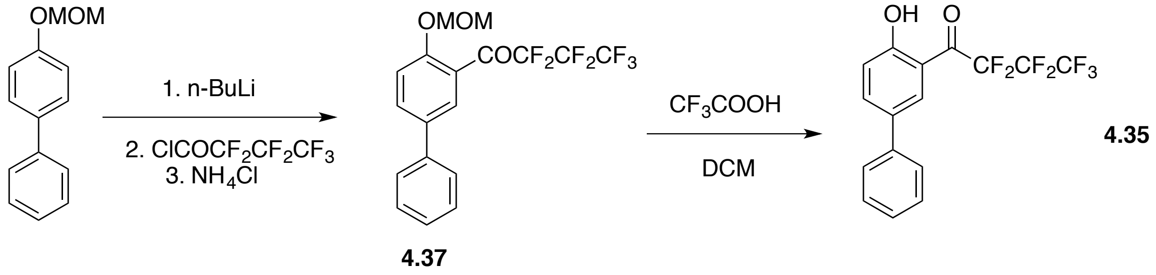

When serine anion was added to the achiral sensor **4.35**, strong fluorescence turn-on was observed at 416 nm with identical intensity for D- and L-enantiomers (Figure 4-62). The different emission wavelength for **4.35** makes it useful in ratiometric sensing in combination with chiral (*S*)-**4.32** as shown in Figure 4-63. We mixed sensor **4.35** with (*S*)-**4.32** in a 1:1 molar ratio. After addition of 10 eq of serine, the emission at 416 nm (blue channel) was identical for two enantiomers, while the emission at 500 nm (green channel) was highly enantioselective. Thus the blue channel can be used to measure the total concentration of serine, while the green channel can be used to determine the enantiopurity. Under UV-irradiation, D- and L-serine gave rise to different colors due to the different ratio at two emission channels.

Figure 4- 62. Fluorescence spectra of **4.35** (0.05 mM) with addition of 10eq D- or L-serine excite at 340 nm in DMSO.

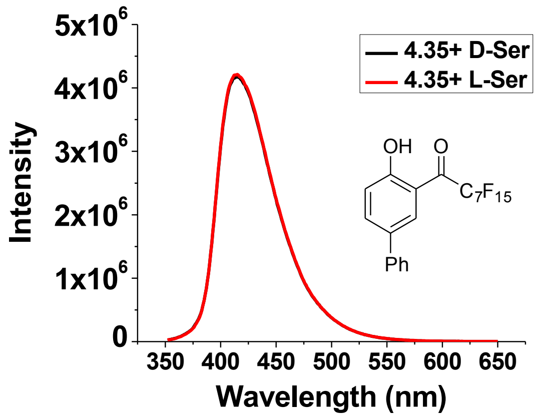

Figure 4- 63. Fluorescence spectra of **4.35** (0.05 mM) + **4.32** (0.05 mM) with addition of 0.5 mM D- or L-serine excited at 363 nm in DMSO.

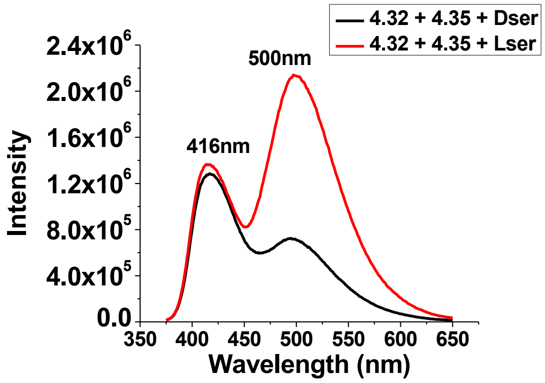

We also tried to achieve sensing of amines through amidation in fluorous solvents by using compound **4.38** (Scheme 4-9). By adding two extra fluorous chains on the 6, 6'-position of BINOL, it is expected that the amide product formed can be soluble in fluorous solvents. However, it is surprising to find that (*S*)-**4.38**, which has higher fluorine contents than BINOL-C_7F_{15}, is almost insoluble in FC-72. In an effort to combine the amide formation process in DMF with the study of fluorous solvents, we prepared a mixture of (*S*)-**4.38** and (*R*)- and (*S*)-2-amino-1-butanol in DMF for 2 h and then diluted it with various fluorous solvents ($MeOC_4F_9$, FC-72, R_fOH = $C_6F_{13}CH_2CH_2OH$). However, while some fluorescence enhancement was observed, only very small enantioselectivity was achieved (Figure 4-64). It seems that with (*S*)-**4.38**, the amidation process still have similar rates for the two enantiomers of a chiral amine. A H_8BINOL backbone structure is required to achieve enantioselectivity for the recognition of amines. We also prepared (*S*)-**4.38** in different solvents and measured fluorescence spectra after a solution of (*R*)- or (*S*)-2-amino-1-butanol or **4.3** in THF was titrated (Figure 4-65 and 66). However, almost no fluorescence change was observed. For **4.38**, the amidation can only occurs in DMF as well.

Scheme 4- 9. Synthesis of (*S*)-**4.38**.

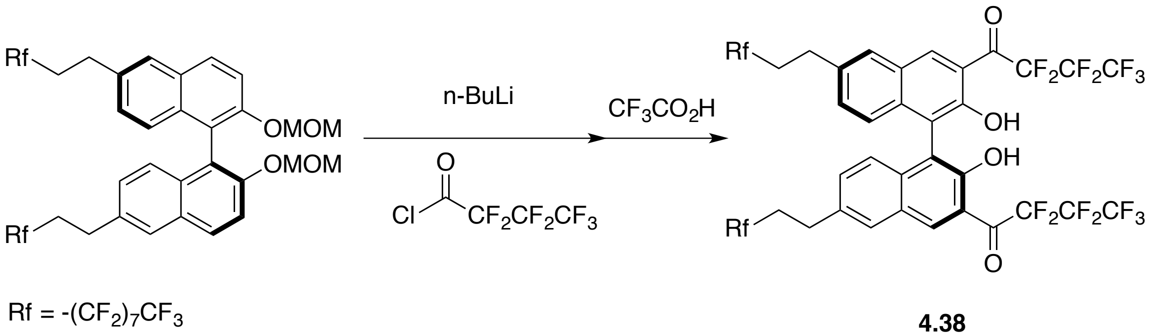

4.38

Figure 4- 64. Fluorescence spectra of (*S*)-**4.38** and (*R*)- or (*S*)-2-amino-1-butanol diluted with various solvents to a total of 2 mL after reacting in DMF (0.2 mL) for 2h (λ_{ex} = 300 nm, slit 3 / 3 nm).

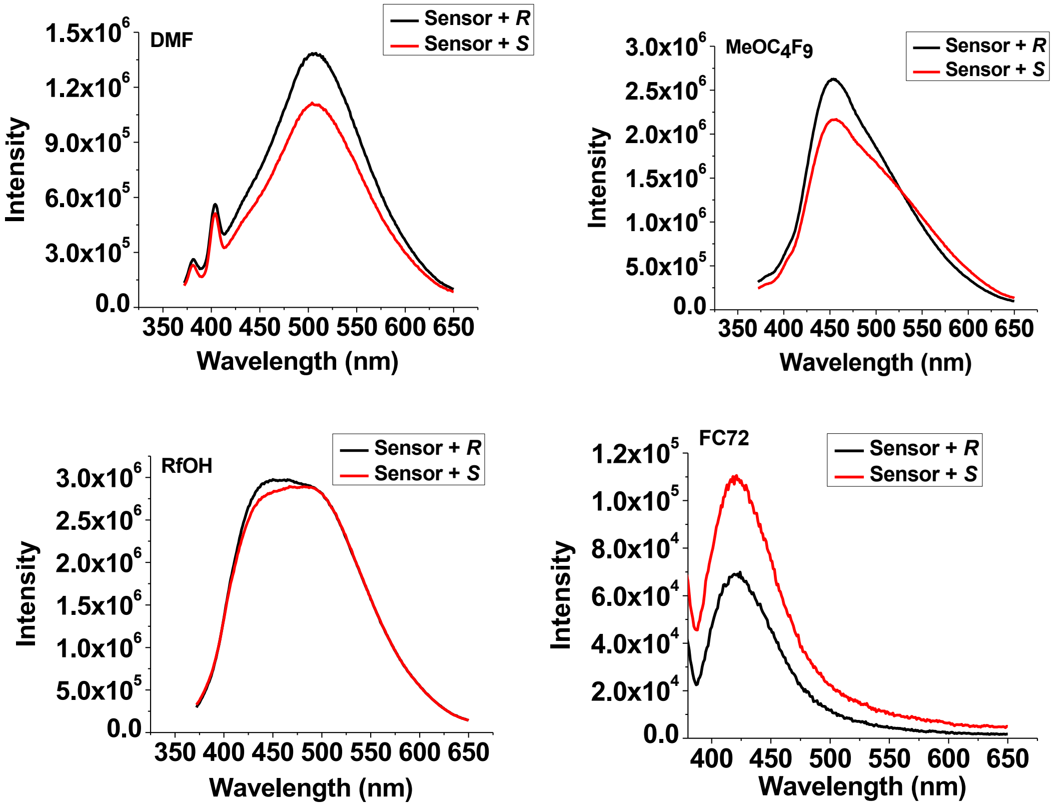

Figure 4- 65. Fluorescence spectra of (*S*)-**4.38** with (*R*) or (*S*)- 2-amino-1-butanol in various solvents (λ_{ex} = 300 nm).

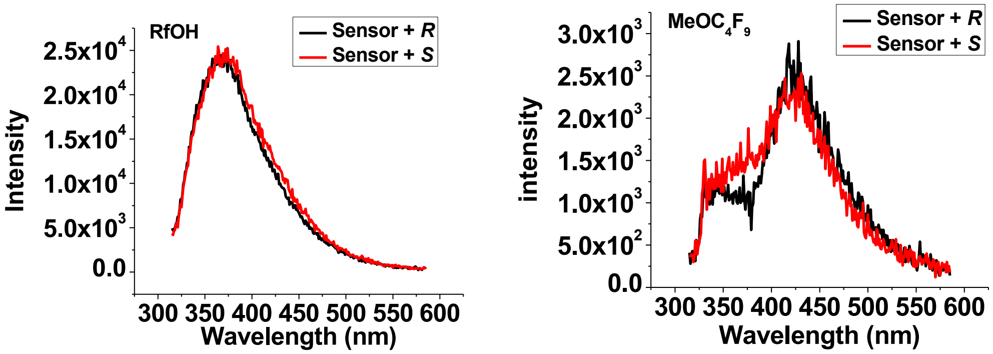

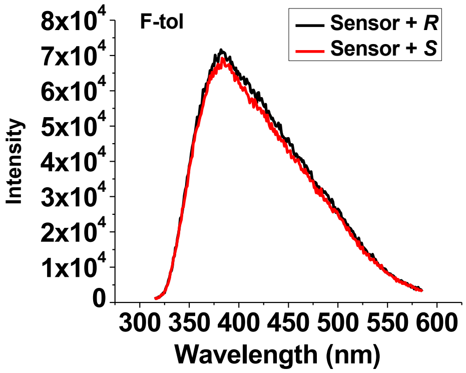

Figure 4- 66. Fluorescence spectra of (*S*)-**4.38** with (*R*) or (*S*)-**4.3** in various solvents (λ_{ex} = 300 nm).

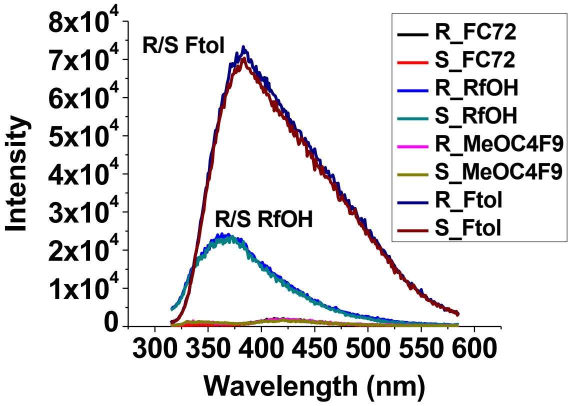

4.3. Conclusion

In conclusion, we have discovered that a H_8BINOL-based perfluoroalkyl ketone exhibits highly enantioselective fluorescent enhancements toward both unfunctionalized and functionalized chiral amines. It greatly expands the substrate scope of the previously reported BINOL-based perfluoroalkyl ketone sensor in the enantioselective fluorescent recognition of chiral amines. A dramatic solvent effect was observed for the reaction of the amines with the perfluoroalkyl ketone sensor. In DMF, cleavage of the perfluoroalkyl group to form amides was observed but not in other solvents. The high enantioselectivity in the fluorescent response of the new sensor toward the chiral amines is found to be due to its different reaction rate with the enantiomers of the chiral amines. The reaction of the sensor with the amines in DMF can be effectively quenched by dilution with another solvent such as THF to give stable fluorescence measurement. This is the first example that the formation of the strong amide bonds under very mild conditions is used for the enantioselective recognition of chiral amines. This work provides a new strategy for the design of molecular sensors for amine recognition.

We also extended the study of amidation in DMF from amine to amino acids. We found that the BINOL-based sensor (*S*)-**4.32** showed pH-dependent fluorescence to amino acids. Unlike the H_8BINOL based sensors, DMSO is a better solvent than DMF for amino acids. While little enantioselectivity was observed for free amino acids, the their TBA salts gave moderate enantioselective emission at 500 nm. The best *ef* value was found in serine, followed by cysteine and threonine. An *ef* value up to 10 can be obtained when large excess of serine was applied. The isolated products from the reaction of (*S*)-**4.32** and serine confirmed that the amide formation is responsible for the emission enhancement. A combination of an achiral sensor with (*S*)-**4.32** enables us to determine total concentrations of amino acid enantiomers at the blue channel emission, and determines *ee* values at the green channel emission.

4.4. Experimental part

4.4.1. General data

All reactions were carried out under N_2 unless otherwise noted. Fluorous reagents were purchased from SynQuest Labs, Inc. All other chemicals were purchased from Sigma Aldrich Chemical Co. or Alfa Aesar. The diamine **4.21** was sublimed under vacuum pump before use. Other chemicals were used without further purification. Methylene chloride and diethyl ether were dried by passing through activated alumina columns under nitrogen. THF and DMF were HPLC grades and used without purification. Optical rotations were measured on a Jasco P-2000 digital polarimeter. NMR spectra were recorded on Varian-600 MHz spectrometer. Chemical shifts for ^{1}H NMR spectra were reported in parts per million relative to a singlet at 7.26 ppm for residual $HCCl_3$ in deuterated chloroform. Chemical shifts for ^{13}C NMR were reported relative to the centerline of a triplet at 77.16 ppm for deuterated chloroform. The ^{19}F NMR spectra were reported in units of part per million (ppm) relative to trifluoroacetic acid (δ -76.55 ppm) as an external reference. Steady-state fluorescence emission spectra were recorded on Horiba FluoroMax-4 spectrofluorometer. High and low resolution mass spectra were obtained from the University of Illinois at Urbana-Champaign (UIUC) Synapt G2SiMass Spectrometry Facility. UV-Vis spectra were produced from a Hewlett-Packard 8452A diode-array spectrophotometer.

4.4.2. Sample preparation for fluorescence measurement:

Stock solutions of (*S*)-**4.2** were freshly prepared with a concentration of 0.5 mM by dissolving (*S*)-**4.2** (5.4 mg) in 0.5 mL THF first, and then diluted to a total volume of 10 mL with DMF [A small amount of THF (5 %) was used since (*S*)-**4.2** doesn't dissolve well in pure DMF]. For amines and amino alcohols, 50 mM or 25 mM stock solutions were freshly prepared in DMF. In the fluorescence enhancement study, the amine solution with designated equivalences was added to a 5 mL volumetric flask, followed by the addition of the (*S*)-**4.2** stock solution (0.1 mL). Extra DMF was added to keep the total volume of the solution at 0.5 mL. The solution was allowed to react at room temperature for 1 h before being diluted to 5 mL with THF, unless otherwise noted.

4.4.3. Synthesis and characterization

Synthesis of (*S*)-1,1'-(2,2'-dihydroxy-5,5',6,6',7,7',8,8'-octahydro-[1,1'-binaphthalene]-3,3'-diyl) bis (2,2,3,3,4,4,5,5,6,6,7,7,8,8,8 pentadecafluorooctan-1-one), (*S*)-4.2.

(1). Under nitrogen, (*S*)-H_8BINOL-MOM[12] (1 mmol, 382.5 mg) was dissolved in anhydrous diethyl ether (12 mL). The solution was cooled to 0 ºC, and n-BuLi (4.0 mmol, 2.5 M in hexane, 1.6 mL) was added dropwise. The reaction mixture was stirred at room temperature for 2 h and cooled to -78 °C by dry ice / acetone. Then perfluorooctanoyl chloride (4.0 mmol, 1.0 mL) was added dropwise. The reaction mixture was stirred at -78 °C for 1 h, and then warmed up to 0 °C to react for additional 2 h to afford a yellow cream-like mixture. Saturated aqueous solution of NH_4Cl (2 mL) was added to quench the reaction at 0 °C. The organic layer was separated, and the aqueous layer was extracted with ethyl acetate (3 × 10 mL). The combined organic extracts were washed with brine, and dried over anhydrous Na_2SO_4. After evaporation of the solvents, the mixture was further dried under vacuum pump to yield a yellow crude product.

(2). Under nitrogen, the above crude product was dissolved in a minimum amount of methylene chloride, and cooled to 0 °C. Trifluroacetic acid (1.0 mL) was added slowly, and the mixture was stirred at room temperature for 1 h. Saturated aqueous solution of $NaHCO_3$ was added slowly to quench the reaction. The organic layer was separated, and the aqueous layer was extracted with CH_2Cl_2 (3 × 10 mL). The combined organic extracts were washed with brine, and dried over anhydrous Na_2SO_4. After evaporation of the solvents, the residue was purified by column chromatography on silica gel eluted with hexane/methylene chloride (15 / 1) to afford compound (*S*)-**4.2** as a yellow oil in 36 % yield, which turned into yellow crystals after sitting at room temperature for 2 days. ^{1}H NMR (600 MHz, Chloroform-d) δ 11.28 (s, 2H), 7.67 (s, 2H), 2.83 (m, 4H), 2.48 (m, 2H), 2.23 (m, 2H), 1.83 – 1.66 (m, 8H). ^{13}C NMR (151 MHz, Chloroform-d) δ 186.49 (t, *J* = 25.7 Hz), 159.59, 150.22, 130.76, 129.78, 124.49, 113.77, 118-106 (m, weak), 29.53, 28.29, 22.67, 22.42. ^{19}F NMR (564 MHz, Chloroform-d) δ -80.84 (t, *J* = 9.7 Hz, 3F), -110.55 (t, *J* = 13.1 Hz, 2F), -120.50 (m, 2F), -120.86 (m, 2F), -121.96 (m, 2F), -122.70 (m, 2F), -126.22 (m, 2F). HRMS Calcd for $C_{36}H_{21}O_4F_{30}$(MH+): 1087.0961. Found: 1087.0933. $[\alpha]_D$ = 18.3 (c = 1.03, $CHCl_3$).

Synthesis of (*R*)-1,1'-(2,2'-Dihydroxy-5,5',6,6',7,7',8,8'-octahydro-[1,1'-binaphthalene]-3,3'-diyl) bis (2,2,3,3,4,4,5,5,6,6,7,7,8,8,8-pentadecafluorooctan-1-one), (*R*)-4.2.

Compound (*R*)-**4.2**, the enantiomer of (*S*)-**4.2**, was synthesized in 42% yield for 2 steps as yellow crystals by using the same procedures for (*S*)-**4.2** but starting with (*R*)-H_8BINOL-MOM. ^{1}H NMR (600 MHz, Chloroform-d) δ 11.29 (s, 2H), 7.69 (s, 2H), 2.83 (m, 4H), 2.49 (m, 2H), 2.24 (m, 2H), 1.86-1.65 (m, 8H). ^{13}C NMR (151 MHz, Chloroform-d) δ 186.52 (t, *J* = 25.5 Hz), 159.62, 150.23, 130.77, 129.80, 124.52, 113.79, 118-107 (m, weak), 29.54, 28.30, 22.68, 22.44. ^{19}F NMR (564 MHz, Chloroform-d) δ -80.84 (t, *J* = 9.7 Hz, 3F), -110.54 (m, 2F), -120.49 (m, 2F), -120.85 (m, 2F), -121.95 (m, 2F), -122.69 (m, 2F), -126.17 (m, 2F). $[\alpha]_D$ = -20.9 (c = 1.04, $CHCl_3$).

Synthesis of (*S*, *S*)-4.9

Under nitrogen, (*S*)-**4.2** (0.300 mmol, 326 mg) was dissolved in a minimum amount of dry THF, then 6 mL of DMF was added, followed by the slow addition of 3-dimethyl-2-butylamine, (*S*)-**4.3** (3.00 mmol, 400 μL). The mixture was allowed to stir at room temperature for 24 h. TLC indicated complete conversion of (*S*)-**4.2** and the mixture showed strong blue fluorescence under UV-lamps. The mixture was poured into 20 mL H_2O, extracted with ethyl acetate (5 × 5 mL). The combined organic extracts were washed with brine, and dried over Na_2SO_4. After evaporation of the solvents, the residue was purified by column chromatography on silica gel eluted with hexane/ethyl acetate (4/1) to afford compound (*S*, *S*)-**4.9** as a white powder in 64 % yield (0.192 mmol, 105 mg). ^{1}H NMR (600MHz, Chloroform-d) δ 12.19 (s, 2H, OH), 7.07 (s, 2H), 6.14 (d, *J* = 9.6 Hz, 2H, NH), 4.09 (m, 2H), 2.78 (m, 4H), 2.49 (m, 2H), 2.16 (m, 2H), 1.82 – 1.63 (m, 8H), 1.17 (d, *J* = 6.8 Hz, 6H), 0.97 (s, 18H). ^{13}C {^{1}H} NMR (151 MHz, Chloroform-*d*) δ 169.42, 156.32, 142.94, 127.56, 125.23, 124.96, 112.41, 52.77, 34.49, 29.62, 27.46, 26.39, 23.09, 22.97,16.30. No signals were observed in ^{19}F NMR. HRMS Calcd for $C_{36}H_{49}N_2O_4$ (MH+): 549.3692, Found: 549.3700. m.p. >260°C (decompose). $[a]_D$ = 7.93 (c=1.04 in $CHCl_3$).

Synthesis of (*S*, *R*)-4.9

Compound (*S*, *R*)-**4.9**, a diastereomer of (*S*, *S*)-**4.9**, was obtained as a white powder in 57% yield with the same procedure as above but by using (*R*)-3, 3-dimethyl-2-butylamine, (*R*)-**4.3**. ^{1}H NMR (600 MHz, Chloroform-*d*) δ 12.12 (s, 2H, OH), 7.06 (s, 2H), 6.09 (d, *J* = 9.6 Hz, 2H, NH), 4.09 (m, 2H), 2.78 (m, 4H), 2.51 (m, 2H), 2.17 (m, 2H), 1.83 – 1.62 (m, 8H), 1.14 (d, *J* = 6.8 Hz, 6H), 0.99 (s, 18H). $^{13}C\{^1H\}$ NMR (151MHz, Chloroform-*d*) δ 169.60, 156.19, 143.01, 127.61, 125.23, 124.88, 112.54, 52.80, 34.51, 29.64, 27.48, 26.43, 23.11, 22.97, 16.24. No signals were observed in ^{19}F NMR. HRMS Calcd for $C_{36}H_{49}N_2O_4$ (MH+): 549.3692, Found: 549.3698. m. p. >260°C (decompose). $[a]_D$ = -72.4 (c=1.02 in $CHCl_3$).

Synthesis of (*S*, *R*, *S*)-4.16

Under nitrogen, (*S*)-**4.2** (0.233 mmol, 253 mg) was dissolved in minimum amount of dry THF, then 4.5 mL of DMF was added, followed by the addition of (1*R*, 2*S*)-(−)-norephedrine (2.33 mmol, 352 mg). The mixture was allowed to react at room temperature for 12 h. TLC indicates a complete conversion of (*S*)-**4.2** and the mixture shows strong blue color under UV-lamp. The mixture was poured into 20 mL H_2O, and extracted with ethyl acetate (5 × 5 mL). The combined organic extracts were washed with brine, and dried over Na_2SO_4. After evaporation of the solvents, the residue was purified by column chromatography on silica gel eluted with hexane/ethyl acetate (3 / 1 to 1 / 1) to afford compound (*S*, *R*, *S*)-**4.16** as a white powder in 77 % yield (0.180 mmol, 117 mg). ^1H NMR (600MHz, Chloroform-d) δ 12.16 (s, 2H, OH), 7.40 – 7.28 (m, 10H), 7.11 (s, 2H), 6.64 (d, *J* = 8.5Hz, 2H, NH), 4.98 (t, *J* = 3.1 Hz, 2H,), 4.49 (m, 2H), 3.03 (s, 2H, HOCH), 2.75 (m, 4H), 2.49 (m, 2H), 2.15 (m, 2H), 1.82 – 1.64 (m, 8H), 1.10 (d, *J* = 6.9 Hz, 6H). ^{13}C $\{^1H\}$ NMR (151 MHz, Chloroform-*d*) δ 170.32, 156.24, 143.34, 140.79, 128.45, 127.91, 127.79, 126.35, 125.63, 125.00, 112.08, 76.04, 50.88, 29.49, 27.50, 23.05, 22.93, 14.12. No signals were observed in ^{19}F NMR. HRMS Calcd for $C_{40}H_{45}N_2O_6$ (MH+): 649.3278, Found: 649.3279. [a]$_D$ = -54.5 (c=1.03 in $CHCl_3$).

Synthesis of (*S*, *S*, *R*)-4.16

Compound (*S*, *S*, *R*)-**4.16**, a diastereomer of (*S*, *R*, *S*)-**4.16**, was obtained as a white powder in 70% yield by using the same procedure as above but starting with (1*S*, 2*R*)-(+)-norephedrine. ^{1}H NMR (600MHz, Chloroform-d) δ 11.90 (s, 2H, OH), 7.40 – 7.28 (m, 10H), 7.14 (s, 2H), 6.63 (d, *J* = 8.4 Hz, 2H, NH), 4.95 (m, 2H), 4.51 (m, 2H), 3.30 (s, 2H, HOCH), 2.73 (m, 4H), 2.50 (m, 4H), 2.18 (m, 2H), 1.80 – 1.61 (m, 8H), 1.07 (d, *J* = 6.7 Hz, 2H). ^{13}C {^{1}H} NMR (151 MHz, Chloroform-d) δ 170.24, 156.04, 143.32, 140.51, 128.41, 127.88, 127.84, 126.31, 125.59, 124.91, 112.07, 76.33, 50.67, 29.44, 27.49, 23.00, 22.89, 14.32. No signals were observed in ^{19}F NMR. HRMS Calcd for $C_{40}H_{45}N_2O_6$ (MH+): 649.3278, Found: 649.3268. [a]$_D$=36.8 (c=1.07 in $CHCl_3$).

Synthesis of (*S*, *R*, *S*)-4.22

Under nitrogen, (*S*)-**4.1** (0.100 mmol, 108 mg) was dissolved in 2 mL DMF, followed by the addition of (1*R*, 2*S*)-(−)-norephedrine (1.00 mmol, 151 mg in 2 mL DMF). The mixture turned into deep red color immediately, which then turned into yellow after a few hours. The mixture was allowed to react for 12 h at room temperature. TLC indicates the complete conversion of (*S*)-**4.1**. The mixture was poured into 15 mL H_2O, and extracted with ethyl acetate (5 × 5 mL). The combined organic extracts were washed with brine, and dried over Na_2SO_4. After evaporation of solvents, the residue was purified by column chromatography on silica gel eluted with hexane/ethyl acetate (1 / 1 to 1 / 3) to afford compound (*S*, *R*, *S*)-**4.22** as a yellow powder in 94 % yield (0.094 mmol, 60.2 mg). ^{1}H NMR (600 MHz, Chloroform-d) δ 12.68 (s, 2H, OH), 8.09 (s, 2H), 7.53 (d, *J* = 8.2 Hz, 2H), 7.40 (m, 6H), 7.34 (m, 4H), 7.28 – 7.23 (m, 4H), 7.13 (t, *J* = 7.3 Hz, 2H), 7.08(d, *J* = 8.6 Hz, 2H, NH), 5.08 (m, 2H), 4.55 (m, 2H), 3.26 (d, *J* = 3.8 Hz, 2H), 1.19 (d, *J* = 6.9 Hz, 6H). ^{13}C {^{1}H} NMR (151 MHz, Chloroform-*d*) δ 170.06, 154.24, 141.05, 136.21, 129.18, 128.79, 128.45, 128.22, 127.67, 127.38, 126.18, 124.67, 124.23, 117.50, 116.70, 75.23, 51.56, 13.34. No signals were observed in ^{19}F NMR. HRMS Calcd for $C_{40}H_{37}N_2O_6$ (MH+): 641.2652, Found: 641.2645. $[a]_D$ = -16.9 (c = 1.03 in $CHCl_3$).

Synthesis of (*S*)-1,1'-(2,2'-dihydroxy-[1,1'-binaphthalene]-3,3'-diyl)bis(2,2,3,3,4,4,4-heptafluorobutan-1-one), (*S*)-4.32

(1). Compound (*S*)-BINOL-MOM (1 mmol, 374 mg) was dissolved in dry diethyl ether (12 mL). The solution was cooled to 0 °C, and n-BuLi (4.0 mmol, 1.6 mL, 2.5 M in hexane,) was added dropwise. The reaction mixture was stirred at room temperature for 2 h and cooled to -78 °C by dry ice / acetone. Then perfluorobutyryl chloride (C_3F_7COCl, 4.0 mmol, 600 μL) was added dropwise. The reaction mixture was stirred at -78 °C for 1 h, and then warmed up to 0 °C to react for additional 1 h to afford a yellow cream-like mixture. Saturated aqueous solution of NH_4Cl (2 mL) was added to quench the reaction at 0 °C. The organic layer was separated, and the aqueous layer was extracted with ethyl acetate (3 x 10 mL). The combined organic extracts were washed with brine, and dried over anhydrous Na_2SO_4. After evaporation of the solvents, the mixture was further dried under vacuum pump to yield a yellow crude product.

(2). The crude product was dissolved in a minimum amount of methylene chloride, and cooled to 0 °C. Trifluroacetic acid (1.0 mL) was added slowly, and the mixture was stirred at room temperature for 1 h. Saturated aqueous solution of $NaHCO_3$ was added slowly to quench the reaction. The organic layer was separated, and the aqueous layer was extracted with CH_2Cl_2 (3 × 10 mL). The combined organic extracts were washed with brine, and dried over anhydrous Na_2SO_4. After evaporation of the solvents, the residue was purified by column chromatography on silica gel eluted with hexane / methylene chloride (10 / 1) to afford compound (*S*)-**4.2** as red solid in 42 % yield for two steps. ^{1}H NMR (600 MHz, Chloroform-*d*) δ 10.56 (s, 2H), 8.77 (d, *J* = 8.64 Hz, 2H), 8.00 (t, *J* = 8.45 Hz, 2H), 7.49 – 7.40 (m, 4H), 7.15 (t, *J* = 8.45 Hz, 2H,). ^{19}F NMR (564 MHz, Chloroform-d) δ -79.84 – -79.89 (m, 3F), -110.20 (t, *J* = 8.61 Hz, 2F), -124.76 – -124.77 (m, 2F). ^{13}C NMR (151 MHz, Chloroform-*d*) δ 187.58 (t, *J* = 25.42 Hz), 155.03, 138.49, 136.46 (t, *J* = 6.9 Hz), 132.32, 131.36, 127.20, 125.26, 124.68, 117.96, 116.70, 119 – 108 (m, weak).

Synthesis of 2,2,3,3,4,4,5,5,6,6,7,7,8,8,8-pentadecafluoro-1- (2-hydroxyphenyl)octan-1-one, 4.23.

Compound **4.23** was synthesized by using Fries rearrangement with a single step protocol. Under nitrogen, a solution of phenol (1 mmol, 94.1 mg) in DCE (4 mL) was cooled to 0°C, followed by addition of perfluorooctanoyl chloride ($C_7F_{15}COCl$, 1.5 mmol, 375 μL) dropwise 0 °C. After 10 min, anhydrous $AlCl_3$ (3.5 mmol, 467 mg) was added in 3-portions over 15 min. The solution was warmed to room temperature over 2 hours, and then was heated to 40 °C. After it was kept at 40 °C for 19 h, the solution was cooled to room temperature and powered to ice water (10 mL). The mixture was extracted with DCM (3 × 10 mL). The combined organic extracts were washed with saturated $NaHCO_3$ (20 mL), then brine (20 mL) and dried over anhydrous Na_2SO_4. The solvents were evaporated and the crude products were re dissolved in diethyl ether (20 mL) and 6 N HCl was added to lower the pH to 7. Saturated $NaHCO_3$ (20 mL) was added to the mixture, which was extracted with diethyl ether (3 × 20 mL). The combined organic extracts were washed with brine (30 mL) and dried over anhydrous Na_2SO_4. After evaporation of the solvents, the residue was purified by column chromatography on silica gel eluted with methylene chloride/ hexane (0 / 1 to 1 / 15) to afford compound **4.23** as yellow oil in 36 % yield. ^{1}H NMR (600 MHz, Chloroform-*d*) δ 11.25 (s, 1H), 7.91 (d, *J* = 7.53 Hz, 1H,), 7.63(t, *J* = 6.62 Hz, 1H), 7.10(d, *J* = 8.53 Hz, 1H), 7.00(t, *J* = 7.67 Hz, 1H). ^{19}F NMR (564 MHz, Chloroform-*d*) δ -80.78 (t, *J* = 9.00 Hz, 3F), -111.23 (t, *J* = 13.62 Hz, 2F), -120.51 – -120.57 (m, 2F), -120.78 – -120.94 (m, 2F), -121.90 – -121.99 (m, 2F), -122.62 – -122.68 (m, 2F), -126.09 – -126.15 (m, 2F).

The Fries rearrangement protocol was not successful when applied to the synthesis of other fluorinate ketone sensors.

Synthesis of 4-(methoxymethoxy)-1,1'-biphenyl, 4.27

Compound 1,1'-Biphenyl-4-ol (1 mmol, 170 mg) was dissolved in 10 mL anhydrous THF and cooled to 0°C. Under stirring, sodium hydride (2 mmol, 80 mg, 60% dispersion in mineral oil) was added in two portions and formation of white precipitate was observed. After 30 min at 0 °C, CH_3OCH_2Cl (MOMCl, 2 mmol, 152 μL) was added slowly. The mixture was warmed to room temperature and stirred for 3 h. After completion as indicated by TLC, the mixture was cooled to 0 °C and quenched by addition of 1 mL H_2O. The mixture was extracted by ethyl acetate (3 × 10 mL). The combined organic extracts were washed with brine, and dried over anhydrous Na_2SO_4. After evaporation of the solvents, the residue was purified by column chromatography on silica gel eluted with hexane/ethyl acetate (15 / 1 to 10 / 1) to afford compound **4.27** as a white solid in 84 % yield. ^{1}H NMR (600 MHz, Chloroform-*d*) δ 7.59 – 7.55 (m, 4H), 7.45 (t, *J* = 7.15 Hz, 2H), 7.34 (t, *J* = 7.15 Hz, 1H), 7.15(d, *J* = 7.9 Hz, 2H), 5.24 (s, 2H), 3.54(s, 3H).

Synthesis of 2,2,3,3,4,4,5,5,6,6,7,7,8,8,8-pentadecafluoro-1-(4-(methoxymethoxy)-[1,1'-biphenyl]-3-yl)octan-1-one, 4.28

A solution of **4.27** (1 mmol, 214 mg) in dry diethyl ether (12 mL) was cooled to 0°C, and n-BuLi (1.25 mmol, 500 μL, 2.5 M in hexane) was added dropwise. The solution was warmed to room temperature and stirred for another 2 h. It was then cooled to -78 °C (dry ice / acetone), and $C_7F_{15}COCl$ (1.25 mmol, 315 μL) was added dropwise. The reaction mixture was stirred at -78 °C for 1 h, and then warmed up to 0 °C to react for additional 2 h to afford a yellow cream-like mixture. Saturated aqueous solution of NH_4Cl (4 mL) was added to quench the reaction at 0 °C. The organic layer was separated, and the aqueous layer was extracted with ethyl acetate (3 × 10 mL). The combined organic extracts were washed with brine, and dried over anhydrous Na_2SO_4. After evaporation of the solvents, the residue was purified by column chromatography on silica gel eluted with hexane / methylene chloride (10 / 1 to 5 / 1) to afford compound **4.28** as a yellow oil in 74 % yield. ^{1}H NMR (600 MHz, Chloroform-*d*) δ 7.76 (d, *J* = 8.53

Hz, 1H), 7.69 (s, 1H), 7.56 (d, *J* = 8.15 Hz, 2H), 7.46 (t, *J* = 7.67 Hz, 2H), 7.39 – 7.35 (m, 2H), 5.28 (s, 2H), 3.53 (s, 3H). ^{19}F NMR (564 MHz, Chloroform-*d*) δ -80.97 (t, *J* = 9.91 Hz, 3F), -115.70 (t, *J* = 12.84 Hz, 2F), -120.63 – -120.67 (m, 2F), -121.09 – -121.15 (m, 2F), -122.01 – -122.09 (m, 2F), -122.74 – -122.81 (m, 2F), -126.23 – -126.27 (m, 2F).

Synthesis of 2,2,3,3,4,4,5,5,6,6,7,7,8,8,8-pentadecafluoro-1-(4-hydroxy-[1,1'-biphenyl]-3-yl)octan-1-one, 4.24

Compound **4.28** (0.74 mmol, 451 mg) was dissolved in 2 mL DCM and the solution was cooled to 0 °C. Trifluroacetic acid (2 mL) was added slowly, and the mixture was stirred at room temperature for 1 h. Saturated aqueous solution of $NaHCO_3$ was added slowly to quench the reaction. The organic layer was separated, and the aqueous layer was extracted with CH_2Cl_2 (3 × 10 mL). The combined organic extracts were washed with brine, and dried over anhydrous Na_2SO_4. After evaporation of the solvents, the residue was purified by column chromatography on silica gel eluted with hexane / methylene chloride (15 / 1) to afford compound **4.24** as yellow solid in 91 % yield. ^{1}H NMR (600 MHz, Chloroform-*d*) δ 11.23 (s, 1H), 8.09 (s, 1H), 7.88 (d, *J* = 8.7 Hz, 1H), 7.50 (dd, *J* = 20.3, 7.3 Hz, 4H), 7.39 (t, *J* = 7.2 Hz, 1H), 7.19 (d, *J* = 8.7 Hz, 1H). ^{19}F NMR (564 MHz, Chloroform-*d*) δ -80.77 (t, *J* = 9.8 Hz, 3F), -110.69 – -111.00 (m, 2F), -120.47 (q, *J* = 12.8, 12.3 Hz, 2F), -120.70 – -120.79 (m, 2F), -121.82 – -121.90 (m, 2F), -122.64 (d, *J* = 18.5 Hz, 2F), -126. 07 – -126.13 (m, 2F).

Synthesis of 2,2,3,3,4,4,4-heptafluoro-1-(4-hydroxy-[1,1'-biphenyl]-3-yl)butan-1-one, 4.35

(1). Compound **4.27** (2.91 mmol, 625 mg) was dissolved in dry diethyl ether (20 mL). The solution was cooled to 0 °C, and n-BuLi (3.64 mmol, 1.46 mL, 2.5 M in hexane,) was added dropwise. The reaction mixture was stirred at room temperature for 2 h and cooled to -78 °C. Then C_3F_7COCl (3.64 mmol, 544 μL) was added dropwise. The reaction mixture was stirred at -78 °C for 1 h, and then warmed up to 0 °C to react for additional 1 h. Saturated aqueous solution of NH_4Cl (4 mL) was added to quench the reaction at 0 °C. The organic layer was separated, and the aqueous layer was extracted with ethyl acetate (3 × 20 mL). The combined organic extracts were washed with brine, and dried over anhydrous Na_2SO_4. After evaporation of the solvents, the mixture was further dried under vacuum pump to yield a yellow crude product.

(2). The crude product was dissolved in a minimum amount of methylene chloride, and cooled to 0 °C. Trifluroacetic acid (3.0 mL) was added slowly, and the mixture was stirred at room temperature for 1 h. Saturated aqueous solution of $NaHCO_3$ was added slowly to quench the reaction. The organic layer was separated, and the aqueous layer was extracted with CH_2Cl_2 (3 × 20 mL). The combined organic extracts were washed with brine, and dried over anhydrous Na_2SO_4. After evaporation of the solvents, the residue was purified by column chromatography on silica gel eluted with hexane/methylene chloride (10 / 1) to afford compound **4.35** as a yellow solid in 75 % yield for two steps. ^{1}H NMR (600 MHz, Chloroform-*d*) δ 11.23 (s, 1H), 8.09 (s, 1H), 7.88 (d, J = 8.7 Hz, 1H), 7.55 – 7.43 (m, 4H), 7.42 – 7.36 (m, 1H), 7.19 (dd, J = 8.8, 2.4 Hz, 1H). ^{19}F NMR (564 MHz, Chloroform-*d*) δ -80.01 (td, J = 9.3, 2.5 Hz, 3F), -111.76 (q, J = 9.8, 8.9 Hz, 2F), -125.00 – -125.05 (m, 2F).

Synthesis of 1,1'-(4,4'-dihydroxy-[1,1'-biphenyl]-3,3'-diyl)bis(2,2,3,3,4,4,5,5,6,6,7,7,8,8,8-pentadecafluorooctan-1-one), 4.25

(1). The MOM protected 4,4'-biphenol was synthesized in 72 % yield by using 4,4'-biphenol (**4.29**, 1 mmol, 186 mg), NaH (4 mmol, 160 mg, 60% dispersion in mineral oil), and MOMCl (4 mmol, 304 μL) as the starting materials following the same procedure described for **4.27** above.

(2). A solution of the MOM protected 4,4'-biphenol (0.72 mmol, 198 mg) in diethyl ether (5 mL) was cooled to 0 °C, and n-BuLi (2.16 mmol, 864 μL, 2.5 M in hexane) was added dropwise. The solution was warmed to room temperature and stirred for another 2 h. It was then cooled to -78 °C (dry ice / acetone), and $C_7F_{15}COCl$ (2.16 mmol, 544 μL) was added dropwise. The reaction mixture was stirred at -78 °C for 1 h, and then warmed up to 0 °C to react for additional 2 h to afford a yellow cream-like mixture. Saturated aqueous solution of NH_4Cl (2 mL) was added to quench the reaction at 0 °C. The organic layer was separated, and the aqueous layer was extracted with ethyl acetate (3 × 10 mL). The combined organic extracts were washed with brine, and dried over anhydrous Na_2SO_4. After evaporation of the solvents, the crude product was further dried under vacuum pump.

(3). This crude product was dissolved in a minimum amount of methylene chloride, and cooled to 0 °C. Trifluroacetic acid (1.0 mL) was added slowly, and the mixture was stirred at room temperature for 1 h. Saturated aqueous solution of $NaHCO_3$ was added slowly to quench the reaction. The organic layer was separated, and the aqueous layer was extracted with CH_2Cl_2 (3 × 10 mL). The combined organic extracts were washed with brine, and dried over anhydrous Na_2SO_4. After evaporation of the solvents, the residue was purified by column chromatography on silica gel eluted with hexane/methylene chloride (15 / 1 to 10 / 1) to afford the final compound **4.25** as a yellow solid in 23 % yield for two steps. ^{1}H NMR (600 MHz, Chloroform-d) δ 11.25 (s, 1H, OH), 8.02 (s, 2H), 7.80(dd, *J* = 8.74, 2.26 Hz, 2H), 7.22(d, *J* = 8.73 Hz, 2H).^{19}F NMR (564 MHz, Chloroform-d) δ -80.94 (t, *J* = 10.02 Hz, 6F), -111.36 (t, *J* = 13.49Hz, 4F), -120.57 – -120.64 (m, 4F), -121.15 – -121.23 (m, 4F), -122.09 – -122.16(m, 4F), -122. 82 – -122.89 (m, 4F), -126.30 – -126.37 (m, 4F).

Synthesis of (*E*)-1,1'-(hex-3-ene-3,4-diylbis(6-hydroxy-3,1-phenylene))bis (2,2,3,3,4,4,5,5,6,6,7,7,8,8,8-pentadecafluorooctan-1-one), 4.26

(1). Starting with (*E*)-Diethylstilbestrol (**4.30**, 3 mmol, 805 mg), NaH (12 mmol, 480 mg, 60 % dispersion in mineral oil), and MOMCl (12 mmol, 912 μL), the MOM-protected product **4.31** was synthesized following the same procedure described for **4.27**, with a yield of 68 %. ^{1}H NMR (600 MHz, Chloroform-*d*) δ 7.12 – 7.10 (m, 4H), 7.03 – 7.01(m, 4H), 5.20 (s, 4H), 3.52(s, 6H), 2.11(q, *J* = 7.53 Hz, 4H,), 0.76 (t, *J* = 7.45 Hz, 6H).

(2). A solution of **4.31** (0.67 mmol, 240 mg) in diethyl ether (10 mL) was cooled to 0 °C, and n-BuLi (2.7 mmol, 1.08 mL, 2.5 M in hexane) was added dropwise. The solution was warmed to room temperature and stirred for another 2 h. It was then cooled to -78 °C (dry ice / acetone), and $C_7F_{15}COCl$ (2.7 mmol, 670 μL) was added dropwise. The reaction mixture was stirred at -78 °C for 1 h, and then warmed up to 0 °C to react for additional 2 h. Saturated aqueous solution of NH_4Cl (2 mL) was added to quench the reaction at 0 °C. The organic layer was separated, and the aqueous layer was extracted with ethyl acetate (3 × 10 mL). The combined organic extracts were washed with brine, and dried over anhydrous Na_2SO_4. After evaporation of the solvents, the crude product was further dried under vacuum pump.

(3). This crude product was dissolved in a 5 mL of methylene chloride, and cooled to 0 °C. Trifluroacetic acid (1.0 mL) was added slowly, and the mixture was stirred at room temperature for 1 h. Saturated aqueous solution of $NaHCO_3$ was added slowly to quench the reaction. The organic layer was separated, and the aqueous layer was extracted with CH_2Cl_2 (3 × 10mL). The combined organic extracts were washed with brine, and dried over anhydrous Na_2SO_4. After evaporation of the solvents, the residue was purified by column chromatography on silica gel eluted with hexane / methylene chloride (15 / 1 to 10 / 1) to afford the final compound **4.26** as a yellow solid in 25% yield for two steps. ^{1}H NMR (600 MHz, Chloroform-d) δ 11.21 (s, 2H, OH), 7.69 (s, 2H), 7.49 (dd, *J* = 8.53Hz, 2.02Hz, 2H), 7.12(d, *J* = 8.60Hz, 2H), 2.12(q, *J* = 7.14Hz, 4H), 0.77(t, *J* = 7.47Hz, 6H). ^{19}F NMR (564 MHz, Chloroform-d) δ -81.00 (t, *J* = 9.85 Hz, 6F,), -111.17 (t, *J* = 13.16 Hz, 4F) -120.58 – -120.64 (m, 4F), -120.99 – -121.05 (m, 4F), -122.10 – -122.13 (m, 4F), -122.83 – -122.87 (m, 4F), -126.30 – -126.36 (m, 4F).

Synthesis of (*S*)-1,1'-(2,2'-dihydroxy-5,5',6,6',7,7',8,8'-octahydro-[1,1'-binaphthalene]-3,3'-diyl)bis(2,2,3,3,4,4,4-heptafluorobutan-1-one), (*S*)-4.33

(1). Compound (*S*)-H_8BINOL-MOM (0.544 mmol, 208 mg) was dissolved in dry diethyl ether (10 mL). The solution was cooled to 0 ºC, and n-BuLi (2.18 mmol, 2.5 M in hexane, 0.87 mL) was added dropwise. The reaction mixture was stirred at room temperature for 2 h and cooled to -78 °C. Then perfluorobutyryl chloride (2.18 mmol, 0.326 mL) was added dropwise. The reaction mixture was stirred at -78 °C for 1 h, and then warmed up to 0 °C to react for additional 2 h. Saturated aqueous solution of NH_4Cl (1 mL) was added to quench the reaction at 0 °C. The organic layer was separated, and the aqueous layer was extracted with ethyl acetate (3 × 10 mL). The combined organic extracts were washed with brine, and dried over anhydrous Na_2SO_4. After evaporation of the solvents, the mixture was further dried under vacuum pump.

(2). The crude product was dissolved in a minimum amount of methylene chloride, and cooled to 0 °C. Trifluroacetic acid (0.5 mL) was added slowly, and the mixture was stirred at room temperature for 1 h. Saturated aqueous solution of $NaHCO_3$ was added slowly to quench the reaction. The organic layer was separated, and the aqueous layer was extracted with CH_2Cl_2 (3 × 10 mL). The combined organic extracts were washed with brine, and dried over anhydrous Na_2SO_4. After evaporation of the solvents, the residue was purified by column chromatography on silica gel eluted with hexane / methylene chloride (15 / 1) to afford compound (*S*)-**4.33** as yellow powder in 42 % yield for two steps. ^{1}H NMR (600 MHz, Chloroform-*d*) δ 11.29 (s, 2H), 7.69 (s, 2H), 2.85 – 2.82 (m, 4H), 2.54 – 2.45 (m, 2H), 2.29 – 2.21 (m, 2H), 1.85 – 1.75 (m, 6H), 1.73 – 1.67 (m, 2H). ^{19}F NMR (564 MHz, Chloroform-*d*) δ -80.05 (t, *J* = 9.5 Hz, 6F), -111.30 – -111.39 (m, 4F), -125.11 – -123.13 (m, 4F).^{13}C NMR (151 MHz, Chloroform-d) δ 186.50 (t, *J* = 26.53 Hz), 159.57, 150.25, 130.75, 129.78, 124.48, 113.76, 119-108 (m, weak), 29.52, 28.29, 22.67, 22.43.

Synthesis of 2,2'-(((*S*)-2,2'-dihydroxy-[1,1'-binaphthalene]-3,3'-dicarbonyl)bis(azanediyl))bis(3-hydroxypropanoic acid), (*S*)-4.36.

DMSO (3 mL) was added to a mixture of (*S*)-**4.32** (0.15 mmol, 102 mg) and tetrabutylammonium L-serine (1.6 mmol, 208 mg) under nitrogen. The mixture was stirred overnight at room temperature. The solution was poured into 30 mL H_2O, then 3 N HCl (2 mL) was added and white precipitate was observed. The mixture was extracted with ethyl acetate (5 × 15 mL). The combined organic extracts were washed with H_2O (20 mL), $NaHCO_3$ (saturated, 20 mL) and brine (40 mL). The organic solvents were evaporated and 10 mL of H_2O was added to the residual. The mixture was placed under sonication for 10 min, and centrifuged to get the white precipitate, which was further washed twice with water. The pure product was obtained after removal of solvents under a vacuum pump. ^{1}H NMR (600 MHz, acetone-d_6) δ 11.84 (s, 2H), 8.80 (s, 2H), 8.64 (d, *J* = 7.8 Hz, 2H), 7.98 (d, *J* = 5.8 Hz, 2H), 7.35 – 7.28 (m, 4H), 7.12 – 7.05 (m, 2H), 4.87 (d, *J* = 3.8 Hz, 2H), 4.19 – 4.08 (m, 4H). ^{13}C NMR (151 MHz, acetone-d_6) δ 171.62, 170.80, 155.62, 137.29, 130.25, 130.12, 129.34, 128.02, 125.23, 124.41, 118.06, 117.88, 62.59, 56.20.

Synthesis of 1,1'-((1*S*)-6,6'-bis(2-((1,1,1,2,3,3,4,4,5,5,6,6,7,7,8,8-hexadecafluoro-8λ^3-octan-2-yl)-λ^2-fluoranyl)ethyl)-2,2'-dihydroxy-[1,1'-binaphthalene]-3,3'-diyl) bis (2,2,3,3,4,4,4-heptafluorobutan-1-one), (*S*)-4.38

(1). Compound **3.17** (0.632 mmol, 800 mg) was dissolved in dry diethyl ether (12 mL). The solution was cooled to 0 °C, and n-BuLi (2.53mmol, 1mL, 2.5 M in hexane,) was added dropwise. The reaction mixture was stirred at room temperature for 2 h and cooled to -78 °C. Then C_3F_7COCl (2.53 mmol, 0.38 mL) was added dropwise. The reaction mixture was stirred at -78 °C for 1 h, and then warmed up to 0 °C to react for additional 1 h. Saturated aqueous solution of NH_4Cl (2 mL) was added to quench the reaction at 0 °C. The organic layer was separated, and the aqueous layer was extracted with methylene chloride (4 × 20 mL). The combined organic extracts were washed with brine, and dried over anhydrous Na_2SO_4. After evaporation of the solvents, the mixture was further dried under vacuum pump to yield the red crude product. TLC showed the formation of a major product.

(2). The crude product was dissolved in methylene chloride (30 mL), and cooled to 0 °C. Trifluroacetic acid (0.6 mL) was added slowly, and the mixture was stirred at room temperature for 1 h. Saturated aqueous solution of $NaHCO_3$ was added slowly to quench the reaction. The organic layer was separated, and the aqueous layer was extracted with CH_2Cl_2 (3 × 20 mL). The combined organic extracts were washed with brine, and dried over anhydrous Na_2SO_4. After evaporation of the solvents, the residue was purified by column chromatography on silica gel eluted with hexane/methylene chloride (15 / 1) to afford compound **4.38** as an orange powder in 29 % yield in two steps. ^{1}H NMR (600 MHz, Chloroform-*d*) δ 10.55 (s, 2H), 8.73 (s, 2H), 7.84 (s, 2H), 7.33 (d, J = 7.5 Hz, 2H), 7.13 (d, J = 8.1 Hz, 2H), 3.17 – 2.94 (m, 4H), 2.58 – 2.36 (m, 4H). ^{19}F NMR (564 MHz, Chloroform-d) δ -79.88 (t, J = 7.8 Hz, 6F), -80.78 (t, J = 8.9 Hz), -110.02 – -110.42 (m), -114.20 – -114.63 (m), -121.52 – -121.94 (m), -122.54 – -122.84 (m), -123.22 – -123.60 (m), -124.63 – -124.83 (m), -125.86 – -126.46 (m).

4.4.4. Mass spectroscopic studies

A solution of (*S*)-**4.2** (0.05 mmol, 54 mg in 0.2 mL THF) and amine (*S*)-**4.3** (0.3 mmol, 40 μL in 6 mL DMF) were prepared in 2 separate vials. The amine solution was poured into the vial containing (*S*)-**4.2**, and the resulting mixture was injected into mass spectrometer immediately after a brief manual shaking.

4.5. References

(1) Reviews on enantioselective fluorescent recognition: (a) Pu, L. *Chem. Rev*. **2004**, 104, 1687–1716. (b) Leung, D.; Kang, S. O.; Anslyn, E. V. *Chem. Soc. Rev*. **2012**, 41, 448–479. (c) Accetta, A.; Corradini, R.; Marchelli, R. *Top. Curr. Chem*. **2011**, 300, 175–216. (d) Pu, L. *Acc. Chem. Res*. **2012**, 45, 150–163. (e) Zhang, X.; Yin, J.; Yoon, J. *Chem. Rev*. **2014**, 114, 4918-4959.

(2) (a) James, T. D.; Sandanayake, K. R. A. S.; Shinkai, S. *Nature* **1995**, 374, 345–347. (b) Lin, J.; Hu, Q. -S.; Xu, M. H.; Pu, L. *J. Am. Chem. Soc*. **2002**, 124, 2088–2089. (c) Li, Z. –B.; Lin, J.; Pu, L. *Angew. Chem. Int. Ed.* **2005**, 44, 1690-1693.

(3) (a) Zhao, J.-Z.; Fyles, T. M.; James, T. D. *Angew. Chem., Int. Ed*. **2004**, 43, 3461–3464. (b) Zhu, L.; Anslyn, E. V. *J. Am. Chem. Soc.* **2004**, 126, 3676–3677. (c) Mei, X. F.; Wolf, C. *J. Am. Chem. Soc*. **2004**, 126, 14736–14737

(4) (a) Irie, M.; Yorozu, T.; Hayashi, K. *J. Am. Chem. Soc*. **1978**, 100, 2236-2237. (b) Iwanek, W.; Mattay, J. *J. Photochem. Photobiol. A: Chem*., **1992**, 67, 209-226.

(5) (a) Pugh, V.; Hu, Q. -S.; Pu, L. *Angew. Chem. Int. Ed.* **2000**, 39, 3638-3641. (b) Huang, Z.; Yu, S. S.; Yu, X. Q.; Pu. L. *Chem. Sci*. **2014**, 5, 3457-3462.

(6) (a) Reetz, M. T.; Sostmann, S. *Tetrahedron*. **2001**, 57, 2515. (b) Liu, S. –L.; Pestano, J. P. C.; Wolf, C. *J. Org. Chem*. **2008**, 73, 4267–4270.

(7) (a) Yorozu, T.; Hayashi, K.; Irie, M. *J. Am. Chem. Soc.* **1981**, 103, 5480-5484**.** (b) Zheng, Y.; Hu, Y. *J. Org. Chem*. **2009**, 74, 5660-5663. (c) He, X.; Zhang, Q.; Liu, X. –H.; Lin, L. –L.; Feng, X. -M. *Chem. Commun*. **2011**, 47, 11641–11643. (d) Jiao, J. –M.; Wei, G.; Li, F.; Mao, X. –R.; Cheng, Y. –X.; Zhu, C. -J. *RSC Adv*. **2014**, 4, 5887-5892.

(8) Wang, C.; Wu, E.; Wu, X. –D.; Xu, X. –C.; Zhang, G. –Q.; Pu, L. *J. Am. Chem. Soc.* **2015**, 137, 3747−3750.

(9) Formation of amides from the reaction of perfluoroalkyl ketones with amines was reported but not used in molecular recognition: (a) Hauptschein, M.; Braun, R. *J. Am. Chem. Soc.* **1955**, 77, 4930–4931. (b) Smith, R. D.; Fawcett, F. S.; Coffman, D. *J. Am. Chem. Soc*. **1962**, 84, 4285-4288. (c) Shchegol'kov, E.; Saloutin, V. *J. Fluorine Chem.* **2007**, 128, 779-788. (d). Howell, J.; Ende, A. *J. Fluorine Chem.* **2008**, 129, 178-184.

(10) (a). Woolfe, G.; Thistletbwaite, P. *J. Am. Chem. Soc.* **1980**,102, 6917-6923. Catalk, J.; (b). Torlblo, F.; Acuna, A. *J. Phys. Chem*. **1982**, 86. 303-306.

(11) Krusic, P.; Roe, D. *Anal. Chem*. **2004**, 76, 3800**-**3803.

(12) Deberardinis, A. M.; Turlington, M.; Ko, J.; Sole, L.; Pu, L. *J. Org. Chem*. 2010, 75, 2836.

Chapter 5. A fluorinated BINAM derived sensor for chiral recognition

5.1. Design and synthesis of (*S*)-5.1

We prepared sensor (*S*)-**5.1** starting with (*S*)-BINAM through two steps reaction involving amidation and aromatic substitution with a 26 % overall yield. The carbonyls in (*S*)-**5.1** are activated by trifluoromethyl groups, which make them good nucleophilic addition sites for chiral molecules. The amide group of (*S*)-**5.1** may form hydrogen bonds with incoming guests, and the bulky pivaloyl groups nearby might create an enhanced enantioselective environment in cooperation with the 1, 1'-binaphthyl backbone.

Scheme 5- 1. Synthesis of (*S*)-**5.1** from (*S*)-BINAM.

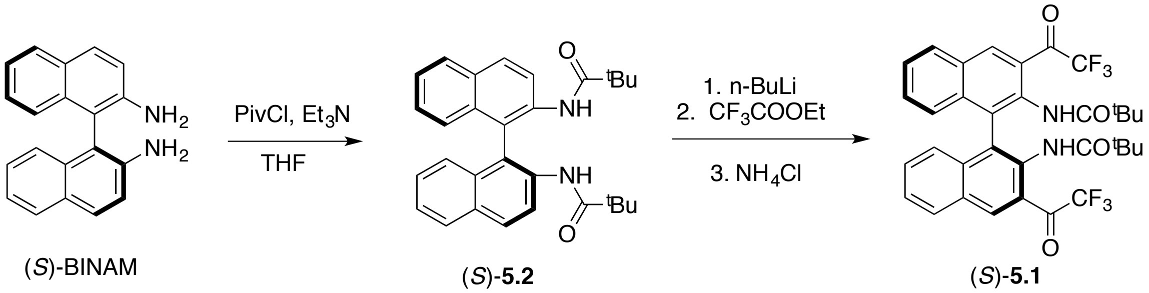

We measured the fluorescence spectra of (*S*)-**5.1** in various solvents (Figure 5-1). (*S*)-**5.1** shows weak fluorescent emission in aprotic solvents like CH_2Cl_2, THF or CH_3CN, and strong emission under the existence of protic solvents like methanol or water. When the amount of water was increased gradually, fluorescence intensity also increased until a saturation point is reached when tested with amino acids (Figure 5-2). They all show a major emission at 357 nm, which is typical for the binaphthyl fluorophore. In CH_2Cl_2 or DMF, it also shows a weak emission at 470 nm, which may be attributed to the effect of the intramolecular NH$\cdots$O=C hydrogen bonding that results in a more planar conjugated system in (*S*)-**5.1**.

Figure 5- 1. Fluorescence spectra of (*S*)-**5.1** (0.01 mM) in various solvents. (λ_{ex} =290 nm, slit = 3.0 / 3.0 nm). The ratios of mixed solvents are 1 / 1 (v / v).

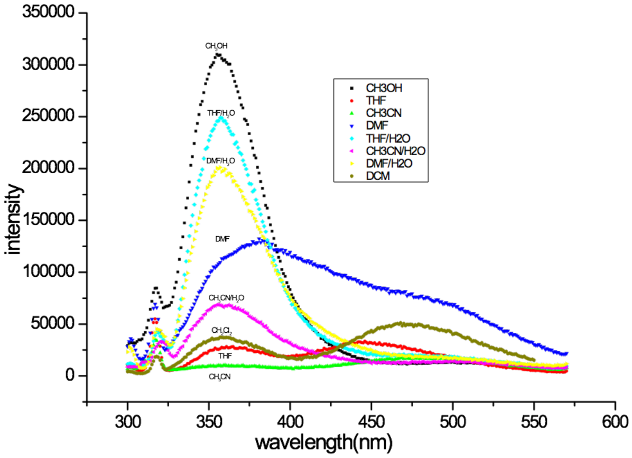

Figure 5- 2. Fluorescence spectra of (*S*)-**5.1** (0.01 mM) with L-serine (1.0 mM) in H_2O / CH_3CN with different ratios (λ_{ex} = 290 nm, slit = 3.0 / 3.0 nm).

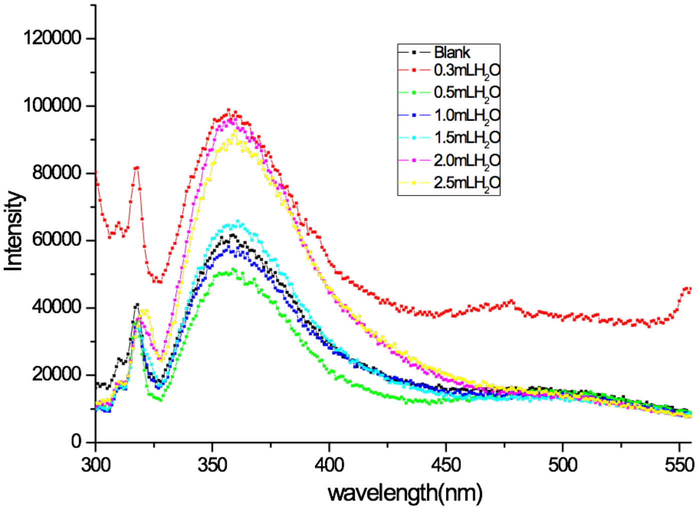

5.2. Fluorescence response of (*S*)-5.1 to chiral molecules

We explored the fluorescence recognition of (*S*)-**5.1** toward amino acids, amino esters, amino alcohols, hydroxyl acids and amines. The enantiomeric fluorescence enhancement ratios *ef* [= (I_S - I_0) / (I_R - I_0)] were summarized in Table 5-1. For amino acids, it shows satisfactory recognition to alanine and serine, with the L-enantiomers cause larger fluorescence enhancement than the D-enantiomers (Figure 5-3). However, no substantial enantioselectivity toward other amino acids like arginine and lysine was observed. D- or L-arginine both caused small fluorescence quenching at 357 nm, while D- or L-Lysine both caused enhancement at 470 nm.

Table 5- 1. The *ef* values of (*S*)-**5.1** to various kinds of chiral molecules.

Amino Acids				Amino Esters		
Ala	Ser	Arg	Lys	Tyr-OMe	Leu-OMe	Ala-OMe-HCl
3.0	3.8	1.1	1.0	1.0	1.1	1.2
Amino Alcohols (1-3)				hydroxy acids (4-6)		
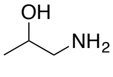	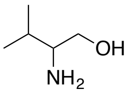	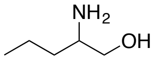		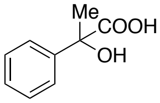	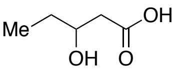	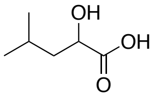
1.1	1.0	1.0		8.9	2.6	1.2

Figure 5- 3. Fluorescence spectra of (*S*)-**5.1** (0.01 mM) with the addition of different amino acids (1.0 mM). (λ_{ex} = 290 nm, slit = 3.0 / 3.0 nm, CH_3CN / H_2O = 4.5 / 0.5 mL).

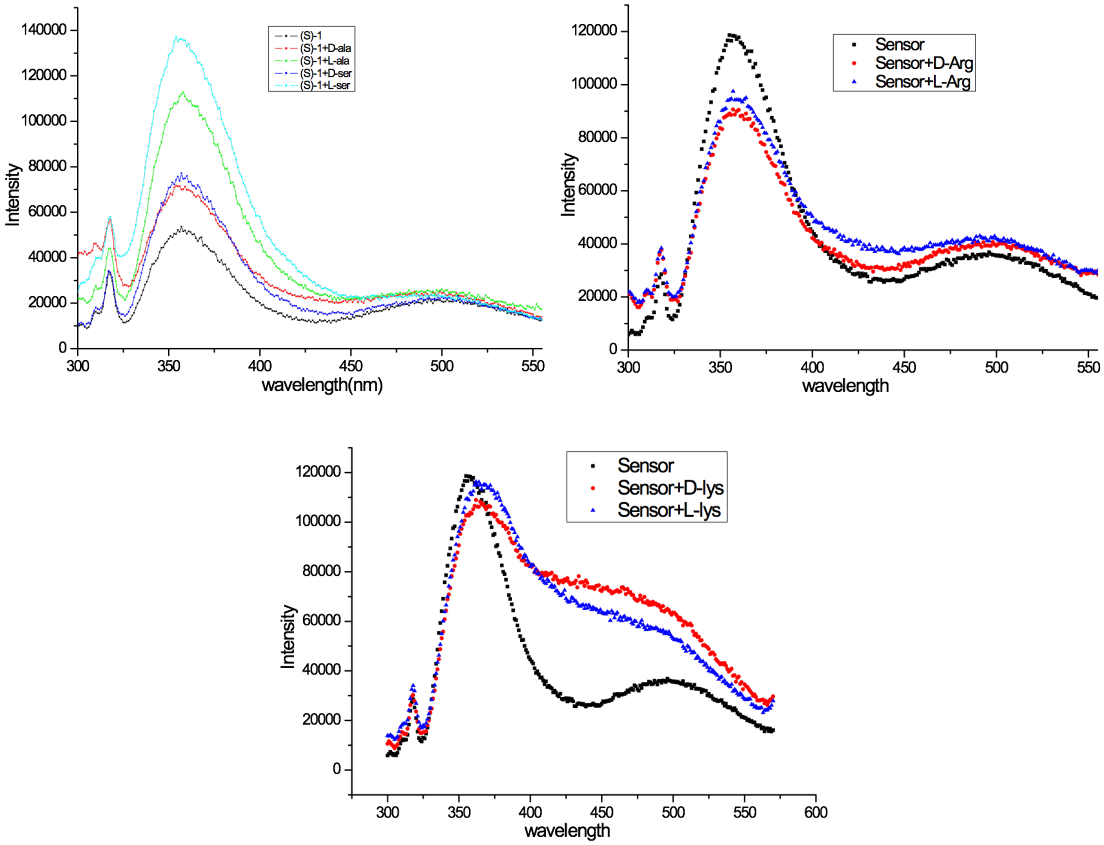

Figure 5- 4. Fluorescence spectra of (*S*)-**5.1** (0.01 mM) with the addition of hydroxyl acids (5.0 mM). (λ_{ex} = 290 nm, slit = 3.0 / 3.0 nm, solvent: CH_2Cl_2).

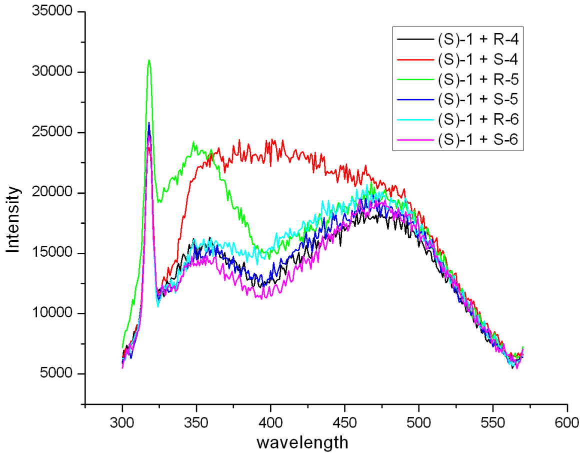

For the amino esters and amino alcohols listed in table 5-1, no enantioselectivity was observed. The hydroxyl acids show better selectivity but with very weak emissions (Figure 5-4). While (*S*)-2-hydroxy-2-phenylpropanoic acid (4) causes some fluorescence enhancement of (*S*)-**5.1**, its *R* form barely makes any changes.

Figure 5- 5. Fluorescence spectra of (*S*)-**5.1** (0.01 mM) with (1*R*, 2*R*)-DAH (top left) or (1*S*, 2*S*)-DAH (top right) at various concentrations; Fluorescence intensity at 474 nm was plotted against the conc. (bottom left) and *ee* (bottom right). 2nd-order fitting was applied (λ_{ex} =290 nm, slit = 3.0 / 3.0 nm, solvent: CH_2Cl_2).

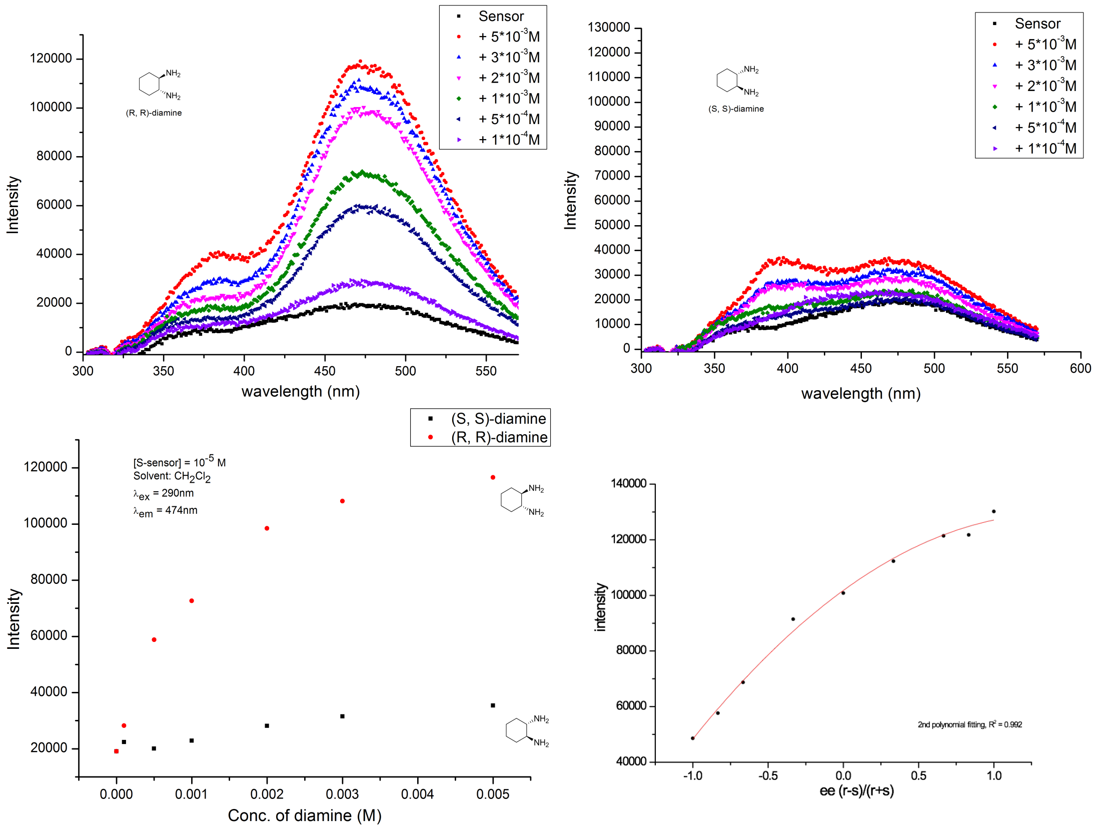

We then tested the fluorescence response of (*S*)-**5.1** toward trans-1, 2-diaminocyclohexane (DAH). Both (1*R*, 2*R*)-DAH and (1*S*, 2*S*)-DAH caused similar fluorescence enhancement of (*S*)-**5.1** at 376 nm, while (1*R*, 2*R*)-DAH caused much stronger emission at 474 nm than its enantiomer (Figure 5-5). For fluorescence intensity at 474 nm (I_{474}), the *ef* is calculated to be 15.8.

As the concentration of DAH increase from 0.1 mM to 5 mM, I_{474} of (1*R*, 2*R*)-DAH increases significantly while that of (1*S*, 2*S*)-DAH barely changes. The emission reaches a saturation point when 5 mM of diamine is added. When (1*R*, 2*R*)-DAH and (1*S*, 2*S*)-DAH are mixed in different ratios to make solutions with enantiomeric excess ranging from -100 % to 100 %, the I_{474} increases nonlinearly with the *ee* values. Additionally, as emission at 376 nm is identical for two enantiomers, thus it can be used to measure the total concentration of mixtures containing both enantiomers. For a give DAH mixture, both concentration and *ee* information can be obtained simultaneously with a single fluorescence measurement.

5.3. Mechanism studies

In order to understand the mechanism for fluorescence recognition, we conducted ^{19}F NMR titration experiments (Figure 5-6). The ^{19}F NMR spectrum of (*S*)-**5.1** in $CDCl_3$ shows a peak at δ -71.75 ppm. When (1*R*, 2*R*)-DAH was added gradually from 1 equiv., two new peaks at -72.82 ppm and -80.63 ppm appeared and kept growing until 10 equiv. of (1*R*, 2*R*)-DAH were added. In contrast, only the peak at -72.82ppm appeared for the titration with (1*S*, 2*S*)-DAH, and 30 equiv. were needed for the reaction to complete. Thus it can be assumed that the nucleophilic addition proceeds faster with the *R*-

enantiomer and two major products are formed simultaneously, compared with one single product for *S*-enantiomer.

Figure 5- 6. ^{19}F NMR titration of (1*R*, 2*R*)-DAH or (1*S*, 2*S*)-DAH to (*S*)-**5.1** in $CDCl_3$.

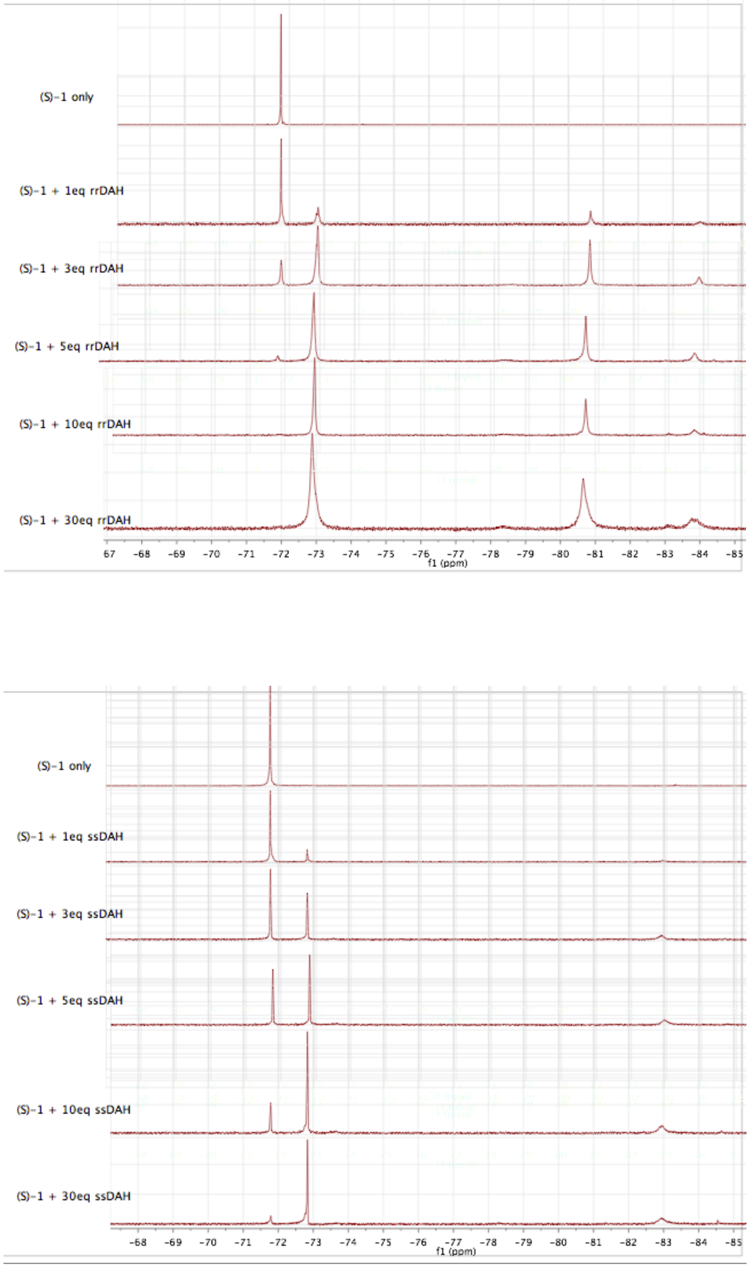

In the titration, the $CDCl_3$ solution of (*S*)-**5.1** (0.5 mL, 5.0 mmol) was prepared in a NMR tube. The $CDCl_3$ solution of (1*S*, 2*S*) or (1*R*, 2*R*)-DAH (2.5 mM) was prepared in a 1 mL volumetric flask as the stock solution. The NMR spectrum of the (*S*)-**5.1** solution was first recorded and the stock solution of the DAH was added to the NMR tube in the following fashion: 2 μL, 4 μL, 4 μL, 10 μL, and then 40 μL (for 1 eq, 3 eq, 5 eq, 10 eq and 30 eq of DAH respectively). The solution was well mixed after each addition and the ^{19}F NMR spectra were recorded immediately. Based on the known reaction of trifluoromethyl ketone with amine, we proposed the reaction routes as shown in Scheme 5-2.

Scheme 5- 2. Reactions between (*S*)-**5.1** and DAH.

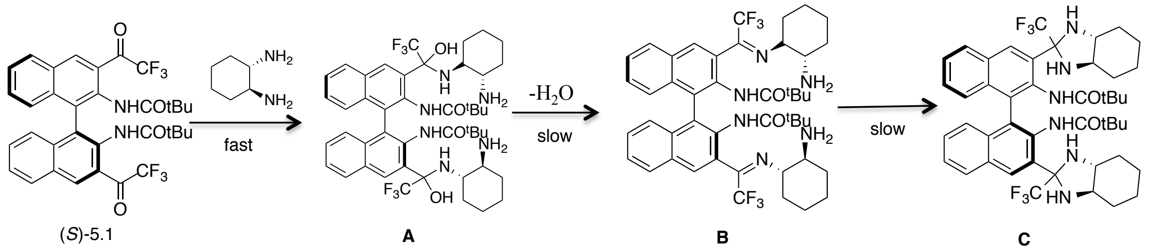

When DAH is added, it first attacks the activated carbonyl group of (*S*)-**5.1** to form the hemiaminal intermediate **A**, which then undergoes elimination to form an imine intermediate **B**. Then the cyclic aminal product **C** can also be formed slowly with the addition of the second amino group to the imine.[1] In the time-scale of sensing, which is finished within 2 hours, the intermediates **A** and **B** should be mainly responsible for observed fluorescence enhancement. We hypothesized that the new ^{19}F NMR signal at -72.82 ppm and fluorescence emission at 376 nm should originate from the hemiaminal intermediate **A**, while the signal at -80.63 ppm and emission at 474 nm come from the imine **B** that has better conjugation. For both enantiomers, the intermediate **A** can be formed with a similar rate, resulting in similar emission at 376 nm to be observed. Due to the orientation difference in space, the formation of the imine **B** is more facile for the *R*-enantiomer than for the *S* one.

5.4. Conclusion

Herein a novel BINAM derived sensor (*S*)-**5.1** was designed and synthesized. Among the substrates tested, the best enantioselectivity was found in the fluorescence recognition of 1, 2-diaminocyclohexane in a ratiometric manner. ^{19}F NMR titration revealed that the enantioselectivity was due to the difference in the rate of the reaction of (*S*)-**5.1** with the diamine. This sensor also shows moderate enantioselectivity toward a few hydroxyl acids and amino acids studied.

5.5. Experimental part

5.5.1. General data

All reactions were carried out under N_2 unless otherwise noted. Fluorous reagents and solvents were purchased from SynQuest Labs, Inc. All other chemicals were purchased from Sigma Aldrich Chemical Co., Alfa Aesar or TCI America. Other chemicals were used without further purification. Methylene chloride and diethyl ether were dried by passing through activated alumina columns under nitrogen. THF, DMF, and DMSO are spectroscopic grades and used without purification. Optical rotations were measured on a Jasco P-2000 digital polarimeter. NMR spectra were recorded on Varian-600 MHz spectrometer. Chemical shifts for 1H NMR spectra were reported in parts per million relative to a singlet at 7.26 ppm for residual HCCl3 in deuterated chloroform. Chemical shifts for ^{13}C NMR were reported relative to the centerline of a triplet at 77.16

ppm for deuterated chloroform. The ^{19}F NMR spectra were reported in units of part per million (ppm) relative to trifluoroacetic acid (δ -76.55 ppm) as an external reference. Steady-state fluorescence emission spectra were recorded on Horiba FluoroMax-4 spectrofluorometer. High and low resolution mass spectra were obtained from the University of Illinois at Urbana-Champaign (UIUC) Synapt G2SiMass Spectrometry Facility. UV-Vis spectra were produced from a Hewlett-Packard 8452A diode-array spectrophotometer.

5.5.2. Synthesis and characterization

Synthesis of (*S*)-2,2'-bis(pivaloylamino)-1,1'-binaphthyl, (*S*)-5.2

Compound (*S*)-**5.2** was synthesized according to a slightly modified literature procedure[3]. Under nitrogen, to a dried 10 mL round-bottom flask with a reflux condenser was charged with (*S*)-BINAMS (1.0 mmol, 284 mg) and TEA (4.0 mmol, 560 μL). 5 mL of dry THF was added, followed by addition of pivaloyl chloride (2.0 mmol, 250 μL). The reaction mixture was refluxed 4 h, and the precipitate was filtered off. After evaporation of the solvent, the residue was purified by column chromatography on silica gel eluted with hexane/ethyl acetate (4 / 1) to afford the product as a white powder in 81 % yield. ^{1}H NMR (300 MHz, Chloroform-*d*): δ 0.75 (d, 18H), 7.15 (d, *J* = 7.9 Hz, 2H), 7.18 (s, 2H), 7.29 – 7.34 (m, 2H), 7.43 – 7.48 (m, 2H), 7.94 (d, *J* = 7.8 Hz, 2H), 8.05 (d, *J* = 9.5 Hz, 2H), 8.48 (d, *J* = 9.5 Hz, 2H).

Synthesis of (*S*)-N,N'-(3,3'-bis(2,2,2-trifluoroacetyl)-[1,1'-binaphthalene]-2,2'-diyl)bis(2,2-dimethylpropanamide), (*S*)-5.1

Compound (*S*)-**5.2** (0.8 mmol, 370 mg) was dissolved in dry ether (10 mL). The solution was cooled to 0 ºC, and n-BuLi (4.8 mmol, 2.5 M in hexane, 2.0 mL) was added dropwise. The reaction mixture was stirred for 4 h at room temperature and cooled to 0°C, and then ethyl trifluoroacetate (4.8 mmol, 0.6 mL) was added slowly. The reaction mixture was allowed to warm to room temperature and stirred for 2 h to afford a cream-like mixture. A saturated aqueous NH_4Cl solution was added to quench the reaction. The organic layer was separated, and the aqueous layer was extracted with ethyl acetate (3 x 20 mL). The combined organic extracts were washed with brine, and dried over Na_2SO_4. After evaporation of the solvent, the residue was purified by column chromatography on silica gel eluted with hexane/methylene chloride (from 1 / 3 to 1 / 10) to afford compound (*S*)-1 as a yellow powder in 32% yield. ^{1}H NMR (300 MHz, Chloroform-d): δ 0.73 (s, 18H), 7.16 (d, *J* = 9.0 Hz, 2H), 7.46 – 7.49(m, 2H), 7.58 – 7.63 (m, 2H), 8.06 (d, *J* = 9.0 Hz, 2H), 8.08 (s, 2H), 8.46 (s, 2H). ^{19}F NMR (300 MHz, Chloroform-d): δ -71.76. ^{13}C NMR (600 MHz, Chloroform-*d*): δ 26.3, 38.6, 116.3 (q, *J* = 286 Hz), 125.0, 126.8, 127.6, 129.9, 130.4, 130.6, 130.7, 131.2, 132.1, 134.0, 178.3, 181.2 (q, *J* = 36 Hz). HRMS Calcd for $C_{34}H_{31}F_6N_2O_4^+$: 645.2188, Found: 645.2192. $[\alpha]^D$ = -169.6 (c = 0.200, $CHCl_3$).

5.6. References

(1) Yu, S.; Pu, L. J. Am. Chem. Soc. **2012**, 134, 20282.

(2) Plaquevent, J., Levillain, J., Guillen, F., Malhiac, C., Gaumont, A. Chem. Rev., **2008**, 108 (12), pp 5035–5060.

(3) Scarborough, C., Popp, B., Guzei, I., Stahl, S. J. Organometallic. Chem. **2005**, 6143.

Chapter 6. Highly fluorinated aldehyde sensors for chiral recognition in fluorous phase

6.1. Introduction

As mentioned in the Chapter 2, fluorous solvents are both hydrophobic and lipophobic, which makes them valuable in fast separation and catalyst recycling. For instance, to find the best reaction conditions for the asymmetric reduction of oxime to amine. A combination of reducing agent, chiral catalyst, solvent and temperature are critical to achieve an optimized *ee* and yield. This process can be tedious in conventional methods, which require sample separation and chromatographic analysis for every condition tested. In addition, further derivation (*i.e.* acetylation) is usually necessary to measure *ee* values of free amines in chiral HPLC.

Scheme 6- 1. A design of rapid *ee* and yield determination using fluorescence.

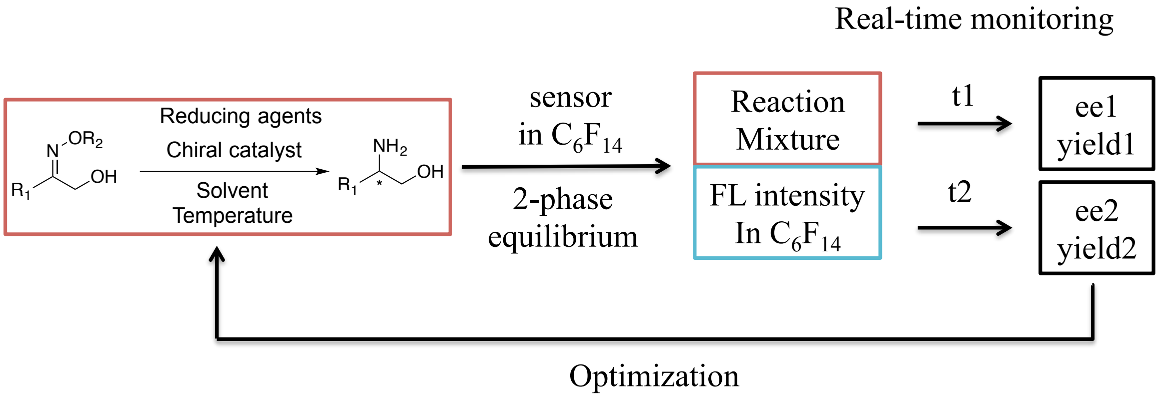
Real-time monitoring
Reducing agents
Chiral catalyst
Solvent
Temperature
N
OR2
R1
OH
NH2
R1
*
OH
sensor
in C_6F_{14}
2-phase
equilibrium
Reaction
Mixture
FL intensity
In C_6F_{14}
t1
t2
ee1
yield1
ee2
yield2
Optimization

In a design shown in Figure 6-1, an aliquot amount of reaction mixture is taken out at different times (t1, t2…) from the reaction mixture and is diluted with an organic solvent. A chiral fluorescent sensor in perfluorohexanes (FC-72) is added, and a fluorescence spectrum in FC-72 is recorded after the two-phase equilibrium. With an established standard curve, the fluorescence intensity can be correlated to the *ee* and yield of the reaction at a specific time. This will enable us to monitor the progress of the reaction conveniently, without disturbing the reaction. As a highly sensitive analysis tool, measuring fluorescence in fluorous solvents is could avoid the interference from other reagents. The information on *ee* and yield will be further used to optimize the reaction conditions. The key issue here would be the development of different kinds of chiral sensors capable of measuring *ee* and yield of products in fluorous solvents. Encouraged by the discovery in fluorous phase, we continue to expand the library of diversified fluorinated sensors for chiral recognition.

Previously, Huang *et al* reported the use of BINOL-CHO as a fluorescent sensor for chiral recognition of amino alcohols and amino acids under the existence of Zn(II).[1] Combined with salicylaldehyde, this method was further improved for simultaneous determination of *ee* and concentration of chiral samples using the emission at 515 nm and 447 nm separately.[2] Based on these reports, we intended to develop new aldehyde sensors that can be used for chiral recognition in the fluorous phase. We designed a series of highly-fluorinated aldehyde chiral sensors for rapid enantiomeric excess (*ee*) determination using fluorescence technique in fluorous solvents.

6.2. Results & Discussion

Compound (*S*)-**6.1** containing two fluorous ponytail chains on the 6, 6'-position of (*S*)-BINOL-CHO is designed for the fluorous phase recognition. (*S*)-**6.1** is synthesized in 4 major steps starting with (*S*)-BINOL using a consecutive bromination / protection, Heck coupling, hydrogenation, nucleophilic addition and deprotection protocol. It needs to be noted that the hydrogenation step to get (*S*)-**6.5** is indispensable for the next step. Otherwise, the n-BuLi would deprotonate the alkenes that have been activated by fluorous chains, and no major product can be obtained.

Scheme 6- 2. Synthesis of (*S*)-**6.1**.

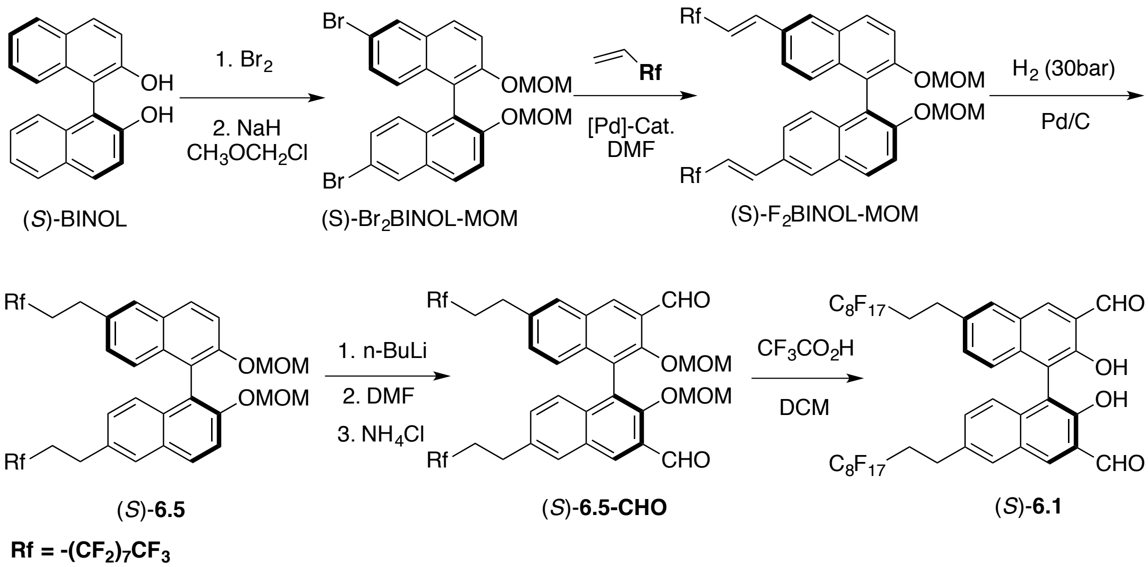
OH
OH
(S)-BINOL
1. Br2
2. NaH
CH3OCH2Cl
Br
OMOM
OMOM
Br
(S)-Br2BINOL-MOM
Rf
[Pd]-Cat.
DMF
Rf
OMOM
OMOM
Rf
(S)-F2BINOL-MOM
H2 (30bar)
Pd/C
Rf
OMOM
OMOM
Rf
(S)-6.5
Rf = -(CF2)7CF3
1. n-BuLi
2. DMF
3. NH4Cl
Rf
CHO
OMOM
OMOM
Rf
CHO
(S)-6.5-CHO
CF3CO2H
DCM
C8F17
CHO
OH
OH
C8F17
CHO
(S)-6.1

Figure 6- 1. Structures of chiral amines studied.

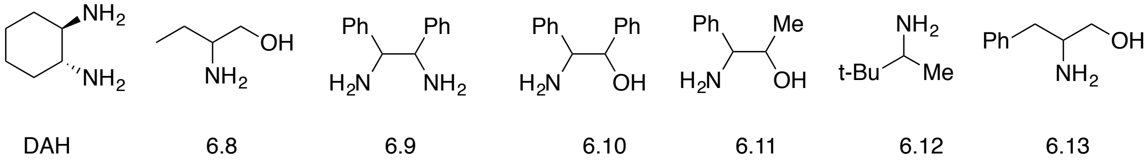
NH2
NH2
DAH
OH
NH2
6.8
Ph
Ph
H2N
NH2
6.9
Ph
Ph
H2N
OH
6.10
Ph
Me
H2N
OH
6.11
NH2
t-Bu
Me
6.12
Ph
OH
NH2
6.13

(*S*)-**6.1** has a fluorine content of 52.3% (wt.) but it is found to be insoluble in fluorous solvents like FC-72. Attempts to use **6.1** at very low concentrations for sensing in fluorous solvents were also not successful due to the low emission intensity. We then proceeded to compare the sensing ability of (*S*)-**6.1** in organic solvents with the previously reported (*S*)-BINOL-CHO sensor[1] that has no fluorous ponytails. For example, (*S*)-BINOL-CHO was shown to have good enantioselective fluorescence toward 2-amino-1-butanol (**6.8**) in methanol under the existence of Zn(II). Under the same conditions, we tested the use of (*S*)-**6.1** and similar enantioselectivity was obtained (Figure 6-2). However, (*S*)-**6.1** gave a smaller fluorescence enhancement toward **6.8** and shows no apparent advantages over (*S*)-BINOL-CHO. The situation is similar for the interaction of amino acids like leucine, with which (*S*)-**6.1** gave smaller fluorescence enhancement as well as a smaller *ef* value.

Figure 6- 2. Fluorescence spectra of (*S*)-**6.1** (0.02 mM left) and (*S*)-BINOL-CHO (0.02 mM, right) treated with (*R*)- or (*S*)-**6.8** in methanol under the existence of zinc acetate (0.02 mM) (λ_{ex} = 330 nm, slit 3/3 nm). Fluorescence intensity at 525 nm was plotted against the equivalents of **6.8**.

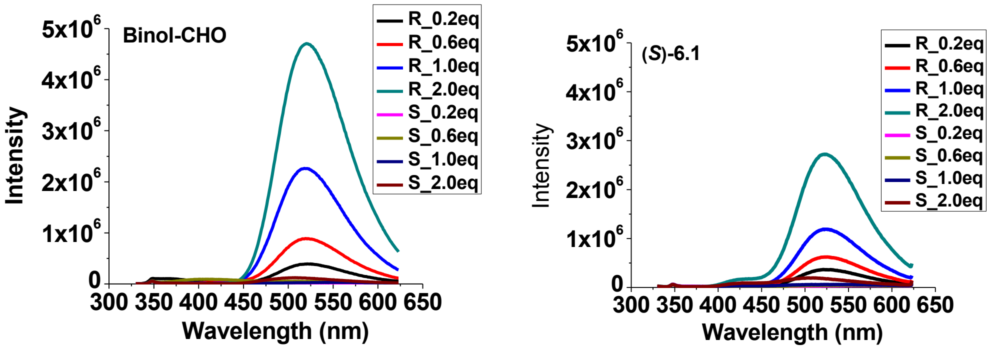

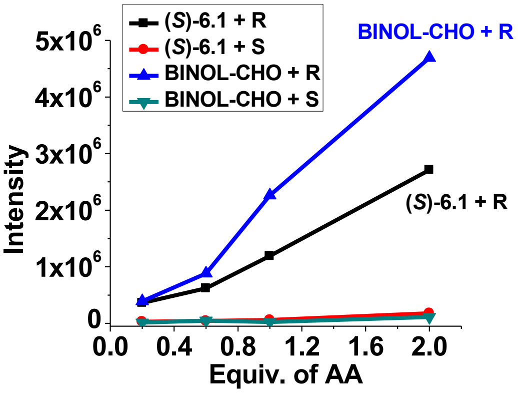

Figure 6- 3. Fluorescence spectra of (*S*)-**6.1** (0.02 mM left) and (*S*)-BINOL-CHO (0.02 mM, right) treated with (*R*)- or (*S*)-leucine in methanol under the existence of zinc acetate (0.02 mM) and TBAOH (10 eq) (λ_{ex} = 330 nm, slit 3 / 3 nm). Fluorescence intensity at 525 nm was plotted against the equivalents of leucine.

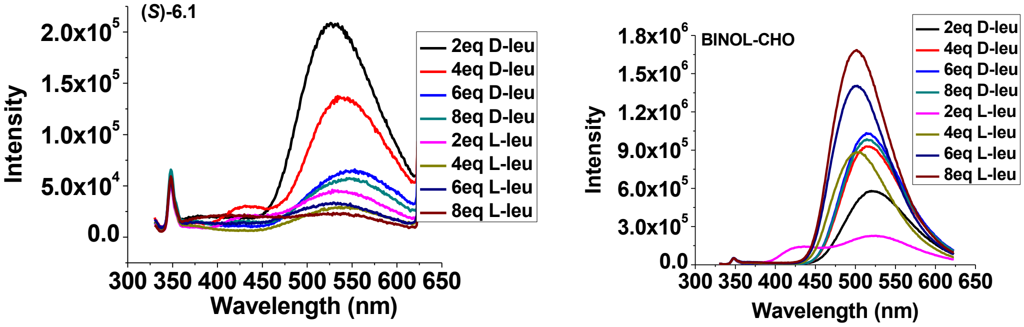

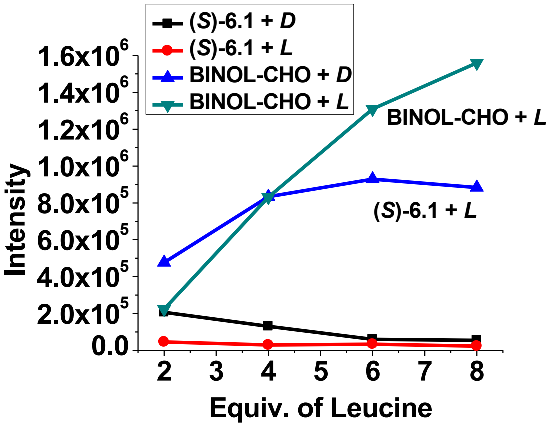

It was found that the zinc(II) promoted chiral recognition worked well in the aprotic solvent toluene (Figure 6-4). In toluene, the (*R*)-**6.8** causes a major emission at 542 nm while the (*S*)-**6.8** at 510 nm, which is a 32 nm blue shift. This is similar for both (*S*)-**6.1** and (*S*)-BINOL-CHO.

Figure 6- 4. Fluorescence spectra of (*S*)-**6.1** (0.02 mM, left) and (*S*)-BINOL-CHO (0.02 mM, right) treated with (*R*)- or (*S*)-**6.8** in toluene under the existence of zinc acetate (0.02 mM) (λ_{ex} = 330 nm, slit 3 / 3 nm). The photo shows the emission under UV-lamp irradiation at 1 eq of **6.8**.

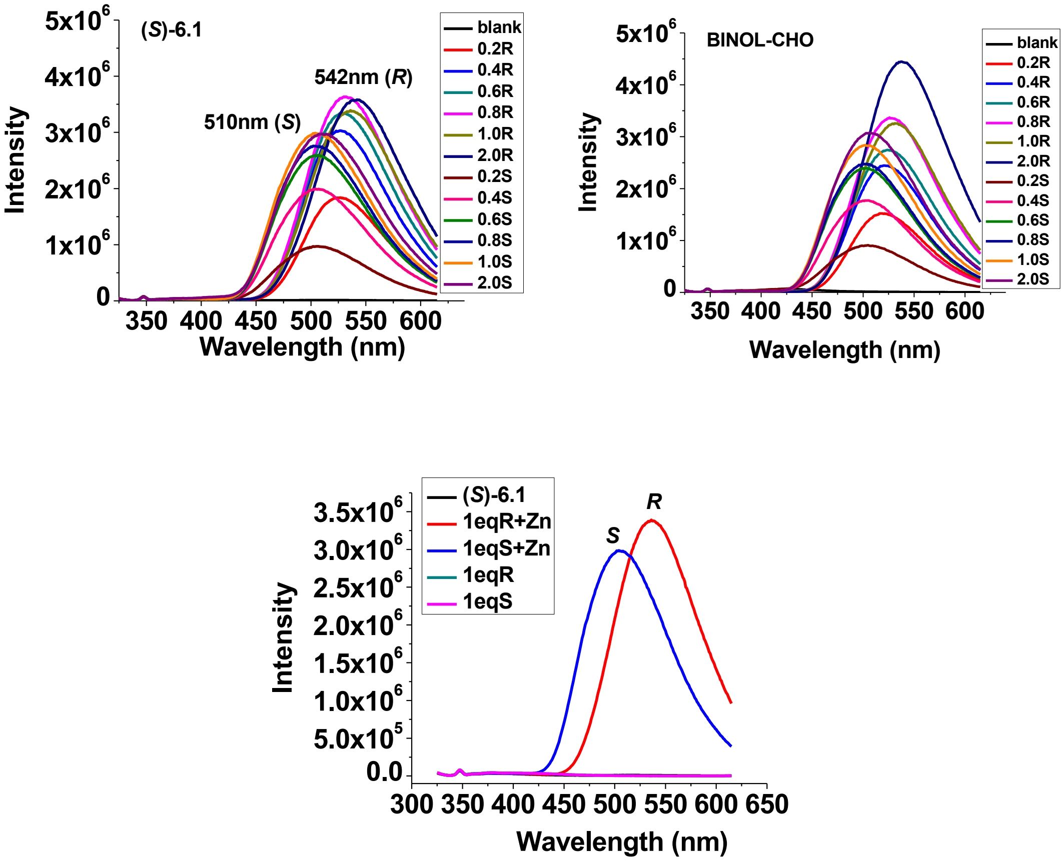

To perform chiral recognition in fluorous phase, we seek to increase the fluorine content of the sensor. A highly fluorinated molecule (*S*)-F$_4$BINOL was synthesized through a bromination and heck coupling protocol starting with (*S*)-BINOL-Hex (Scheme 6-3). (*S*)-F$_4$BINOL has fluorine content of 62.6% and shows good solubility in FC-72 and other fluorous solvents. It also has much brighter blue emission than (*S*)-BINOL due to the extended π-conjugation as observed under a UV-lamp irradiated at 254 nm.

Scheme 6- 3. Synthesis of (*S*)-**6.2** containing 4 fluorous ponytails.

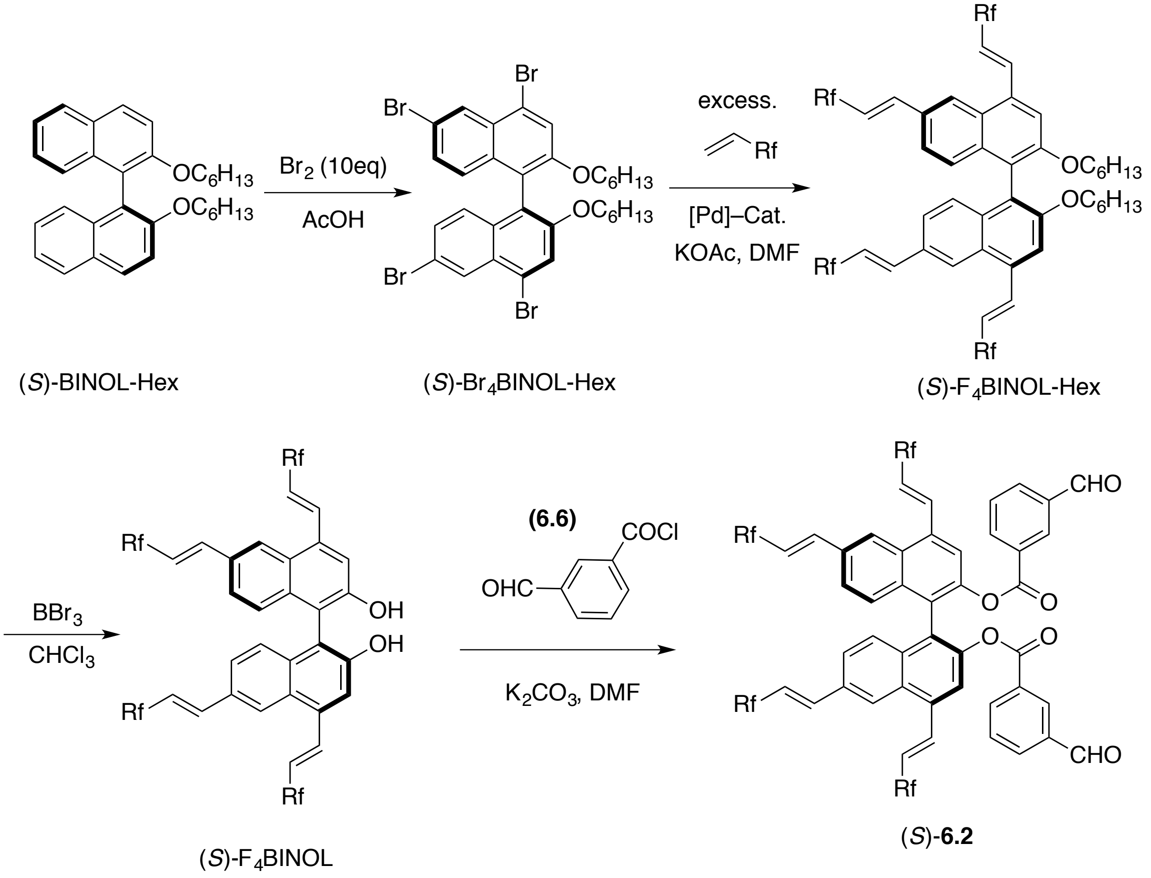
OC6H13
OC6H13
(S)-BINOL-Hex
Br2 (10eq)
AcOH
Br
Br
Br
Br
OC6H13
OC6H13
(S)-Br4BINOL-Hex
excess.
Rf
[Pd]–Cat.
KOAc, DMF
Rf
Rf
Rf
Rf
OC6H13
OC6H13
(S)-F4BINOL-Hex
BBr3
CHCl3
Rf
Rf
Rf
Rf
OH
OH
(S)-F4BINOL
(6.6)
COCl
OHC
K2CO3, DMF
Rf
Rf
Rf
Rf
CHO
CHO
O
O
O
O
(S)-6.2

Scheme 6- 4. Attempted synthesis of aldehyde sensor (*S*)-**6.15**.

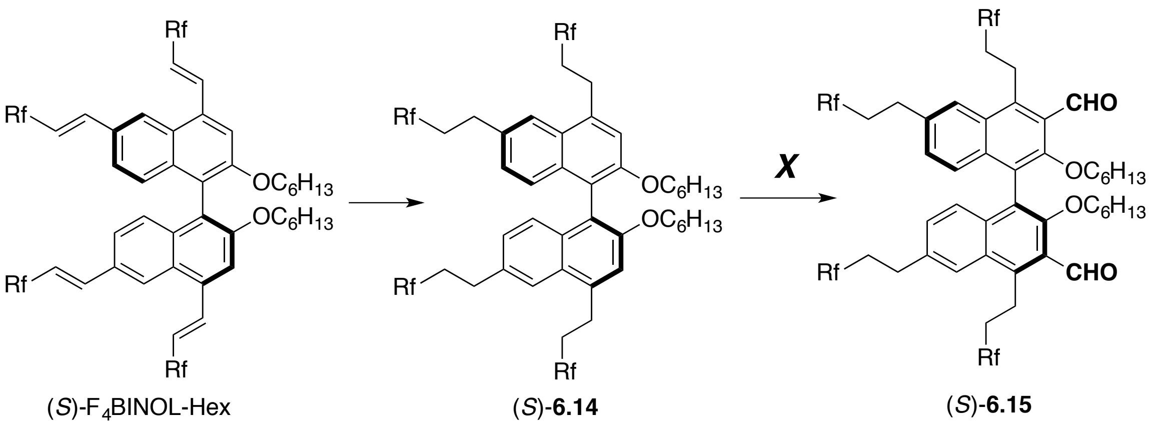

We first tried to synthesize the compound (*S*)-**6.15**, an anlogue of (*S*)-**6.1**, that has the aldehyde groups on the 3, 3'-positions of BINOL (Sccheme 6-4). After reducing (*S*)-BINOL-Hex to (*S*)-**6.14**, it was found that the formylation on BINOL was not possible even under harsh conditions. Most of the starting material was left unreacted. This is very likely due to the large steric effects at the 3- and 3'-positions of BINOL.

We then turned to the acylation of the hydroxyl group of F_4BINOL, and end up obtaining (*S*)-**6.2** in good yield (Scheme 6-3). (*S*)-**6.2** bears two formyl groups that are quite far away from the chiral center. This sensor shows significantly weaker emission than F_4BINOL and moderate solubility in flurous solvents.

The fluorescence response of (*S*)-**6.2** to (1*R*, 2*R*)- and (1*S*, 2*S*)-DAH was tested as shown in Figure 6-5. When less than 1 eq of DAH was added, no change in fluorescence was observed. With the addition of more DAH, fluorescence intensity at 395 nm started to increase and reached plateau soon with 10-fold enhancement at 4 eq of DAH. We plotted the fluorescence intensity at 395 nm against the amounts of DAH and only observed very small enantioselectivity (*ef* =1.4 when 4 eq of DAH was used). Besides fluorous solvents, we also tried several organic solvents with or without the use of zinc(II), as shown in Figure 6-6.

Figure 6- 5. Fluorescence spectra of (*S*)-**6.2** (0.05 mM) with DAH (0.4-10 eq) in FC-72 (4 % DCM, λ_{ex} = 320 nm, slit 3 / 3 nm).

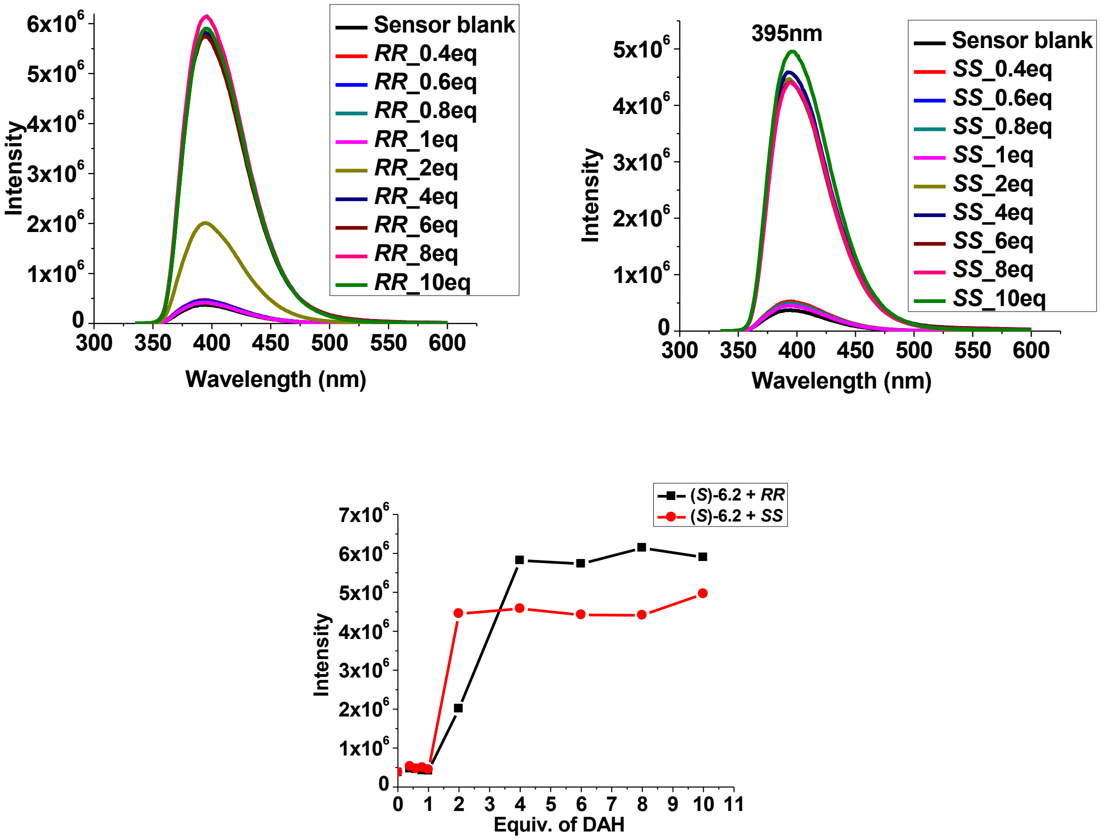

Figure 6- 6. Fluorescence spectra of (*S*)-**6.2** (0.05 mM) with DAH (4 eq) in various solvents (λ_{ex} = 320 nm, slit 3 / 3 nm).

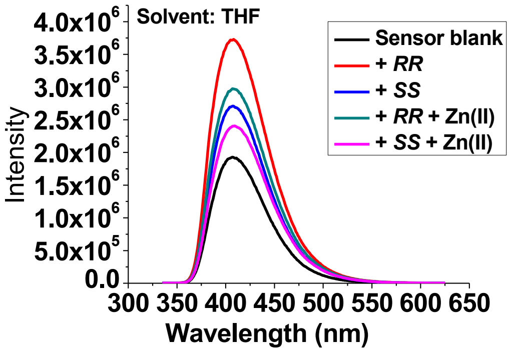

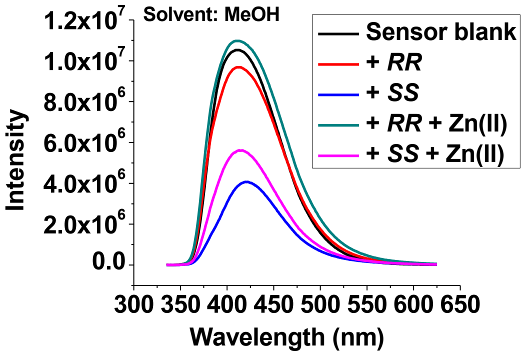

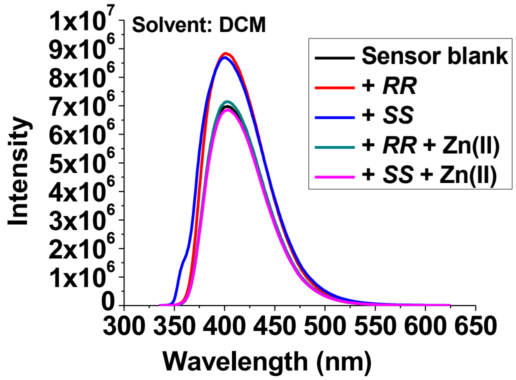

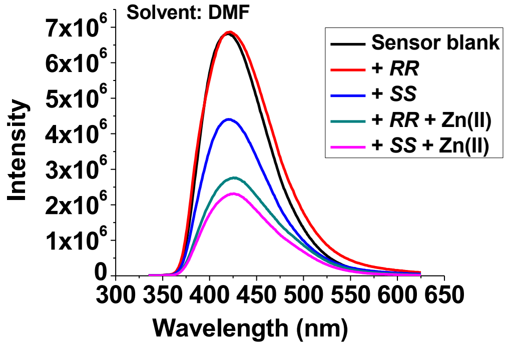

Generally, in organic solvents (*S*)-**6.2** gives much stronger fluorescence background compared with in fluorous solvents. In THF, a 2-fold fluorescence enhancement was observed when (1*R*, 2*R*)-DAH was added to the sensor. The *ef* values obtained were 4.5 and 2.2 with or without the use of zinc acetate. In methanol, emission of (*S*)-**6.2** was quenched with good enantioselectivity. No enantioselectivity was observed when DCM was the solvent. In DMF, it showed that (1*R*, 2*R*)-DAH didn't change much of the emission while the other enantiomer quenched it. Addition of zinc acetate quenched the emission for both of them. We summarized the *ef* values in Table 6-1. The enantioselectivity is highly dependent on the solvent used. Even though we did get moderate enantioselectivity in THF and methanol, the magnitude of emission enhancement or quenching was very small. The strong background emission from sensor itself was disadvantageous for an accurate sensing and *ee* determination in organic solvents.

Table 6- 1. A summary of *ef* values of (*S*)-**6.2** toward DAH in various solvents.

ef	FC-72	THF	MeOH	DCM	DMF
(*S*)-**6.2**	1.4	4.5	7.7	1.0	–
(*S*)-**6.2** + Zinc(II)	–	2.2	10.9	1.0	1.1

We prepared the mixtures of (1*R*, 2*R*)- and (1*S*, 2*S*)-DAH in different ratios for *ee* ranging from -100% to 100%, at a total concentration of 30 μM in 5 mL DCM [*ee* = (*RR* - *SS*) / (*RR* + *SS*)]. To these solutions were added solutions of (*S*)-**6.2** in FC-72 (5 μM, 5 mL). The two-layer solutions were then left on the shaker for 1 h to allow a two-phase equilibrium. We then measured the emission spectra of each layer and established a relationship between the emission intensity and *ee* values (Figure 6-7). As *ee* increases from -100 % to 100 %, we observed a non-linear increase in emission intensity at both organic and fluorous phases. The higher emission intensity in DCM could be attributed to the dominant distribution of DAH in organic solvent. However, the range of intensity change is too small for an accurate *ee* determination.

Figure 6- 7. Correlation of *ee* to fluorescence intensity in a DCM / FC-72 biphasic system (λ_{ex} = 320 nm, slit 3 / 3 nm). Emission intensities at 395 nm were plotted against *ee* values.

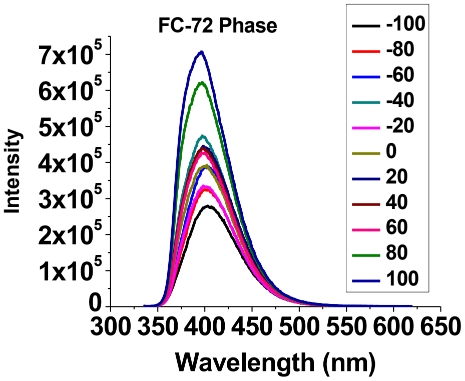

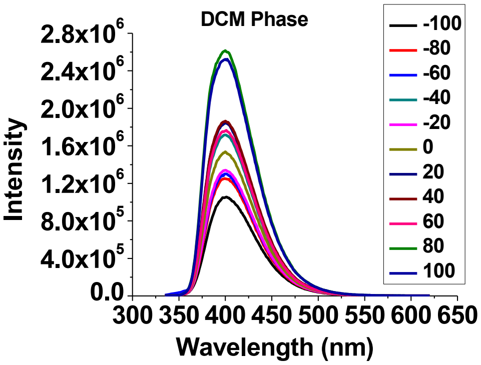

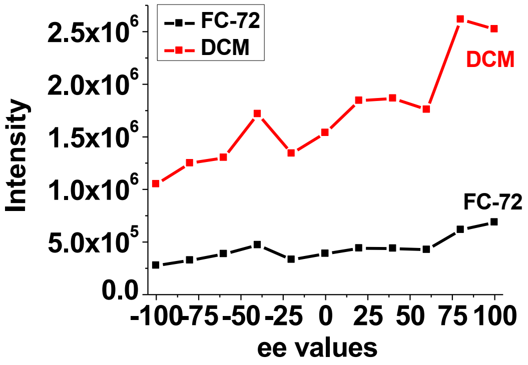

The relative low enantioselectivity of (*S*)-**6.2** to amines is probably due to the long distance between the reactive binding sites (aldehyde group) and BINOL chiral core. For better chiral recognition, we designed compound (*S*)-**6.3** and (*S*)-**6.4**, which have the aldehyde group at the ortho-position instead of meta-position as in **6.2** (Scheme 6-5). These two compounds were synthesized from the reaction between F_4BINOL and **6.7**, which was prepared from the reduction of 2-cyanobenzyl bromide by DIBAL-H. (*S*)-**6.4** can be obtained much easier with the use of excess amount of **6.7**. (*S*)-**6.3**, on the other hand, can only be isolated with difficulty at around 30% yield. Formation of **6.3** was always accompanied by the coexistence both **6.4** and F_4BINOL, even only 1 eq of **6.7** was used. This was likely due to the fact that **6.3** has low solubility in DMF while **6.4** and F_4BINOL have better solubility. A slow injection of **6.7** (1 eq, 3 h) into the reaction mixture was not efficient as well. Higher reaction temperature was also not suitable due to unexpected side reactions.

Scheme 6- 5. Synthesis of (*S*)-6.3 and (*S*)-6.4.

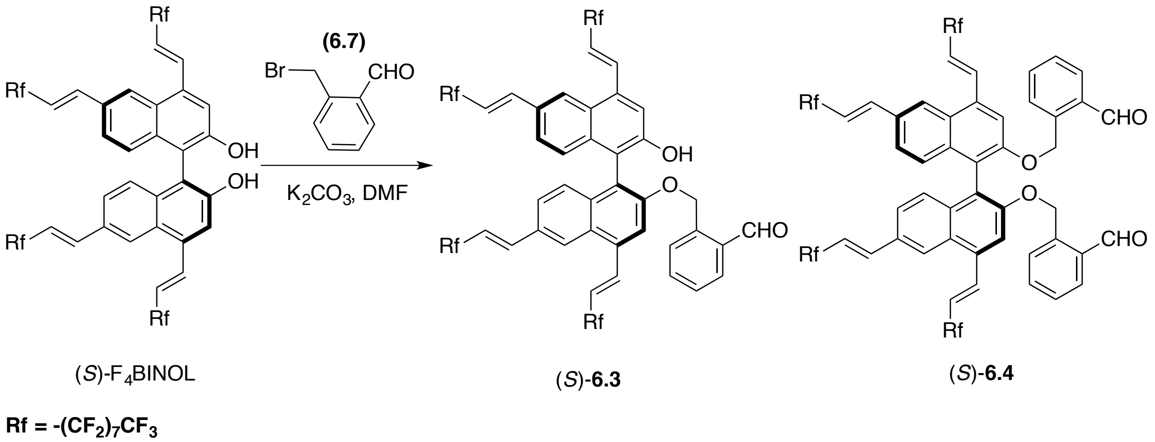

It is assumed that the free hydroxyl group in (*S*)-**6.3** might work as an addition hydrogen binding site to the incoming chiral guest, therefore increase the enantioselectivity. (*S*)-**6.3** was highly soluble in various fluorous solvents including FC-72 and only slightly soluble in common organic solvents. (*S*)-**6.4**, on the other hand, has moderate solubility in both fluorous and organic solvents.

We first tested the response of (*S*)-**6.3** toward 1, 2-diaminocyclohexane (DAH) in perflurohexanes (FC-72) as shown in Figure 6-8. (*S*)-**6.3** blank shows very bright blue emission at 412 nm. Addition of 1 eq of DAH caused significant fluorescence quenching. No substantial change in the emission spectra was observed after 2 eq of DAH was added. The enantioselectivity toward two enantiomers was also negligible.

We then tried to increase the reaction time and studied fluorescence sensing in different solvents including FC-72, perfluorotoluene, methoxyperfluorobutane ($MeOC_4F_9$ or HFE-7100), perfluorodecalin, DCM and MeOH as depicted in Figure 6-9. In all solvents except methanol, addition of DAH quenched the emission of (*S*)-**6.3** significant with very small enantioselectivity (*ef* < 1.1). In methanol, (*S*)-**6.3** has very weak emission intensity mainly due to the low solubility. Addition of DAH in methanol slightly increased the emission intensity.

Figure 6- 8. Fluorescence spectra of (*S*)-**6.3** (0.01 mM) with DAH (1-10 eq) in FC-72/ 2 % DCM recorded 1 h after mixing (λ_{ex} = 335 nm, slit 3 / 3 nm).

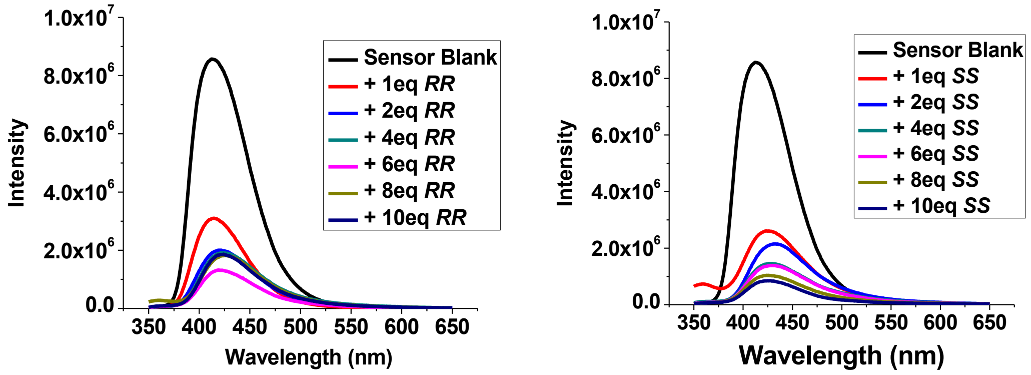

Figure 6- 9. Fluorescence spectra of (*S*)-**6.3** (0.01 mM) with DAH (10 eq) in different solvents recorded 3 h after mixing (λ_{ex} = 335 nm, slit 3 / 3 nm).

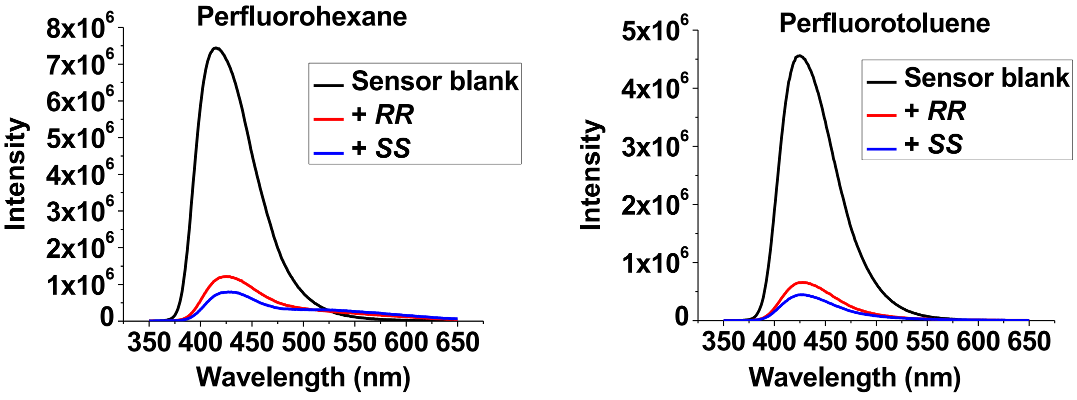

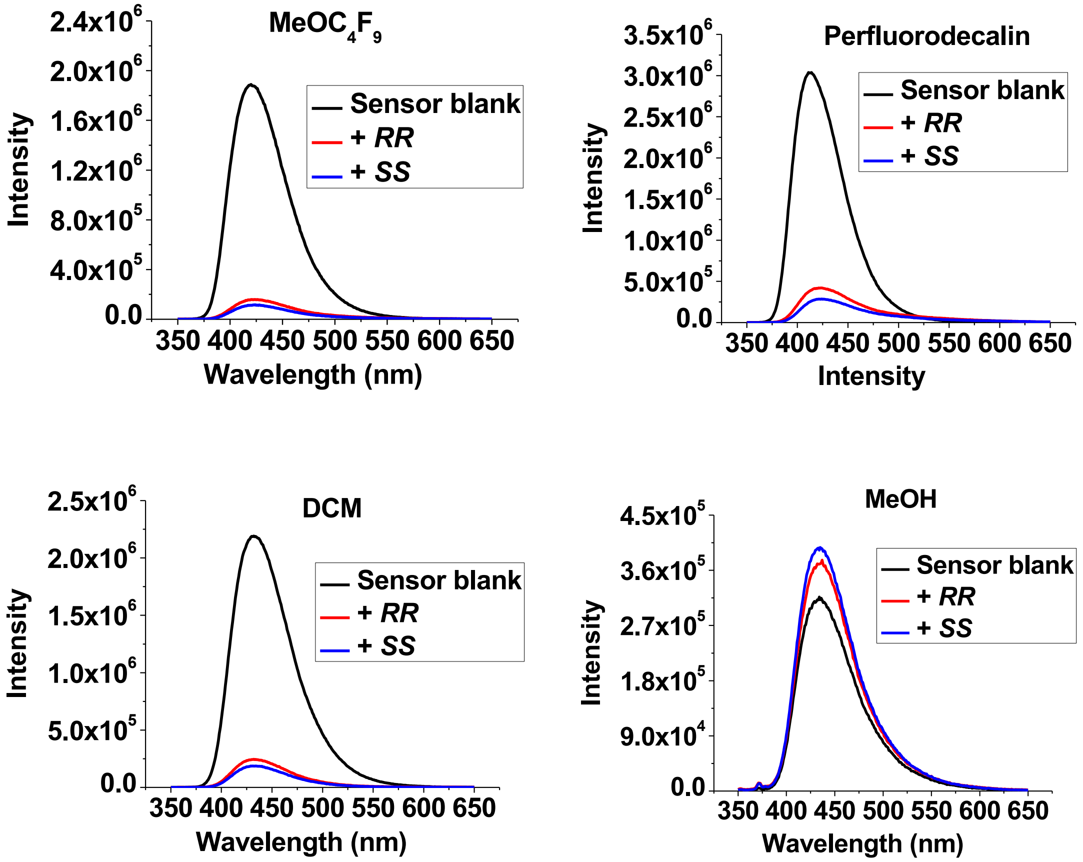

Figure 6- 10. Fluorescence spectra of (*S*)-**6.3** (0.1 mM) with DAH (10 eq, left) and **6.8** (20 eq, right) in FC-72 recorded 3 h, 6 h, 9 h after mixing (λ_{ex} = 335 nm, slit 2 / 2 nm).

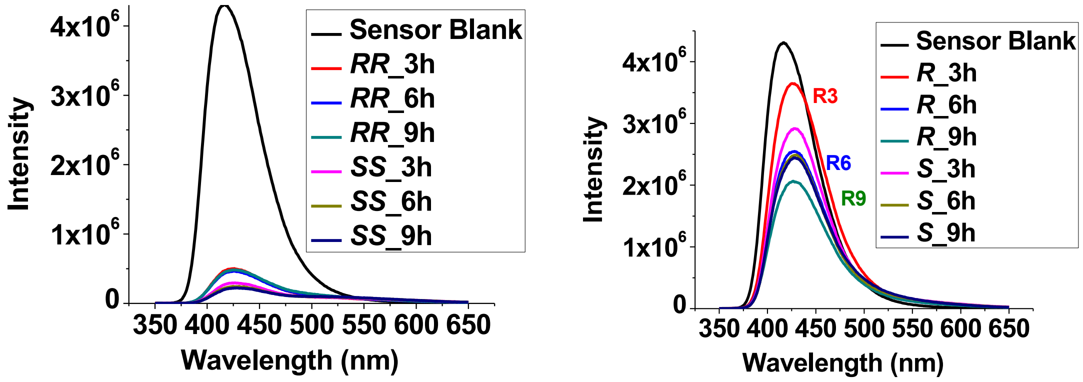

As shown in Figure 6-10 above, we also tested the use of higher concentration of sensor (0.1 mM) and increased reaction time in FC-72. However we did not gain any improvement in enantioselectivity. We also tested the use of (*R*)- or (*S*)-2-amino-1-butanol (**6.8**) under the same conditions. **6.8** resulted in less fluorescence quenching and the emission was unstable when it was monitored 9 h. The enantioselectivity was also not satisfactory (*ef* < 1.2).

Compound (*S*)-**6.3**-DAH can be prepared by refluxing (*S*)-**6.3** and (1*R*, 2*R*)-DAH at 1:1 molar ratio in FC-72 / DCM. It could be purified by simply washing the mixture with DCM as the product is not very soluble in organic solvents. As DAH quenches the fluorescence of (*S*)-**6.3**, the product (*S*)-**6.3**-DAH has much weaker fluorescence than (*S*)-**6.3**. This confirms that the quenching is a result of imine formation. We then studied the interaction of DAH or **6.8** with (*S*)-**6.3**-DAH**,** but no substantial fluorescence change was observed. In another experiment, we prepared a mixture of (*S*)-**6.3** and (1*S*, 2*S*)-DAH in situ and added (*R*)- or (*S*)- 2-amino-1-butanol (**6.8**) continuously in various equivalents (Figure 6-11). A fluorescence turn-on up to 1.5-fold was observed without enantioselectivity.

Scheme 6- 6. Reaction between **6.3** and DAH to form (*S*)-**6.3**-DAH.

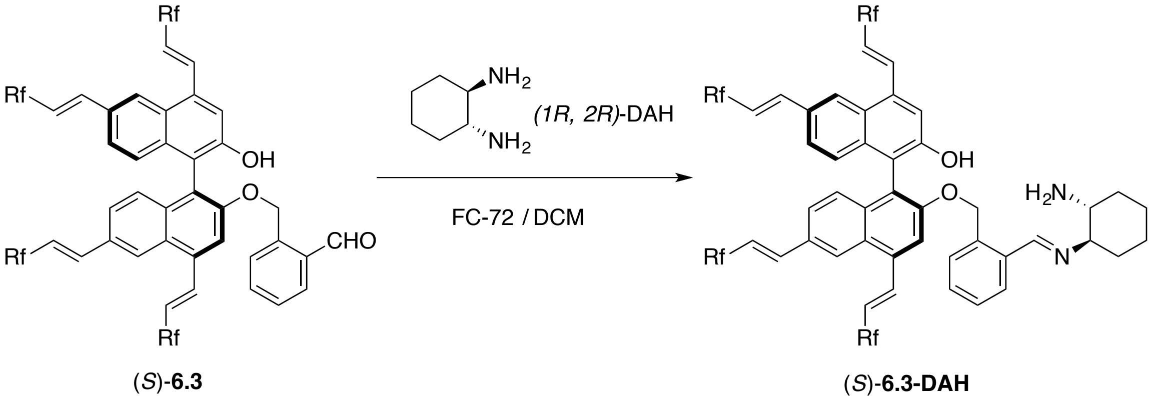

Figure 6- 11. Fluorescence spectra of (*S*)-**6.3** (0.01 mM) + (1*S*, 2*S*)-DAH (1 eq) with addition of **6.8** (4-40 eq) in 4 % DCM / FC-72. Emission intensity at 412 nm was plotted against equivalents of **6.8**.

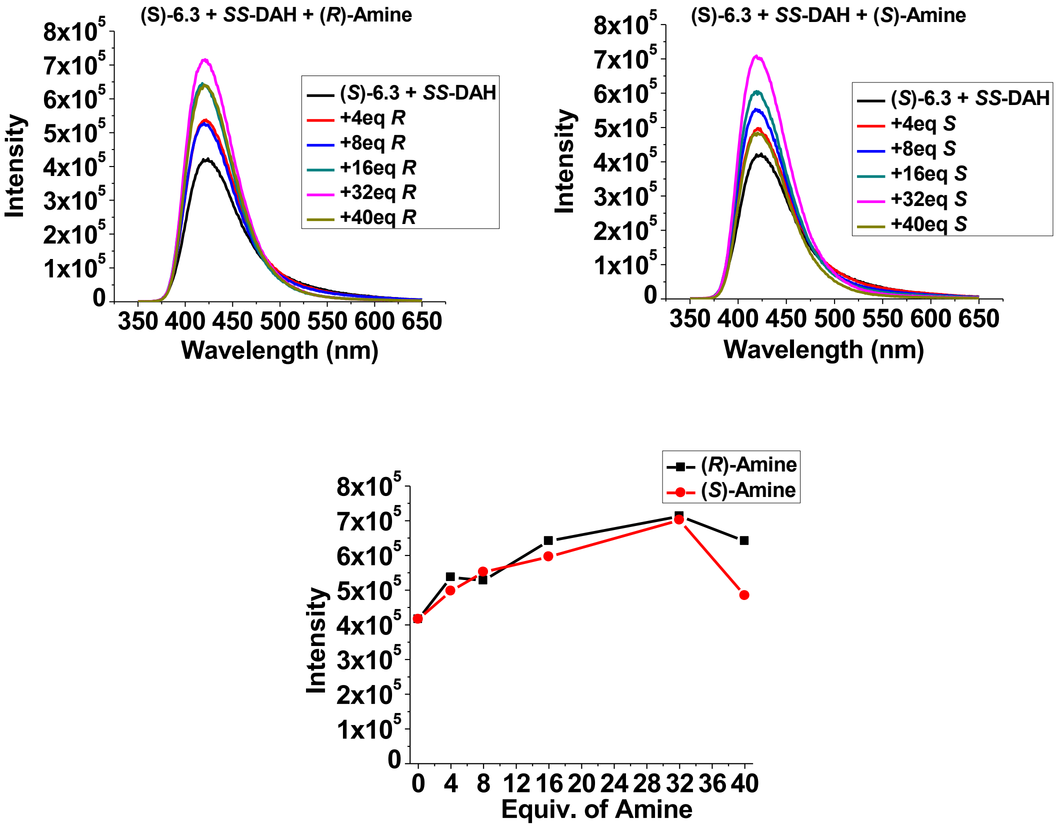

As shown above, we did not obtained good enantioselectivity to in the fluorescence recognition of amines by using (*S*)-**6.3** either in fluorous or organic solvents. We then examined the feasibility of sensing in biphasic systems. (*S*)-**6.3** was dissolved in 2mL FC-72 at 0.05 mM, while (1*R*, 2*R*) or (1*S*, 2*S*)-DAH was dissolved in 0.5 mL methanol at 1 to 8 equivalents separately. The two solutions was then mixed and left on the shaker for 1h to reach a 2-phase equilibrium.

Figure 6- 12. Fluorescence spectra of (*S*)-**6.3** (0.05 mM) in FC-72 (2 mL), with DAH at different equivalents in methanol (0.5 mL) layer (λ_{ex} = 335 nm, slit 2/2 nm).

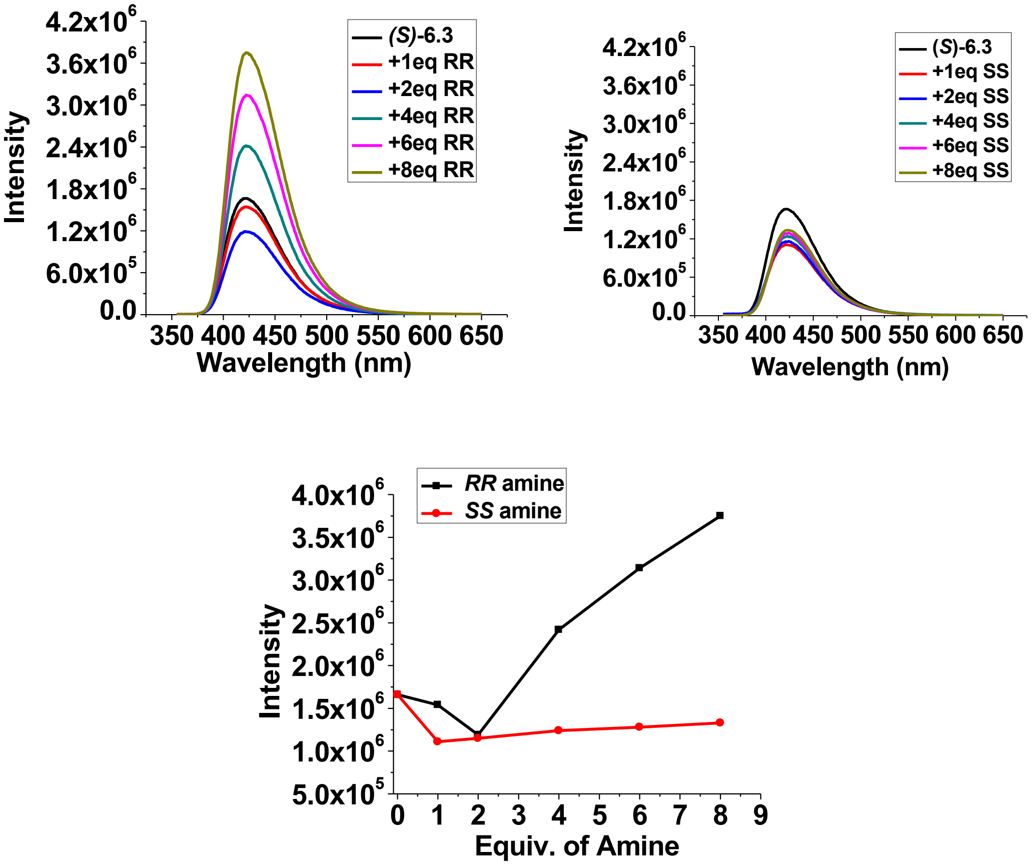

After equilibrium the fluorescence spectra of FC-72 phase was measured as shown in Figure 6-12. Addition of DAH below 2 eq caused similar fluorescence quenching as shown above. However, when more than 2 eq of DAH was added, the (1*R*, 2*R*)-DAH resulted in stronger fluorescence emission than the (1*S*, 2*S*)-DAH enantiomer. An *ef* value of around 4 was obtained when 8 eq of DAH was used, which is much better than results in the single-phase system. We also added zinc acetate (1 eq) to the methanol layer and tested its effect on enantioselectivity. However, we observed lower enantioselectivity at 8 eq of DAH, and more DAH (32 eq) was needed to achieve an *ef* value of 5 (Figure 6-13).

Figure 6- 13. Fluorescence spectra of (*S*)-**6.3** (0.05 mM) in FC-72 (2 mL), with DAH at 8 eq or 32 eq and zinc acetate (1 eq) in the methanol (0.5 mL) layer (λ_{ex} = 335 nm, slit 2 / 2 nm).

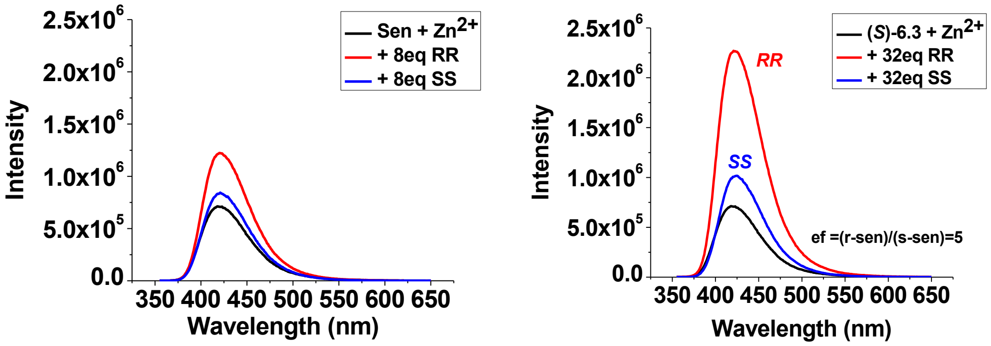

We then make a direct comparison about the effects of zinc acetate on fluorescent emission (Figure 6-14). It seems that the addition of Zn^{2+} only decreased the intensity slightly and made no substantial changes to enantioselectivity. Because the 2-phase system works to improve the enantioselectivity compared with the 1-phase system, we studied the effects of the volume of methanol (Figure 6-15). It shows that a smaller amount of methanol gives slightly better enantioselectivity. So in further studies we maintained the amount of the organic solvent at 0.5mL. The use of too much or too little organic solvent will make the phase separation slow and difficult.

Figure 6- 14. Fluorescence spectra of (*S*)-**6.3** (0.05 mM) in FC-72 (2 mL), and DAH (8 eq) with or without and zinc acetate (1 eq) in methanol (0.5 mL) layer (λ_{ex} = 335 nm, slit 2/2 nm).

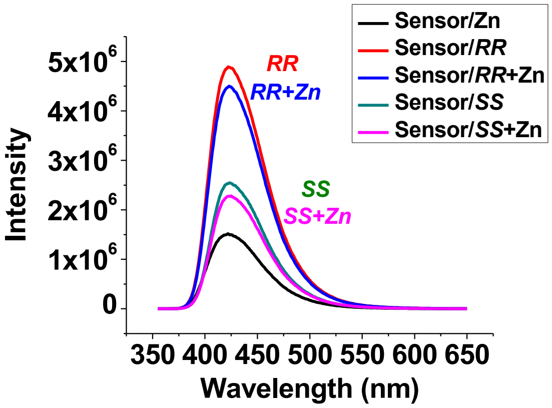

Figure 6- 15. Fluorescence spectra of (*S*)-**6.3** (0.05 mM) in FC-72 (2 mL), and DAH (8 eq) in methanol from 1 mL to 6 mL (λ_{ex} = 335 nm, slit 2 / 2 nm).

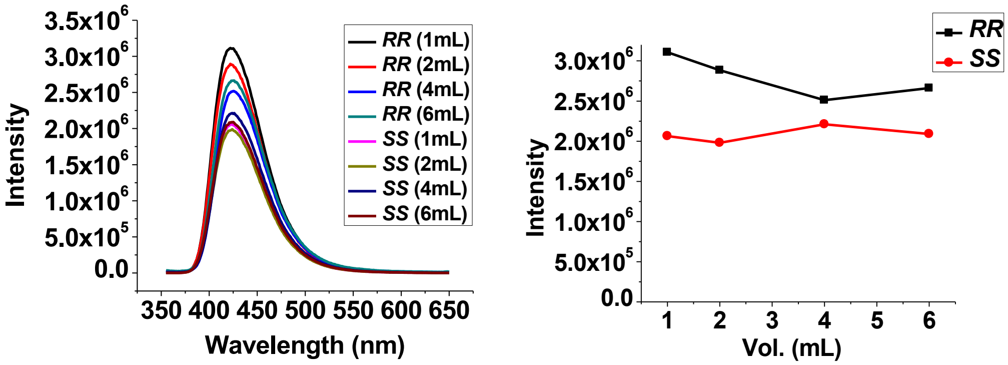

Figure 6- 16. Fluorescence spectra of (*S*)-**6.3** (0.05 mM) in FC-72 (2 mL), and DAH (8 eq) in different solvents (0.5 mL) (λ_{ex} = 335 nm, slit 2 / 2 nm).

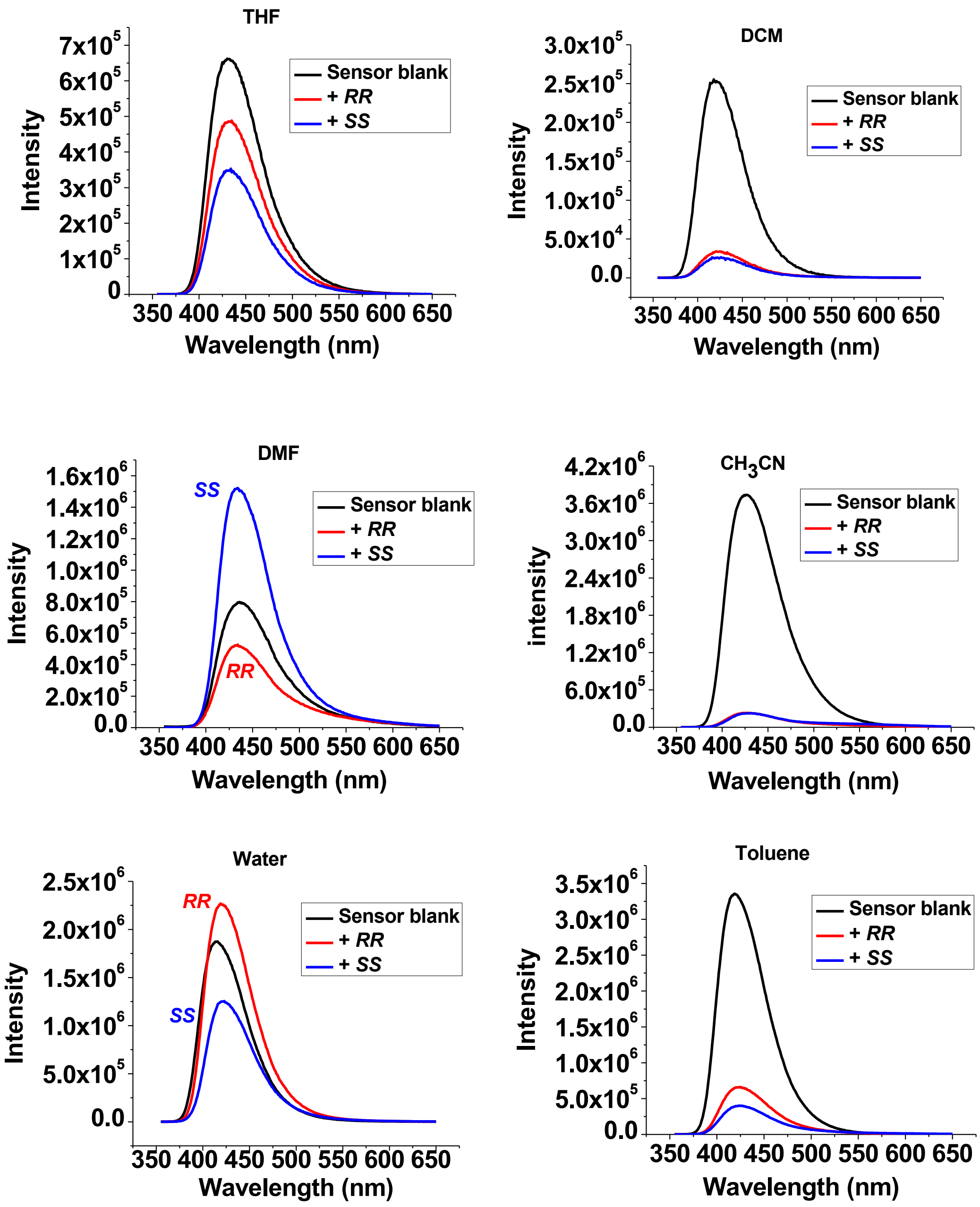

Table 6- 2. A summary of *ef* values in a 2-phase system with (*S*)-**6.3** and DAH in different solvents.

	THF	DCM	DMF	CH_3CN	Toluene	Water
ef	1.7	1.0	2.6	1.0	1.1	1.6

When the extraction was performed in DCM, Toluene or acetonitrile, almost no enantioselectivity was obtained (Figure 6-16). Moderate enantioselectivity was obtained for THF and water. Among them, DMF gives the best enantioselectivity with *ef* = 2.6. In contrast with other solvents, in DMF the (1*S*, 2*S*)-DAH resulted in higher emission intensity than the (1*R*, 2*R*)-DAH. In Figure 6-16, we observed fluorescence quenching for the (1*R*, 2*R*)-DAH and enhancement for (1*S*, 2*S*)-DAH. However, this was likely due to the experimental errors. When we double-check this condition with various equivalents of DAH, both enantiomers caused fluorescence quenching (Figure 6-17). We still observed moderate enantioselectivity when 2 to 8 eq of DAH was used. Beyond 12 eq, almost complete fluorescence quenching was obtained for both enantiomers. This reflects the difficulty to obtain reproducible data in a 2-phase system, which is highly dependent on the equilibrium status of the two phases. This problem was more prominent in fluorescence study, which is highly sensitive to trivial changes in concentration and other variables.

Figure 6- 17. Fluorescence spectra of (*S*)-**6.3** (0.05 mM) in FC-72 (2 mL), and DAH at 2-20 eq in DMF (0.5 mL) (λ_{ex} = 335 nm, slit 2 / 2 nm). Fluorescence intensity at 430 nm was plotted against equivalents of DAH.

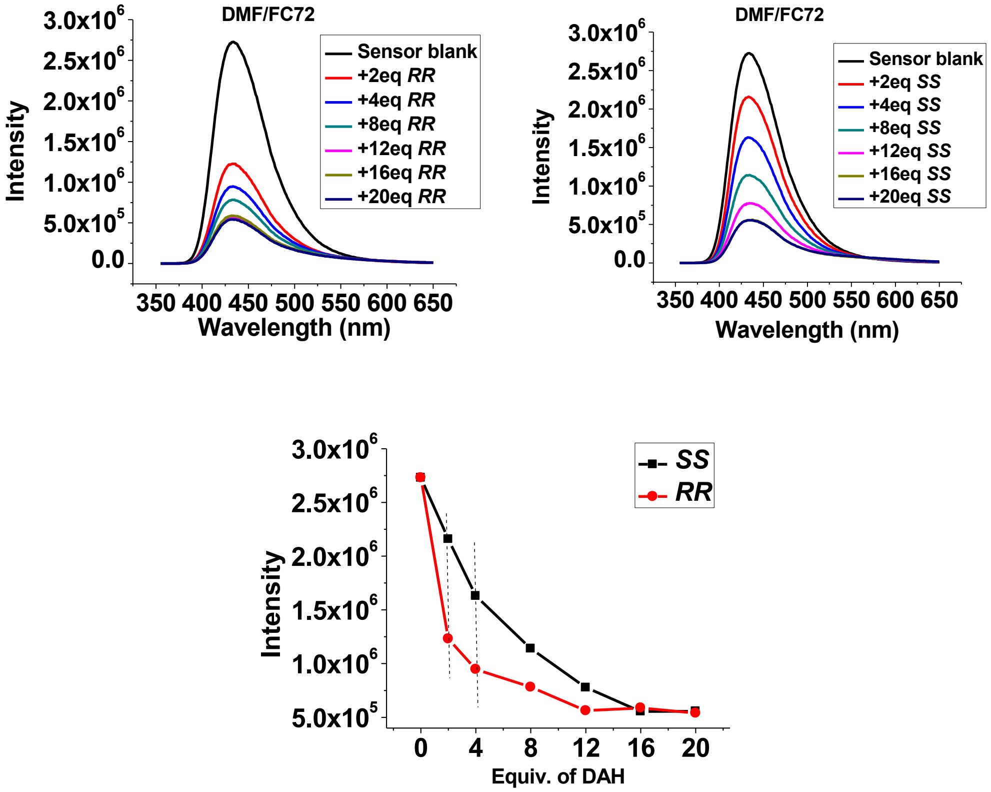

It seems that methanol was the best option among all the organic solvents tested. In the FC-72 - methanol biphasic system, we successfully established a relationship between the fluorescence intensity (FC-72 layer) and *ee* values (methanol layer). As shown in Figure 6-18, the intensity and *ee* values demonstrate a good linear relationship. Using this as a standard curve, the mixtures of DAH at any *ee* values in methanol could be easily obtained by fluorescence measurement in the fluorous phase without affecting the DAH sample.

Figure 6- 18. Relationship between *ee* and emission intensity in a FC-72 / methanol biphasic system. Emission intensities at 420 nm were plotted against *ee* values ([**6.3**] = 0.05 mM, [rrDAH + ssDAH] = 8 eq, λ_{ex} = 335 nm, slit 2 / 2 nm).

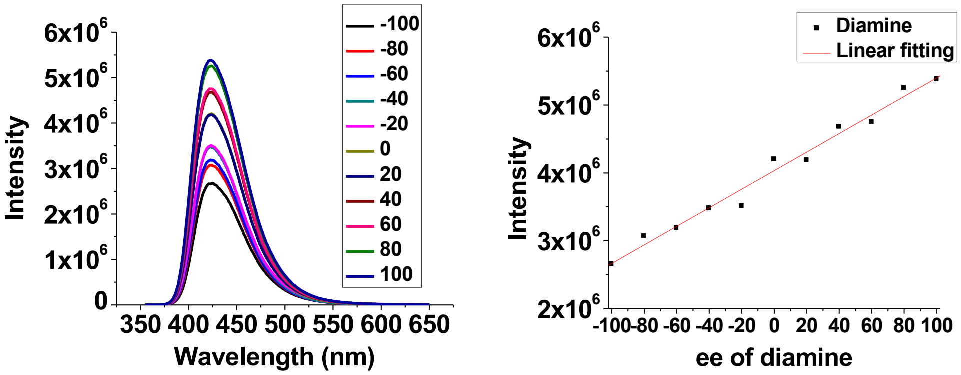

Scheme 6- 7. A representative diagram of *ee* determination in a biphasic system.

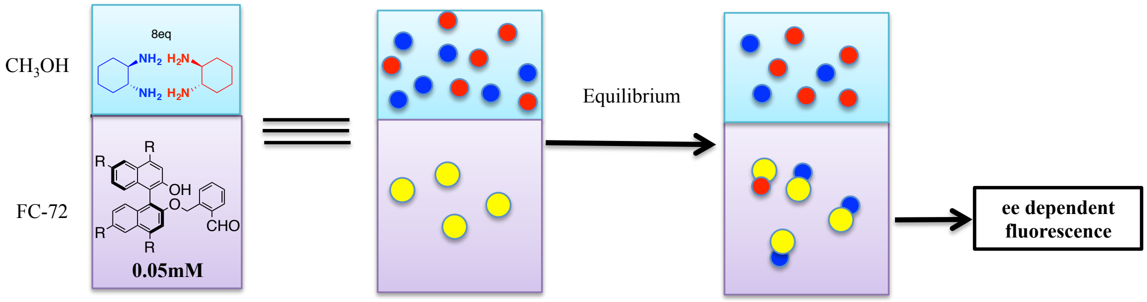

When the chiral sensor (*S*)-**6.3** in FC-72 reacts with DAH in methanol, it is possible that it has higher reacting rate with one enantiomer than the other one, which could result in an *ee* dependent fluorescence intensity [Scheme 6-7, yellow: (*S*)-**6.3**, blue: (1*R*, 2*R*)-DAH, red: (1*S*, 2*S*)-DAH]. We also reduced the concentration of (*S*)-**6.3** to examine its effect on enantioselectivity (Figure 6-19). In general, lower concentration of the sensor results in lower enantioselectivity. The *ef* values of 2.5 and 1.4 were obtained for the sensor concentrations of 10 μM and 0.4 μM respectively. At sensor concentration of 40 nM and 4 nM, only very weak fluorescence responses were observed. However, the strong emission of (*S*)-**6.3** would be potentially useful for sensing at extremely low concentrations.

Figure 6- 19. Fluorescence spectra of (*S*)-**6.3** at various concentrations in FC-72 (2 mL), and DAH (0.4 mM) in 0.5 mL methanol (λ_{ex} = 335n m, slit 2 / 2 nm).

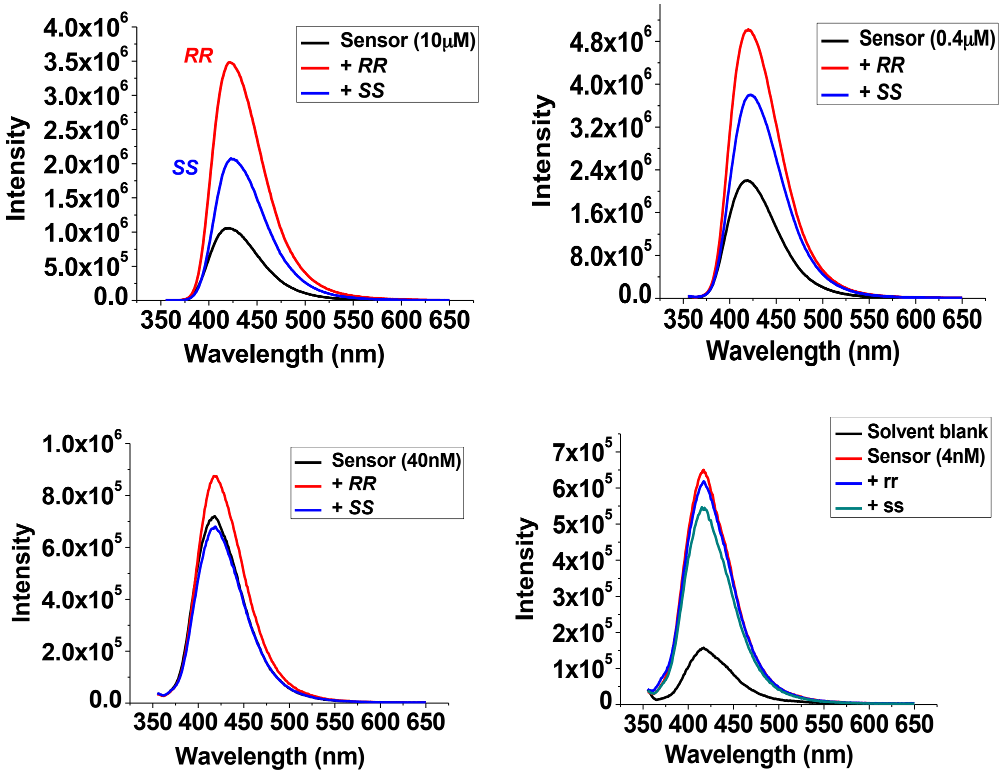

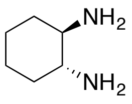

DAH

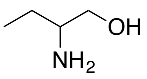

6.8

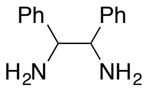
Ph
Ph
H2N
NH2
6.9

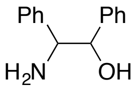

6.10

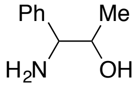

6.11

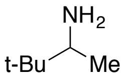

6.12

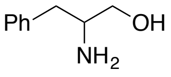

6.13

Compared with DAH, (*S*)-**6.3** gave very small enantioselectivity to 2-amino-1-butanol (**6.8**) with or without the existence of zinc acetate (Figure 6-20). Only 1.5-fold fluorescence enhancement was received with excess amount of **6.8**. We also checked the sensing of a wide range of aromatic amino alcohols, they all gave around 2-5 fold fluorescence enhancements with *ef* values up to 1.2 (Figure 6-21). In the sensing of amino acids like serine or cysteine, we didn't observe any enantioselectivity.

Figure 6- 20. Fluorescence spectra of (*S*)-**6.3** (5 μM) in FC-72 (2 mL). **6.8** (36 eq) with or without zinc acetate (1eq) were added in methanol (0.5mL) layer (λ_{ex} = 335 nm, slit 2 / 2 nm).

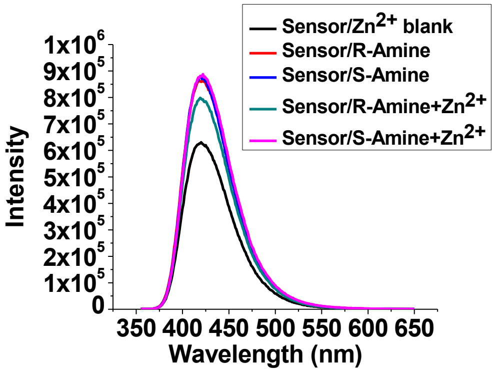

Figure 6- 21. Fluorescence spectra of (*S*)-**6.3** (0.05 mM) in FC-72 (2 mL), with various kinds of amino alcohols (16 eq) in 0.5 mL methanol (λ_{ex} = 335 nm, slit 2 / 2 nm).

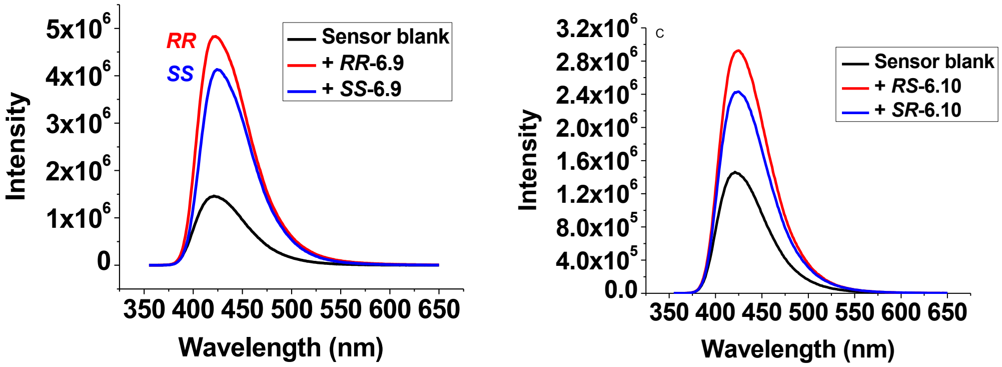

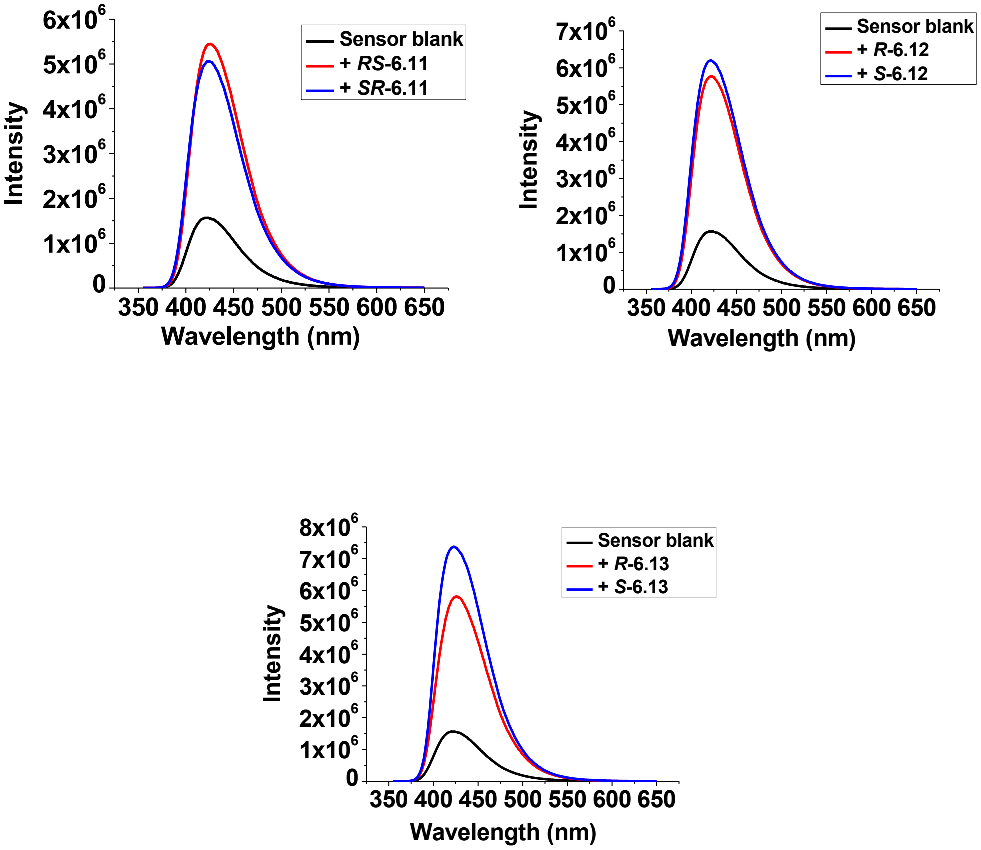

Figure 6- 22. Fluorescence spectra of (*S*)-**6.3** (0.05 mM) in FC-72 (2 mL), with amino acids (Ser or Cys, 16 eq) in 0.5 mL methanol (5 % of H_2O, $\lambda_{ex} = 335$ nm, slit 2 / 2 nm).

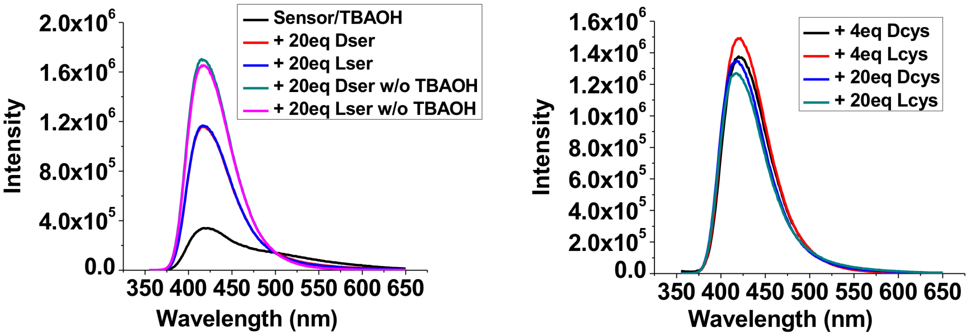

We next studied the recognition of DAH using (*S*)-**6.4**, the analogue of (*S*)-**6.3**. It shows weaker emission than **6.3** and lower solubility in FC-72. When (*S*)-**6.4** was used in the biphasic system for chiral recognition of DAH, we observed 10-fold fluorescence enhancement but with no enantioselectivity (Figure 6-22). The intensity reaches plateau after 6eq of DAH was used. Addition of Zn^{2+} also has makes no difference to the enantioselectivity.

Figure 6- 23. Fluorescence spectra of (*S*)-**6.4** (0.05 mM) in FC-72 (2 mL), with 1-8 eq of DAH in 0.5 mL methanol (λ_{ex} = 335 nm, slit 2 / 2 nm).

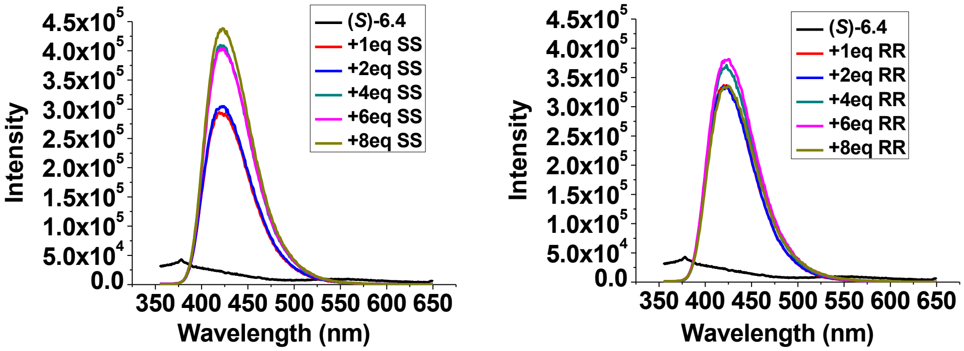

Scheme 6- 8. Synthesis of (*S*)-**6.4**-PEA by condensation.

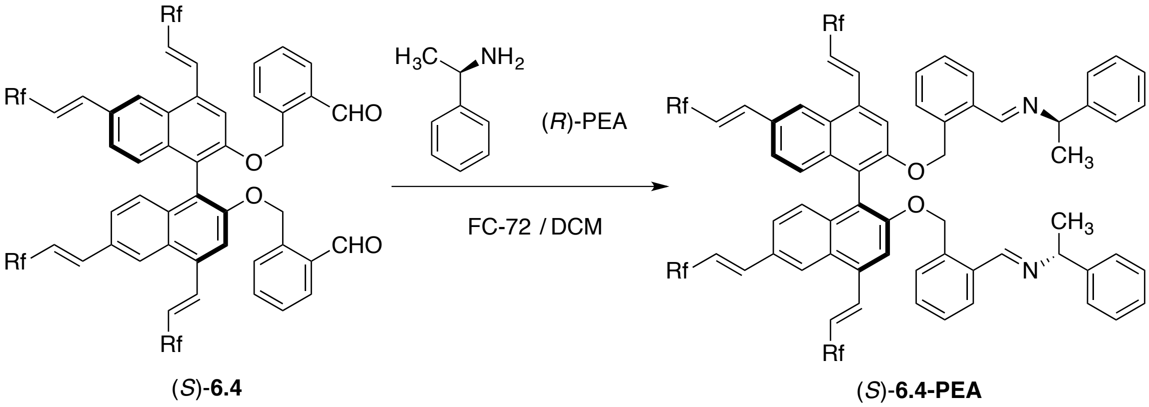

We then synthesized the compound (*S*)-**6.4**-PEA by condensation of (*S*)-**6.4** with excess (*R*)- phenylethyl amine (PEA) in high yield (Scheme 6-8). After reaction, the product can be easily isolated by washing and sonicating with DCM for several times. It is assumed that addition of another chiral amine to (*S*)-**6.4**-PEA would undergo an imine exchange reaction, which might induce enantioselective fluorescence response. To the solution of (*S*)-**6.4**-PEA in THF or methanol, we added DAH but found no fluorescence change. Addition of various cations like Zn(II), Cu(II) or Yb(III) to promote coordination were also not effective (Figure 6-24 to 26).

Figure 6- 24. Fluorescence spectra of (*S*)-**6.4**-PEA (5 μM) + DAH (10 eq) with Zn (II) (1 eq) in THF or methanol (λ_{ex} = 340 nm, slit 1 / 1 nm).

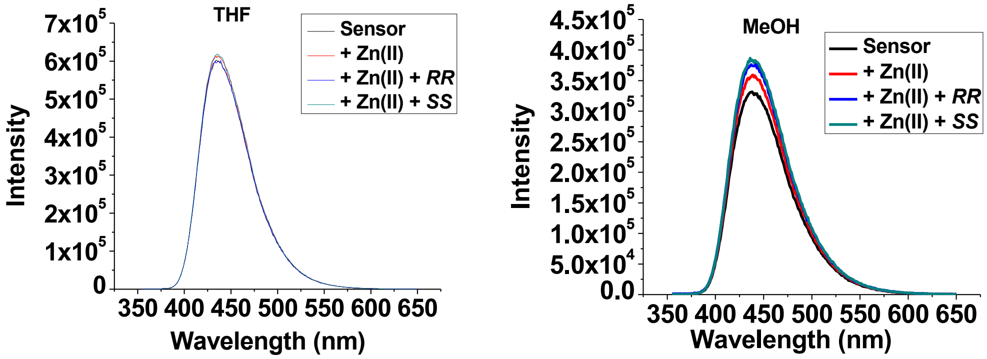

Figure 6- 25. Fluorescence spectra of (*S*)-**6.4**-PEA (5 μM) + DAH (10 eq) with or without Cu (II) (1 eq) in THF or methanol (λ_{ex} = 340 nm, slit 1 / 1 nm).

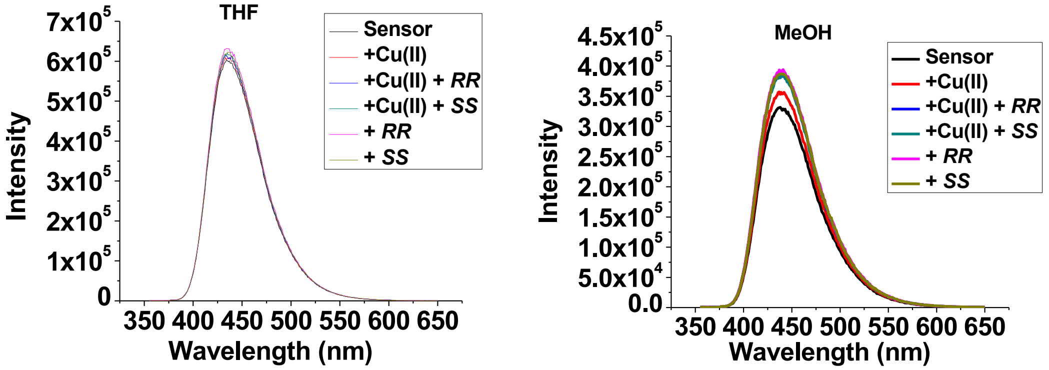

Figure 6- 26. Fluorescence spectra of (*S*)-**6.4**-PEA (5 μM) + DAH (10 eq) with Yb (III) (1 eq) in THF or methanol (λ_{ex} = 340 nm, slit 1 / 1 nm).

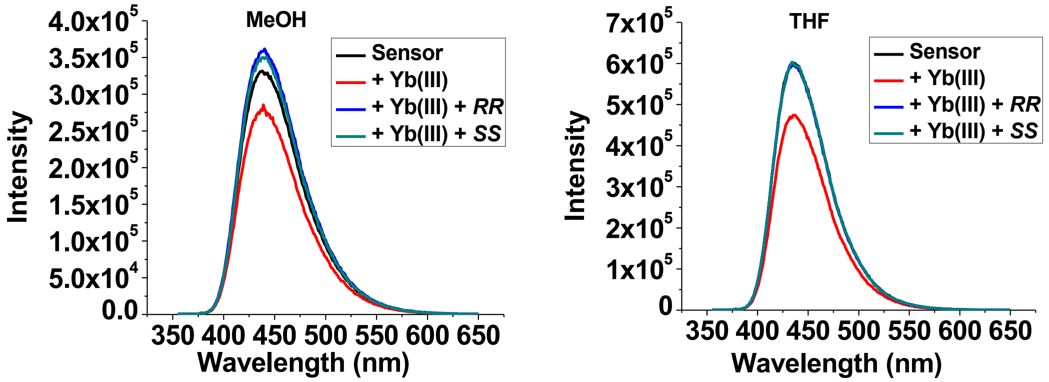

6.3. Conclusion

Among all of the highly fluorinated aldehyde sensors tested, (*S*)-**6.3** gave the best enantioselectivity toward 1,2-diaminocyclohexanes (DAH) in a biphasic FC-72/methanol system, with an *ef* value up to 4. The enantioselectivity was higher compared with the use of a single fluorous phase. We established a linear relationship between the enantiomeric excess values of DAH in methanol with fluorescence intensity in FC-72. However, the recognitions of amino alcohols and amino acids are not efficient, with *ef* values less than 1.2 were obtained. For **6.2-6.4**, addition of zinc (II) or other cations didn't show substantial effects on the emission spectra as observed in **6.1** or BINOL-CHO. The chiral sensing ability of **6.2-6.4** was limited by the fact that the aldehyde groups are not directly located on the BINOL backbone and the reactions with amines are not very enantioselective. However, with F_4BINOL on hand, it would be relatively easy to design a series of fluorinated chiral sensors with better enantioselectivity in the future.

6.4. Experimental part

The synthesis of (*S*)-**6.5** was described in Chapter 3.

***S*ynthesis of (*S*)-6.5-CHO**

A solution of (*S*)-**6.5** (1 mmol, 1.27 g) in dry diethyl ether (20mL) was cooled to 0°C, and n-BuLi (4 mmol, 1.6 mL, 2.5 M in hexane) was added dropwise. The solution was warmed to room temperature and stirred for another 2 h. It was then cooled to 0 °C, and anhydrous DMF (5 mmol, 0.39 mL) was added dropwise. The reaction mixture was stirred at 0 °C for 30 min, and then warmed up to room temperature for additional 3 h to afford a yellow cream-like mixture. Saturated aqueous solution of NH_4Cl (4 mL) was added to quench the reaction at 0 °C. The organic layer was separated, and the aqueous layer was extracted with ethyl acetate (3 x 10 mL). The combined organic extracts were washed with brine, and dried over anhydrous Na_2SO_4. After evaporation of the solvents, the residue was purified by column chromatography on silica gel eluted with hexane / ethyl acetate (10 / 1 to 6 / 1) to afford the compound as a yellow solid in 56 % yield. ^1H NMR (600 MHz, Chloroform-*d*) δ 10.54 (s, 2H), 8.57 (s, 2H), 7.91 (s, 2H), 7.29 (d, J = 8.7 Hz, 2H), 7.19 (d, J = 8.8 Hz, 2H), 4.75 (d, J = 6.3 Hz, 2H), 4.69 (d, J = 6.3 Hz, 2H), 3.09 (t, *J* = 8.3 Hz, 4H), 2.87 (s, 6H), 2.53 – 2.41 (m, 4H). ^{19}F NMR (564 MHz, Chloroform-*d*) δ -81.04 (t, *J* = 10.1 Hz, 6F), -114.31 – -114.85 (m, 4F), -121.60 – -121.91 (m, 4F), -121.91 – -122.25 (m, 8F), -122.74 – -123.03 (m, 4F), -123.48 – -123.59 (m, 4F), -126. 27 – -126.41 (m, 4F). ^{13}C NMR (151 MHz, Chloroform-*d*) δ 190.62, 154.17, 137.36, 135.67, 132.00, 130.59, 130.45, 129.41, 129.05, 126.86, 126.00, 120.49 –106. 31(m, weak), 100.82, 57.13, 32.62 (t, *J* = 21.96 Hz), 26.45 (m, , *J* = 3.89 Hz).

Synthesis of (*S*)-6.1

(*S*)-**6.5-**CHO (0. 567 mmol, 750 mg) was dissolved in a minimum amount of DCM and cooled down to 0 °C. 3 mL of trifluoroacetic acid (TFA) was added slowly at 0 °C. The mixture was warmed to room temperature and allowed to react for additional 30 min. It was then cooled down to 0 °C, and saturated $NaHCO_3$ was added slowly until no bubble formation was observed. The mixture was diluted with DCM (30 mL) and extracted. The aqueous layer was extracted with DCM (3 × 20 mL). The combined organic extracts were washed with water (50 mL), brine (80 mL), and then dried over anhydrous Na_2SO_4. After evaporation of solvents, the residue was purified by column chromatography on silica gel eluted with hexane / DCM (1 / 15 to 1 / 10) to afford (*S*)-**6.1** as a bright yellow powder in a yield of 87 %. ^{1}H NMR (600 MHz, Chloroform-*d*) δ 10.58 (s, 2H), 10.19 (s, 2H), 8.30 (s, 2H), 7.83 (s, 2H), 7.28 (d, *J* = 8.8, 2H), 7.18 (d, *J* = 8.7 Hz, 2H), 3.08 – 3.03 (m, 4H), 2.50 – 2.39 (m, 4H). ^{19}F NMR (564 MHz, Chloroform-*d*) δ -80.79 (t, *J* = 9.9 Hz, 6F), -114.54 (t, *J* = 16.6 Hz, 4F), -121.60 – -122.08 (m, 12F), -122.75 (s, 4F), -123.47 (s, 4F), -126.12 – -126.19 (m, 4F).

Synthesis of (*S*)-Br$_4$BINOL-Hex

(1). The hexyl protected (*S*)-BINOL-Hex was prepared. To a solution of (*S*)-BINOL (5.72 g, 20 mmol) in acetonitrile (100 mL) was added potassium carbonate (100 mmol, 13.8 g) and 1-bromohexane (100 mmol, 14 mL). The mixture was refluxed under N_2 for 12 h, and TLC indicated a complete conversion. The solution was cooled down to room temperature and evaporated to remove the solvent. 50 mL of hexane was added and the solution was filtered to remove the precipitates. The precipitate was washed with hexane, and the filtrate was collected. After evaporation of solvents, the residue was purified by column chromatography on silica gel eluted with hexane / DCM (1 / 30 to 1 / 10) to afford (*S*)-BINOL-Hex as colorless oil in 95 % yield.

(2). Under nitrogen, the product obtained was dissolved in glacial acetic acid (120 mL) and bromine (190 mmol, 9.9 mL) was added slowly at room temperature. The reaction was allowed to stay at room temperature for 5 h, and TLC indicated a moderate conversion. Longer reaction time doesn't improve the reaction much. The solution was extracted directly with hexane (5 × 60 mL). The combined hexane extract was washed with saturated $NaHSO_3$ (2 × 40 mL), saturated $NaHCO_3$ (2 × 40 mL), water (100 mL) and brine (100 mL). Note: be careful of the release of gas during extraction. The washed hexane extract was dried over anhydrous Na_2SO_4. After evaporation of solvents, the residue was purified by column chromatography on silica gel eluted with hexane / DCM (1 / 30 to 1 / 10) to afford (*S*)-Br$_4$BINOL-Hex as colorless oil in a yield of 54 %. ^{1}H NMR (600 MHz, Chloroform-*d*) δ 8.42 (s, 2H), 7.73 (s, 2H), 7.31 (dd, *J* = 5.9, 3.1 Hz, 2H), 7.00 (dd, *J* = 9.0, 5.7 Hz, 2H), 4.01 – 3.89 (m, 4H), 1.49 – 1.37 (m, 4H), 1.16 – 0.84 (m, 17H), 0.80 – 0.76 (m, 6H).

Synthesis of (*S*)-F$_4$BINOL-Hex

To a 50mL round bottom flask was added (*S*)-Br$_4$BINOL-Hex (1.97 mmol, 1.52 g), potassium acetate (6 eq, 11.8 mmol, 1.17 g). Herrmann's catalyst (3 mol %, 55 mg) was then added in glove box, followed by addition of dry DMF (35 mL) and 1H, 1H, 2H-Perfluoro-1-decene ($CH_2CHC_8F_{17}$, 11.9 mmol, 3.2 mL). The mixture was heated at 120 °C with rigorous stirring for 24 h. After cooled down to room temperature, the solution was poured into ice water (150 mL) and extracted with diethyl ether / hexane mixture (20 mL / 20 mL, 5 times). The combined organic extracts were washed with H_2O (100 mL), brine (100 mL) and dried over anhydrous Na_2SO_4. After evaporation of the solvents, the residue was purified by column chromatography on silica gel eluted with hexane/ethyl acetate (30 / 1 to 15 / 1) to afford (*S*)-F$_4$BINOL-Hex as highly viscous oil in 65 % yield. ^{1}H NMR (600 MHz, Chloroform-*d*) δ 8.07 - 8.03 (m, 4H), 7.54 (s, 2H), 7.40 (d, *J* = 9.0 Hz, 2H), 7.31 (d, *J* = 16.1 Hz, 2H), 7.18 (d, *J* = 8.9 Hz, 2H), 6.44 – 6.33 (m, 2H), 6.24 – 6.14 (m, 2H), 3.96 - 4.05 (m, 4H), 1.45 (d, *J* = 7.3 Hz, 4H), 1.06 – 0.91 (m, 11H), 0.70 (t, *J* = 6.9 Hz, 5H). ^{19}F NMR (564 MHz, Chloroform-*d*) δ -81.12 (dt, *J* = 19.6, 9.9 Hz, 12F), -111.04 – -111.33 (m, 8F), -121.30 – -121.35 (m, 4F), -121.50 – -121.59 (m, 4F), -121.82 – -122.31 (m, 16F), -122.77 – -123.21 (m, 12F), -123.28 – -123.47 (m, 4F), -126.24 – -126.50 (m, 8F). ^{13}C NMR (151 MHz, Chloroform-*d*) δ 155.33, 139.6 (t, J=8.9Hz), 135.20 (t, J=8.9Hz), 129.94, 126.95, 126.81, 125.29, 124.07, 122.22, 118.97 (t, J=23.81Hz), 114.51, 120.47 – 106.52 (m, weak), 69.73, 31.37, 29.32, 25.51, 22.59, 13.74. . M.S. (MALDI, low resolution): 2230.953, calculated 2231.017.

Synthesis of (*S*)-F_4BINOL

A solution of (*S*)-F_4BINOL-Hex (0.93 mmol, 2.09 g) in chloroform (80 mL) was cooled down to -78 °C (dry ice / acetone). Boron tribromide (6 eq, 5.58 mmol, 0.53 mL) was added slowly while rigorous stirring. The cool bath was removed and the solution was allowed to react at room temperature for 24 h, with TLC indicated a good conversion. The solution was cooled to 0 °C and quenched by addition of water dropwise while stirring. The solvent was evaporated and the residual was dissolved in ethyl acetate (30 mL). 30 mL of water was added and the organic layer was separated. The aqueous layer was washed with ethyl acetate / hexane (15 mL / 15 mL, 3 times). The combined organic extracts was washed with $NaHCO_3$ and brine, and then dried with anhydrous Na_2SO_4. After evaporation of the solvents, the residue was purified by column chromatography on silica gel eluted with hexane/ethyl acetate (15 / 1 to 10 / 1) to afford (*S*)-F_4BINOL as a white solid in 75 % yield. ^{1}H NMR (598 MHz, Chloroform-*d*) δ 8.06 (s, 2H), 8.00 (d, *J* = 15.9 Hz, 2H), 7.57 (s, 2H), 7.51 (d, *J* = 8.9 Hz, 2H), 7.33 (d, *J* = 16.0 Hz, 2H), 7.18 (d, *J* = 8.9 Hz, 2H), 6.47 – 6.38 (m, 2H), 6.28 – 6.18 (m, 2H), 5.14 (s, 2H). M.P. 123–125 °C. M.S. (MALDI, low resolution): 2062.966, calculated 2062.693.

Synthesis of (*S*)-6.2

(1). The reactant 3-formylbenzoyl chloride (**6.6**) was prepared by refluxing a mixture of 3-formylbenzoic acid (2 mmol, 300 mg) and thionyl chloride (16 mmol, 1.2 mL) in anhydrous toluene (10 mL) overnight. After cooled down to room temperature, the solution was evaporated and placed under vacuum pump to get **6.6**. Formation of **6.6**

was confirmed by comparing its ^{13}C NMR with the acid. After vacuum dry, **6.6** was dissolved in anhydrous THF (10 mL) for further use.

(2). To a round-bottom flask containing (*S*)-F_4BINOL (0.5 mmol, 1.02 g) in anhydrous THF (20 mL) was added triethylamine (2 mmol, 0.28 mL) at 0 °C. After 30 min, the solution of **6.6** in THF was added. The mixture was stirred at room temperature for 16 h, and TLC indicated good conversion. Water was then added to quench the reaction. The solution was extracted with ethyl acetate (3 × 30 mL). The combined organic extracts was washed with brine, and then dried over anhydrous Na_2SO_4. After evaporation of the solvents, the residue was purified by column chromatography on silica gel eluted with hexane/ethyl acetate (20 / 1 to 8 / 1) to afford (*S*)-**6.2** as white solid in 85 % yield. ^{1}H NMR (600 MHz, Chloroform-*d*) δ 9.95 (s, 2H), 8.20 (s, 2H), 8.10 (s, 2H), 8.06 – 7.94 (m, 6H), 7.73 (s, 2H), 7.61 – 7.50 (m, 4H), 7.41 (d, J = 8.7 Hz, 2H), 7.36 (d, J = 14.9 Hz, 2H), 6.43 – 6.26 (m, 4H). ^{19}F NMR (564 MHz, Chloroform-*d*) δ -80.85 (s, 12F), -111.08 – -111.95 (m, 8F), -121.24(s, 4F), -121.41(s, 4F), -121.95(s, 16F), -122.75 – -122.93 (m, 12F), -123.12 (s, 4F), -126.18 (s, 8F).

Synthesis of 2-(bromomethyl) benzaldehyde (6.7)

Compound **6.7** was synthesized following the reported procedure.[3] A solution 2-(bromomethyl) benzonitrile (10.2 mmol, 2.0 g) in dry DCM (35 mL) was purged with argon for 30 min and then cooled to 0 °C under argon. A solution of 1 M DIBAL-H in heptane (11.2 mmol, 11.2 mL) was injected slowly over 30 min. The mixture was slowly warmed to room temperature with stirring in a period of 3 h by removing the ice bath. Then it was cooled to 0 °C again and poured into an Erlenmeyer flask containing ice (40

g) and precooled HBr (6.0 N, 40 mL). The mixture was stirred vigorously for 1 h without darkening. It was then extracted 3 times with DCM (60 mL). The combined organic extract was washed with 1N $NaHCO_3$, brine, and then dried over anhydrous Na_2SO_4. After evaporation of the solvents, the residue was further purified by a flash column chromatography on silica gel to afford **6.7** as brown liquid in quantitative yield. It turns into brown crystals after leaving in the freezer (-20 °C) for several days. ^{1}H NMR (600 MHz, Chloroform-*d*) δ 10.24 (s, 1H), 7.87 – 7.79 (m, 1H), 7.56 (q, *J* = 7.2 Hz, 1H), 7.53 – 7.43 (m, 2H), 4.94 (s, 2H).

Synthesis of (*S*)-6.3

To a mixture of (*S*)-F_4BINOL (0.25 mmol, 510 mg), K_2CO_3 (0.25 mmol, 35 mg) and **6.7** (0.25 mmol, 50 mg) was added anhydrous DMF (10 mL) under nitrogen. The mixture was heated to 70 °C with vigorous stirring for 24 h. After cooled down to room temperature, the solution was poured into ice water (15 mL) and extracted with diethyl ether (20 mL, 5 times). The combined organic extracts were washed with H_2O (60 mL), brine (60 mL) and dried over anhydrous Na_2SO_4. After evaporation of solvents, the residue was carefully purified by column chromatography on silica gel eluted with hexane/ethyl acetate (20 / 1 to 8 / 1) to afford (*S*)-**6.3** as pale yellow solid in 26 % yield. The low yield was due to the co-existence of (*S*)-F_4BINOL and (*S*)-**6.4**. A 2nd separation by column chromatography was usually needed to get (*S*)-**6.3** with high purity. ^{1}H NMR (600 MHz, Chloroform-*d*) δ 10.12 (s, 1H), 8.21 – 8.12 (m, 4H), 7.88 (d, *J* = 7.4 Hz, 1H), 7.80 (s, 1H), 7.69 (s, 1H), 7.64 (d, *J* = 9.1 Hz, 1H), 7.58 – 7.53 (m, 2H), 7.50 – 7.43 (m, 3H), 7.40 (d, *J* = 8.6 Hz, 3H), 7.25 (d, *J* = 8.9 Hz, 1H), 7.21 (d, *J* = 7.8 Hz, 1H), 6.61 –

6.46 (m, 2H), 6.43 – 6.30 (m, 2H), 5.80 (d, *J* = 14.6 Hz, 1H), 5.70 (d, *J* = 14.6 Hz, 1H), 5.30 (s, 1H). M.S. (MALDI, low resolution): 2179.109, calculated (**7.3**-H) 2179.828.

Synthesis of (*S*)-6.4

Compound (*S*)-**6.4** can be synthesized as a white solid using the same method above but using 4eq of **6.7**, in a yield of 74%. ^{1}H NMR (600 MHz, Chloroform-*d*) δ 9.95 (s, 2H), 8.07 – 8.00 (m, 4H), 7.70 (d, *J* = 7.6 Hz, 2H), 7.58 (s, 2H), 7.42 (d, *J* = 9.0, 2H), 7.37 – 7.30 (m, 4H), 7.23 (d, *J* = 9.0 Hz, 2H), 7.17 (t, *J* = 7.7 Hz, 2H), 6.99 (d, *J* = 7.8 Hz, 2H), 6.35 (q, *J* = 12.2 Hz, 2H), 6.21 (q, *J* = 12.3 Hz, 2H), 5.54 (s, 4H). M.P. 104 – 106°C.

Synthesis of (*S*)-7.4-PEA

To a mixture of (*S*)-**6.4** (0.0865 mmol, 200 mg) and (*R*)-phenylethyl amine (10 eq, 0.865 mmol, 0.11 mL) was added 10 mL methanol. The solution was heated to reflux for 6 h. After cooled down to room temperature, the solvent was evaporated. The residual was washed with DCM (HPLC grade) for 5 times, and then hexane (HPLC grade) for 3 times. It was then dried under vacuum pump to get (*S*)-**6.4**-PEA in 79% yield as pale yellow powder. ^{1}H NMR (600 MHz, Chloroform-*d*) δ 8.34 (s, 2H), 8.01 (t, *J* = 8.0 Hz, 4H), 7.56 (s, 2H), 7.49 (d, *J* = 7.5 Hz, 2H), 7.37 (d, *J* = 8.5 Hz, 2H), 7.32 (d, *J* = 7.6 Hz, 5H), 7.29 – 7.25 (m, 9H), 7.21 – 7.17 (m, 6H), 6.94 – 6.92 (m, 4H), 6.29 – 6.13 (m, 5H), 5.60 (d, *J* = 14.7 Hz, 2H), 5.52 (d, *J* = 14.9 Hz, 2H), 4.30 (q, *J* = 6.2, 5.5 Hz, 2H), 1.49 (d, *J* = 6.6 Hz, 6H).

6.5. References

(1) Huang, Z.; Yu, S.; Wen, K.; Yu, X.; Pu, L. *Chem. Sci.* **2014**.

(2) Huang, Z.; Yu, S.; Zhao, X.; Wen, K.; Xu, Y.; Yu, X.; Xu, Y.; Pu, L. *Chem. - A Eur. J.* **2014**, *20* (50), 16458.

(3) Zhang, X. X.; Lippard, S. J. *J. Org. Chem.* **2000**, *65* (17), 5298.

Chapter 7. Attempted research: conjugation of fluorophore with chiral backbone for enantioselective recognition

7.1. Introduction

In the development of fluorescence sensing, researchers have spared no effort in exploiting new fluorophores with longer emission wavelengths at the visible and near infrared regions. Long wavelength light has deeper tissue penetration, less sample damage and is not easily interfered by background emission. This is especially important for biological or medical imaging. Recently, *Zeng et al* pioneered the use of a (*S*)-SPIRO derived aldehyde sensor for enantioselective *in vitro* imaging of *L*- and *D*- amino acids under the existence of zinc.[1] However, the relative low emission wavelength (~450 nm) and low quantum yield of SPIRO fluorophores limit its implication for intracellular studies and high-throughput screening. Herein, we seek to incorporate organic dyes that have red-emission and high quantum yield into chiral backbone to achieve enantioselective sensing at visible regions.

7.2. Results & Discussion

7.2.1 Enantioselective recognition of chiral acid

The sensor (*S*)-**7.1** was synthesized starting with (*S*)-BINOL-MOM and Rhodamine-B through 4 steps with a total yield of 13 % (Scheme 7-1). The structure of (*S*)-**7.1** is characteristic for the conjugation of a chiral BINOL center with the rhodamine dye that can show emission at red wavelength, which is rarely studied in enantioselective fluorescent recognitions.

Scheme 7- 1. Synthesis of Rhodamine-BINOL conjugate (*S*)-**7.1**.

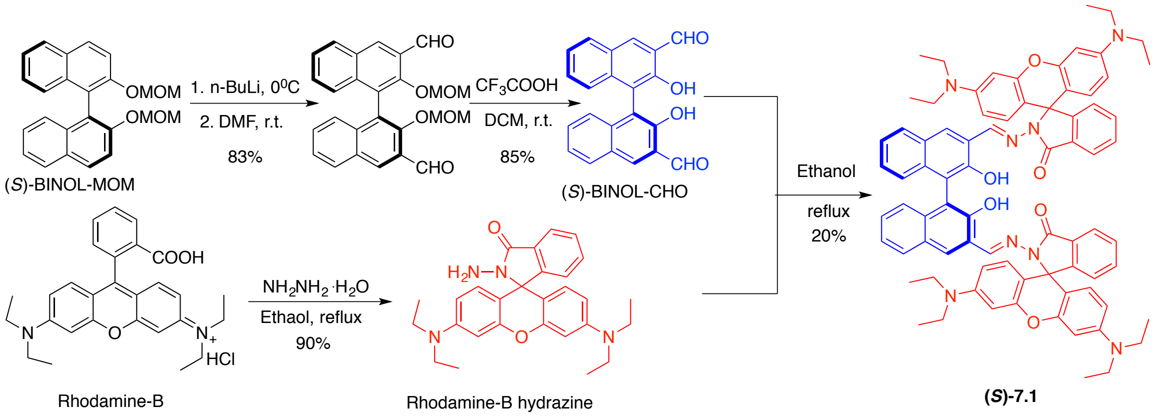
OMOM
OMOM
(S)-BINOL-MOM
1. n-BuLi, 0^{0}C
2. DMF, r.t.
83%
CHO
OMOM
OMOM
CHO
CF$_3$COOH
DCM, r.t.
85%
CHO
OH
OH
CHO
(S)-BINOL-CHO
COOH
N
O
N+
HCl
Rhodamine-B
NH$_2$NH$_2$·H$_2$O
Ethaol, reflux
90%
O
H$_2$N–N
N
O
N
Rhodamine-B hydrazine
Ethanol
reflux
20%
N
O
N
N
N
O
OH
OH
O
N
N
N
O
N
(S)-7.1

It is widely known that the five-membered spiro-ring of rhodamine hydrazine lactam can undergo ring-opening when exposed to acid, and the two forms can coexist in equilibrium at different ratios depending on the condition.^{2} This property should remain intact when Rhodamine B is bound to the BINOL chiral center (Scheme 7-2).

Scheme 7- 2. Acid/base promoted ring opening/closure of Rhodamine B.

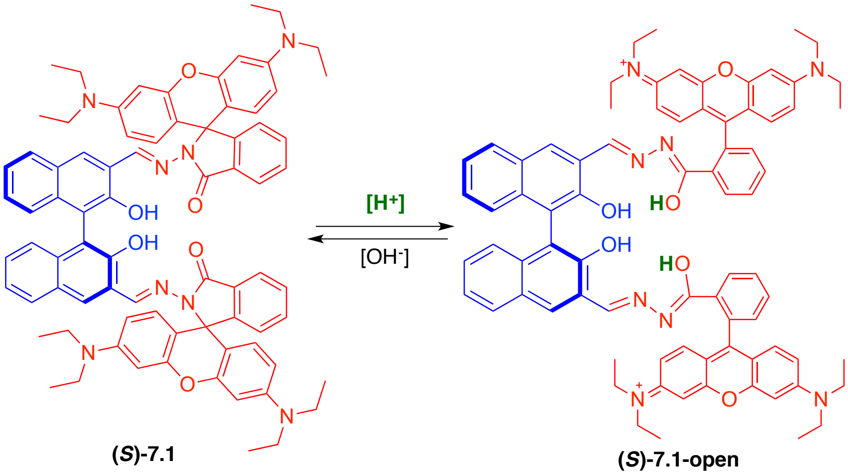
N
O
N
N
N
O
OH
OH
O
N
N
N
O
N
(S)-7.1
[H+]
[OH-]
+N
O
N
N
N
OH
HO
OH
HO
N
N
+N
O
N
(S)-7.1-open

We tried to utilize this property to achieve enantioselective fluorescent recognition of (*S*)-**7.1** to chiral α-hydroxyl acids and amino acids. Two enantiomers of chiral acids may result in different degree of ring-opening, thus different fluorescence intensity, due to their distinct spatial orientation. Although numerous studies have been reported for the fluorescent recognition of ions and small molecules using rhodamine and its derivatives since the pioneering work of Czarnik,[3] no work has been reported for enantioselective recognition of chiral molecules using rhodamine-B as far as we know.

(*S*)-**7.1** produces weak fluorescence at long wavelength in solvents like CH_3CN, THF and H_2O, and shows moderate emission in DCM and methanol (Figure 7-1). For all of the solvents used, the solutions are colorless at 0.01 mM. This is consistent with the knowledge that the spiro-form of rhodamine usually has weaker emission than the open form. The ring opening usually leads to substantial fluorescence turn-on.

Figure 7-1. Fluorescence spectra of (*S*)-**7.1** (0.01 mM) in different solvents (λ_{ex} = 530 nm, slit = 3.0 / 3.0 nm).

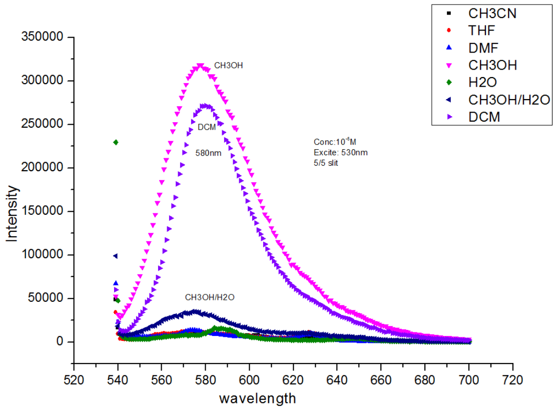

When chiral acids are added, the color changes to pink only for solutions in DCM and methanol, which indicate the large fluorescence enhancement. However, among all the solvents tested, the best enantioselectivity was observed for CH_3CN in which (*S*)-**7.1** is almost non-emissive, though the fluorescence enhancement is smaller than that in DCM and methanol. In acetonitrile, (*S*)-**7.1** has moderate ability to discriminate two enantiomers of α-hydroxyl acids or amino acids at the emission of 580 nm. For the α-hydroxyl acids, the *R* enantiomers always display larger fluorescent enhancement than the *S* forms (Figure 7-2).

Figure 7- 2. Fluorescence spectra of (*S*)-**7.1** (0.01 mM) with or without addition of hydroxyl acids (5 mM). (λ_{ex} =530 nm, slit = 5.0 / 5.0 nm, solvent: CH_3CN).

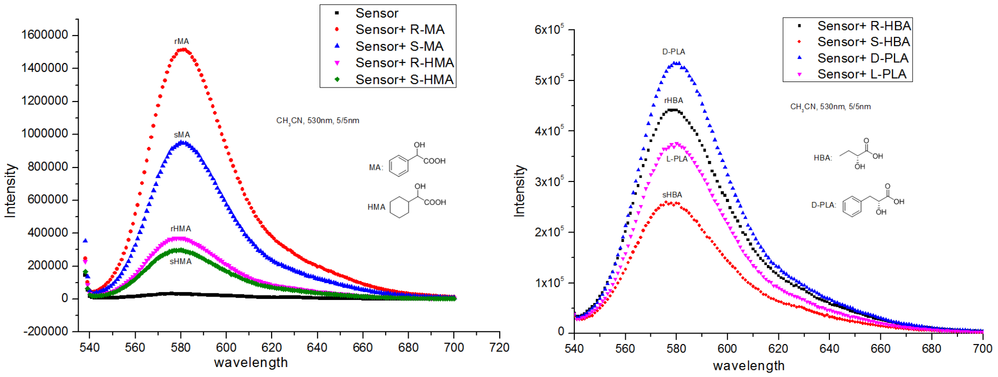

We tested the fluorescence intensity at 580 nm (I_{580}) with the addition of mandelic acid in different concentrations. It shows that the (*R*)-mandelic acid always causes stronger fluorescence enhancement than the (*S*)-mandelic acid, and the *ef* values almost keep constant at concentration ranges higher than 5 mM (Figure 7-3). Herein, *ef* is defined as $(I_R - I_0) / (I_S - I_0)$, where I_0 is the original fluorescence intensity of sensor and I_R, I_S are fluorescence intensities after addition of *R*- or *S*- enantiomer.

It is believed that when the acid interacts with the rhodamine, the chiral environment created by the adjacent BINOL moiety may display chiral discrimination to the incoming acid, whose proton is not completely ionized in the aprotic solvents. We attempted to detect this chemical process by ^{1}H NMR, but unfortunately that we did not observe the appearance of any new peaks or any signal shifts. This might due to the fact that only an extremely small group of hydroxyl acids are able to cause the ring opening of rhodamine. Even though the use of protic solvents like methanol or water was able to facilitate the ring opening process by increasing the ionization of acid, even lower *ef* values were obtained.

Figure 7- 3. Fluorescence spectra of (*S*)-**7.1** (0.01 mM) with addition of mandelic acid at various concentrations. Fluorescence intensity at 580 nm was plotted against concentration. (λ_{ex} =530 nm, slit = 5.0 / 5.0 nm, solvent: CH_3CN)

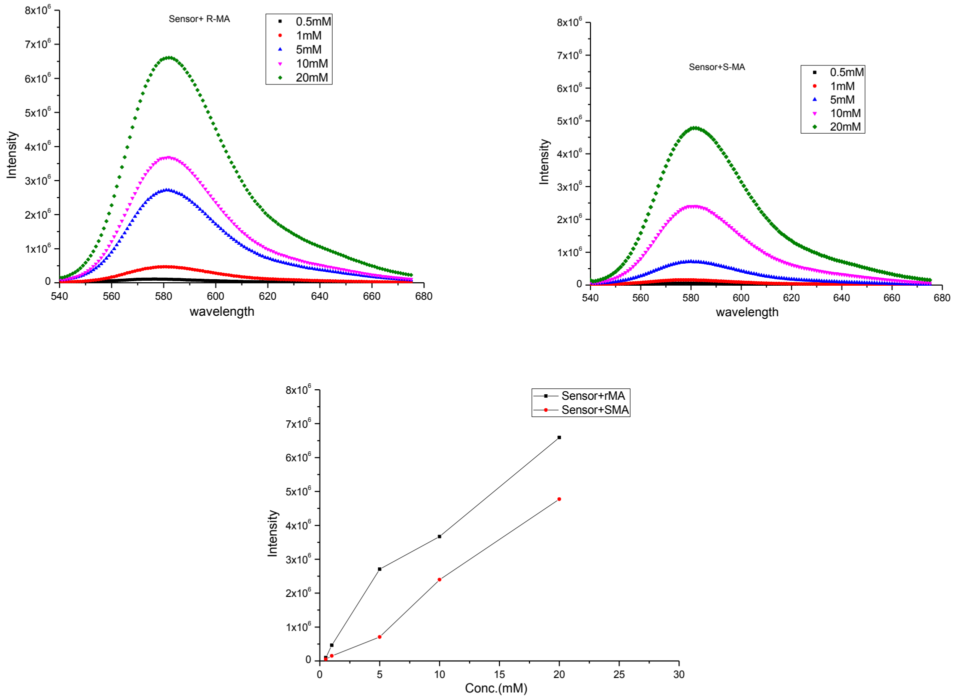

We summarized the *ef* values of (*S*)-**7.1** (0.01 mM) toward different chiral acids (5 mM) in acetonitrile. The selectivity (*ef*) to hydroxyl acids was up to 1.8, while that to amino acids tested was up to 2.6 (Table 7-1). To further improve the enantioselectivity, we tested the addition of zinc cation, which could coordinate with oxygen or nitrogen atoms and might result in a more rigid structure with increased fluorescence enhancement. The addition of 5 eq of $ZnCl_2$ or $Zn(NO_3)_2$ causes about 10-fold fluorescence enhancement, while $Zn(OAc)_2$ does not cause any enhancement but shifts the emission wavelength from 583 nm to 568 nm (Figure 7-4)

Table 7- 1. The *ef* values of (*S*)-**7.1** to hydroxyl acids and amino acids.

MA	HMA	HBA	PLA	Asp	Ser	Val	Ph-Ala-OMe·HCl
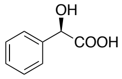	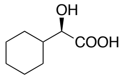	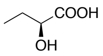	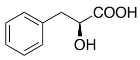	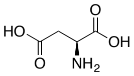	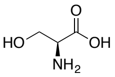	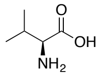	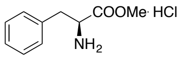
1.6	1.3	1.8	1.5	1.3	2.6	1.4	1,4

Figure 7-4. Fluorescence spectra of (*S*)-**7.1** (0.01 mM) with addition of Zn(II) at various equivalents. (λ_{ex} = 530 nm, slit = 2.0 /2.0 nm, solvent: methanol).

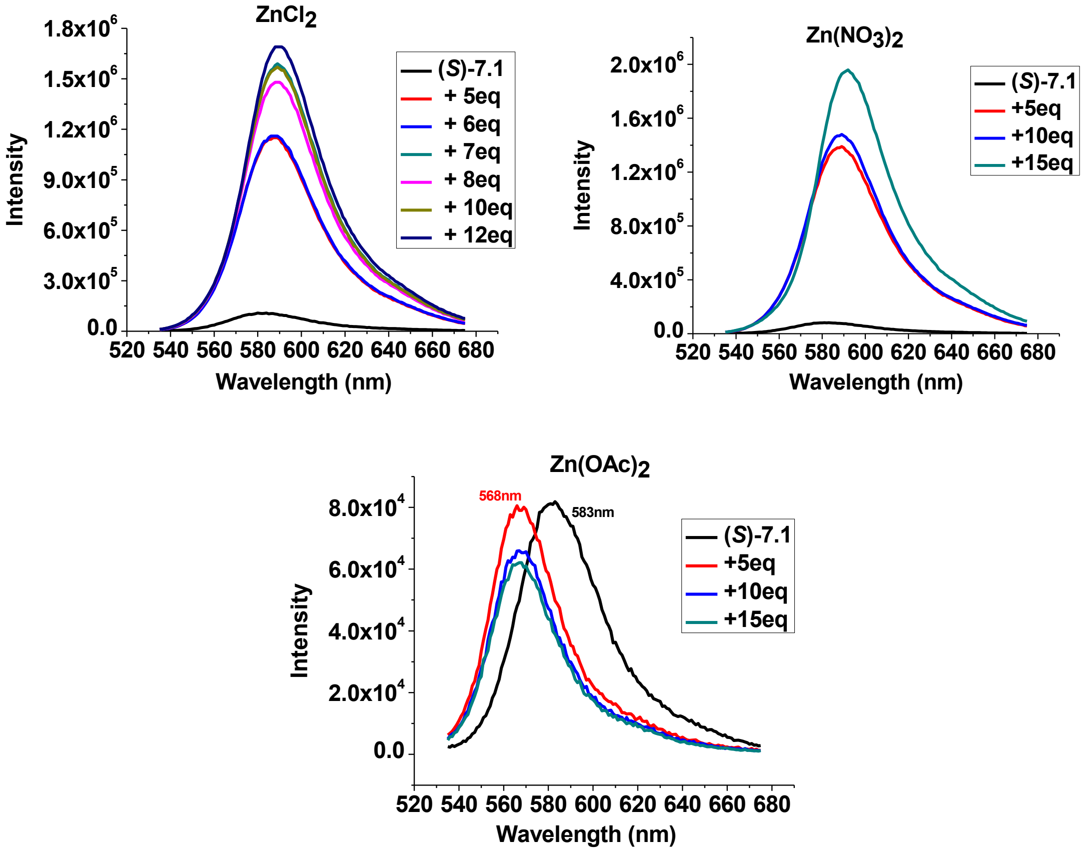

When $ZnCl_2$ was used as an additive for the chiral recognition, it did not induce any improved enantioselectivity (Figure 7-5). With Zn (II), increased emission intensity was observed when acid was added. However, the enantioselectivity almost disappeared completely. It seems that the chiral BINOL moiety is not sufficient enough to control the enantioselective ring opening on the rhodamine moiety, as the conjugate is still pretty flexible.

Figure 7- 5. Fluorescence spectra of (*S*)-**7.1** (0.01 mM) + chiral acids (0.1 mM) with or without $ZnCl_2$ (0.1 mM). (λ_{ex} = 530 nm, slit = 2.0 / 2.0 nm, solvent: methanol).

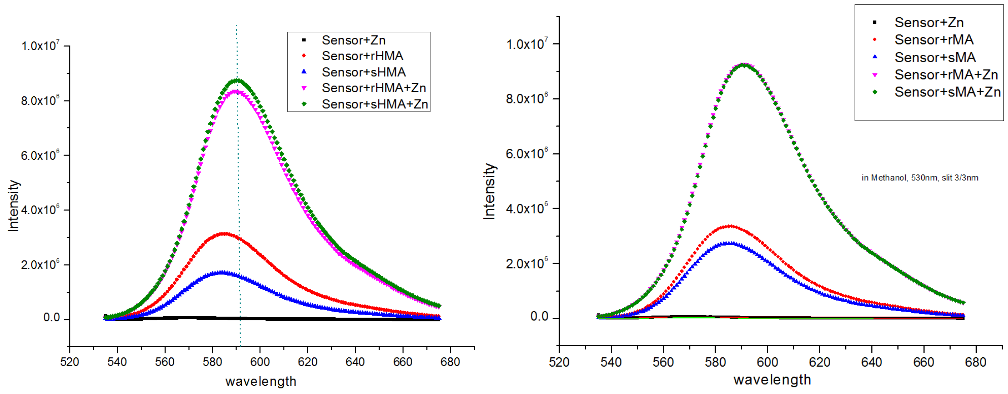

When mandelic acid was added to (*S*)-**7.2** in methanol, it shows a new absorption peak at 560 nm, which is responsible for the fluorescent emission at 580 nm. But in the circular dichroism measurement, no CD signal is observed at 560 nm, indicating the lack of chirality for this polarized absorption (Figure 7-6). We also tested the recognition to chiral amines and alcohols, but no significant enantioselectivity was observed.

Figure 7- 6. UV-Vis absorption spectra of (*S*)-**7.1** (0.01 mM) with addition MA (5 mM) in methanol (left), and its circular dichroism spectra (right).

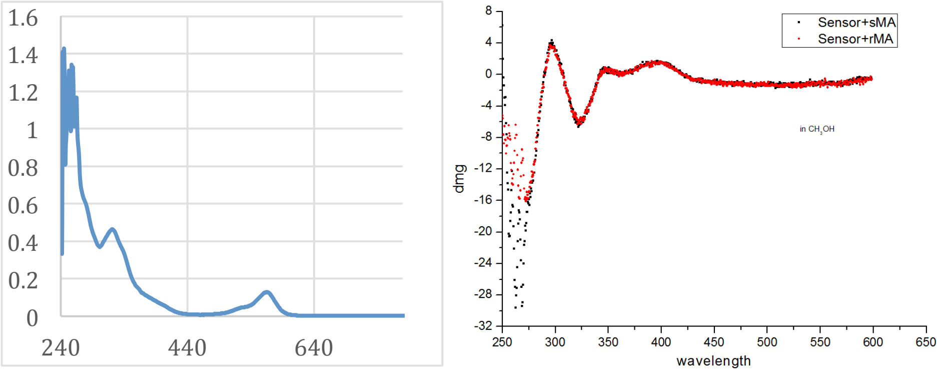

7.2.2. Enantioselective recognition of amines with Resorufin conjugate

Resorufin, which can emit at around 600 nm, has been widely used in the fluorescent and colorimetric sensing of cations, anions and biomolecules[4–6]. Its ester or ether form is usually weakly emissive, while the anionic form is strongly emissive.

An intense fluorescence turn-on can thus be obtained through C-O bond cleavage. Bearing this in mind, we designed a sensor (*S*)-**7.2**, which is an ester connecting H_8BINOL and resorufin. The reaction between (*S*)-H_8BINOL-COOH and resorufin was not successful using the general protocol for peptide synthesis with EDC or HATU. (*S*)-**7.2** was synthesized by the reaction of the acyl chloride (*S*)- H_8BINOL-COCl with resorufin sodium in moderate yields (*S*cheme 7-3).

Scheme 7- 3. Synthesis of Resorufin-H$_8$BINOL conjugate (*S*)-**7.2**.

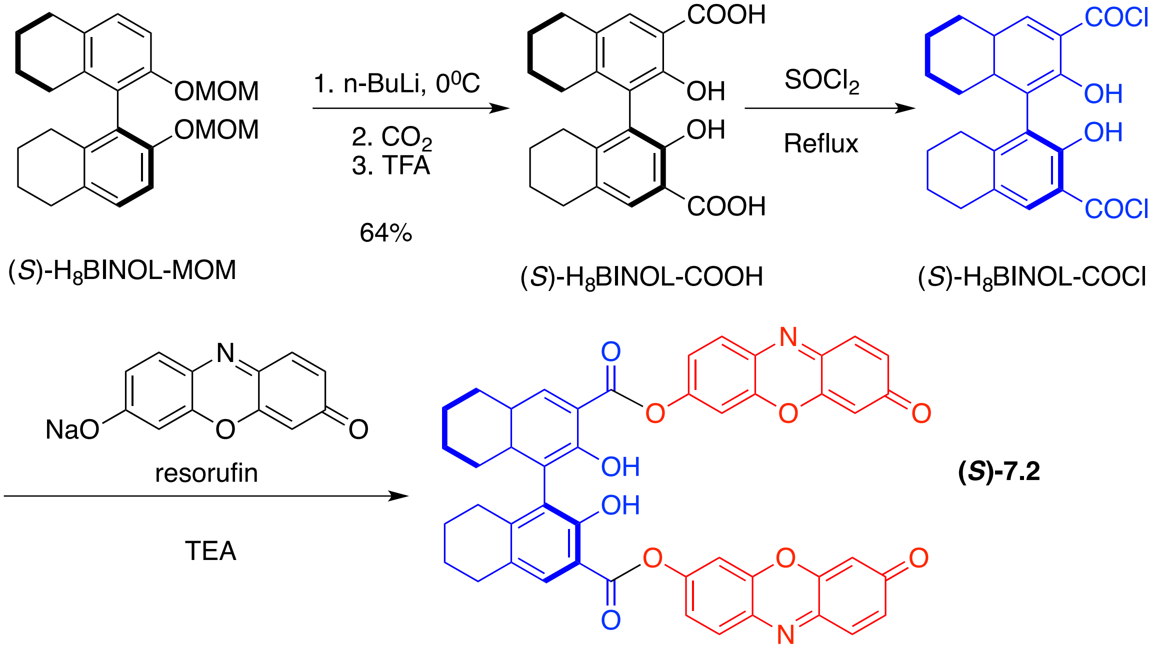
OMOM
OMOM
(S)-H8BINOL-MOM
1. n-BuLi, 0°C
2. CO2
3. TFA
64%
COOH
OH
OH
COOH
(S)-H8BINOL-COOH
SOCl2
Reflux
COCl
OH
OH
COCl
(S)-H8BINOL-COCl
NaO
N
O
O
resorufin
TEA
(S)-7.2

(*S*)-**7.2** is a chiral ester, which should be able to react readily with amines to form amide and free resorufin (Scheme 7-4). The H$_8$BINOL derived amide is expected to have strong emission at around 450 nm as shown in Chapter 4. The free resorufin would give emission at around 600 nm. Therefore, this rational design could enable ratiometric sensing of amines. We wish to use one of the emissions to indicate concentration of amine, while the other one to indicate the enantiomeric excess. A single fluorescence analysis would be enough to make a comprehensive analysis, which should be more convenient than HPLC methods. Recently, this concept was successfully applied to the sensing of amines and amino acids using an imine exchange reaction.[7]

Scheme 7- 4. Substitution of Resorufin with amine for ratiometric sensing.

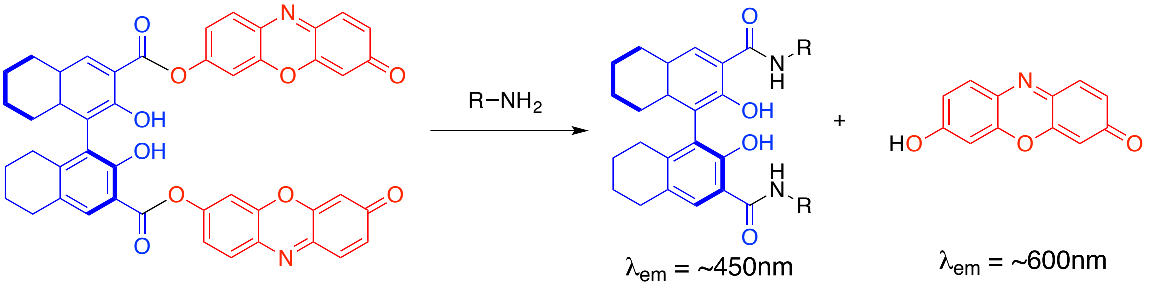

We first checked the background emission of (*S*)-**7.2** in various solvents as shown in Figure 7-7. It is weakly emissive in DCM, CH3CN, CH3OH and mixed solvents containing 90 % water. However, in DMF it shows major dual emission at 595 and 613 nm, consistent with the emission of resorufin.[5] A weak emission was also observed at 494 nm in THF.

Figure 7- 7. Fluorescence spectra of (*S*)-**7.2** (0.05 mM) in various solvents (λ_{ex} = 332 nm, slit 2 / 2 nm).

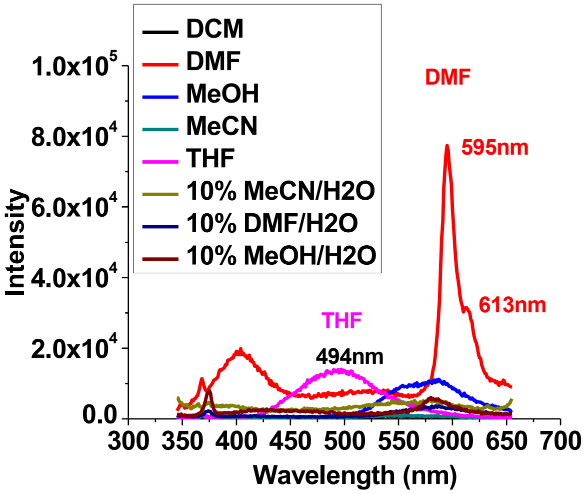

We then tested the efficiency of (*S*)-**7.2** (0.05 mM) in chiral recognition of trans-1, 2-diaminocyclohexane (DAH, 5 mM) in DMF. At 1 h after mixing, no substantial fluorescence change was observed. By increasing the reaction time to 5 and 8 h, we observed a new peak at 457 nm, which is consistent with the emission of the H_8BINOL amide (Scheme 7-4). For enantioselectivity, an *ef* value of 1.3 (λ_{em} = 457 nm) was calculated at 5 h reaction time. During this period, there's also 1.6-fold emission enhancement at 610 nm without enantioselectivity. Thus, the emission at 457 nm can be used to determine enantiomeric excess of DHA while that at 610 nm can be used to determine their total concentration. However, the enantioselectivity was not satisfactory and requires further improvement.

Figure 7- 8. Fluorescence spectra of (*S*)-**7.2** with addition of *RR* or *SS*-DAH over 1-8 h.

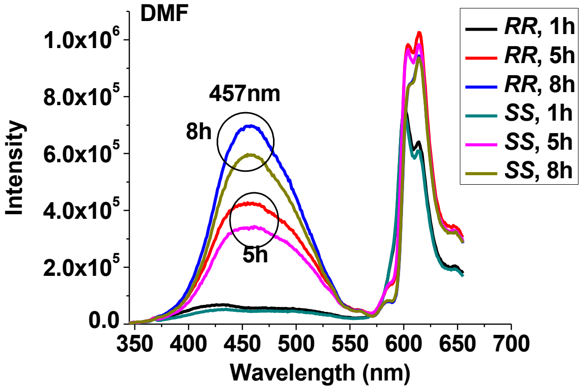

Figure 7- 9. Fluorescence spectra of (*S*)-**7.2** (0.05 mM) with DAH (5 mM) in various solvents overtime.

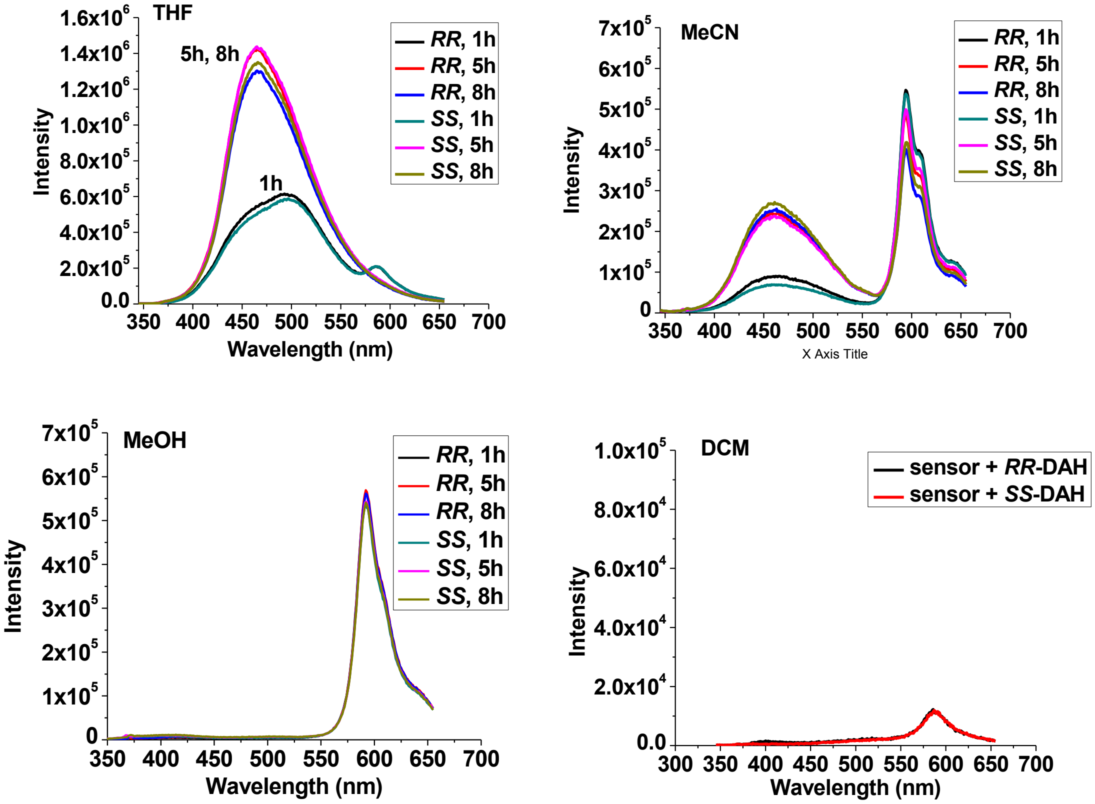

We then turned to other solvents to optimize the sensing condition using the same concentrations of sensor and amine (Figure 7-9). For THF and acetonitrile, we still observed new emission at around 450 nm, but the enantioselectivity was lower than in DMF. No emission at 610 nm was observed in THF. For methanol and DCM, no fluorescence response was observed. As DMF is the optimized solvent for chiral recognition, we mix it with water for the sensing of amino acid (Figure 7-10). Over 4 h reaction time, we observed 8-fold fluorescence enhancement at 610 nm without enantioselectivity. No emission was observed at 450 nm, which is due to the lower nucleophilicity of amino acid than free amine.

Figure 7- 10. Fluorescence spectra of (*S*)-**7.2** (0.05 mM) with serine (5 mM) in 10 % H_2O / DMF overtime.

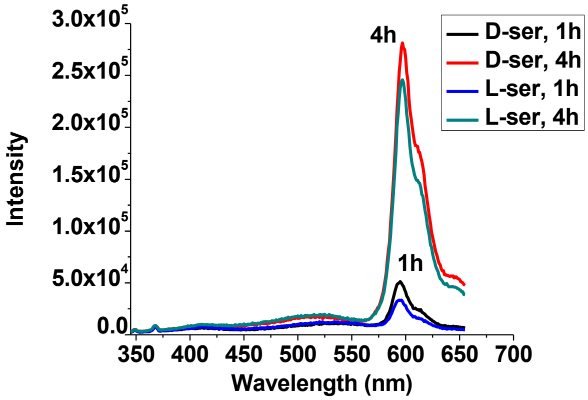

In an attempt to improve selectivity, we tested several additives, which are Cs_2CO_3, triethylamine (TEA), and zinc acetate. These basic additives are assumed to be able to increase the reaction rates between the sensor and amine. As seen in Figure 7-11, in DMF addition of TEA made no difference to the emission spectra. Unexpectedly, cesium carbonate and zinc acetate quench the emission at both 454 nm and 610 nm. In the protic solvent methanol, these additives induced no change in fluorescence at all. In THF, only the addition of zinc acetate caused increased emission intensity at 455 nm but without enantioselectivity.

Figure 7- 11. Fluorescence spectra of (*S*)-**7.2** (0.05 mM) and DAH (5 mM) with additive (0.05 mM) in various solvents at 3 h after mixing.

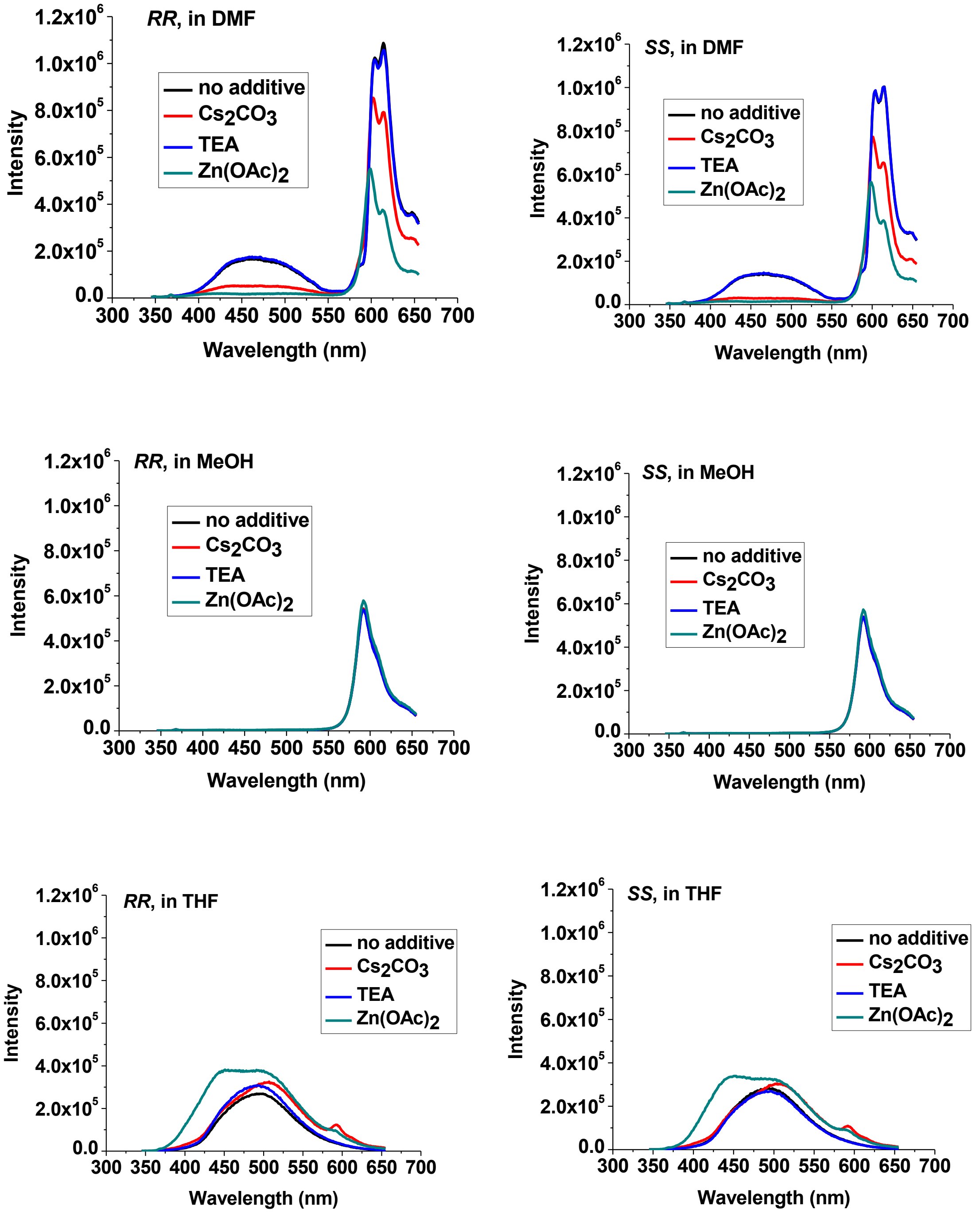

Besides the diamines, we also tested the chiral recognition of (*R*)- and (*S*)-2-amino-1-butanol in various solvents (Figure 7-12). In methanol and THF, *ef* values of about 1.1 were obtained without additives. No enantioselectivity was observed for DMF and acetonitrile. In all cases, the use of additive couldn't improve selectivity.

Figure 7- 12. Fluorescence spectra of (*S*)-**7.2** (0.05 mM) and 2-amino-1-butanol (5 mM) with or without additive (0.05 mM) in various solvents at 3 h after mixing.

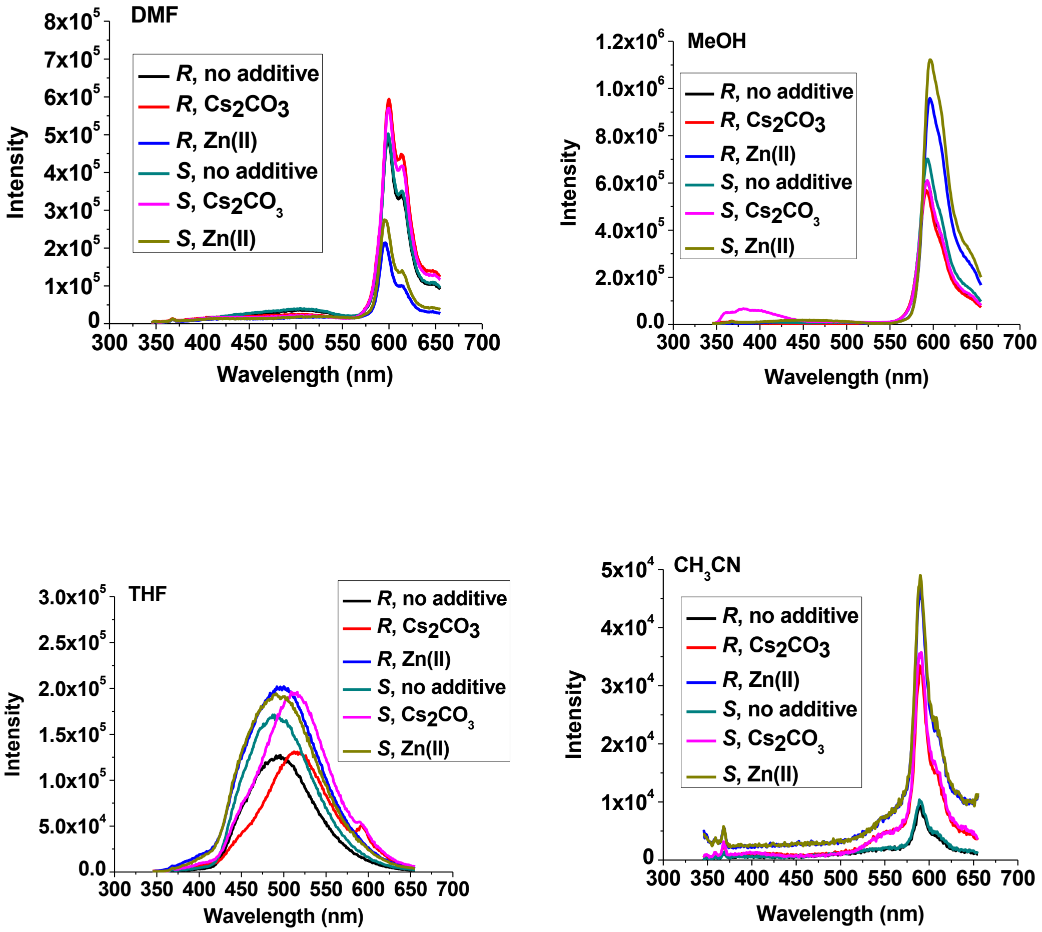

7.3. Conclusion

The conjugation of chiral backbone with fluorophores that have long emission wavelength and high quantum yield could be a new direction in the design of enantioselective sensors. It would largely expand the chiral sensor available, especially the ones that have visible or even NIR emission. The Rhodamine-BINOL (**7.1**) and Resorufin-H_8BINOL (**7.2**) sensor we developed showed promising results in the chiral recognition of hydroxyl acids and free amines and worth further development. However, the enantioselectivity (*ef* < 2) was not satisfactory, mainly due to the large distance between the reaction sites and chiral backbone. Moving the binding sites closer to the chiral center would be necessary to achieve better selectivity.

7.4. Experimental part

Synthesis of (*S*)-2,2'-bis(methoxymethoxy)-[1,1'-binaphthalene]-3,3'-dicarbaldehyde, (*S*)-MOM-BINOL-CHO

To a solution of (*S*)-BINOL-MOM (1 mmol, 373 mg) in dry diethyl ether (12 mL) at 0 °C, a solution of 2.5 M n-BuLi in hexane (3.5 mmol, 1.4 mL) was added dropwise. The mixture was warmed to room temperature and allowed to react for 3 h. Then it was cooled down to 0 °C, and anhydrous DMF (4 mmol, 0.44 mL) was added dropwise. The mixture was warmed to room temperature and reacted for additional 2 h. Saturated NH_4Cl (aq.) was added to quench the reaction at 0 °C. The mixture was extracted with ethyl acetate (3 × 20 mL). The combined organic extract was washed with H_2O (30 mL), then brine (50 mL), and dried with anhydrous Na_2SO_4. After evaporation of the solvents, the residue was purified by column chromatography on silica gel eluted with hexane /

ethyl acetate (15 / 1 to 6 / 1) to afford the desired product as white solid in 83 % yield. ^{1}H NMR (600 MHz, Chloroform-*d*) δ 10.55 (s, 2H), 8.61 (s, 2H), 8.08 (d, *J* = 8.3 Hz, 2H), 7.52 (t, *J* = 7.5 Hz, 2H), 7.43 (t, *J* = 7.7 Hz, 2H), 7.22 (d, *J* = 7.9 Hz, 2H), 4.73 (d, *J* = 6.3 Hz, 2H), 4.69 (d, *J* = 6.3 Hz, 2H), 2.88 (s, 6H).

Synthesis of (*S*)-2,2'-dihydroxy-[1,1'-binaphthalene]-3,3'-dicarbaldehyde, (*S*)-BINOL-CHO

To a solution of (*S*)-MOM-BINOL-CHO (6.6 mmol, 2.84 g) in DCM (20 mL) was added CF_3COOH (5 mL) slowly at 0 °C. The mixture was allowed to react at room temperature for 30 min. Saturated $NaHCO_3$ (aq.) was added slowly to quench the reaction at 0 °C until no bubble formation. The mixture was extracted with DCM (4 × 40 mL). The combined organic extract was washed with H_2O (100 mL), then brine (100 mL), and dried with anhydrous Na_2SO_4. After evaporation of solvents, methanol (20 mL) was added to the residue. The slurry formed was sonicated and centrifuged. The liquid phase was removed. Methanol (20 mL) was added and the process was repeated for 3 times. The pure product was obtained as yellow powder in 85 % yield. ^{1}H NMR (600 MHz, Chloroform-*d*) δ 10.58 (s, 2H), 10.19 (s, 2H), 8.34 (s, 2H), 8.00 (d, *J* = 9.4 Hz, 2H), 7.45 – 7.38 (m, 4H), 7.21 (d, *J* = 9.7 Hz, 2H).

Synthesis of 2-amino-3',6'-bis(diethylamino)spiro[isoindoline-1,9'-xanthen]-3-one, Rhodamine-B hydrazine

To a solution of rhodamine B (2.09 mmol, 1 g) in 40 mL methanol, excess amount of hydrazine hydrate (4 mL, 85 %) was added. The mixture was refluxed under nitrogen for 3 hours. After cooled down to room temperature, the solvent was removed and HCl (40 mL, 1 N) was added while stirring. After 10 min, NaOH (1 N) was added to adjust the pH to 9 – 10 with the formation of precipitate. The precipitate was filtered and washed with H_2O, and then dried under vacuum pump. The product was obtained as orange powder in 90 % yield. No further purification was needed for the next step, though high purify can be obtained by recrystallization in water / methanol. ^{1}H NMR (300 MHz, Chloroform-*d*) δ 8.01 – 7.90 (m, 1H), 7.55 – 7.41 (m, 2H), 7.19 – 7.07 (m, 1H), 6.55 – 6.40 (m, 4H), 6.29 (dd, *J* = 8.8, 2.6 Hz, 2H), 3.61 (s, 2H), 3.34 (q, *J* = 7.1 Hz, 8H), 1.17 (t, *J* = 7.0 Hz, 12H).

Synthesis of 2,2''-(((1*E*,1'*E*)-((*S*)-2,2'-dihydroxy-[1,1'-binaphthalene]-3,3'diyl)bis(methanylylidene)) bis(azanylylidene)) bis (3',6'-bis(diethylamino)spiro[isoindoline-1,9'-xanthen]-3-one), (*S*)-7.1.

Compound (*S*)-**7.1** was synthesized from the condensation of (*S*)-BINOL-CHO and Rhodamine-B hydrazine. Under nitrogen, activated M.S. (4A) was added to a dried 100mL round-bottom flask with reflux condenser, followed by the charge of (*S*)-2,2'-dihydroxy-[1,1'-binaphthalene]-3,3'-dicarbaldehyde (0.4 mmol, 137 mg) and Rhodamine-B hydrazine (1.0 mmol, 457 mg). 50 mL anhydrous ethanol was added and the mixture was refluxed overnight. After filtration of M.S. and evaporation of the solvent, the residue was purified by column chromatography on silica gel eluted with hexane/ethyl acetate (1 / 1) to afford (*S*)-2 as a yellow powder in 20 % yield, which can be further recrystallized from methanol / DCM. ^{1}H NMR (300 MHz, Chloroform-*d*): δ 1H NMR 11.08 (s, 2H), 8.38 (s, 2H), 7.96 (d, *J* = 7.8Hz, 2H), 7.72 (d, *J* = 7.6Hz, 2H), 7.58 (s, 2H), 7.49-7.40 (m, 4H), 7.19–6.99(m, 8H), 6.58–6.43 (m, 8H), 6.26 (broad s, 4H), 3.34-3.30 (m, 16), 1.17–1.14 (m, 24H).

Synthesis of (*S*)-2,2'-dihydroxy-5,5',6,6',7,7',8,8'-octahydro-[1,1'-binaphthalene]-3,3'-dicarboxylic acid, (*S*)-H_8BINOL-COOH

Under nitrogen, (*S*)-H_8BINOL-MOM (3.67 mmol, 1.4 g) was dissolved in anhydrous diethyl ether (30 mL). The solution was cooled to 0 ºC, and 2.5 M n-BuLi in hexane (14.75 mmol, 5.9 mL) was added dropwise. The reaction mixture was stirred at room temperature for 2 h and cooled to -78 °C by dry ice/acetone. A round bottom flask containing dry ice was connected to a tube filled with moisture absorbing silica gel, which was further connected to the reaction mixture allowing CO_2 bubbling in the solution. The mixture was warmed to room temperature and CO_2 was bubbled into the solution for additional 30min. Then CO_2 was removed and the mixture was cooled to 0ºC. 5 mL of CH_3COOH was added, and the solution was stirred at room temperature for 30 min. TLC shows good conversion, with a major blue spot shown at the bottom (EA / Hexane = 1 / 1) under the UV-lamp. Water was added to quench the reaction, and the mixture was extracted 3 times with diethyl ether (4 × 20 mL). The combined organic extracts were washed with brine, and dried over anhydrous Na_2SO_4. After evaporation of the solvents, the residue was purified by column chromatography on silica gel eluted with hexane/ethyl acetate (3 / 1 to 1 / 3) to afford compound (*S*)-H_8BINOL-COOH in 64 % yield. ^{1}H NMR (600 MHz, Chloroform-*d*) δ 10.35 (s, 2H), 7.70 (s, 2H), 2.83 – 2.76 (m, 4H), 2.44 – 2.42(m, 2H), 2.23 – 2.17 (m, 2H), 1.81 – 1.65 (m, 8H).

Synthesis of bis(3-oxo-3*H*-phenoxazin-7-yl)2,2'-dihydroxy-4a,5,5',6,6',7,7',8,8a,8'-decahydro-[1,1'-binaphthalene] -3,3'-dicarboxylate, (*S*)-7.2.

The (*S*)-H_8BINOL-COCl needed was made in-situ by refluxing (*S*)-H_8BINOL-COOH (1.24 mmol, 479 mg) in thionyl chloride (12 mL) for 16 h and then removing the solvent with evaporator and vacuum pump. A dispersed solution of resorufin sodium (3.72 mmol, 875 mg) in DCM (60 mL) was prepared, and triethylamine (4.5 mmol, 0.63 mL) was added under nitrogen. To this mixture was added the solution of (*S*)-H_8BINOL-COCl (1.24 mmol) in DCM (5 mL). After stirring for 12 h, the mixture was filtered to remove unreacted resorufin sodium. The filtrate was washed with water (50 mL), then 1 M $NaHCO_3$, and brine. The solution was dried over anhydrous Na_2SO_4. After evaporation of the solvents, the product was obtained with good purity. ^{1}H NMR (600 MHz, Chloroform-*d*) δ 10.20 (s, 2H), 7.88 (s, *2*H), 7.86 (s, 2H), 7.46 – 7.43 (d, *J* = 9.8 Hz, 2H), 7.26 – 7.22 (m, 2H), 6.88 (d, *J* = 11.6 Hz, 2H), 6.35 (s, 2H), 2.90 – 2.81 (m, 4H), 2.58 – 2.49 (m, 2H), 2.32 – 2.25 (m, 2H), 1.85 – 1.73 (m, 8H). NMR (151 MHz, Chloroform-*d*) δ 186.44, 168.54, 157.09, 153.11, 149.38, 148.73, 147.02, 144.59, 135.44, 134.97, 131.71, 131.48, 130.24, 129.47, 124.17, 119.58, 110.19, 108.97, 107.52, 29.41, 28.01, 22.88, 22.77.

7.5. References

(1) Zeng, C.; Zhang, X.; Pu, L. *Chem. - A Eur. J.* **2016**, 2432.

(2) Li, X. H.; Gao, X. H.; Shi, W.; Ma, H. M. *Chem. Rev.* **2014**, *114* (1), 590.

(3) D, V.; Ford, F.; Anthony, C. *J. Am. Chem. Soc* **1997**, *119*, 7386.

(4) Zhou, M.; Diwu, Z.; Panchuk-Voloshina, N.; Haugland, R. P. *Anal. Biochem.*

1997, *253* (253), 162.

(5) Kim, H. N.; Ren, W. X.; Kim, J. S.; Yoon, J. *Chem. Soc. Rev.* **2012**, *41* (8), 3210.

(6) Choi, M. G.; Hwang, J.; Eor, S.; Chang, S. K. *Org. Lett.* **2010**, *12* (24), 5624.

(7) Wen, K.; Yu, S.; Huang, Z.; Chen, L.; Xiao, M.; Yu, X.; Pu, L. *J. Am. Chem. Soc.* **2015**, *137* (13), 4517.

Appendix

Appendix for Chapter 3

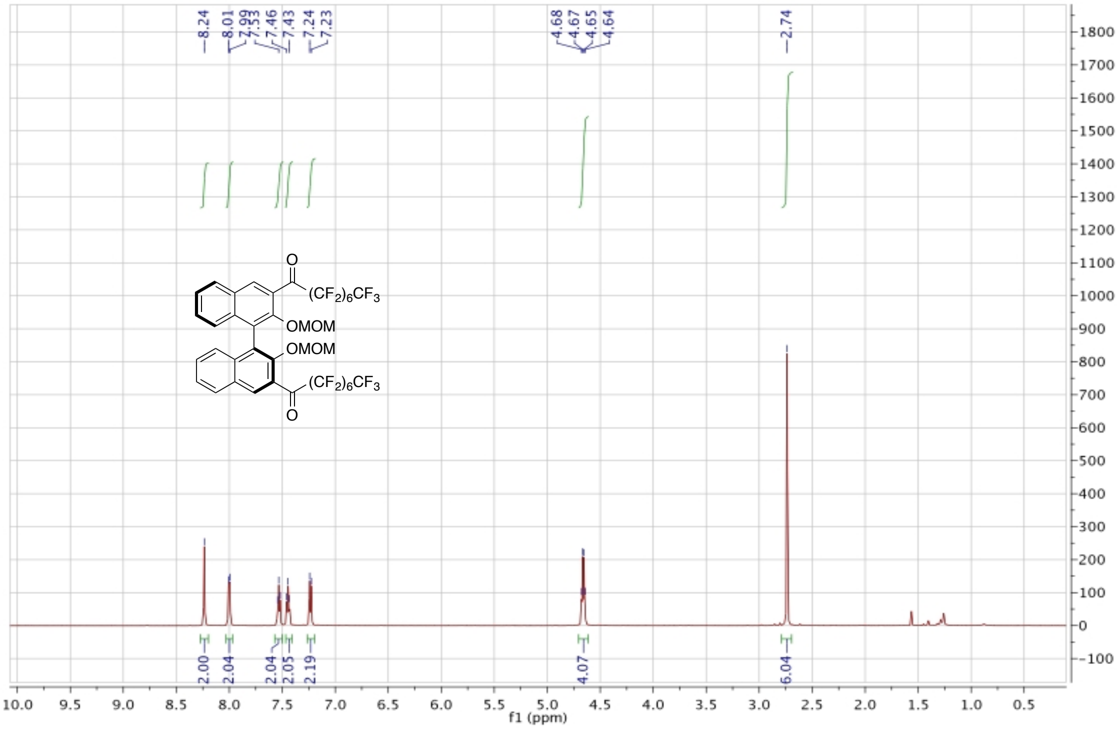

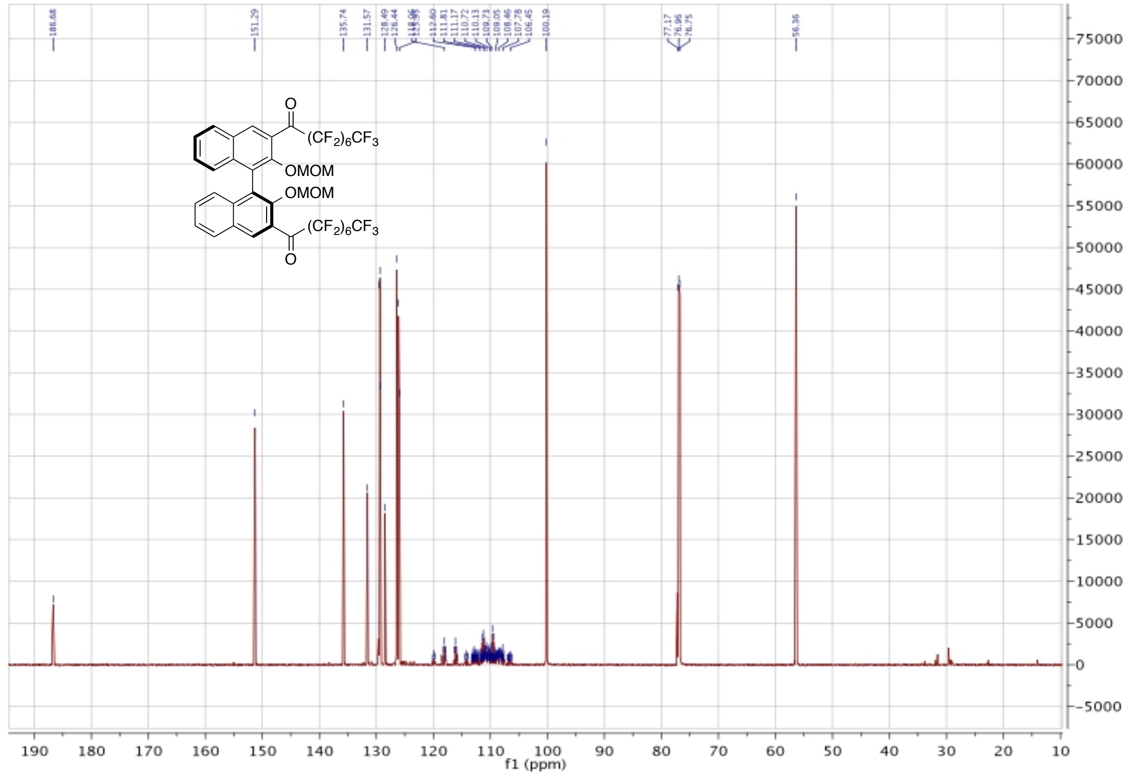

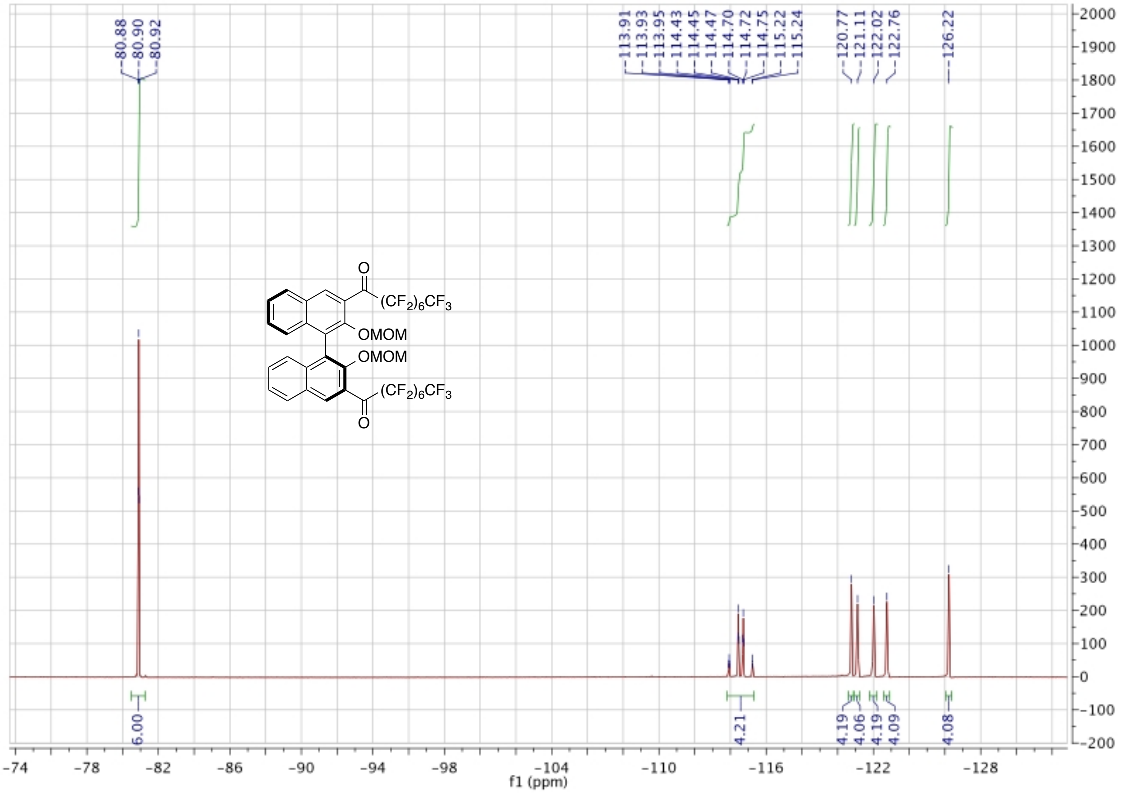
-80.88
-80.90
-80.92
-113.91
-113.93
-113.95
-114.43
-114.45
-114.47
-114.70
-114.72
-114.75
-115.22
-115.24
-120.77
-121.11
-122.02
-122.76
-126.22
6.00
4.21
4.19
4.06
4.19
4.09
4.08
O
(CF2)6CF3
OMOM
OMOM
(CF2)6CF3
O
-74
-78
-82
-86
-90
-94
-98
-104
-110
-116
-122
-128
f1 (ppm)
2000
1900
1800
1700
1600
1500
1400
1300
1200
1100
1000
900
800
700
600
500
400
300
200
100
0
-100
-200

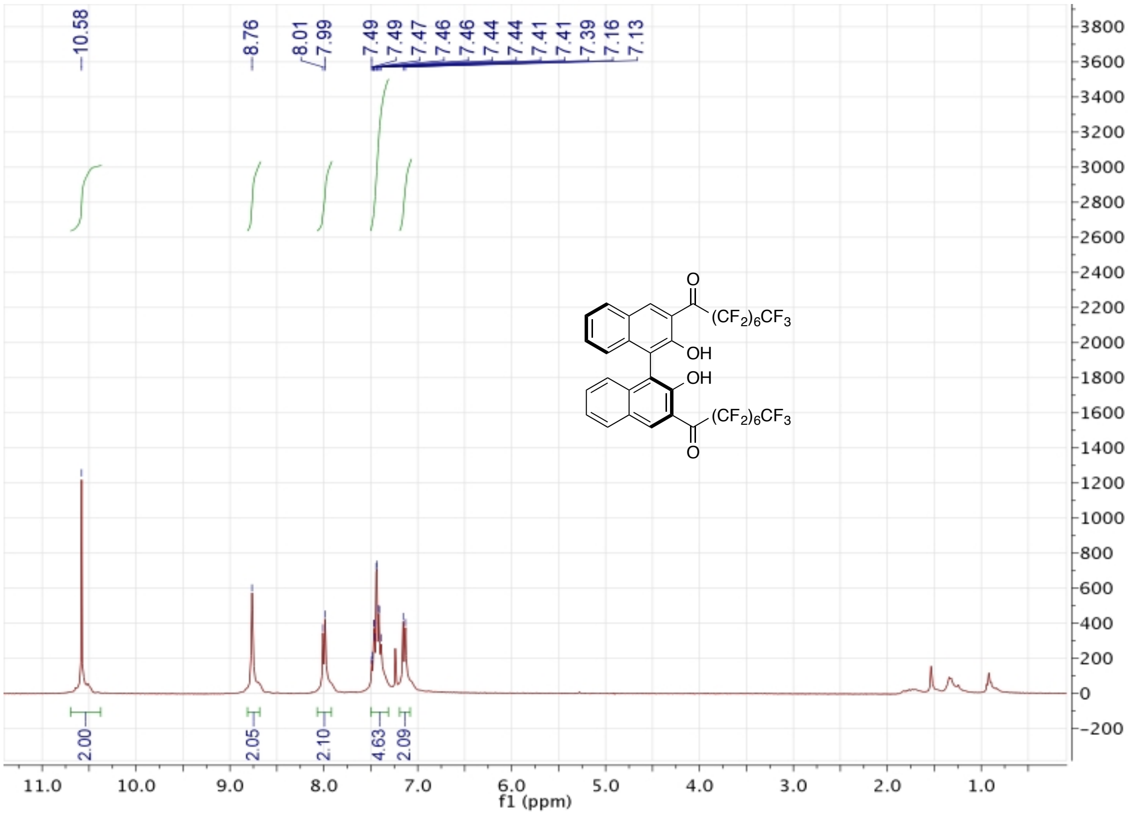
10.58
8.76
8.01
7.99
7.49
7.49
7.47
7.46
7.46
7.44
7.44
7.41
7.41
7.39
7.16
7.13
2.00
2.05
2.10
4.63
2.09
O
(CF2)6CF3
OH
OH
(CF2)6CF3
O
11.0
10.0
9.0
8.0
7.0
6.0
5.0
4.0
3.0
2.0
1.0
f1 (ppm)
3800
3600
3400
3200
3000
2800
2600
2400
2200
2000
1800
1600
1400
1200
1000
800
600
400
200
0
-200

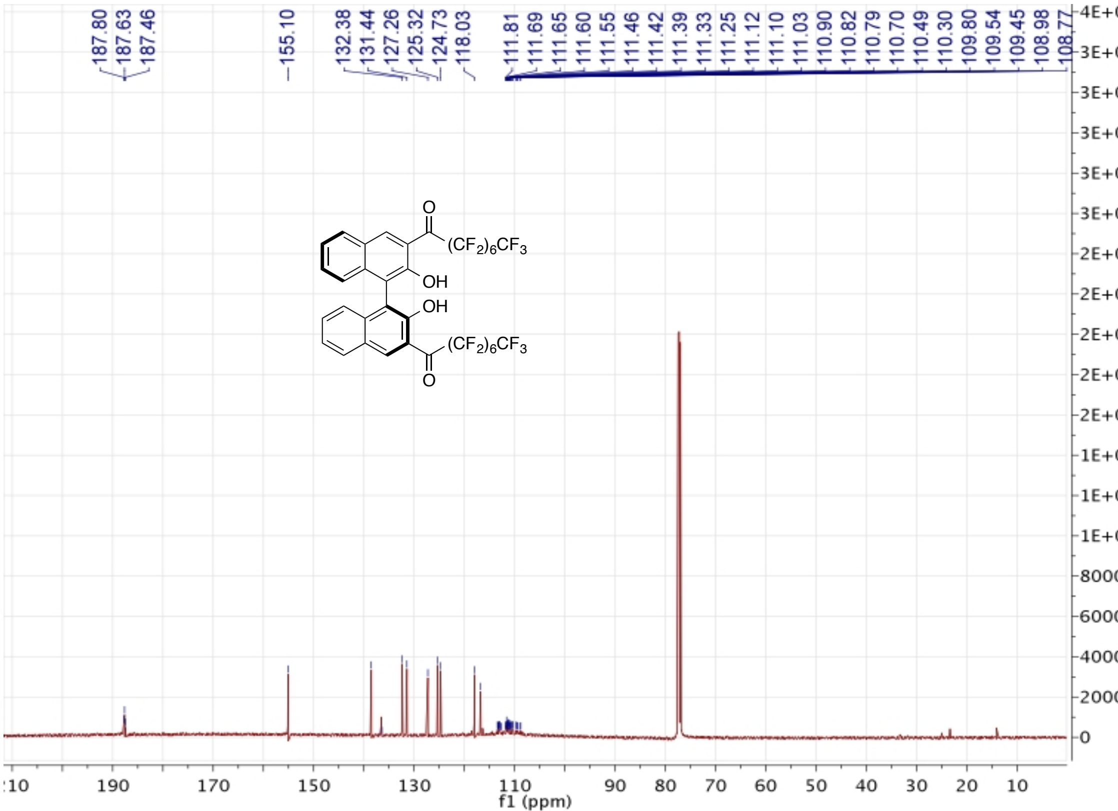
187.80
187.63
187.46
155.10
132.38
131.44
127.26
125.32
124.73
118.03
111.81
111.69
111.65
111.60
111.55
111.46
111.42
111.39
111.33
111.25
111.12
111.10
111.03
110.90
110.82
110.79
110.70
110.49
110.30
109.80
109.54
109.45
108.98
108.77
O
(CF2)6CF3
OH
OH
(CF2)6CF3
O
4E+05
3E+05
3E+05
3E+05
3E+05
3E+05
2E+05
2E+05
2E+05
2E+05
2E+05
1E+05
1E+05
1E+05
80000
60000
40000
20000
0
10
190
170
150
130
110
90
80
70
60
50
40
30
20
10
f1 (ppm)

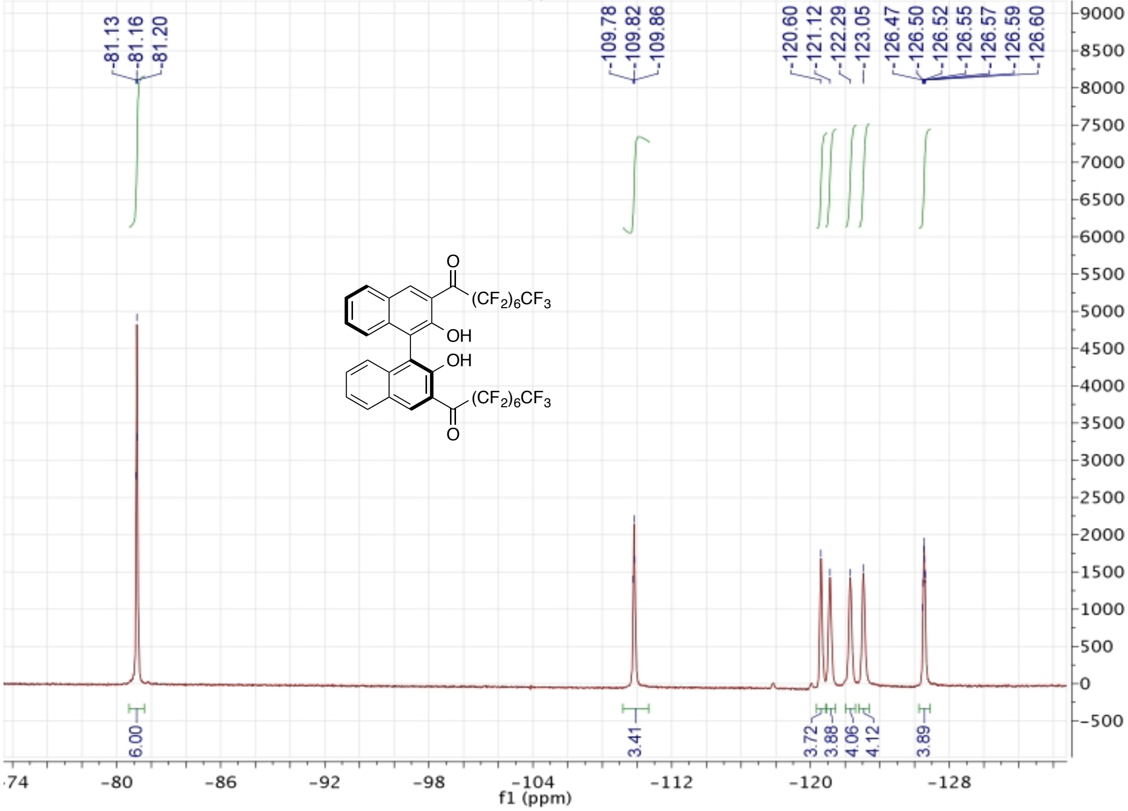
-81.13
-81.16
-81.20
-109.78
-109.82
-109.86
-120.60
-121.12
-122.29
-123.05
-126.47
-126.50
-126.52
-126.55
-126.57
-126.59
-126.60
O
(CF2)6CF3
OH
OH
(CF2)6CF3
O
9000
8500
8000
7500
7000
6500
6000
5500
5000
4500
4000
3500
3000
2500
2000
1500
1000
500
0
-500
6.00
3.41
3.72
3.88
4.06
4.12
3.89
-74
-80
-86
-92
-98
-104
-112
-120
-128
f1 (ppm)

NMR spectra of (*R*)-**3.6**

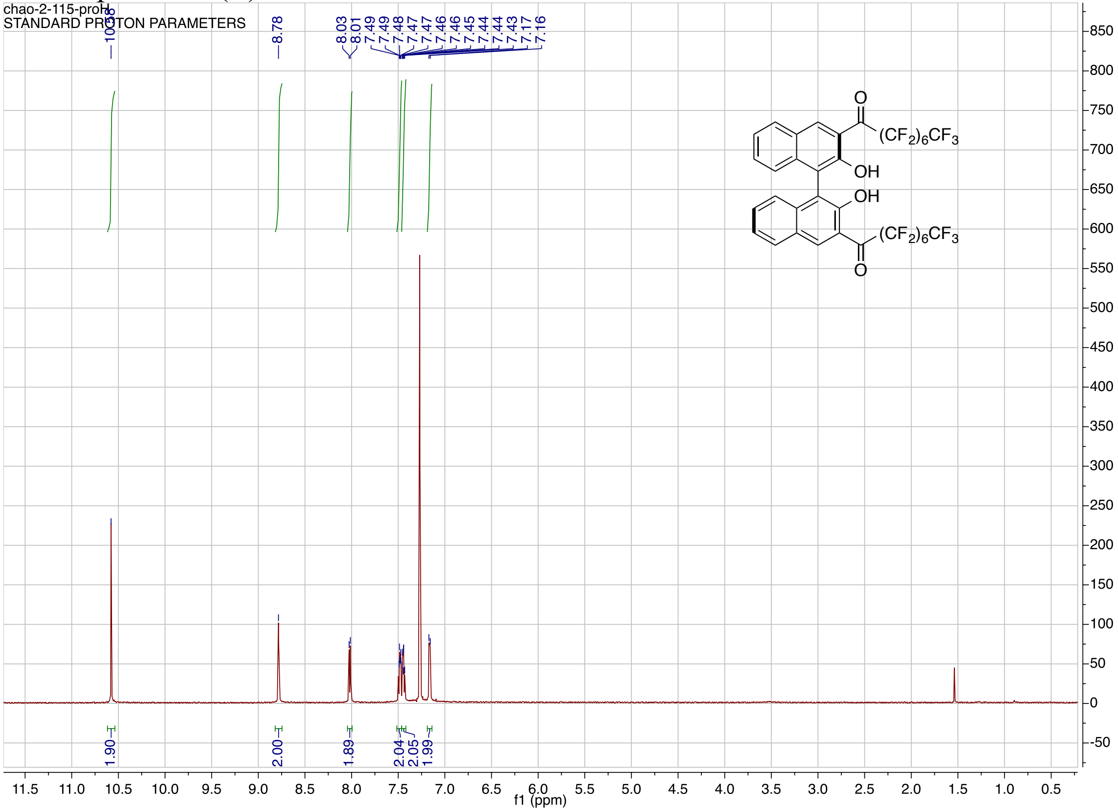

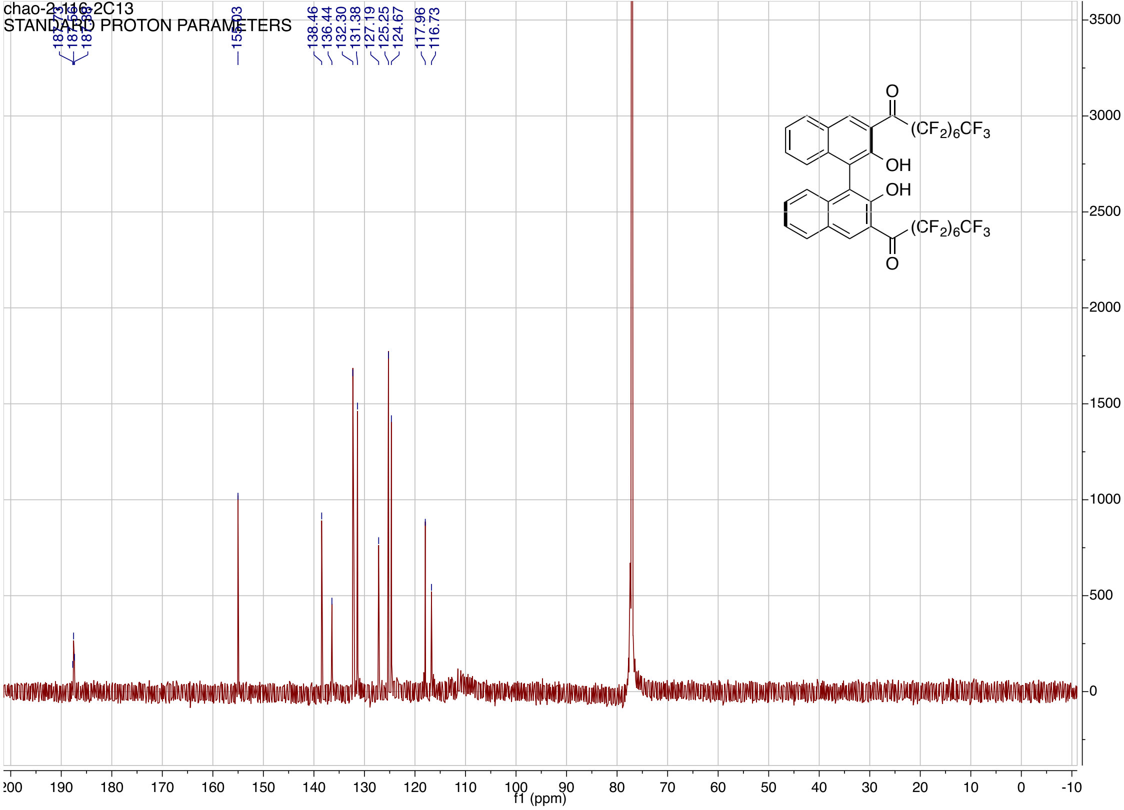

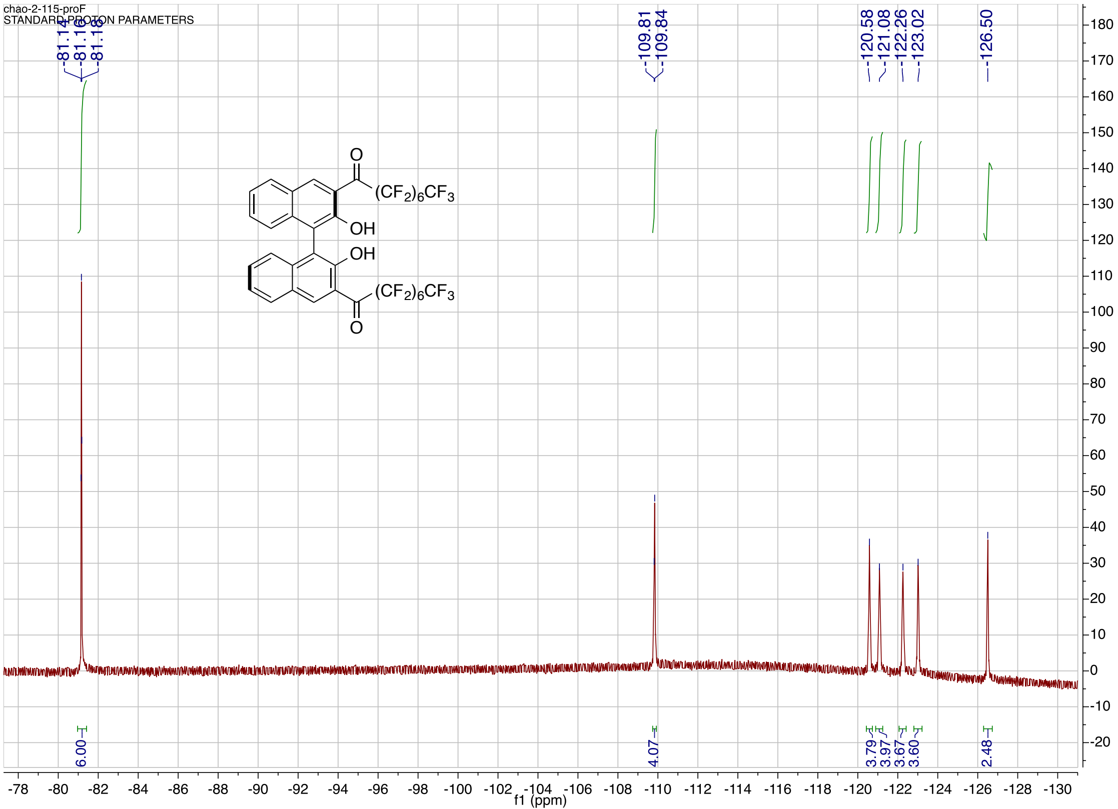
chao-2-115-proF
STANDARD PROTON PARAMETERS
-81.14
-81.16
-81.18
-109.81
-109.84
-120.58
-121.08
-122.26
-123.02
-126.50
O
$(CF_2)_6CF_3$
OH
OH
$(CF_2)_6CF_3$
O
6.00
4.07
3.79
3.97
3.67
3.60
2.48
f1 (ppm)
-78 -80 -82 -84 -86 -88 -90 -92 -94 -96 -98 -100 -102 -104 -106 -108 -110 -112 -114 -116 -118 -120 -122 -124 -126 -128 -130
180 170 160 150 140 130 120 110 100 90 80 70 60 50 40 30 20 10 0 -10 -20

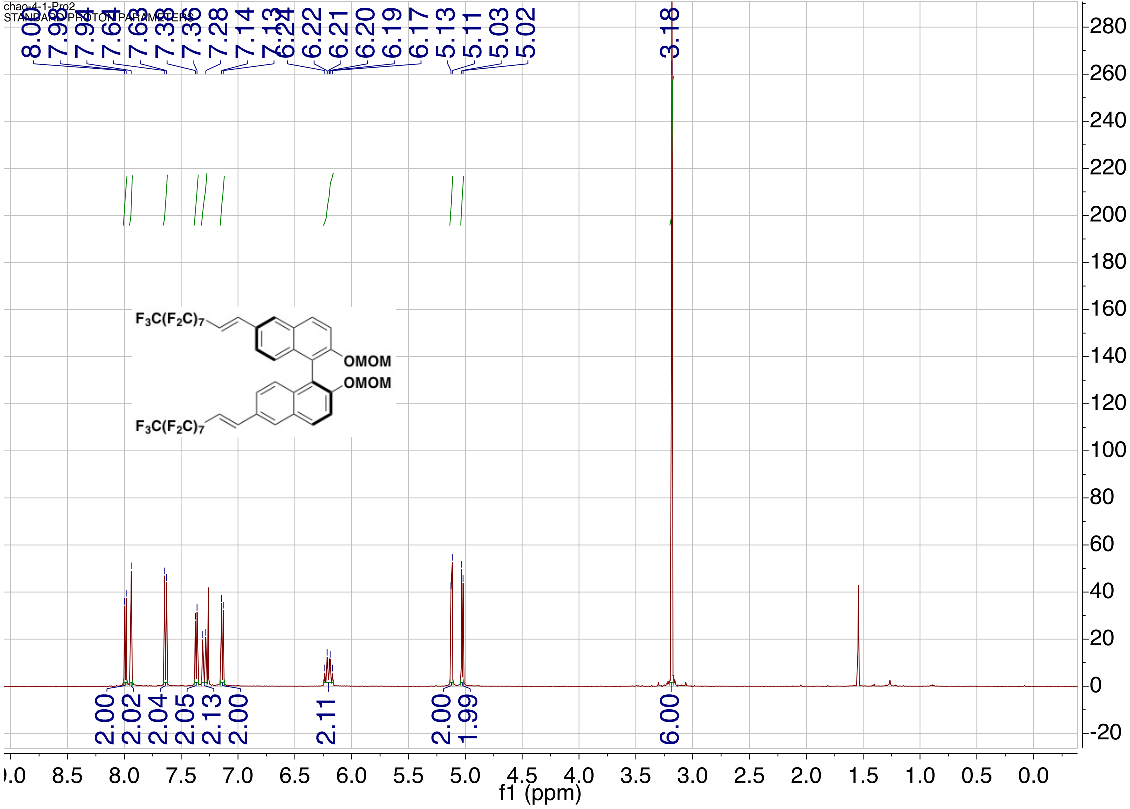
chao-4-1-Pro2
STANDARD PROTON PARAMETERS
8.00
7.98
7.94
7.64
7.63
7.38
7.36
7.28
7.14
7.13
6.24
6.22
6.21
6.20
6.19
6.17
5.13
5.11
5.03
5.02
3.18
$F_3C(F_2C)_7$
OMOM
OMOM
$F_3C(F_2C)_7$
2.00
2.02
2.04
2.05
2.13
2.00
2.11
2.00
1.99
6.00
f1 (ppm)
9.0 8.5 8.0 7.5 7.0 6.5 6.0 5.5 5.0 4.5 4.0 3.5 3.0 2.5 2.0 1.5 1.0 0.5 0.0
280 260 240 220 200 180 160 140 120 100 80 60 40 20 0 -20

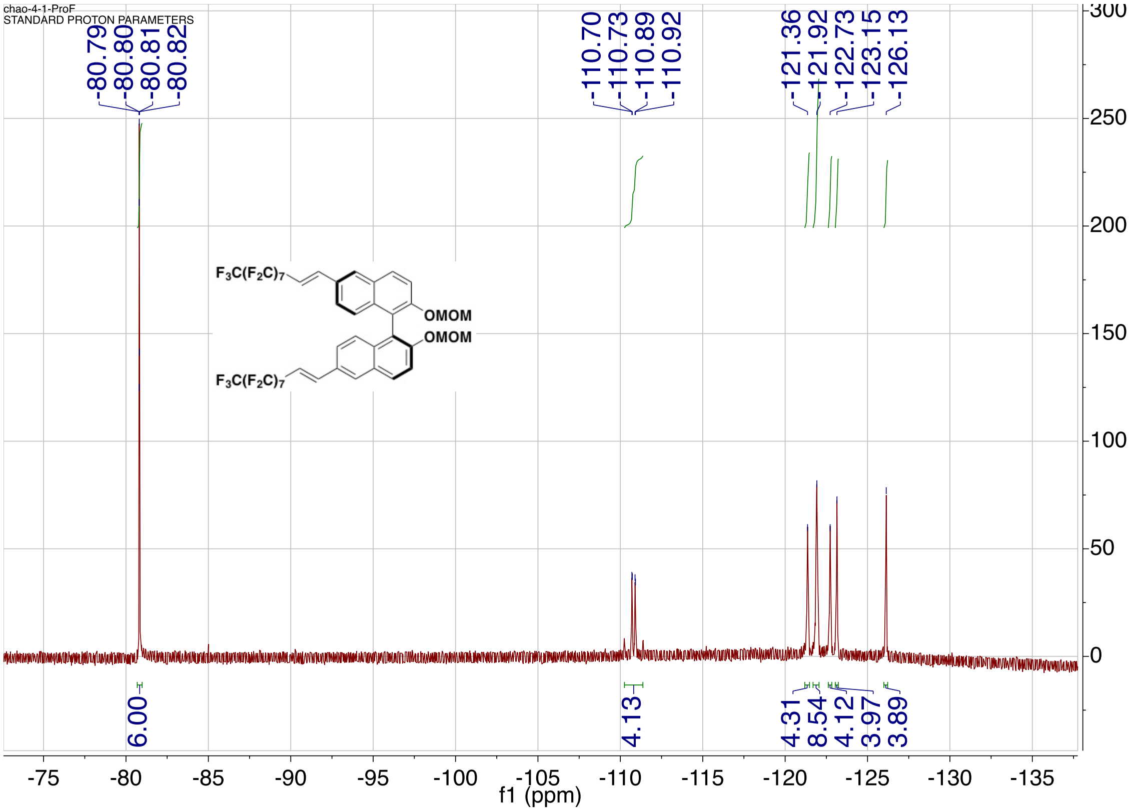
chao-4-1-ProF
STANDARD PROTON PARAMETERS
-80.79
-80.80
-80.81
-80.82
-110.70
-110.73
-110.89
-110.92
-121.36
-121.92
-122.73
-123.15
-126.13
F₃C(F₂C)₇
OMOM
OMOM
F₃C(F₂C)₇
6.00
4.13
4.31
8.54
4.12
3.97
3.89
300
250
200
150
100
50
0
-75
-80
-85
-90
-95
-100
-105
-110
-115
-120
-125
-130
-135
f1 (ppm)

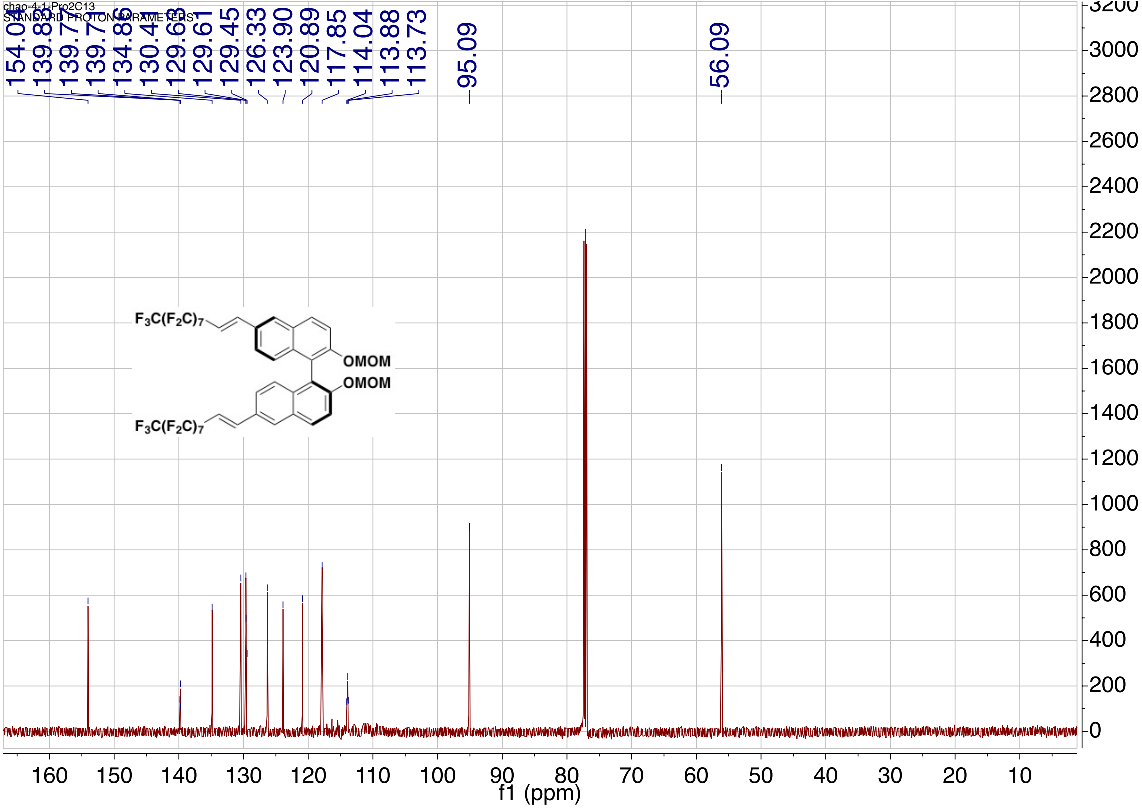
chao-4-1-Pro2C13
STANDARD PROTON PARAMETERS
154.04
139.83
139.77
139.76
134.86
130.41
129.63
129.61
129.45
126.33
123.90
120.89
117.85
114.04
113.88
113.73
95.09
56.09
F₃C(F₂C)₇
OMOM
OMOM
F₃C(F₂C)₇
3200
3000
2800
2600
2400
2200
2000
1800
1600
1400
1200
1000
800
600
400
200
0
160
150
140
130
120
110
100
90
80
70
60
50
40
30
20
10
f1 (ppm)

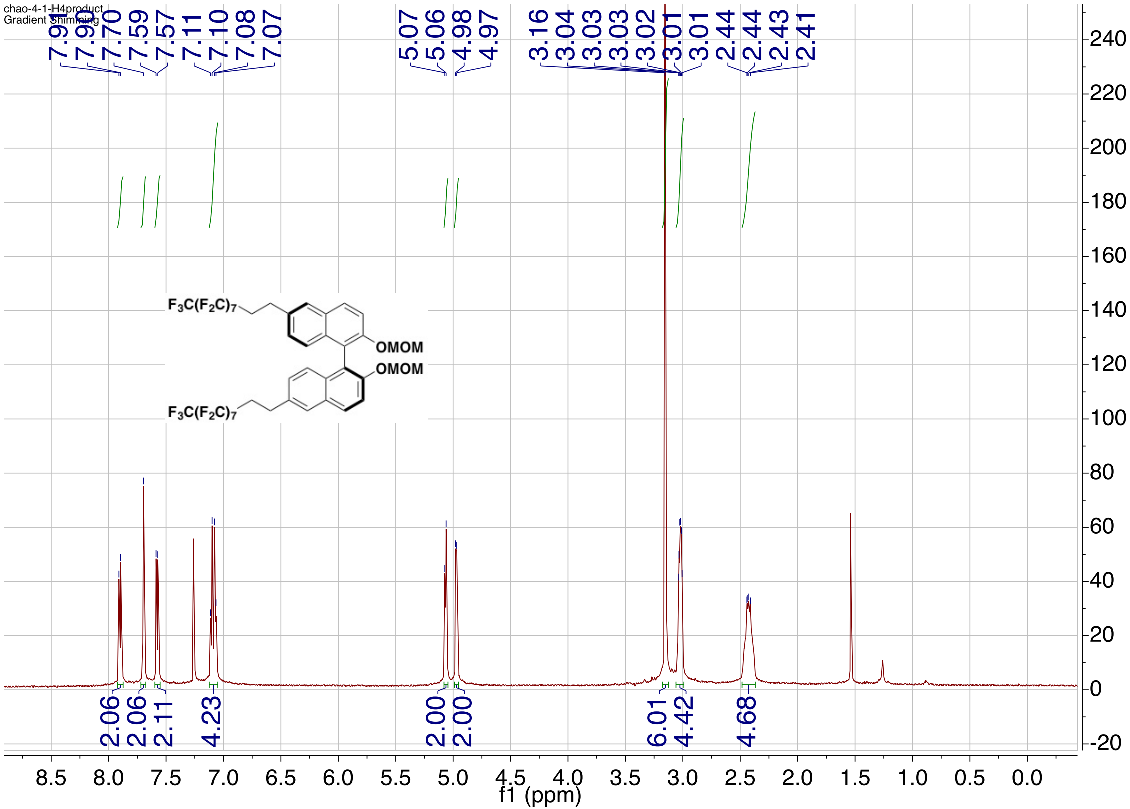
chao-4-1-H4product
Gradient Shimming
7.91
7.90
7.70
7.59
7.57
7.11
7.10
7.08
7.07
5.07
5.06
4.98
4.97
3.16
3.04
3.03
3.03
3.02
3.01
3.01
2.44
2.44
2.43
2.41
F3C(F2C)7
OMOM
OMOM
F3C(F2C)7
2.06
2.06
2.11
4.23
2.00
2.00
6.01
4.42
4.68
240
220
200
180
160
140
120
100
80
60
40
20
0
-20
8.5
8.0
7.5
7.0
6.5
6.0
5.5
5.0
4.5
4.0
3.5
3.0
2.5
2.0
1.5
1.0
0.5
0.0
f1 (ppm)

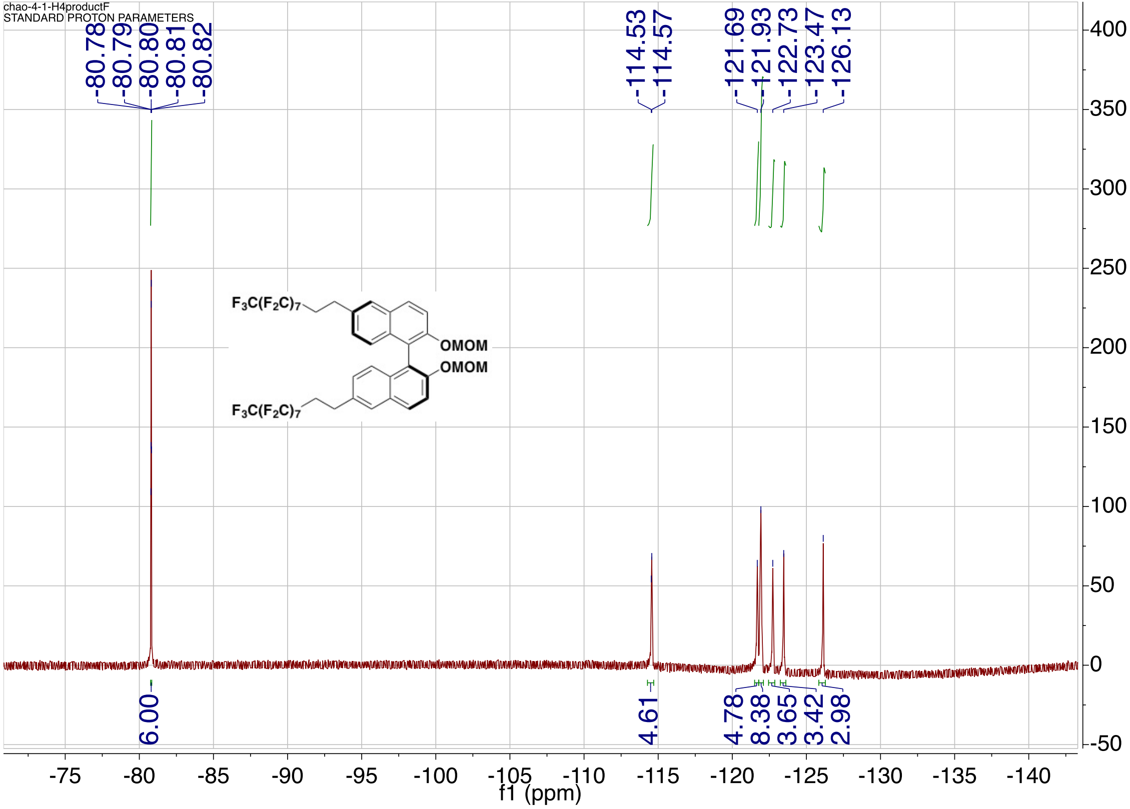
chao-4-1-H4productF
STANDARD PROTON PARAMETERS
-80.78
-80.79
-80.80
-80.81
-80.82
-114.53
-114.57
-121.69
-121.93
-122.73
-123.47
-126.13
F3C(F2C)7
OMOM
OMOM
F3C(F2C)7
6.00
4.61
4.78
8.38
3.65
3.42
2.98
400
350
300
250
200
150
100
50
0
-50
-75
-80
-85
-90
-95
-100
-105
-110
-115
-120
-125
-130
-135
-140
f1 (ppm)

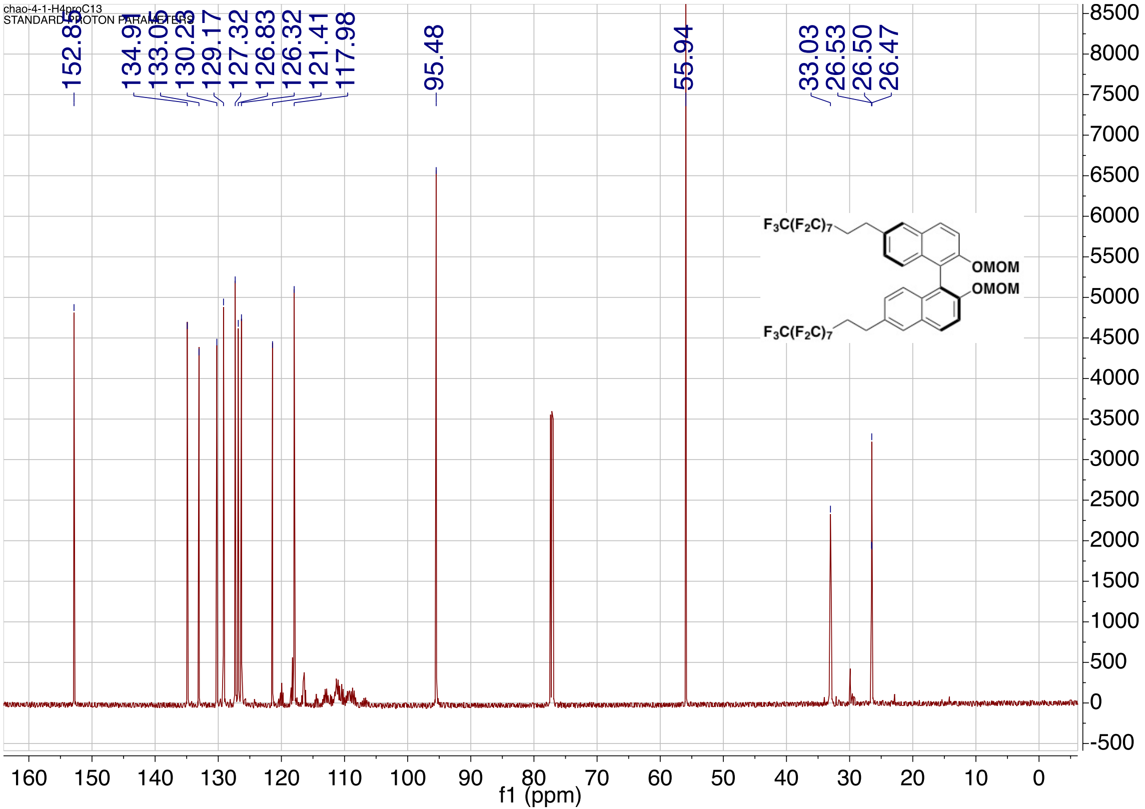
chao-4-1-H4proC13
STANDARD PROTON PARAMETERS
152.85
134.91
133.05
130.23
129.17
127.32
126.83
126.32
121.41
117.98
95.48
55.94
33.03
26.53
26.50
26.47
$F_3C(F_2C)_7$
OMOM
OMOM
$F_3C(F_2C)_7$
8500
8000
7500
7000
6500
6000
5500
5000
4500
4000
3500
3000
2500
2000
1500
1000
500
0
-500
160 150 140 130 120 110 100 90 80 70 60 50 40 30 20 10 0
f1 (ppm)

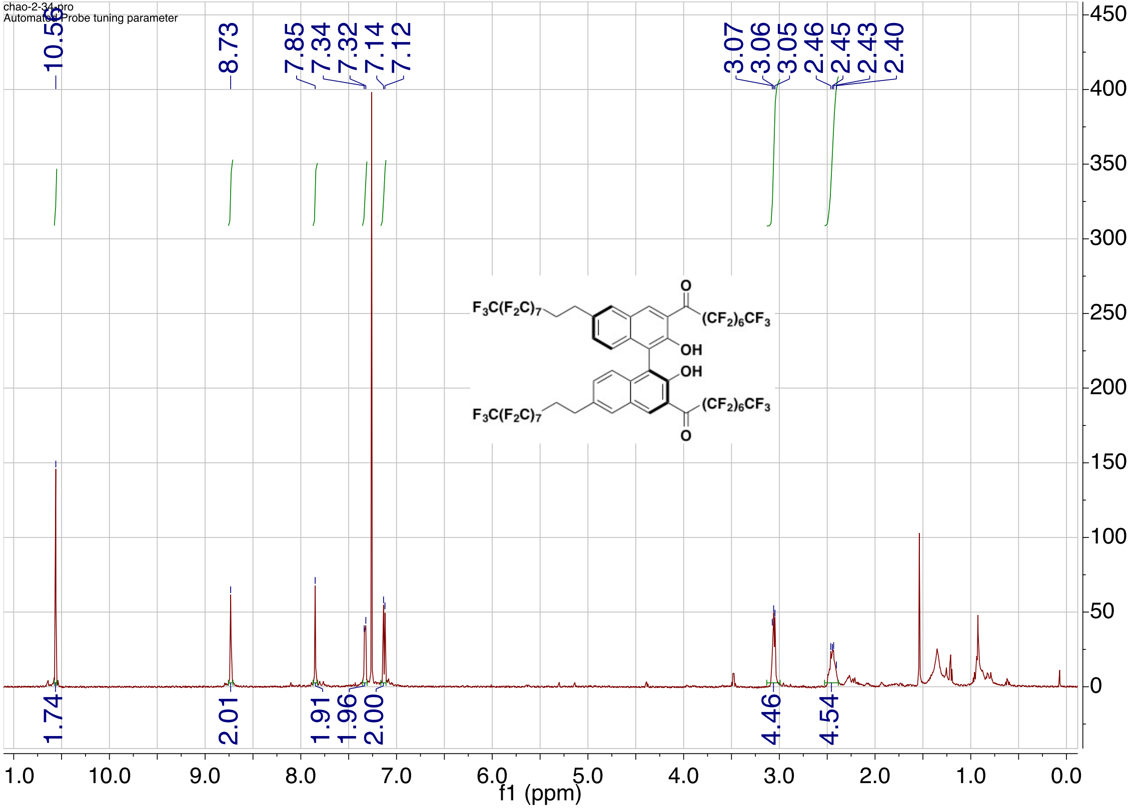
chao-2-34.pro
Automated Probe tuning parameter
10.56
8.73
7.85
7.34
7.32
7.14
7.12
3.07
3.06
3.05
2.46
2.45
2.43
2.40
$F_3C(F_2C)_7$
O
$(CF_2)_6CF_3$
OH
OH
$F_3C(F_2C)_7$
$(CF_2)_6CF_3$
O
1.74
2.01
1.91
1.96
2.00
4.46
4.54
450
400
350
300
250
200
150
100
50
0
1.0 10.0 9.0 8.0 7.0 6.0 5.0 4.0 3.0 2.0 1.0 0.0
f1 (ppm)

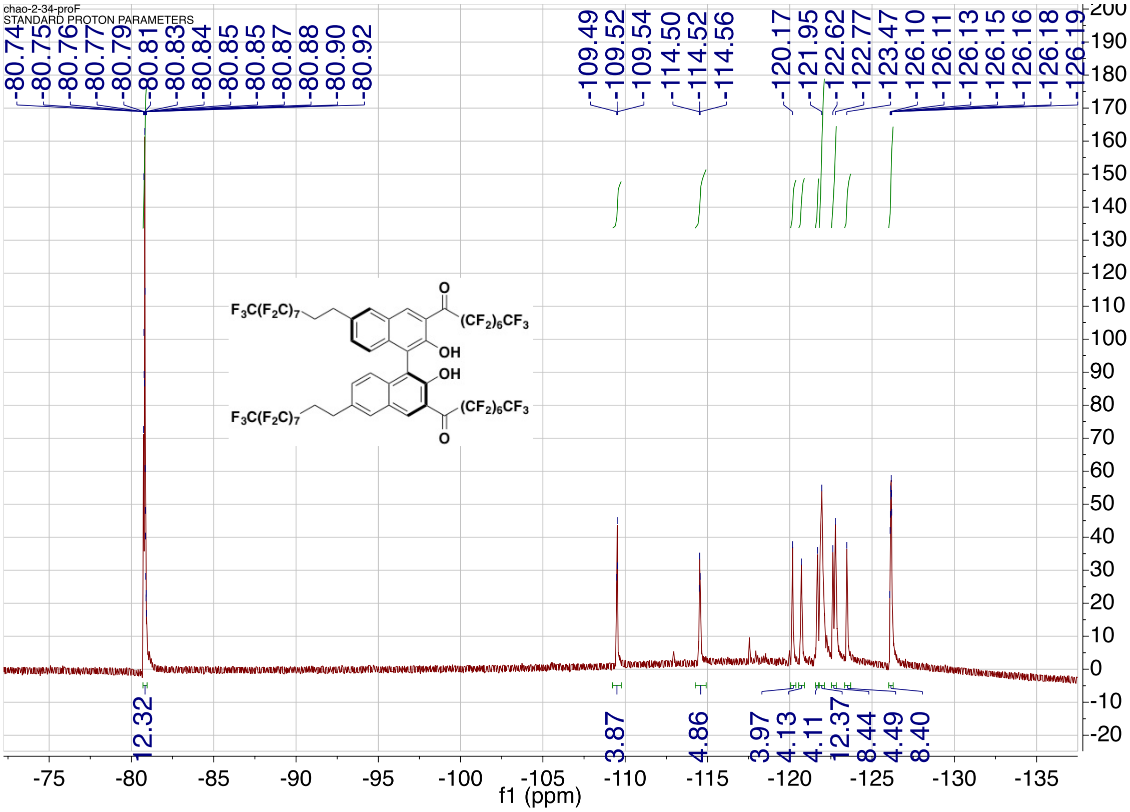

Mass spectrum of the precipitate isolated from (*S*)-**3.6** and (*R*)-**3.7**

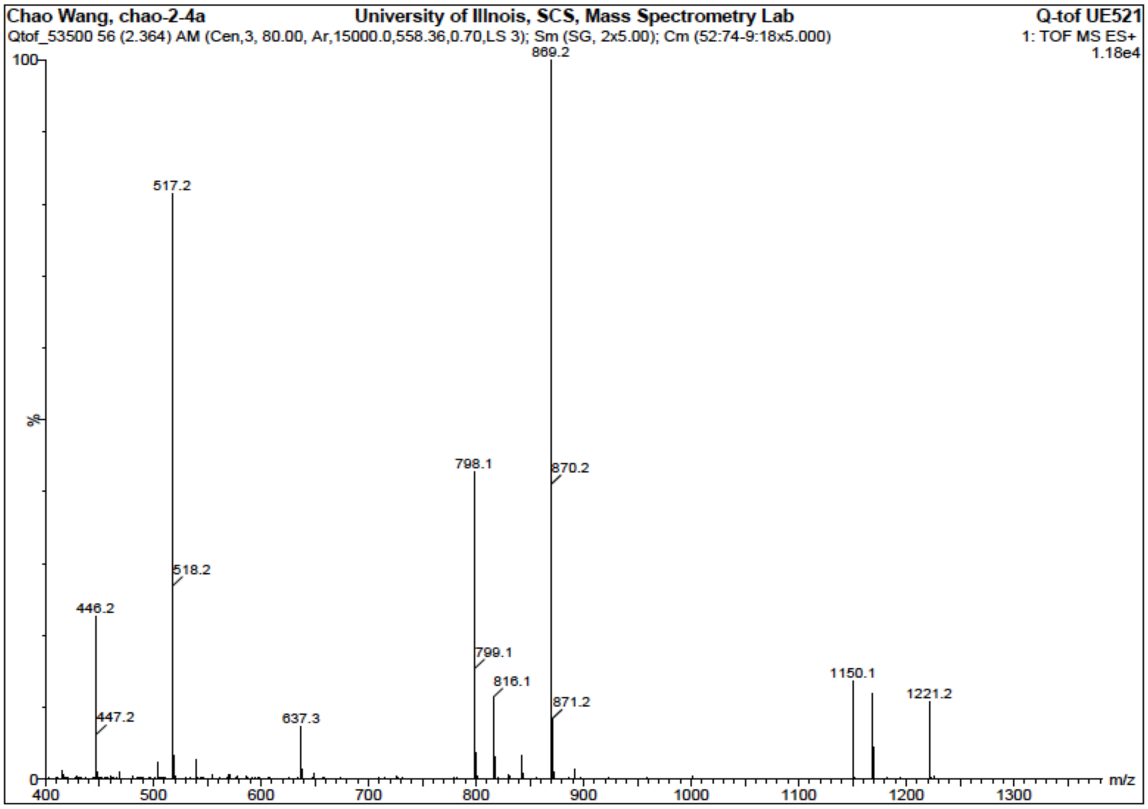

Mass spectrum of the reaction mixture of (*S*)-**3.6** and (*R*)-**3.7**.

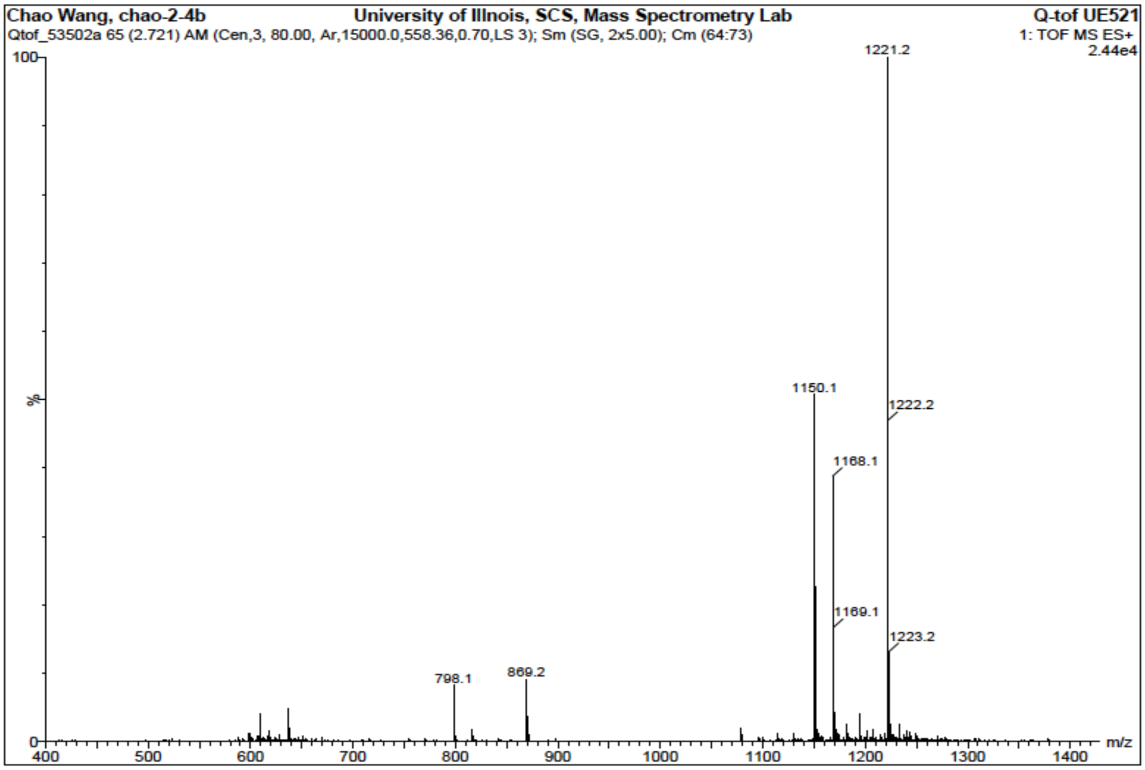

Mass spectrum of the reaction mixture of (*S*)-**3.6** and (*S*)-**3.7**.

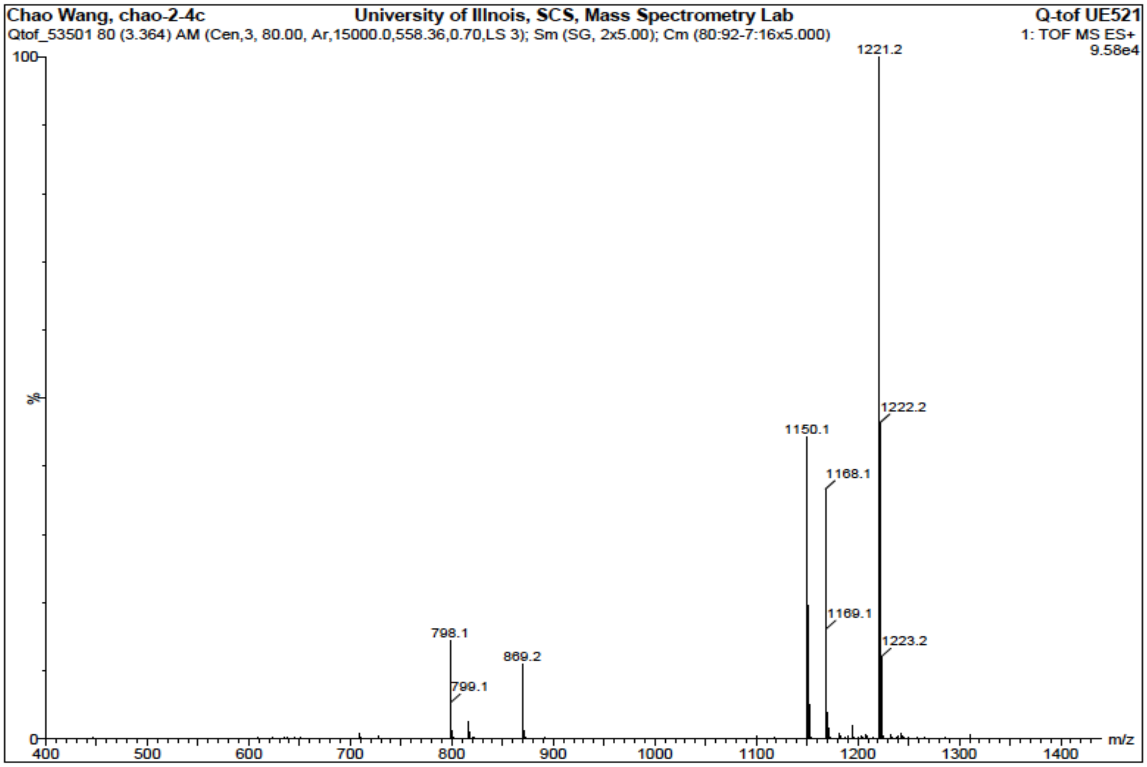

IR spectra of (*S*)-**3.6**.

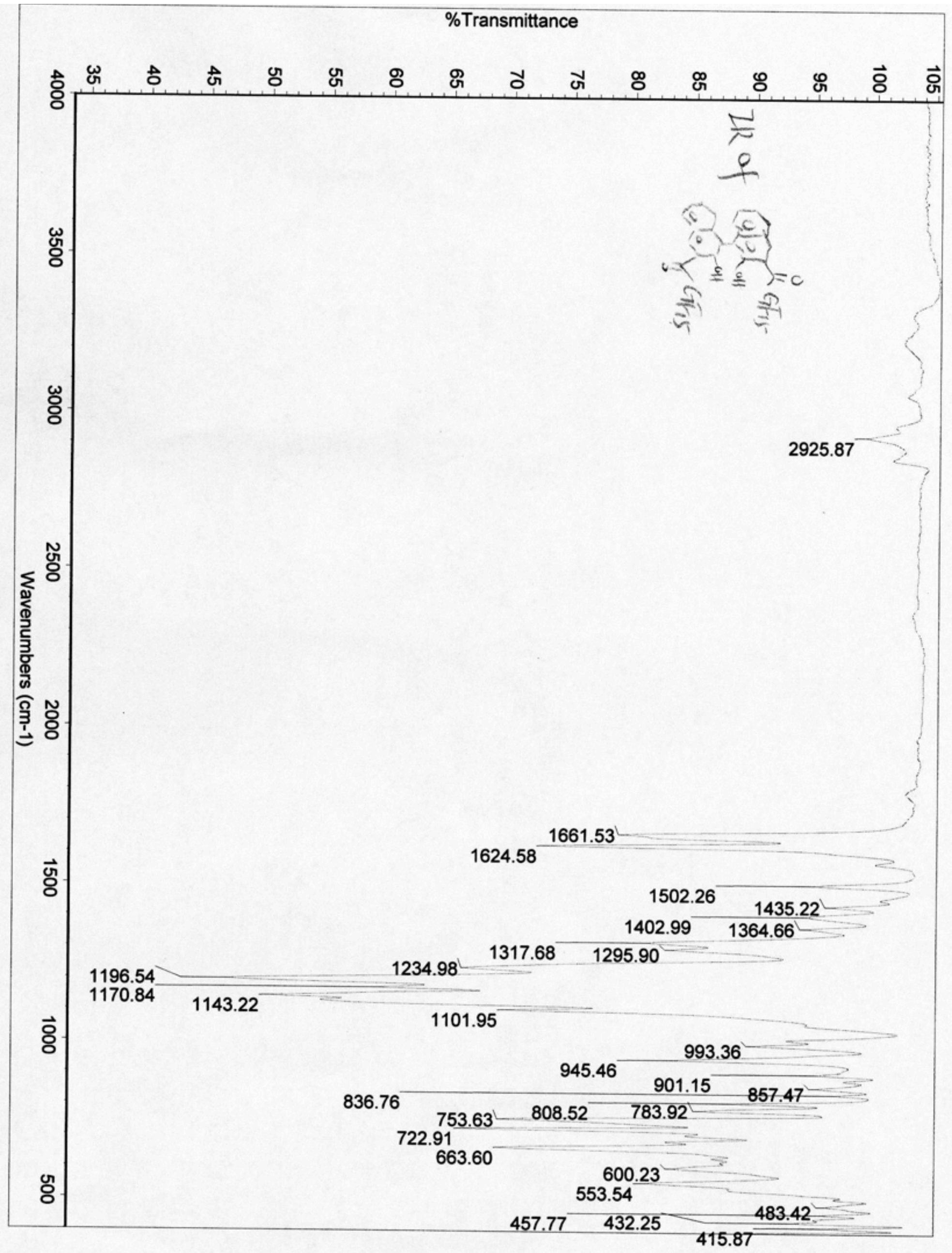

IR spectra of the precipitate isolated from the mixture of (*S*)-**3.6** and (*R*)-**3.7**.

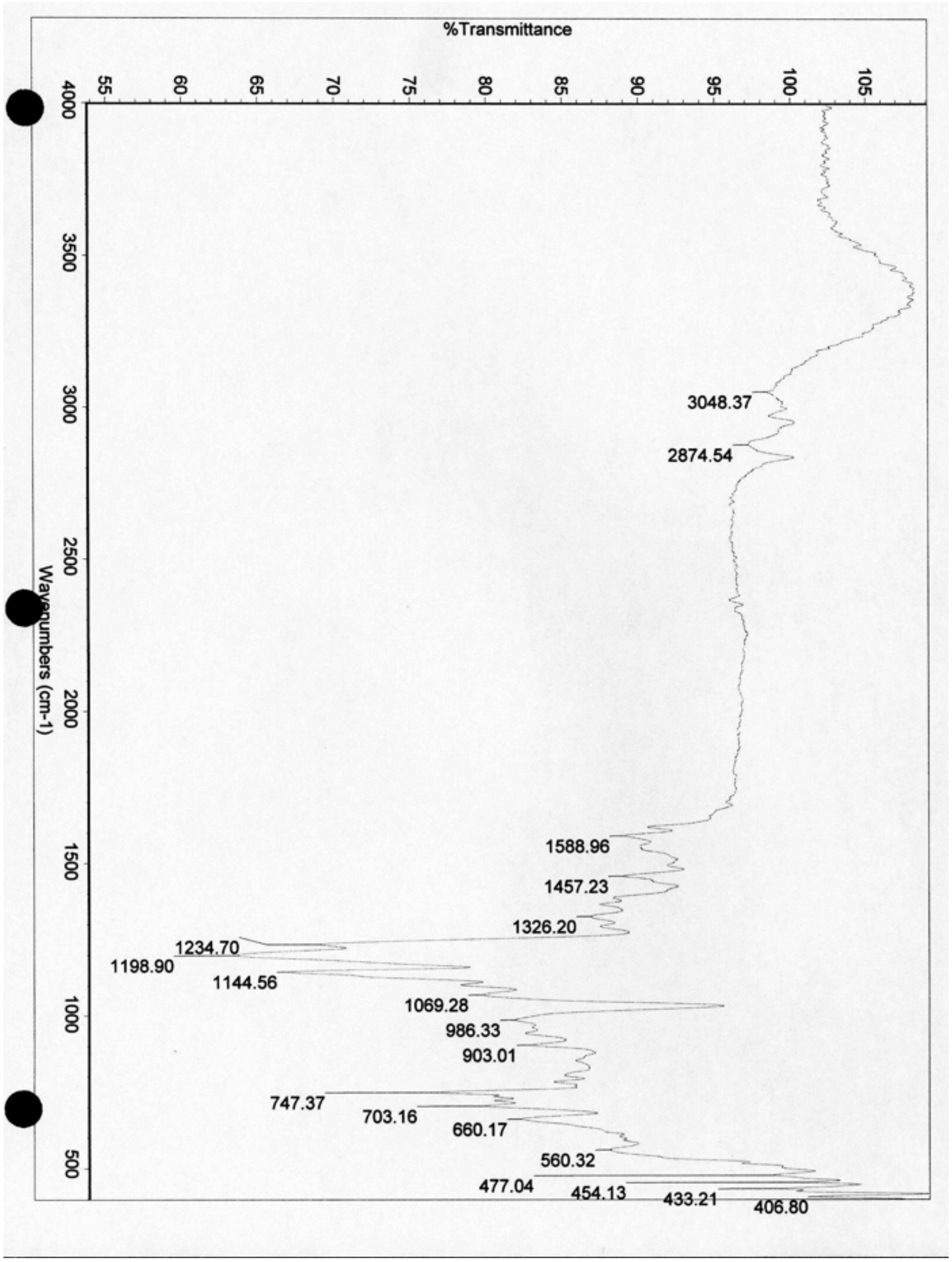

Appendix for Chapter 4

Mass spectra were recorded at 0 min, 30 min and 1 h after mixing the sensor and amine

0min

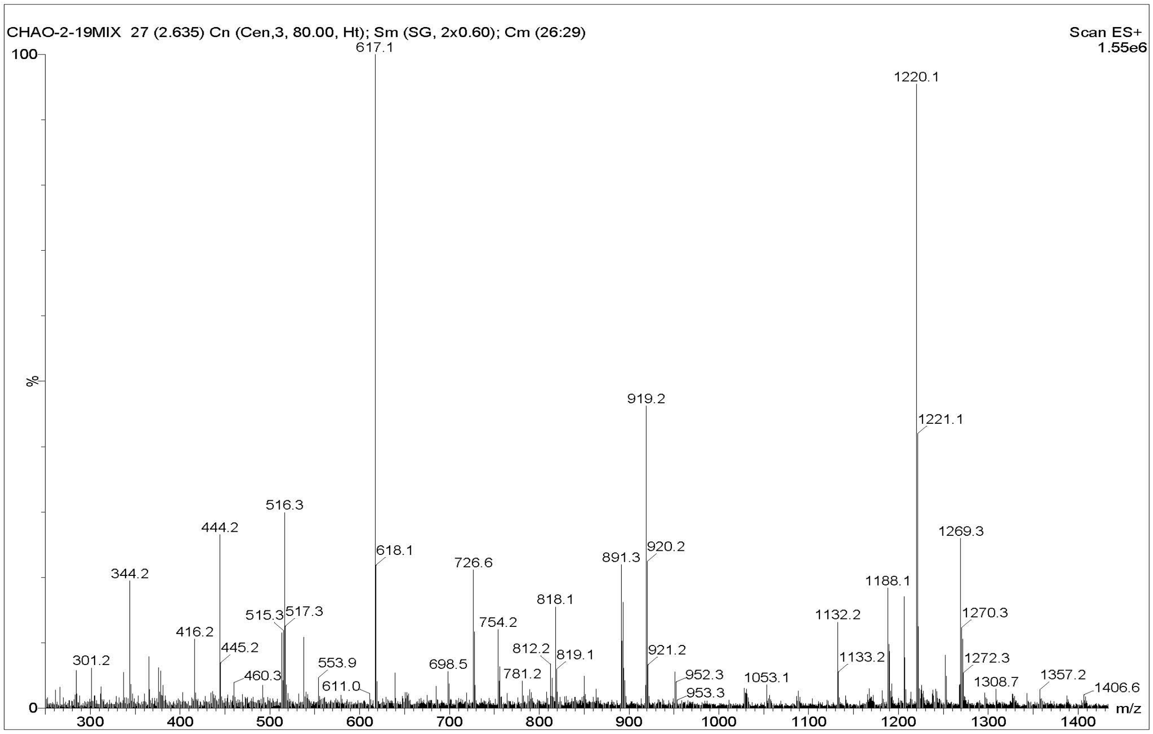

30min

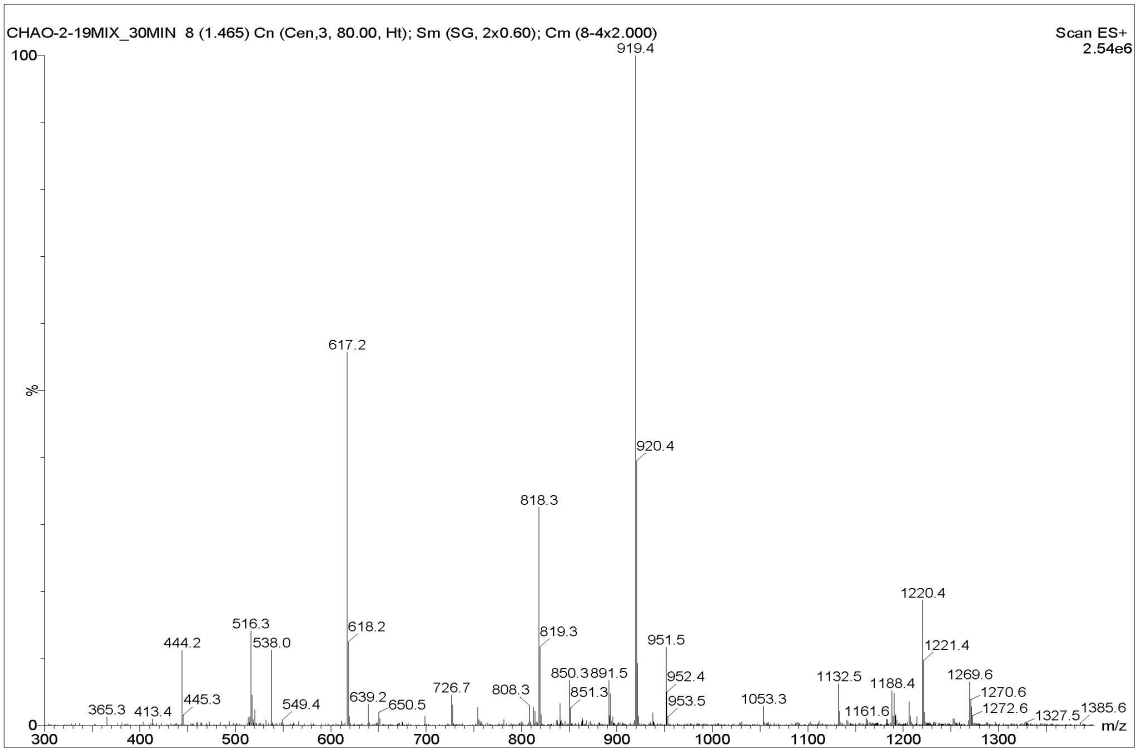

1h

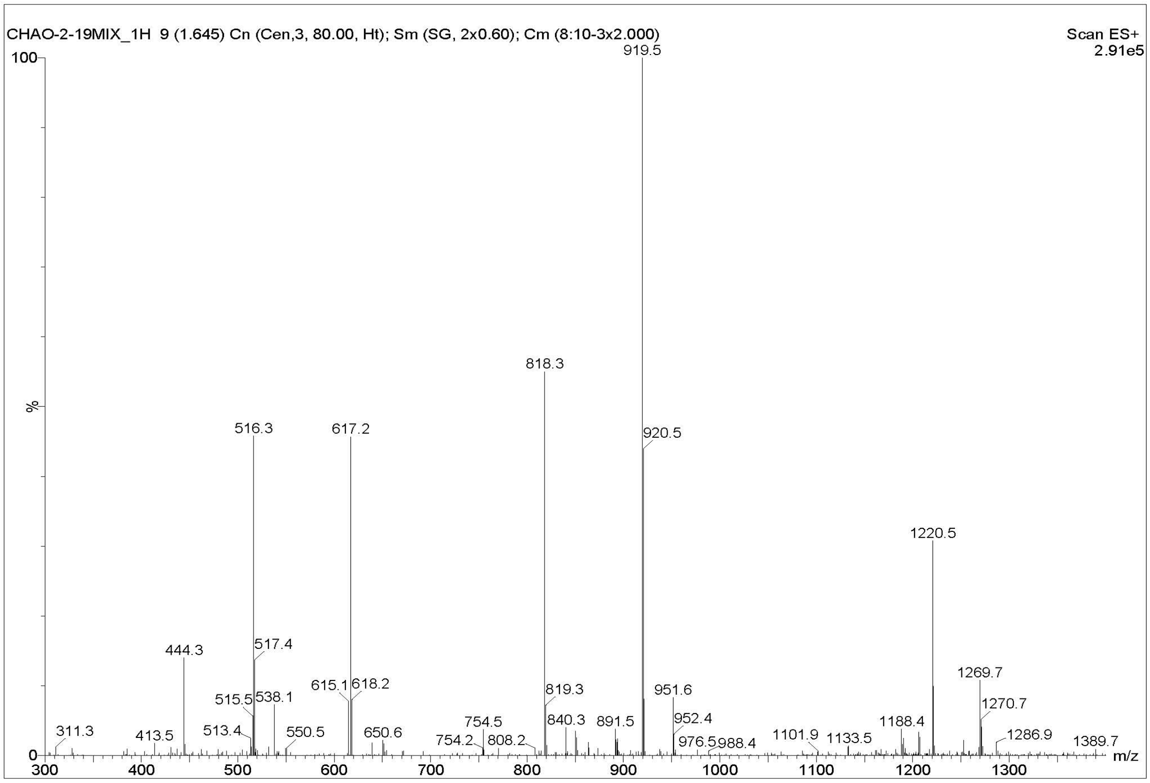

^{1}H NMR of (*S*)-H$_8$BINOL-MOM

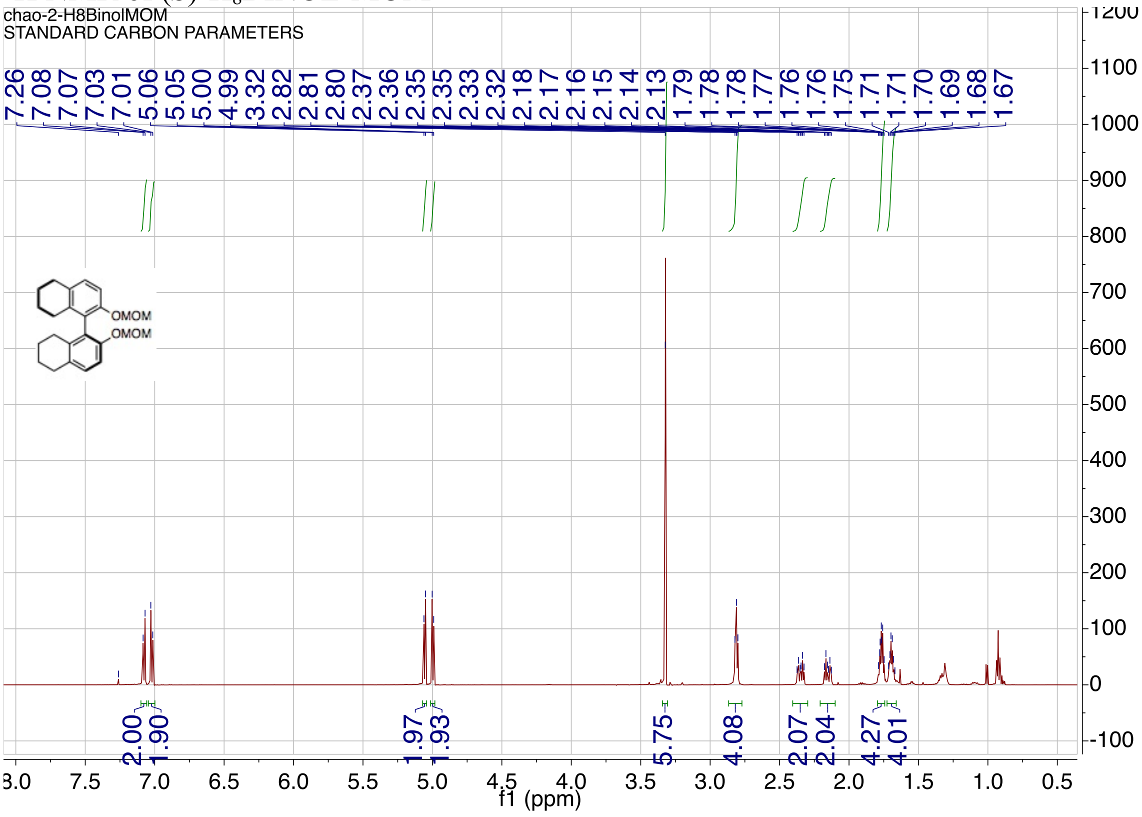

^{1}H NMR of (*R*)-H$_8$BINOL-MOM

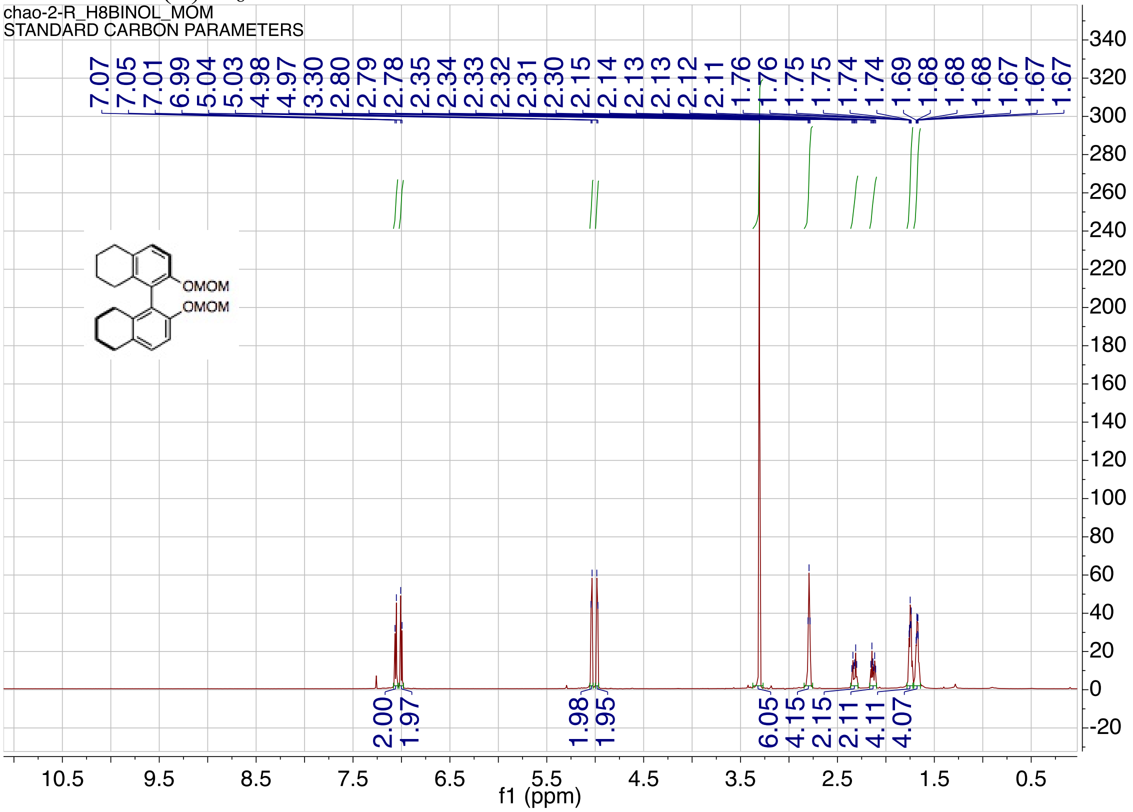

NMR of (*S*)-**4.2**

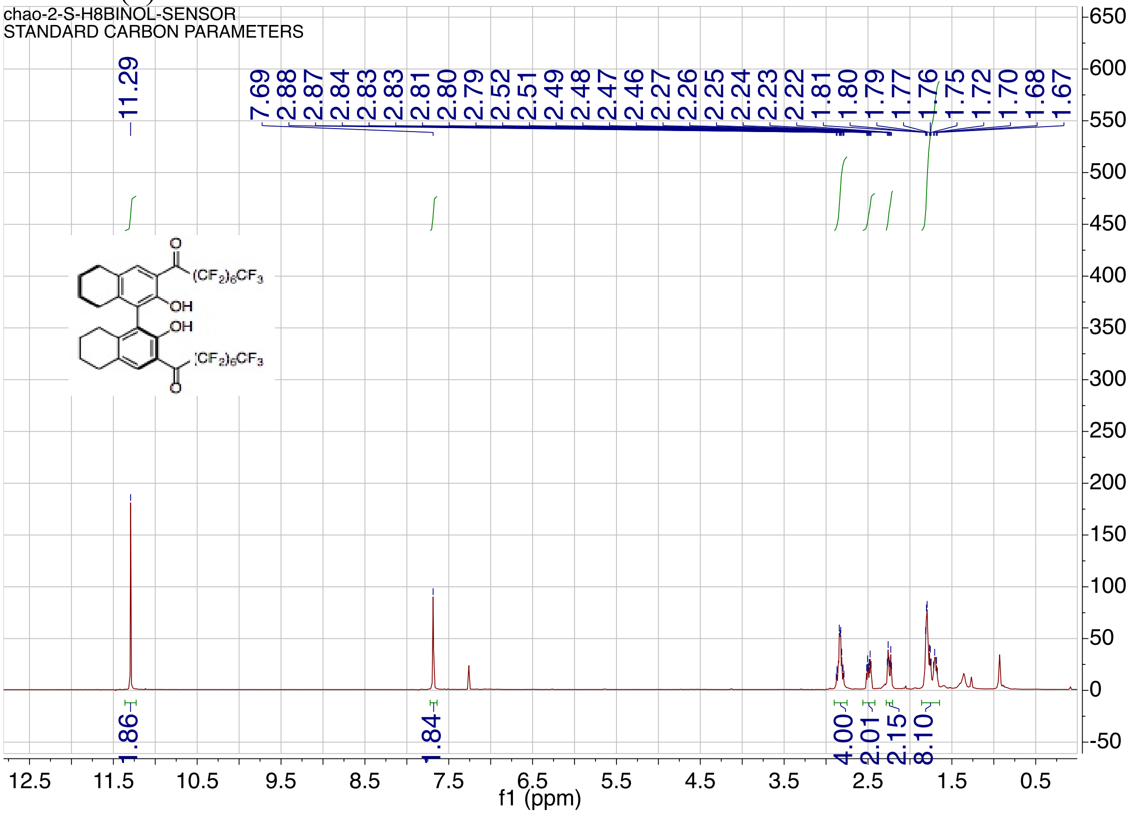

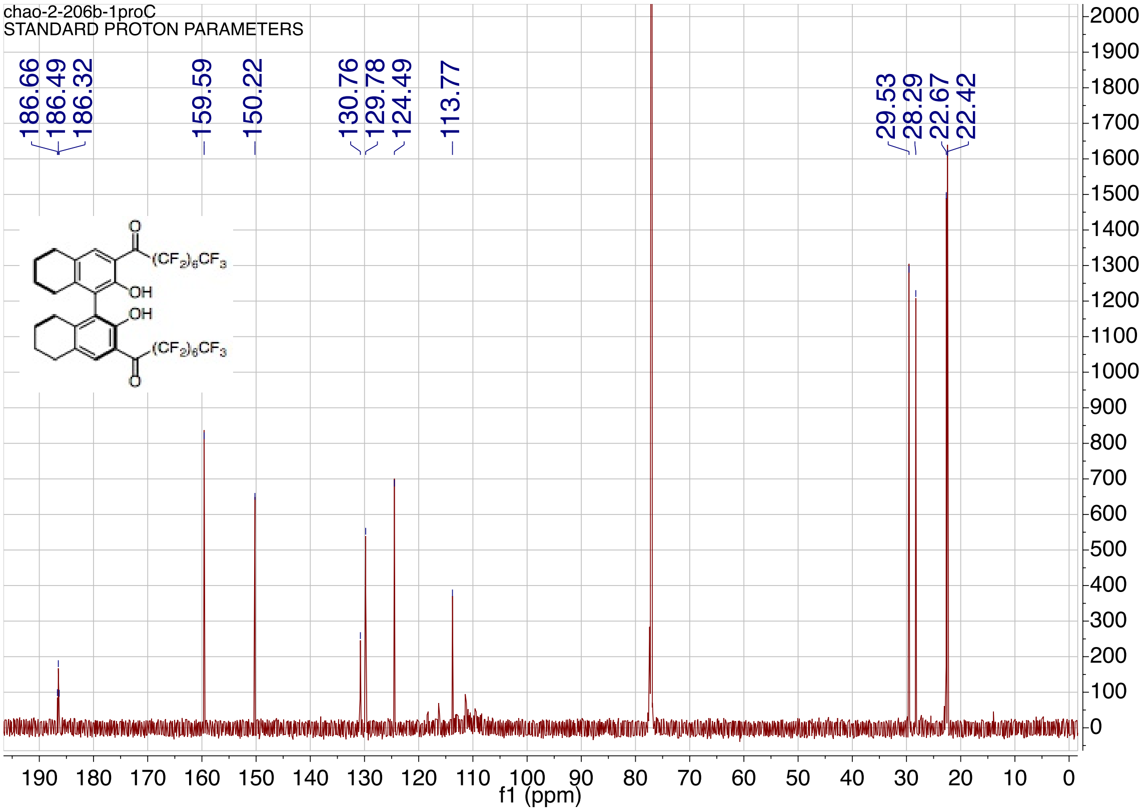
chao-2-206b-1proC
STANDARD PROTON PARAMETERS
186.66
186.49
186.32
159.59
150.22
130.76
129.78
124.49
113.77
29.53
28.29
22.67
22.42
O
(CF2)6CF3
OH
OH
(CF2)6CF3
O
2000
1900
1800
1700
1600
1500
1400
1300
1200
1100
1000
900
800
700
600
500
400
300
200
100
0
190
180
170
160
150
140
130
120
110
100
90
80
70
60
50
40
30
20
10
0
f1 (ppm)

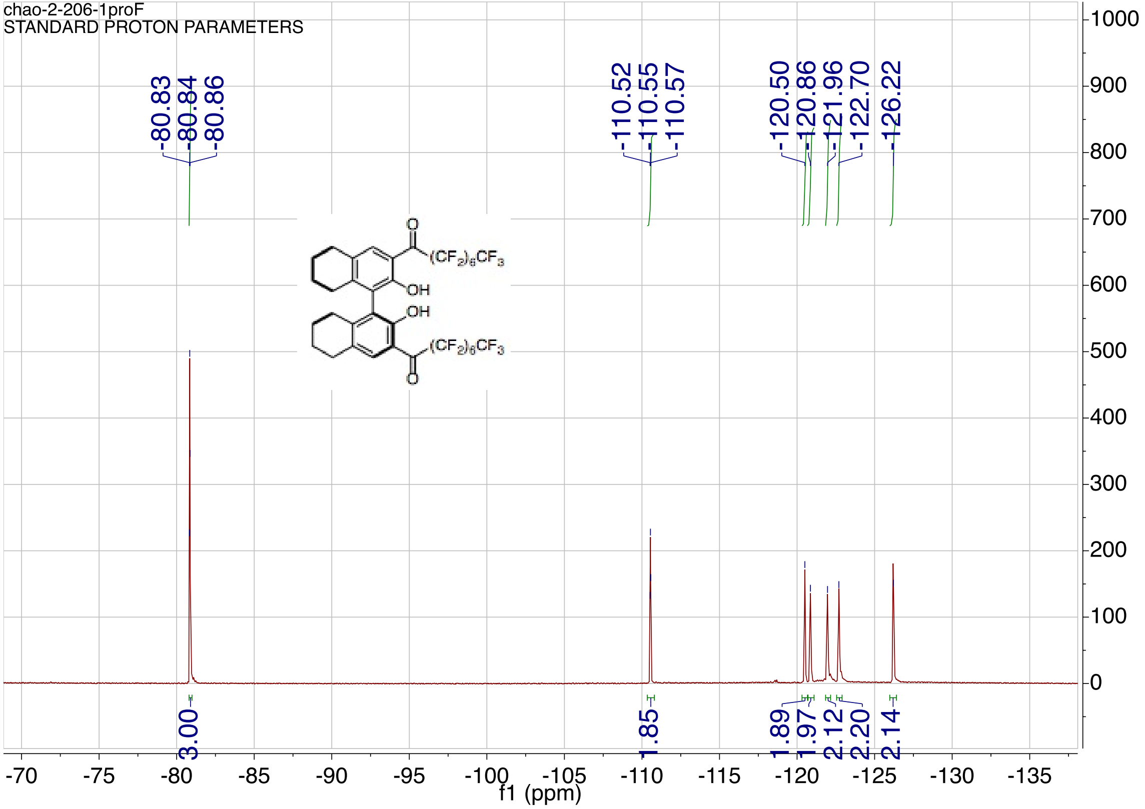
chao-2-206-1proF
STANDARD PROTON PARAMETERS
-80.83
-80.84
-80.86
-110.52
-110.55
-110.57
-120.50
-120.86
-121.96
-122.70
-126.22
O
(CF2)6CF3
OH
OH
(CF2)6CF3
O
3.00
1.85
1.89
1.97
2.12
2.20
2.14
1000
900
800
700
600
500
400
300
200
100
0
-70
-75
-80
-85
-90
-95
-100
-105
-110
-115
-120
-125
-130
-135
f1 (ppm)

NMR of (*R*)-**4.2**

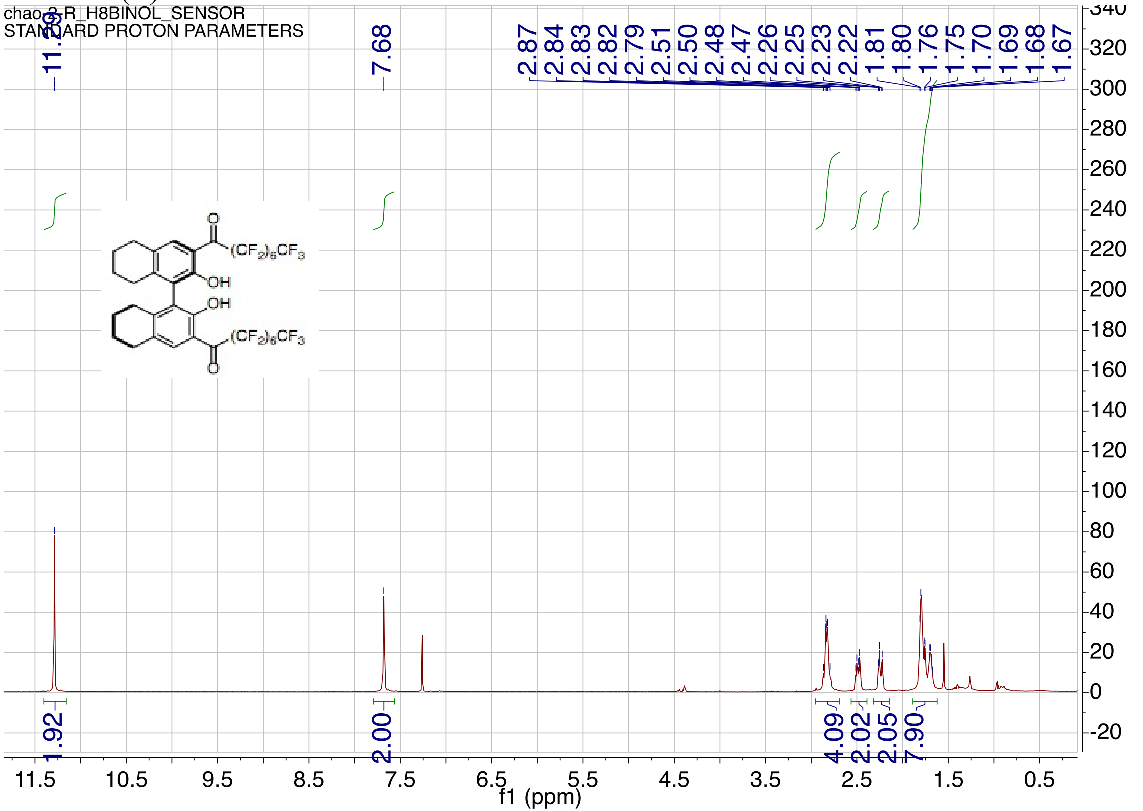
chao-2-R_H8BINOL_SENSOR
STANDARD PROTON PARAMETERS
11.29
7.68
2.87
2.84
2.83
2.82
2.79
2.51
2.50
2.48
2.47
2.26
2.25
2.23
2.22
1.81
1.80
1.76
1.75
1.70
1.69
1.68
1.67
O
(CF2)6CF3
OH
OH
(CF2)6CF3
O
1.92
2.00
4.09
2.02
2.05
7.90
11.5
10.5
9.5
8.5
7.5
6.5
5.5
4.5
3.5
2.5
1.5
0.5
f1 (ppm)
340
320
300
280
260
240
220
200
180
160
140
120
100
80
60
40
20
0
-20

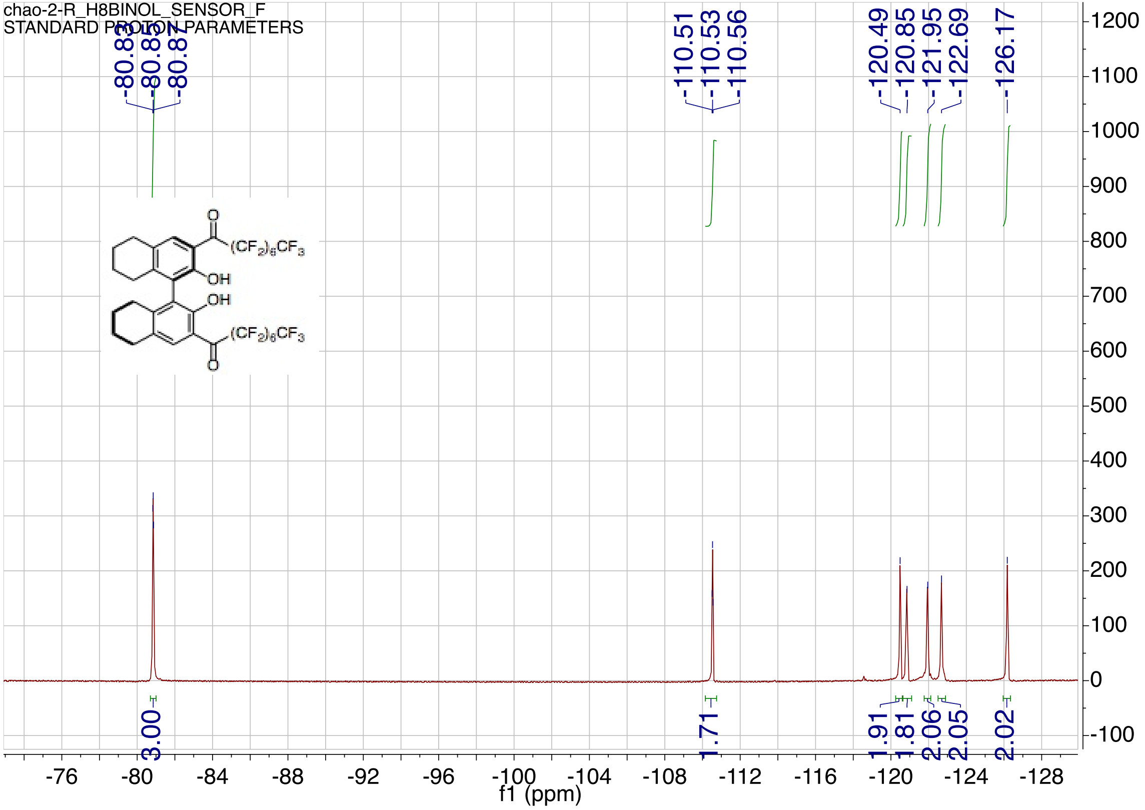
chao-2-R_H8BINOL_SENSOR_F
STANDARD PROTON PARAMETERS
-80.83
-80.85
-80.87
-110.51
-110.53
-110.56
-120.49
-120.85
-121.95
-122.69
-126.17
O
(CF2)6CF3
OH
OH
(CF2)6CF3
O
3.00
1.71
1.91
1.81
2.06
2.05
2.02
-76
-80
-84
-88
-92
-96
-100
-104
-108
-112
-116
-120
-124
-128
f1 (ppm)
1200
1100
1000
900
800
700
600
500
400
300
200
100
0
-100

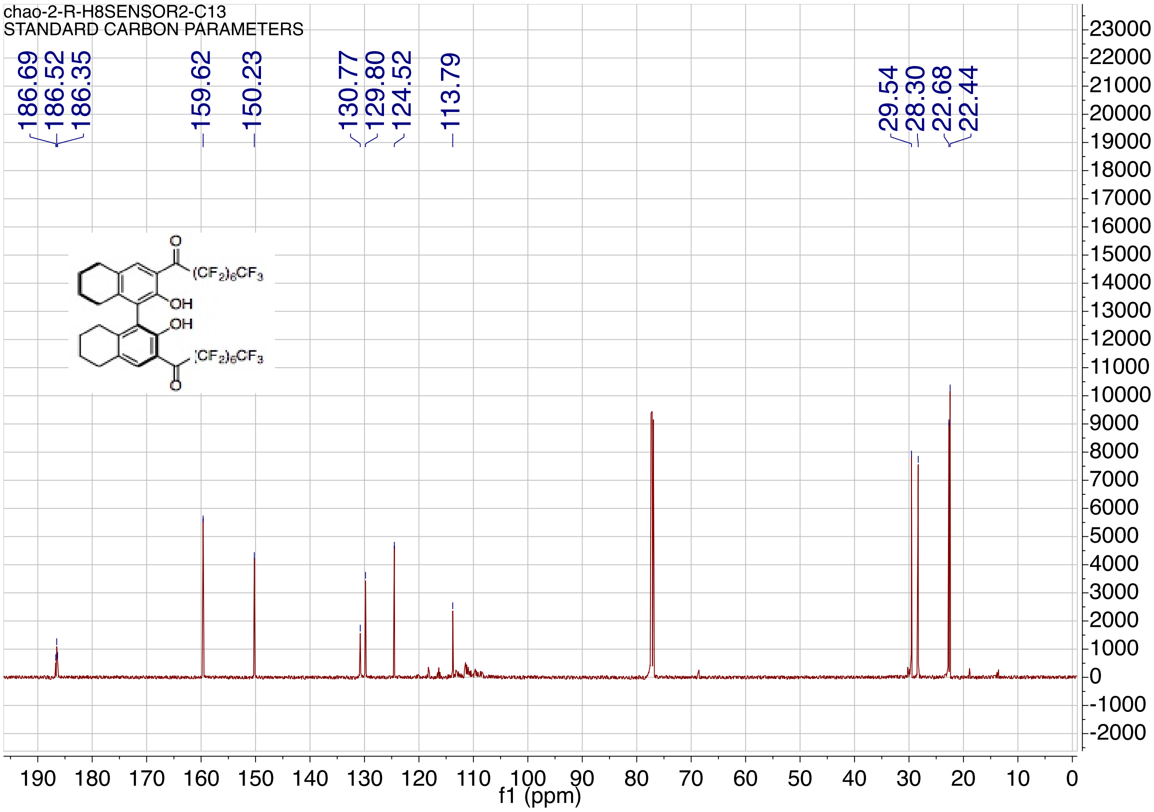
chao-2-R-H8SENSOR2-C13
STANDARD CARBON PARAMETERS
186.69
186.52
186.35
159.62
150.23
130.77
129.80
124.52
113.79
29.54
28.30
22.68
22.44
O
$(CF_2)_6CF_3$
OH
OH
$(CF_2)_6CF_3$
O
f1 (ppm)

NMR of (*S*, *S*)-**4.9**

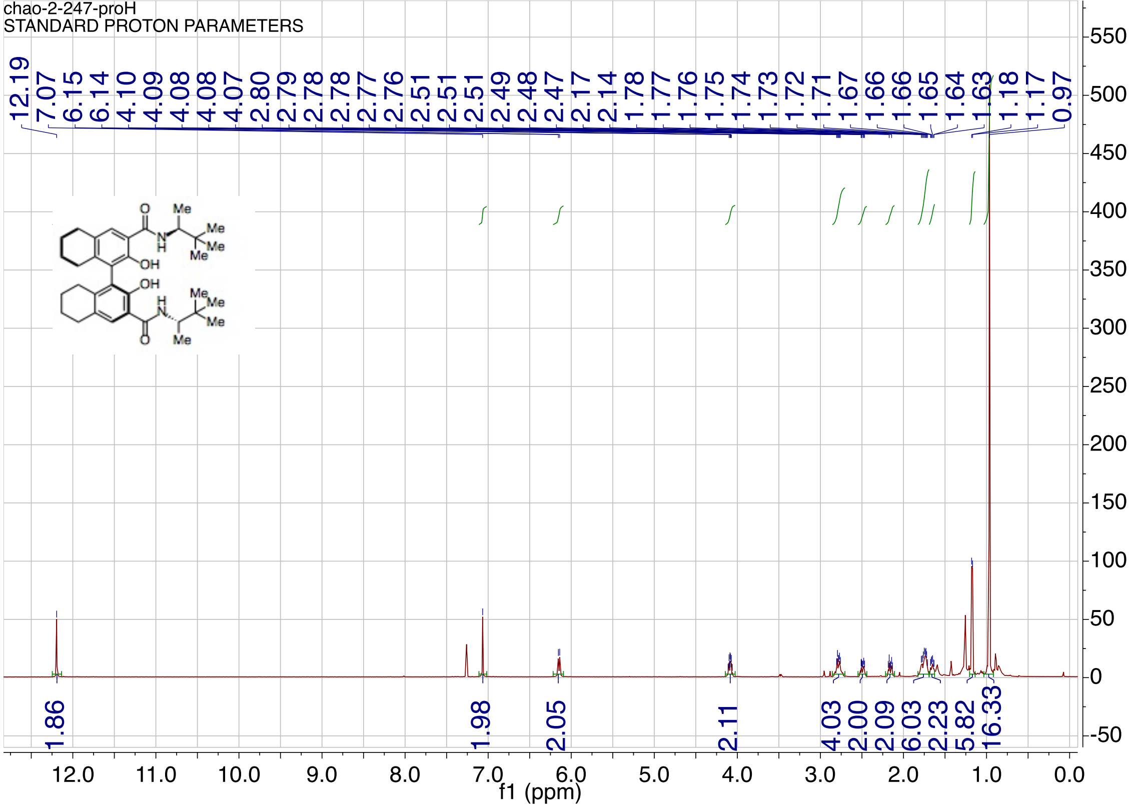
chao-2-247-proH
STANDARD PROTON PARAMETERS
12.19
7.07
6.15
6.14
4.10
4.09
4.08
4.08
4.07
2.80
2.79
2.78
2.78
2.77
2.76
2.51
2.51
2.51
2.49
2.48
2.47
2.17
2.14
1.78
1.77
1.76
1.75
1.74
1.73
1.72
1.71
1.67
1.66
1.66
1.65
1.64
1.63
1.18
1.17
0.97
1.86
1.98
2.05
2.11
4.03
2.00
2.09
6.03
2.23
5.82
16.33
Me
Me
Me
Me
OH
OH
Me
Me
Me
Me
f1 (ppm)

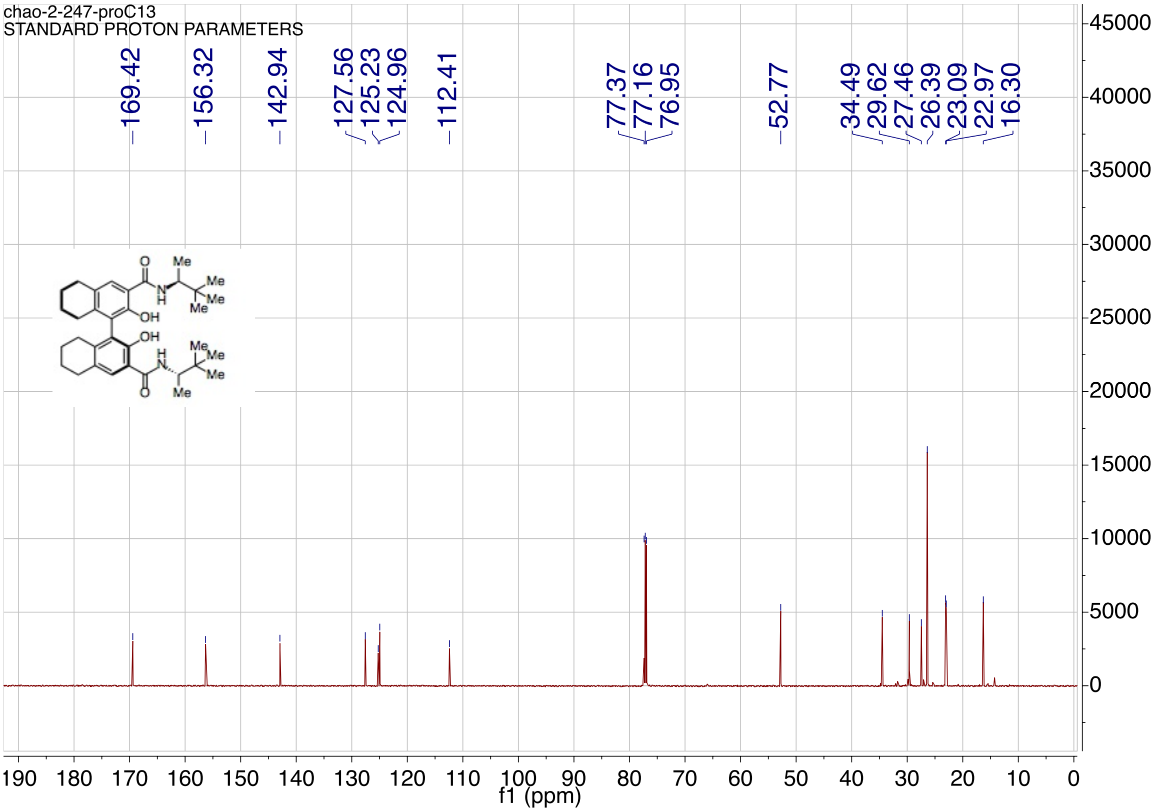
chao-2-247-proC13
STANDARD PROTON PARAMETERS
169.42
156.32
142.94
127.56
125.23
124.96
112.41
77.37
77.16
76.95
52.77
34.49
29.62
27.46
26.39
23.09
22.97
16.30
O
Me
N
H
Me
Me
Me
OH
OH
H
N
Me
Me
Me
O
Me
45000
40000
35000
30000
25000
20000
15000
10000
5000
0
190 180 170 160 150 140 130 120 110 100 90 80 70 60 50 40 30 20 10 0
f1 (ppm)

NMR of (*S, R*)-**4.9**

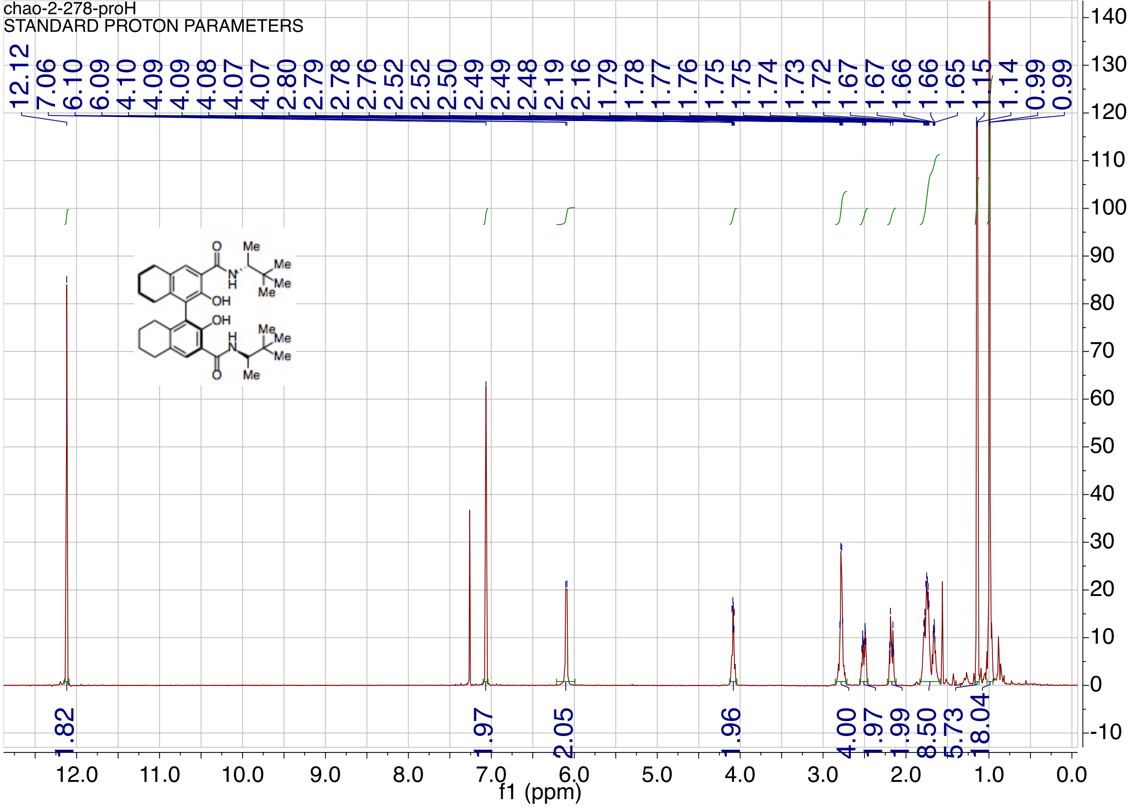
chao-2-278-proH
STANDARD PROTON PARAMETERS
12.12
7.06
6.10
6.09
4.10
4.09
4.09
4.08
4.07
4.07
2.80
2.79
2.78
2.76
2.52
2.52
2.50
2.49
2.49
2.48
2.19
2.16
1.79
1.78
1.77
1.76
1.75
1.75
1.74
1.73
1.72
1.67
1.67
1.66
1.66
1.65
1.15
1.14
0.99
0.99
O
Me
N
H
Me
Me
Me
OH
OH
H
N
Me
Me
Me
O
Me
1.82
1.97
2.05
1.96
4.00
1.97
1.99
8.50
5.73
18.04
140
130
120
110
100
90
80
70
60
50
40
30
20
10
0
-10
12.0 11.0 10.0 9.0 8.0 7.0 6.0 5.0 4.0 3.0 2.0 1.0 0.0
f1 (ppm)

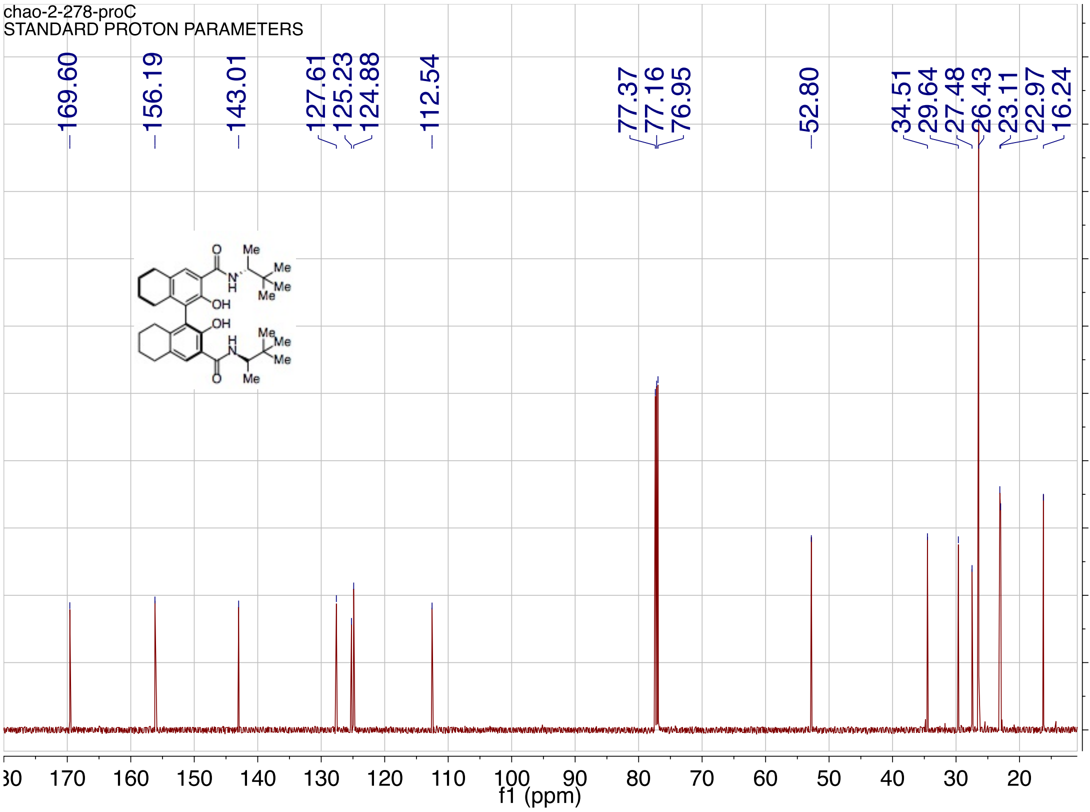

NMR for (*S*, *R*, *S*)-**4.16**

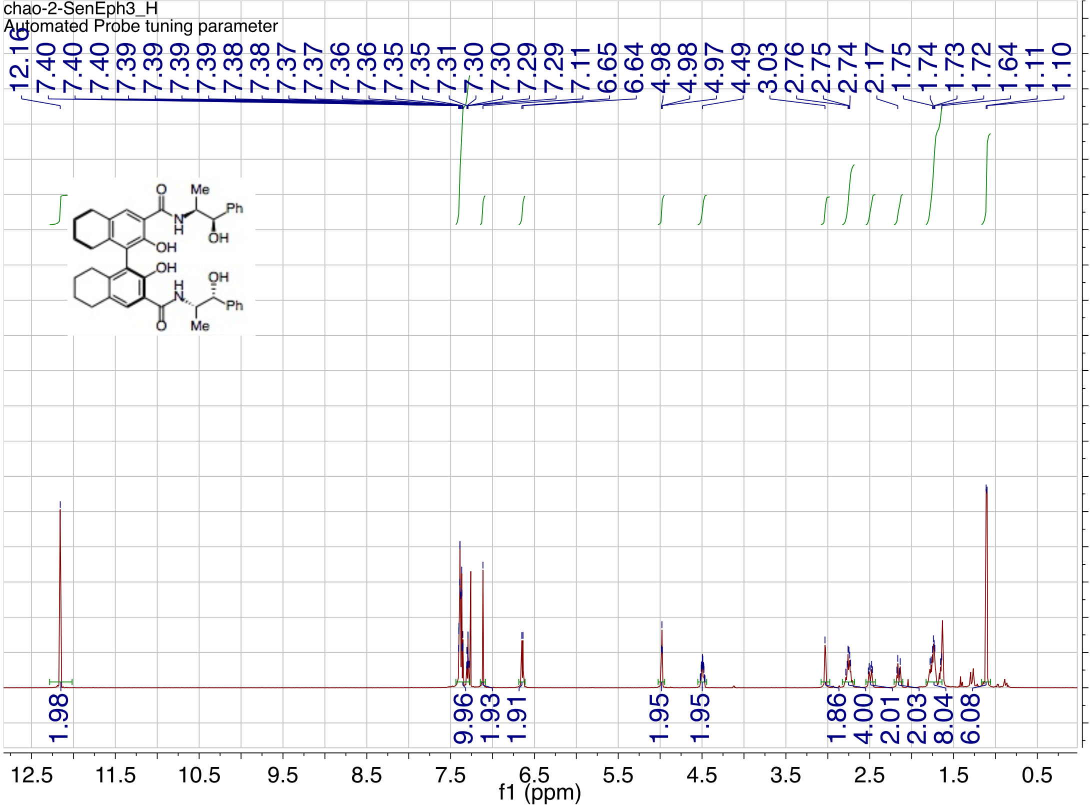

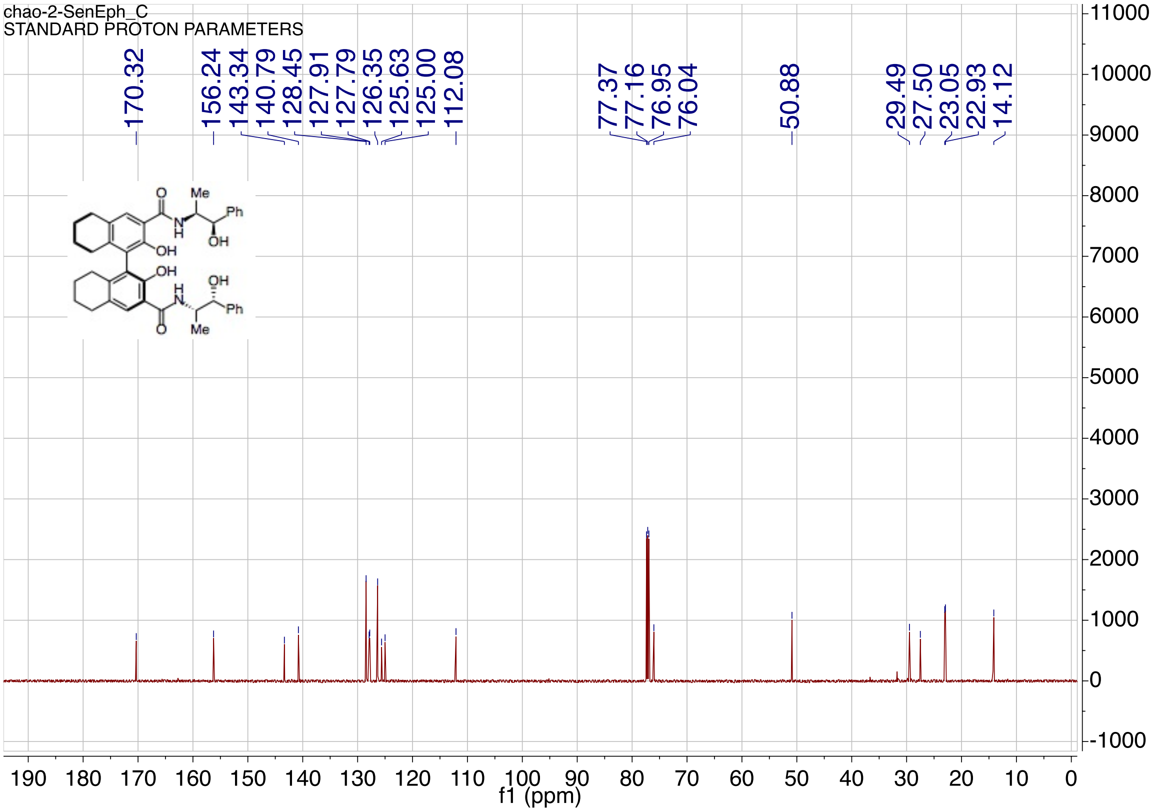

NMR of (*S, S, R*)-**4.16**

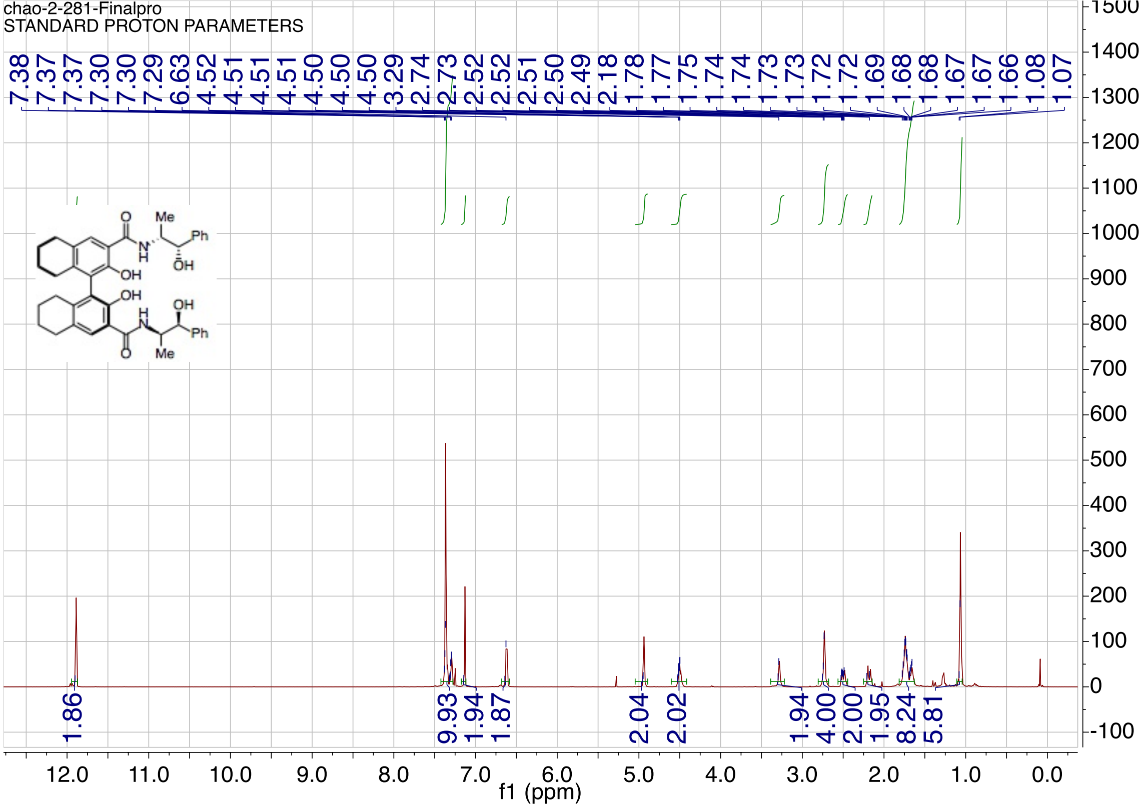

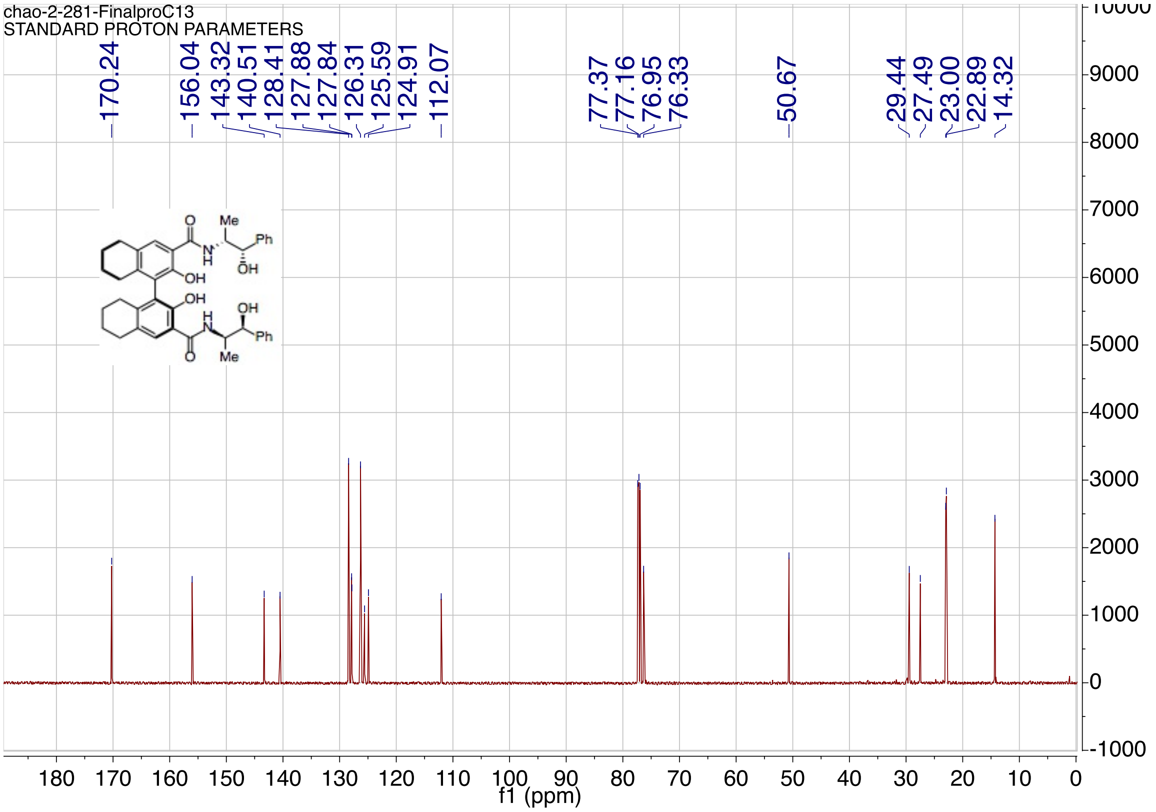

NMR of (*S*, *R*, *S*)-**4.22**

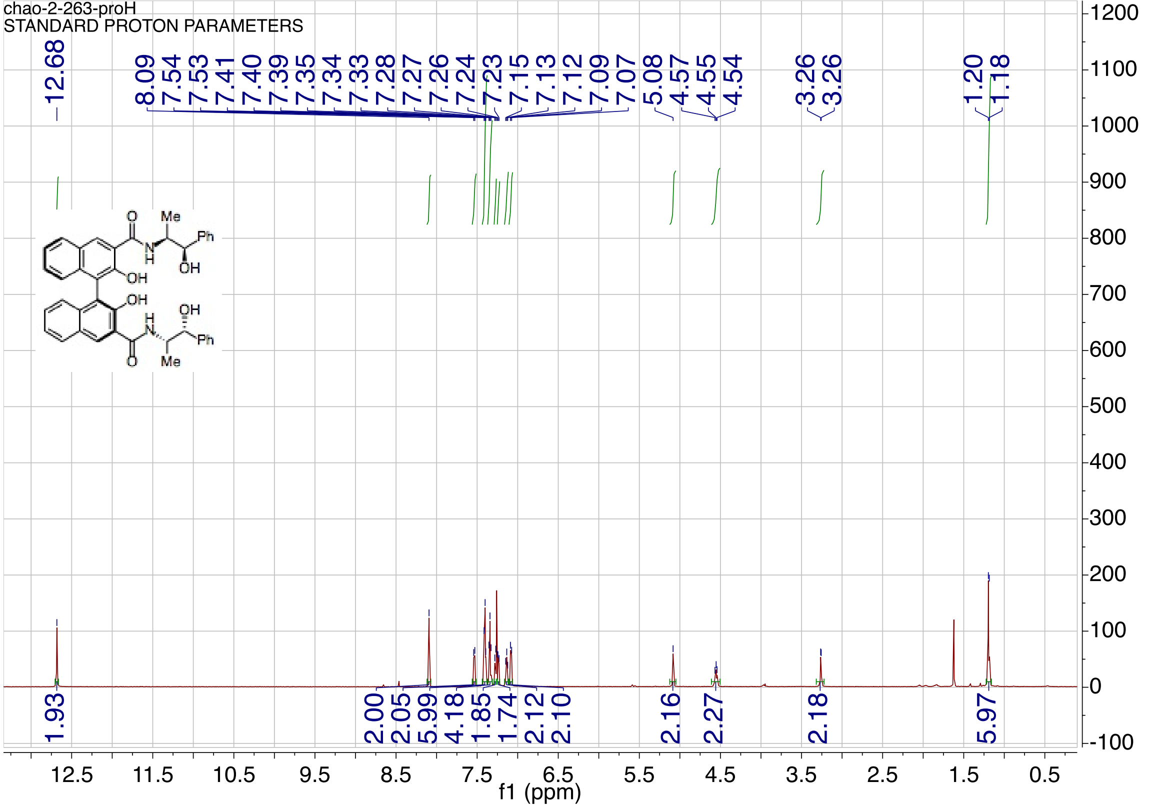

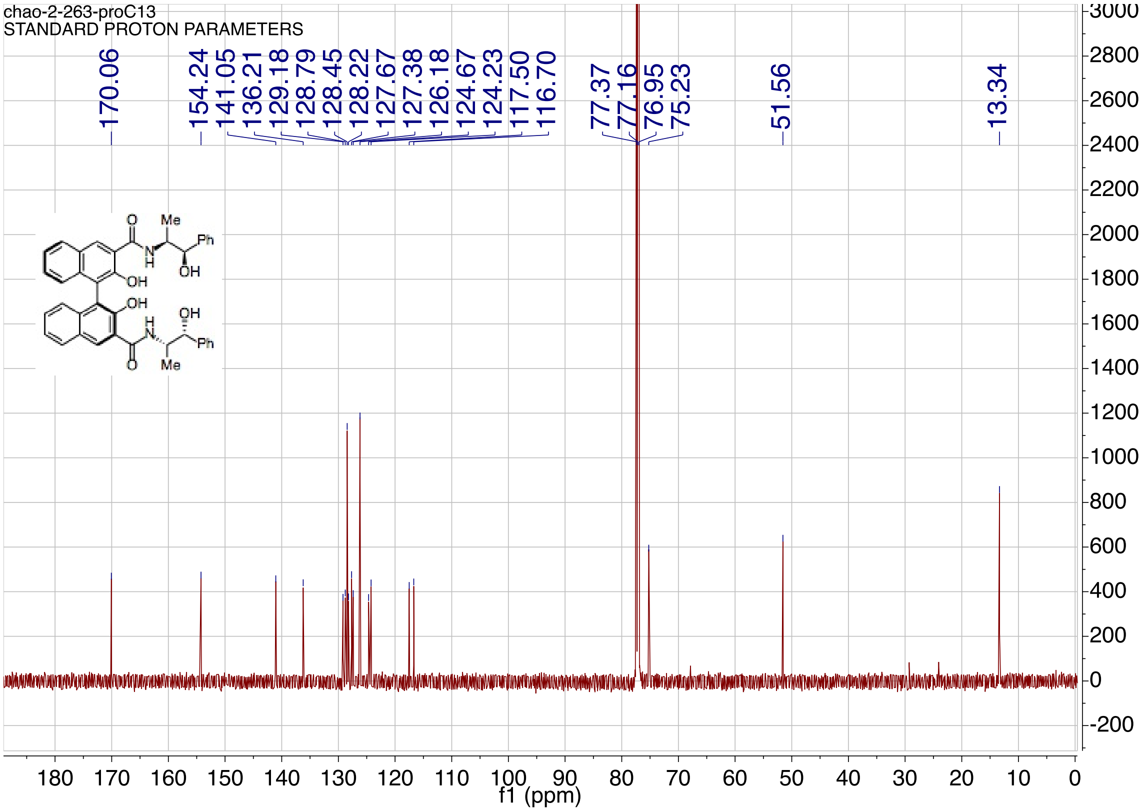
chao-2-263-proC13
STANDARD PROTON PARAMETERS
170.06
154.24
141.05
136.21
129.18
128.79
128.45
128.22
127.67
127.38
126.18
124.67
124.23
117.50
116.70
77.37
77.16
76.95
75.23
51.56
13.34
O
Me
N
H
Ph
OH
OH
OH
H
N
OH
Ph
O
Me
3000
2800
2600
2400
2200
2000
1800
1600
1400
1200
1000
800
600
400
200
0
-200
180
170
160
150
140
130
120
110
100
90
80
70
60
50
40
30
20
10
0
f1 (ppm)

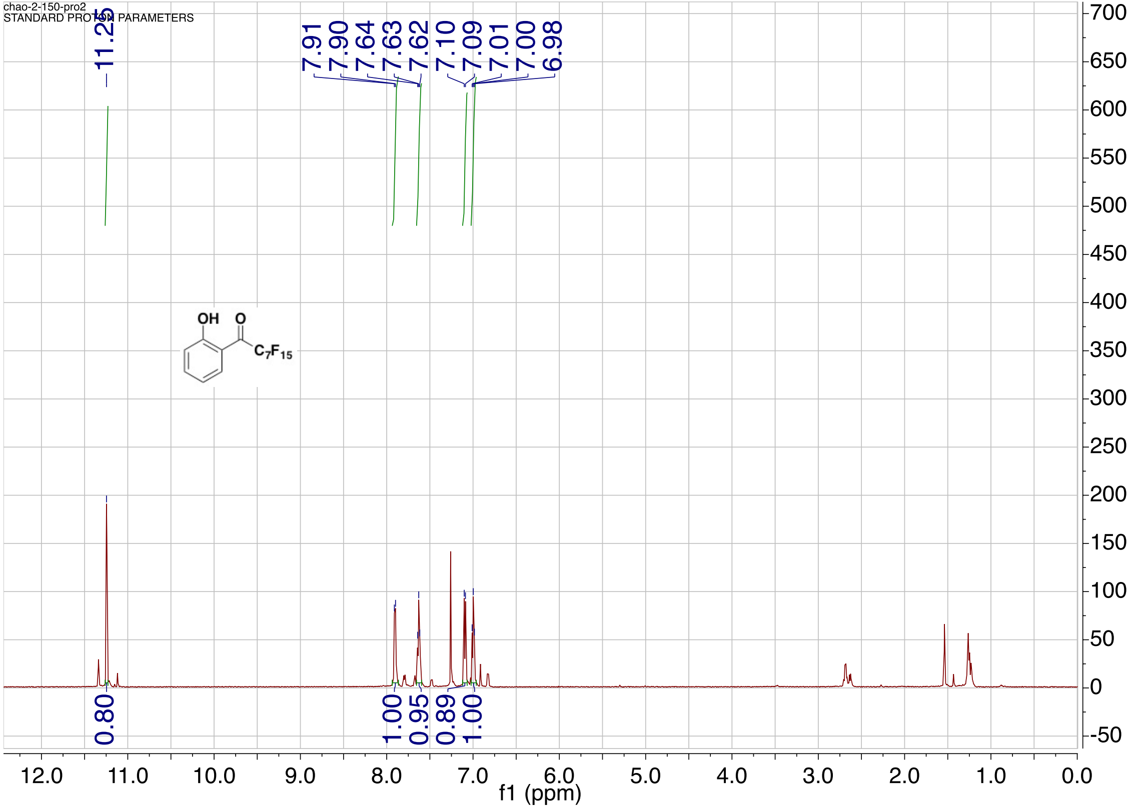
chao-2-150-pro2
STANDARD PROTON PARAMETERS
11.25
7.91
7.90
7.64
7.63
7.62
7.10
7.09
7.01
7.00
6.98
OH
O
C7F15
0.80
1.00
0.95
0.89
1.00
700
650
600
550
500
450
400
350
300
250
200
150
100
50
0
-50
12.0
11.0
10.0
9.0
8.0
7.0
6.0
5.0
4.0
3.0
2.0
1.0
0.0
f1 (ppm)

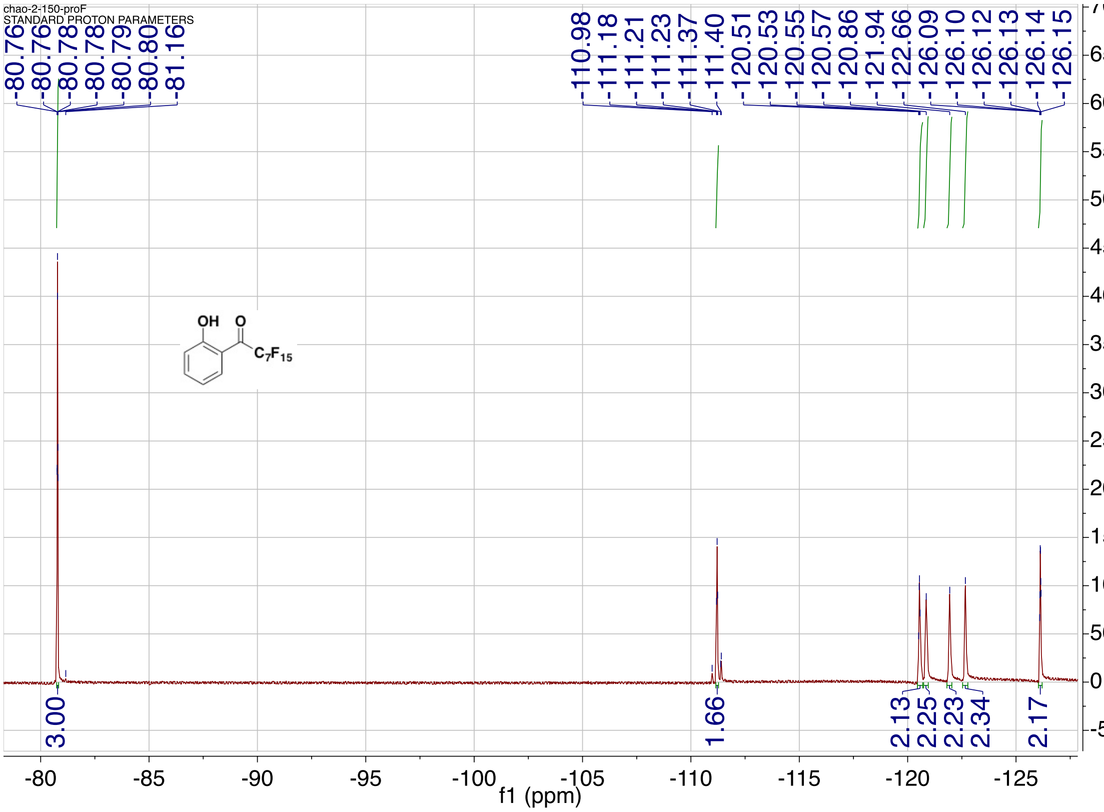
chao-2-150-proF
STANDARD PROTON PARAMETERS
-80.76
-80.76
-80.78
-80.78
-80.79
-80.80
-81.16
-110.98
-111.18
-111.21
-111.23
-111.37
-111.40
-120.51
-120.53
-120.55
-120.57
-120.86
-121.94
-122.66
-126.09
-126.10
-126.12
-126.13
-126.14
-126.15
OH
O
C7F15
3.00
1.66
2.13
2.25
2.23
2.34
2.17
700
650
600
550
500
450
400
350
300
250
200
150
100
50
0
-50
-80
-85
-90
-95
-100
-105
-110
-115
-120
-125
f1 (ppm)

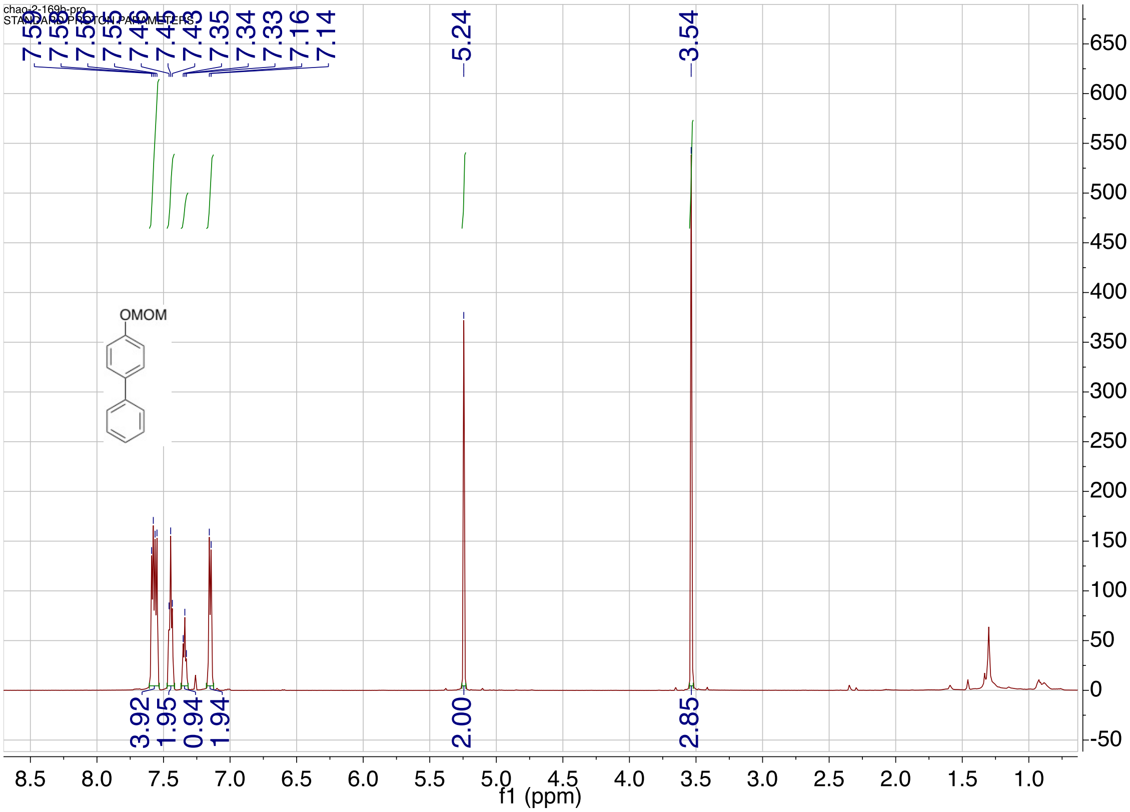
chao-2-169b-pro
STANDARD PROTON PARAMETERS
7.59
7.58
7.56
7.55
7.46
7.45
7.43
7.35
7.34
7.33
7.16
7.14
5.24
3.54
OMOM
3.92
1.95
0.94
1.94
2.00
2.85
650
600
550
500
450
400
350
300
250
200
150
100
50
0
-50
8.5
8.0
7.5
7.0
6.5
6.0
5.5
5.0
4.5
4.0
3.5
3.0
2.5
2.0
1.5
1.0
f1 (ppm)

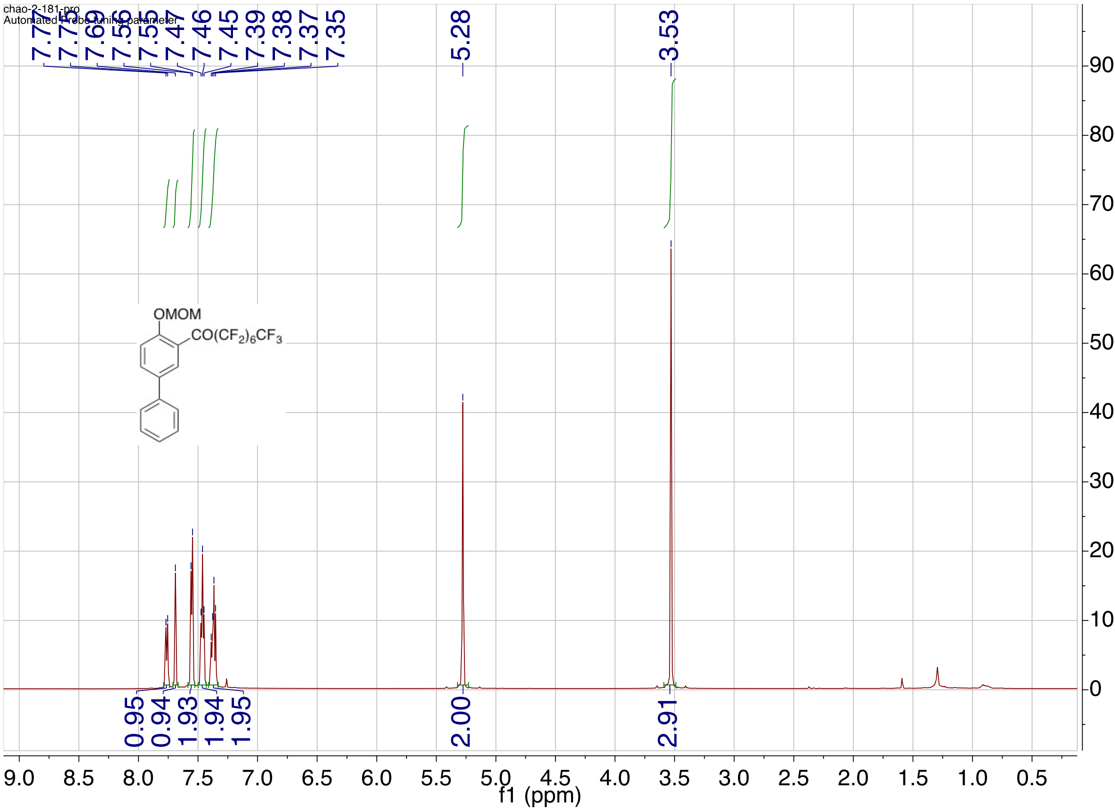
chao-2-181-pro
Automated Probe tuning parameter
7.77
7.75
7.69
7.56
7.55
7.47
7.46
7.45
7.39
7.38
7.37
7.35
5.28
3.53
OMOM
CO(CF2)6CF3
0.95
0.94
1.93
1.94
1.95
2.00
2.91
900
800
700
600
500
400
300
200
100
0
9.0
8.5
8.0
7.5
7.0
6.5
6.0
5.5
5.0
4.5
4.0
3.5
3.0
2.5
2.0
1.5
1.0
0.5
f1 (ppm)

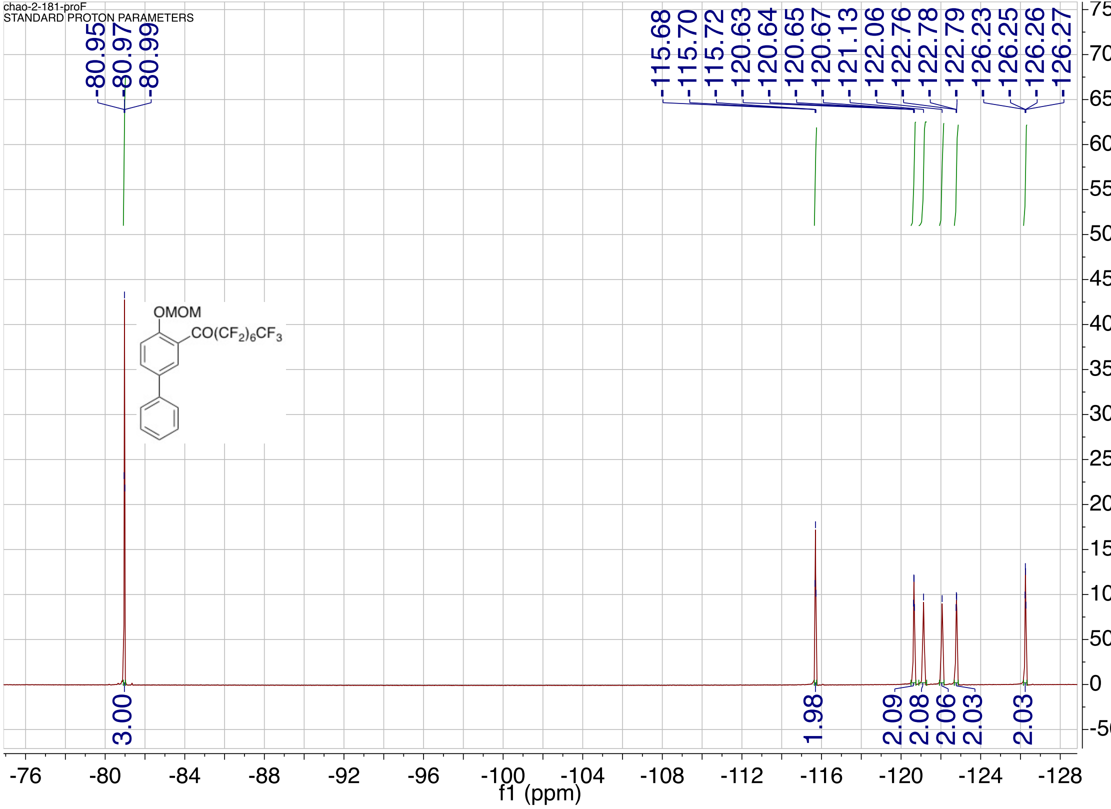
chao-2-181-proF
STANDARD PROTON PARAMETERS
-80.95
-80.97
-80.99
-115.68
-115.70
-115.72
-120.63
-120.64
-120.65
-120.67
-121.13
-122.06
-122.76
-122.78
-122.79
-126.23
-126.25
-126.26
-126.27
OMOM
CO(CF2)6CF3
3.00
1.98
2.09
2.08
2.06
2.03
2.03
750
700
650
600
550
500
450
400
350
300
250
200
150
100
50
0
-50
-76
-80
-84
-88
-92
-96
-100
-104
-108
-112
-116
-120
-124
-128
f1 (ppm)

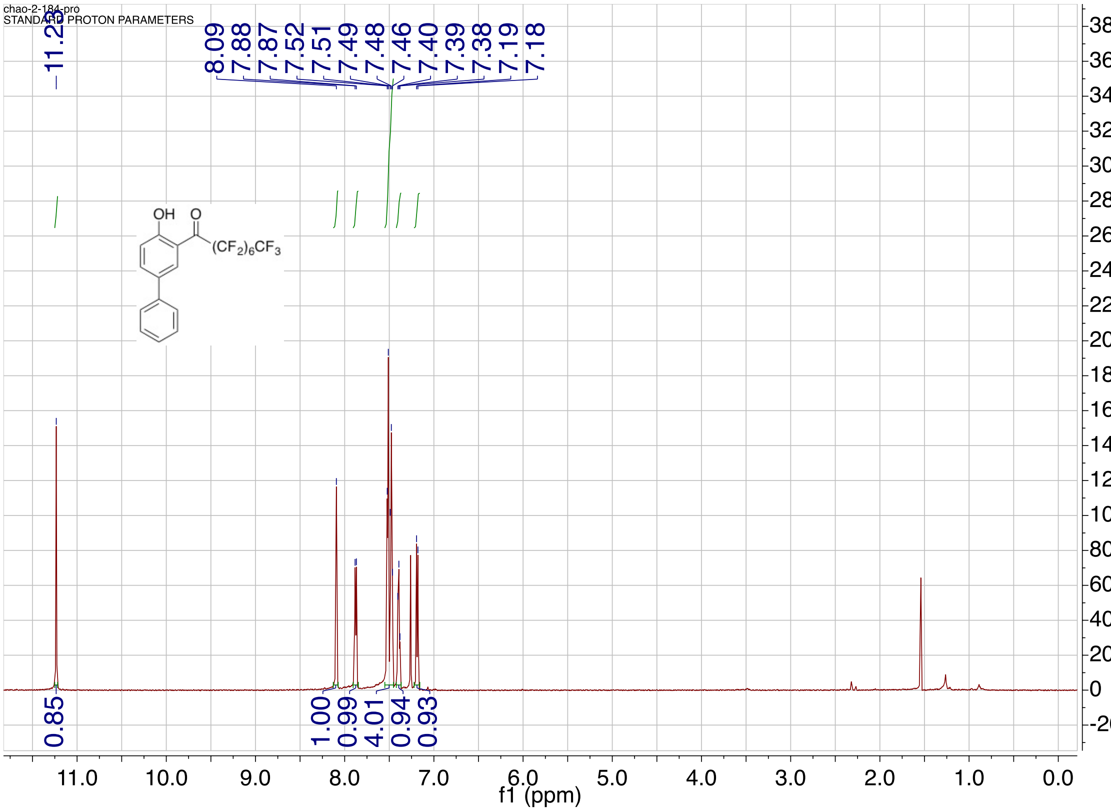
chao-2-184-pro
STANDARD PROTON PARAMETERS
11.25
8.09
7.88
7.87
7.52
7.51
7.49
7.48
7.46
7.40
7.39
7.38
7.19
7.18
OH
O
(CF2)6CF3
0.85
1.00
0.99
4.01
0.94
0.93
11.0
10.0
9.0
8.0
7.0
6.0
5.0
4.0
3.0
2.0
1.0
0.0
f1 (ppm)
380
360
340
320
300
280
260
240
220
200
180
160
140
120
100
80
60
40
20
0
-20

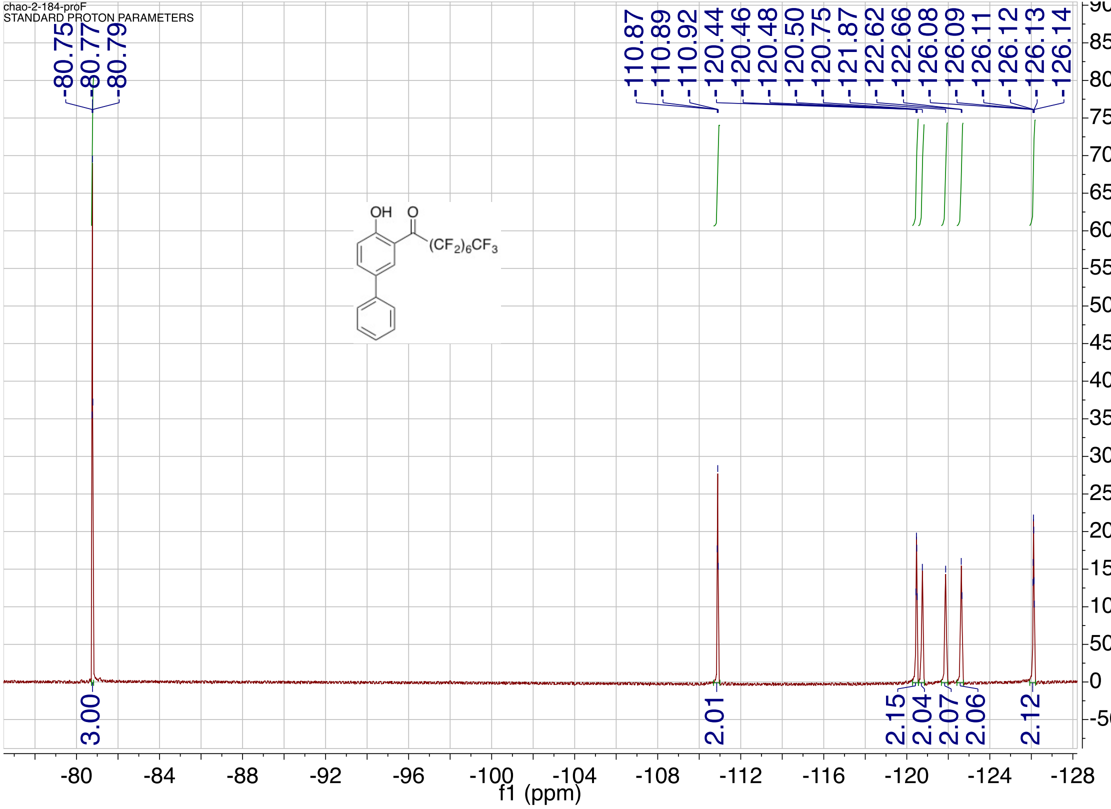
chao-2-184-proF
STANDARD PROTON PARAMETERS
-80.75
-80.77
-80.79
-110.87
-110.89
-110.92
-120.44
-120.46
-120.48
-120.50
-120.75
-121.87
-122.62
-122.66
-126.08
-126.09
-126.11
-126.12
-126.13
-126.14
OH
O
(CF2)6CF3
3.00
2.01
2.15
2.04
2.07
2.06
2.12
-80
-84
-88
-92
-96
-100
-104
-108
-112
-116
-120
-124
-128
f1 (ppm)
900
850
800
750
700
650
600
550
500
450
400
350
300
250
200
150
100
50
0
-50

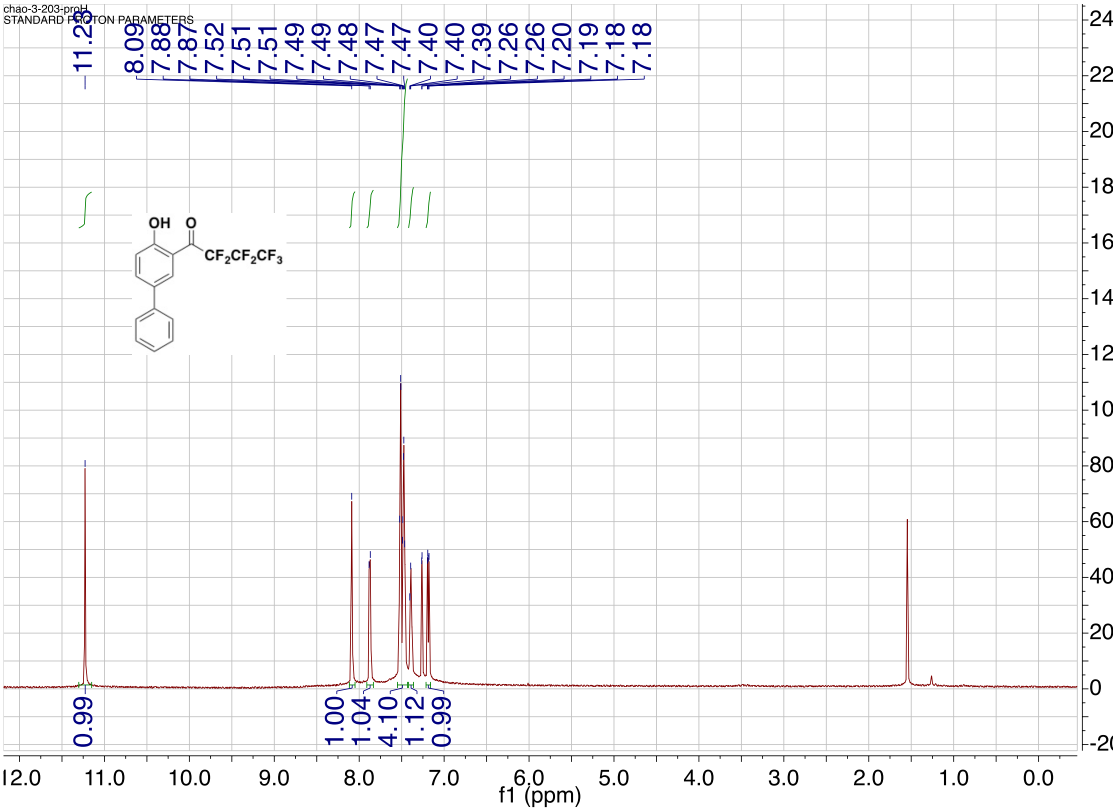
chao-3-203-proH
STANDARD PROTON PARAMETERS
11.25
8.09
7.88
7.87
7.52
7.51
7.51
7.49
7.49
7.48
7.47
7.47
7.40
7.40
7.39
7.26
7.26
7.20
7.19
7.18
7.18
OH
O
CF2CF2CF3
0.99
1.00
1.04
4.10
1.12
0.99
240
220
200
180
160
140
120
100
80
60
40
20
0
-20
12.0
11.0
10.0
9.0
8.0
7.0
6.0
5.0
4.0
3.0
2.0
1.0
0.0
f1 (ppm)

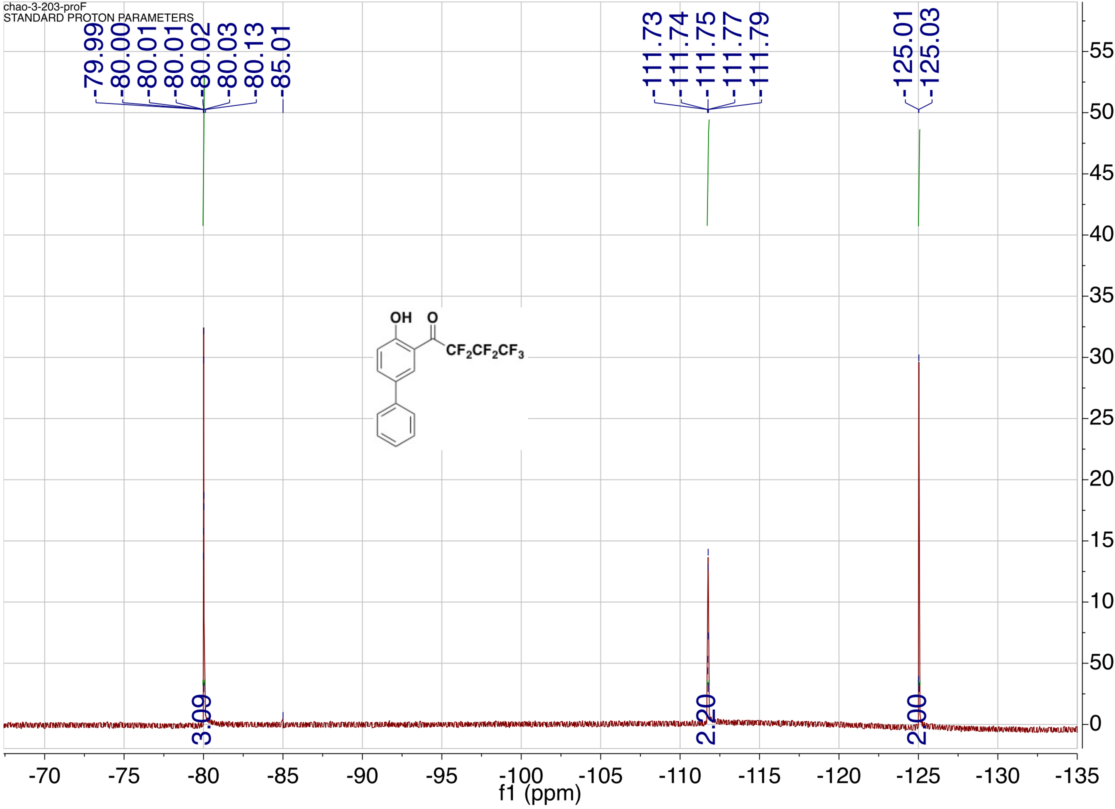
chao-3-203-proF
STANDARD PROTON PARAMETERS
-79.99
-80.00
-80.01
-80.01
-80.02
-80.03
-80.13
-85.01
-111.73
-111.74
-111.75
-111.77
-111.79
-125.01
-125.03
OH
O
CF2CF2CF3
3.09
2.20
2.00
550
500
450
400
350
300
250
200
150
100
50
0
-70
-75
-80
-85
-90
-95
-100
-105
-110
-115
-120
-125
-130
-135
f1 (ppm)

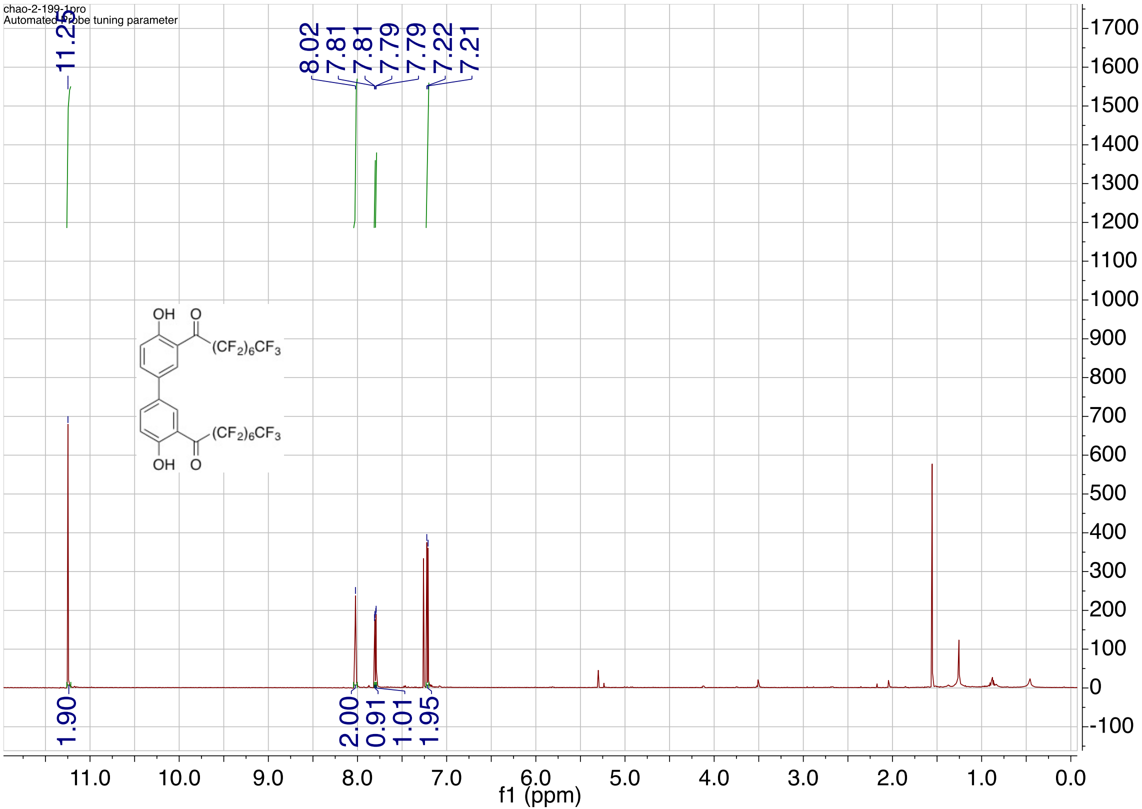
chao-2-199-1pro
Automated Probe tuning parameter
11.25
8.02
7.81
7.81
7.79
7.79
7.22
7.21
OH
O
(CF2)6CF3
(CF2)6CF3
OH
O
1.90
2.00
0.91
1.01
1.95
1700
1600
1500
1400
1300
1200
1100
1000
900
800
700
600
500
400
300
200
100
0
-100
11.0
10.0
9.0
8.0
7.0
6.0
5.0
4.0
3.0
2.0
1.0
0.0
f1 (ppm)

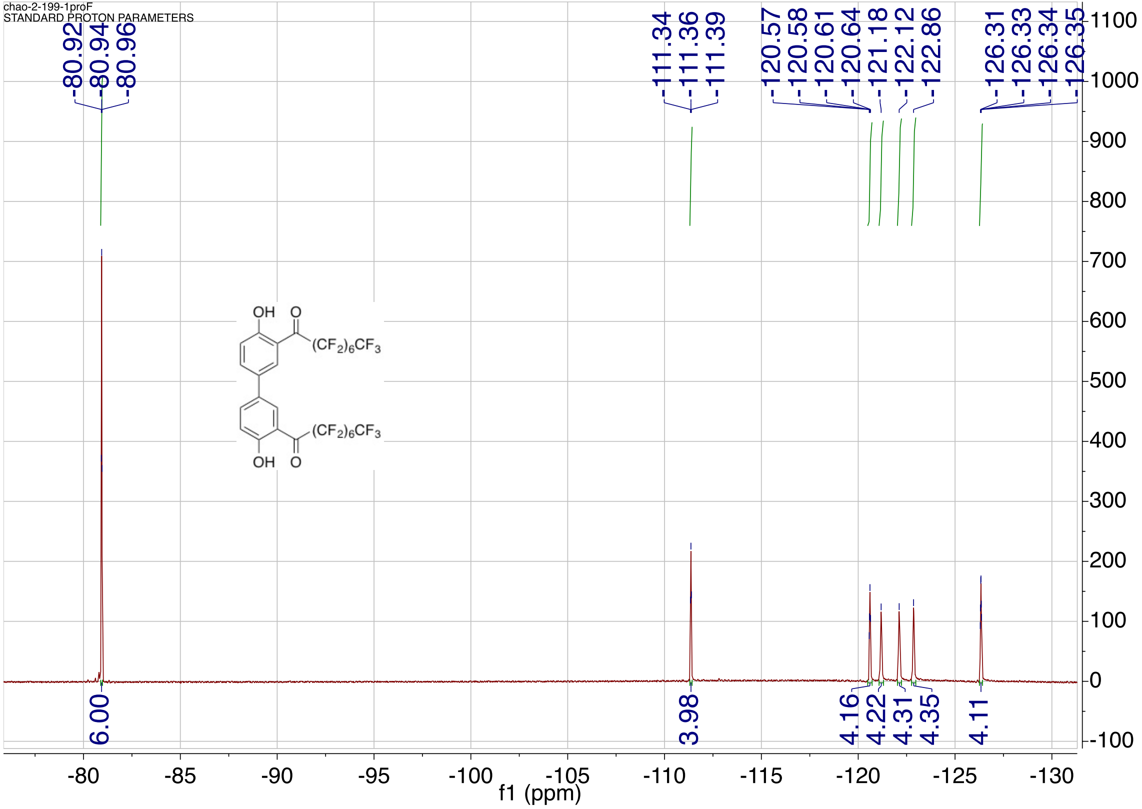
chao-2-199-1proF
STANDARD PROTON PARAMETERS
-80.92
-80.94
-80.96
-111.34
-111.36
-111.39
-120.57
-120.58
-120.61
-120.64
-121.18
-122.12
-122.86
-126.31
-126.33
-126.34
-126.35
OH
O
(CF2)6CF3
(CF2)6CF3
OH
O
6.00
3.98
4.16
4.22
4.31
4.35
4.11
1100
1000
900
800
700
600
500
400
300
200
100
0
-100
-80
-85
-90
-95
-100
-105
-110
-115
-120
-125
-130
f1 (ppm)

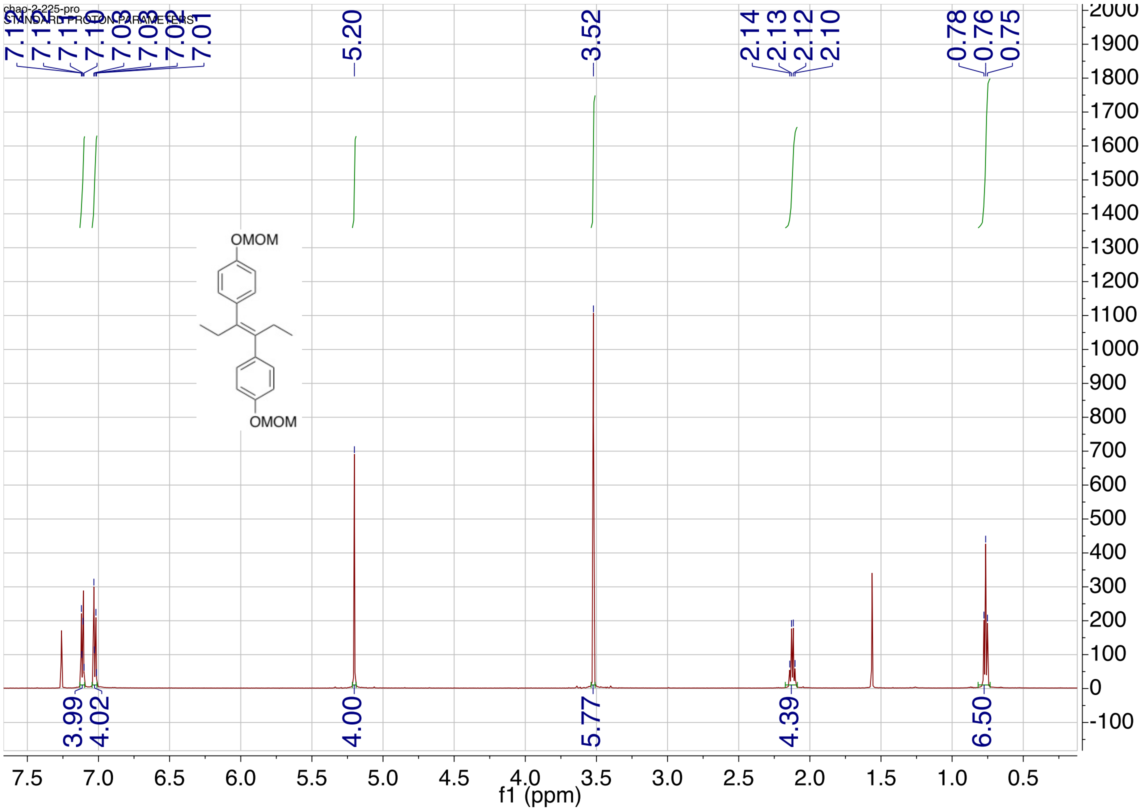
chao-2-225-pro
STANDARD PROTON PARAMETERS
7.12
7.12
7.11
7.10
7.03
7.03
7.02
7.01
5.20
3.52
2.14
2.13
2.12
2.10
0.78
0.76
0.75
OMOM
OMOM
3.99
4.02
4.00
5.77
4.39
6.50
2000
1900
1800
1700
1600
1500
1400
1300
1200
1100
1000
900
800
700
600
500
400
300
200
100
0
-100
7.5
7.0
6.5
6.0
5.5
5.0
4.5
4.0
3.5
3.0
2.5
2.0
1.5
1.0
0.5
f1 (ppm)

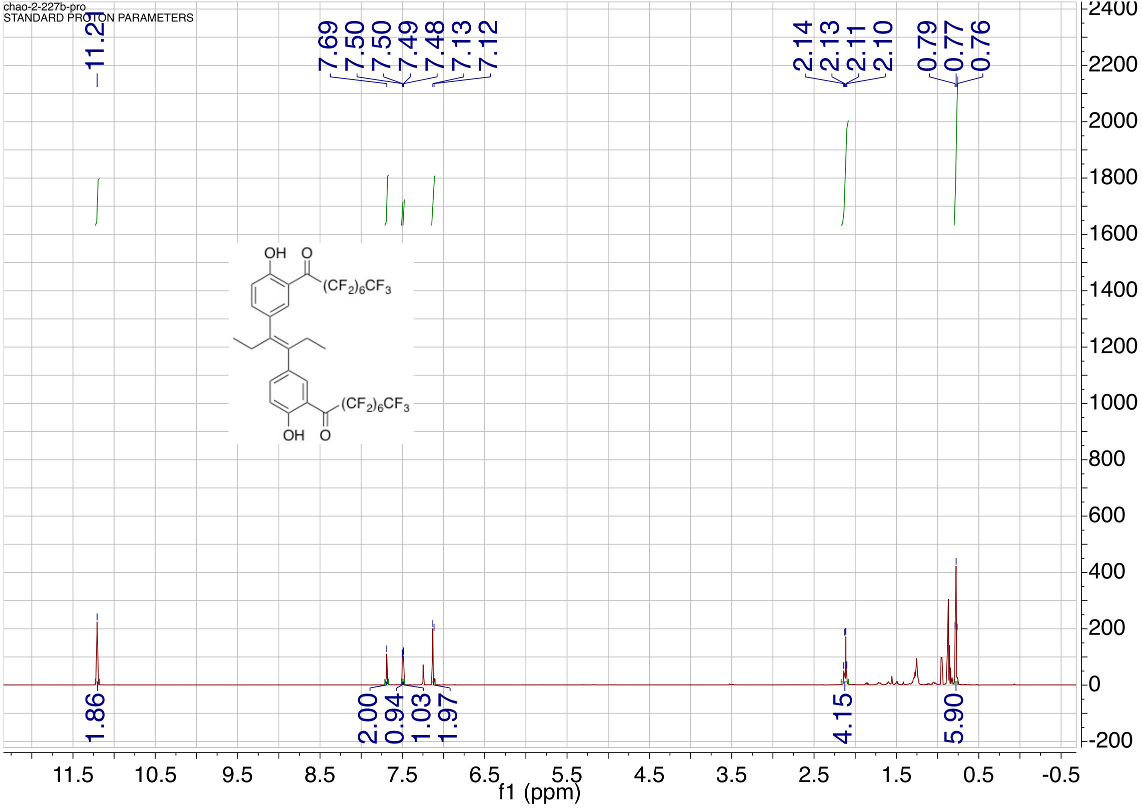
chao-2-227b-pro
STANDARD PROTON PARAMETERS
11.24
7.69
7.50
7.50
7.49
7.48
7.13
7.12
2.14
2.13
2.11
2.10
0.79
0.77
0.76
OH
O
$(CF_2)_6CF_3$
$(CF_2)_6CF_3$
OH
O
1.86
2.00
0.94
1.03
1.97
4.15
5.90
2400
2200
2000
1800
1600
1400
1200
1000
800
600
400
200
0
-200
11.5
10.5
9.5
8.5
7.5
6.5
5.5
4.5
3.5
2.5
1.5
0.5
-0.5
f1 (ppm)

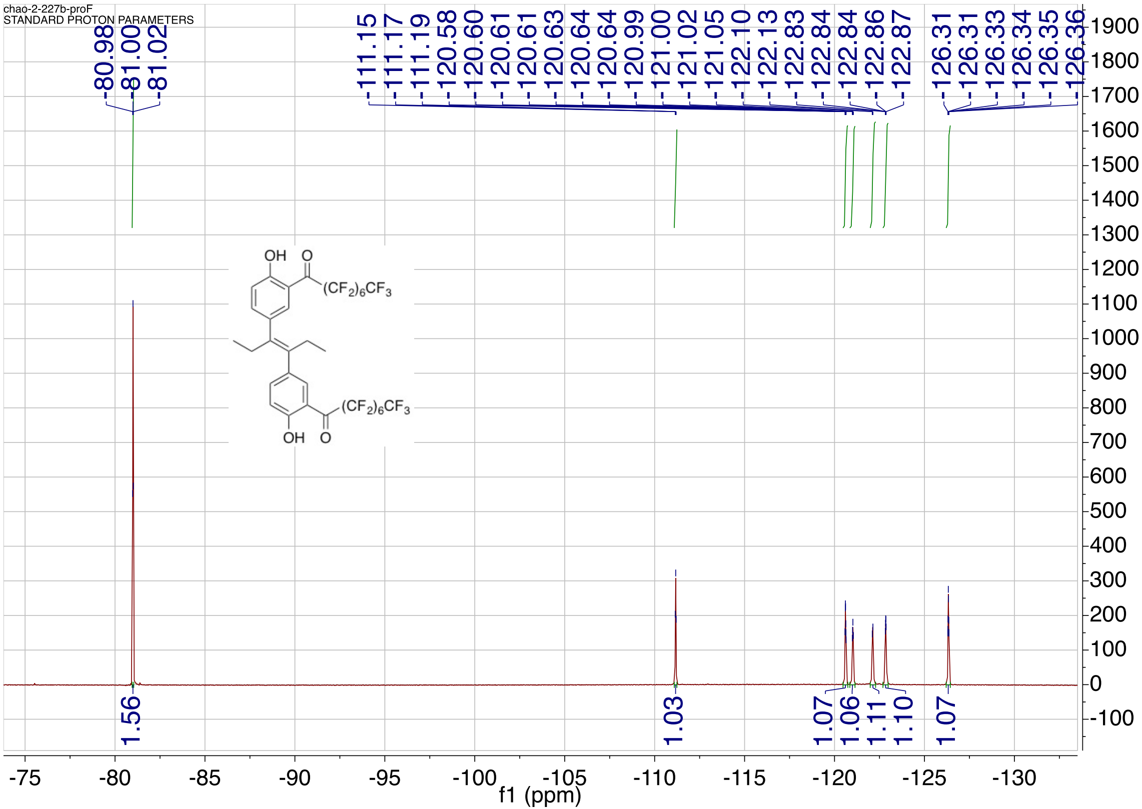
chao-2-227b-proF
STANDARD PROTON PARAMETERS
-80.98
-81.00
-81.02
-111.15
-111.17
-111.19
-120.58
-120.60
-120.61
-120.61
-120.63
-120.64
-120.64
-120.99
-121.00
-121.02
-121.05
-122.10
-122.13
-122.83
-122.84
-122.84
-122.86
-122.87
-126.31
-126.31
-126.33
-126.34
-126.35
-126.36
OH
O
(CF2)6CF3
(CF2)6CF3
OH
O
1.56
1.03
1.07
1.06
1.11
1.10
1.07
1900
1800
1700
1600
1500
1400
1300
1200
1100
1000
900
800
700
600
500
400
300
200
100
0
-100
-75
-80
-85
-90
-95
-100
-105
-110
-115
-120
-125
-130
f1 (ppm)

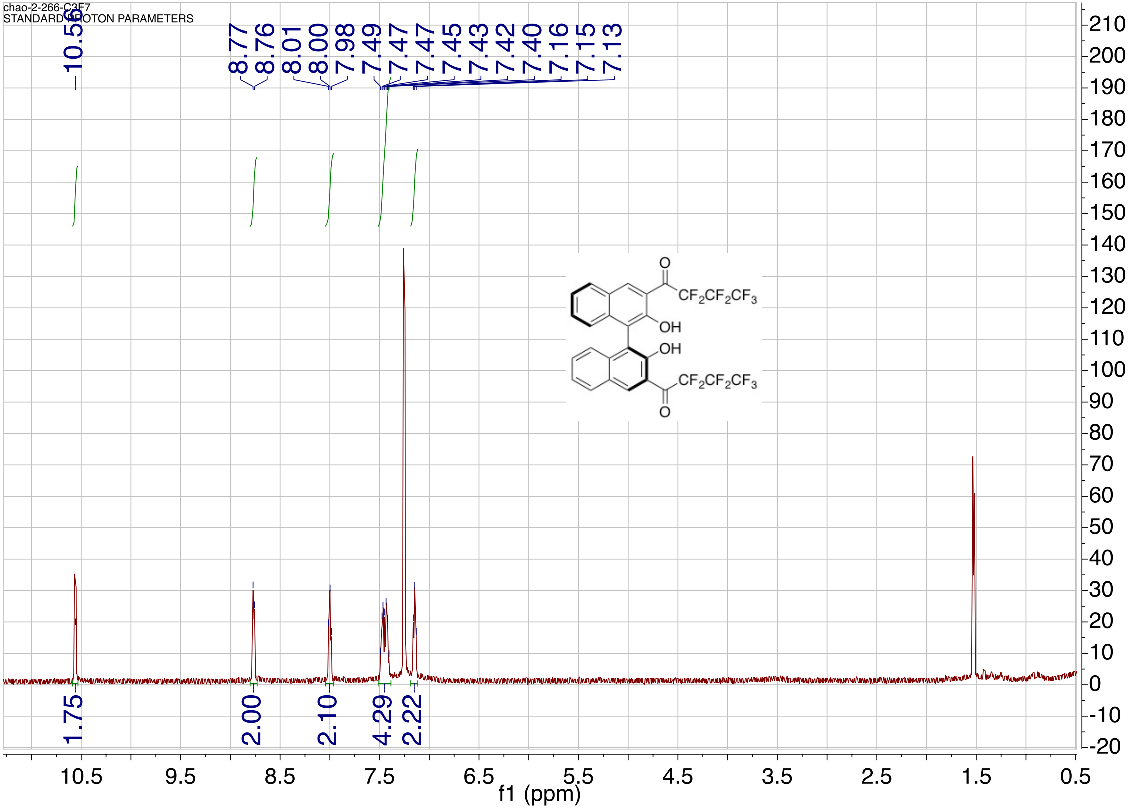
chao-2-266-C3F7
STANDARD PROTON PARAMETERS
10.56
8.77
8.76
8.01
8.00
7.98
7.49
7.47
7.47
7.45
7.43
7.42
7.40
7.16
7.15
7.13
O
CF2CF2CF3
OH
OH
CF2CF2CF3
O
1.75
2.00
2.10
4.29
2.22
210
200
190
180
170
160
150
140
130
120
110
100
90
80
70
60
50
40
30
20
10
0
-10
-20
10.5
9.5
8.5
7.5
6.5
5.5
4.5
3.5
2.5
1.5
0.5
f1 (ppm)

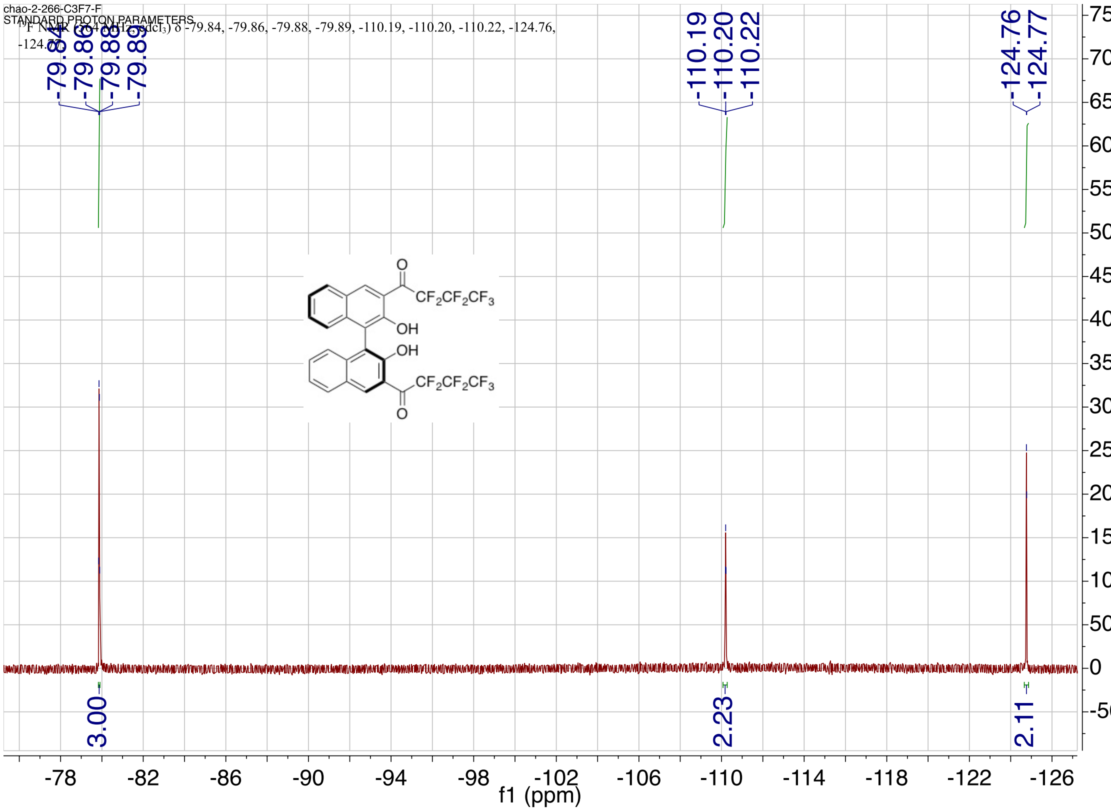

^{19}F NMR (564 MHz, cdcl$_3$) δ -79.84, -79.86, -79.88, -79.89, -110.19, -110.20, -110.22, -124.76, -124.77.

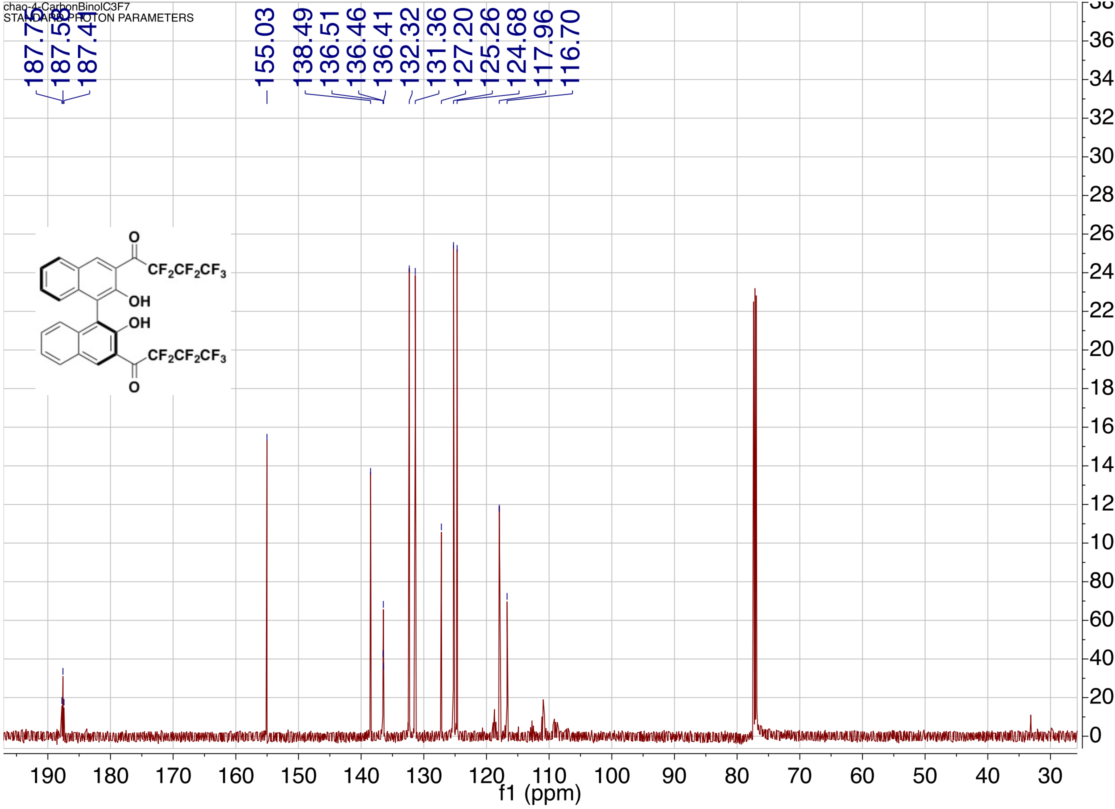

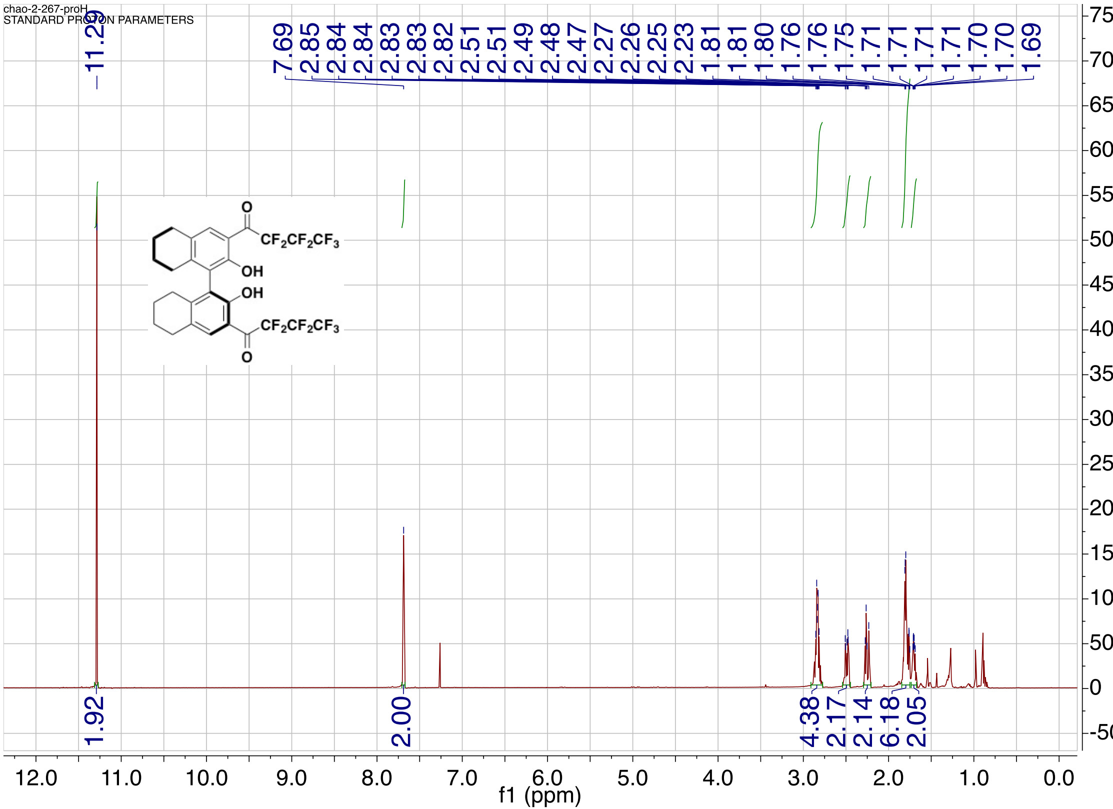
chao-2-267-proH
STANDARD PROTON PARAMETERS
11.29
7.69
2.85
2.84
2.84
2.83
2.83
2.82
2.51
2.51
2.49
2.48
2.47
2.27
2.26
2.25
2.23
1.81
1.81
1.80
1.76
1.76
1.75
1.71
1.71
1.71
1.71
1.70
1.70
1.69
O
CF2CF2CF3
OH
OH
CF2CF2CF3
O
1.92
2.00
4.38
2.17
2.14
6.18
2.05
12.0
11.0
10.0
9.0
8.0
7.0
6.0
5.0
4.0
3.0
2.0
1.0
0.0
f1 (ppm)
750
700
650
600
550
500
450
400
350
300
250
200
150
100
50
0
-50

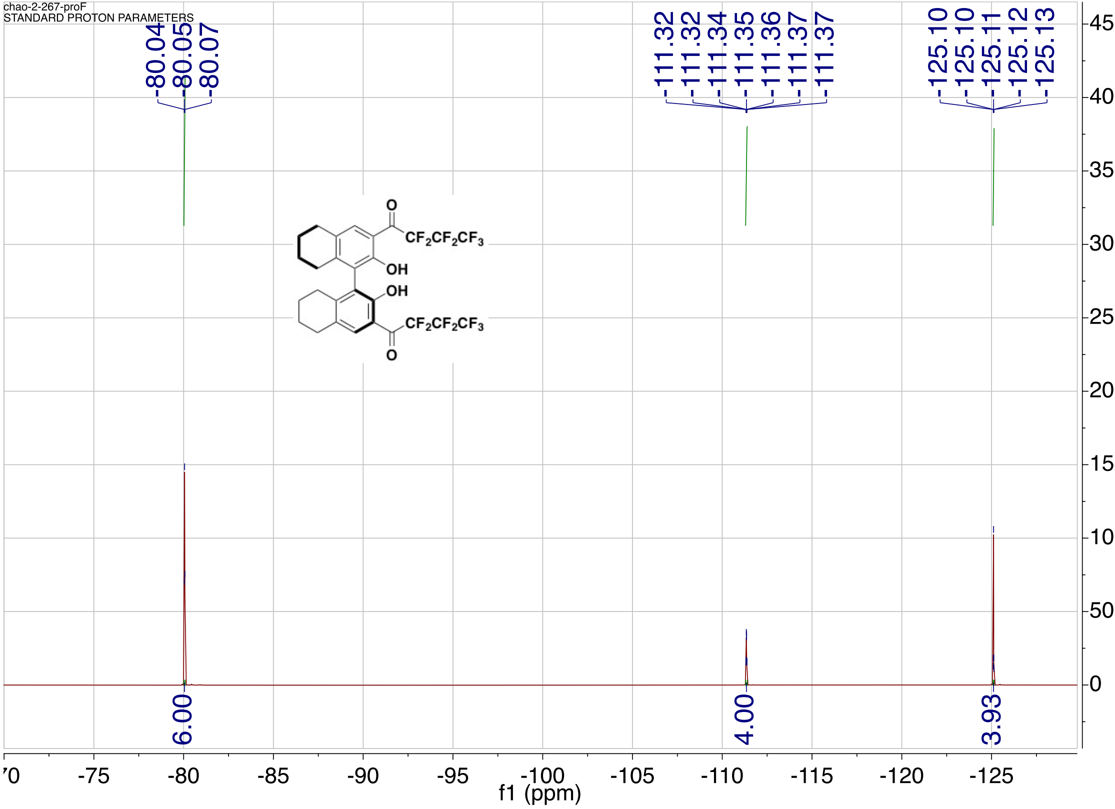
chao-2-267-proF
STANDARD PROTON PARAMETERS
-80.04
-80.05
-80.07
-111.32
-111.32
-111.34
-111.35
-111.36
-111.37
-111.37
-125.10
-125.10
-125.11
-125.12
-125.13
O
CF2CF2CF3
OH
OH
CF2CF2CF3
O
6.00
4.00
3.93
-70
-75
-80
-85
-90
-95
-100
-105
-110
-115
-120
-125
f1 (ppm)
4500
4000
3500
3000
2500
2000
1500
1000
500
0

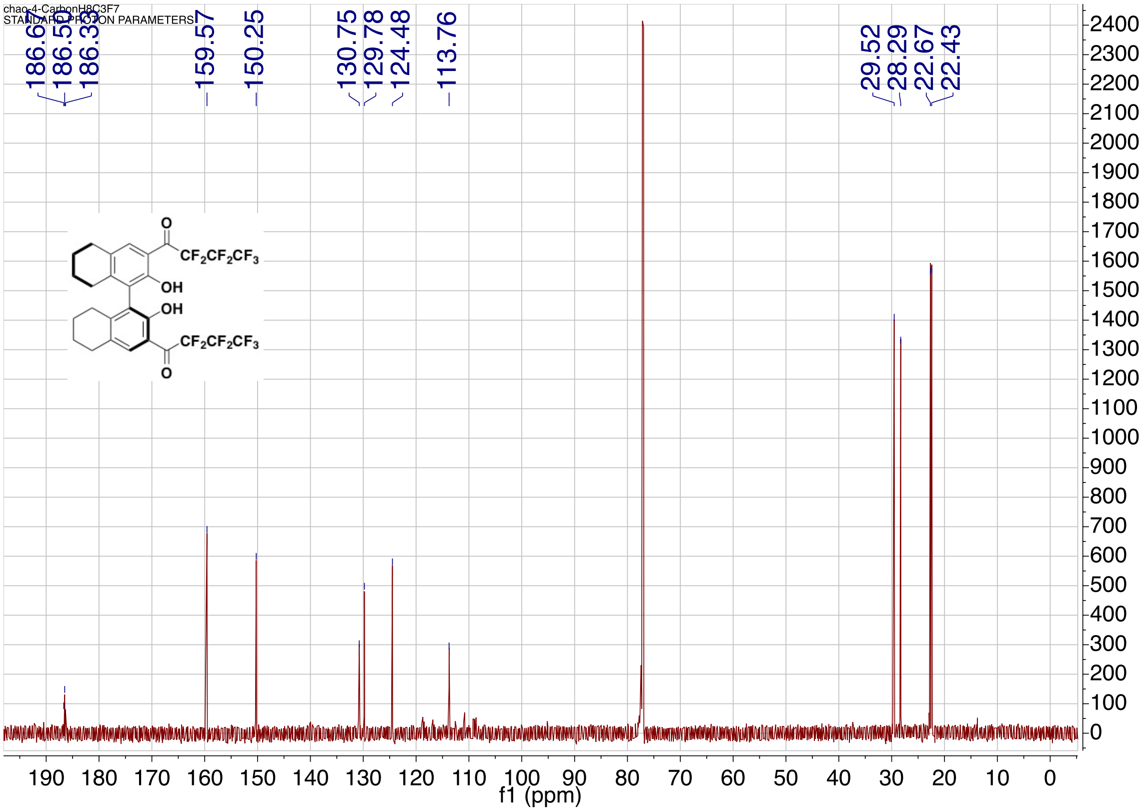
chao-4-CarbonH8C3F7
STANDARD PROTON PARAMETERS
186.67
186.50
186.33
159.57
150.25
130.75
129.78
124.48
113.76
29.52
28.29
22.67
22.43
O
CF2CF2CF3
OH
OH
CF2CF2CF3
O
2400
2300
2200
2100
2000
1900
1800
1700
1600
1500
1400
1300
1200
1100
1000
900
800
700
600
500
400
300
200
100
0
190 180 170 160 150 140 130 120 110 100 90 80 70 60 50 40 30 20 10 0
f1 (ppm)

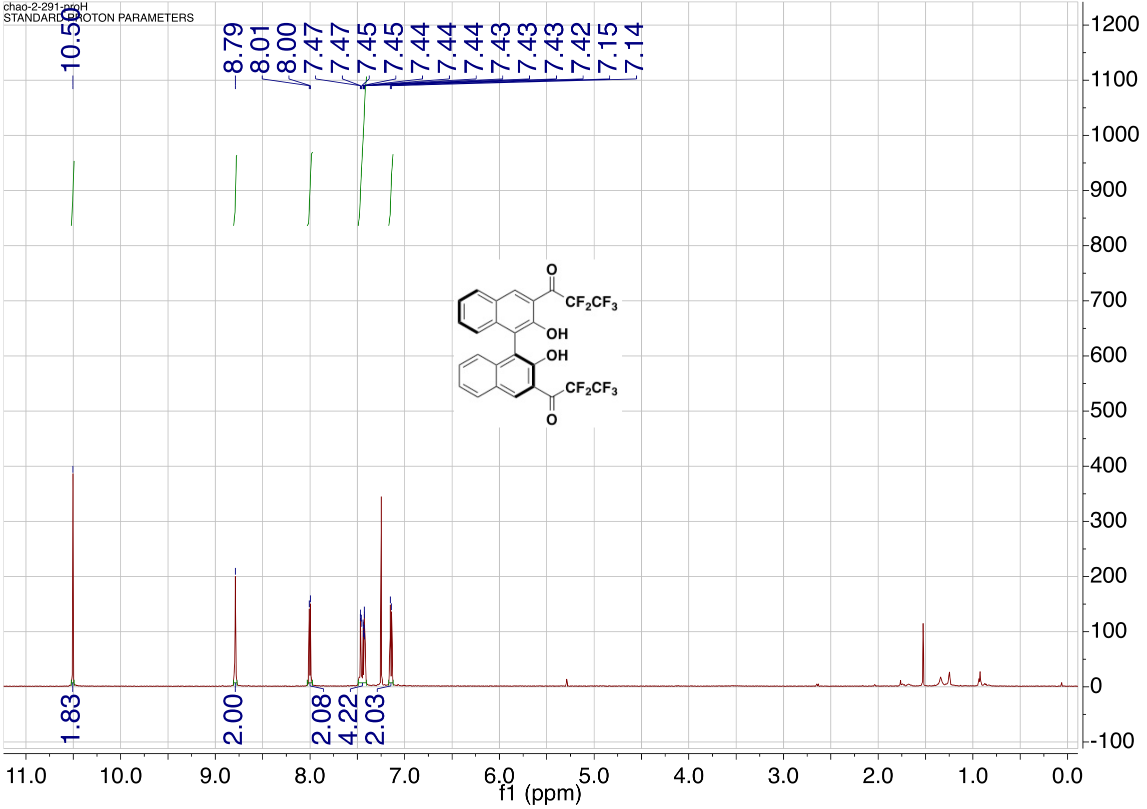
chao-2-291-proH
STANDARD PROTON PARAMETERS
10.50
8.79
8.01
8.00
7.47
7.47
7.45
7.45
7.44
7.44
7.44
7.43
7.43
7.43
7.42
7.15
7.14
O
CF2CF3
OH
OH
CF2CF3
O
1.83
2.00
2.08
4.22
2.03
1200
1100
1000
900
800
700
600
500
400
300
200
100
0
-100
11.0 10.0 9.0 8.0 7.0 6.0 5.0 4.0 3.0 2.0 1.0 0.0
f1 (ppm)

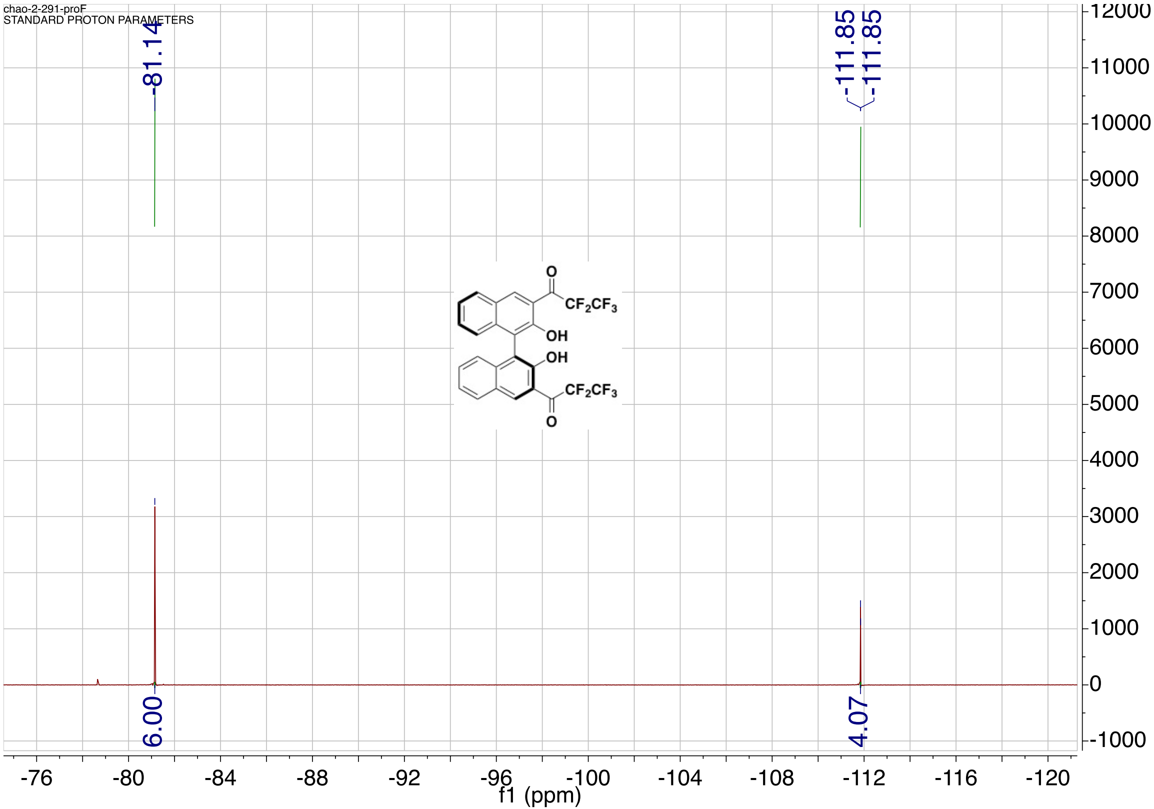
chao-2-291-proF
STANDARD PROTON PARAMETERS
-81.14
-111.85
-111.85
6.00
4.07
CF2CF3
OH
OH
CF2CF3
O
O
12000
11000
10000
9000
8000
7000
6000
5000
4000
3000
2000
1000
0
-1000
-76
-80
-84
-88
-92
-96
-100
-104
-108
-112
-116
-120
f1 (ppm)

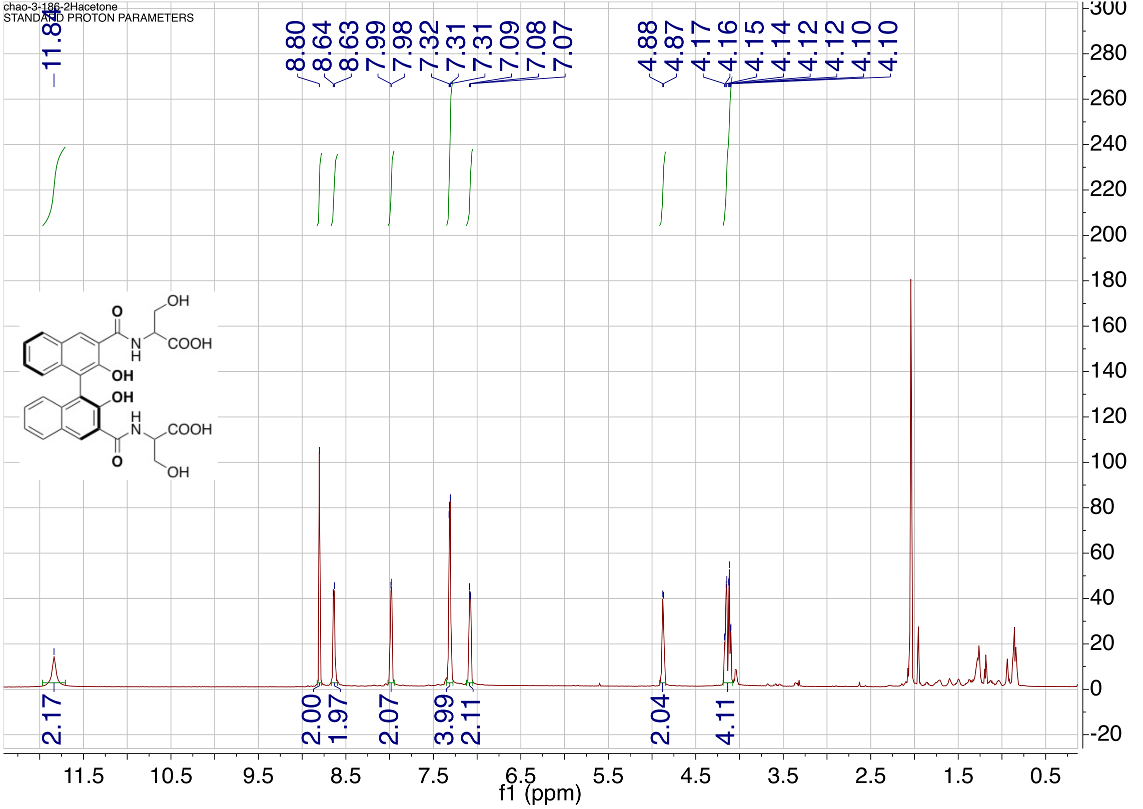
chao-3-186-2Hacetone
STANDARD PROTON PARAMETERS
11.84
8.80
8.64
8.63
7.99
7.98
7.32
7.31
7.31
7.09
7.08
7.07
4.88
4.87
4.17
4.16
4.15
4.14
4.12
4.12
4.10
4.10
2.17
2.00
1.97
2.07
3.99
2.11
2.04
4.11
OH
O
N
H
COOH
OH
OH
H
N
COOH
O
OH
300
280
260
240
220
200
180
160
140
120
100
80
60
40
20
0
-20
11.5
10.5
9.5
8.5
7.5
6.5
5.5
4.5
3.5
2.5
1.5
0.5
f1 (ppm)

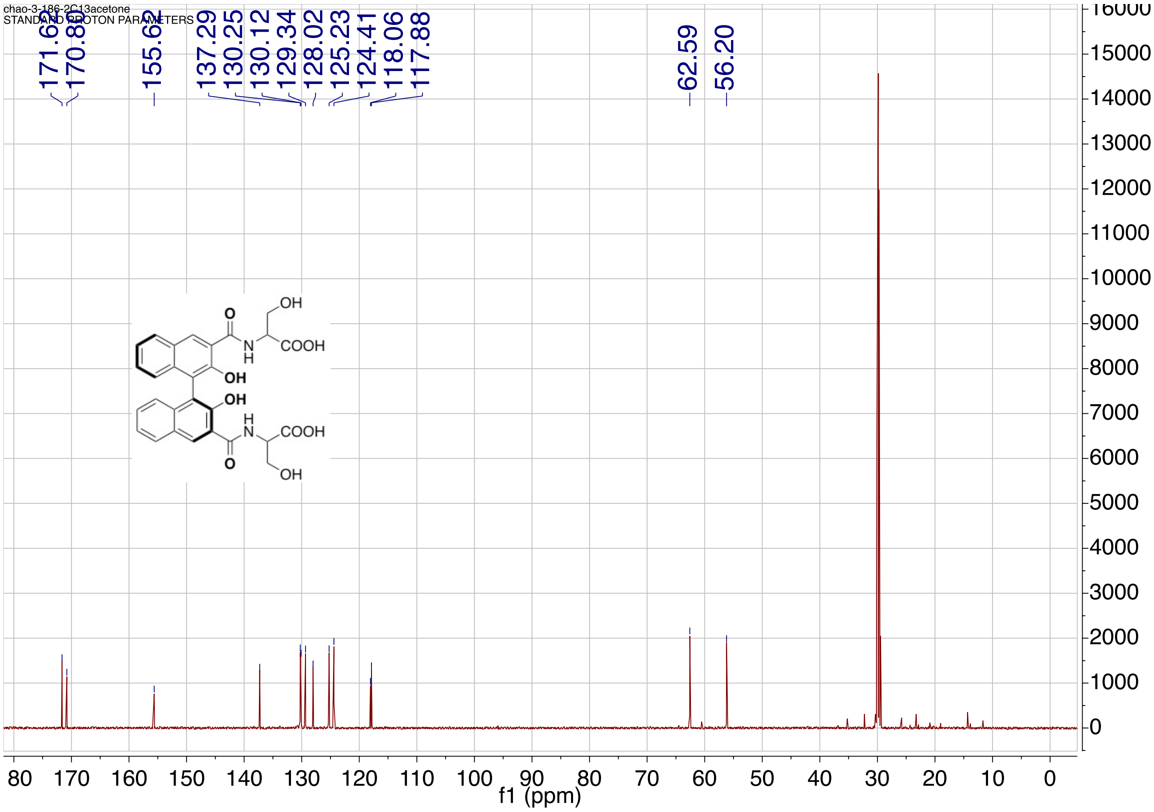
chao-3-186-2C13acetone
STANDARD PROTON PARAMETERS
171.62
170.80
155.62
137.29
130.25
130.12
129.34
128.02
125.23
124.41
118.06
117.88
62.59
56.20
OH
O
N
H
COOH
OH
OH
H
N
COOH
O
OH
16000
15000
14000
13000
12000
11000
10000
9000
8000
7000
6000
5000
4000
3000
2000
1000
0
80 170 160 150 140 130 120 110 100 90 80 70 60 50 40 30 20 10 0
f1 (ppm)

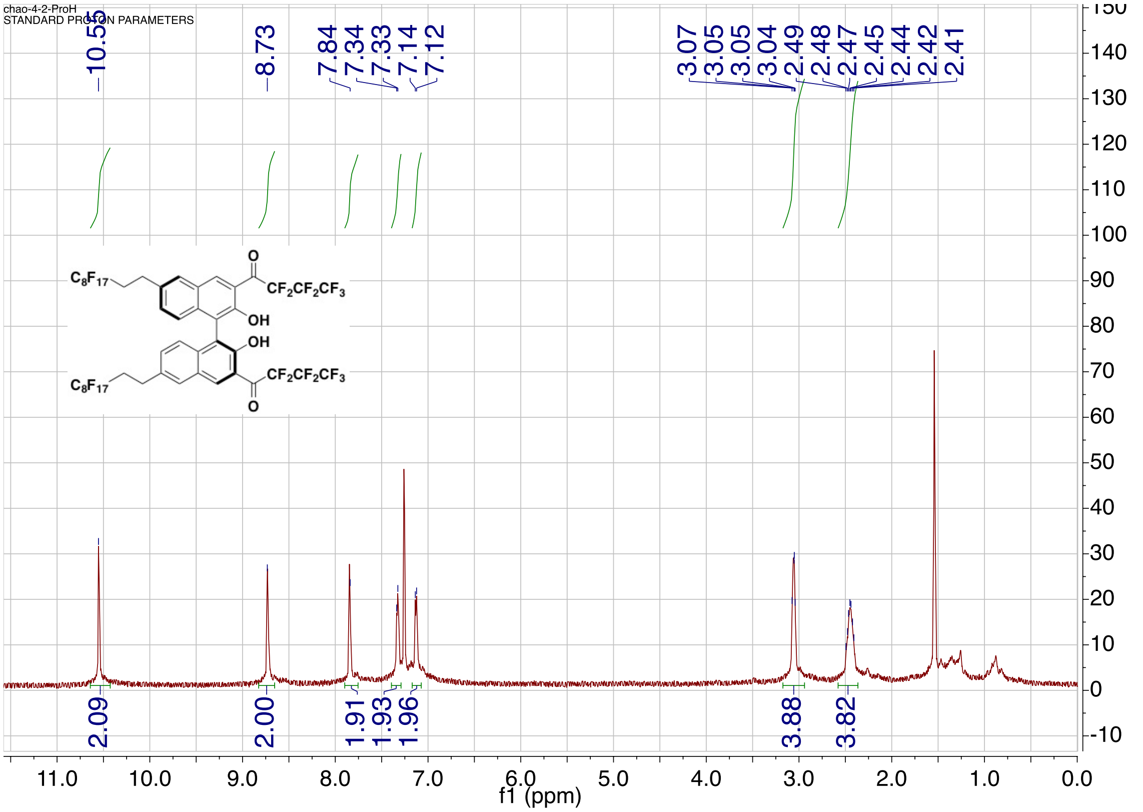
chao-4-2-ProH
STANDARD PROTON PARAMETERS
10.55
8.73
7.84
7.34
7.33
7.14
7.12
3.07
3.05
3.05
3.04
2.49
2.48
2.47
2.45
2.44
2.42
2.41
C8F17
O
CF2CF2CF3
OH
OH
C8F17
CF2CF2CF3
O
2.09
2.00
1.91
1.93
1.96
3.88
3.82
150
140
130
120
110
100
90
80
70
60
50
40
30
20
10
0
-10
11.0 10.0 9.0 8.0 7.0 6.0 5.0 4.0 3.0 2.0 1.0 0.0
f1 (ppm)

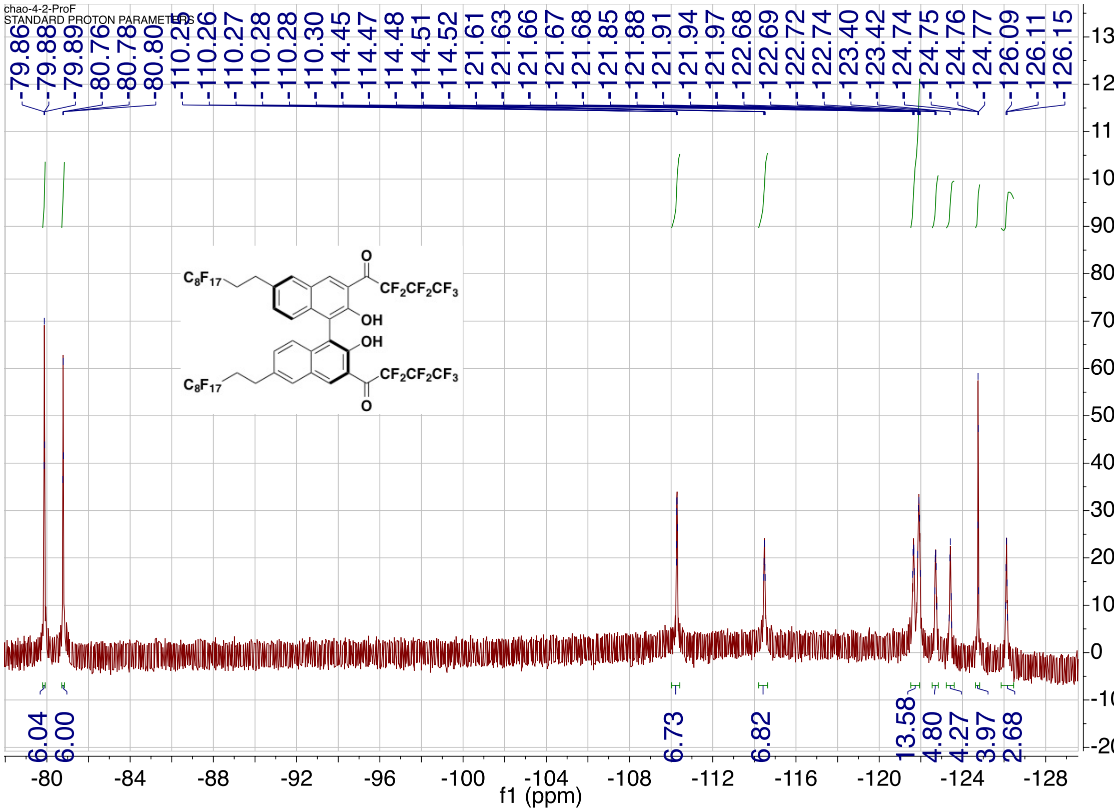
chao-4-2-ProF
STANDARD PROTON PARAMETERS
-79.86
-79.88
-79.89
-80.76
-80.78
-80.80
-110.25
-110.26
-110.27
-110.28
-110.28
-110.30
-114.45
-114.47
-114.48
-114.51
-114.52
-121.61
-121.63
-121.66
-121.67
-121.68
-121.85
-121.88
-121.91
-121.94
-121.97
-122.68
-122.69
-122.72
-122.74
-123.40
-123.42
-124.74
-124.75
-124.76
-124.77
-126.09
-126.11
-126.15
C_8F_{17}
O
$CF_2CF_2CF_3$
OH
OH
C_8F_{17}
$CF_2CF_2CF_3$
O
6.04
6.00
6.73
6.82
13.58
4.80
4.27
3.97
2.68
130
120
110
100
90
80
70
60
50
40
30
20
10
0
-10
-20
-80
-84
-88
-92
-96
-100
-104
-108
-112
-116
-120
-124
-128
f1 (ppm)

Appendix for Chapter 5

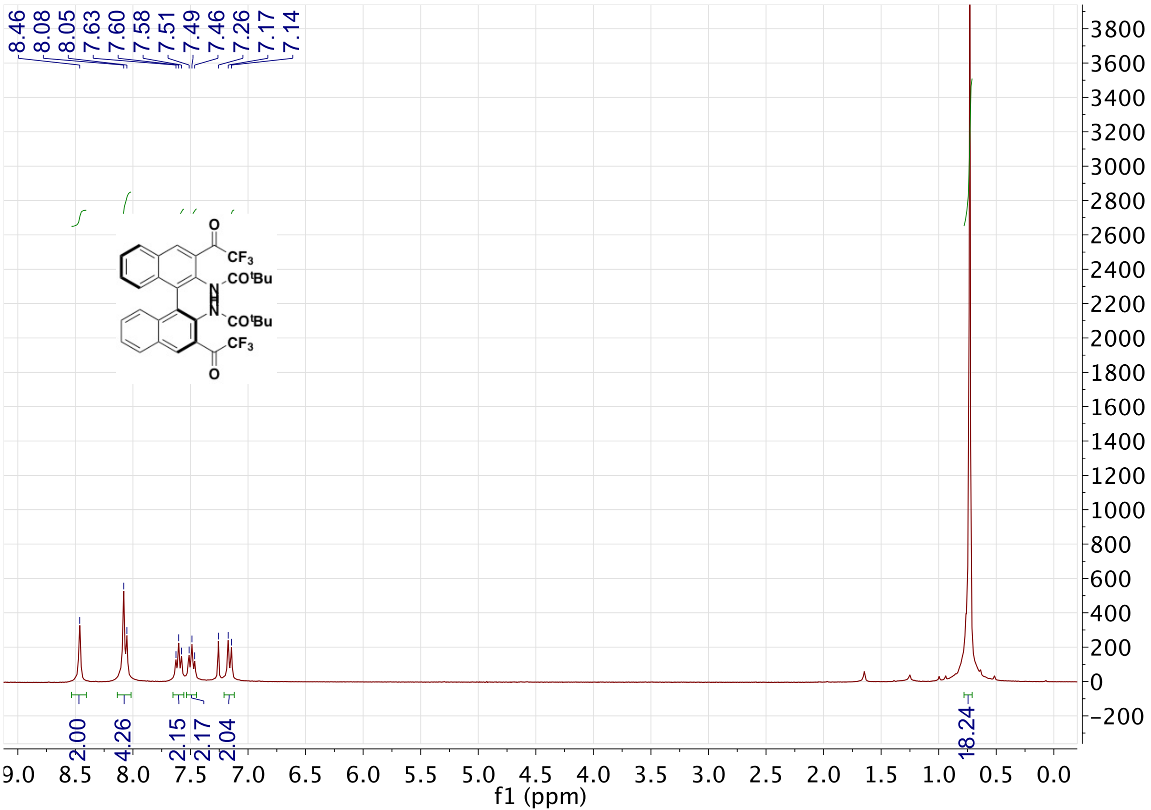

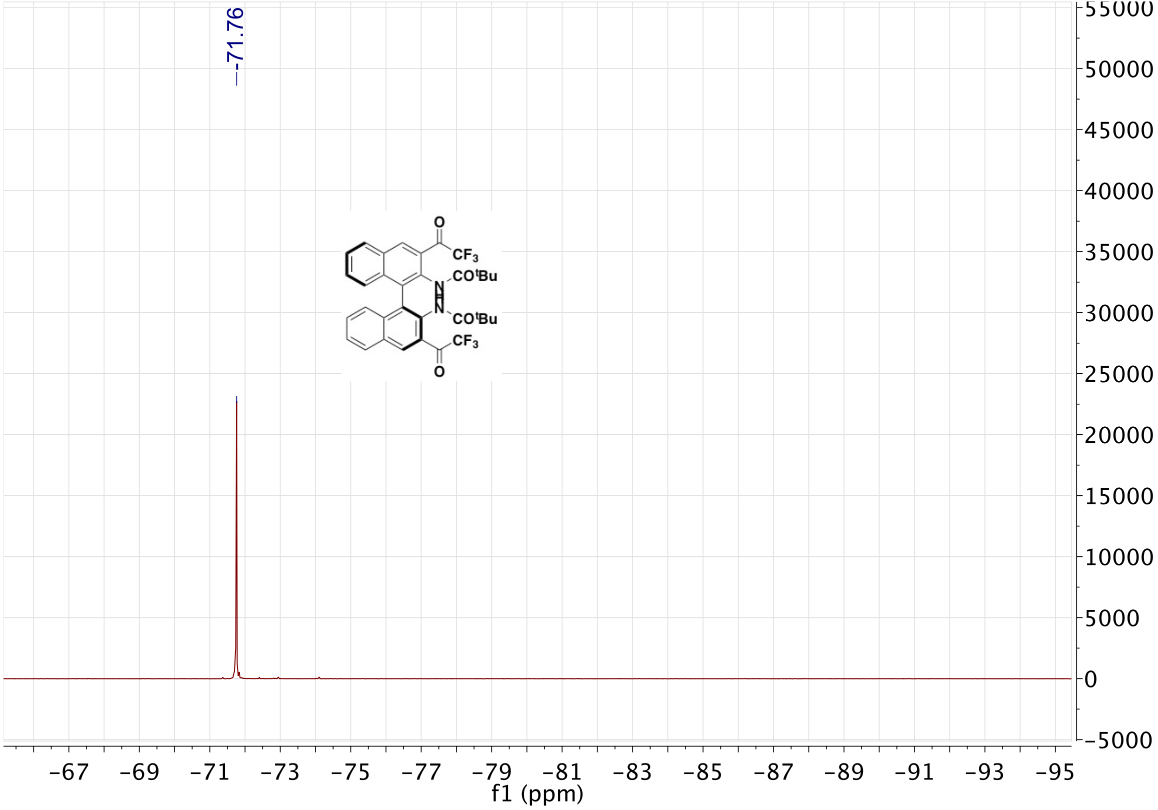

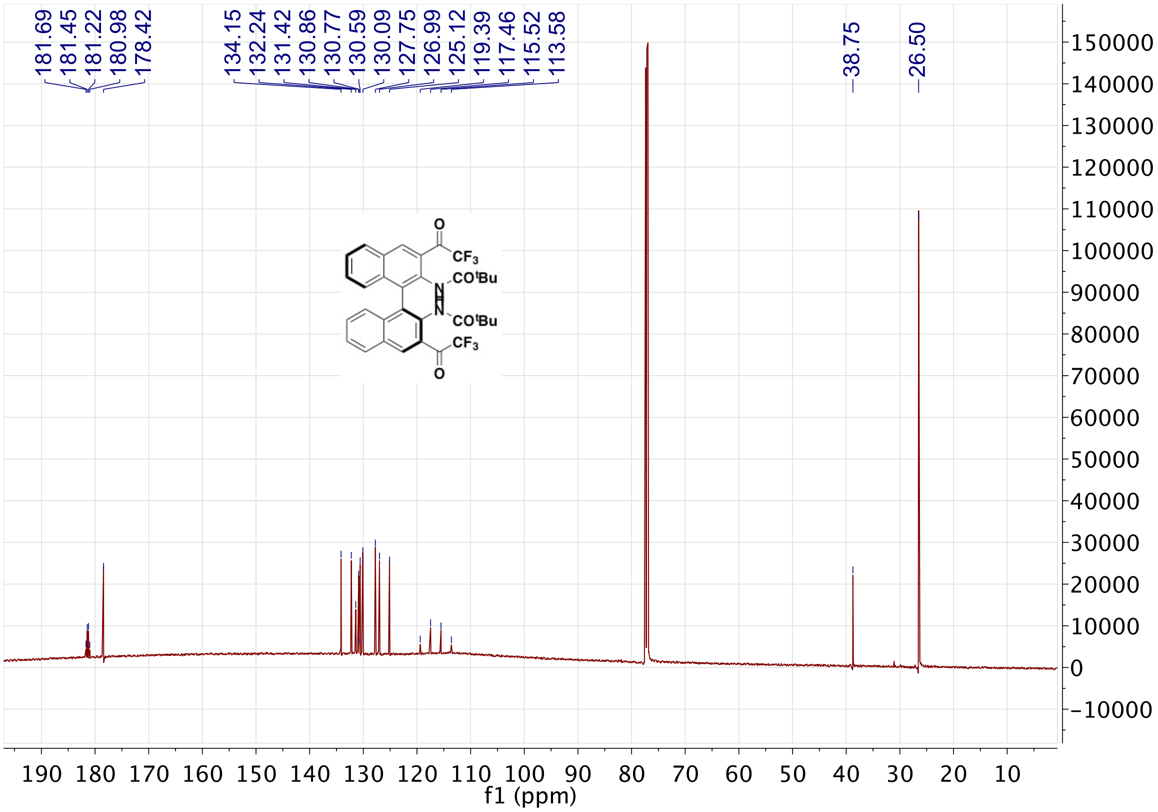
181.69
181.45
181.22
180.98
178.42
134.15
132.24
131.42
130.86
130.77
130.59
130.09
127.75
126.99
125.12
119.39
117.46
115.52
113.58
38.75
26.50
O
CF3
N
COtBu
H
N
H
COtBu
CF3
O
150000
140000
130000
120000
110000
100000
90000
80000
70000
60000
50000
40000
30000
20000
10000
0
−10000
190 180 170 160 150 140 130 120 110 100 90 80 70 60 50 40 30 20 10
f1 (ppm)

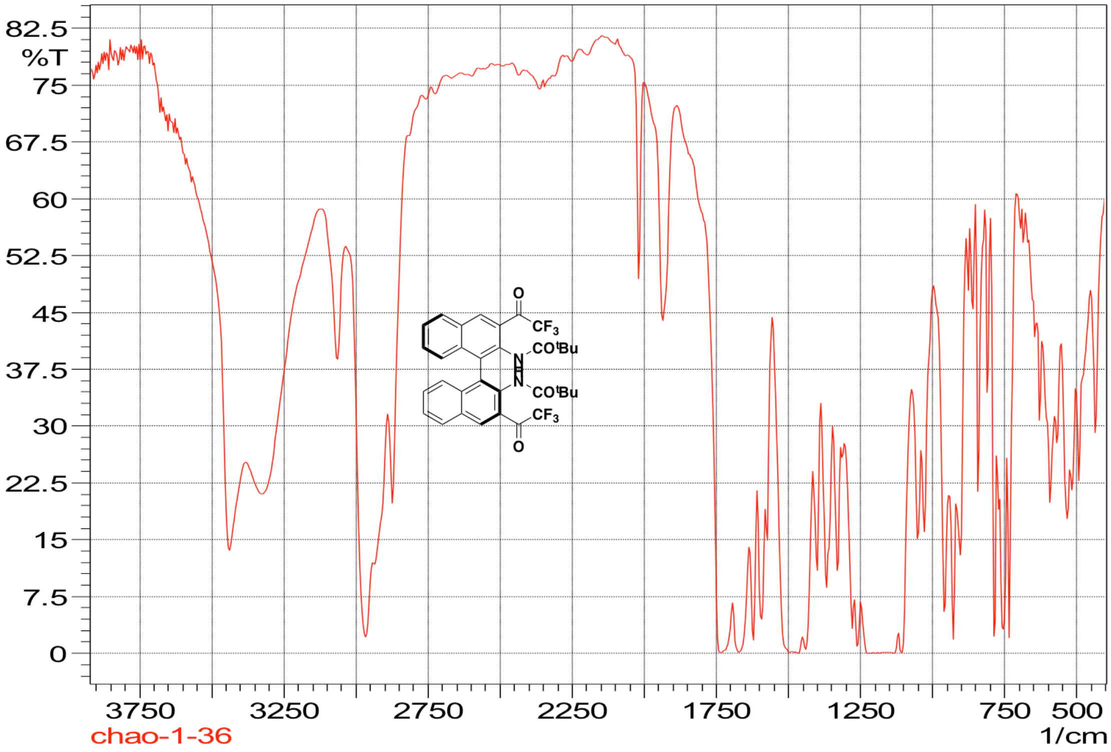
82.5
%T
75
67.5
60
52.5
45
37.5
30
22.5
15
7.5
0
O
CF3
N
H
COtBu
N
H
COtBu
CF3
O
3750
3250
2750
2250
1750
1250
750
500
chao-1-36
1/cm

Appendix for Chapter 6

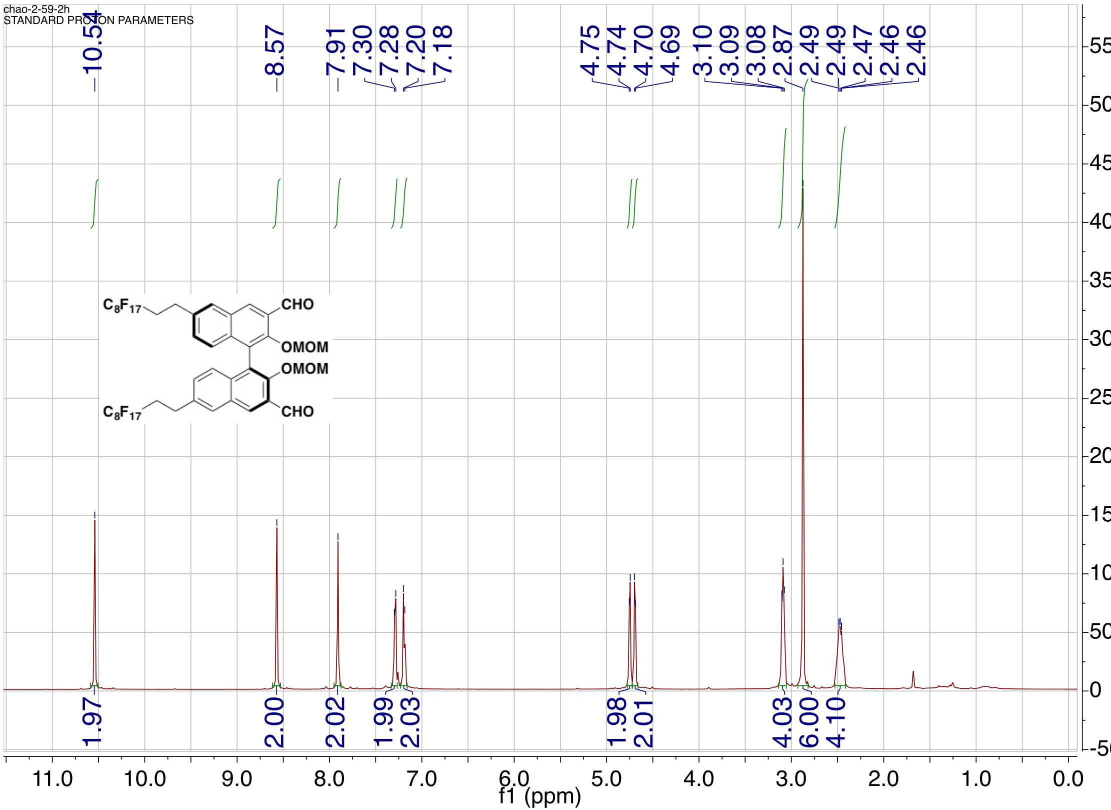

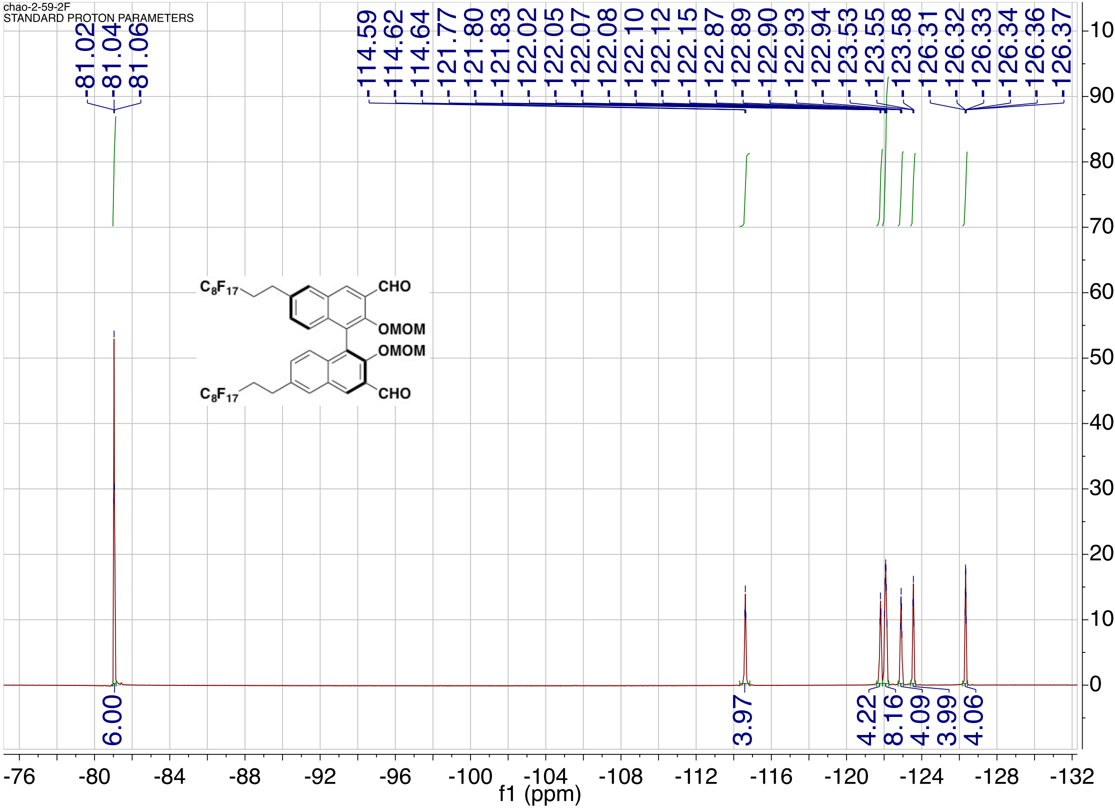

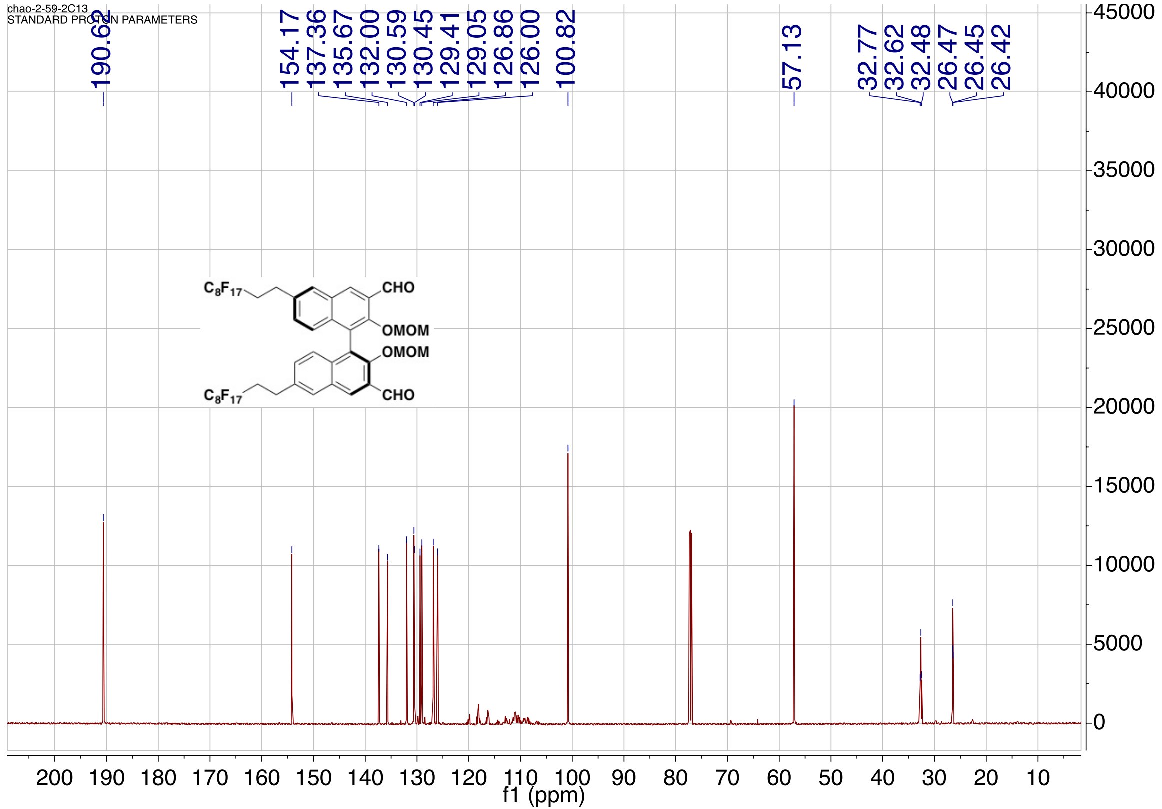
chao-2-59-2C13
STANDARD PROTON PARAMETERS
190.62
154.17
137.36
135.67
132.00
130.59
130.45
129.41
129.05
126.86
126.00
100.82
57.13
32.77
32.62
32.48
26.47
26.45
26.42
C_8F_{17}
CHO
OMOM
OMOM
C_8F_{17}
CHO
45000
40000
35000
30000
25000
20000
15000
10000
5000
0
200 190 180 170 160 150 140 130 120 110 100 90 80 70 60 50 40 30 20 10
f1 (ppm)

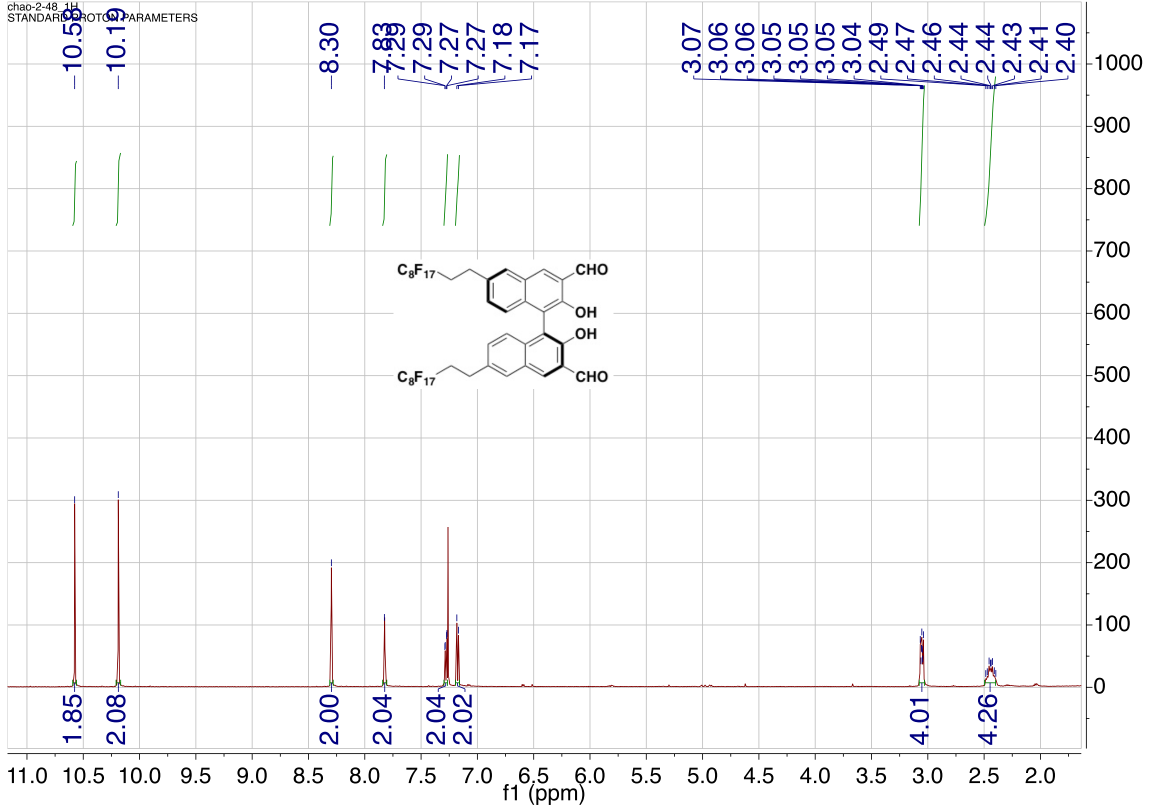
chao-2-48_1H
STANDARD PROTON PARAMETERS
10.58
10.19
8.30
7.83
7.29
7.29
7.27
7.27
7.18
7.17
3.07
3.06
3.05
3.05
3.05
3.04
2.49
2.47
2.46
2.44
2.44
2.43
2.41
2.40
C_8F_{17}
CHO
OH
OH
C_8F_{17}
CHO
1000
900
800
700
600
500
400
300
200
100
0
1.85
2.08
2.00
2.04
2.04
2.02
4.01
4.26
11.0 10.5 10.0 9.5 9.0 8.5 8.0 7.5 7.0 6.5 6.0 5.5 5.0 4.5 4.0 3.5 3.0 2.5 2.0
f1 (ppm)

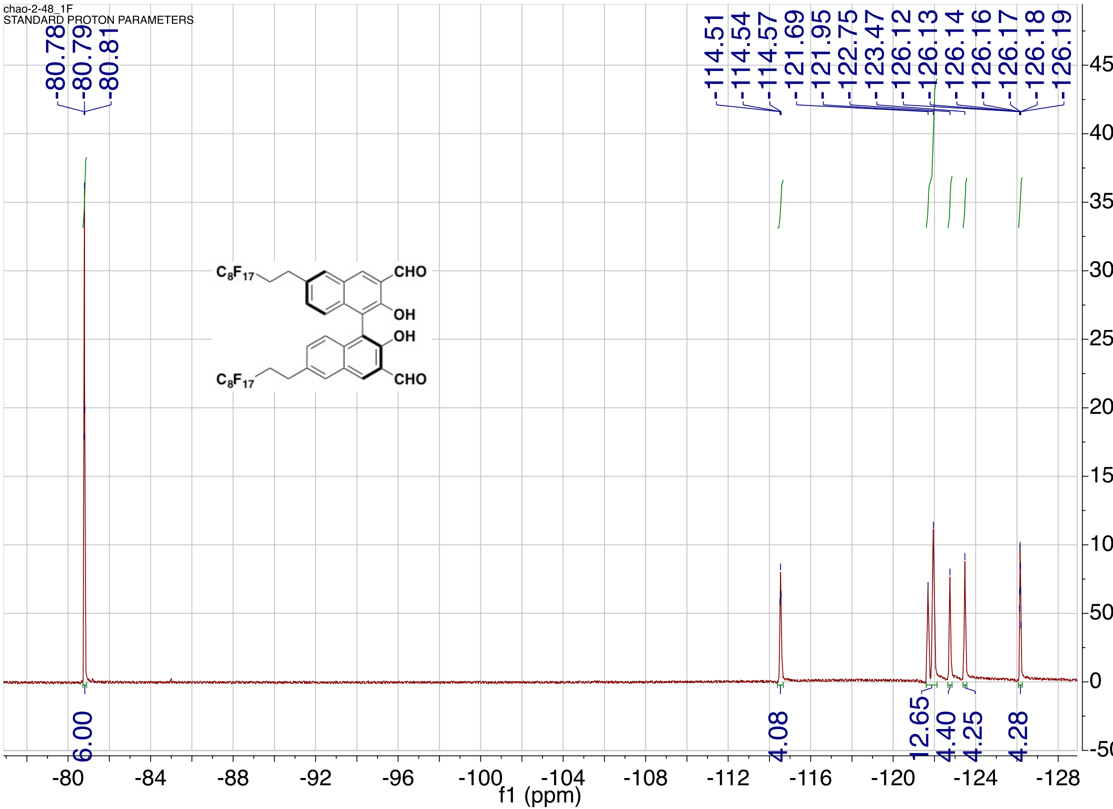
chao-2-48_1F
STANDARD PROTON PARAMETERS
-80.78
-80.79
-80.81
-114.51
-114.54
-114.57
-121.69
-121.95
-122.75
-123.47
-126.12
-126.13
-126.14
-126.16
-126.17
-126.18
-126.19
C8F17
CHO
OH
OH
C8F17
CHO
6.00
4.08
12.65
4.40
4.25
4.28
450
400
350
300
250
200
150
100
50
0
-50
-80
-84
-88
-92
-96
-100
-104
-108
-112
-116
-120
-124
-128
f1 (ppm)

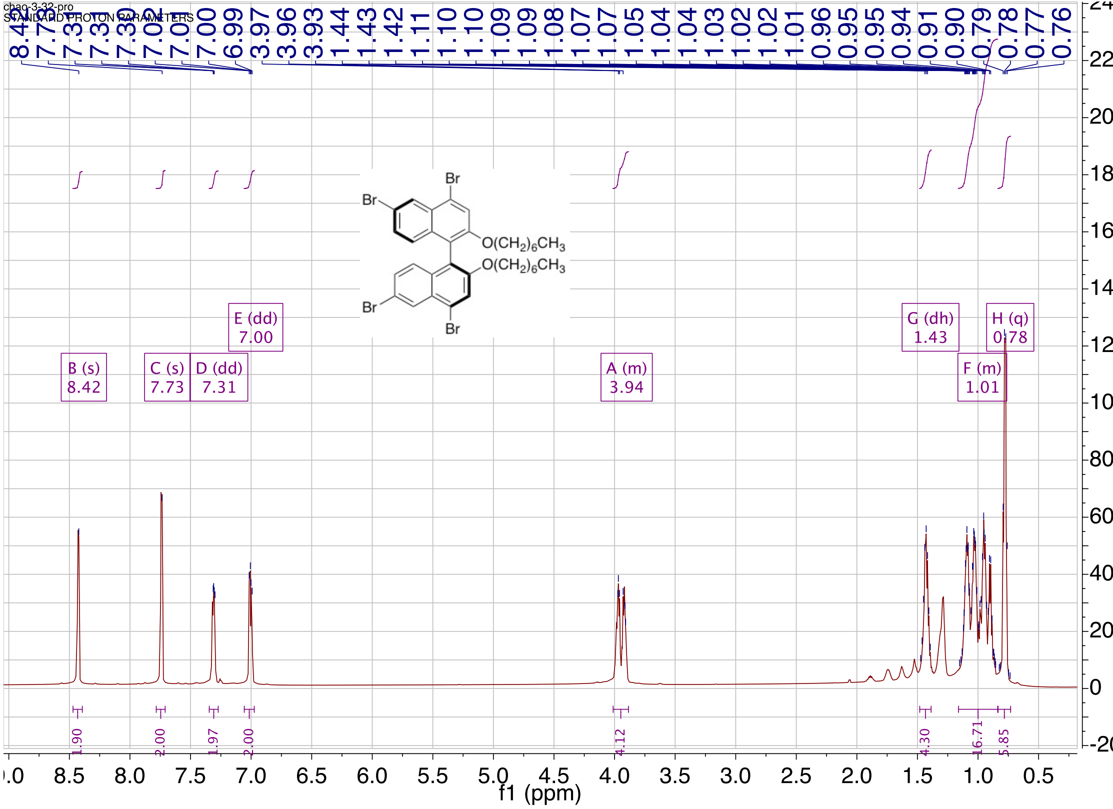
chao-3-32-pro
STANDARD PROTON PARAMETERS
8.42
7.73
7.31
7.31
7.30
7.02
7.01
7.00
6.99
3.97
3.96
3.93
1.44
1.43
1.42
1.11
1.10
1.10
1.09
1.09
1.08
1.07
1.07
1.05
1.04
1.04
1.03
1.02
1.02
1.01
0.96
0.95
0.95
0.94
0.91
0.90
0.79
0.78
0.77
0.76
Br
Br
O(CH2)6CH3
O(CH2)6CH3
Br
Br
E (dd)
7.00
B (s)
8.42
C (s)
7.73
D (dd)
7.31
A (m)
3.94
G (dh)
1.43
H (q)
0.78
F (m)
1.01
1.90
2.00
1.97
2.00
4.12
4.30
16.71
5.85
240
220
200
180
160
140
120
100
80
60
40
20
0
-20
9.0
8.5
8.0
7.5
7.0
6.5
6.0
5.5
5.0
4.5
4.0
3.5
3.0
2.5
2.0
1.5
1.0
0.5
f1 (ppm)

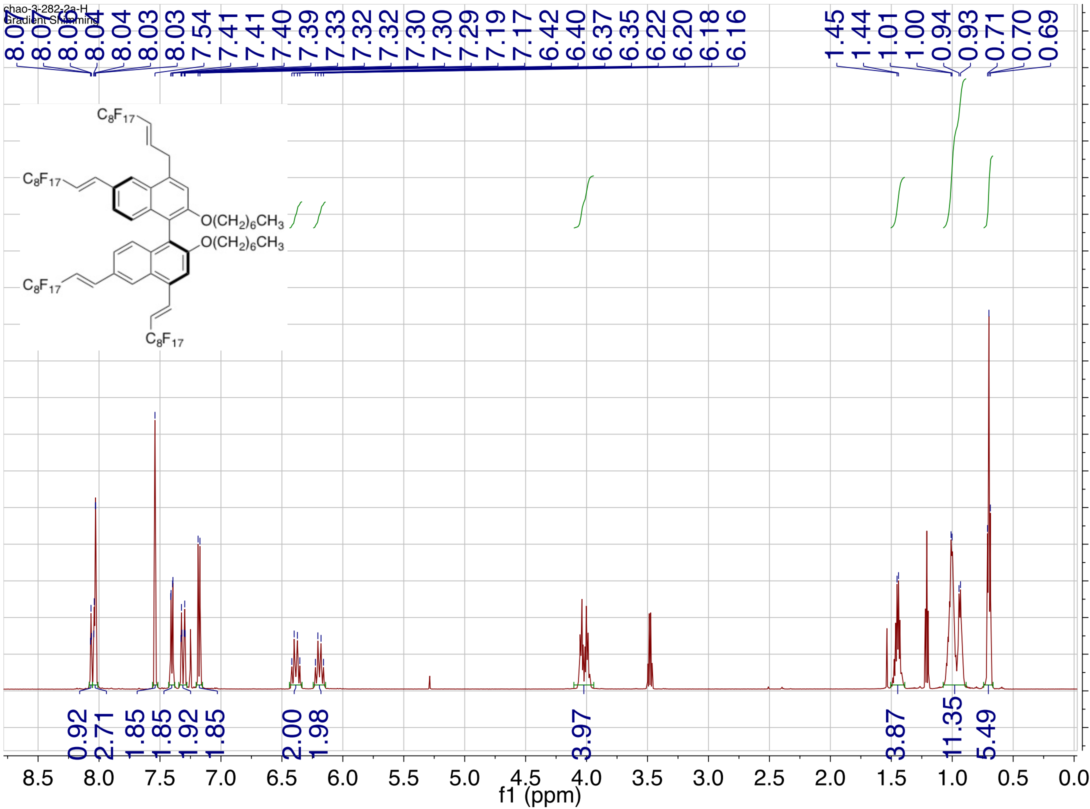
chao-3-282-2a-H
Gradient Shimming
8.07 8.07 8.05 8.04 8.04 8.03 8.03 7.54 7.41 7.41 7.40 7.39 7.33 7.32 7.32 7.30 7.30 7.29 7.19 7.17 6.42 6.40 6.37 6.35 6.22 6.20 6.18 6.16
1.45 1.44 1.01 1.00 0.94 0.93 0.71 0.70 0.69
C_8F_{17}
C_8F_{17}
$O(CH_2)_6CH_3$
$O(CH_2)_6CH_3$
C_8F_{17}
C_8F_{17}
0.92 2.71 1.85 1.85 1.92 1.85 2.00 1.98 3.97 3.87 11.35 5.49
8.5 8.0 7.5 7.0 6.5 6.0 5.5 5.0 4.5 4.0 3.5 3.0 2.5 2.0 1.5 1.0 0.5 0.0
f1 (ppm)
360 340 320 300 280 260 240 220 200 180 160 140 120 100 80 60 40 20 0 -20

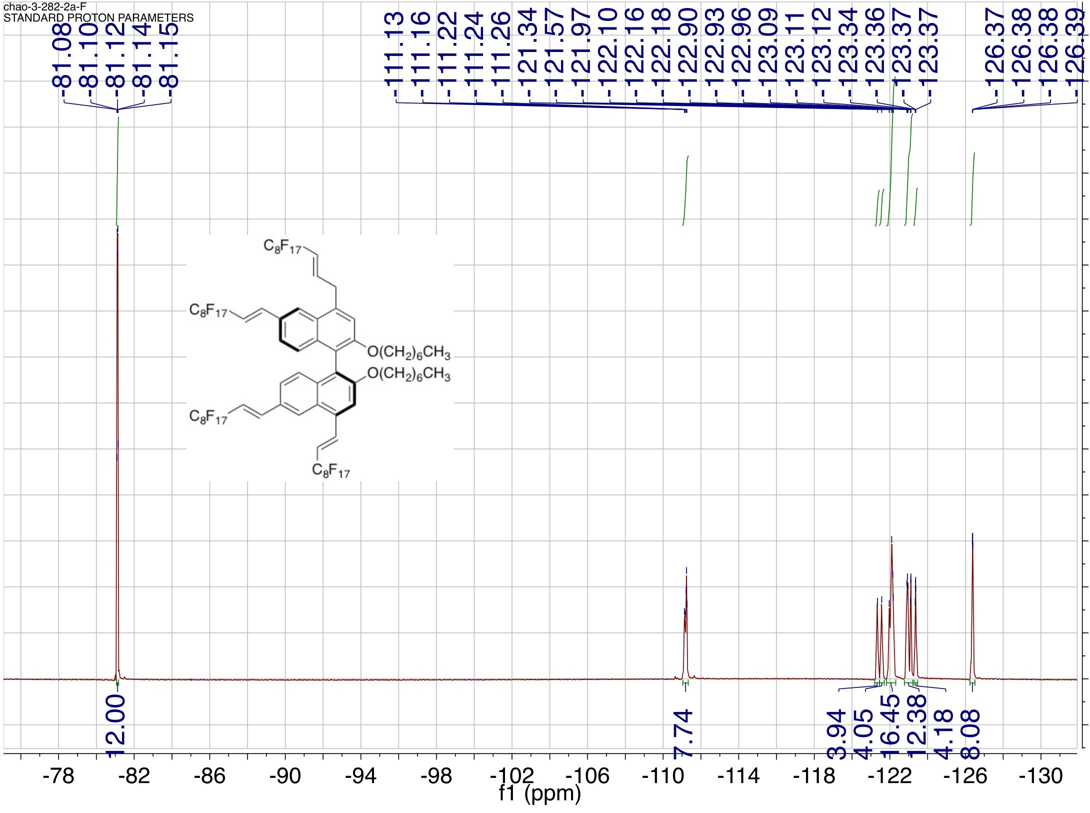
chao-3-282-2a-F
STANDARD PROTON PARAMETERS
-81.08 -81.10 -81.12 -81.14 -81.15
-111.13 -111.16 -111.22 -111.24 -111.26 -121.34 -121.57 -121.97 -122.10 -122.16 -122.18 -122.90 -122.93 -122.96 -123.09 -123.11 -123.12 -123.34 -123.36 -123.37 -123.37
-126.37 -126.38 -126.38 -126.39
C_8F_{17}
C_8F_{17}
$O(CH_2)_6CH_3$
$O(CH_2)_6CH_3$
C_8F_{17}
C_8F_{17}
12.00 7.74 3.94 4.05 16.45 12.38 4.18 8.08
-78 -82 -86 -90 -94 -98 -102 -106 -110 -114 -118 -122 -126 -130
f1 (ppm)
280 260 240 220 200 180 160 140 120 100 80 60 40 20 0 -20

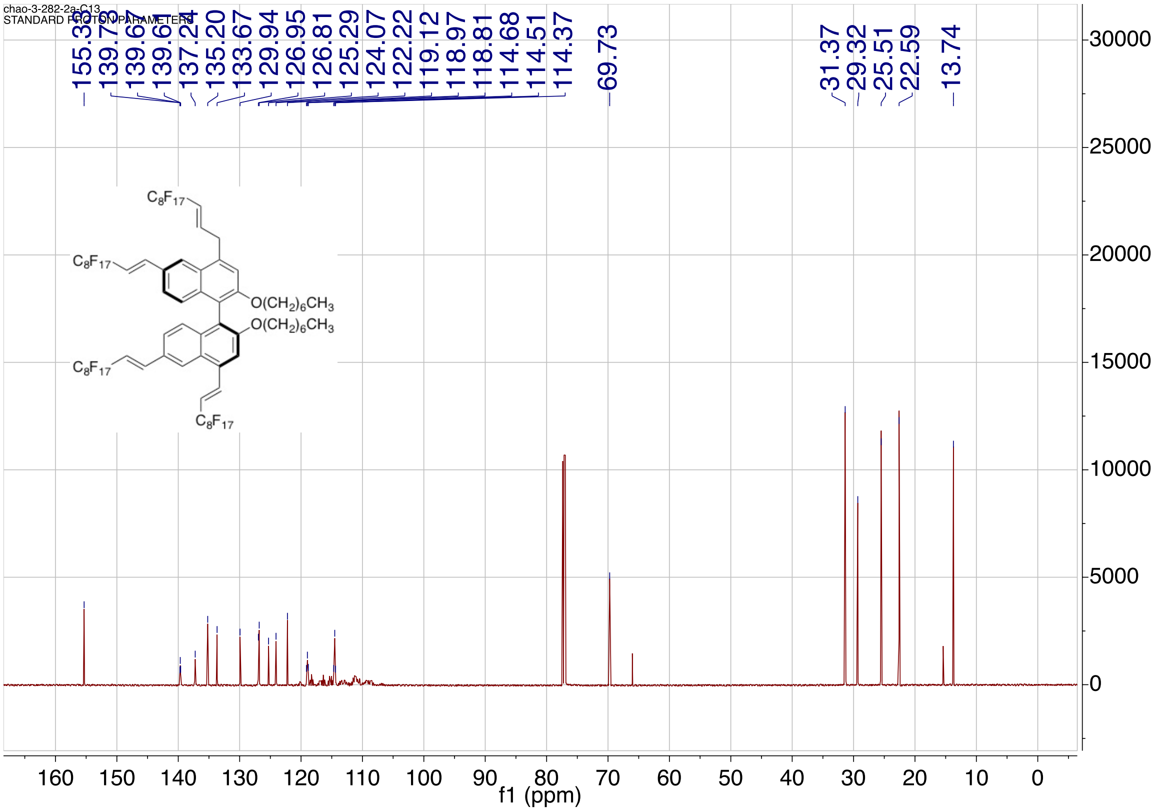
chao-3-282-2a-C13
STANDARD PROTON PARAMETERS
155.33
139.73
139.67
139.61
137.24
135.20
133.67
129.94
126.95
126.81
125.29
124.07
122.22
119.12
118.97
118.81
114.68
114.51
114.37
69.73
31.37
29.32
25.51
22.59
13.74
C_8F_{17}
C_8F_{17}
$O(CH_2)_6CH_3$
$O(CH_2)_6CH_3$
C_8F_{17}
C_8F_{17}
30000
25000
20000
15000
10000
5000
0
160
150
140
130
120
110
100
90
80
70
60
50
40
30
20
10
0
f1 (ppm)

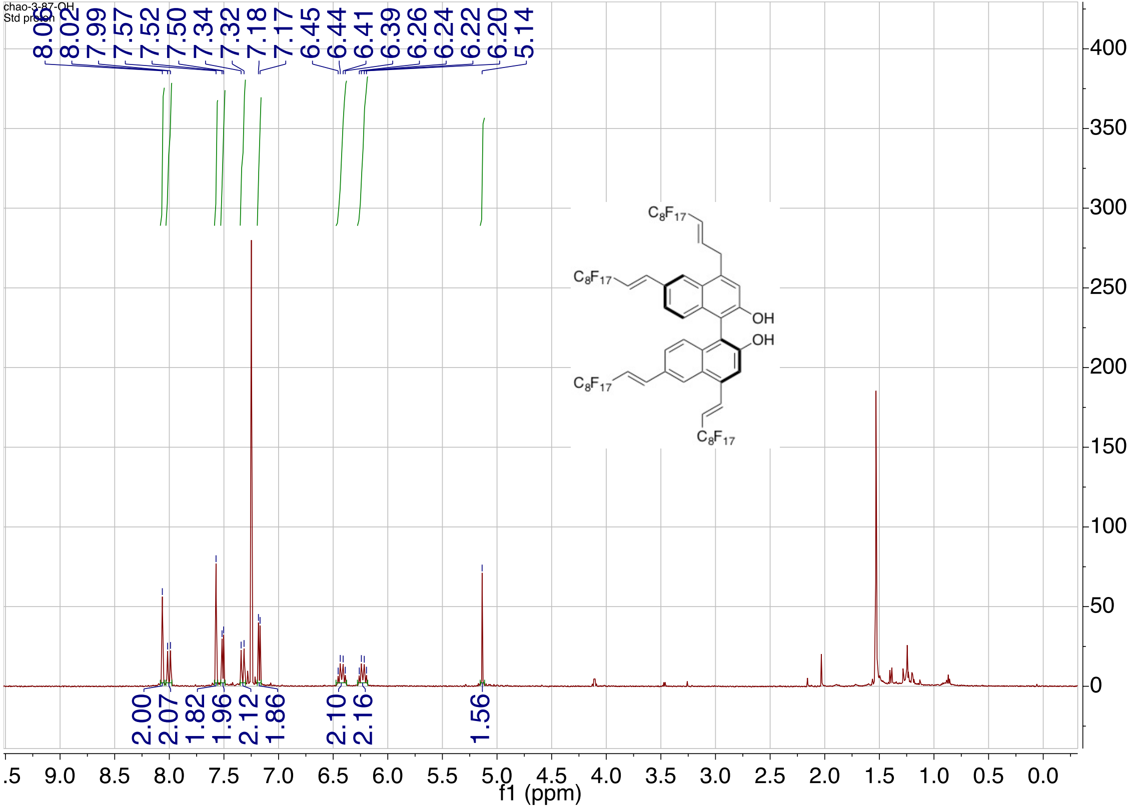
chao-3-87-OH
Std proton
8.06
8.02
7.99
7.57
7.52
7.50
7.34
7.32
7.18
7.17
6.45
6.44
6.41
6.39
6.26
6.24
6.22
6.20
5.14
C_8F_{17}
C_8F_{17}
OH
OH
C_8F_{17}
C_8F_{17}
2.00
2.07
1.82
1.96
2.12
1.86
2.10
2.16
1.56
400
350
300
250
200
150
100
50
0
.5
9.0
8.5
8.0
7.5
7.0
6.5
6.0
5.5
5.0
4.5
4.0
3.5
3.0
2.5
2.0
1.5
1.0
0.5
0.0
f1 (ppm)

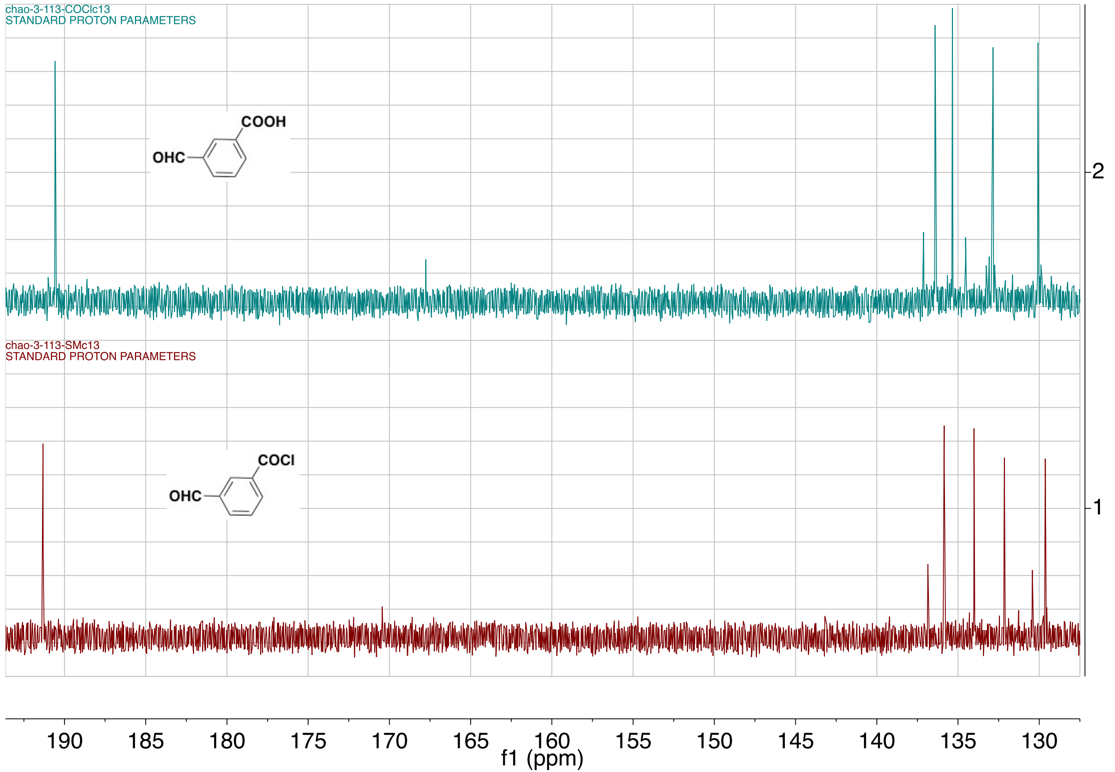
chao-3-113-COClc13
STANDARD PROTON PARAMETERS
COOH
OHC
chao-3-113-SMc13
STANDARD PROTON PARAMETERS
COCl
OHC
2
1
190
185
180
175
170
165
160
155
150
145
140
135
130
f1 (ppm)

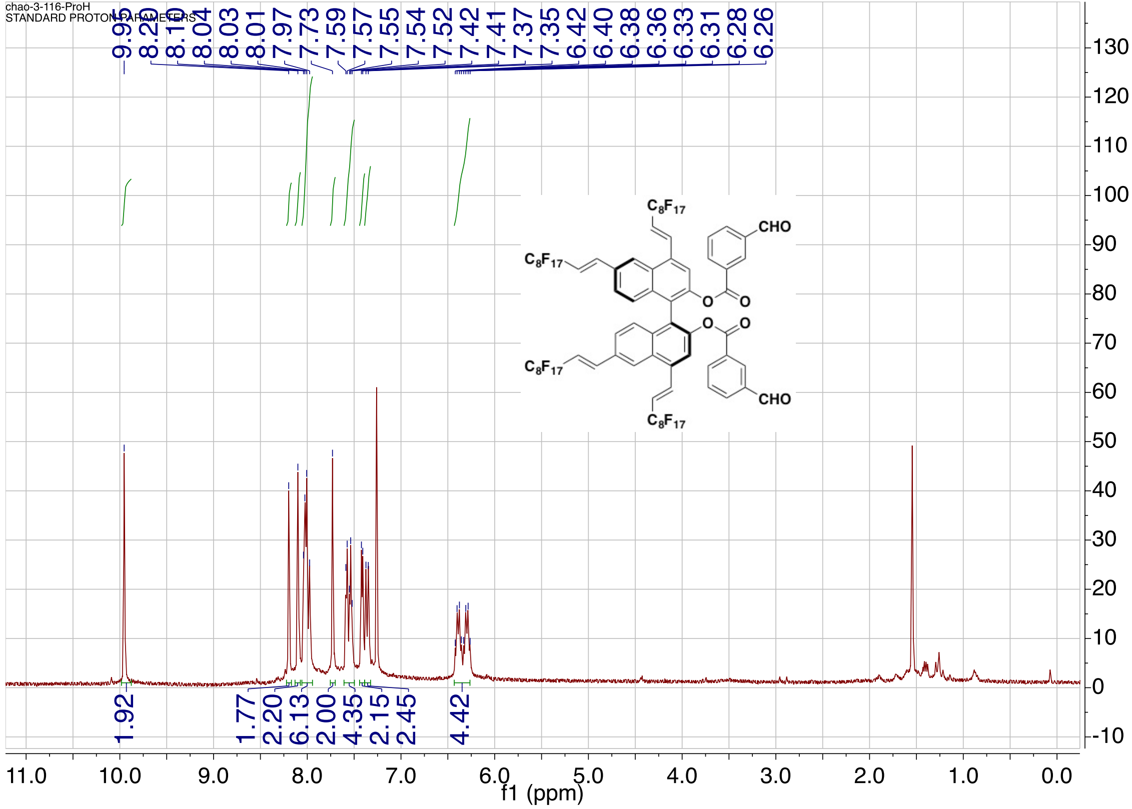
chao-3-116-ProH
STANDARD PROTON PARAMETERS
9.95
8.20
8.10
8.04
8.03
8.01
7.97
7.73
7.59
7.57
7.55
7.54
7.52
7.42
7.41
7.37
7.35
6.42
6.40
6.38
6.36
6.33
6.31
6.28
6.26
C_8F_{17}
CHO
C_8F_{17}
O
O
O
O
C_8F_{17}
CHO
C_8F_{17}
1.92
1.77
2.20
6.13
2.00
4.35
2.15
2.45
4.42
130
120
110
100
90
80
70
60
50
40
30
20
10
0
-10
11.0
10.0
9.0
8.0
7.0
6.0
5.0
4.0
3.0
2.0
1.0
0.0
f1 (ppm)

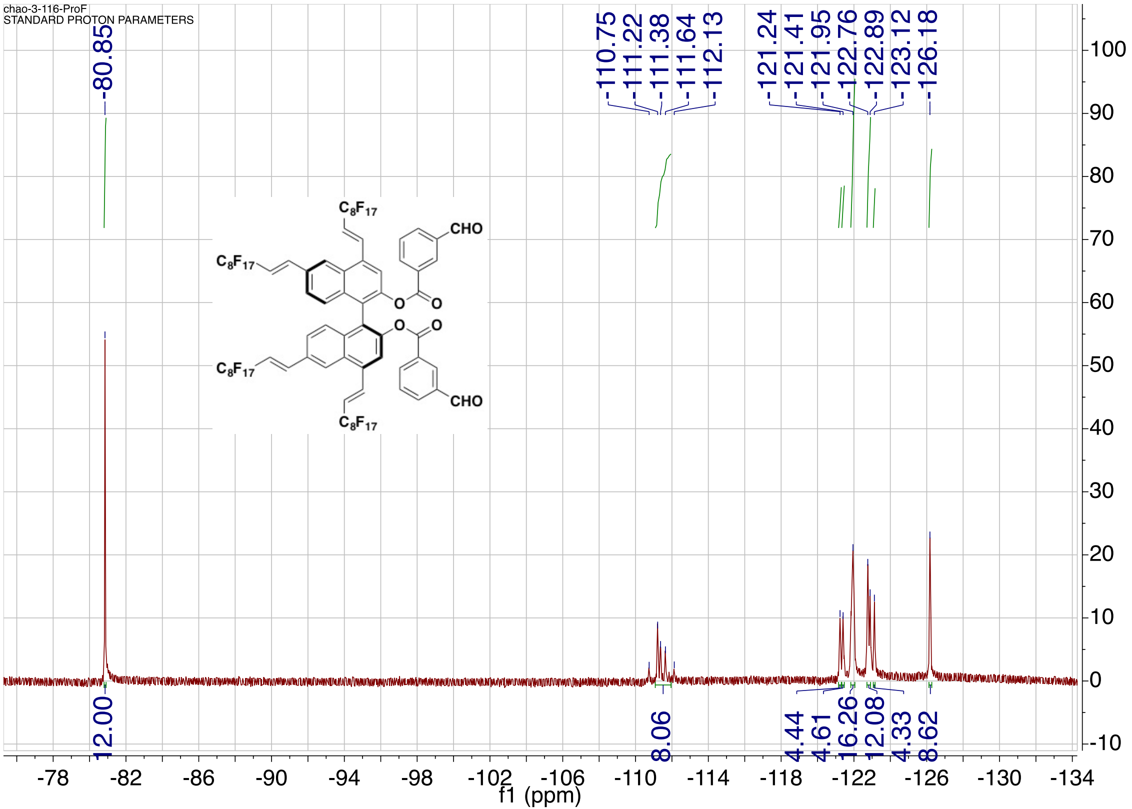
chao-3-116-ProF
STANDARD PROTON PARAMETERS
-80.85
-110.75
-111.22
-111.38
-111.64
-112.13
-121.24
-121.41
-121.95
-122.76
-122.89
-123.12
-126.18
C8F17
CHO
O
O
O
O
C8F17
C8F17
CHO
C8F17
12.00
8.06
4.44
4.61
16.26
12.08
4.33
8.62
100
90
80
70
60
50
40
30
20
10
0
-10
-78
-82
-86
-90
-94
-98
-102
-106
-110
-114
-118
-122
-126
-130
-134
f1 (ppm)

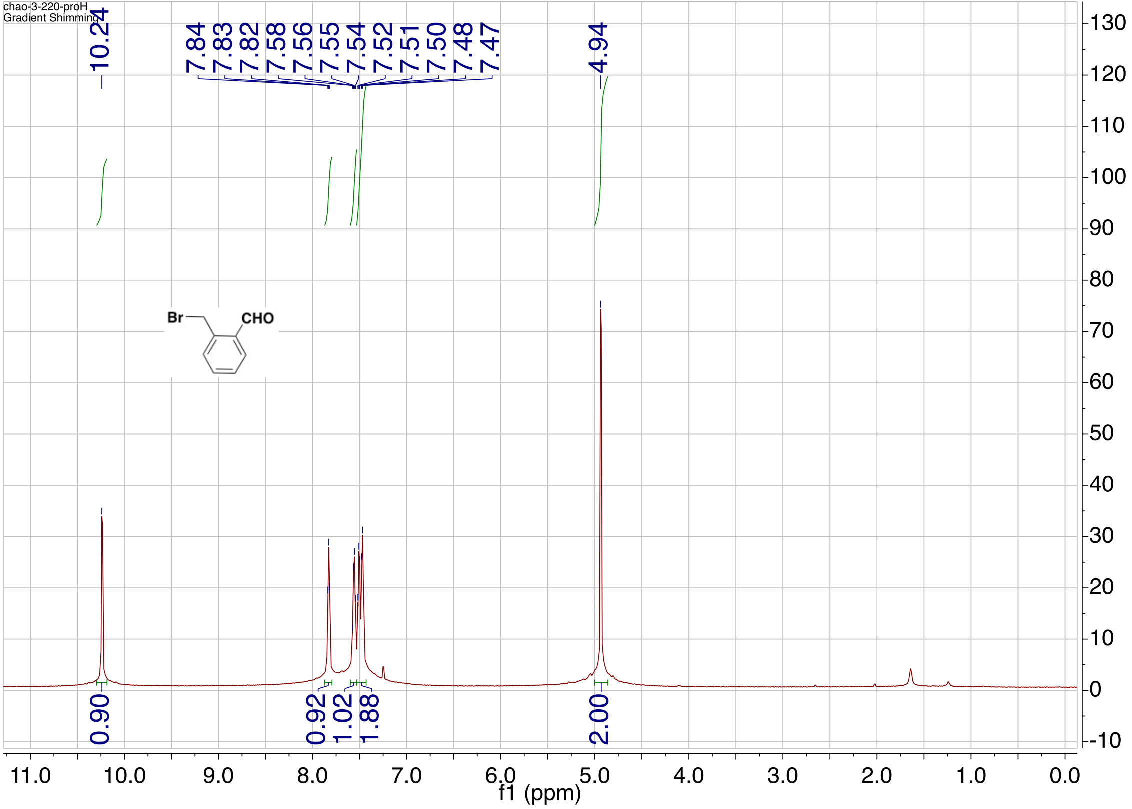
chao-3-220-proH
Gradient Shimming
10.24
7.84
7.83
7.82
7.58
7.56
7.55
7.54
7.52
7.51
7.50
7.48
7.47
4.94
Br
CHO
0.90
0.92
1.02
1.88
2.00
130
120
110
100
90
80
70
60
50
40
30
20
10
0
-10
11.0
10.0
9.0
8.0
7.0
6.0
5.0
4.0
3.0
2.0
1.0
0.0
f1 (ppm)

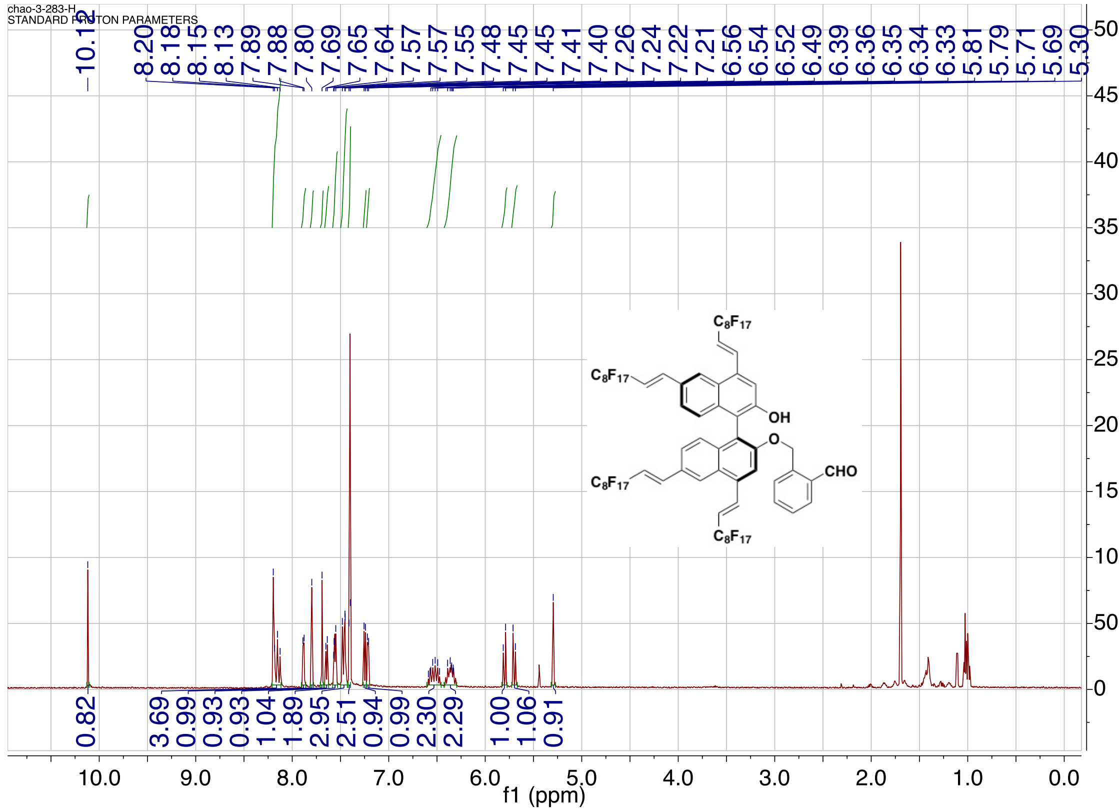
chao-3-283-H
STANDARD PROTON PARAMETERS
10.12
8.20 8.18 8.15 8.13 7.89 7.88 7.80 7.69 7.65 7.64 7.57 7.57 7.55 7.48 7.45 7.45 7.41 7.40 7.26 7.24 7.22 7.21 6.56 6.54 6.52 6.49 6.39 6.36 6.35 6.34 6.33 5.81 5.79 5.71 5.69 5.30
0.82
3.69 0.99 0.93 0.93 1.04 1.89 2.95 2.51 0.94 0.99 2.30 2.29
1.00 1.06 0.91
C8F17
C8F17
OH
O
CHO
C8F17
C8F17
500
450
400
350
300
250
200
150
100
50
0
10.0
9.0
8.0
7.0
6.0
5.0
4.0
3.0
2.0
1.0
0.0
f1 (ppm)

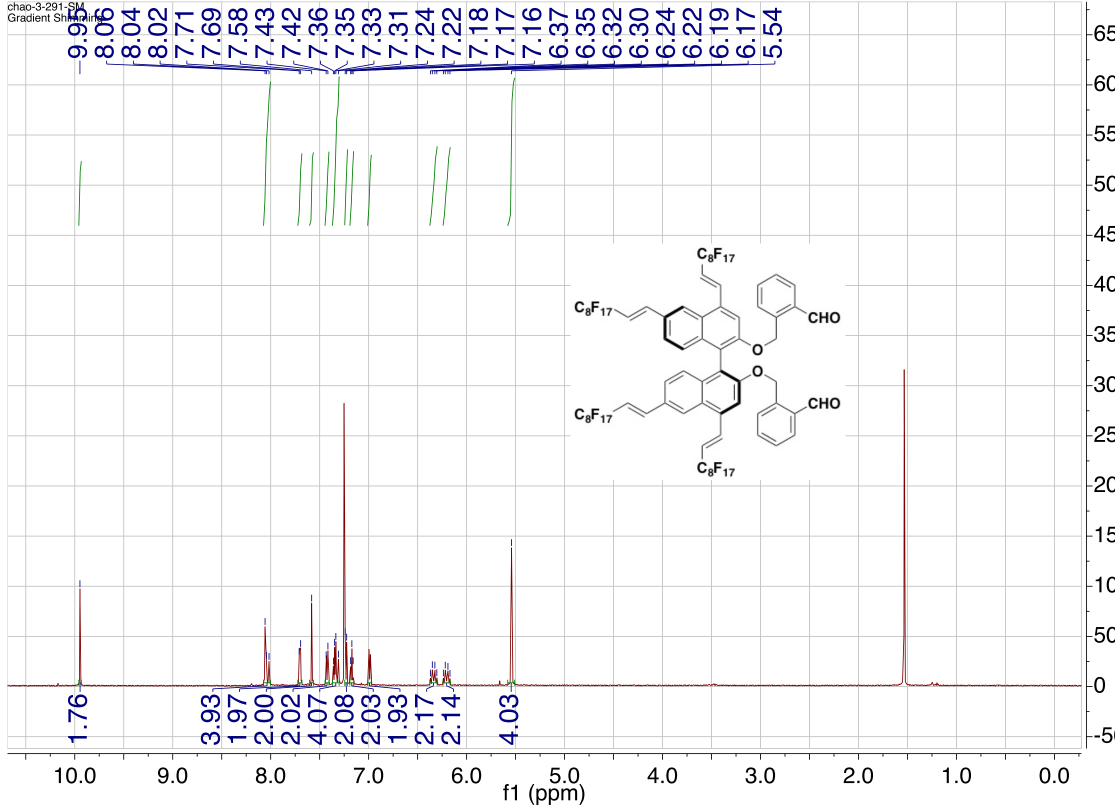
chao-3-291-SM
Gradient Shimming
9.96
8.06 8.04 8.02 7.71 7.69 7.58 7.43 7.42 7.36 7.35 7.33 7.31 7.24 7.22 7.18 7.17 7.16 6.37 6.35 6.32 6.30 6.24 6.22 6.19 6.17 5.54
1.76
3.93 1.97 2.00 2.02 4.07 2.08 2.03 1.93 2.17 2.14
4.03
C8F17
C8F17
CHO
O
O
CHO
C8F17
C8F17
650
600
550
500
450
400
350
300
250
200
150
100
50
0
-50
10.0
9.0
8.0
7.0
6.0
5.0
4.0
3.0
2.0
1.0
0.0
f1 (ppm)

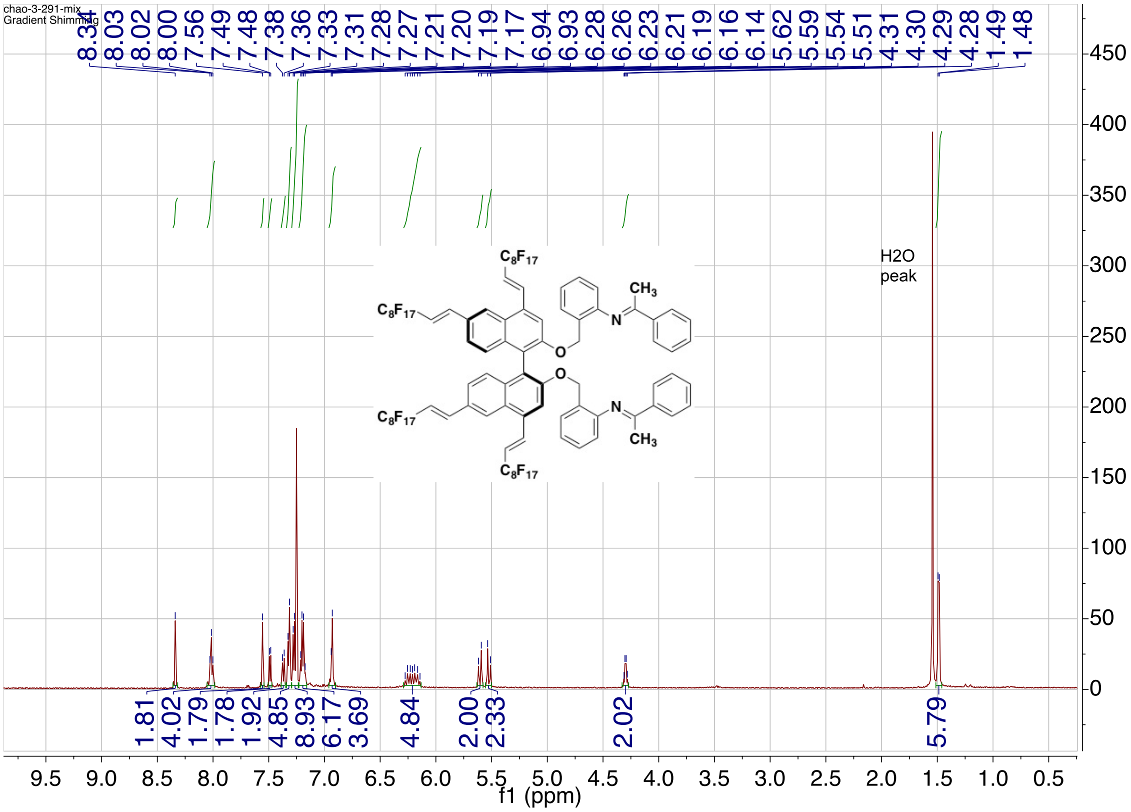
chao-3-291-mix
Gradient Shimming
8.34
8.03
8.02
8.00
7.56
7.49
7.48
7.38
7.36
7.33
7.31
7.28
7.27
7.21
7.20
7.19
7.17
6.94
6.93
6.28
6.26
6.23
6.21
6.19
6.16
6.14
5.62
5.59
5.54
5.51
4.31
4.30
4.29
4.28
1.49
1.48
H2O
peak
C_8F_{17}
C_8F_{17}
C_8F_{17}
C_8F_{17}
O
O
N
N
CH_3
CH_3
1.81
4.02
1.79
1.78
1.92
4.85
8.93
6.17
3.69
4.84
2.00
2.33
2.02
5.79
450
400
350
300
250
200
150
100
50
0
9.5
9.0
8.5
8.0
7.5
7.0
6.5
6.0
5.5
5.0
4.5
4.0
3.5
3.0
2.5
2.0
1.5
1.0
0.5
f1 (ppm)

Appendix for Chapter 7

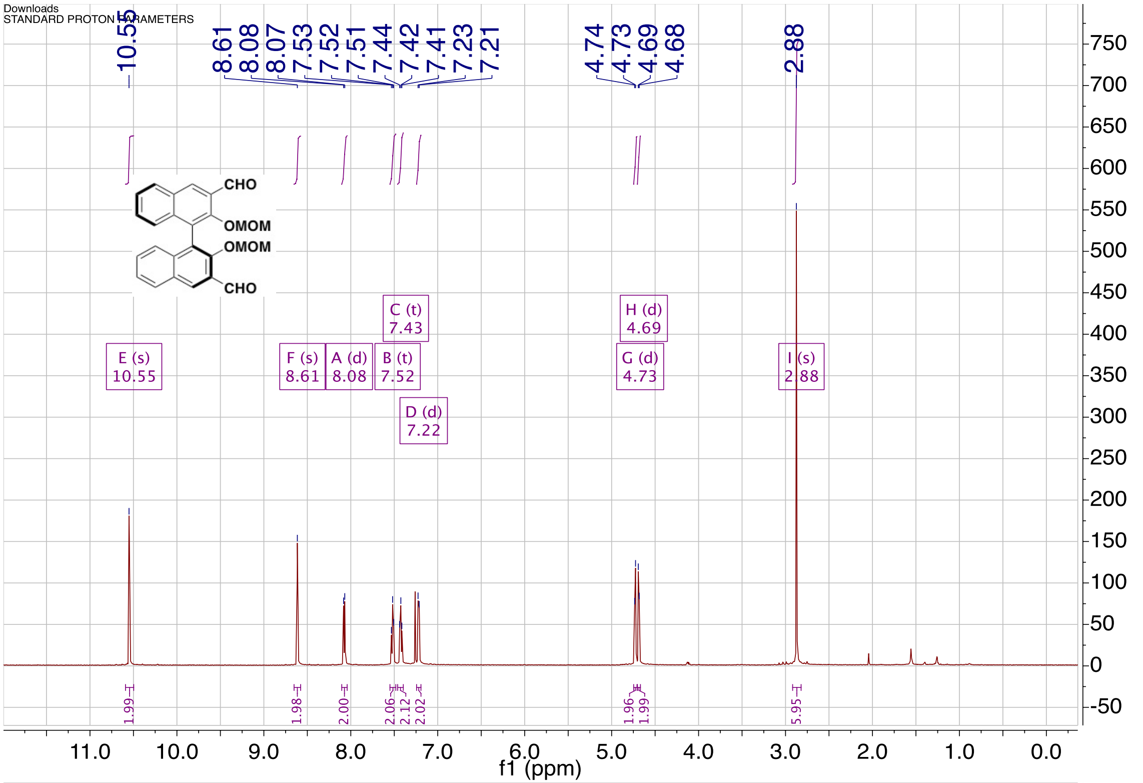

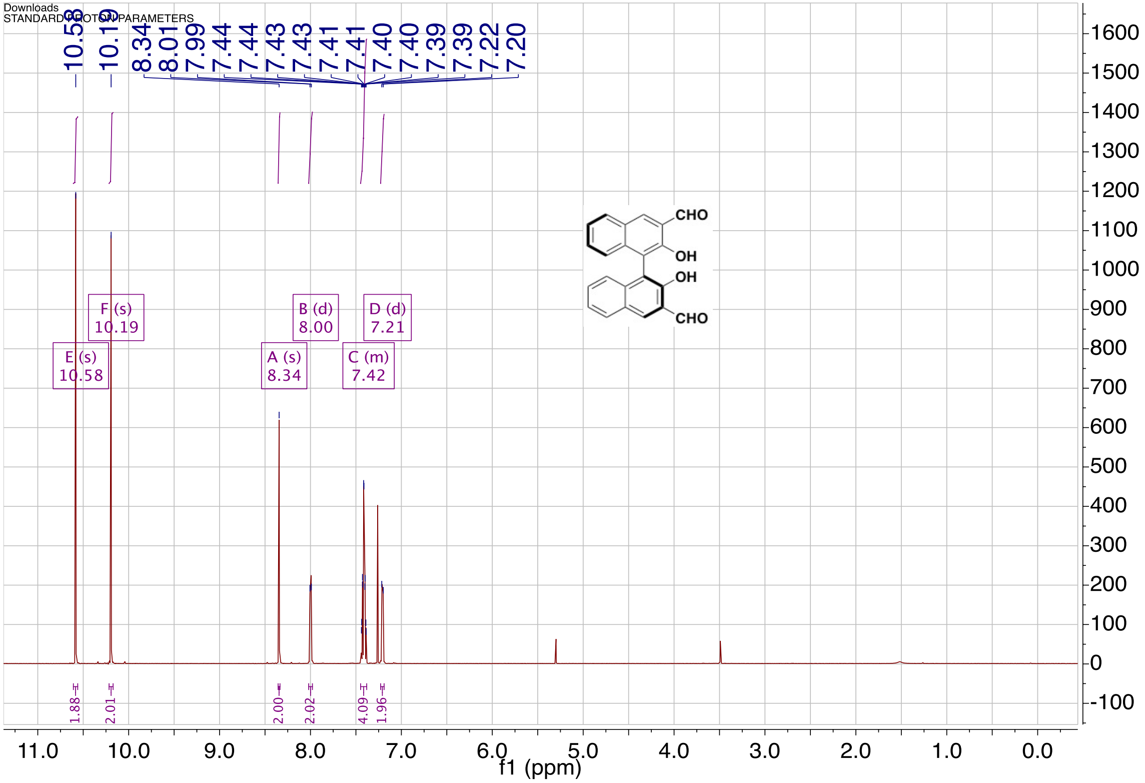

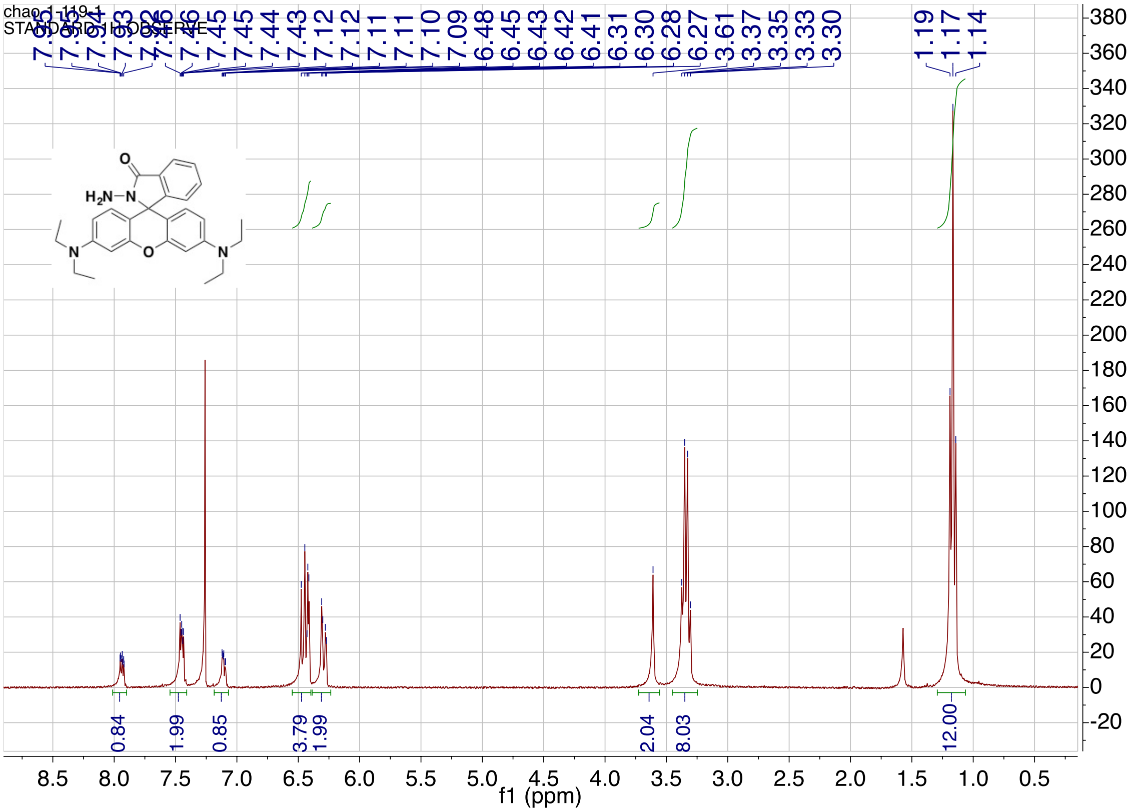
chao-1-119-1
STANDARD 1H OBSERVE
7.95 7.95 7.94 7.93 7.92 7.46 7.46 7.45 7.45 7.44 7.43 7.12 7.12 7.11 7.11 7.10 7.09 6.48 6.45 6.43 6.42 6.41 6.31 6.30 6.28 6.27 3.61 3.37 3.35 3.33 3.30 1.19 1.17 1.14
O
H2N
N
O
N
N
0.84 1.99 0.85 3.79 1.99 2.04 8.03 12.00
8.5 8.0 7.5 7.0 6.5 6.0 5.5 5.0 4.5 4.0 3.5 3.0 2.5 2.0 1.5 1.0 0.5
f1 (ppm)
380 360 340 320 300 280 260 240 220 200 180 160 140 120 100 80 60 40 20 0 -20

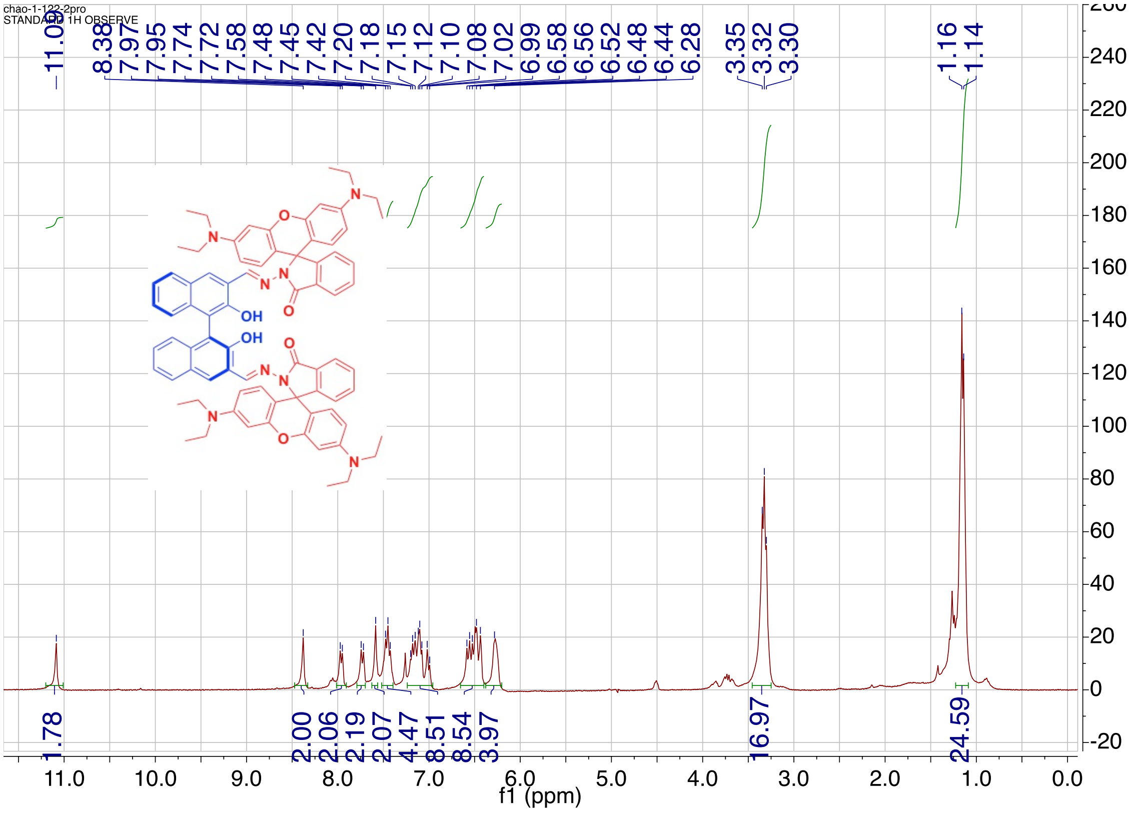
chao-1-122-2pro
STANDARD 1H OBSERVE
11.09 8.38 7.97 7.95 7.74 7.72 7.58 7.48 7.45 7.42 7.20 7.18 7.15 7.12 7.10 7.08 7.02 6.99 6.58 6.56 6.52 6.48 6.44 6.28 3.35 3.32 3.30 1.16 1.14
N
O
N
N
O
OH
OH
O
N
N
N
O
N
1.78 2.00 2.06 2.19 2.07 4.47 8.51 8.54 3.97 16.97 24.59
11.0 10.0 9.0 8.0 7.0 6.0 5.0 4.0 3.0 2.0 1.0 0.0
f1 (ppm)
240 220 200 180 160 140 120 100 80 60 40 20 0 -20

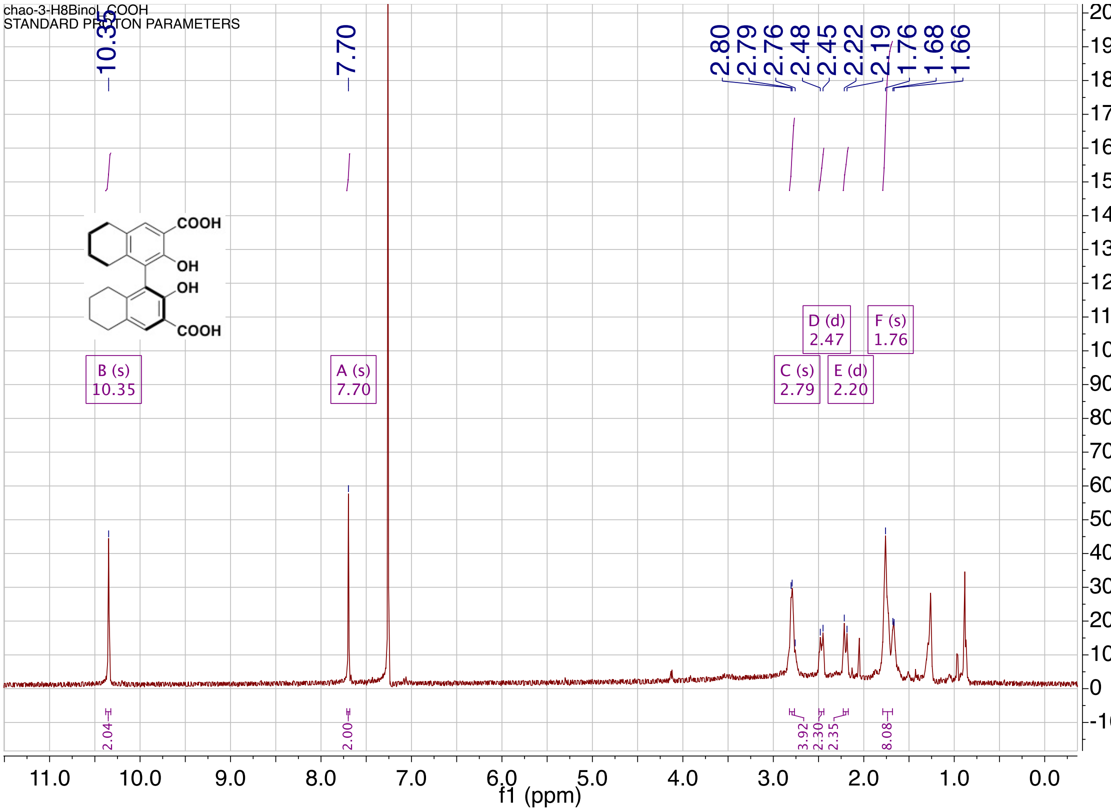
chao-3-H8Binol_COOH
STANDARD PROTON PARAMETERS
10.35
7.70
2.80 2.79 2.76 2.48 2.45 2.22 2.19 1.76 1.68 1.66
COOH
OH
OH
COOH
B (s) 10.35
A (s) 7.70
C (s) 2.79
D (d) 2.47
E (d) 2.20
F (s) 1.76
2.04
2.00
3.92
2.30
2.35
8.08
200 190 180 170 160 150 140 130 120 110 100 90 80 70 60 50 40 30 20 10 0 -10
11.0 10.0 9.0 8.0 7.0 6.0 5.0 4.0 3.0 2.0 1.0 0.0
f1 (ppm)

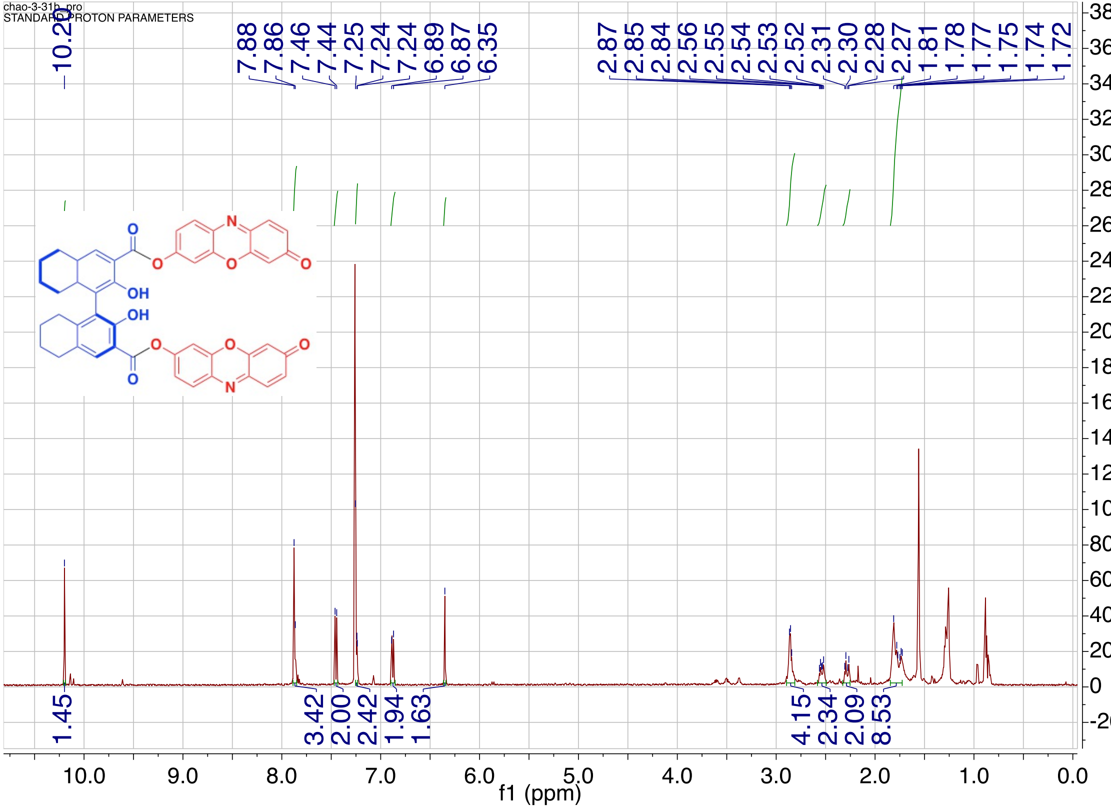
chao-3-31b_pro
STANDARD PROTON PARAMETERS
10.20
7.88 7.86 7.46 7.44 7.25 7.24 7.24 6.89 6.87 6.35
2.87 2.85 2.84 2.56 2.55 2.54 2.53 2.52 2.31 2.30 2.28 2.27 1.81 1.78 1.77 1.75 1.74 1.72
O
N
O
O
OH
OH
O
O
O
N
O
1.45
3.42
2.00
2.42
1.94
1.63
4.15
2.34
2.09
8.53
380 360 340 320 300 280 260 240 220 200 180 160 140 120 100 80 60 40 20 0 -20
10.0 9.0 8.0 7.0 6.0 5.0 4.0 3.0 2.0 1.0 0.0
f1 (ppm)

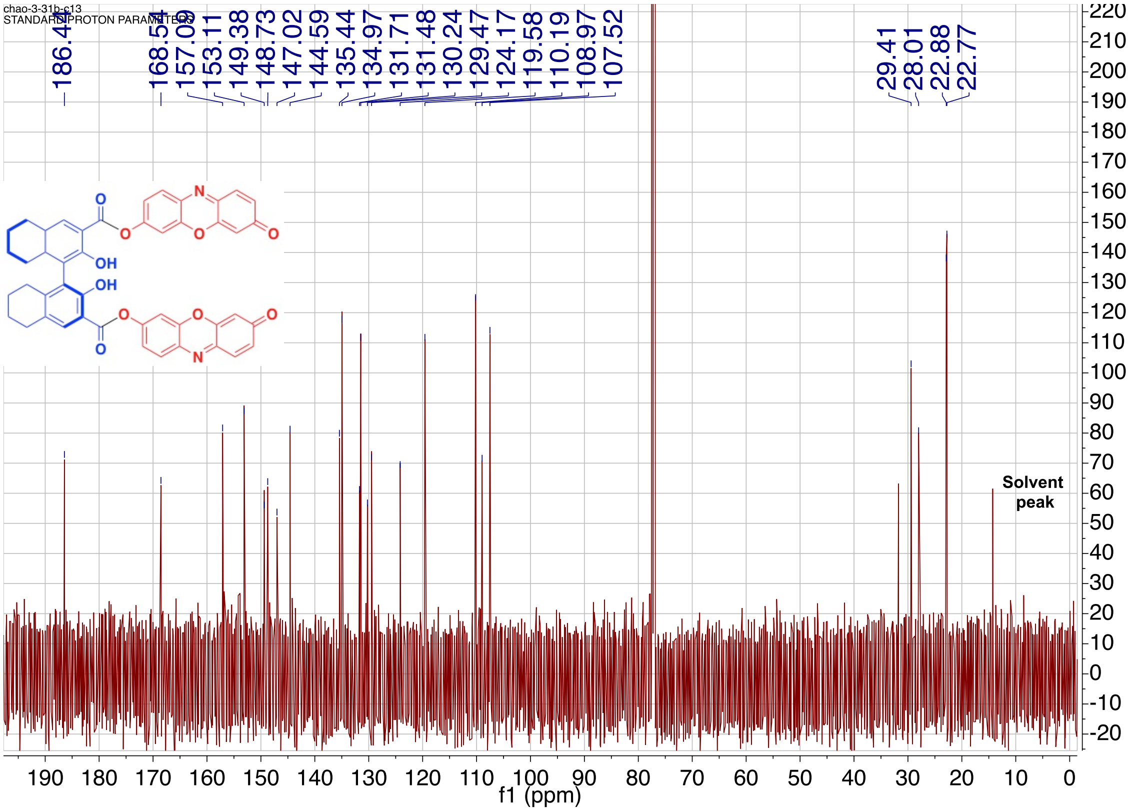
chao-3-31b-c13
STANDARD PROTON PARAMETERS
186.44
168.54
157.09
153.11
149.38
148.73
147.02
144.59
135.44
134.97
131.71
131.48
130.24
129.47
124.17
119.58
110.19
108.97
107.52
29.41
28.01
22.88
22.77
O
N
O
O
OH
OH
O
O
O
N
O
O
Solvent peak
220
210
200
190
180
170
160
150
140
130
120
110
100
90
80
70
60
50
40
30
20
10
0
-10
-20
190
180
170
160
150
140
130
120
110
100
90
80
70
60
50
40
30
20
10
0
f1 (ppm)